CHEMICAL REVIEWS

pubs.acs.org/CR

Review

Designing Sites in Heterogeneous Catalysis: Are We Reaching Selectivities Competitive With Those of Homogeneous Catalysts?

Francisco Zaera*

Cite This: https://doi.org/10.1021/acs.chemrev.1c00905

Read Online

ACCESS | Metrics & More | Article Recommendations

ABSTRACT: A critical review of different prominent nanotechnologies adapted to catalysis is provided, with focus on how they contribute to the improvement of selectivity in heterogeneous catalysis. Ways to modify catalytic sites range from the use of the reversible or irreversible adsorption of molecular modifiers to the immobilization or tethering of homogeneous catalysts and the development of well-defined catalytic sites on solid surfaces. The latter covers methods for the dispersion of single-atom sites within solid supports as well as the use of complex nanostructures, and it includes the post-modification of materials via processes such as silylation and atomic layer deposition. All these methodologies exhibit both advantages and limitations, but all offer new avenues for the design of catalysts for specific applications. Because of the high cost of most nanotechnologies and the fact that the resulting materials may exhibit limited thermal or chemical stability, they may be best aimed at improving the selective synthesis of high value-added chemicals, to be incorporated in organic synthesis schemes, but other applications are being explored as well to address problems in energy production, for instance, and to design greener chemical processes. The details of each of these approaches are discussed, and representative examples are provided. We conclude with some general remarks on the future of this field.

CONTENTS

Received: October 25, 2021

1. INTRODUCTION

The modern holy grail of catalysis has become selectivity.[1−3] In the early days of Berzelius, catalysts were introduced as substances used to accelerate reaction rates.[4] In those times, the reactions being promoted were relatively simple, and typically did not yield many byproducts. However, the applications of chemical catalysis have expanded enormously over the years, and now address many complex chemical synthesis processes.[5,6] As the targets of catalysts have become more sophisticated, the ability to promote the proper reactions selectively, discriminating against other pathways, has become increasingly more difficult. For instance, with organic molecules having multiple unsaturations, how can one of those bonds be hydrogenated without affecting the others?[7−9] In oxidation processes, how can complete oxidation, which ultimately produces carbon dioxide and water, be avoided?[10−13] In organic synthesis, how can stereochemistry and enantiochemistry be directed?[14−17] These challenges require careful design of catalysts involving the control of many molecular details.[3] Because of concerns associated with the excessive consumption of feedstocks, the need to minimize the use of expensive separation and purification methods, and the desire to avoid polluting byproducts, improving selectivity is often more important than speeding up reactions in industrial processes.[1]

From a molecular point of view, selectivity in catalysis can be controlled by forcing the reactants to traverse the potential energy surface toward a particular transition state; that transition state is expected to induce the appropriate electronic and geometrical changes needed to form the desired products.[3,18−24] In this light, what is needed is a catalyst with reaction sites that favor such transition states. In particular, one can conceive a molecule or solid with "pockets" having the right shape, where the only way for reactants to access them is by adopting the right configuration for conversion. This "lock and key" model is one often used to understand enzymatic catalysis.[25−28] In addition, the temporary bonding between reactant and catalysts can take place at particular atoms or sites of the latter where appropriate electron donation or electron withdrawing may occur as needed. The challenge is to be able to develop catalysts with well-defined and identical sites displaying these desirable structural and electronic characteristics.

The demanding requirements on the structural and electronic characteristics of catalytic sites are best met at a molecular level. Enzymes in particular, having complex molecular structures, carry out catalytic functions in living organisms under mild conditions and with exquisite selectivity.[29] However, although they are certainly used in some applications, enzymes are in general finicky and hard to preserve outside living organisms, and typically promote reactions at slow rates. They are, therefore, difficult to use in industrial settings.[30−33] Instead, most practical processes, especially those dealing with sophisticated synthesis such as in the pharmaceutical, agro, and fine chemical industries, rely on the use of homogeneous catalysts.[6,34−36] Often, these consist of organometallic or other metal organic compounds where metal centers act as binding sites for reaction while the surrounding ligands provide the appropriate geometrical and electronic characteristics required to promote the desired reaction.[37,38] The main drawback of homogeneous catalysis is that, because the catalyst is added to the same solution that contains the reactants and products, expensive and energy-consuming separation processes are needed afterwards.[39,40] In fact, because many metals are toxic, the requirements for the purification step in medical and food-related applications are quite stringent and sometimes near to impossible to fulfill. Many homogeneous catalysts also have the tendency to decompose after a limited number of turnovers.[41]

The ideal solution to these problems lies in heterogeneous catalysis, where the catalyst, typically a solid, exists in a different phase to that of the reaction mixture (a gas or a liquid solution). The main limitation here is that it is not trivial to generate complex catalytic sites with identical structural and electronic characteristics in large numbers in solids. To the extent that the processes to be catalyzed are relatively simple, such as in oil refining and in the manufacture of basic chemicals such as ammonia, hydrogen, and syn gas, this problem can be overcome; heterogeneous catalysis has for a long time been at the center of the production of simple products such as small olefins, ammonia, sulfuric acid, hydrogen cyanide, formaldehyde, and vinyl acetate, as well as in the hydrodesulfurization (HDS), cracking, and reforming of fossil fuels.[42,43] The three-way catalyst is another excellent example of the success of heterogeneous catalysis, in that case for environmental remediation applications.[44,45] On the other hand, in difficult organic syntheses, the state of the art does not, in general, provide sufficient tools to design the appropriate solids to promote the reactions involved with acceptable selectivities.[46] This, however, may be changing. Several approaches have been advanced in recent years to produce solids with the well-defined and complex structures that may facilitate the transition from homogeneous to heterogeneous catalysis for the manufacture of fine and speciality chemicals.[21,47−56]

In this report, we provide a critical review of the main routes taken to address this issue. We start our discussion in Section 2 with the immobilization or tethering of homogeneous catalysts, organic functionalities, or enzymes on surfaces. Next, in Section 3, we introduce the way catalytic surfaces can be modified via the adsorption of modifiers, discrete molecules that can act as co-catalysts and/or help define the structural details of the catalytic site. These modifiers can be added reversibly, typically from liquid solutions (where their adsorption-desorption equilibria can be adjusted), or irreversibly, relying on strong bonding between the modifier and the surface, as in the case of self-assembly monolayers (SAMs). Alternatively, the catalytic site can be designed and built entirely on solid surfaces without any molecular components. One prominent new approach in this category is single-site catalysis, an idea introduced in Section 4. In parallel, some research groups have been attempting to harness the recent advances seen in nanotechnology to synthesize solids with complex but well-defined structures that may promote specific catalysis. Some of this work has focused on metal nanostructures (Section 5), but additional effort has been directed at oxides and other non-metallic nanomaterials as well (Sections 6 and 7). Finally, existing solids may be modified afterwards, via the deposition of thin films on their surfaces or by other treatments, as reported in Section 8. We end with a general discussion of the advantages and limitations of each of

https://doi.org/10.1021/acs.chemrev.1c00905
Chem. Rev. XXXX, XXX, XXX−XXX

the approaches discussed here, and with a personal outlook for this field.

2. IMMOBILIZATION OF HOMOGENEOUS CATALYSTS ON SURFACES

One of the oldest approaches for the design of highly selective heterogeneous catalysts has been by immobilizing, grafting, or tethering homogeneous catalysts on solid surfaces.[57−62] Particular selectivity in catalysis can be obtained with organometallic and metal organic complexes, and much effort has been directed over the years toward the effective addition of those to porous solid surfaces, typically to oxides[63−65] but also to other materials such as polymers.[66,67] To provide stability, metal organic complex additions to solids often rely on a form of covalent bonding, but the use of other noncovalent interactions has in some instances proven successful as well.[68] More complex molecules, enzymes in particular, have been immobilized to produce highly selective heterogeneous catalysts. Examples of this approach are provided next.

2.1. Direct Grafting of Organometallic and Metal Organic Catalysts to Surfaces

Much effort has been directed over the years toward immobilizing homogeneous catalysts on solids in a way that allows them to retain their catalytic performance, in particular their high selectivity for the desired process. In many instances, organometallic and metal organic catalysts are grafted on solids via direct coordination to specific sites on the surface, typically hydroxyl groups on solid oxides. In this approach, sometimes referred to as surface organometallic chemistry,[69] the surface acts as one of the ligands in the coordination sphere of the metal center, and replaces another ligand from the original compound. Although this methodology has been tested for decades,[64,70−73] it has regained prominence in recent years under the banner of "single-site" catalysis, as discussed in more detail later in this review (Section 4.1).[65,74−81] One nice example of coordinatively attaching homogeneous organometallic catalysts to surfaces is that of a silica-grafted dihydride pincer complex used for olefin hydrogenation (Figure 1).[82,83]

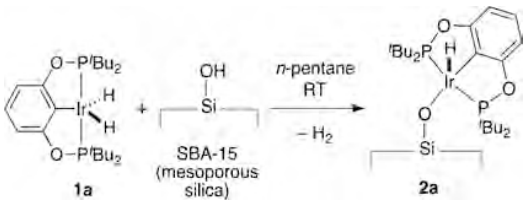

Figure 1. Schematics of a process followed to graft a dihydride pincer complex [IrH$_2$(POCOP), (POCOP = 1,3-bis((di-*tert*-butylphosphino)oxy)benzene, **1a**] onto mesoporous silica (SBA-15), forming a 16-electron iridium(III)monohydride species [IrH(O−SBA-15)(POCOP)] (**2a**).[83] Reproduced with permission from ref 83. Copyright 2014 American Chemical Society.

In another case, two novel tris(tert-butoxy)siloxy palladium(II) complexes were covalently grafted onto the surface of mesoporous silica to produce a heterogeneous catalyst capable of selectively promoting the semihydrogenation of 1-phenyl-1-propyne to (Z)-1-phenyl-1-propene.[84] On carbon nanotubes, the surface was derivatized with pyridine to act as a coordinating ligand for the anchoring of an Fe porphyrin to promote the electrocatalytic reduction of oxygen (ORR).[85]

Immobilization of organometallic complex can also be used to heterogenize molecular photoactive centers, or even photosensitizers.[86−89] In a recent example, [Re(bpy)(CO)$_3$Cl] was deposited on a bpy-derivatized mesoporous organosilica surface (bpy-PMO) via a ligand exchange reaction to form a new immobilized Re(CO)$_3$Cl(bpy−PMO) photocatalytic center (Figure 2).[90] Unfortunately, the activity of this

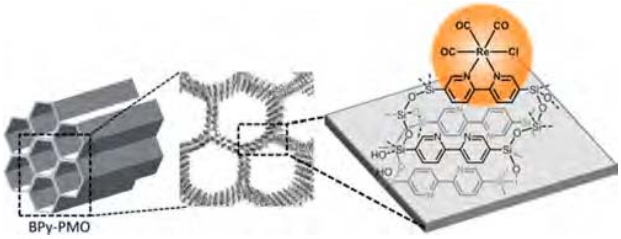

Figure 2. Immobilization of a molecular rhenium-based photosensitizer on an organosilica mesoporous support.[90] Reproduced with permission from ref 90. Copyright 2018 Wiley-VCH Verlag GmbH & Co. KGaA, Weinheim.

heterogeneous Re complex for the photocatalytic reduction of CO_2 was lower than that of the corresponding homogeneous Re complex, presumably because of a reduced phosphorescence lifetime resulting from immobilization. This is a common problem with photoactive molecules as they interact with solids, a phenomenon that is often accompanied by a red shift in light absorption energy. In the Re(CO)$_3$Cl(bpy−PMO) system, additional photocatalytic activity enhancement could be accomplished via the co-immobilization of the [Ru(bpy)$_3$]$^{2+}$ photosensitizer on the PMO surfaces. In another study, both a Ru(II)(bpy-dicarboxylic acid−2H)(4-picoline)(N-(3-(triethoxysilyl)propyl)isonicotinamide) photoactive catalyst and a [Ru(bpy)$_2$(4,4-(PO$_3$H$_2$)$_2$bpy)]Br$_2$ photosensitizer were immobilized successfully on a TiO_2 surface and used for the splitting of water with visible light.[91] Going one step further, a third research group tethered molecular Ru- and Co-complexes to a n-type TiO_2 anode and a p-type NiO cathode, respectively, using pyridine-2,6-dicarboxylic acid and the [Ru(bpy)$_2$(4,4′-(PO$_3$H$_2$)$_2$bpy)]^2 photosensitizer, to promote both the corresponding oxygen evolution (OER) and hydrogen evolution (HER) reactions in a full water-splitting photoelectrochemical device;[92] other tethered organic photosensitizers were tested at a later stage.[93] In a fourth example, the polyoxometalate [(PW$_9$O$_{34}$)$_2$Co$_4$(H$_2$O)$_2$]$^{10-}$ ion was immobilized in the hexagonal channels of the Zr(IV) porphyrinic MOF-545 hybrid framework to be used as an all-in-one heterogeneous photocatalytic system for visible-light-driven water oxidation with the catalyst and the photosensitizer within the same porous solid material.[94] On a p-type NiO photocathode, an immobilized 4-[bis(4-{5-[2,2-dicyanovinyl]-thiophene-2-yl}phenyl)amino]benzoic acid organic dye (P1) has been combined with immobilized carbon monoxide dehydrogenase (an enzyme) for the selective visible-light promotion of the reduction of CO_2 to CO at low potentials.[95]

The coordinated complexes used in these applications typically consist of a single metal center surrounded by the appropriate organic ligands, but in some instance small metal clusters have been immobilized as well;[77,96] the use of multiple metal atoms affords the creation of more complex adsorption sites on the surface.[97,98] Figure 3 shows some of the metal clusters that have been successfully deposited on solid

https://doi.org/10.1021/acs.chemrev.1c00905
Chem. Rev. XXXX, XXX, XXX−XXX

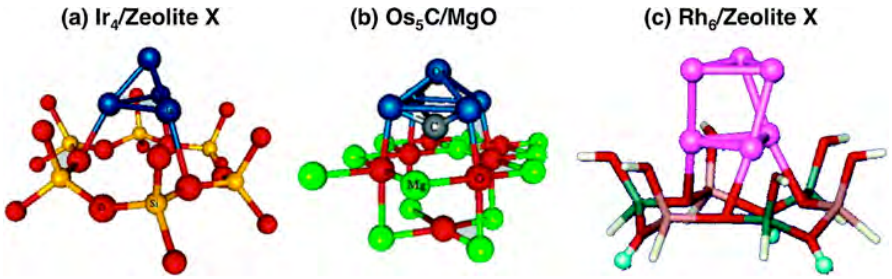

Figure 3. Structures of some of the metal clusters that have been successfully dispersed on solid surfaces: (a) Ir_4 on Zeolite X; (b) Os_5C on MgO; and (c) Rh_6 on Zeolite X.[99] Reproduced with permission from ref 96. Copyright 2006 American Chemical Society.

substrates, on oxides such as SiO_2 or MgO.[96,99] The coordinated ligand is often CO, but multicenter metalorganic complexes with other ligands have been immobilized on solid surfaces too, typically on silica or related oxides. Examples in this category include the reported grafting of $[Fe\{\mu^1\text{-}C_6H_2(CH_3)_3\}\{\mu^2\text{-}C_6H_2(CH_3)_3\}]_2$,[100] and $[Fe(II)\{N(SiHMe_2)_2\}_2]_2$[101] on silica substrates. Cases of the deposition of larger (thiol- or phospine-based) clusters include a series of $Au_n(PPh_3)_y$ (n = 8, 9, 11, and 101, variable y), immobilized on titania nanoparticles (NPs).[102] One important observation common to many of these reports is that, although deposition can sometimes be performed with preservation of the molecular structure, these clusters do tend to undergo partial decomposition, decarbonylation in the case of metal carbonyls, especially when exposed to catalytic conditions; this is the case in the examples in Figure 3.[103,104] In fact, in some instances the ligand loss, breakup, and reformation of the clusters have been shown to be reversible.[105] Unfortunately, with very few exceptions,[106] no catalytic tests have been carried out with any of these supported clusters. Moreover, activation of the molecular clusters can lead to ligand decomposition and metal sintering. For instance, the grafting of $[AgN(SiMe_3)_2]_4$ on silica was shown to result in the formation of 2 nm Ag NPs, with the advantage that the resulting catalyst proved capable of selectively hydrogenate alkynes to alkenes.[107] The use of $[CuOSi(OtBu)_3]_4$ and $[CuOtBu]_4$ was also shown to lead to the formation of Cu NPs, with control on the final oxidation state of the Cu atoms made possible via the choice of the precursor.[108,109]

2.2. Tethering of Organometallic Catalysts

One drawback with the direct coordination of organometallic catalysts to solids is that the new interactions may affect the electronic properties of the metal center and alter catalytic performance.[75] Alternatively, tethering may be carried out via the insertion of a short organic linker, using so-called "click" chemistry.[110−118] A number of reliable and sturdy routes have been developed for the covalent tethering of discrete molecules to oxide surfaces this way.[119−122] An example of this approach is that of the immobilization of a (NHC)NN-pincer complex on MCM-41 (a silica mesoporous material) reported by the Corma group (Figure 4). Tethering in that case was accomplished via a reaction of a propyltriethoxysilane moiety, added to the imidazolium salt used as precursor for the chelating N-heterocyclic carbene (NHC) pyridine pyrrolidine ligands, with the surface.[123] Surprisingly, the resulting catalysts showed significant increases in reactivity and enantioselectivity compared with those obtained with the corresponding soluble complexes, and the production of the S isomer always, regardless of whether the organometallic precursor had a

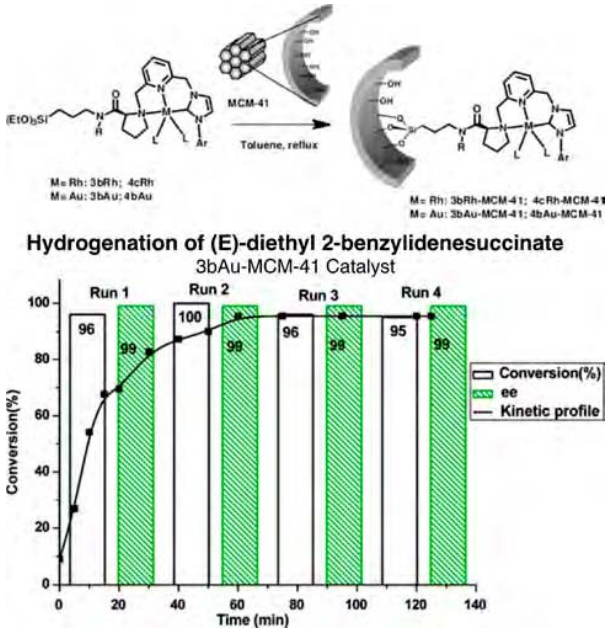

Figure 4. Top: Scheme for the tethering of (NHC)NN-pincer complexes on MCM-41 using click chemistry.[123] Bottom: Results from recycling tests showing the activity (% Conversion) and enantioselectivity (ee = enantiomeric excess) of a gold-based catalyst over four consecutive runs. Reproduced with permission from ref 123. Copyright 2010 Springer Science+Business Media, LLC.

mesityl or an isopropyl group (an inversion of enantioselectivity potentially attributable to the confinement effect of the porous support). The immobilized catalyst was also quite stable, retaining its performance over four consecutive catalytic runs (Figure 4, bottom). In another example, [Cu(I)(tris(pyridylmethyl)amine)] and [Mn(II)(tris(pyridylmethyl)amine)] were successfully tethered to a silica substrate via a copper-catalyzed azide alkyne cycloaddition (CuAAC, the original "click" chemistry)[124,125] and tested for the epoxidation of 1-octene.[126] An important conclusion from that work was that the catalytic performance was dependent on the density of the metalorganic catalyst tethered on the surface, with yields decreasing with increasing coverage. In a third case, a [Fe(III)(biuret-amide)] complex was immobilized onto mesoporous silica NPs via the same CuAAC click chemistry to produce an efficient peroxidase mimic.[127] A surface coverage dependence was also seen with Ni[N,N-bis(2-pyridylmethyl)-N-{(1-tertbutyl-1H-1,2,3-triazol-4-yl)methyl}amine] CuAAC-tethered to silica in terms of the catalytic activity toward alkane oxidation, but some leaching was seen at low coverages that

https://doi.org/10.1021/acs.chemrev.1c00905
Chem. Rev. XXXX, XXX, XXX−XXX

could be inhibited by increasing the surface density of the catalyst.[128] Co(II)-, Fe(II)-, and Cu(II)-salen complexes have been tethered to silica using 3-aminopropyltriethoxysilane (APTES) as the linker to produce catalysts selective in the oxidation of the alcohol group in 5-hydroxymethyl-2-furfural (HMF).[129]

Less common but also possible is the tethering of homogeneous catalysts to other surfaces: witness, for instance, the covalent attachment of a catalytically active Co complex to a B-doped p-type conductive diamond via the appending of peripheral acetylene groups to a Co-porphyrin complex followed by CuAAC linking to a surface decorated with alkyl azides; the resulting surface was successfully used for the electrocatalytic reduction of CO_2 to CO in an acetonitrile solution.[130] On graphene oxide (GO), $RuCl_2(PPh_3)_3$ was tethered to the surface using APTES as the linker to produce a recyclable heterogeneous catalyst with enhanced catalytic performance toward the hydrogenation of olefins and ketones compared with the homogeneous analogue.[131] An interesting alternative route to tethering homogeneous catalysts is via their *in situ* assembly, as in the case of a Cu-salen catalyst used to promote olefin epoxidations prepared on GO via the sequential modification of the surface with trimethoxysilane (APTMS), condensation of salicylaldehyde on the resulting groups, and addition of a Cu(II) salt to form the Cu-salen complex on the surface (Figure 5).[132] GO and other carbon-based materials have in fact become a popular choice as a support for this type of catalysts in recent times (see Section 6.4).[133−135]

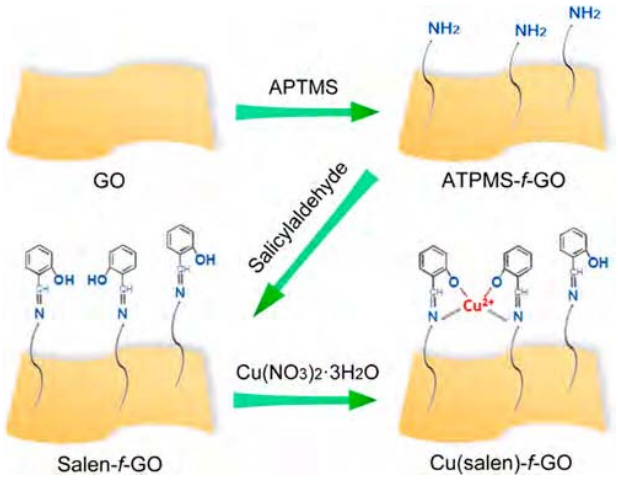

Figure 5. Synthetic scheme for the *in situ* assembly of a Cu-salen catalyst tethered to a GO surface, used for the promotion of olefin epoxidations.[132] Reproduced with permission from ref 132. Copyright 2014 American Chemical Society.

Another popular type of support onto which homogeneous catalysts are tethered is polymers.[136−138] An example of the use of click chemistry to tether organometallic catalysts on polymers is the synthesis of monofunctionalized Mn- and Co-salen complexes attached via a stable phenylene-acetylene linker to a norbornene monomer used for subsequent polymerization (Figure 6).[66] The resulting catalysts were successfully tested for both the asymmetric epoxidation of olefins and the hydrolytic kinetic resolution of epoxides: all polymeric catalysts showed catalytic activities and selectivities comparable to the original catalysts reported by Jacobsen, and

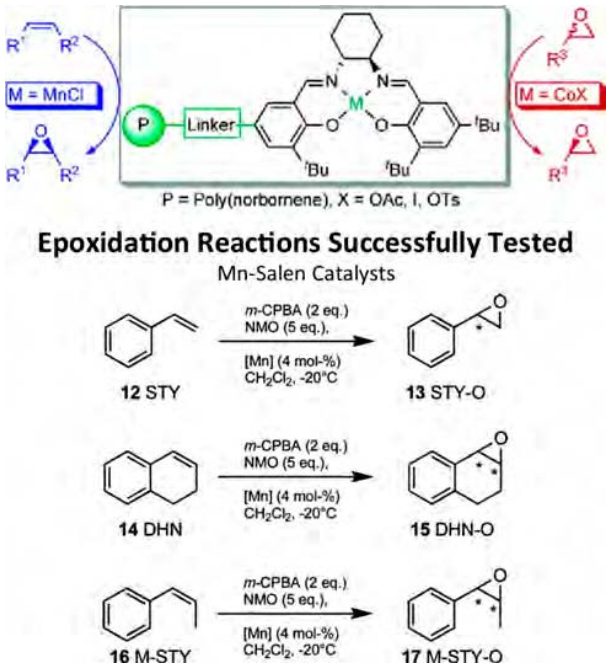

Figure 6. Top: Scheme for the preparation of an architecture of salen-based catalysts tethered to polymer matrices via short linkers.[66] Bottom: Some of the epoxidation reactions successfully promoted by these immobilized catalysts. Reproduced with permission from ref 66. Copyright 2006 American Chemical Society.

higher than their homopolymer analogues. Studies with these polymer-based systems have also provided corroborating proof of the fact that, with salen salts, catalyst density and site isolation are key factors, the same as in the examples provided above with silica substrates. One additional advantage of using polymers as supports for catalyst tethering is that, in addition of the ability to add linkers via the click chemistry described above, with these solids it is also possible to incorporate the linkers directly into the monomers used to synthesize the polymers.[139] This approach can provide a great degree of control on surface concentration and site distribution. Further control of the swelling of the resins can be harnessed to add selectivity.[140−144]

The methods for complexing metal ions with organic ligands tethered to solid surfaces can go beyond simple individual or bidentate coordination in discrete metalorganic complexes. More flexible coordination modes may be particularly useful for redox catalysts, where changes in the oxidation state of the metal center may lead to changes in coordination number or structure. In an example from our laboratory, a new selective hydrocarbon oxidation heterogeneous catalyst was developed by tethering an iron-coordinated cavitand to the surfaces of SBA-15, a mesoporous silica material (Figure 7).[145] This catalyst was shown to catalyze the oxidation of cyclic hydrocarbons at room temperature and to be quite robust and easy to recycle. The architecture in this case turned out to be somewhat complex, with the roles of the cavitand scaffold being the prevention of the catalytic Fe ions from interacting directly with the silica surface and the provision of a controlled environment for reversible redox catalysis. In another example, a catalyst with multiple metal centers was prepared by first grafting poly(amidoamine) dendrimers on carbon nanotubes and then appending those with polypyridyl ligands to

https://doi.org/10.1021/acs.chemrev.1c00905
Chem. Rev. XXXX, XXX, XXX−XXX

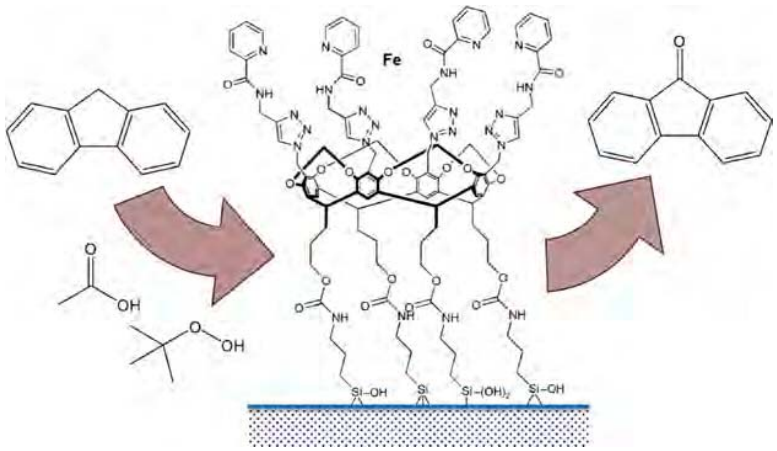

Figure 7. Proposed structure of a Fe-cavitand-derivatized SBA-15 catalyst used for the selective oxidation of non-functionalized saturated C−H bonds (fluorene in this example).[145] Adapted with permission from ref 145. Copyright 2013 American Chemical Society.

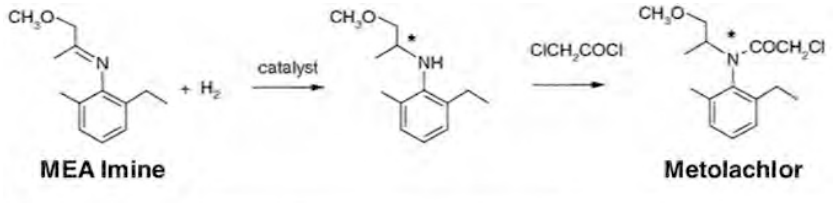

	free		extractable	immobilized, silica gel		immobilized, polystyrene
	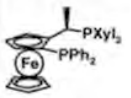		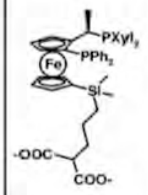	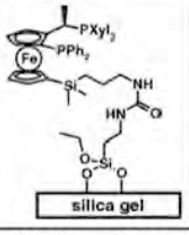		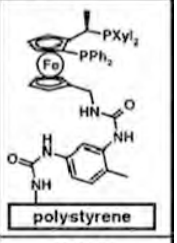
S/C	50,000	120,000	120,000	50,000	120,000	50,000
time	1h	2.1h	3h	8h	10h	30h
ee	79%	80%	79%	78%	78%	74%
separation			extraction > 90%	filtration 95%		filtration 95%

Figure 8. Top: Reactions used in the preparation of metolachlor.[58,153] Bottom: Results from tests on the hydrogenation of N-(2-methyl-6-ethyl phenyl)-1-methoxypropyl-2-imine (MEMI, labeled here as MEA imine) with free, extractable, and immobilized Josiphos-based metal catalysts. Reproduced with permission from ref 153. Copyright 2014 Elsevier Ltd.

functionalize with iron(II)-benzoylformate complexes; this design was aimed at mimicking artificial non-heme oxygenase for the selective catalytic oxidation of organic molecules.[146] Tethered calixarenes have also been used to create new surface sites with controlled accessibility,[147−149] and even to control stereoselectivity.[150]

Particularly challenging has been the promotion of asymmetric and chiral reactions with useful stereo-, regio-, or enatio-selectivity using heterogeneous catalysts, an area that has received much attention in recent years.[114,151,152] One interesting example of the use of tethered organometallic complexes for this use in industry is in the synthesis of (S)-metolachlor, a chiral tertiary amine used as an herbicide. A research team at Solvias developed an heterogeneous process for this process based on an metal complex containing a Josiphos derivative with R = 3,5-xylyl.[58,153] As indicated by the data reported in Figure 8, tethering that complex to a silica surface resulted in a new heterogeneous catalyst that retained the initial enantioselectivity of the original homogeneous catalyst (compare entries 1 versus 3) but showed significantly less total activity, presumably because of mass transport limitations. Ultimately the low activity, combined with the additional synthetic cost, led Solvias to discard this option for their industrial process. Nevertheless, the experience provided valuable lessons for the design of future immobilized catalysts.[58]

The same parameters discussed above in connection with other tethered and immobilized catalysts are relevant to chiral tethered catalysts as well. For one, there are some examples where the tethered chiral catalyst contains several metal centers: as an example, a di-Rh(II) tetraprolinate catalyst tethered to silica has been successfully used to promote a range

https://doi.org/10.1021/acs.chemrev.1c00905
Chem. Rev. XXXX, XXX, XXX−XXX

of enantioselective transformations in donor/acceptor carbenoids.[154] Magnetic supports can also be used to assist with catalyst separation, as in the case of the chiral Cu-bis(oxazoline) complex tethered to a mesoporous silica foam with magnetic NPs grafted to its pore surface; the resulting material was used successfully to promote enantioselective Henry reactions with nitromethane and aryl aldehydes.[155] One important aspect of chiral catalysis promoted by tethered homogeneous complexes is that the enantioselectivity is highly sensitive to structural factors associated with both the complex itself and the support. This was made evident, for example, in a study of an Ir Lewis-acid chiral catalyst tethered to polystyrene macrobeads using different linkers: the anchored catalysts displayed superior enantioselectivity during the promotion of the Friedel−Crafts alkylation of indole with α,β-unsaturated 2-acyl imidazole than the original homogeneous catalyst, but similar to those obtained with their structural homogeneous homologues (Figure 9).[156] In another example, the enantio-

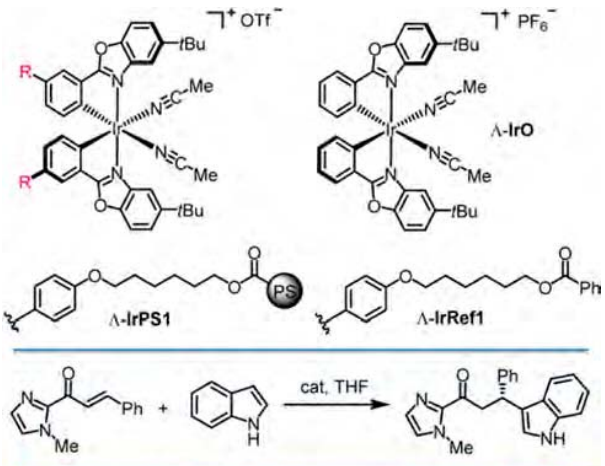

Catalyst	Time (h)	Conversion (%)	(R) ee (%)
Λ-IrO	16	98	93
Λ-IrPS1	72	70	97
Λ-IrRef1	44	>99	98

Figure 9. Effect of tethering on the performance of an enantioselective Friedel−Crafts Ir(III)-based catalyst.[156] Shown are the structures of the homogeneous (top, Λ-IrO) and tethered (center-left, Λ-IrPS1) Ir(III) complexes, together with a reference compound where the linker is bonded to the homogeneous catalyst (center-right, Λ-Ref1). Bottom: Results from catalytic runs on the addition of indole to α,β-unsaturated 2-acyl imidazole, showing both total conversion and ee. Adapted with permission from ref 156. Copyright 2017 American Chemical Society.

selectivity of asymmetric cyclopropanation reactions promoted by Cu-pyridineoxazoline complexes was shown to improve markedly upon immobilization, allegedly because of a synergistic effect between the polymeric backbone and the bulky substituent in the chiral oxazoline ring around the Cu center due to their proximity.[157] It should be said that enantioselectivity with tethered organometallic catalysts, if improved, almost always comes at the expense of lower overall activity; this is certainly the case in the example in Figure 9.[158]

2.3. Tethering of Organic Functionalities

In addition to organometallic complexes, other organic functionalities have also been added to solids to incorporate new chemistry or improve their catalytic activity.[159−163] The most common examples of this have been the addition of acidic or basic organic groups to solid oxides, usually silica porous materials, in many cases using the linking and click chemistry mentioned in the previous section.[119,120] Many oxides, aluminosilicates in particular, have both Brønsted- and Lewis-acid sites already, but the molecular nature of those can vary among sites within a given solid, and control on the acid strength is limited;[164−167] the same can be said of basic or nucleophilic solids.[168] Tethering of molecular acid or base functionalities provides a way to better control the nature of those catalytic sites, and even to tune their strength. Examples of tethered acid organocatalysts and of reactions promoted by them are provided in Figure 10; a similar long list exists for basic catalysts.[163]

There are three general approaches to the incorporation of functionalities into solids:[163,169] (1) during the synthesis of such solid, typically a sol-gel process when dealing with oxides, by simultaneous reacting the precursor used to make the solid and organic compounds with terminal groups capable of reacting with those during co-condensation (condensable inorganic silica species and silylated organic compound to make silica-based catalysts);[170] (2) by grafting the organic component onto the surface of already-made solid matrixes, either using conventional immobilization or click reactions;[171] and (3) by using organic precursors with dual terminal groups that can condense and form periodic mesoporous solids (bis-silylated reactants to make silica).[172] These schemes are summarized in Figure 11. All three approaches have proven successful, but perhaps the most commonly used, and the one that more closely relates to the theme of this subsection, is the second. It is perhaps also the most flexible.

One example of acid-functionalized catalysts made by the second (grafting) method is that of the covalent attachment of sulfonic acid-containing aryl radicals on the surface of ordered mesoporous carbon depicted in Figure 12.[173] This material was shown to exhibit high surface area, uniform pore size distribution, high activity, and good stability for acid-catalyzed reactions such as esterifications and condensations. In another study, four different sulfonic acids were grafted onto silica-coated magnetic NP supports to produce easily removable solid acid catalysts.[174] The acidic functionality was shown to promote the deprotection of benzaldehyde dimethylacetal, and the catalyst to retain its sulfonic acid moieties in recycling experiments. A similar approach was followed by a different research group to produce sulfamic acid-functionalized magnetic Fe_3O_4 nanoparticles, for the promotion of the one-pot synthesis of α-amino nitriles in water.[175] A fourth case is that of the preparation of amine-functionalized MCM-41 materials for the promotion of nitroaldol (Henry) reactions:[176] high selectivity was achieved with secondary and tertiary (but not primary) amine groups. Perhaps more interestingly, the least sterically hindered amines were found to be the most active, suggesting that the size of the pores in MCM-41 affects this catalysis. In a more recent example, sulfonic groups have been tethered to porous carbon supports for the promotion of reactions related to biodiesel production.[177]

An example involving the use of chiral molecules to add enantioselectivity to reactions catalyzed by basic/nucleophilic groups from our laboratory illustrates some key aspects of the surface organic-derivatization approach (Figure 13).[178] First, we showed that the point of bonding to the surface can affect catalytic performance: two synthetic routes were explored for

https://doi.org/10.1021/acs.chemrev.1c00905
Chem. Rev. XXXX, XXX, XXX−XXX

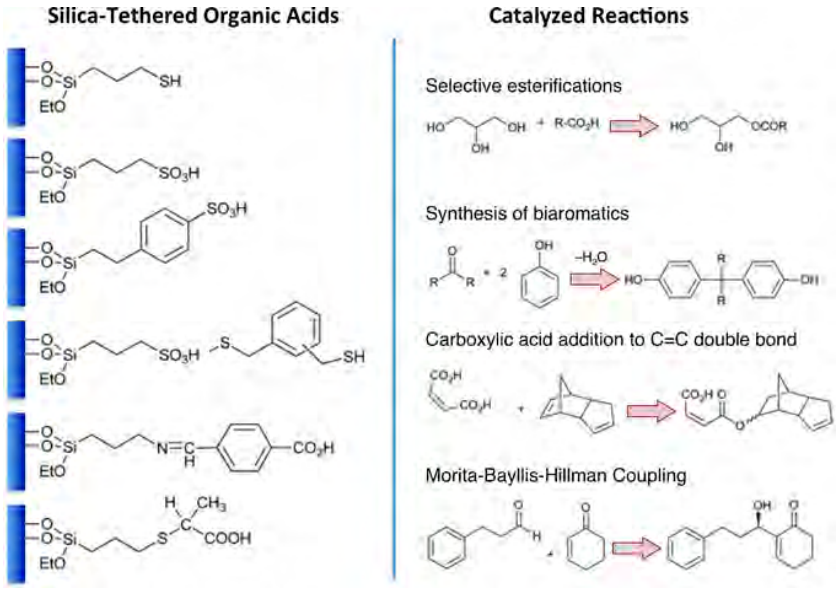

Figure 10. Examples of molecular organoacid functionalities tethered to silica surfaces (left) and of organic reactions catalyzed by them (right).[163]

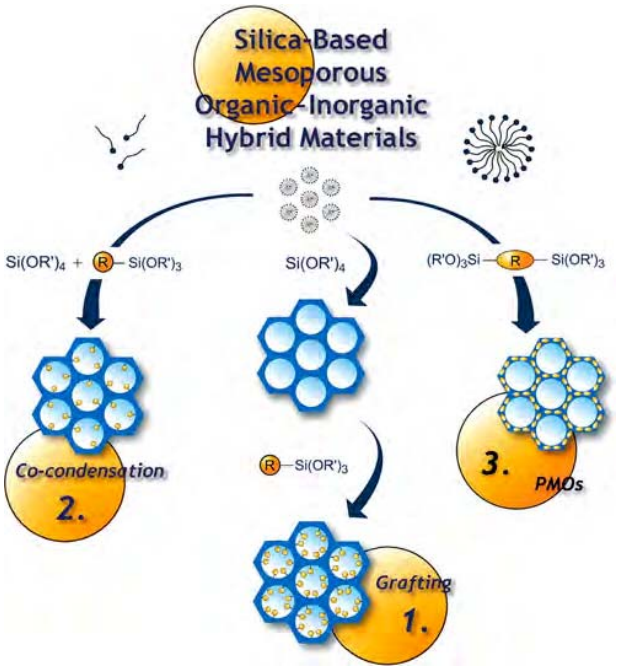

Figure 11. Main synthetic strategies used for the synthesis of catalysts based on functionalized organosilicas.[169] Reproduced with permission from ref 169. Copyright 2006 Wiley-VCH Verlag GmbH & Co. KGaA, Weinheim.

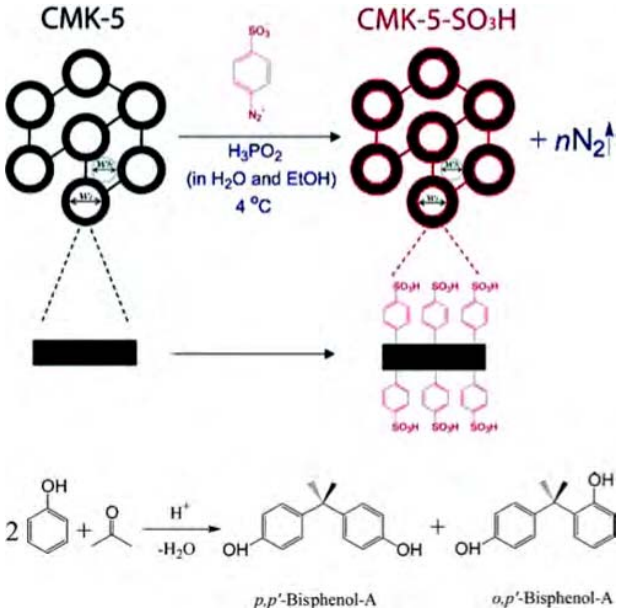

Figure 12. Top: Reaction used for the functionalization of CMK-5, an ordered mesoporous carbon material, with sulfonic acid groups. Bottom: Acid-catalyzed formation of bisphenol-A, a reaction successfully catalyzed by the acid-derivatized carbon. Reproduced with permission from ref 173. Copyright 2007 American Chemical Society.

the grafting of cinchonidine (Cd), adding 3-isocyanatopropyltriethoxysilane (ICPTEOS) to the alcohol position to make a carbamate link, and attaching 3-mercaptopropyltriethoxysilane (MerPTEOS) at the vinyl position to make a mercapto bond.[179] In addition, a loss of enantioselectivity was observed upon tethering because of a combination of factors, namely, the nonselective catalytic activity of the solid itself, the activity of surface OH species, and the direct bonding of the Cd molecule to the surface. These effects could be minimized via silylation of the surface (a surface silanol-capping treatment to be discussed in more detail later in this review, Section 8.1), by choosing appropriate solvents, and by selecting the best attaching position, but it is clear that the surface plays an active role in these tethered catalysts beyond providing a solid platform for the heterogenization of molecular catalysts. An independent study by another research group has shown that controlling acid−base interactions on the surface of the catalyst is also important in designing cooperative catalysis. In particular, amine-silanol cooperativity in solids made by tethering amine groups to silica supports were shown to be critical to the promotion of nitroaldol condensation, and that

https://doi.org/10.1021/acs.chemrev.1c00905
Chem. Rev. XXXX, XXX, XXX−XXX

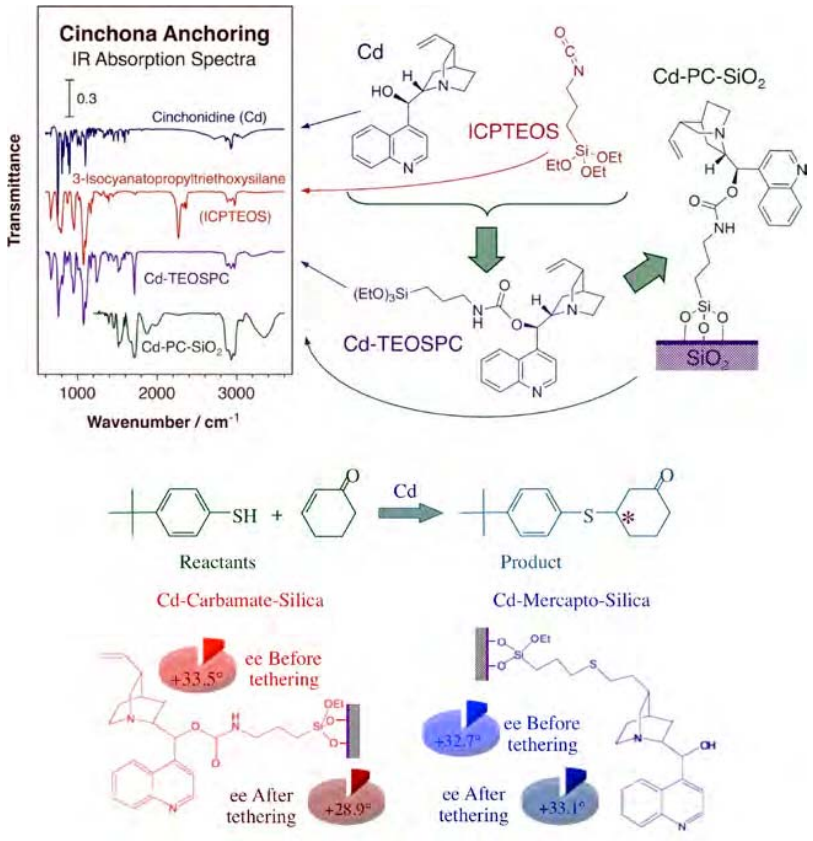

Figure 13. Top: Infrared absorption spectroscopy (IR) evidence for the success of the tethering of cinchonidine (Cd) to a silica surface using click chemistry and 3-isocyanatopropyltriethoxysilane (ICPTEOS) as the linker. Bottom: ee results obtained via the promotion of the addition of p-tert butylbenzenethiol to 2-cyclohexene-1-one using two types of catalysts, tethered via the OH (carbamate, left) and vinyl (mercapto, right) moieties of Cd. Adapted with permission from ref 178. Copyright Springer Science+Business Media, LLC 2011.

Figure 14. Examples of organocatalysts, salen ligands with or without Mo ions, tethered to the surface of a periodic mesoporous organosilica (PMO).[188] Reproduced with permission from ref 188. Copyright 2021 Wiley-VCH GmbH.

such cooperativity can be tuned by adjusting the linker length and pore size;[180] silylation of the surface was shown to turn off this cooperativity.[181] An anhydrous synthesis of aminosilica materials from alkyl halide-functionalized mesoporous SBA-15 silica by post-grafting amination has also been reported as a way to improve activity in acid−base bifunctional catalysis

https://doi.org/10.1021/acs.chemrev.1c00905
Chem. Rev. XXXX, XXX, XXX−XXX

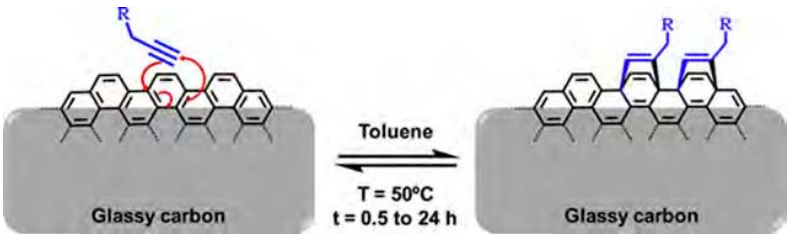

Figure 15. Reaction scheme for the functionalization of the surface of glassy carbon with ferrocen (R)-terminated propargyl groups via Diels–Alder condensation with surface dienes.[193] Reproduced with permission from ref 193. Copyright 2019 American Chemical Society.

compared to traditional amine-grafted materials, presumably because of an increase in the spacing between the amine groups obtained with the new synthesis.[182]

More complex organic functionalities can be tethered to porous oxide materials for use in catalysis too. For instance, silica-tethered pyrrolidine–triazole proved to be a good insoluble and recyclable organocatalyst for the enantioselective Michael addition of ketones to nitroalkenes.[183] Cytosine-functionalized SBA-15 was shown to exhibit high activity for Knoevenagel reactions.[184] 3,3′-bis(2,4,6-triisopropylphenyl)-1,1′-binaphthyl-2,2′-diyl hydrogen phosphate, a phosphoric acid–based catalysts commonly referred to as TRIP, was successfully immobilized on polystyrene, using a copolymerization-based strategy, to produce a robust and recyclable heterogeneous catalyst for the asymmetric allylboration of aldehydes.[185] A resin-supported peptide catalyst with an N-terminal primary amino group was developed for the asymmetric epoxidation of enones through iminium activation.[186] An interesting recent example is that of 4,4′,4′′,4′′′-porphyrin-5,10,15,20-tetrayltetrabenzoic acid tethered to a periodic mesoporous organosilica, which was successfully used for the cycloaddition of epoxide and CO_2, a carbon-capture reaction.[187] Figure 14, illustrates a case where a mesoporous-silica-based catalyst was decorated with a salen ligand to promote the epoxidation of cyclohexene, and further functionalized with MoO_2^{2+} ions to aid in the preparation of cyclic carbonates.[188] Yet another type of periodic mesoporous organosilica, made by coupling hexachlorocyclotriphosphazene with APTES, proved able to promote the same reaction.[189] A complex chiral amino carbamate tethered to silica was designed as a recyclable catalyst for the conversion of cyclohexanone to (E)-β-nitrostyrene, a prototypical Michael addition.[190]

Supports other than silica, alumina, or other common oxides can be used to tether catalytic organic functionalities as well. For example, proline immobilized on a polystyrene matrix proved to be recyclable and to produce pure enantiomeric and diastereomeric aldol adducts in asymmetric aldol reactions under continuous flow conditions.[191] In another case, proline tethered to carbon nanotubes (CNTs) via an aniline linker was tested for the promotion of the synthesis of 2-amino-4H-pyran derivatives.[192] An interesting tethering new chemistry is that used for grafting ethynyl ferrocen covalently onto a glassy carbon electrode via a Diels-Alder reaction; the resulting material was successfully tested for reversible electro redox conversions (Figure 15).[193] In general, carbon-based supports have become popular for uses in this type of molecular catalyst tethering.[194] An example of yet another kind of support is that of the aminosilane-grafted SiO_2–ZrO_2 polyamide-imide hollow fibers developed to promote the tandem conversion of glucose or fructose to HMF.[195] There are in principle many permutations of supports, linkers and organic functionalities that can be used to make this type of tethered catalysts.

2.4. Tethering of Enzymes

More complexity can be added to the catalytic sites of solids by immobilizing enzymes. Enzymes offer a unique level of selectivity and operate under mild conditions. On the other hand, their stability under the harsh conditions encountered in many industrial processes is limited. Immobilization of enzymes on solid surfaces may help protect their structural integrity, and also simplify downstream processing and improve operational stability. Depending on the methodology used, it has been reported that immobilization may improve the functional properties of some enzymes too, and even their selectivity during catalysis.[196−199] However, it may also affect the behavior of such enzymes: the type and extent of bonding to the surface and of the changes induced by the surrounding microenvironment, especially in porous materials, can affect the ability of enzymes to perform as well as when free in solution.[200] Although the incorporation of enzymatic catalysis to industrial processes is still a nascent and evolving field, there are already a number of excellent reviews on this area, in particular in reference to enzyme immobilization.[32,200−206]

Several approaches for enzyme immobilization have been tested,[200,205,207−209] with mixed success. Adsorption or binding to a support through hydrophobic or ionic interactions is in principle a straightforward method for enzyme immobilization, but physical binding is in general too weak to keep the enzyme bound to the surface in the presence of water, the solvent typically used in enzymatic catalysis.[201,210] Entrapment or encapsulation of enzymes within a solid matrix, typically a polymer or sol-gel-made silica, can minimize but not fully prevent leaching of the enzyme from the solid,[208] and puts additional constrains on the sturdiness of the enzyme, as the matrix needs to be synthesized *in situ* in the presence of the enzyme; reactive species or toxic solvents, for instance, can denature enzymes.[211] Covalent binding can provide adequate stability against leaching, improve recyclability, and also resolve issues of solubility. An example of the latter is the case of the immobilization of ketoreductase on a solid resin via covalent binding at two points between amine and epoxide groups to facilitate its operation in organic solvents: the production of (R)-1-(3,5-bis(trifluoromethyl)phenyl)ethanol, a key chiral intermediate in the synthesis of EMEND (a orally active neurokinin-1 receptor antagonist used for chemotherapy-induced vomiting), could be made with this catalyst in 98% yield and with >99% ee (Figure 16).[199] On the negative side, this so-called cross-linking is impractical with enzymes that deactivate easily, as there is no practical way to regenerate the tethered enzymes. Tethering may also lead to losses in enzyme flexibility, and typically dilutes activity. Despite all these limitations, however, tethering of enzymes to a variety of

https://doi.org/10.1021/acs.chemrev.1c00905
Chem. Rev. XXXX, XXX, XXX−XXX

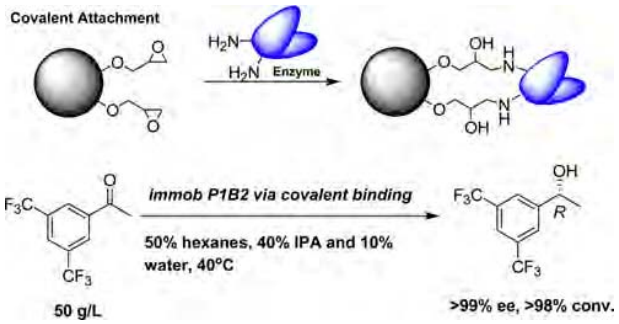

Figure 16. Example of the use of multipoint covalent enzyme tethering to improve catalytic performance.[199] Top: tethering reaction. Bottom: catalytic reaction, with performance data. The key gain from immobilization of the enzyme in this case was the ability to carry out the reaction in organic solvents, which exhibit higher solubility for the reactants and products. Reproduced with permission from ref 199. Copyright 2015 American Chemical Society.

solids, including polymers[212] and inorganic solids,[213,214] also brings many benefits and has been amply tested and is actively pursued at the present time.

One important observation deriving from studies on the immobilization of enzymes is that the surface of the support often plays a role in the behavior of the catalyst.[203,206,210,215−217] Typically, immobilization affects enzymatic catalysis in negative ways, but in some instances it can improve performance, by, for instance, facilitating operation in organic solvents as in the example in (Figure 16), or by increasing pH tolerance or heat stability. In addition, the interaction of enzymes with surfaces increases structural rigidity,[218,219] minimizes enzyme aggregation,[220,221] blocks possible inhibition sites,[196,222] and stabilizes multimeric enzymes,[223−225] preventing dissociation-related inactivation[224] and even stabilizing a hyperactivated form of the enzyme, as in the case of lipases immobilized on hydrophobic supports.[226−229] In one example of surfaces influencing enzymatic catalysis, it was shown that hydrophobic supports enhance the catalytic activity of lipase by more than an order of magnitude compared to that seen in solution (Figure 17); the change in catalytic behavior was traced back to the fact that hydrophobic surfaces appear to force the immobilized lipase into its more active open configuration.[230] In another study, with soybean peroxidase immobilized on graphene and single- and multiwalled CNTs, a correlation was identified between the curvature of the substrate, which presumably affects the extent of distortion of the immobilized enzyme, and catalytic activity.[231] A clear illustration of electronic effects associated with enzyme immobilization is that of horseradish peroxidase on graphene-related materials, where the oxygen functionalities of the support induce changes in electronic conductivity that interfere with enzymatic processes: both graphene and GO lead to significant reduction in enzymatic stability because of the alteration of the conformation of the enzyme, but reduced GO was shown to enhance enzymatic activity 7-fold because of its capacity to quench superoxide radicals.[232]

Some processes are ideally suited for enzymatic catalysis, and in those immobilization has been a useful route to improve recyclability and overall catalytic performance. A high-profile example of the application of immobilized enzymes in industry is the isomerization of glucose to fructose catalyzed by glucose isomerase.[200,233] More recently, there has been much interest

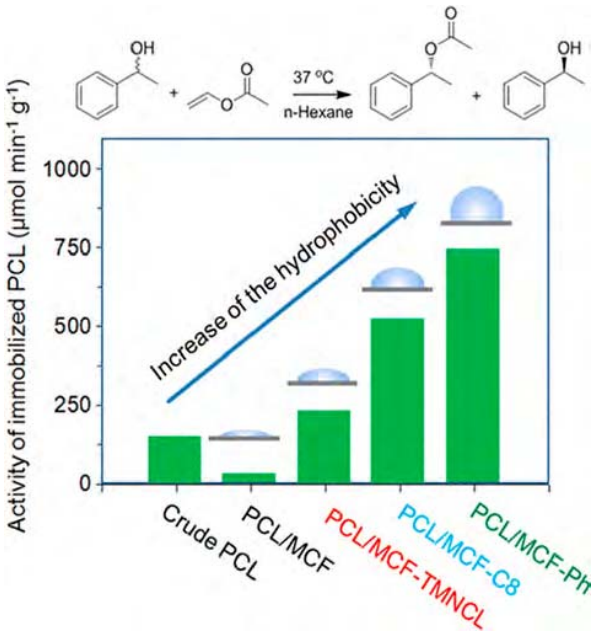

Figure 17. Specific activity of lipase from *Pseudomonas cepacia* (PCL) immobilized onto siliceous mesocellular foams (MCF) with various hydrophobic/hydrophilic surfaces for the promotion of the non-aqueous transesterification reaction of racemic 1-phenylethanol (the reaction indicated at the top).[230] The data clearly show that increases in hydrophobicity (characterized by measurements of the water contact angle) lead to increases in specific activity. The surface modifiers used were N-trimethoxysilylpropyl-N,N,N-trimethylammonium chloride (TMNCL), n-octyl triethoxysilane (C8), and phenethyltrimethoxysilane (Ph). Reproduced with permission from ref 216. Copyright 2015 American Chemical Society.

in using immobilized enzymes in biorefining and other bio-inspired green processes, to, for instance, promote the conversion of carbohydrates to furfural and HMF.[234−236] However, the number of industrial processes that use immobilized enzymes is relatively small, among other reasons because of the high cost associated with the synthesis of these immobilized catalysts.[237] In addition, many natural enzymes often fail to meet the stringent operational requirements required in specific industrial applications. To address that latter shortcoming, protein engineering has been implemented in some instances to modify the structure of proteins, to create enzymes with improved functional properties such as higher stability, specific activity, minimized inhibition by reaction products, or selectivity towards non-natural substrates.[203,238−240] In one example, a new biocatalyst was developed by immobilizing a modified enzyme, made via mutagenesis of the wild-type penicillin acylase (PA) from Escherichia coli, on glyoxyl Eupergit C250L, a modified industrial support (Figure 18).[241] The resulting catalyst showed improved activity compared to the original PA for the synthesis of cephalexin (99% versus 76%), cefaclor (99% versus 65%) and cefprozil (99% versus 60%), and also better stability. Site-directed mutagenesis can also be used specifically to improve on the way that enzymes are immobilized on the support.[242−244] For example, in one study the orientation of ferredoxin-NADP$^+$ (NADP = nicotinamide adenine dinucleotide phosphate) reductase immobilized onto a modified Au electrode was accomplished by introducing a genetically engineered metal binding site on a selected region of the

https://doi.org/10.1021/acs.chemrev.1c00905
Chem. Rev. XXXX, XXX, XXX−XXX

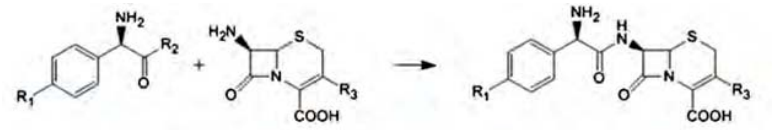

Reactant 1 (Acyl Donor)	R_1	R_2	Reactant 2 (Nucleus)	R_3	Product (Antibiotic)
D-PGA or D-PGME	H	NH_2	7-ADCA	CH_3	Cephalexin
	H	OCH_3	7-ACCA	Cl	Cefaclor
D-HPGME	OH	OCH_3	7-APRA	$CH{=}CH{-}CH_2$	Cefprozil

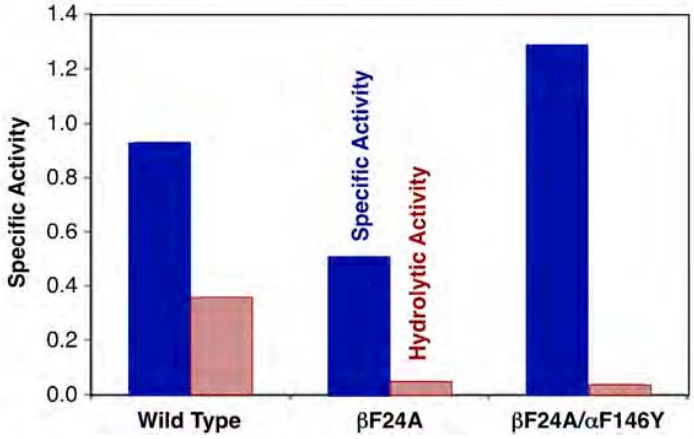

Figure 18. Performance of three immobilized penicillin acylase catalysts, the wild type and versions modified via mutagenesis in position β24 alone and in positions α146 and β24 (βF24A/αF146Y); used for the production of cephalosporins (D-(−)-phenylglycine amide −D-PGA−, D-phenylglycine methyl ester −D-PGME−, and 4-hydroxy-D-(−)-phenylglycine methyl ester −D-HPGME−).[241] Top: Catalyzed reaction and substrates tested. Bottom: Specific synthetic (desired main path, blue) and hydrolytic (undesired side reactions, red) activities measured with D-PGME at 28 °C, expressed as micromole per minute (μmol/min) of cephalexin synthesized or hydrolyzed per milligram of enzyme.

protein surface and covering the Au surface with a self-assembled monolayer of thiols appended with nitrilotriacetic acid groups complexed with metal transition ions.[245] In another case, site-directed mutagenesis of the penicillin acylase surface from Escherichia coli was specifically designed to increase multipoint covalent attachment to the substrate, in this case glyoxyl-agarose.[246] An investigation where cysteine residues were introduced in *Escherichia coli* inorganic pyrophosphatase at specific sites in order to control binding to Au NPs concluded that site-directed orientation and surface density can modulate the activity of immobilized proteins, and also that orientation has a greater effect than density.[247] Protein engineering may be applied to the material on the surface where the enzyme is immobilized as well. This was the case in a study where magnetite NPs were coated with a genetically functionalized lipid membrane tuned to immobilize a phosphohydrolase, with the aim of producing a recyclable biocatalyst for the degradation of ethyl-paraoxon (a commonly used pesticide).[248]

It is clear that enzymes can provide unparalleled selectivity in specific reactions and that immobilization of enzymes not only helps with process design but can also improve catalytic performance. Yet, because of the fragility of many enzymes and the cost of their preparation and purification, the number of practical examples available for the use of immobilized enzymes as catalysts in industrial processes is still limited. More work is needed to make this approach more common.

2.5. Multifunctional Catalysts

Solid catalysts can be conceived to contain more than one functionality. The advantages of using such catalysts are several, in particular the ability to simplify process engineering in multistep chemical synthesis. The design of catalytic processes in tandem, to perform a sequence of cascade reactions, is particularly valuable for the synthesis of fine chemicals, because such combined systems reduce the number of isolation and purification steps required. A lesser number of steps leads to a reduction in waste generation and to savings in energy, either because of the elimination of heat-based processing (i.e., distillation, recrystallization, etc.) and/or thanks to the reduced requirement of solvents in purification steps.[249] Moreover, immobilization of incompatible catalytic functionalities such as acids and bases, oxidizers and reducers, amines and metals, enzymes and acids, etc., can afford their use in the same vessel, and interferences with reactants and/or products can be avoided this way as well. Solid catalysts also solve the problems of solubility often encountered in homogeneous catalysis. Finally, if properly placed spatially within the support (with complementary functionalities next to each other, for instance), multifunctional immobilized catalyst can be conceived to promote processes involving kinetically unstable intermediates.[250]

Multifunctional catalysts can be used in different modes, either by allowing for cooperative effects in specific chemical steps involving two or more different surface sites, or by promoting various chemical reactions.[251−254] These applica-

https://doi.org/10.1021/acs.chemrev.1c00905
Chem. Rev. XXXX, XXX, XXX−XXX

tions have been referred to in the literature by using different, sometimes overlapping, terms, including (1) cascade (or domino) processes, where the catalyst promotes sequential steps going from reactants to intermediates to products; (2) more generic tandem, cooperative, or one-pot conversions, involving multiple steps that not necessarily required sequentiality (and with reactants added all at once or in a stepwise manner); and (3) catalysts with dual (or multiple) sites that perform in a synergistic fashion to promote a specific reaction. Some debate has ensued in the literature to better define and distinguish among these options,[255,256] but much confusion remains, and the different terms are often used indistinctively; here we do not intend to resolve this issue but rather focus on illustrating how solid catalysts can sustain several functionalities and be used to design complex catalytic processes. It should also be noted that sometimes one given catalytic site can itself promote cascade processes, as with acid sites on solid oxides;[257] this is not the focus of this section either. It is also possible to combine homogeneous and heterogeneous catalysts in one pot to carry out cascade conversions, as in the recent example where an asymmetric bifunctional organocatalytic nitro-Mannich reaction was coupled with a gold-catalyzed allene hydroamination step for the enantioselective preparation of trisubstituted pyrrolidine derivatives.[258] However, such approach may defeat the gains from using all-heterogeneous systems, and is also not to be discussed in this review. The basic idea behind the use of all-heterogeneous multifunctional catalysts for cascade reactions is illustrated in Figure 19.

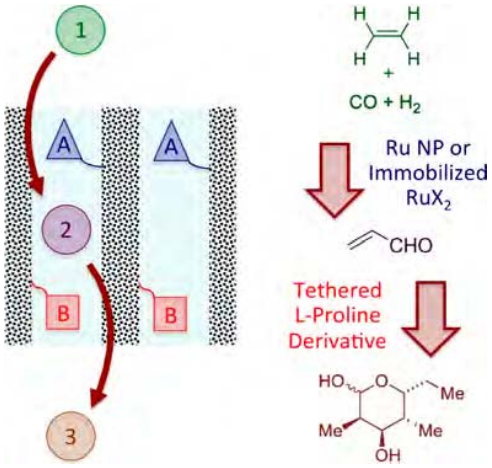

Figure 19. Left: Schematic illustration of the mechanism of cascade catalytic reactions promoted by molecular functionalities tethered on the surfaces of porous solids. Right: Hypothetical cascade process, in this case a two-step synthesis involving the hydroformylation of ethylene on a Ru-based catalyst followed by the proline-promoted trimerization of the resulting acrolein.

There are several ways by which solid catalysts can be made to contain two or more different functionalities. Perhaps the most straightforward is by using materials with intrinsic catalytic activity and adding a second type of site to them. For instance, oxide substrates, even nominally inert ones such as silica, display acid or base sites capable of promoting specific organic reactions, and can therefore be used as good starting materials to make bifunctional catalysts. Figure 20 illustrates this idea with an example where molecular amines tethered to

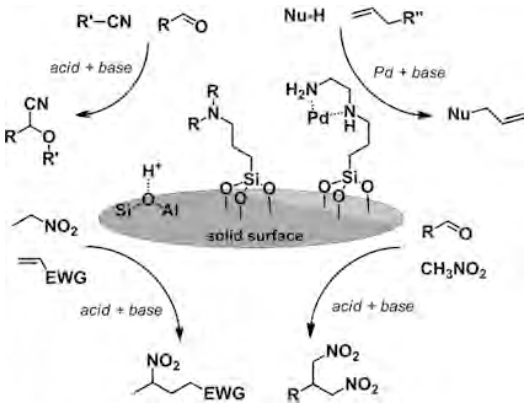

Figure 20. Bifunctional and trifunctional catalysts made out of tethered molecular amines, complexed Pd ions, and solid acid sites, used for the promotion of several nucleophilic addition reactions.[259] Reproduced with permission from ref 259. Copyright 2014 The Japan Petroleum Institute.

aluminosilicate supports, which expose both Lewis- and Brønsted-acid sites, were used to promote a number of nucleophilic addition reactions.[259] It is interesting to note that in this example the authors also added Pd ions, which formed a complex with some of the surface-tethered amine groups (a way by which they could be retained on the surface), and in that form assisted with a variety of C–C bond-forming reactions. The synergistic behavior between amine tethered groups and surface silanol sites was tested by Bass and coworkers, who showed that capping the latter via silylation (a deactivation process discussed in more detail later in this review, Section 8.1) leads to the poisoning of the catalytic activity toward the Knoevenagel condensation of isophthalaldehyde with malonitrile seen without silanol capping.[260] Also, a systematic study of aminated silica catalysts has highlighted the effects of amine structure and base strength on the acid–base cooperative promotion of aldol condensations: it was found that the arrangement of the amine active sites depends on the amine type used (primary versus secondary versus tertiary, aliphatic versus aromatic), and influences the rate of reaction: primary amines are more active than tertiary amines, for instance.[261] Nevertheless, even tertiary amines that cannot promote C–C coupling reactions in solution show catalytic activity when tethered to silica, again highlighting the importance of the amine-silanol cooperative interaction.[262]

A related bifunctional architecture is one where the performance of catalysts based on metal NPs, dispersed on porous materials or in core–shell or other nanostructures, is augmented by the addition of a molecular organofunctionality. For instance, amine groups have been tethered to a Pd/MCM-41 catalysts to promote the one-pot tandem Sonogashira-Henry reaction.[263] Unfortunately, this catalyst performed poorly. We in our laboratory developed a synthetic protocol to tether cinchonidine selectively to silica sites directly adjacent to Pt NPs to bestow enantioselectivity to the hydrogenation of ethyl pyruvate, and showed that this leads to a better performance than that obtained with catalysts where the molecular modifier is added randomly on the silica surface (Figure 21).[264] The examples above involve the addition of small molecular functionalities, but larger molecules such as an enzyme can be incorporated as well. For instance, the one-pot synthesis of R-1-phenylethyl acetate starting from acetophe-

https://doi.org/10.1021/acs.chemrev.1c00905
Chem. Rev. XXXX, XXX, XXX–XXX

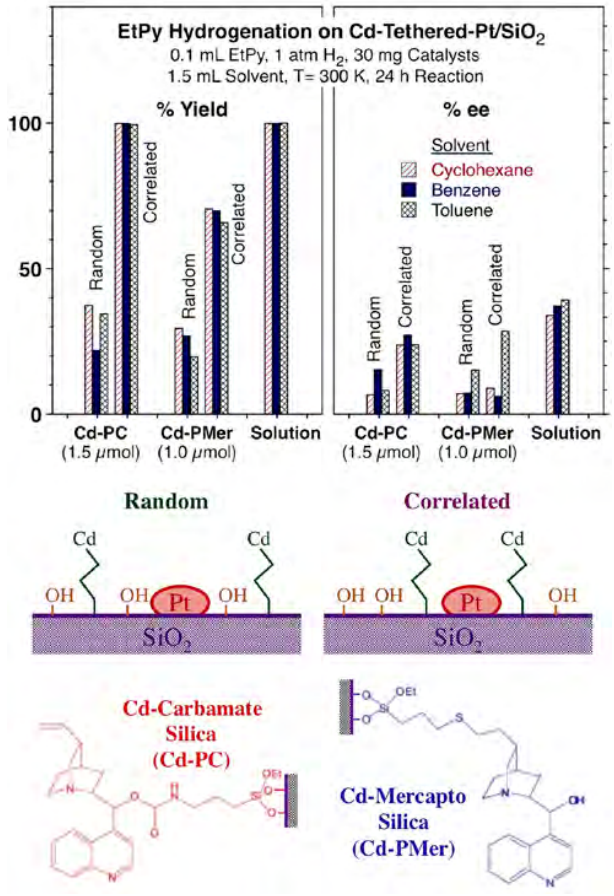

Figure 21. Effect of correlated surface modification on catalytic performance.[264] The example is for SBA-15-supported Pt catalysts modified via cinchonidine (Cd) tethering to add enantioselectivity to the hydrogenation of alpha-keto esters. Both yields (left) and ees (right) are reported for the hydrogenation of ethyl pyruvate promoted by catalysts where Cd was distributed on the silica surface randomly versus in a correlated way around the Pt NPs, and where the tethering was done via either carbamate or mercapto links, as indicated at the bottom. The results in three different solvents are shown, and contrasted to equivalent catalysis with the Cd modifier free in solution. The general observation is that tethering selectively next to the Pt NPs improves catalytic performance. Adapted with permission from ref 264. Copyright 2015, The Royal Society of Chemistry.

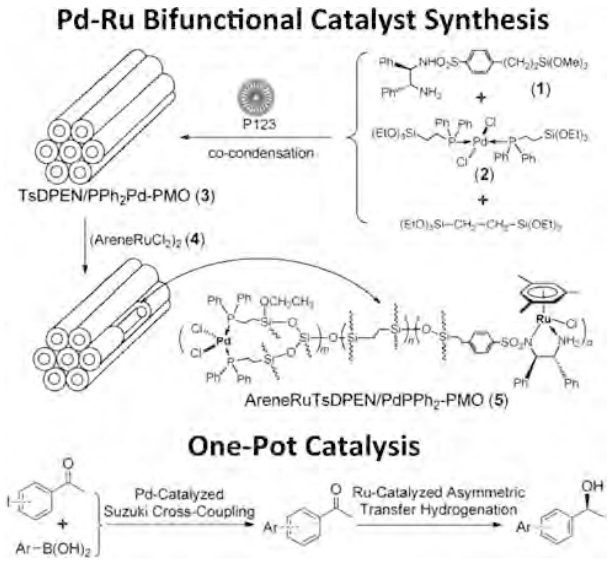

Figure 22. Example of the synthesis of bifunctional catalysts using sol-gel chemistry.[267] Top: Synthetic steps leading to a mesoporous silica material derivatized with Pd and Ru complexes. Bottom: two-step coupling process promoted by this catalyst. Reproduced with permission from ref 267. Copyright 2014 Wiley-VCH Verlag GmbH & Co. KGaA, Weinheim.

none hydrogenation has been possible over supported Pd catalysts when combined with immobilized lipase.[265] In another case, a catalyst made by tethering glucosidase to the outside surface of a Au@SiO_2 core−shell nanostructure was used to carry out a tandem process where 4-nitrophenyl-β-glucopyranoside is hydrolyzed (by the glucosidase) to generate 4-nitrophenol, an intermediate that is then reduced to 4-aminophenol (by the Au nanoparticles).[266]

A second option for the preparation of multifunctional heterogeneous catalysts is via one-pot direct synthesis. For instance, specific agents can be added to the reaction mixture during the sol-gel preparation of oxides such as silica, as exemplified by the case of the co-condensation of trialkoxysilane-terminated Pd and Ru complexes with 1,2-bis(triethoxysilyl)ethylane following the scheme shown in Figure 22 to create a bifunctionalized mesoporous organosilica catalyst capable of promoting the sequential Pd-catalyzed cross-coupling of haloacetophenones with arylboronic acids and the Ru-catalyzed asymmetric transfer hydrogenation to produce chiral biaryl alcohols in aqueous solutions with high efficiency and enantioselectivity.[267] Another illustration of this approach comes from the synthesis of ordered nanoporous polymer resins via self-assembly of lyotropic liquid crystal monomers; the resulting material contained both acid and base sites and could catalyze a model tandem process consisting of the acid-promoted deacetalization of benzaldehyde dimethyl acetal to benzaldehyde followed by a base-promoted nitroaldol (Henry) step to yield β-nitrostyrene.[268] A variation of this methodology consists of first incorporating specific organic groups within the silica network during its synthesis and then derivatizing those further after the solid is made. In fact, this is what was done to add the Ru sites to the catalyst in Figure 22. Another example is one where an acid−base bifunctional catalyst was made by first hydrolyzing 1,4-bis(triethoxysilyl)-benzene and APTES (in the presence of cetyltrimethylammonium bromide, CTAB, a surfactant) to make amine-functionalized mesoporous phenylene-bridged silica and then protecting the exposed amine groups, sulfonating at the bridging phenylene units by simple treatment with chlorosulfonic acid, and deprotecting the amino groups by thermal treatment.[269] Interestingly, in a study that directly compared MCM-41-based acid−base catalysts made using direct synthesis versus via post-synthetic grafting (to be discussed next), it was determined that the latter is more efficient in promoting the one-pot deacetalization-Knoevenagel and deacetalization-Henry reaction sequences; the relative poor performance of the former was explained by a combination of lower density of active sites on the surface and the possibility of some of those being trapped inside the silica network and therefore inaccessible for catalysis.[270] This latter conclusion may not be general, as the reverse trend was reported by another research group, however;[271] resolving this discrepancy would

https://doi.org/10.1021/acs.chemrev.1c00905
Chem. Rev. XXXX, XXX, XXX−XXX

be useful, as it would help determine the optimum synthetic route for bifunctional catalysts.

Many multifunctional heterogeneous catalysts are made by immobilizing two or more individual molecular catalytic motifs on one single solid support using the type of tethering chemistry described previously. The bulk of examples in the literature of this type of tandem catalysts often involves the addition of acid (sulfonic) and base (amine) molecular groups to solid oxide supports. In an early example from the Davis' group, a catalyst made via the simultaneous tethering of primary-amine and sulfonic-acid groups on SBA-15 proved active for the promotion of the aldol condensation of 4-nitrobenzaldehyde with acetone.[272,273] The behavior of catalysts made via co-condensation and post-tethering synthetic methods were contrasted in terms of their ability to promote aldol condensations: not much difference was detected between the two, but what did make a difference was the nature of the acidic functionality, as the native silanol groups proved to have a better cooperative effect than added carboxylic functionalities.[180] A different synthetic approach to acid−base bifunctional silica catalysts has been provided by Shiju and coworkers, by which the surface is first amine-functionalized using APTES and then partially titrated with phosphotungstic acid ($H_3PW_{12}O_{40}$): the resulting material was shown to promote the model one-pot tandem deacetalization-Henry sequence of reactions (Figure 23).[274] Another acid−base bifunctional catalyst was designed to promote the one-pot conversion of cellulose to HMF via a three-step process: hydrolysis of the oligomers with the help of acid sites, base-promoted isomerization of the resulting glucose monomers to fructose, and acid-catalyzed interconversion of fructose to HMF.[275] More recently, glucose isomerase, immobilized inside the pores of an amine-functionalized silica support, was used as the active phase for the glucose-to-fructose isomerization step; the combination of this catalyst with a second Brønsted-acid ($-SO_3H$) functionalized mesoporous silica afforded the one-pot transformation of glucose to HMF.[276] Post-modification of solid supports to add multiple functionalities, often acid and base sites, has also been successfully tested with other materials such as polymers and other carbon-based materials. For instance, acid−base bifunctional microporous organic nanotubes were recently made via a combination of hypercrosslinking core−shell brush copolymers and post-functionalization, and successfully evaluated for the test acid-catalyzed acetal hydrolysis plus base-catalyzed Knoevenagel tandem sequence of reactions.[277] More than two functionalities can be added to solid catalysts as well: witness the example of the simultaneous tethering of Cu(I)-pyridyltriazol, TEMPO, and *N*-methylimidazole (NMI) sites on azide-functionalized silica particles (via CuAAC click chemistry) to promote the aerobic oxidation of alcohols; NMI is known to accelerate the reaction by decreasing the Cu(II)/Cu(I) reduction potential.[278−280]

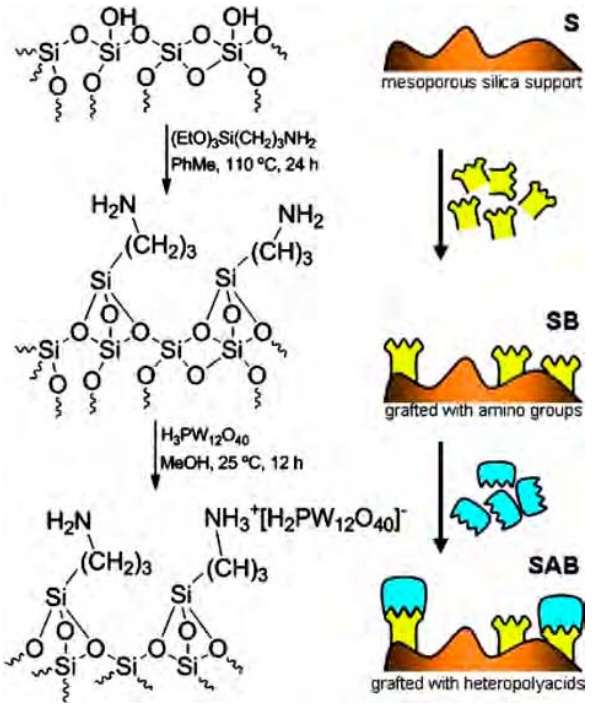

Figure 23. Synthetic protocol to produce acid−base bifunctional heterogeneous catalysts where a silica support is first derivatized with amine groups (using APTES) and then partially titrated to add phosphotungstic acid ($H_3PW_{12}O_{40}$).[274] Reproduced with permission from ref 274. Copyright 2011 Wiley-VCH Verlag GmbH & Co. KGaA, Weinheim.

Tandem reactions may be carried out sequentially, even with one single multifunctional catalyst, by spacing the exposure of the catalyst to the different reactants in time. This may be needed under certain circumstances, but it adds complexity to the design of the catalytic process; it is more desirable to be able to carry out the conversion all at once, by adding one single reaction mixture at the start. More interesting, albeit more difficult to accomplish, is the possibility of conceiving processes with multifunctional catalysts that display spatial compartmentalization. This may not only afford proper separation of incompatible functionalities, but also, at least in principle, improve the kinetics of the overall conversion by matching the rates of the different steps, minimizing mass transport bottlenecks and optimizing the transfer of unstable intermediates from one site to the next before decomposition. In fact, in some instances it may be desirable to have two or more functionalities placed in adjacent sites, because they may exhibit a cooperative or synergistic behavior that may help promote certain catalytic conversions. When tethered functionalities are expected to cooperate with solid surface sites such as silanols in silica, the interactions can be tuned by varying the length of the linker: in cases involving tethered aminoalkylsilanes and surface silanols, for instance, short linkers were shown to limit the amine-silanol cooperativity and to result in lower catalytic activity in aldol condensations; three carbons proved sufficient to optimize catalytic performance, and no additional changes were seen with longer chains (Figure 24).[281]

More commonly, two organofunctionalities may be added to the solid support in a concerted fashion. Several strategies have been tested to control the distribution of the different tethered functionalities within the solid at a molecular level in those cases.[250,282] One is by using an imprinting agent during the synthesis of the solid,[283] as, for instance, in the case of the sol-gel synthesis of porous silica where a carbamate-protected APTES with two or three of such units bonded to a central aromatic ring was added to the regular tetraethoxysilane (TEOS) sol-gel reagent; once the solid was formed, methanol/aqueous sodium bicarbonate washing was used to break the carbamate bonds and release the aromatic ring scaffold, leaving behind two or three amine groups tethered to the silica surface

https://doi.org/10.1021/acs.chemrev.1c00905
Chem. Rev. XXXX, XXX, XXX−XXX

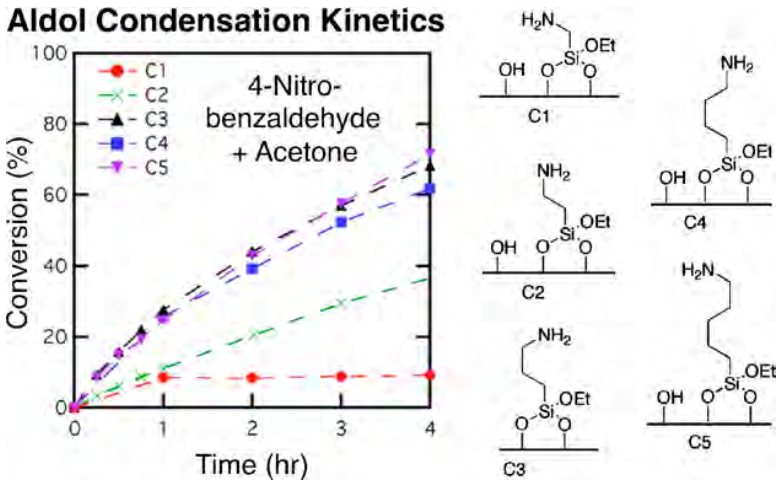

Figure 24. Effect of chain length on the catalytic activity of amine groups tethered to a SBA-15 silica surface.[281] Shown are the kinetics of the aldol condensation of 4-nitrobenzaldehyde with acetone: low activity is seen with short alkyl linker chains, but approximately similar behavior is obtained with chains with three carbons or longer. Reproduced with permission from ref 281. Copyright 2012 American Chemical Society.

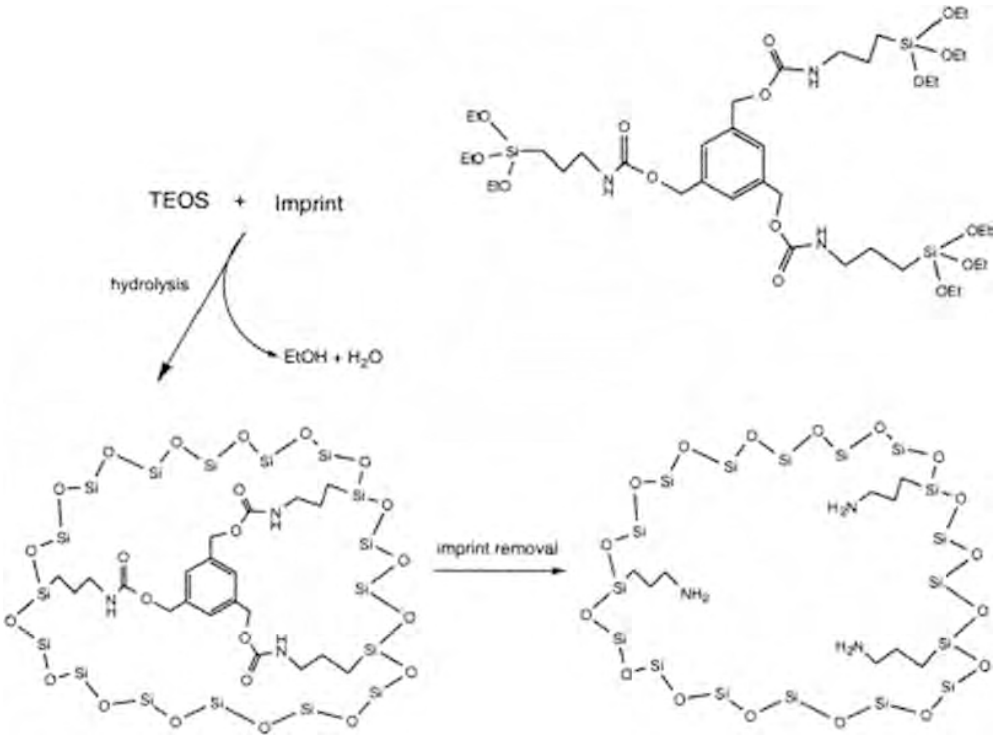

Figure 25. Imprinting synthetic route for the derivatization of silica surfaces with aminopropyl groups in a correlated fashion.[159] In this case, three amine groups are carbamate-protected on a single aromatic ring, and terminated with triethoxysilane groups to help incorporate the molecules to silica during a sol-gel synthesis. The benzene-carbamate groups are then remove by washing with a solvent. Reproduced with permission from ref 159. Copyright 2002 American Chemical Society.

in predetermined relative positions (Figure 25).[284] A second approach here is site pairing. Propyltriethoxysilane-terminated disulfides can be used for this purpose to produce pairs of sulfonic acid sites (after oxidation), for instance.[159,285] Tests on the promotion of the condensation of phenol and acetone to produce bisphenol-A proved that the resulting proximity of pairs of sulfonic acid groups on silica leads not only to a clear increase in total activity but also to higher regioselectivity.[285] In a separate study, a decrease in spatial distance between the sulfonic-acid groups prepared with such disulfide precursors was found to increase the acid strength of the resulting solid catalyst. However, catalytic performance for the promotion of the methanol esterification of palmitic acid could not be simply related to the effects induced by the spatial location of the acid sites.[286] Finally, the two functionalities may be incorporated within the same organic fragment. For instance, catalysts prepared by tethering of discrete pairs of sulfonic acid and thiol groups were proven more active than materials containing randomly distributed acid and thiol groups in the condensation of either acetone or cyclohexanone with phenol; increasing the

https://doi.org/10.1021/acs.chemrev.1c00905
Chem. Rev. XXXX, XXX, XXX−XXX

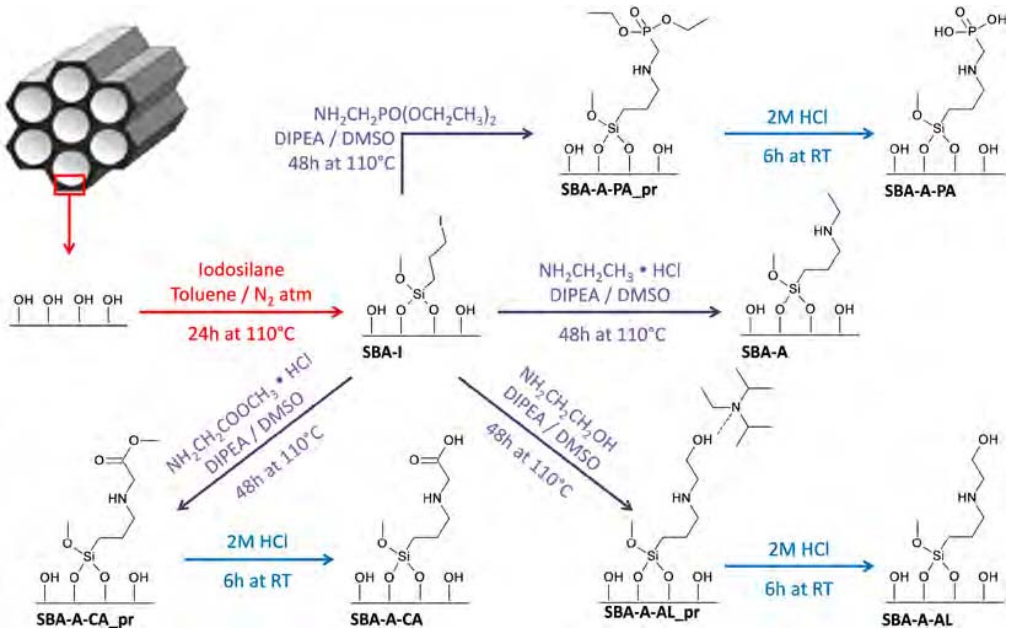

Figure 26. Stepwise synthetic schemes for the tethering of single molecular fragments with dual acid−base functionalities.[290] Reproduced with permission from ref 290. Copyright 2015 Elsevier Inc.

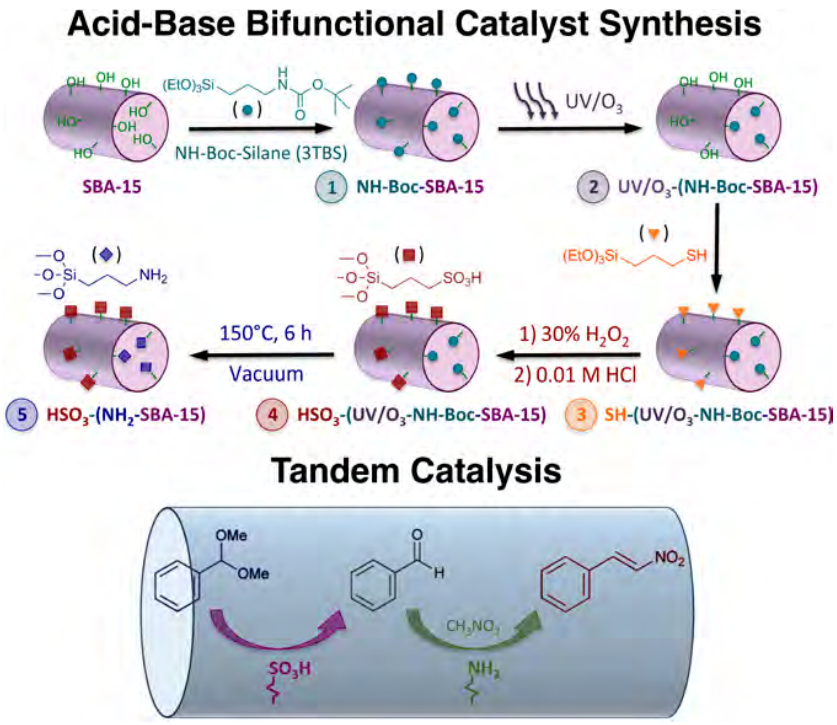

Figure 27. Top: Synthetic strategy to make acid−base multifunctional solid catalysts. Bottom: Sequence of deacetylation and Henry reactions used to test this catalyst. Reproduced with permission from ref 291. Copyright 2018 American Chemical Society.

acid/thiol distance in the paired materials was shown to result in decreases in both activity and selectivity.[287]

Another option is the simple derivatization of the solid with one single type of organic fragment such as amino acids containing multiple functionalities, as in the example of cysteine and cysteamine tethered on a silica support by means of a photoinitiated thiol−ene click reaction; this catalyst could easily promote the aldol condensation of 4-nitrobenzaldehyde with acetone.[288] A more sophisticate example is that of the solid catalyst that was functionalized with a chiral proline-like group at the end of a linker chain containing another amine groups; this catalyst, after protonation of one of the two amine groups to make it an acid−base catalyst, proved active in the aldol reaction between acetone and p-nitrobenzaldehyde, with an activity that decreased with increasing acid strength.[289] A dual organofunctionality can be built *in situ*

https://doi.org/10.1021/acs.chemrev.1c00905
Chem. Rev. XXXX, XXX, XXX−XXX

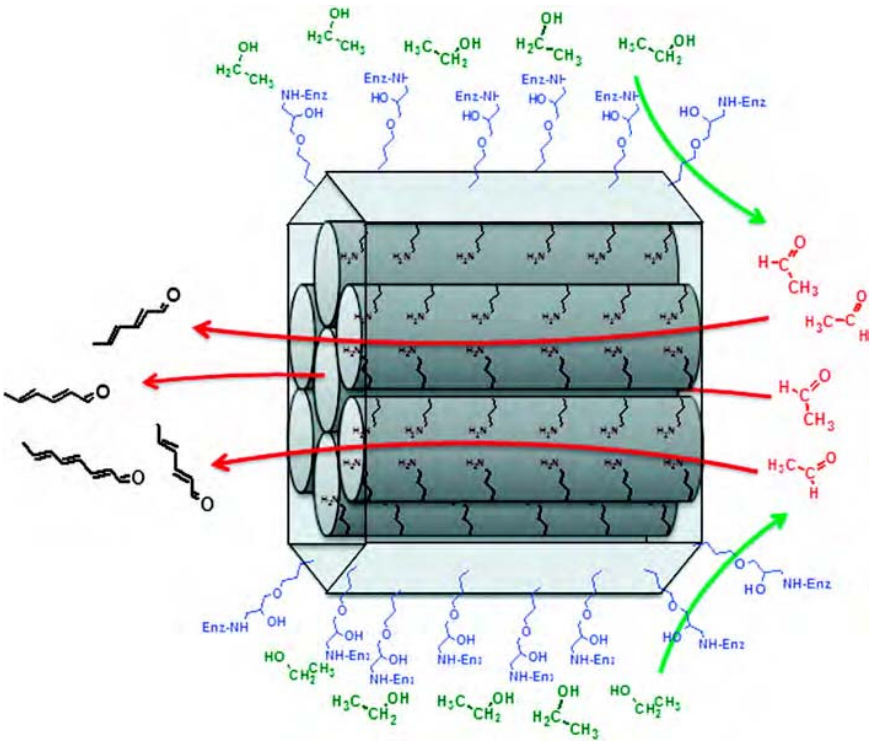

Figure 28. Bifunctional catalyst made out of alcohol oxidase tethered to the outer walls of a silica support with pores terminated on amino groups (incorporated by adding APTES during the synthesis of the solid).[299] This catalyst was proven to successfully promote a sequence of ethanol oxidation (green arrows) and aldol condensation of the resulting acetaldehyde (red arrows) steps. Reproduced with permission from ref 299. Copyright 2013 American Chemical Society.

on the surface in a stepwise fashion. This is what was reported by the Jones' group in the case of SBA-15 first derivatized with iodosilane, after which the terminal iodide group was replace with ethylamine, ethanolamine, methyl aminoacetate, or diethyl aminomethylphosphonate (Figure 26); specific trends were identified for the catalysis of aldol reactions as a function of the strength of the acid site.[290]

In some instances, the interest is to place two orthogonal molecular functionalities in different regions of the solid, a compartmentalization defined at a nanometer scale. To illustrate the type of synthetic approaches available to attain this type of phase separation, we cite an example from our laboratory where both simple acid and base groups where immobilized on the same mesoporous material (SBA-15).[291] A number of steps, including group protecting and deprotecting, needed to be strung together to add the acid and base functionalities without neutralizing each other: (1) the addition of Boc-protected APTES; (2) the controlled use of UV/ozonolysis to selectively remove the exterior groups; (3) the decoration of the exterior sites freed in Step 2 with 3-mercaptopropyltriethoxysilane; (4) the selective oxidation of the mercaptan groups to sulfonic acid; and (5) the pyrolytic deprotection of the amine (Figure 27). The resulting catalyst contained sulfonic acid functionality on its external surface and entrance of the pores and amino groups deep inside those pores, at coverage ratios that could be controlled by tuning the exposure time during the UV/ozonolysis step. This catalyst was successfully tested for the promotion of the model deacetylation-Henry cascade reaction: optimum performance was seen with the catalyst having an overall 1:2 acid:base molar ratio.[291] A different group followed a similar sequence of steps but using CTAB during the thiol addition (which was done first) to block the pores and thus prevent access to the amine, which consequently ended up tethered only to the otter surfaces of the catalysts.[292] A third example is that of a selective functionalization with acid (carboxylic) and base (amine) groups at the outer and inner surfaces of hollow silica nanospheres, respectively; these were also successfully tested for the promotion of the deacetalization-Henry cascade reaction.[293] In yet another recent case, compartmentalization of the active sites was accomplished by segregating acid sites on the silica surface and base sites within the polymer domains of SBA/MCM-SH-poly(styrene-*co*-2-(4-vinylbenzyl)-isoindoline-1,3-dione) mesoporous silicate-polymer composite materials; the use of large polymer units confined the associated functionalities to the external surfaces.[294] Shell cross-linked micelles is another way to compartmentalize functionalities: in one case, amphiphilic poly(2-oxazoline) triblock copolymers were used as starting materials to develop a two-chamber nanoreactor with acid sites in the shell and base sites in the core to promote the prototypical deacetalization-Henry reaction.[295]

Polymers are also good supports for the design of synthetic strategies to separate different molecular functionalities within one solid catalyst. For instance, hyper-cross-linked polymers with both acid and base sites have been synthesized by a three-step Friedel-Crafts reaction-based approach involving the synthesis of a microporous organic support using a SiO_2@PS(19) core−shell composite as the precursor (see Section 7.1 for more details on these nanostructures), the addition of acid sites (mostly on the external shell of the sphere) using acetyl sulfate, and a final decoration step using 2-(hydroxymethyl)-

https://doi.org/10.1021/acs.chemrev.1c00905
Chem. Rev. XXXX, XXX, XXX−XXX

isoindoline-1,3-dione as the amine precursor; this catalyst was successfully tested for the promotion of deacetalization-Henry and deacetalization-Knoevenagel reactions.[296] An example not involving acid−base system is that of the immobilization of two incompatible transition metals on a core−shell micellar support: the orthogonal functional groups on the side chain of a amphiphilic triblock copolymer of poly(2-oxazoline), used as the support, were covalently cross-linked and conjugated to two metal catalysts in different domains of the micelle: to a Co complex at the hydrophobic core to catalyze the hydration of alkynes, and to a separate Rh complex in the hydrophilic shell to promote the asymmetric transfer hydrogenation of the intermediate ketone into a chiral alcohol.[297] 2,2,6,6-tetramethyl-1-piperidinyloxyl (TEMPO) and Rh N-tosylated 1,2-diphenyl-1,2-ethylenediamine (Rh-TsDPEN) moieties have been spatially positioned into the hydrophilic corona and the hydrophobic micelle core of poly(2-oxazoline)-based shell cross-linked micelles, respectively, to promote one-pot redox-driven deracemizations of secondary alcohols in aqueous media.[298] Differences in size can also be used to attain spatial separation of functionalities, particularly if the active component is an enzyme (Figure 28).[299,300]

It should be indicated that, while innovative in their construction, most reported heterogeneous tandem catalysts address simple reactions that illustrate proof of principle but may not be of great value for practical applications.[254] The use of the deacetylation-condensation (Henry or Knoevenagel) sequences to test the multifunctional catalysts in many of the examples cited above illustrates this point. Another common example is that of the oxidation of styrene followed by simple reduction to 1-phenylethanol,[251] a case that nicely illustrates asymmetric reactivity but produces a compound that is a feedstock itself. The true impact of the heterogeneous tandem catalysis concept lies in the addition of value to simple feedstocks via C−C bond constructions and the application to more complex, challenging reactions. This has been demonstrated by the Dumesic group in their use of a Pd/MgO-ZrO_2 bifunctional aldol condensation/hydrogenation catalyst for the conversion of furfural, obtained from biomass sources, to large water-soluble organic precursors for the synthesis of alkanes.[301−303] The implementation of multifunctional catalysts with well-defined spatial definition to practical applications also remains a challenge for the future; there are only limited ways to control functionality placing, and kinetic matching is also quite difficult. To these specific issues, one needs to add the generic limitations associated with the design and use of catalysts with tethered molecular functionalities mentioned before. These include stability, recyclability, and cost. There may be processes where the high value of the products may justify wrestling with these shortcomings, however, in particular in fine chemical production.

2.6. Decomposition and Leaching

It is clear that the immobilization of molecular catalysts, be organometallic or metal organic compounds, organic functionalities, or enzymes, is the approach that promises the highest level of selectivity in heterogeneous catalysis. As discussed later in this review (Sections 5 and 6), modern nanotechnologies may provide new avenues for the preparation of solids with complex and well-defined structures, but the resulting catalytic surface sites in those cases cannot yet achieve the same level of structural detail possible with molecular synthesis. On the other hand, immobilized molecular catalysts face some important shortcomings that limit their use,[304] and there is a trade off associated with the immobilization of molecular structures on solids.[64] If their interactions with the surface are weak, as in the case of physical adsorption, chances are that the molecular catalyst will leach out of the solid during catalysis.[305] Even with some covalently bonded tethered catalysts, leaching because of chemical decomposition, via detachment of the metal from the ligands in organometallic catalysts, is possible. In Figure 29 we provide an example, for the case of a carbon-tethered Rh complex used for hydroamination and dihydroalkoxylation reactions: high turnover numbers, close to 1000, were achieved with these catalyst, but a few percent of the Rh content was lost in each cycle, and a drop in hydroamination conversion from >98% to 72% was measured by the fourth consecutive run.[306] This may be a particularly acute problem with immobilized catalysts based on Rh,[307−309] Pd,[310−312] and other transition metals.[313−318] Alternative mechanisms for the loss of activity with tethered catalysts include clustering of the metal ions into metal NPs[312,319] and the hydrolysis of silane bonds.[110] It is interesting that in some instances structural or electronic changes in the tethered catalysts may be required for their activation; in those cases, an increase (rather than a decrease) in activity is seen in reusability tests.[145,320] However, these are the exception rather than the rule. At the other extreme, namely, if the interaction between the support and the tethered functionality is strong, as in cases involving covalent bonding, the catalysts are hard to regenerate once the molecular functionality decomposes. For instance, tethered amine organofunctionalities have been shown to deactivate starting at temperatures below 200 °C.[321] In one of the few mechanistic studies on the decomposition of tethered catalysts, with Pd-pincer complexes bonded to silica supports, it was suggested that such process may occur through exchange of the phosphorus or sulfur ligand within one arm of the pincer ligand with triethylamine followed by a β-hydrogen elimination of the base and a rapid second ligand exchange.[321] It is unfortunate that, even though these problems are well known and generally recognized by the catalysis community, they have not been studied explicitly in much detail; leaching of tethered or immobilized molecular catalysts, for example, is often mention in passing if at all as part of studies of catalyst stability.

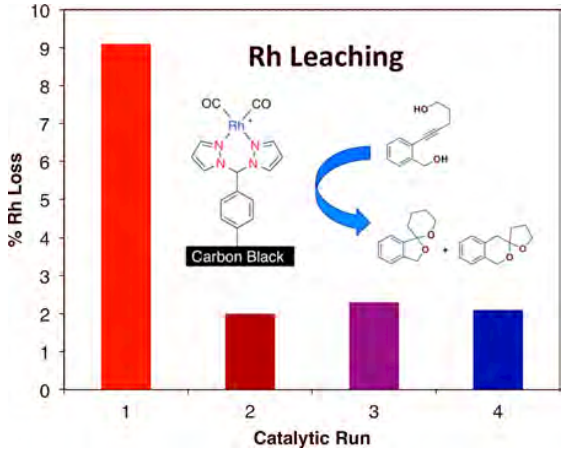

Figure 29. Metal leaching during dihydroalkoxylation catalysis using a carbon support functionalized with a $[Rh(CO)_2(\mu\text{-}Cl)]_2$ organometallic complex.[306]

https://doi.org/10.1021/acs.chemrev.1c00905
Chem. Rev. XXXX, XXX, XXX−XXX

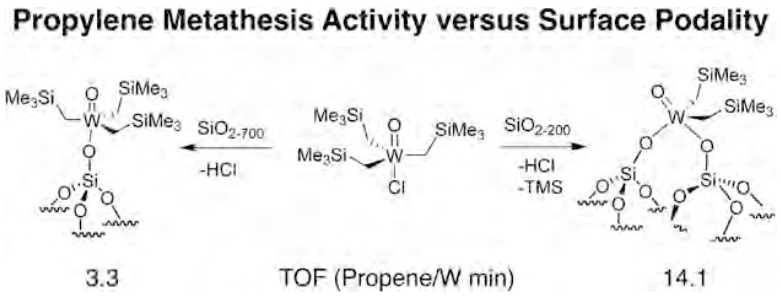

Figure 30. Effect of podality on the performance of grafted organometallic catalysts.[325] In this case, a tungsten complex was bonded to a silica surface via one (left) or two (right) oxo ligands. The latter resulted in a much more active catalyst for propene metathesis, as indicated by the turnover frequency (TOF) values reported below the reaction scheme. Reproduced with permission from ref 325. Copyright 2016 American Chemical Society.

A second challenge relates to the role of the surface of the solid in the processes promoted by the immobilized molecular catalysts. In many instances, an inert solid with high surface area is chosen for these applications in the hope that they only provide a platform to heterogenize the catalyst and do not participate in any conversion. However, this often turns out not to be the case. With organometallics, for instance, their grafting often involves surface sites acting as ligands that coordinate to the metal center.[75] On silica, for instance, the surface may be viewed as equivalent to a siloxo ligand.[322] This organometallic-surface complexation provides a strong interaction for immobilizing the metal center, but the structural and electronic properties of the surface site are never able to exactly match those of an analogous free ligand, and therefore may produce heterogeneous catalysts with different behavior. The picture is further complicated by the fact that the surface can act as a substitute for more than one ligand, increasing the so-called "podality".[64,75,323,324] With $[\equiv SiO)_xWO(CH_2SiMe_3)_{3-x}]$ (x = 1, 2) grafted tungsten complexes, for instance, it was shown that the bipodal catalyst (x = 2) is significantly more active in promoting propylene metathesis than the monopodal (x = 1) counterpart (Figure 30).[325] In another example, with a tethered rather than grafted catalyst, Rh_2(trifluoroacetate)$_4$ was complexated to SBA-15 derivatized with amino (APTES) groups either alone or in combination with carboxylic ligands; the latter was clearly superior for the promotion of the cyclopropanation of styrene with ethyl diazoacetate.[326] More subtle but also important is the position at which the ligand bonds to both the linker used for tethering and the immobilized metal ion-ligand: for instance, it has been possible to tune the regio- and stereo-selective of C−H functionalization reactions using a tethered chiral Rh_2(S-ortho-Cl-(1,2,2-triarylcyclopropane carboxylate)$_4$ catalyst by varying the ligand immobilization position.[327] A similar effect related to the point of tethering within the molecular functionalities can be seen with non-metallic organic groups, as illustrated in the examples shown in Figures 13 and 21.[178,179] It is interesting that in those studies it was found that the enantioselectivity of the thiol addition to 2-cyclohexen-1-one decreases not only upon tethering of the cinchona alkaloid catalyst to a silica surface but also if physical mixtures of the homogeneous catalyst with pure silica are used; this is a case where the acid sites of the support independently promote undesirable side reactions (the non-enantioselective coupling of the reactants).[179] As also discussed above, silanol surface groups can act in a cooperative way with other tethered functionalities to promote tandem reactions. These effects may in some cases be beneficial to the catalytic process,[328] but more often are detrimental because homogeneous catalysts have typically been optimized prior to considering their immobilization on solid surfaces.[329]

The influence of the surface on the molecular catalytic center can be minimized via tethering using "click" chemistry and longer linkers, as discussed already (Sections 2.2, 2.3, and 2.4). However, in that case the flexibility of the linker may allow for the molecular functionality to approach surface sites nearby.[178,179] We witness one example of this issue when we tethered cinchona alkaloids on silica supports: a loss of enantioselectivity during the promotion of the addition of aromatic thiols to a conjugated cyclohexanone was observed, which could be accounted for by a combination of at least three effects: (1) the nonselective catalytic activity of the surface of the solid itself; (2) the activity of the OH species generated by hydrolysis of some of the Si-alkoxy groups in the trialkoxy moieties used to bind many linkers to oxide surfaces; and (3) the bonding of the molecule to be tethered directly to the surface.[179] Fortunately, several approaches are available to minimize these problems, including the silylation of the active OH surface groups of the support (discussed in more detail in this review, Section 8.1), the selection of solvents to minimize hydrolysis or alcoholysis reactions, and the regioselective binding of the molecular catalyst (the cinchona alkaloid) to minimize its ability to interact with the surface. The hydrophobicity or hydrophilicity of the surface is another factor, as already discussed above in connection with the immobilization of enzymes (Section 2.4). Finally, porous solids are often used as supports in order to achieve high surface areas, sometimes even to retain big molecular discrete catalysts, enzymes in particular, within the solid to minimize leaching,[208] but those pores may impose geometrical constrains on the ability of molecular catalysts to adopt their required structure and interact with the reactants for optimum promotion of reactions,[330] especially with large molecular catalysts such as enzymes (as mentioned before, Section 2.4).[331,332] To the specific limitations imposed by the local structure of the pores, additional consideration needs to be given to mass transport limitations of reactants and products to and from the catalytic site,[333] although this is a problem common to all heterogeneous catalysts. It should be mentioned that the complexity of solid surfaces can also provide unique opportunities, since they can display large atomic assemblies difficult to reproduce via molecular synthesis. The advantages of using such multiatom surface sites as catalysts by themselves will be discussed later in this review, but here it needs to be

https://doi.org/10.1021/acs.chemrev.1c00905
Chem. Rev. XXXX, XXX, XXX−XXX

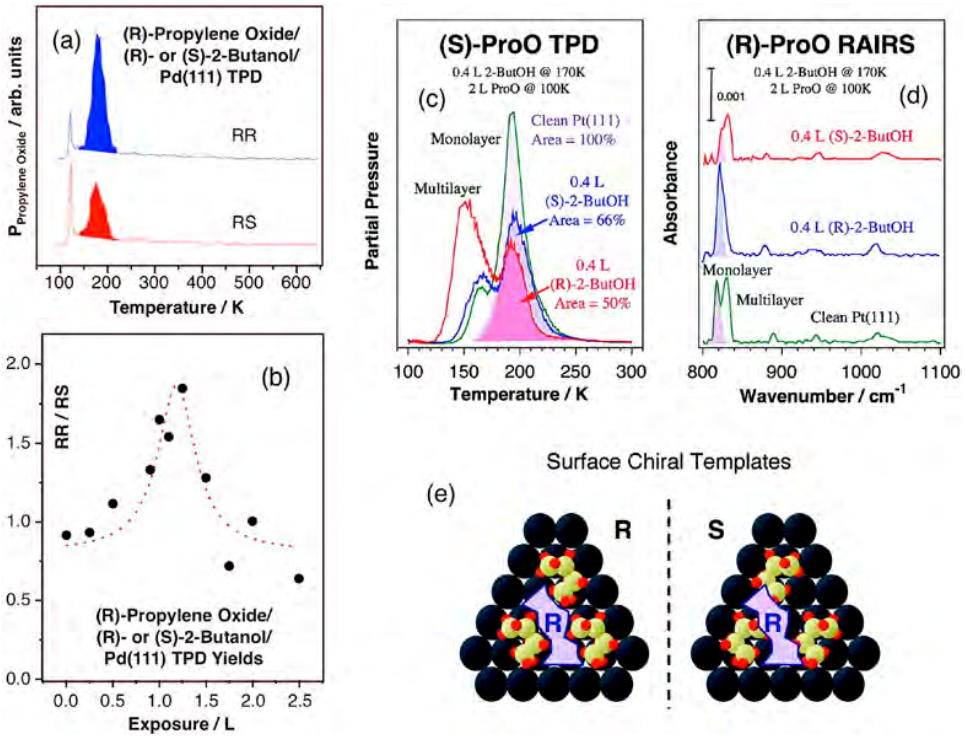

Figure 31. Examples of chiral imprinting on model surfaces using enantiopure adsorbates. (a) Typical contrasting temperature-programmed desorption (TPD) traces for (R)-propylene oxide (PO) adsorbed on a Pd(111) surface modified with a submonolayer coverage of either (R)- or (S)-2-butoxide surface species. It can be seen that there is a larger uptake on the surface with the (R)-2-butoxide layer than with the analogous (S)-2-butoxide modifier. (b) Enantiomeric TPD (R)-PO/(R)-2-butoxide versus (R)-PO/(S)-2-butoxide yield ratios as a function of initial 2-butanol exposure for the system exemplified in (a) showing optimum enantiomeric differentiation (RR being more favorable than RS) at an exposure of ~1.2 L (about a quarter of a monolayer). Reproduced with permission from ref 364. Copyright 2002 American Chemical Society. (c) TPD, and (d) reflection-absorption infrared spectra (RAIRS) from similar PO/2-butoxide combinations on Pt(111), showing again an enhanced monolayer PO uptake for the SS and RR combinations relative to the SR and RS counterparts. Reproduced with permission from ref 371. Copyright 2008 American Chemical Society. (e) Model proposed for the formation of supramolecular surface chiral templates, where three molecules of the enantiopure templating agents (2-butoxide adsorbates) form a pocket of specific chirality on the surface: the (R) purple structure fits nicely in the chiral site left by the (R)-butoxides but not on that defined by the (S) enantiomers. Reproduced with permission from ref 3. Copyright 2009 American Chemical Society.

acknowledged that they can also be coupled with molecular functionalities to help shape the catalytic site, add a second catalytic element, or help with additional adsorption sites for the reactants.[334,335]

All the effects listed above can in some instances be incorporated in the design of heterogeneous catalysts, and may in fact help improve the catalytic performance of the molecular functionalities being immobilized. More often, however, the presence of solid surfaces affects molecular catalysts in negative ways. Because of these issues of catalytic stability and surface interference, and also because of cost, the use of immobilized molecular catalysts in industry has been limited. It may still be worth using this approach for the synthesis of complex and expensive products requiring high selectivity, such as, for instance, enantiopure chiral pharmaceuticals, but it is unlikely for this approach to become common in industrial applications where profits are marginal and catalyst cost is a deciding factor.

3. ADSORBATES AS CO-CATALYSTS OR CATALYST MODIFIERS

Another way to incorporate molecular features to surfaces is by adsorbing appropriate molecules directly from the gas or liquid phases during the course of the catalytic process. This can perhaps be seen as a hybrid approach, in between homogeneous and heterogeneous catalysis, given that a molecular compound is required and constitutes part of the catalytic site. This modifier may bond reversibly on the surface, in which case it may need to be added to the reaction mixture to attain appropriate surface coverages under catalytic conditions, or, alternatively, it may be attached more strongly and irreversibly to the solid, becoming part of the heterogeneous catalyst. Below we briefly discuss a few key examples of this approach.

3.1. Chiral Modifiers

As mentioned above, a molecular agent can be added temporarily and reversibly to the catalysts by establishing an adsorption-desorption equilibrium of such modifier, mixed with the reaction mixture, on the surface. A particular case where this idea has shown some promise is in the bestowing of enantioselectivity to typical transition-metal-based heterogeneous hydrogenation catalysts by using chiral modifiers. Chirality is quite relevant to many products in the pharmaceutical and agro industries:[336−339] because life on earth has evolved to favor one chirality over the other, much of the biochemistry of living organisms runs with pure enantiomers.[340−342] The direct production of enantiopure chiral compounds is arguably the most stringent test of selectivity in catalysis.[3] To bias the hydrogenation of achiral

https://doi.org/10.1021/acs.chemrev.1c00905
Chem. Rev. XXXX, XXX, XXX−XXX

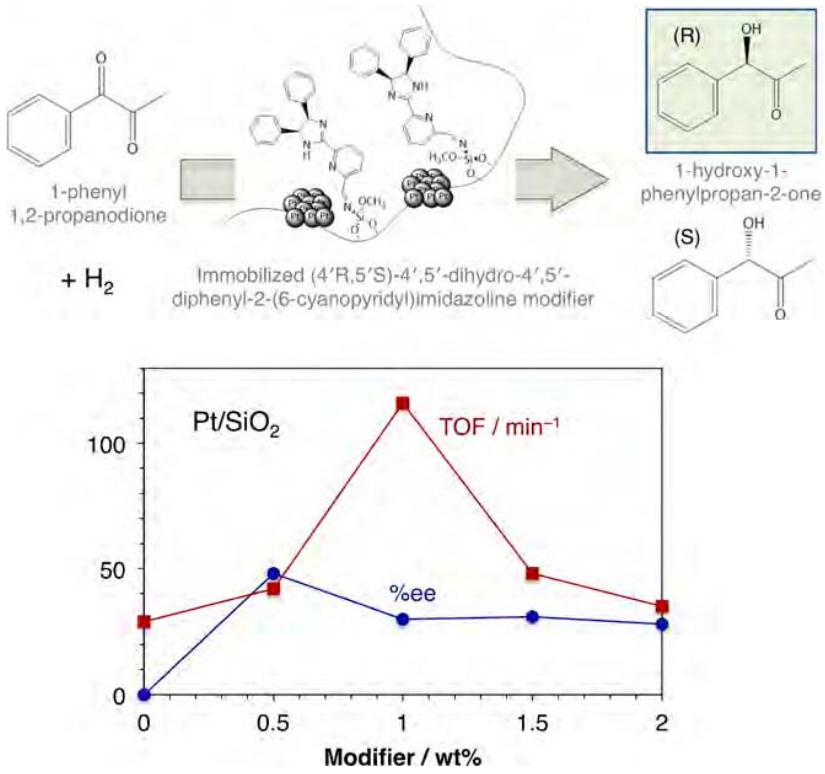

Figure 32. Example of chiral modification of Pt/SiO_2 hydrogenation catalysts via the immobilization of a non-cinchona chiral modifier.[419] Top: reaction scheme, highlighting the reactant (1-phenyl-1,2-propanodione), the products ((R)- and (S)-1-hydroxy-1-phenylpropan-2-one), and the catalysts with its surface modified via the tethering of (4′R,5′S)-4′,5′-dihydro-4′,5′-diphenyl-2-(6-cyanopyridyl)imidazoline. Bottom: catalytic performance in terms of TOF and %ee as a function of the chiral modifier surface coverage. Adapted with permission from ref 419. Copyright 2015 Elsevier B.V.

compounds toward the preferential formation of one of the enantiomers over the other requires a chiral environment, and, although some surfaces are known to be chiral,[343−345] it is difficult to produce solid catalysts that expose only one handedness. Instead, a local chiral environment can be recreated on surfaces by an adsorbed chiral compound.[17,346]

Two related families of chiral modifiers have been put forward and proven to impart enantioselectivity to hydrogenation catalysts.[16,347,348] In one, tartaric acid has been added to nickel catalysts to promote the enantioselective hydrogenation of β-ketoesters.[347,349−352] The scope of this reaction is quite limited, as it only works for a small group of uninteresting molecules,[353−355] but these systems have nevertheless generated quite a bit of interest in the surface-science community because of their simplicity.[356−358] The challenge in explaining how this modifier works is that, because tartaric acid is such a small molecule, it is not likely to provide, by itself, a local chiral environment around solid catalytic sites with enough structural details to promote enantioselective hydrogenation steps. Instead, the focus has been on exploring the idea of the formation of adsorbate suprastructures on the surface via the organization of the individual molecules in specific patterns.[359−361] The premise is that such suprastructures may create a template with open spaces having chiral characteristics, the sites that may show enantioselective adsorption and reactivity. In fact, experiments on selected model surfaces and molecular combinations have proven this to be possible,[362,363] as illustrated by the examples with 2-butanol (templating molecule) and propylene oxide (enantioselectivity probe) on Pd and Pt surfaces shown in Figure 31.[364−369] In the end, however, although some interesting kinetic effects leading to large enantioselective effects on surface reactions have been identified,[370] the extension of the understanding derived from studies on model surfaces to actual catalytic systems is still missing.

The more promising and more studied second group of chiral modifiers is based on cinchona alkaloids, which were originally added to platinum catalysts to enantioselectively hydrogenate α-ketoesters. The reaction was originally reported in the late '70s by Orito and coworkers,[372,373] and has been studied extensively ever since.[16,347,374−380] Excellent enantioselectivities have been reported with particular α-ketoesters such as ethyl pyruvate,[381−383] but the scope of this reaction, as in the case of the tartaric acid-modified nickel catalysts, is limited. There is a little more flexibility in this case, though, as examples have been identified for the promotion of hydrogenations with related reactants such as ketones,[377,384−386] other carbonyl-containing organic molecules,[387,388] and even reactants with C═C double bonds,[16] as well as for related reactions such as asymmetric C−C bond couplings.[389] Transition metals other than Pt (Pd, Rh Ir) have proven useful as well,[375,390,391] and the range of possible modifiers has been extended from cinchona-related[377,392−401] to amino acids[402,403] and other aromatics (e.g., indans and indols)[404] Catalytic performance can also be tuned using different supports,[394,405] solvents,[399,406−409] reaction conditions[410−412] and surface structures (metal NP size).[413−416] There have even been attempts to tether the chiral modifier to the surface of the

https://doi.org/10.1021/acs.chemrev.1c00905
Chem. Rev. XXXX, XXX, XXX−XXX

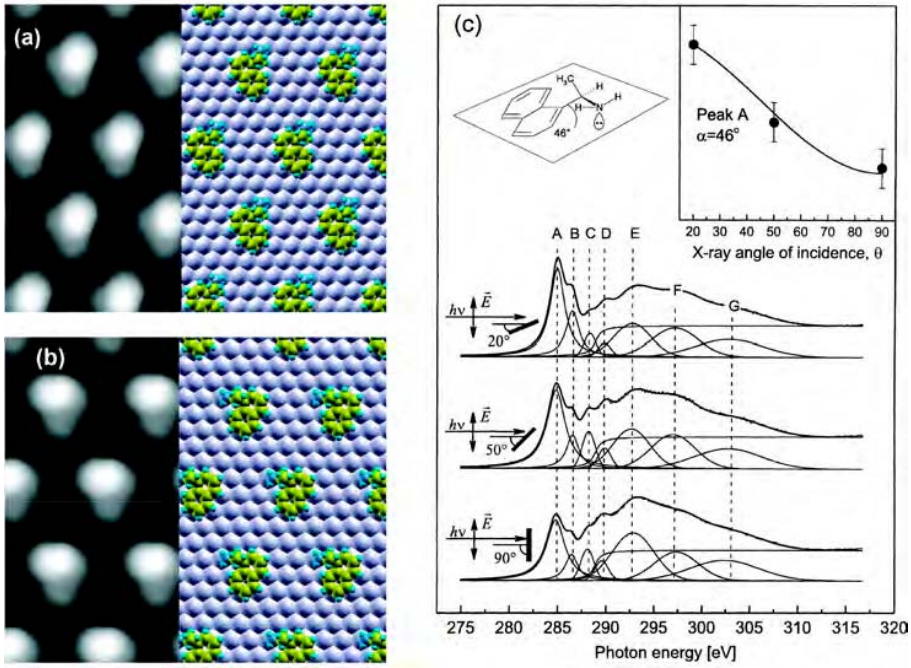

Figure 33. Evidence for the flat adsorption geometry that NEA adopts on metal surfaces under UHV conditions. Left: STM images and corresponding overhead views of DFT-optimized structures for the (a) exo- and (b) endo-conformers of NEA on Pd(111).[422] Right (c): Normalized carbon K-edge NEXAFS spectra for a monolayer of (S)-NEA on Pt(111). The inset shows the normalized intensity for Peak A as a function of photon incidence angle, and at the top-left a proposed structure with the aromatic ring parallel to the surface based on these data.[428] Reproduced with permission from refs 422 and 428. Copyright 2011 American Chemical Society and 2001 Elsevier Science B.V., respectively.

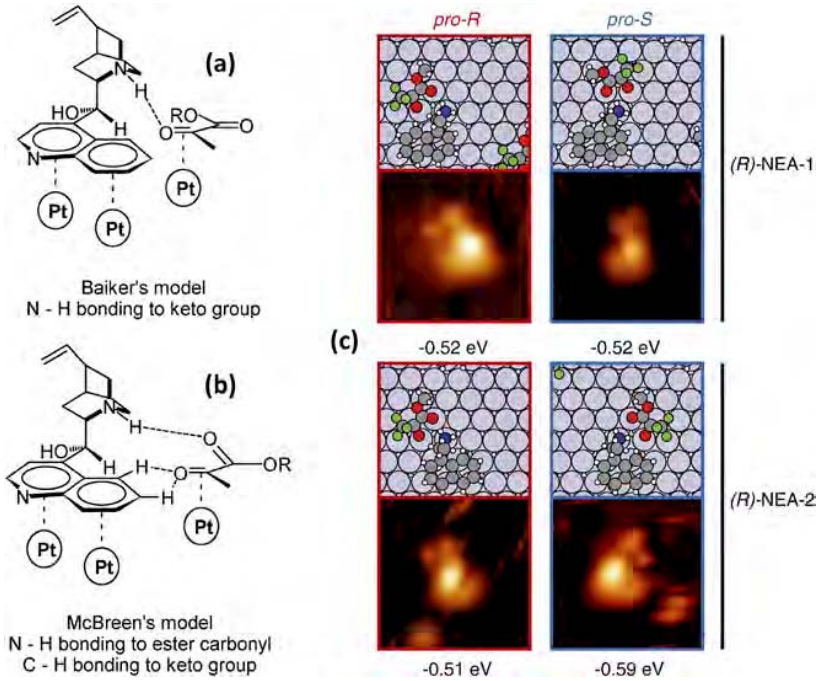

Figure 34. Schematic presentations of the (a) one-point[436] and (b) three-point[438] activated surface complexes proposed to form upon the surface interaction of cinchona alkaloid modifiers with ketoester reactants during the hydrogenation of the latter promoted by metal catalysts. Reproduced with permission from ref 379. Copyright 2007 American Chemical Society. (c) STM images and corresponding DFT atomic illustrations and adsorption energy values for the most common complexes observed with methyltrifluoropyruvate/(R)-NEA on a Pt(111) surface. Reproduced with permission from ref 442. Copyright 2014 Elsevier B.V.

support to make all-heterogeneous enantioselective catalysts, but that approach has only shown limited success, and does not provide a way to prevent decomposition of the surface species and deterioration of the catalytic performance over

https://doi.org/10.1021/acs.chemrev.1c00905
Chem. Rev. XXXX, XXX, XXX−XXX

time.[264,417,418] In Figure 32, a case is reported that exemplifies some of the varied components listed above: (4′R,5′S)-4′,5′-dihydro-4′,5′-diphenyl-2-(6-cyanopyridyl)imidazoline was covalently immobilized on a Pt/SiO_2 catalyst to add enantioselectivity to the hydrogenation of 1-phenyl-1,2-propanodione to 1-hydroxy-1-phenylpropan-2-one.[419] The enantioselectivity effect of the modifier is only moderate, but one important observation is that both enantioselectivity and, in particular, activity depend on the coverage of the modifier on the silica surface, with the catalyst reaching optimum performance at intermediate values.

Multiple modern surface-science studies have been carried out to understand the details of the chiral modification of solid surfaces with cinchona-type modifiers, using 1-(1-naphthyl)-ethylamine (NEA) in particular as a simplified modifier.[17,346,420,421] Much of that work has been performed under ultrahigh vacuum (UHV) conditions, as needed to operate the techniques used, which include scanning tunneling microscopy (STM),[420,422−424] reflection-absorption infrared absorption spectroscopy (RAIRS),[362,420,424−427] temperature-programmed desorption (TPD),[362,426] near-edge X-ray absorption fine structure (NEXAFS),[428,429] X-ray photoelectron spectroscopy,[428,429] and molecular beams,[362,430] and the experimental work has been complemented with quantum mechanics calculations, mainly using density functional theory (DFT).[422,431] One main conclusion from those studies has been that adsorption of the chiral modifier takes place through the aromatic ring (the naphthyl ring with NEA, a quinoline analog with cinchona alkaloids), and that, at low coverages at least, the ring lies parallel to the surface plane. Representative data supporting this conclusion are provided in Figure 33.

Additional experiments have also been carried out on the coadsorption of chiral modifiers with ketoesters, prototypical reactants, in order to understand the mechanism that drives enantioselectivity in these systems. In contrast with the case of the addition of tartaric acid of Ni surfaces, the cinchona alkaloid modifiers have a molecular structure large enough to, by themselves, provide the chiral local environment required to direct the hydrogenation steps during catalysis. Accordingly, most models start from the assumption that the reactant and modifier form weak 1:1 adducts or complexes on the surface.[432−435] The initial proposal, put forward by Baiker and coworkers, was based on a one-point hydrogen bond between the amine group of the quinuclidine ring of cinchona alkaloids and the oxygen atom of the keto group of the reactant (Figure 34a),[436,437] but that scheme was later refined by McBreen and coworkers to include additional interactions, in a 3-point model (Figure 34b)[438] akin to what has been previously reported for enzymes.[439] Results from recent STM experiments such as those shown in Figure 34c, aided by DFT calculations, have provided direct visualization of how heterogeneous asymmetric induction with single-site resolution is sufficient to distinguish stereochemical conformations.[423,440,441] Notice in particular the different relative positions and orientations of (R)-NEA when interacting with pro-(R) (top-left case in Figure 34c) versus pro-(S) (Figure 34c, bottom-right) methyltrifluoropyruvate, and also the subtle differences in energies involved (-0.52 eV vs −0.59 eV, for a $\Delta E \approx 7$ kJ/mol).[423]

The UHV work discussed in the previous paragraph shows how modern surface-science studies have been able to provide a molecular-level picture of catalytic sites on the surface of heterogeneous catalysts for subtle enantioselective processes. It highlights the need of the addition of discrete molecular modifiers to achieve the level of structural detail in the catalytic site required for demanding enantioselective reactions. Unfortunately, the UHV/surface-science research approach is incomplete, as it does not consider all the elements involved in catalysis. For one, practical catalysts consist of small metal NPs with rough surfaces, not flat and ordered crystallographic planes. There is in fact some evidence that variations in the size of the metal NPs may affect catalytic performance: larger particles, with more basal planes, appear to, in general (but not always),[443] perform better.[374,415,444,445] A recent report has also shown that enantioselectivity is promoted by (111) but not by (100) facets of Pt, and this effect is combined with a second dependence on particle size, presumably because larger NPs contain larger facets where the modifier:reactant complex can be better accommodated (Figure 35).[416]

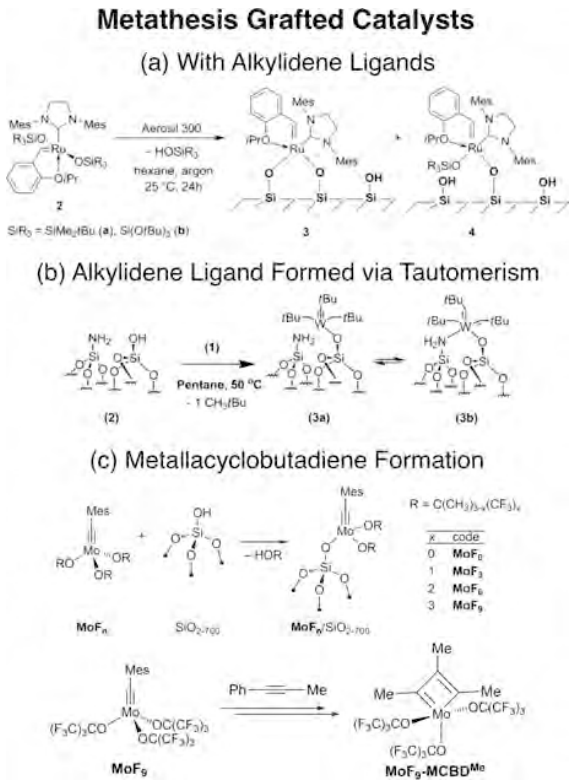

Figure 35. Effect of facet orientation and NP size on the enantioselectivity of the hydrogenation of ethyl pyruvate (EtPy) on a cinchonidine (Cd)-modified Pt/Graphite catalyst.[416] Three sets of catalysts were prepared and annealed at increasing temperatures to alter the fraction of (111) facets exposed, and that fraction was then correlated with catalytic performance. A linear dependence was identified, but the preparation method also affected performance, presumably because it created NPs with different size distributions.

More important is the need to consider the role of the solvent. For one, our *in situ* infrared absorption spectroscopy (IR) studies[446,447] have shown that adsorption of modifiers from solution yields species quite distinct from those seen under vacuum, or even from the free molecules in solution.[448−450] We have also shown that the adsorption geometry of cinchona alkaloids from solution onto Pt surfaces changes with surface coverage, from the flat-lying configuration seen under UHV at low coverages to a more tilted arrangement

https://doi.org/10.1021/acs.chemrev.1c00905
Chem. Rev. XXXX, XXX, XXX−XXX

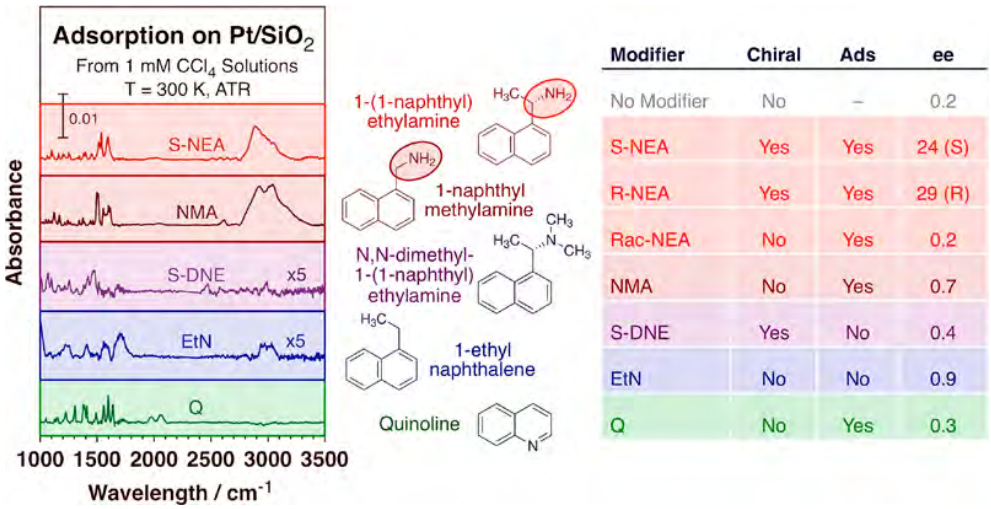

Modifier	Chiral	Ads	ee
No Modifier	No	–	0.2
S-NEA	Yes	Yes	24 (S)
R-NEA	Yes	Yes	29 (R)
Rac-NEA	No	Yes	0.2
NMA	No	Yes	0.7
S-DNE	Yes	No	0.4
EtN	No	No	0.9
Q	No	Yes	0.3

Figure 36. Left: Attenuated total reflection (ATR) IR spectra for, from top to bottom, S-NEA, 1-NMA, S-DNE, 1-ethylnaphthalene (EtN), and quinoline (Q) adsorbed from 1 mM CCl_4 solutions onto the surface of a supported Pt/SiO_2 catalyst.[450] Right: Corresponding ee for the catalytic hydrogenation of ethyl pyruvate.[454] Adapted with permission from ref 450. Copyright 2017 Elsevier B.V.

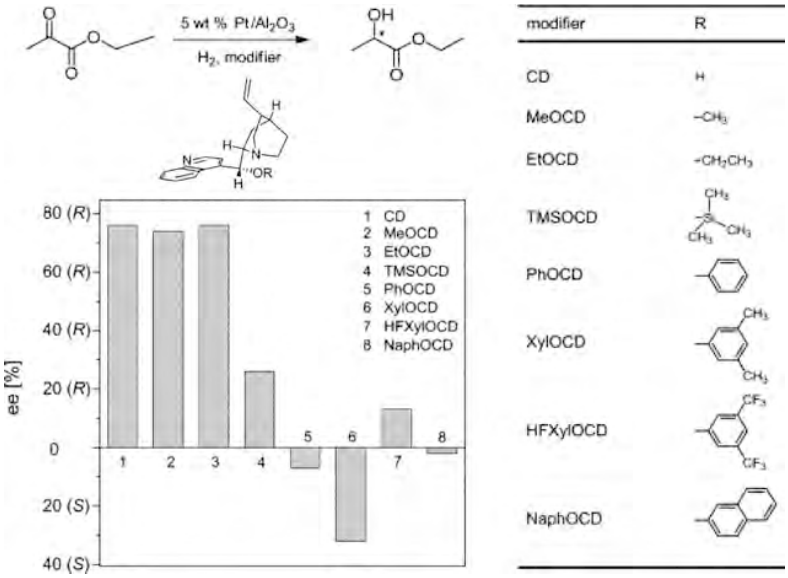

Figure 37. Inversion of enantioselectivity versus the bulkiness of the ether function (R) of the cinchona modifier used in the hydrogenation of ethyl pyruvate promoted by a Pt/Al_2O_3 catalyst.[476] What is reported here is that preference for the enantiomeric identity of the ethyl lactate product flips from predominantly (R) to net (S) with increasing size of the R substitution. Reproduced with permission from ref 476. Copyright 2004 Elsevier Inc.

as the surface becomes more crowded.[450,451] This change in geometry was found to correlate with enantioselectivity in catalysis. Indeed, our initial work on this suggested that it is the flat adsorption geometry the one that provides the chiral environment for enantioselective hydrogenation, and that, counterintuitively, adding more modifier to the reaction mixture leads to the tilting of the aromatic ring of the modifier and with that to a deterioration of, not an improvement in, enantioselectivity.[19,451] However, our proposed adsorption geometry of the active modifier has been recently challenged;[421,452] this issue is still not fully resolved. Curiously, with NEA at least, we have also shown that adsorption may be controlled by the amine nitrogen atom, not the aromatic ring as implied by the surface-science studies carried out under UHV. Indeed, a correlation between the availability of that N atom for bonding and both adsorption and catalytic performance was identified (Figure 36): adsorption seems to require a primary amine group, only available in NEA and 1-naphthylmethylamine (NMA) (among the modifiers probed), and no enantioselectivity can be obtained without modifier adsorption even if the modifier is chiral (like in the case of (S)-N,N-dimethyl-1-(1-naphthyl)ethylamine (S-DNE).[450,453,454]

Several other considerations concerning these chiral-modified catalytic processes have not been fully addressed to date. It has been recognized, for instance, that the cinchona alkaloids have many internal-rotation degrees of freedom,[362,408,431,455−458] but it is not yet clear how those become reduced upon adsorption and complexation with the reactant (if at all).[459,460] In fact, it is not even known if the modifier:reactant adduct mentioned before forms directly on

https://doi.org/10.1021/acs.chemrev.1c00905
Chem. Rev. XXXX, XXX, XXX−XXX

the surface or previously in solution. Certainly, the nature of the solvent is critical,[461] affecting not only enantioselectivity but also total activity; it would seem that better solvents for the modifier facilitate reversible adsorption,[462] and with that improve catalytic performance.[3,406,463−467] The competitive adsorption of different modifiers defines the nature of the surface modification as well,[468−470] and can even lead to enantioselectivity inversion from the preferential production of one enantiomer to the other;[397,399,471−475] an early example of this type of inversion, due to changes in the bulkiness of the ether function of the modifier, is illustrated in Figure 37.[476] The silanol groups of silica supports may also interact with the chiral modifier, and in some cases improve enantioselectivity.[477] The presence of gases in the solvent is another factor to take into consideration,[478] in particular because hydrogen preconditioning of the surface appears to be necessary for catalyst activation in many circumstances; such pretreatments may even affect the adsorption geometry.[479,480] Finally, protonation of the modifier may also affect catalytic performance.[481−483] None of these factors are easy to emulate with model systems under vacuum conditions.

There are a few other examples of the use of adsorbed molecular modifiers to control enantioselectivity in heterogeneous catalysis.[484] For instance, a catalyst consisting of Ru NPs supported on CNTs could be made enantioselective for the asymmetric hydrogenation of acetophenone by adding (1S,2S)-1,2-diphenyl-1,2-ethanediamine to the reaction mixture as a chiral modifier.[485] In another example, the synthesis of iodomethyl dihydrobenzofuran promoted by a Pd/SiO_2 catalyst was made enantioselective via the addition of a chiral sulfinamide phosphine modifier.[486] Ir NPs can also be made enantioselective for the hydrogenation of ketones via the addition of a chiral secondary phosphine oxide.[487] Another example is that of the use of chiral N-heterocyclic carbenes to modify Pd/Fe_3O_4 catalysts during the promotion of asymmetric α-arylations.[488] Molecular modification can also be applied to non-metallic catalysts. With MgO catalysts, for instance, the promotion of a tandem conversion involving the Claisen-Schmidt condensation of benzaldehydes with acetophenones to yield chalcones on Lewis-base O^{2-} sites followed by an asymmetric epoxidation on Brønsted hydroxyls could be made enantioselective by adding a diethyl tartrate salt to the solution, which forms strong hydrogen bonds with the −OH surface groups on MgO and directs the delivery of nucleophilic oxygen in a surface peroxide species (also added from solution, as the oxidant) stereoselectively to produce the chiral epoxy ketones (Figure 38);[489] similar MgO-promoted asymmetric Henry and Michael reactions aided by (S)-(−)-1,1′-bi(2-naphthol) are possible as well.[490] In a somewhat different approach to molecular surface modification (not related to enantioselectivity), it has been reported that the acidity and redox properties of SiO_2-supported $H_{3+n}PV_nMo_{12-n}O_{40}$ (n = 0−4) Keggin clusters, used for the promotion of the selective one-step low-temperature oxidation of methanol to dimethoxymethane, can be titrated dynamically during catalysis via the addition of either 2,6-di-*tert*-butylpyridine or pyridine to the reaction mixture, thus preventing the undesirable methanol dehydration side reaction.[491] The reversibility of the adsorption of the modifier in most of the cases mentioned above were not tested or discussed, though. In general terms, it is safe to say that the number of examples in this area is quite small; the use of reversibly-adsorbed molecular modifiers in heterogeneous catalysis has yet to be exploited to its fullest.

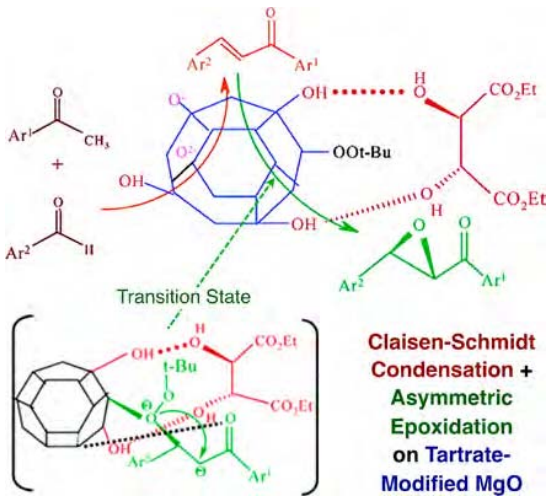

Figure 38. Proposed mechanism for the tandem Claisen-Schmidt condensation of benzaldehydes with acetophenones followed by an asymmetric epoxidation using MgO NPs as catalyst, *tert*-butyl hydroperoxide as oxidant, and diethyl tartrate as chiral modifier to drive the enantioselectivity of the epoxidation step.[489] Reproduced with permission from ref 489. Copyright 2004 American Chemical Society.

3.2. Molecular Mediators in Electrocatalysis and Photocatalysis

The addition of reversibly adsorbed discrete modifiers may also be required to attain the desired performance in electro-, photo-, and photoelectro-catalysis. It is indeed common in electrocatalysis to use molecular agents in solution to shuttle electrons via reversible redox chemistry, and in photocatalysis (and photoelectrocatalysis) to use photosensitizers capable of adsorbing light and converting that excitation into activated electrons. It should be noted that in many of the examples in this section the main catalyst is in fact molecular; the surface of electrodes in electrocatalysts often acts as a collector or donor of electrons, to close the redox cycle. Nevertheless, we include these systems in our discussion because without a heterogeneous interface the catalytic process would not possible.

Electrochemistry affords direct access to radical species useful in synthetic organic chemistry for the selective addition of organic functionality to produce commodity chemicals and complex natural products.[492,493] There are three broad modalities of how electrocatalysis can be implemented (Figure 39).[494] The catalytic reaction can take place directly at the surface of the electrode, which may be inactive (and only promote electron transfer) or activated (Figure 39, top two modalities). In these cases, the electrode provides little flexibility in terms of selectivity, as it tends to impose high kinetic barriers and to oxidize or reduce species from solution indiscriminately, with the only control typically being the applied potential. Moreover, the high-energy species (radicals, cations and anions) resulting from reactions at electrodes tend to accumulate in the double layer that forms above the surface during electrochemical processes, sometimes decomposing and depositing unwanted impurities leading to electrode deactivation.[495] Only a small family of useful conversions has proven feasible using this approach, processes such as dimerizations and other couplings,[496−501] including intramolecular cyclizations.[502−505] Reaction specificity can also be added to electrocatalysis by using redox-active species as mediators

https://doi.org/10.1021/acs.chemrev.1c00905
Chem. Rev. XXXX, XXX, XXX−XXX

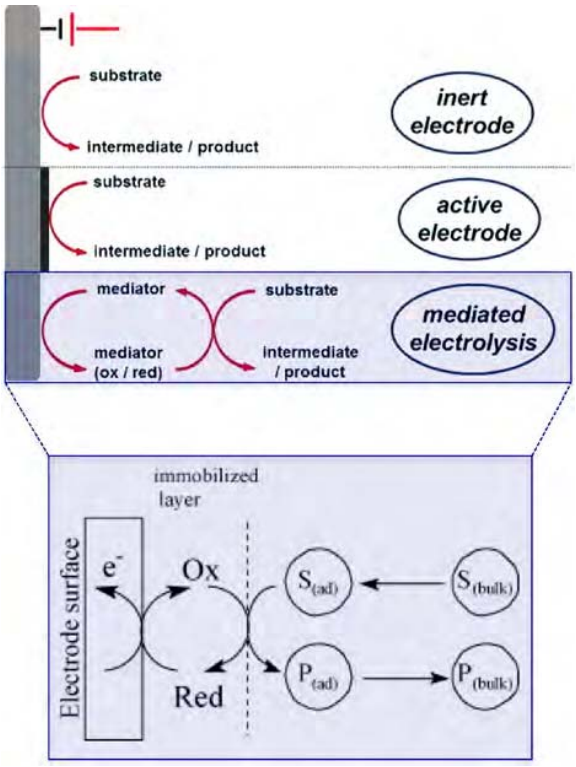

Figure 39. Operational types of electrocatalysis. Only the third type, mediated electrolysis (shown in detail at the bottom), where a molecular mediator (electrocatalyst) participates, is discussed in detail in this review. Adapted with permission from refs 507 and 494. Copyright 2007 Elsevier B.V. and 2018 The Authors.

(the third modality; Figure 39, bottom),[494] an approach that usually affords the use of milder potentials too.[506] These mediators are in fact often the actual catalysts, either by selectively targeting a specific functional group in a complex substrate to aid in the electrochemical redox step, or by offering control over the selectivity of downstream reactions involving electrochemically generated reactive intermediates. Redox-active molecular catalysts that interact directly with electrodes and mediate electron transfer between the electrode and the substrate are known as electrocatalysts.[506]

Electrocatalysts in organic syntheses have mainly been used as electron transfer agents or hydrogen-atom-abstraction catalysts, to promote reactions such as alkene functionalization[508,509] and alcohol oxidation (for fuel cell applications, for instance),[510,511] and more recently carbon dioxide conversion.[512,513] In the past these mediators have often been small ions, radicals or molecules such as halogen, sulfonium or ammonium ions, nitroxyl radicals, amines, imidazoles, fluorenes, benzoquinones, or ferrocenes,[505,508,514−523] but there are also examples involving more complex molecules such as organometallics, as discussed in more detail below.[507,524,525] These mediators are commonly used in simple reactions such as water splitting/oxidation,[526,527] but those processes are beyond the scope of our review. Instead, here we focus on more involved organic conversions, where selectivity may become a key consideration. Early examples of the use of electrocatalysis in organic synthesis include epoxidations of olefins, which can be promoted by using metal (Ru,[528,529] Fe,[530−532] Mn,[533−535] Cr[536−538]) oxo compounds, including metaloporphyrins.[539] Such metal-oxo species are often electrogenerated *in situ* from metal-aquo complexes, and reduced back at the electrode surface after reaction with the olefin. Another partial oxidation reaction sometimes assisted by electrocatalysts is the conversion of alcohols to aldehydes or ketones, for which metal complexes with Ru,[528,540,541] Rh,[542] Ir,[543] and Ni[544,545] have been used. It appears that in many cases selective oxidation is achievable thanks to the formation of specific peroxide and superoxide intermediates at the metal center, in oxygen reduction reaction (ORR) steps analogous to those seen in enzymatic catalysis (Figure 40);[546−549] the electrogenerated superoxide species can function as a base, a nucleophile, an oxidant, a reductant, an electron transfer shuttle, or a free radicals.[547]

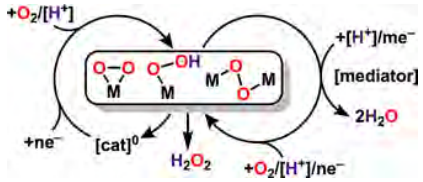

Figure 40. Peroxides and superoxides as intermediates coordinated to metal complexes to promote the ORR in electrocatalysis.[548] Reproduced with permission from ref 548. Copyright 2020 American Chemical Society.

Metal complexes have been shown to be particularly useful electrocatalysts for the promotion of organic synthesis reactions.[525,550−554] Many of the complexes used for this, typically based on transition metals, are good catalysts in their own right. Nevertheless, a combination of organometallic chemistry and electrochemistry is required when redox steps are involved and the organic substrates are not electroactive or cannot be converted selectively via direct electron transfer activation. Because selectivity is typically provided by the molecular catalyst, electrocatalysis in these systems often involves two sequential steps, chemical activation of organic substrates by the transition metal followed by electron transfer between the electrode and that activated complex (Figure 41a). Alternatively, the role of the electrodes may be to provide (or extract) electrons to recycle the active catalyst after its oxidation (reduction) during the catalytic step (Figure 41b). In these two mechanisms, the main interaction of the reactant is with the organometallic complex, and catalytic activity and, more importantly, catalytic selectivity are primarily defined by the structural details of such complex; these are cases of electrode assisted homogeneous catalysis. Yet a third mechanism for electrocatalysis promoted with organometallic mediators is one where the latter acts as a shuttle to help transfer electrons from (to) the electrode to (from) the reactant (Figure 41c). Because in this process no new organometallic species are formed (since the electron transfer only involves outer-sphere orbitals), no additional structural features that can help with selectivity are provided by the mediator; no further discussion of this modality will be provided in this review.

Metal-complex-assisted electrocatalysis can promote both oxidation and reduction reactions, and may involve one- or two-electron activations. Ni complexes, including Ni-salen, are popular: examples of electrocatalytic processes promoted by those include electroreductive carboxylations,[555−557] electroreductive couplings,[558,559] and reductive cyclizations.[560] In

https://doi.org/10.1021/acs.chemrev.1c00905
Chem. Rev. XXXX, XXX, XXX−XXX

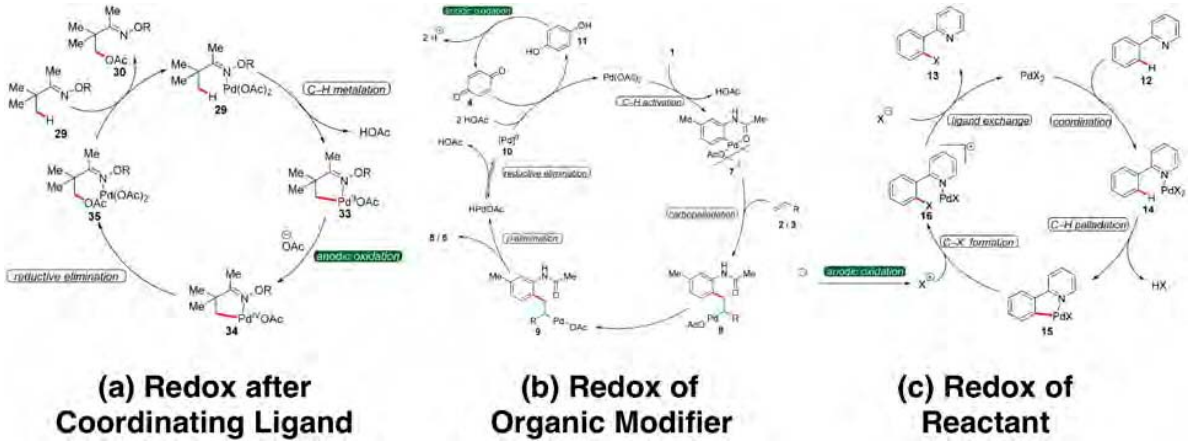

Figure 41. Types of organometallic mediated electrocatalysis in organic synthesis.[553] Reproduced with permission from ref 553. Copyright 2018 American Chemical Society.

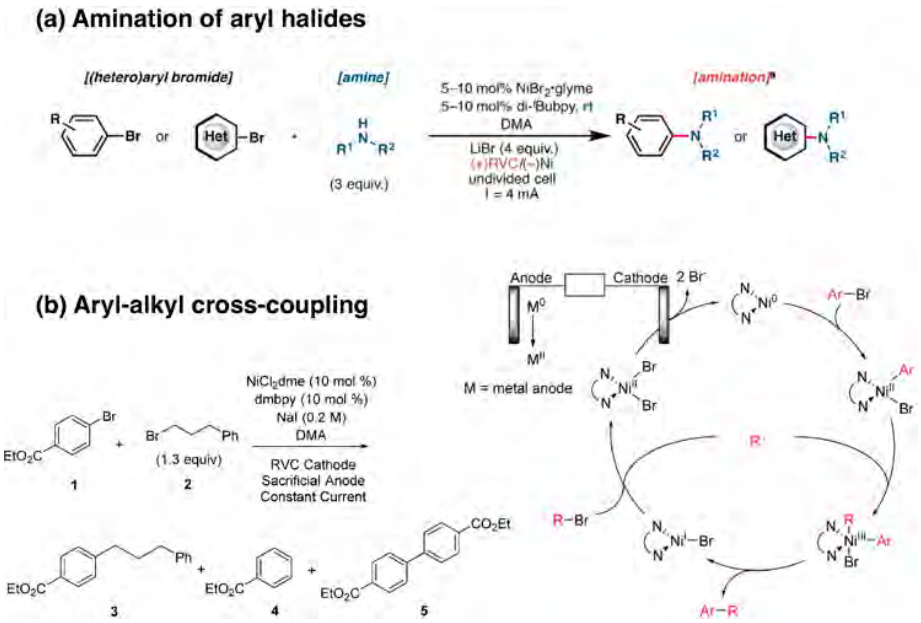

Figure 42. Organic synthesis promoted by Ni-bpy electrocatalysts. (a) Amination of aryl halides;[561] (b) aryl-alkyl cross-coupling, with proposed mechanism.[562] Adapted with permission from refs 561 and 562. Copyright 2017 Wiley-VCH Verlag GmbH & Co and 2017 American Chemical Society, respectively.

Figure 42 two recent examples are provided where Ni-bpy complexes were used to help with the amination of aryl halides (Figure 42a)[561] and with aryl-alkyl cross-couplings (Figure 42b).[562] Other organometallic electrocatalysts include Mn(II) salts, used for the oxidative vicinal difunctionalization (diazidation, dichlorination, halotrifluoromethylation) of alkenes,[508] Pd acetate, employed for C−H activation,[563,564] Co acetate, to promote a [4+2] annulation of sulfonamides with alkynes,[565] and Co chloride, for the oxychlorination of alkenes.[566] The development of organometallic electrocatalysts for the electrocatalytic promotion of specific organic synthesis reactions selectively is still in its infancy, but much progress has been seen in recent years and more is expected in the near future.

In many of the examples cited above, either selectivity is not a critical issue or it is not dependent on the nature of the mediator. However, in highly demanding reactions where regio-, stereo-, or enantio-selectivity is required, directing such selectivity is most viable via the tuning of the molecular structure of the mediator. The use of chiral electrocatalysts to produce enantiopure products has gained particular attention in recent years. One approach derives directly from the surface modification methodology discussed in the previous section, where a reversibly adsorbing chiral modifier is added to the solution to promote the formation of a weak adduct with the reactant that, when bound to the surface, forces a particular stereochemistry thanks to the resulting chiral environment.[509,567,568] In an early example of this, the electrochemical reduction of 4-methylcoumarin and 5-methoxy-4-methylcoumarin in the presence of optically active amines was shown to afford optically active dihydrocoumarins.[569] The synthesis of 2-hydroxy-2-phenylpropionic acid (atrolactic acid) from acetophenone via CO_2 electrocatalytic fixation could be made enantioselective, to produce either the (R) or the (S)

https://doi.org/10.1021/acs.chemrev.1c00905
Chem. Rev. XXXX, XXX, XXX−XXX

enantiomer, by adding cinchonidine or cinchonine to the solution, respectively.[570] In a study on the alkaloid-induced electrocarboxylation of 4-methylpropiophenone, enantiodiscrimination was shown to depend on the nucleophilic quinuclidine nitrogen atom and the OH group of the modifiers.[571] A cinchonidine-aided electroreduction of acetophenone was shown to yield two main products, the optically active (that is, chiral) alcohol, and the dimer product pinacol, which showed no optical rotation (Figure 43).[572] Quite

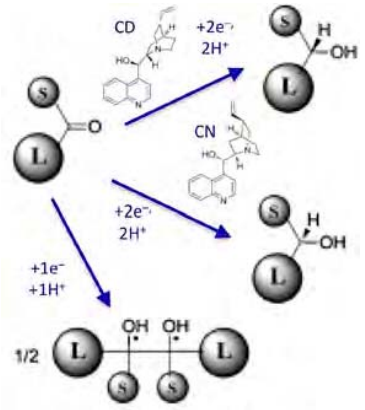

Figure 43. Example of an electrocatalytic hydrogenation made enantioselective via the addition of cinchona alkaloid modifiers, with acetophenone as the reactant.[572] Adapted with permission from ref 572. Copyright 2013 Elsevier Ltd.

recently, the addition of cinchonidine to the reaction mixture was shown to bestow enantioselectivity to a Ag−Cu bimetallic cathode in the asymmetric electroreduction of ethyl benzoylformate.[573] These are all interesting examples of the use of chiral modifiers to direct enantioselectivity in surface reactions, but, as in the case of chiral modifications of thermal hydrogenation catalysts discussed before, the scope has proven to be quite limited so far. Notice too that the modifiers and reactants (cinchona alkaloids and α-ketoesters and related carbonyl containing compounds) are often the same or similar to those used in the analogous thermal chemistry. Presumably, the electrode in these cases is added mainly to provide an alternative way to generate the surface atomic hydrogen required for the hydrogenation reaction, as substitute for the activation of molecular hydrogen required in thermal catalysis. It is promising to see that the idea of chiral modification can be extended to electrocatalytic systems, but more work is still needed to make it general.

Other examples of stereo- and enantioselectivity in electrocatalysis follow the mechanisms already discussed above in connection with non-chiral processes.[574,575] In particular, electrochemical activation may involve the formation of a complex between the reactant and a chiral catalyst in solution. Examples here include that of the α-alkylation of aldehydes electrocatalytically promoted with chiral tertiary amines to produce enantiopure α-alkylated aldehydes,[576] the more recent case of the asymmetric Lewis-acid catalyzed electrochemical alkylation mediated by a nickel chiral complex,[577] and the electrocatalytically-driven oxidative cross-coupling of 2-acyl imidazoles with silyl enol ethers aided by a chiral Lewis acid Rh-based catalysis to produce non-racemic 1,4-dicarbonyls.[578] The diagram in Figure 44 is for a process where anodic oxidation and aldehyde organocatalytic α-arylation steps were

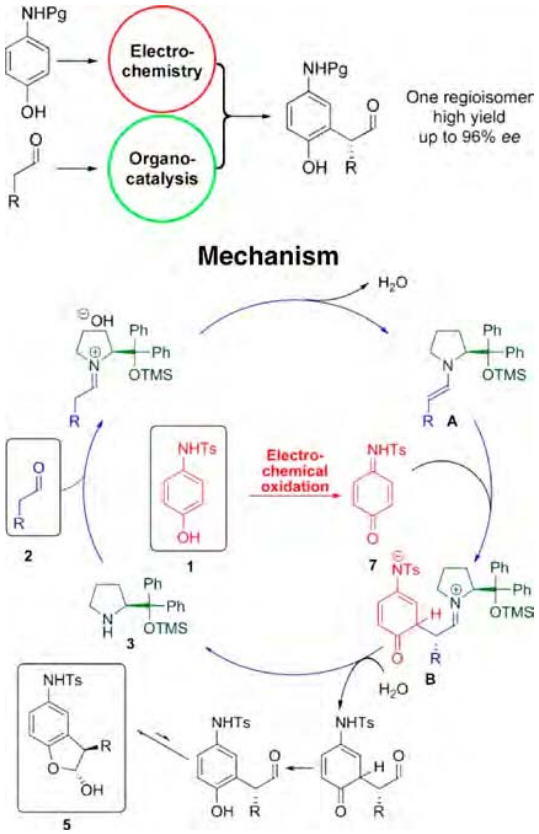

Figure 44. Proposed mechanism for the electrochemical/organocatalytic sequence shown on the top. TMS = trimethylsilyl, Ts = 4-toluenesulfonyl. Reproduced with permission from ref 579. Copyright 2010 Wiley-VCH Verlag GmbH & Co. KGaA, Weinheim.

combined to access an enantiopure dihydrobenzofuran.[579] Some enantioselective electrocarboxylations have been reported as well.[580] In all these examples, complexation between the electrocatalyst and the reactant occurs first, in solution, after which the new complex (or one of the compounds involved) approaches the surface of the electrode to undergo the required electron transfer, or reacts with a second reactant pre-reduced or pre-oxidized at the electrode surface. These processes can be seen as similar to the reversible surface modification discussed before, except that here the chiral modifier may participate directly in the redox steps; with the cinchona alkaloid, the role of the electrode is to provide atomic hydrogen, a step independent of the adsorption and conversion of the reactant. Nevertheless, in both cases the key reactions still proceed on the surface of the electrode, and require the modification of the local environment by the modifier to achieve stereo- or enantio-selectivity.

More indirect mechanisms are viable as well. For instance, a cascade process may be designed in which redox steps can be coupled with subsequent catalytic steps involving chiral mediators, as in the reported enantioselective Ni-catalyzed electrochemical synthesis of biaryl atropisomers (Figure 45a),[581] or the catalytic asymmetric electrochemical oxidative coupling of tertiary amines with simple ketones.[582] Alternatively, a mediator may reduce or oxidize the reactant and be regenerated afterwards at the surface of the electrode. An early example here is the asymmetric epoxidation of olefins using an optically active Mn-salen complex reported by Tanaka and co-

https://doi.org/10.1021/acs.chemrev.1c00905
Chem. Rev. XXXX, XXX, XXX−XXX

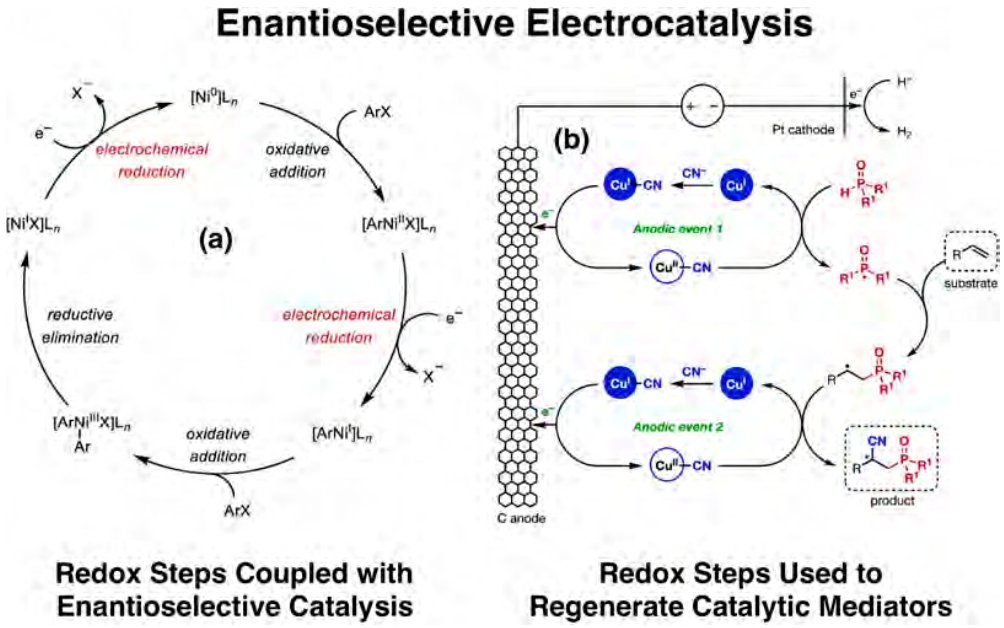

Figure 45. Examples of proposed catalytic cycles for enantioselective electro-promoted reactions where the redox steps are decoupled from the chiral chemistry. Left (a): Enantioselective Ni-catalyzed electrochemical synthesis of biaryl atropisomers, where the electrode is used to reduce the catalyst to facilitate subsequent oxidative addition and reductive elimination steps.[581] Right: Enantioselective Cu-catalyzed electrocatalytic cyanofunctionalization of vinylarenes.[584] In this case, the anode helps with the side Cu-CN complex oxidation step. Reproduced with permission from refs 581 and 584. Copyright 2020 and 2019 American Chemical Society, respectively.

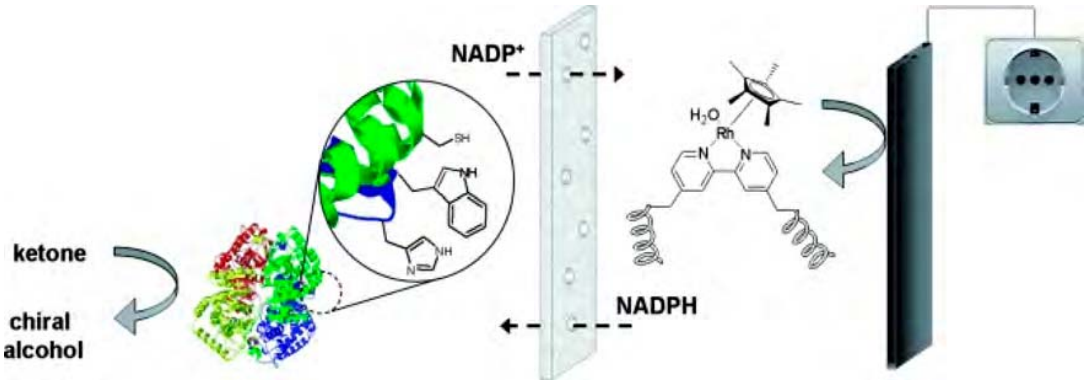

Figure 46. Example of enantioselective enzyme-based electrocatalysis, in this case for the chiral hydrogenation of ketones to alcohols promoted by NAD-phosphate ($NADP^+$).[587] A Rh-bpy-derivatized soluble membrane was added to physically separate the redox and catalytic steps. Reproduced with permission from ref 587. Copyright 2009 Wiley-VCH Verlag 4998 GmbH&Co. KGaA, Weinheim.

workers.[583] Another more recent case is that of the enantioselective electrocatalytic cyanofunctionalization of vinylarenes reported by Fu et. al. (Figure 45b).[584] Because in these schemes the catalytic selectivity is attained in the liquid phase, away from the surface, they are less relevant to the focus of this review.

Even more subtle selectivity can be achieved in electrocatalytic system by using enzymes. However, although this has been an area of great interest for a number of years, the number of useful enzyme-aided electrocatalytic systems developed to date is still small. Enzymes are delicate, and the environment and conditions where they can operate may be incompatible with those required for the chemical reaction of interest. Nevertheless, electron transfer in electrochemistry can provide a viable mechanism for regenerating enzymes after reduction or oxidation steps.[575,585] This is, for instance, what happens during the electrocatalytic promotion of the hydrogenation of cyclohexanone with thermophilic nicotinamide adenine dinucleotide (NAD)-dependent alcohol dehydrogenase (TADH).[586] In another case, an approach based on the spatial separation of the enzymatic and redox chemistry using a bpy-derivatized water-soluble polymeric mediator was developed to minimize the rapid enzyme inactivation typical in electroenzymatic synthesis of chiral alcohols: in that case, a Rh complex formed at the polymer acted as a redox mediator (Figure 46).[587] Like in non-enzymatic cases, electrocatalytic systems can also be conceived where a reactant is oxidized or reduced at the surface of an electrode to produce an active intermediate that then reacts further at an enzymatic site in solution; chloroperoxidase can be used, for instance, to enantioselectively catalyze an asymmetric sulfoxidation via the prior reduction of atomic oxygen to a peroxide

https://doi.org/10.1021/acs.chemrev.1c00905
Chem. Rev. XXXX, XXX, XXX−XXX

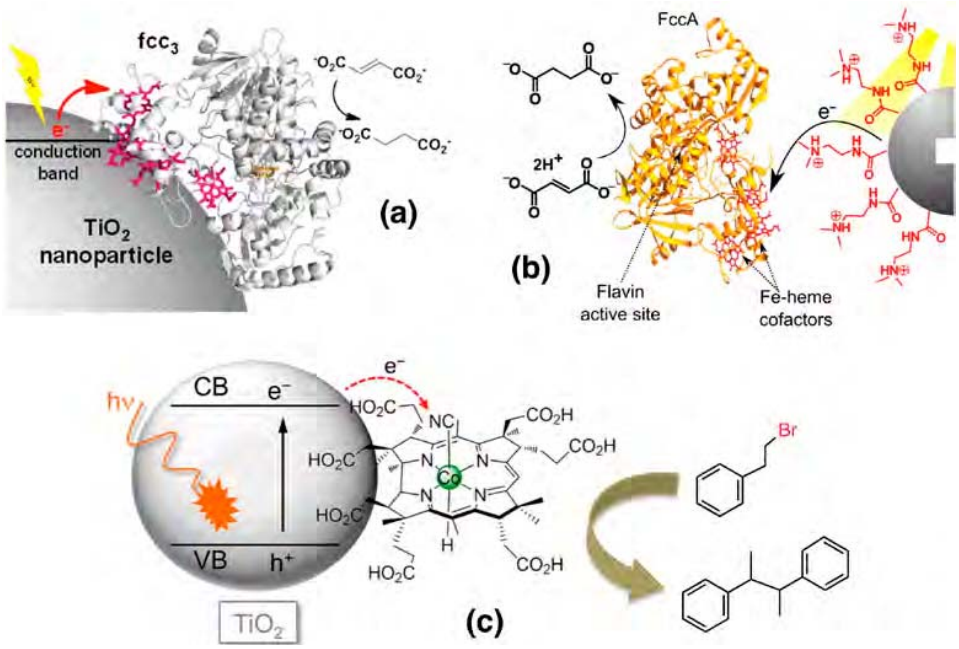

Figure 47. Examples of photocatalytically promoted conversions using discrete molecular mediators. (a) Hydrogenation of fumarate to succinate promoted by flavocytochrome c3 adsorbed on a TiO_2 NP.[606] (b) Hydrogenation of fumarate to succinate promoted by fumarate reductase adsorbed on carbon dots.[607] (c) Debromination of phenethyl bromide and coupling to 2,3-diphenylbutane promoted by B12(cobalamin)-dependent enzyme adsorbed on TiO_2.[608] Adapted with permission from refs 606, 607, and 610. Copyright 2014, 2016, and 2019 American Chemical Society, respectively.

intermediate.[588] Again, in these examples selectivity is provided by the enzyme in solution, not the surface, and in that sense could be viewed as cases of selectivity in homogeneous, not heterogeneous, catalysis. Virtually no examples exist for the direct catalytic reduction or oxidation of the reactant on the surface of an electrode while attached to an enzyme, where the latter provides the environment required for selective conversion as in the non-enzymatic examples discussed above. On the other hand, in a few cases enzymes have been immobilized on the surface of electrodes, forcing all steps of the electrocatalyst to occur on the solid surface.[589−591] These are specific cases of the immobilized catalysis that are discussed in more detail elsewhere in this Review (Section 2.4).

Photocatalysts can also be combined with molecular modifiers, in this case called photosensitizers, to help define surface sites and help with selectivity in catalytic conversions. There are several similarities between electrocatalysis and photocatalysis.[506] For one, like in indirect electrocatalysis, where catalytic processes may be initiated via reduction or oxidation of the mediator rather than the substrate, indirect photoredox processes typically begin by exciting the photosensitizer rather than the reactant; the excited state of the sensitizer can then serve as the catalyst for the oxidation or reduction of the reactant via a photoelectron transfer process. In fact, some electrocatalysts are also good photosensitizers, a good example of this being 2,3-dichloro-5,6-dicyano-1,4-benzoquinone (DDQ).[592,593] On the other hand, some photocatalytic systems have been constructed where the photosensitizer is not molecular but rather a semiconductor NP, and the catalytic site the discrete molecular modifier.[594,595] Much effort has been dedicated to the use of photosensitized heterogeneous catalysts for simple reactions such as hydrogen production[594] and CO_2 reduction,[596−598] yet, the examples where photosensitizer-modified photocatalysis has been used to direct selectivity in complex reactions are rare. In terms of molecular photosensitizers, porphyrins or other organometallic compounds have also been used, in combination with solid (carbon, Pt) surfaces, mainly for the promotion of the same simple reactions mentioned above, namely, water reduction[599] and the conversion of CO_2 to acetylene:[600−604] in these, the porphyrin transfers electrons to the surface after photoexcitation to promote the catalytic reaction. It should be noted that, although the conversion of CO_2 to hydrocarbons is difficult to promote in general, no particular demands are imposed on the catalytic site in terms of shape or structural details, and the porphyrin does not contribute to defining such site. Perhaps more interesting from the point of view of selectivity are combinations of photoactive (sometimes dye-sensitized) NPs with discrete catalysts, usually enzymes but also porphyrins and other organometallics, which have been tested for the reduction of alkenes (Figure 47a,b),[605−607] and for reductive dehalogenation reactions (Figure 47c).[608,609] In those examples, the roles are reversed: it is the NPs that is photoactive, and the discrete modifier the one responsible for the selective catalytic conversion. Since enzymes are often immobilized (or just deposited/adsorbed) on the surface of the NPs, these can be seen as true heterogeneous catalysts. To date, though, the number of examples of this type of enzyme-assisted photocatalysis is low.

In principle, it is possible to combine electro- and photoexcitations to fine-tune the type of reactions discussed above.[611] Photovoltaic cells have indeed been used to conduct electrochemical oxidations[524,612] and other reactions requiring the generation of reactants with high reduction potentials such as aryl radicals.[613] However, the examples of this to date are sparse, and mostly rely on indirect mechanisms that, as we

https://doi.org/10.1021/acs.chemrev.1c00905
Chem. Rev. XXXX, XXX, XXX−XXX

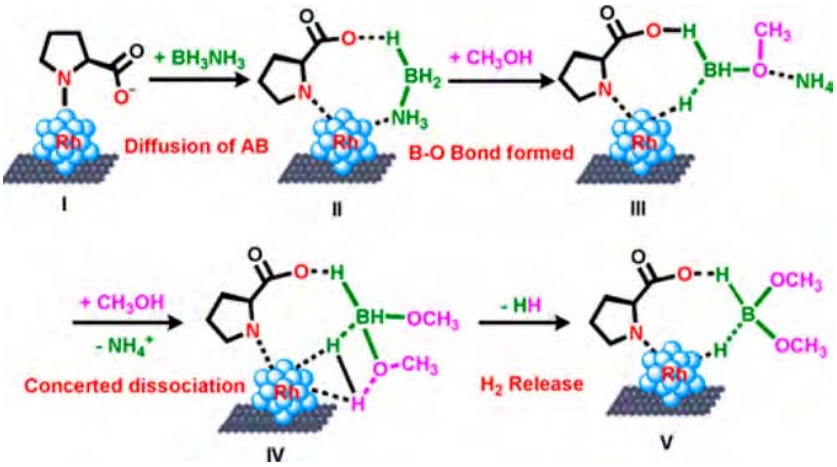

Figure 48. Example of the use of amino acids to modify the surface and improve the activity and selectivity of heterogeneous catalysts. Shown is the proposed mechanism for the methanolysis of ammonia borane catalyzed by Rh catalysts modified with L-proline.[636] Reproduced with permission from ref 636. Copyright 2019 Wiley-VCH Verlag GmbH & Co.

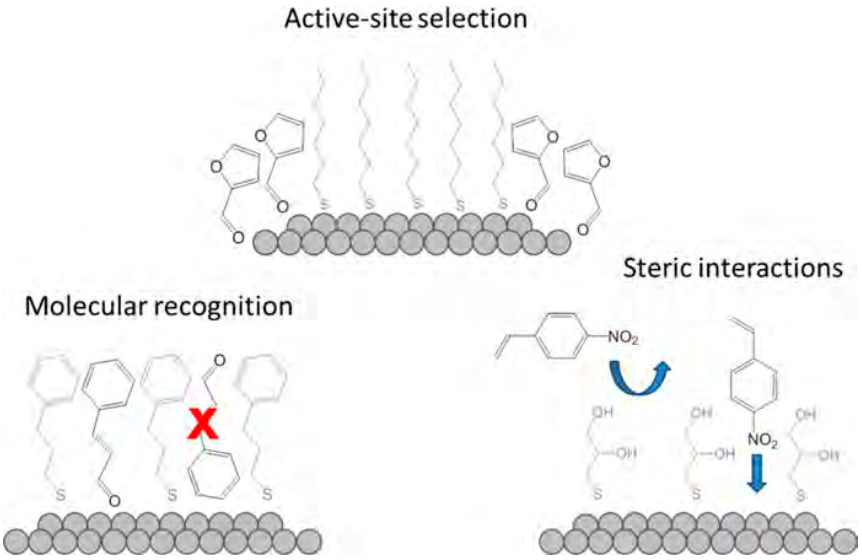

Figure 49. Proposed mechanisms for the way SAMs participate as modifiers of catalytic sites for the improvement of selectivity.[643] Reproduced with permission from ref 643. Copyright 2014 American Chemical Society.

have discussed above, do not require special surface sites as the catalysis takes place in the liquid phase. The idea of designing photoelectrocatalytic processes for selective organic synthesis is enticing, but lies in the future.

3.3. Self-Assembly Monolayers and Other Non-Covalent Adsorbates

In the systems discussed in this section so far, a molecular modifier is added to the reaction mixture, in solution, to aid with the definition of the structure of the catalytic site. This is accomplished on solid surfaces via the adsorption of those modifiers, either prior to the uptake of the reactant and the start of the catalytic reaction, or after forming a complex or adduct with the reactant in solution. In many instances, this adsorption is reversible. The addition of molecular modifiers via reversible adsorption provides several advantages, among them the ability of the catalyst to continuously regenerate itself. However, because the "co-catalyst" is added to the solution, this approach defeats the purpose of transitioning to heterogeneous catalysts in that the added modifier needs to be separated from the reaction mixture and the product purified as in homogeneous catalytic processes.

The irreversible adsorption of molecular modifiers circumvents this shortcoming. In some instances, this is already what happens with the modifiers described above. For instance, in the chiral modification of nickel catalyst with tartaric acid for the promotion of β-ketoester hydrogenations, there is some evidence that indicates that deprotonation occurs upon adsorption, and that the actual chiral modifier is a tartrate anion;[614−621] such species is likely to be bound irreversible to the surface. Surface modification with amino acids, which may form irreversibly-adsorbed zwitterions on metal surfaces,[369,622−627] has also been considered,[628−632] although the success of this approach in catalysis is still under investigation; only a handful of examples of the use of such modifiers are available in the literature to date (Figure 48).[633−636] In fact, even in the case of cinchona alkaloid modification, where the adsorption is believed to be reversible in solution, irreversible

https://doi.org/10.1021/acs.chemrev.1c00905
Chem. Rev. XXXX, XXX, XXX−XXX

adsorption has been tested in gas phase, with limited success.[637,638] Finally, because of their high molecular weight and because they display multiple organic functionalities, some of the enzymes used as modifiers in the electrocatalysts discussed in the previous sub-section are also likely to adsorb irreversibly on surfaces. In this section we explore the possibility of functionalizing the surfaces of heterogeneous catalysts with modifiers that bind irreversibly but via non-covalent bonds.

One non-covalent way to modify the surface of heterogeneous catalysts is via the addition of self-assembled monolayers (SAMs). This is an approach that has been greatly advanced by the Medlin group.[639−648] In their first report on this topic, they indicated that selectivity during the hydrogenation of unsaturated epoxides with Pd catalysts can be enhanced by adding *n*-alkanethiol SAMs to the surface.[639] The role of the SAM in this case was determined to be primarily indirect, via the destabilization of adsorbates to favor bond-making reactions over bond-breaking steps. SAMs can also be used to selectively block surface sites, the terraces on metal NPs in the case of the hydrogenation of furfural (Figure 49, top).[649] A third mechanism for the intervention of SAMs in catalysis is as a steric agent to block access to the surface of bulky reactants or products (Figure 49, bottom-right): in one case, SAMs facilitated the hydrogenation of polyunsaturated to mono-unsaturated fatty acids but inhibited further hydrogenation to the fully, "kink"-shaped, saturated species.[650] Finally, a more proactive SAM role was seen in the selective hydrogenation of cinnamaldehyde on Pt catalysts, which was shown to be aided by the addition of phenylated SAMs thanks to aromatic stacking interactions between the phenyl rings of the reactant and the SAM (Figure 49; bottom-left).[641]

Other groups have provided additional examples of the use of SAMs to modify the surfaces of metal-based heterogeneous catalysts.[651] For instance, several publications have reported the use of SAMs to improve selectivity in Au- or Pd-catalyzed half-hydrogenation conversions of alkynes to alkenes.[652−655] SAMs have also been used to modify the catalytic conversion of alcohols,[656−658] like in the case of the Pd-promoted isomerization of allyl alcohols to carbonyl analogues, where performance was optimized by tuning both NP size and SAM surface coverage.[659] One particularly interesting example is that of the thiolate-mediated selective oxidation of benzyl alcohol promoted by carbon-supported Au clusters, because in that case not only selectivity but also absolute activity for the production of the desirable benzaldehyde product was reported to increase (Figure 50).[660] Lastly, like in the examples discussed above with reversibly-adsorbed modifiers, SAMs can be used to control enantioselectivity.[661] For instance, the deposition of homochiral cysteine SAMs on Au(111) has been used to direct enantioselectivity during the electrocatalytic redox conversion of catechin and epicatechin.[662] In a study from our own laboratory, cinchonidine-terminated thiol-based SAMs were added to both colloidal Pt NPs and Pt NPs dispersed on a solid oxide support to direct the enantioselectivity of the hydrogenation of ethyl pyruvate.[418] Significant improvements in both activity and selectivity were seen with the colloidal NPs upon chiral SAM modification because of a kinetic effect associated with increases in cinchonidine residence time on the surface, whereas more nuanced compromises between activity and selectivity were identified when using supported catalysts.

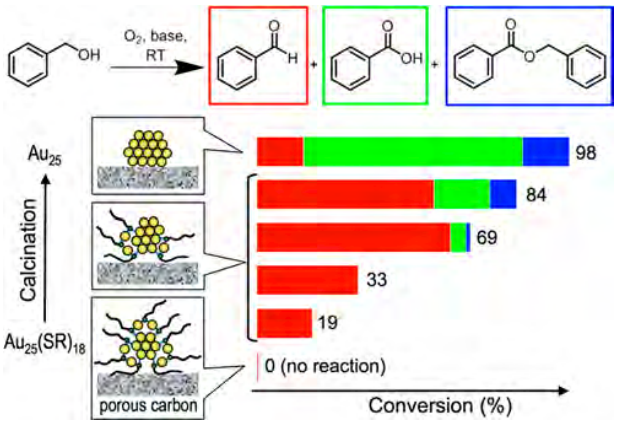

Figure 50. Conversion and selectivity data for the aerobic oxidation of benzyl alcohol on thiol ($SC_{12}H_{25}$)-SAMs-modified carbon-supported Au_{25} NPs as a function of the severity of the calcination post treatment (which increases from bottom to top in the bar graph).[660] Optimum performance (69% conversion, 90% selectivity) was reached after partial SAMs removal (4 h calcination at 450 °C). Reproduced with permission from ref 660. Copyright 2014 American Chemical Society.

Surface modification by non-covalent molecular agents is also common in many new catalysts because of the way they are prepared. Indeed, self-assembly approaches to the preparation of metal NPs such as via colloidal chemistry involve the use of surfactants that may not be fully removed during subsequent treatments. The role that those organic residues play in catalysis has been somewhat controversial (as discussed later in this Review, Section 5.4),[50,651,663−667] but in some cases they have been added purposely to modify the activity of the metal surface.[668,669] It needs to be remembered that even if surfactants only play an indirect role in affecting the characteristics of catalysts during both the synthesis and catalysis stages, those effects need to be clearly delineated. For instance, in a study on the hydrogenation of *p*-chloronitrobenzene and cinnamaldehyde using colloid-prepared Au NPs, although significant variations in catalytic behavior were seen with different surfactants, they were ascribed to changes in NP size rather than to intrinsic modification of the surface chemistry by the adsorbed organic fragments.[670] Figure 51 provides an example where the activity of polymer-supported Ru−Co bimetallic catalysts, used for the room-temperature chemoselective reduction of nitroarenes, was altered by tuning the electronic properties of the supporting polymer: faster conversion was attained with electron-deficient polystyrenes.[671] Also, surfactants can affect the shape of metal NPs, and that way direct selectivity in catalysis.[672]

In the majority of cases, however, it is clear that the surface species resulting from the addition of surfactants directly affect catalytic performance. The effects of these adsorbates on catalysis may be ascribed to the properties of the individual molecular units: by systematically diluting active ligands with inert ones, Ghosh and coworkers excluded cooperative effects and highlighted the role of the morphology of the ligand shell, in their case the promoting contribution of sulfonic acid layers to the esterification of carboxylic acids on Au NPs.[673] In a separate investigation where primary alkylamines were used to modify the Pt-catalyzed hydrogenation of alkynes to alkenes, it was determined that activity and selectivity can both be tuned by adjusting the relative adsorption energies of the capping

https://doi.org/10.1021/acs.chemrev.1c00905
Chem. Rev. XXXX, XXX, XXX−XXX

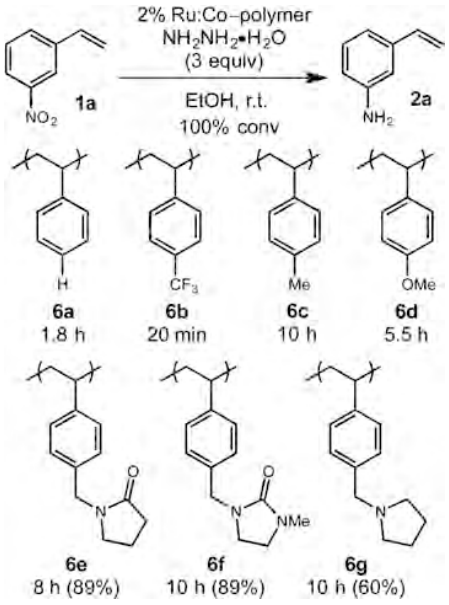

Figure 51. Effect of the electronic properties of the organic matter in polymer-supported Ru−Co bimetallic catalysts on the rate of reduction of nitroarenes to aromatic amines. Electron-rich and Lewis-base polymers slow down the reaction.[671] Reproduced with permission from ref 671. Copyright 2015 American Chemical Society.

agents relative to the alkyne reactants and alkene products (Figure 52; in this case unsupported Pt NPs were used as the catalyst).[674] In some examples the effect of the ligands has been explained via a modification of the electronic structure of the metal NPs.[675] For example, the poly(diallyldimethyl-

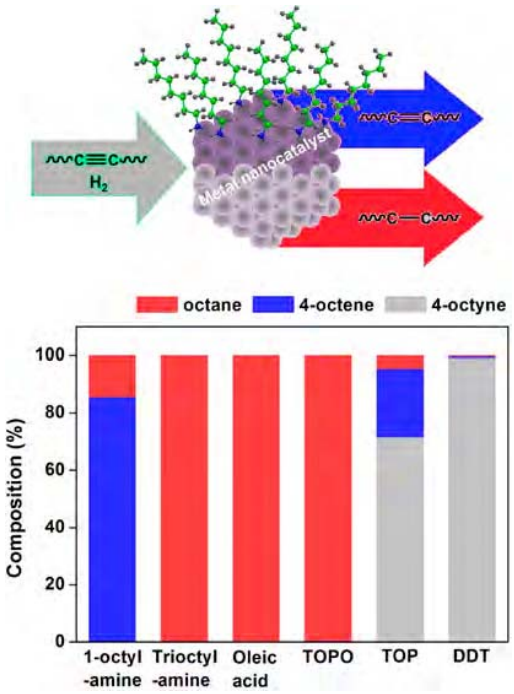

Figure 52. Effect of the surfactant on the selectivity of the hydrogenation of 4-octyne to 4-octene and octane promoted by Pt NPs.[674] Adapted with permission from ref 674. Copyright 2012 American Chemical Society.

ammonium chloride) stabilization of Pt and Pd NPs that was shown to lead to a more efficient promotion of the hydrogenation of 4-nitrophenol with $NaBH_4$ was explained by a charge-transfer modification of the surface of the metal.[676] In another report, the electronic properties of catalysts made out of Pt nanowires were modified via ethylenediamine adsorption to improve the selectivity of the partial hydrogenation of nitroaromatics toward the production of *N*-hydroxylanilines: it was claimed that electron donation from ethylenediamine to the Pt surface makes the latter electron rich.[677] More often, though, the modification of catalysts by surfactants may be a collective effect associated with steric factors, as in the example of the aerobic oxidation of benzyl alcohol by Au/SiO_2 in liquid phase, where the use of PVP as a capping agent enhances selectivity toward benzaldehyde production; that behavior was justified by a model where a competitive coupling step is blocked by the adsorbates.[678] In another case, the selective hydrogenation of furanic aldehydes to furfuryl alcohols using Ni catalysts could also be directed by capping the metal NPs with organic molecules during their colloidal synthesis because of the added steric hindrance.[679] An extreme example is that of the asymmetric hydrogenation of β-keto esters over α-amino acid-functionalized Pt nanoparticles, because it was claimed that in this system the modifier induces a switch in reaction mechanism from stepwise H atom incorporation (a classical Langmuir-Hinshelwood mechanism) to a pathway where the addition of the two hydrogen atoms to the carbonyl group of the reactant is concerted and mediated by the amino group of the ligand.[680]

On the whole, the studies of non-covalent surface modification at the colloidal NP synthetic stage for the control of catalytic performance has so far been sparse and unsystematic; the main focus in this field has been on extracting correlations with NP morphology instead. Consequently, the full potential of this approach is still to be demonstrated. Another important observation here is the fact that most SAMs and surfactant modification studies of catalysts have involved metal NPs; other types of solids are seldom considered in this research. One notable exception is the recent work on the use of carboxylates to tune selectivity during the ammoxidation of hydroxyaldehyde toward the desired hydroxynitrile product on manganese oxide catalysts, an effect that was attributed to a selective decrease in hydroxyl adsorption affinity of the oxide surface.[681,682] A second case is that of the dehydration of alcohols over TiO_2 catalysts modified with various phosphonic-acid SAMs, where the changes in catalytic behavior upon surface modification were explained by a balance between transition state stabilization and active site blocking effects.[683] Hopefully, more examples will become available in the near future.

4. SINGLE-SITE CATALYSIS

In the preceding discussion, we have talked about the addition of molecular functionality to solid surfaces to develop selective heterogeneous catalysts. In those, selectivity is provided mainly by the added discrete molecule, be it an organometallic catalyst, an enzyme, or an organic functionality. Alternatively, elements can be added to surfaces in order to build surface sties as part of the solid structure. There is presently an interest in developing individual and isolated catalytic sites on solid surfaces to create new selective heterogeneous, so-called single-site[22,60,684−686] or single-atom,[687−692] catalysts (a distinction is sometimes made between these two terms,[690] but in this

https://doi.org/10.1021/acs.chemrev.1c00905
Chem. Rev. XXXX, XXX, XXX−XXX

review we will group them together). The recent advances in this direction are surveyed and discussed next.

4.1. Isolated Metal Atoms from Organometallics

One way to create catalytic sites on the surfaces of solid catalysts is via the adsorption and further processing of organometallic precursors. We have already discussed the design of heterogeneous catalyst via the grafting or tethering of organometallic catalysts (Sections 2.1 and 2.2), but in this case the idea is to (partially) decompose the adsorbed species, in a controlled manner, to create a new surface site, possible involving atoms from the original solid as well. This distinction is, to some extent, arbitrary, as even during grafting some decomposition, or at least ligand exchange, takes place. Nevertheless, we will here attempt to emphasize the recent work in this area under the banner of single-site catalysis.[22,77,98,686,693]

Perhaps the first issue that needs to be considered when talking about metal single-site catalysis is the nature of the support upon which the organometallic molecules are adsorbed and partially decomposed. The vast majority of dispersed catalysts are prepared on high-surface-area porous oxides, quite often on silica[75,77,685,694,695] but in a few instances also on other common oxides such as alumina,[695−697] titania,[698−700] ceria,[701] and magnesia,[698,702] and also on mixed oxides, silicoaluminas in particular.[703] Coordination of organometallics to these surfaces takes place predominantly at terminal M−OH groups, silanols in the case of silica.[22,75,77,685] Still, several structural options are available, as silanols (for instance) mainly exist as isolated groups (≡Si−OH) but can also be present on the surface in geminal (=Si(OH)$_2$) or vicinal (=Si(OH)−O−Si(OH)=) forms, a fact that affords multiple ligand substitution and coordination of discrete metal complex to the surface.[685,694,695,704−707] Even if the primary coordination is via ligand displacement by a single isolated silanol group, additional coordination is also possible to adjacent siloxane bridges (≡Si−O−Si ≡), as in the case of the Ta-based catalysts for alkene metathesis shown in Figure 53a.[708] With acidic supports such as alumina, monocoordinated complexes can also interact with adjacent Brønsted- or Lewis-acid sites, and possibly react with those to form bridged bicoordinated species:[703,709,710] this is, for instance, what was proposed for the W-based metathesis catalysts shown in Figure 53b.[711] All these new multiply coordinated metal species exhibit chemistry different to that seen with their free counterparts in solution, or even with the monocoordinated analogues, offering some flexibility in terms of the design of single-site catalysis. Design of single sites with multiply coordinated metal centers is aided by the fact that the density of hydroxyl surface groups in oxides, which directly affects the relative preference between single and double bonding of organometallic species to the surface, can be tuned to some extent via appropriate chemical or thermal treatments (the latter activates partial dehydration).[712−714]

A second consideration when discussing so-called single sites made via grafting of organometallic compounds is the changes that may be induced upon further treatment of the surface. As mentioned above, the surface may actually be treated prior to the grafting reaction, mainly to control the density of reacting (hydroxyl) sites. Similarly, the solid can be processed after grafting, via calcination or thermolysis. Extreme processes such as high-temperature calcination are likely to burn all organic ligands, and even promote the incorporation of the metal

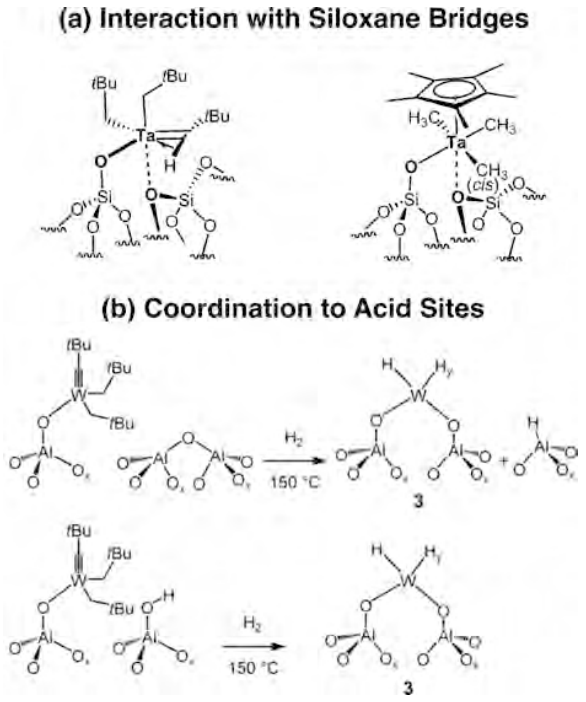

Figure 53. Examples of catalysts based on organometallics grafted to silica exhibiting multiple coordination to the surface. (a) Ta complexes bonded to a siloxy group but also showing a secondary interaction with an adjacent siloxane bridge.[708] (b) Reaction of a W complex, initially coordinated to a alumina hydroxyl group, with adjacent Al−O−Al bridges or Al−OH surface species to form multiply coordinated sites.[711] Reproduced with permission from refs 708 and 711. Copyright 2004 American Chemical Society and 2005 Wiley-VCH Verlag GmbH & Co. KGaA, Weinheim.

atoms into the oxide lattice[715] or the sintering of the individual metal atoms to form metal NPs.[700,716] On the other hand, more controlled treatments, perhaps heating to lower temperatures and in the presence of hydrogen or an inert gas, can lead to well-defined transformations. In fact, many of the bicoordinated species used as examples in the previous paragraph were produced via thermal activation of initial monocoordinated intermediates.[709,711] Another common consequence of thermally treating organometallic species grafted on oxide surfaces is the inducement of the replacement of the original ligands for hydroxo or other oxygen-based coordinations (under oxidizing conditions, Figure 54),[717,718] or for hydrides (under reducing conditions, Figure 53b).[709]

Single-site catalysts prepared via partial decomposition of grafted organometallic precursors have been used to promote several types of reactions. Much work has been directed at the design of catalysts for metathesis. The metals in catalysts made by conventional methods tend to form dispersed NPs, and are by and large not efficient at promoting the formation of the alkylidene intermediate involved in the metathesis mechanism; isolated metal atoms are required for such a step. Metal-grafted single-site catalysts designed for metathesis may already contain the alkylidene or alkylidyne ligand needed to initiate metathesis (Figure 55a),[65,719−721] reach that intermediate via tautomerism from other configurations (Figure 55b),[722] or be preconditioned to form alkylidene or alkylidyne species upon exposure to the reaction mixture.[704,723,724] Examples also exist on the detection of metallacyclobutadiene intermediates on the

https://doi.org/10.1021/acs.chemrev.1c00905
Chem. Rev. XXXX, XXX, XXX−XXX

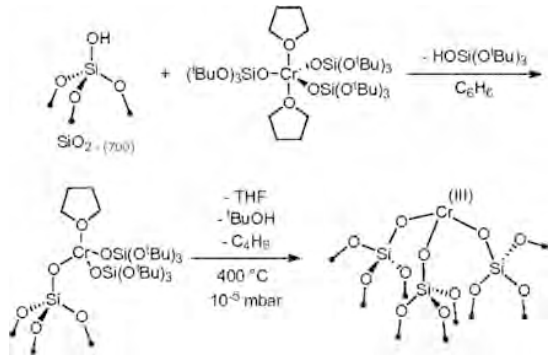

Figure 54. Example of the synthesis of single-site catalysts via the grafting and ligand exchange of organometallic precursors. In this case $Cr(OSi(O^tBu)_3)_3(THF)_2$ is initially bonded to silica via the displacement of one of the tris(*tert*-butoxy)siloxy ligands by a silanol surface group (and the elimination of tris(*tert*-butoxy)silanol), and further converted into a $(\equiv SiO)_3Cr(III)$ site upon heating in vacuum.[718] Reproduced with permission from ref 718. Copyright 2014 National Academy of Sciences.

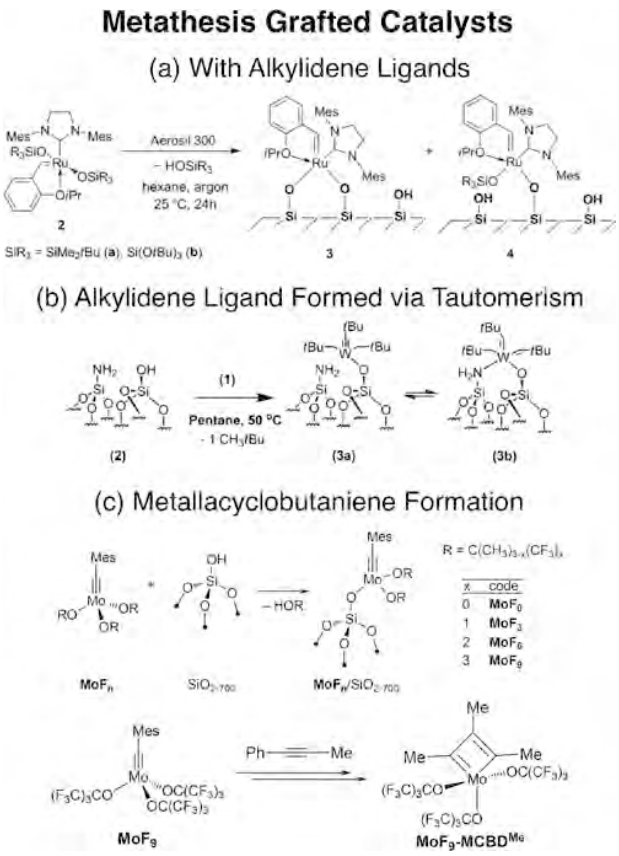

Figure 55. Examples of single-site metathesis catalysts prepared via the grafting of organometallic precursors. (a) Immobilization of Ru-carbene metathesis catalysts on silica.[719] (b) Active $[(\equiv Si-NH_2-)(\equiv Si-O-)W(=CHtBu)_2(CH_2tBu)]$ catalyst formed via tautomerization of an initial $[\equiv Si-NH_2][(\equiv Si-O)W(\equiv CtBu)(CH_2tBu)_2]$ intermediate.[722] (c) Immobilization of a Mo-carbyne species on a silica surface, and formation of a metallacyclobutadiene intermediate via reaction with an alkyne.[725] Reproduced with permission from refs 719, 722, and 725. Copyright 2011 Wiley-VCH Verlag GmbH& Co. KGaA, Weinheim, 2016 Wiley-VCH Verlag GmbH & Co. KGaA, Weinheim, and 2017 American Chemical Society.

tethered metal-grafted catalysts (Figure 55c).[725] In many instances, the solid catalysts end up performing better than the homogeneous homologues, an observation that has been explained in terms of two effects: the blocking of bimolecular decomposition pathways upon grafting of the organometallic compounds on the surface,[726] and the fact that the surface siloxy groups are small and weak σ-donors with electronic properties similar to those of O^tBu_{F3} groups.[727]

This type of grafted single-site catalysts have also been used for related reactions requiring olefin or alkyne coordination such as alkene dimerizations, oligomerizations, and polymerizations.[728−732] The development of single-site models for Ziegler−Natta and Phillips type catalysts using the organometallic grafting approach has been a particular focus, for which an activator or co-catalyst is often needed, at least on silica.[718,733−736] There have also been significant advances on the use of grafted single-site catalysts to promote the hydrogenation of organic reactants.[82,84,737,738] For instance, a catalyst prepared by grafting organozirconium complexes on sulfated oxides was shown to be quite selective toward the hydrogenation of benzene in the presence of other unsaturated molecules, presumable because of the control that can be exerted on the Zr−support bond distance, which provides the appropriate steric hindrance to block access to bulkier arene reactants (Figure 56).[739] Activation of alkanes is also desirable, and sometimes possible, with this type of grafted-metal catalysts.[740]

In summary, the development of single-site catalysts via the grafting of organometallic complexes is promising, especially as a way to design selective processes for the conversion of organic feedstocks. The level of molecular detail on the catalytic site obtained this way is hard to match with the all-

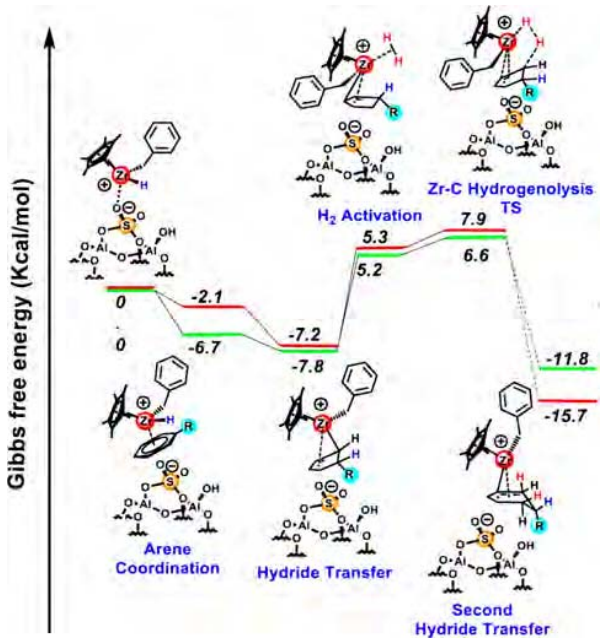

Figure 56. Comparative Gibbs free energy profiles for the hydrogenation of benzene (red traces) versus toluene (green) over a $Cp^*Zr(H)Bz^+$/sulfated-alumina catalyst, highlighting the energy differences that drive selectivity toward the former reaction.[739] Reproduced with permission from ref 739. Copyright 2005 American Chemical Society.

https://doi.org/10.1021/acs.chemrev.1c00905
Chem. Rev. XXXX, XXX, XXX−XXX

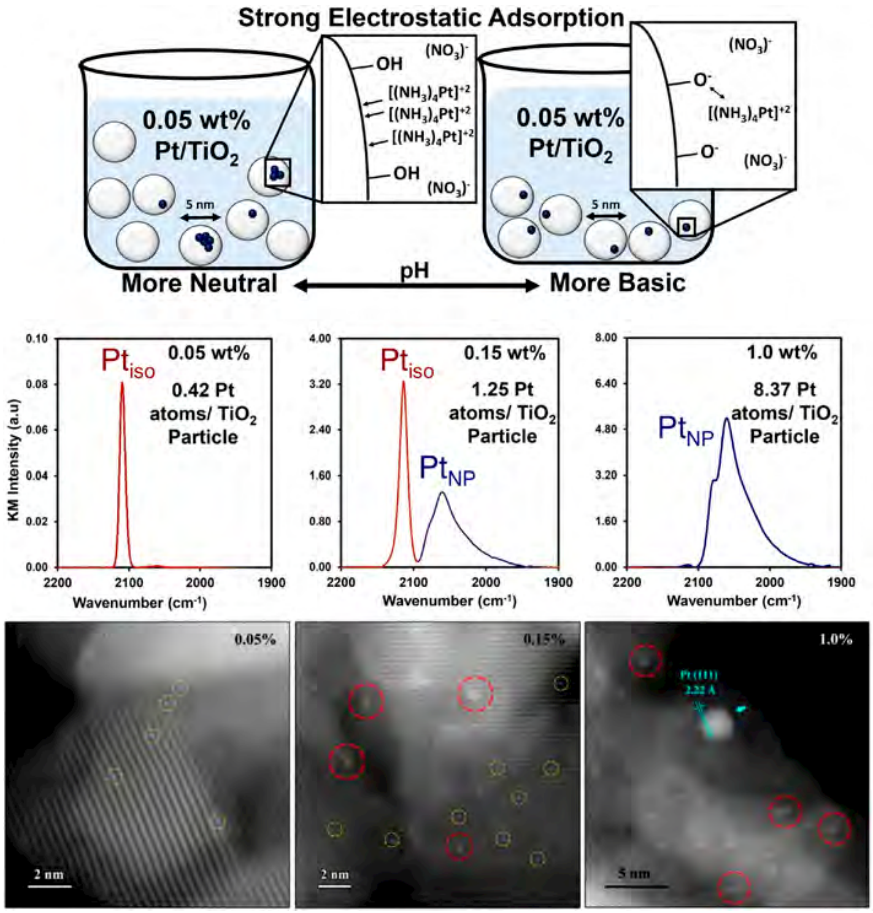

Figure 57. Top: Impregnation-based synthesis of catalysts with site-isolated Pt on TiO_2.[747] Center: IR spectra of carbon monoxide adsorbed on Pt/TiO_2 produced by using three different loadings, employed to probe and follow the evolution of the nature of the metal on the surface from isolated Pt atoms (Pt_{iso}) to Pt NPs. Bottom: Corresponding STEM images indicating the nature, isolated versus clustered, of the Pt sites. Adapted with permission from ref 747. Copyright 2017 American Chemical Society.

solid synthetic methods discussed in the next sections of this review. On the other hand, these catalysts are somewhat fragile, especially if they need to retain some of the original ligands of the organometallic precursor, and are therefore prone to decomposition. This limits the conditions under which they can be used, in particular to low temperatures, and with that the range of reactions that can be promoted with them. Another point to be considered is the fact that the heterogeneity of the surfaces of the original oxides almost always leads to the formation of several types of catalytic sites, as seen in some of the examples provided above, an occurrence that affects selectivity. In addition, control over the nature of the coordination of the metal to the surface is limited, relying mostly on the type and distribution of surface hydroxyl groups in the case of oxide supports. Nevertheless, these catalysts are some of the most promising for uses in metathesis and polymerizations.[741]

4.2. Monoatomically Dispersed Metal Atoms

In many applications, the interest is to create catalysts with individual, naked, metal atoms dispersed on a support.[742] Because these catalysts do not require ligands coordinated to the metal, they can be prepared by other synthetic routes, not starting from organometallic precursors as discussed in the previous section. Moreover, they can potentially be more stable, as they do not contain organic ligands prone to oxidation or decomposition, although sintering may still be a problem. The challenge remains to develop methods to obtain the proper metal dispersion, assuring that the metal phase is indeed present on the surface in uniform and presumably atomic form.

Several synthetic strategies have been developed to obtain atomic dispersion and produce single-atom metal-based heterogeneous catalysts.[743] The most common by far, perhaps due to their simplicity, are impregnation and coprecipitation.[744−746] These are in fact also typical procedures for the synthesis of traditional metal-based heterogeneous catalysts. In general, however, they yield metal NPs with a distribution of sizes dispersed on the solid support; the normal impregnation and coprecipitation techniques need to be properly adapted to be useful in the synthesis of single-atom catalysts. The simplest way to accomplish this is by selecting high-surface-area supports and lowering the metal loading until reaching metal-to-oxide-NP ratios below one; the viability of such an approach has been nicely tested by Christopher and coworkers.[747−750] In their initial report, which they have since generalized to other systems, stable isolated Pt sites (Pt_{iso}) were created on titania supports by using small (~5 nm) titania NPs; monoatomic Pt dispersion was corroborated by a combination of carbon monoxide-IR titration experiments and scanning transmission electron microscopy (STEM) imaging

https://doi.org/10.1021/acs.chemrev.1c00905
Chem. Rev. XXXX, XXX, XXX−XXX

(Figure 57).[747] Others have reported the successful use of this method to produce single-atom catalysts as well.[751−754] There is still the possibility that nucleation followed by preferential deposition may lead to metal NP formation even with these low-concentration solutions, though, so the atomic dispersion in the final catalysts needs to be carefully verified by imaging or by spectroscopic means.

Sintering during synthesis can be minimized by performing the appropriate deposition chemistry at low temperatures, with the aim of lowering the probability of atomic diffusion on the surface. For instance, atomic Pt has been dispersed on various substrates, including mesoporous carbon, graphene, carbon nanotubes, titanium dioxide NPs, and zinc oxide nanowires, via photochemical reduction of a frozen (−25 °C) chloroplatinic acid solution using ultraviolet light (Figure 58).[755] In another

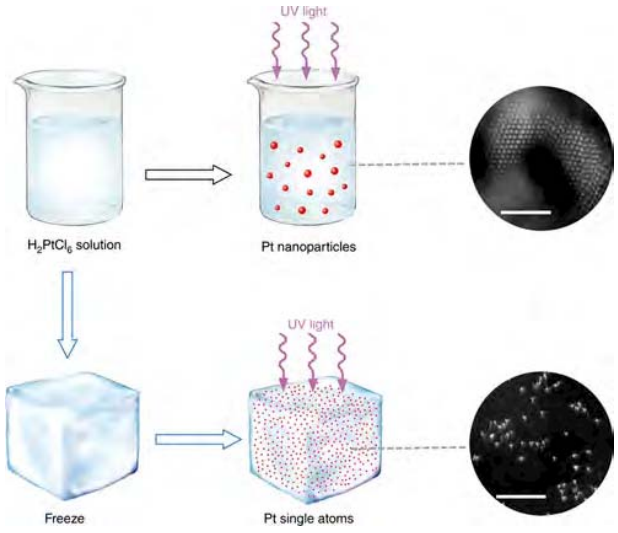

Figure 58. Schematic illustration of a single-atom catalyst preparation method based on a combination of solvent freezing and photocatalytic activation.[755] As indicated by the electron microscopy images on the right, the conventional photochemical reduction of H_2PtCl_6 aqueous solutions leads to the formation of Pt NPs (top row), but agglomeration can be prevented via the prior freezing of the solution (bottom) (scale bar, 2 nm). Reproduced with permission from ref 755. Copyright 2017, Springer Nature.

case, atomically-dispersed Pt supported on nitrogen-doped mesoporous carbon substrates could be attained by carrying out the deposition from solution at low (−40 °C) temperature.[756] Zhou and co-workers reported the successful synthesis of atomically dispersed Pd single-atom catalysts on nitrogen-doped graphene by using a similar freeze-drying-assisted method.[757] Monodispersed Ni/Y_2O_3-based catalysts were analogously prepared by freeze-drying a solution containing the two precursors, $Ni(NO_3)_2{\cdot}6H_2O$ and $Y(NO_3)_3{\cdot}6H_2O$, together with the GO support.[758] Highly diluted solutions are still needed for this method to succeed, since the freezing component is meant to prevent sintering but does not modify the initial metal ion dispersion on the support.

Unfortunately, the low metal content of catalysts synthesized by this approach limits their activity, and therefore their practical applicability. To address such limitation, solid supports may be designed with specific defect sites onto which adsorption of the metal precursor may be favored. In one case, it was reported that MoS_2 monolayer sheets could be decorated with isolated Co atoms bonded covalently to S basal vacancies to improve the activity, selectivity, and stability of the catalyst for the hydrodeoxygenation of 4-methylphenol to toluene; the success of the decoration and single-atom site formation was ascribed to the presence of a large density of sulfur vacancies at S−Mo interfaces.[759] In another recent example, a single-atom Ru catalyst was prepared via the filling of metal vacancies in a nickel hydroxide support with Ru^{3+} ions.[760] Following a slightly different approach, a Pt/titania water splitting photocatalyst was recently reported where the oxide support was made in tubular form to create well-distributed defects where monoatomic Pt deposition could be attained (Figure 59).[761] What all these examples have in common is the high density of single-atom sites that was reached.

Metal single sites can also be produced by using chemical vapor deposition (CVD), mainly in its most modern version, atomic layer deposition (ALD).[762−764] ALD is a versatile technique for the deposition of thin films with monolayer control, as we discuss in more detail later in this review (Section 8.2). An interesting example that illustrates the flexibility of this approach was provided by Zhang et. al, who used sequential ALD steps with $MeCpPtMe_3$ and $Ru(EtCp)_2$ precursors to create Pt−Ru diatomic bimetallic sites on nitrogen-doped CNTs: the Pt complex reacts and deposits Pt atoms selectively at the surface nitrogen atoms of the carbon-based support, and the Ru organometallic then adds preferentially at the newly created Pt sites (Figure 60).[765] Key to the success of this methodology is the ability to create surface sites on the original supporting material with the appropriate chemistry for binding the ALD precursor. Also, the higher the surface density of such sites than can be created, the better; this is why many examples of the use of ALD for the preparation of single-atom catalysis involve carbon-based supports.[766,767] Other less common methods to synthesize single-atom site catalysts include ion exchange,[768] chemical etching,[769,770] electrochemical[771] or photochemical[755] reactions, and microwave,[772] shockwave,[773] ball-milling,[774] or metal-ligand[775] or ionic-liquid[776] self-assembly assisted methods.

Success in obtaining and maintaining atomic dispersion depends to a great extent on the nature of the support and its interaction with the individual metal atoms. Stronger metal-support interactions can lead to less sintering and better catalyst stability, but may also affect the electronic properties of the catalytic site, and with that catalytic performance. This may be the most evident when single-metal atoms are dispersed in ionic or polar supports, as many oxides are. Ion exchange and filling of ion vacancies are possible mechanisms for single-atom site formation on oxides, as already illustrated above, but that requires the initial deposition of metal ions, which may then be partially (but typically not fully) reduced. Charge transfer between the isolated metal atoms and the support can be viewed as an extreme case of the so-called strong-metal-support-interaction (SMSI) that has been extensively studied and discussed in the literature, especially when reducible oxides such as titania or ceria are involved.[777−780] However, the case of single metal atoms on oxide supports is likely to be more complex. In a recent study, it was reported that a SMSI can indeed occur on TiO_2-supported Pt single atoms, but at a much higher reduction temperatures than those required with Pt NPs.[781] Moreover, it was established that the Pt single atoms involved in this SMSI are not covered by the TiO_2

https://doi.org/10.1021/acs.chemrev.1c00905
Chem. Rev. XXXX, XXX, XXX−XXX

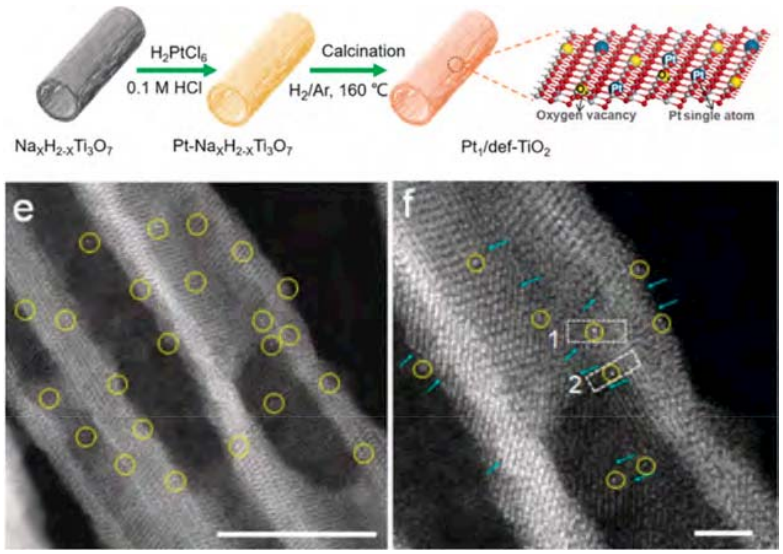

Figure 59. Top: Synthetic scheme for the preparation of high-density single-atom Pt catalysts dispersed on a titania support.[761] Bottom: High-angle annular dark-field (HAADF) STEM images of the resulting catalyst, highlighting the position of the individual Pt atoms. (Scale bars: (e) 10 nm and (f) 2 nm). Adapted with permission from ref 761. Copyright 2020 Wiley-VCH Verlag GmbH & Co. KGaA, Weinheim.

support or embedded in the subsurface of the solid, as with metal NPs. The suppression of the capacity of the metal single atoms to adsorb even simple molecules such as carbon monoxide was instead ascribed to a saturation in coordination according to the 18-electron rule that applies to transition metals.[781] In a separate theoretical study of a Pt/CeO_2 catalyst that combined DFT and first-principles Born−Oppenheimer molecular dynamics (BOMD), it was concluded that imagining the charge around the metal in these single-atom catalysts as static is an oversimplification, and that the dynamics of the interaction among several well-defined charge states needs to be taken into consideration (Figure 61).[782] Ultimately, though, it is clear that the electronic properties of single metal atoms are modified by the support, and that such charge transfers can modify catalytic behavior. Much discussion has been had in particular on the oxidation state of supported Au catalysts.[783]

Additional consideration needs to be given to the phisical properties of the support used to make these single-site catalysts. For instance, even within one given support, structural effects are possible, as the nature of the facet of the solid exposed can alter the metal deposition. In one example, it was shown that single Pt atoms can be readily ALD on the (110) and (100) facets of CeO_2 but not on the (111) plane.[784] Also, the material of the support can help with catalyst preparation: atomic dispersion of metals on carbon-containing supports, for example, is often easier to achieve than on oxides, as individual defect sites can be readily created on the surface of those materials to preferentially bind single metal atoms. Graphene has become a particularly popular support for the making of single-site catalysts, as already illustrated in Figure 60 (and discussed in more detail in Section 6.4).[767,785] In fact, covalent bonding of metal atoms to carbon surface defects may also take place with minimal charge transfer, a fact that may provide more control on the catalytic performance of the metal. Still, the surface will always influence the chemical properties of the single metal atoms, and therefore those are never expected to behave as if they were fully metallic.[786] This has become particularly evident with catalysts exposed or treated with water or steam, as water-containing environments often affect the performance of the catalyst is significant ways. An example is shown in Figure 62, in which catalysts made out of individual Pt^{2+} ions dispersed on CeO_2 were activated for CO oxidation at 150 °C via a steam treatment at 750 °C.[744] The authors explain this activation on the basis of DFT results showing that the steam helps with the diffusion of bulk oxygen vacancies within the oxide support to the surface, and by relying on data from their titration with adsorbed water, which dissociates to create two adjacent surface hydroxyl groups (Figure 62); these new OH moieties, produced in sites adjacent to the Pt ion, assist in the activation of carbon monoxide during its oxidation. These examples point to the fact that, because the support often plays some role in the overall catalysis, flexibility in the selection of supports to improve on atom dispersion is limited; instead, once the support is selected, metal dispersion must be controlled by other means.

In general, it is clear that the isolation of metals as single atoms within the surface of catalysts adds to the degree of control of the catalytic site when compared with dispersed metal NPs, which often display a range of sizes and shapes. On the other hand, the fact that the catalytic site is comprised of a single metal atom limits the degrees of freedom available to the design of atomic ensembles to be used to control reaction selectivity, and also the ability to tune the electronic properties or oxidation state. Moreover, atomically dispersed catalysts may not be stable, and are therefore likely not to survive the extreme temperature and pressure conditions of many catalytic processes. It is perhaps for this reason that most single-atom metal catalysts in this category have been used for mild processes,[52] either electrochemical[689,760,765,769−771,774,787] or photochemical[757,758,761,788] catalysis, or for the promotion of low-temperature reactions such as hydrocarbon hydrogenations,[652,737−739,751,766,789−791] although a few other conversions have been tested with these catalysts as well.[721,737,768] The lack of site complexity and the low stability may be reasons why the use of these catalysts have to date not often been extended to more complex processes where selectivity imposes more stringent requirements on the catalytic site.[690,789,792] It is

https://doi.org/10.1021/acs.chemrev.1c00905
Chem. Rev. XXXX, XXX, XXX−XXX

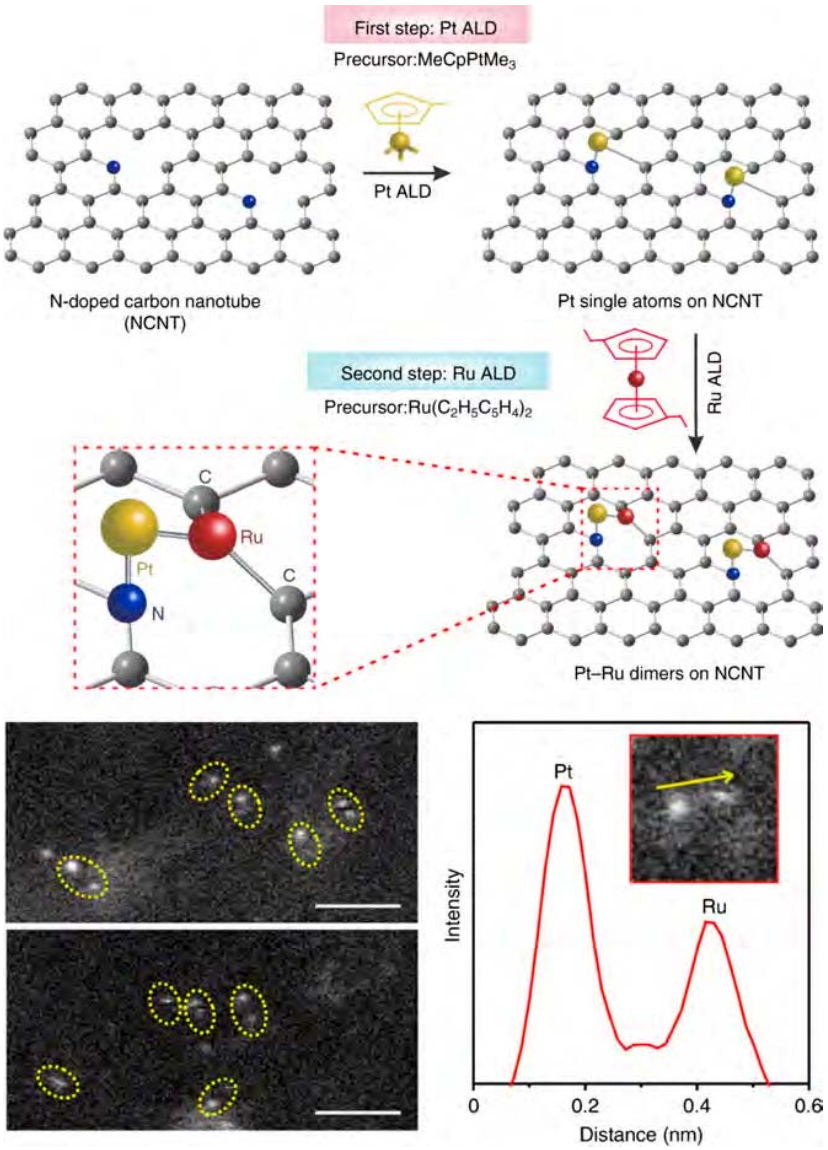

Figure 60. Single-site Pt−Ru dimeric catalytic sites prepared using ALD.[765] Top: Schematics of the ALD sequence. Bottom: Aberration-corrected HAADF-STEM images of Pt−Ru dimers dispersed on N-doped CNTs (scale bar: 1 nm) and example of the intensity profile of the Pt−Ru dimers. Reproduced with permission from ref 765. Copyright 2019 Springer Nature.

also important to realize that although the metal itself may exist in atomic form and therefore in a well-defined state on the surface, the surrounding surface atomic ensembles may display multiple structures and electronic properties; atomic dispersion of metals is not, in itself, a warranty of uniform catalytic sites.[687,793] Nevertheless, the single-atom approach is still in its infancy, and has shown much promise in certain catalytic applications.

4.3. Single-Site Alloys

An alternative way to isolate atoms of a specific metal within a catalyst is by diluting that metal in bimetallic solid-supported and dispersed NPs, to create so-called single-atom alloy (SAA) catalysts.[794,795] Bimetallic catalysts have in fact been used extensively in catalysis for decades (Section 5.3):[796−798] arguments have been made to justify the effectiveness of this approach either in terms of the creation of two types of surfaces, each with its own catalytic functionality, or as a way to create NPs that in essence display unique electronic properties, often (but not always) a weighted average of the electronic properties of the individual components.[799−802] In some instances, alloying has also been used to create new sites with unique ensembles of atoms, an old idea that has recently been extended to SAA catalysts.[803,804] The difference here, when compared to other more traditional bimetallic catalysts, is that in SAA the component of interest must be present on the surface of the NPs in isolated form, far from other atoms of the same metal. There have also been multiple instances of supported metallic catalysts that have been modified via the addition of small amounts of a second element, atoms such as N, S or Cl, or sometimes another metal (alkaline metals such as K or Na, for instance).[805−807] Those elements are likely to be well dispersed and present on the surface in isolated form, but in such cases the addition of the minority element aims to modify the properties of the main catalytic component. Here,

https://doi.org/10.1021/acs.chemrev.1c00905
Chem. Rev. XXXX, XXX, XXX−XXX

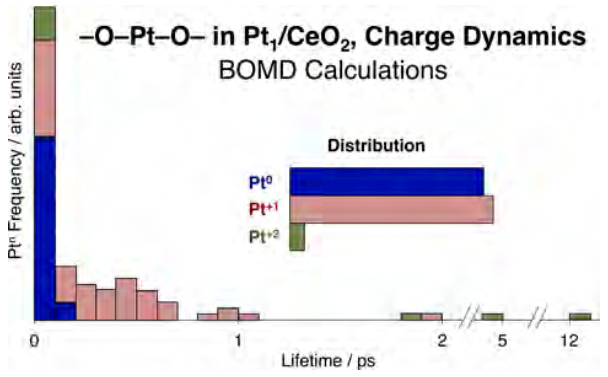

Figure 61. Charge distribution statistics in a Pt_1/CeO_2 single-atom catalyst, as estimated from BOMD calculations.[782] Shown is the lifetime distribution of the various Pt oxidation states for a double-coordinated −O−Pt−O structure, together with the total average time fractions that the metal exist in each of the three possible oxidation states.

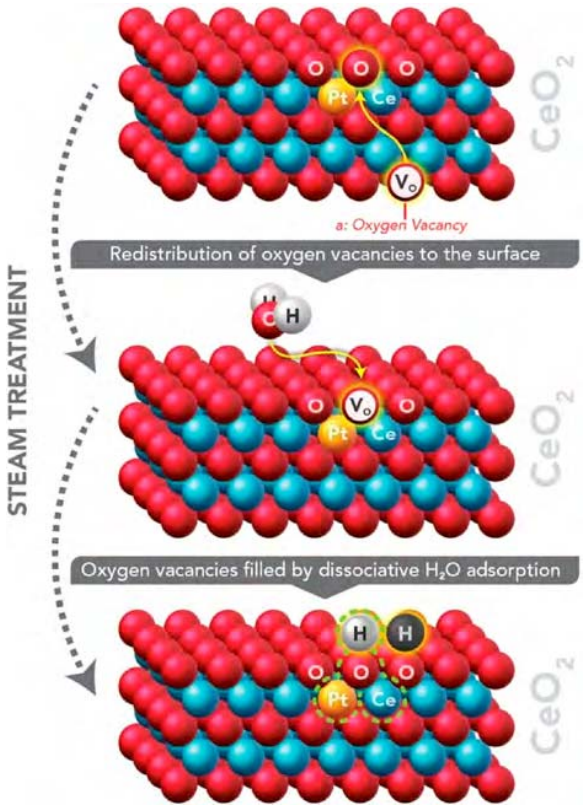

Figure 62. Surface modification of a Pt_1/CeO_2 single-atom catalyst induced by a high-temperature steam treatment, as estimated from DFT calculations.[744] The steam helps with the segregation of bulk CeO_x oxygen vacancies to the surface and with their filling; this produces hydroxyl surface groups adjacent to the Pt^{2+} site that assist with CO oxidation catalysis. Reproduced with permission from ref 744. Copyright 2017, The Authors, some rights reserved; exclusive licensee American Association for the Advancement of Science.

the isolated metal atoms are expected to be main catalytic sites by themselves.

Several synthetic methods have been developed to prepare SAA catalysts. The most straightforward are those derived from the traditional protocols followed to prepare bimetallic materials, adapted by controlling the relative amounts of the elements added and the pretreatment conditions. Specifically, SAA catalysts have been synthesized by co-precipitation,[808] incipient wetness co-impregnation,[809−811] and sequential reduction.[812] Other methods more specifically design for the preparation of SAAs have also been reported, including galvanic replacement (Figure 63)[813−815] and sequential acid etching and electrochemical leaching.[816] It should be indicated that, upon surveying of the literature, it would appear that examples of SAA catalysts are still limited, mostly consisting of late transition metals (Pd, Pt, Rh, Ni, Ru) alloyed into coinage metal (Cu, Ag, Au) NPs. Their uses have typically been limited to mild and simple reactions such as CO oxidation,[817] alkene,[818,819] alkynes,[810,813,820,821] and carbonyl[808,809,822,823] hydrogenations, alcohol[812,824] and organic acid[825] dehydrogenations, reduction of nitrogen-containing reactants,[811,826] and electrocatalysis.[804,827] In one case, Cu NPs were used as "antenna" to collect light and transfer the ensuing electronic excitation to a single Ru atom to photocatalytically promote a low-temperature methane dry reforming.[828]

One crucial difference between SAA catalysts and the single metal atom catalysts discussed in the preceding section is that instead of bonding to carbon-based materials, oxides, or other insulator or semiconductor surfaces, the isolated metal atoms in SAAs are embedded in metallic NPs. The electronic interactions between metals in alloys are complex and potentially more intimate than in bonds with non-metallic surfaces, as already mentioned.[799−801] At an extreme, it may be possible to isolate the electronic structure of the minority metal atom within the metallic matrix of the majority component by judiciously selecting the latter to exhibit minimum orbital overlap, in which case the atomic electronic bands of the isolated metal may become narrow and look more like those of a single atom, akin to what is seen in molecular metal complexes (Figure 64).[802] Yet, even in that case it is difficult to control the final oxidation state or tune the ensuing catalytic chemistry; these systems are in any case the exceptions, perhaps the reason for the limited selection of metal pairs used for SAA. Moreover, the main element in SAA catalysts is typically another transition metals, and most transition metals are active in some if not most catalytic environments. In fact, the majority SAA catalysts conceived to date have attempted to take advantage of this property: processes promoted by SAA have typically been designed to involve multiple elementary steps, with the isolated and main metal elements playing central roles in promoting different reactions within the overall mechanism.

Perhaps the best-studied SAA system in recent years is that of Pt (or Pd) atoms diluted in Cu NPs. The premise for the use of this combination is that Cu can be selective in the promotion of some hydrocarbon conversions under reducing conditions, but its effectiveness as a catalyst is hampered by its inability to activate molecular hydrogen, the crucial initial step in most hydrogenation processes. In the SAA scheme, that step may be promoted by a few isolated Pt atoms on the surface. Large surface coverages of Pt are to be avoided, however, as those would overtake the activity of the Cu surface and promote hydrocarbon conversions in a non-selective way. Support for this mechanistic scheme has been provided by data from a series of elegant experiments from the Sykes group using model surfaces and a controlled UHV environment. By using TPD in combination with high-resolution STM (HR-STM), they have shown that the addition (via evaporation) of

https://doi.org/10.1021/acs.chemrev.1c00905
Chem. Rev. XXXX, XXX, XXX−XXX

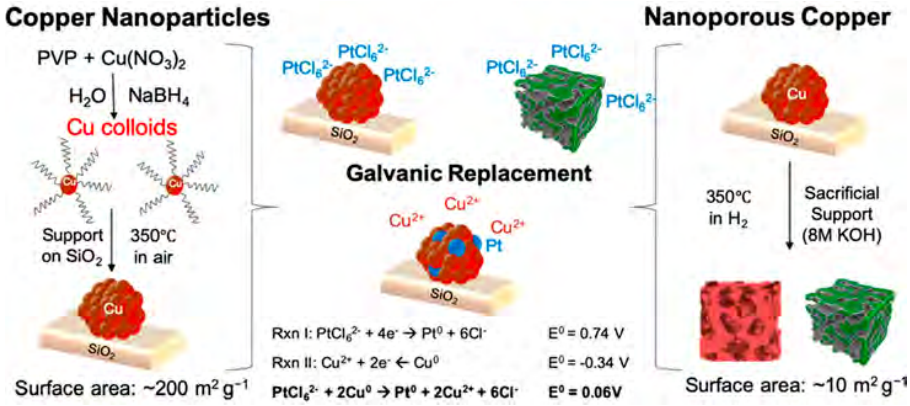

Figure 63. Schematic representation of the galvanic replacement method for the synthesis of NP (left) and nanoporous (right) SAA catalysts.[795] In this case the host metal is Cu, which can be present in either metallic (red) or oxidized (green) state. Subsequent exposure to a $PtCl_6^{2-}$ solution induces the replacement of individual atoms and the deposition of isolated Pt. Reproduced with permission from ref 795. Copyright 2020 American Chemical Society.

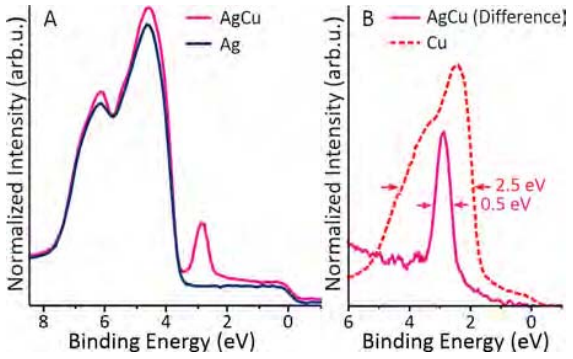

Figure 64. Example of a SAA where the electronic band structure of the minority element (Cu in this case, 0.3% diluted in Ag) resembles that of an isolated atom, as in metal complexes.[802] The thing to notice here is that the peak at a binding energy of ~2.5 eV in the red trace shown in Panel (a), which corresponds to the Cu 3d state, is quite narrow: this is better observed in the difference spectrum, AgCu minus pure Ag, plotted together with a Cu reference spectrum in Panel (b). Adapted with permission from ref 802 provided by Dr. Greiner.

isolated Pd or Pt atoms substantially lowers the energy barrier for the uptake of hydrogen on Cu(111) single-crystal surfaces (Figure 65).[829−831] STM studies were also used to assess the atomic dispersion and surface positioning of the added atoms (Pd, Pt),[830,832] and DFT calculations were performed to complement the experimental work and fully evaluate the changes in the energetics of the H_2 activation, adsorption and desorption on the modified Cu(111) surfaces.[830,831,833,834] The conclusion from that work was that, indeed, the isolated Pt/Pd sites are the ones responsible for the H−H bond activation step, at least under UHV.[835]

In additional TPD experiments with adsorbed acetylene or styrene, the Sykes group has also shown that the addition of the second metal (Pd) renders the Cu(111) surface, which is by itself inactive toward hydrogenation reactions with H_2, capable of producing ethylene or ethylbenzene, respectively, while avoiding the extensive dehydrogenation steps seen on pure Pd.[829] Similar experiments with butadiene on Pt−Cu(111) pointed to the ability of these systems to selectively stop at the production of butene (Figure 66a).[818] Studies with formic acid on the same SAA surface pointed to a selectivity for dehydrogenation over dehydration (Figure 66b),[825] and tests with ethanol identified an increased dehydrogenation activity upon Pt addition.[824] Again, these experiments were all carried out under UHV and using model surfaces, but some of the proposed reactions and selectivities were successfully tested by the Flytzani-Stephanopoulos group in kinetic experiments with dispersed SAA catalysts.[688,818,825] Two things have become clear from the work cited above: (1) SAA catalysts do clearly exhibit unique catalytic behavior, different to that of the individual metallic components, in hydrogenations as well as in other reactions;[688,808,809,818,836,837] and (2) under UHV, it is clear that the main role of the added second metal (Pd, Pt) is to activate molecular hydrogen and promote hydrogen-incorporation reactions.[820,830,833,834,838]

Unfortunately, the conclusions from studies under UHV with model surfaces do not always extrapolate directly to realistic catalytic conditions, where catalysts usually consist of metal NPs dispersed on a high-surface-area support and are exposed to atmospheric pressures (or liquid solutions) of the reactants. This disconnect between the two regimes has been long acknowledged and discussed in the surface-science literature, and referred to as the "materials" (or "structural")[21,839−843] and "pressure"[8,840,844,845] gaps, respectively. What is missing is an understanding of what may happen to the surface of real SAA catalysts during catalysis. In the particular case of the Cu-based SAA catalysts, two effects have been identified relevant to our discussion. The first is the fact that the surface of the Cu metal NPs can be easily oxidized, as indicated by recently X-ray photoelectron spectroscopy (XPS) data reported by our group: the $CuPt_x$ NPs appear to be covered by a thin CuO_x film during catalysis (Figure 67a).[808] A second effect relates to the knowledge that the single-atom phase may diffuse into the bulk of the NPs and may therefore not be directly available during catalysis. Carbon monoxide IR titration experiments carried out in our laboratory suggested that this may be the case (Figure 67b).[808] A similar failure to detect CO adsorption on the minority metal in $CuPd_x/SiO_2$ catalysts has been reported by others as well,[810] but this still needs to be corroborated by carrying out the experiments *in situ* under reaction conditions (preliminary data from our group do support this conclusion).[808] CO-induced segregation has also been identified recently for a couple of SAA systems using ambient-pressure XPS,[846,847] although no similar

https://doi.org/10.1021/acs.chemrev.1c00905
Chem. Rev. XXXX, XXX, XXX−XXX

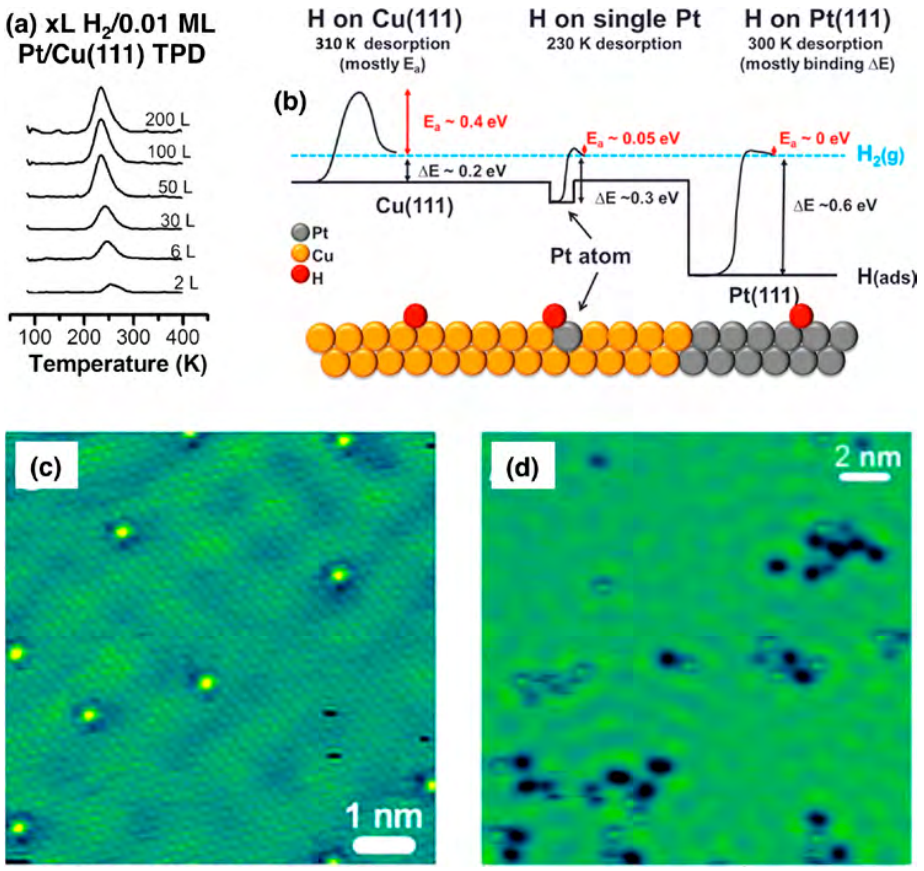

Figure 65. Evidence for the role of the isolated Pt atoms in Cu−Pt SAA surfaces as the phase that activates molecular hydrogen. (a) H_2 TPD traces from Pt/Cu(111) SAAs.[830] (b) Estimated energetics of H_2 activation on pure Cu (left), pure Pt (right), and a single Pt atom on a Cu surface (center).[831] The SAA configuration lowers the activation barrier for H−H bond scission compared to that in pure Cu but retains a weak metal-H binding, a property beneficial for hydrogenation catalysis. (c) STM image of 0.01 ML Pt dispersed on a Cu(111) surface, indicating the atomic dispersion of the Pt atoms.[830] (d) STM image of atomic H adsorbed on Cu, made possible by the initial activation of H_2 on the Pt SAA sites.[830] Adapted with permission from refs 830 and 831. Copyright 2015 and 2018 American Chemical Society.

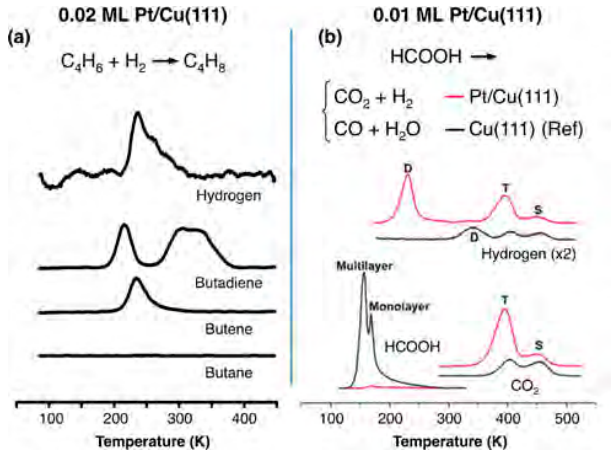

Figure 66. TPD results on Pt/Cu(111) indicating the increased selectivity induced by the addition of Pt to the surface toward the (a) hydrogenation of butadiene to butene[818] and the (b) dehydrogenation (versus dehydration) of formic acid.[825] Reproduced with permission from refs 818 and 825. Copyright 2015 The Authors and 2017 American Chemical Society, respectively.

behavior appears to be operational with H_2 in the case of Cu−Pt SAA.[848] It is also interesting to note that no isotope scrambling within H_2-D_2 mixtures was seen in experiments with $CuPd_x$ alloy films until a ∼15 mol % Pd content was reached, a result that implies than no Pd atoms are accessible on the surface of diluted alloys for this catalysis.[849] Even under UHV, CO oxidation on Pt-doped O-dosed Cu surfaces has been shown to lead to the diffusion of the Pt atoms underneath the Cu−O layer.[817]

Finally, a more recent report from our group on the use of $CuPt_x$/SBA-15 catalysts for the selective hydrogenation of unsaturated aldehydes provides kinetic data indicating the direct participation of the added Pt in defining catalytic selectivity.[822] Specifically, a rapid decrease in catalytic activity was observed with all catalysts as the reaction proceeded (in a batch reactor), an observation that was ascribed to the blocking of catalytic sites by the products because of their stronger adsorption compared to that of the reactant. It was determined that selectivity is controlled by the relative values of the initial rate constants for hydrogenation to the unsaturated alcohol versus to the saturated aldehyde, which were found to vary by up to an order of magnitude as a function of Pt content in the catalyst in spite of the fact that the hydrogenation steps are presumed to occur on Cu, not Pt, sites (Figure 68). In general, significant changes in equilibrium and kinetic parameters were seen across the series of $CuPt_x$/SBA-15 catalysts tested versus the value of x (the molar

https://doi.org/10.1021/acs.chemrev.1c00905
Chem. Rev. XXXX, XXX, XXX−XXX

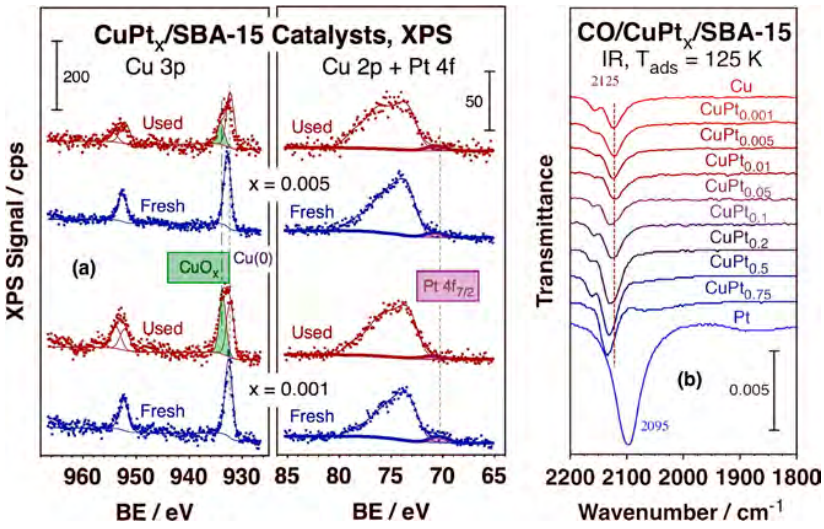

Figure 67. Surface characterization of $CuPt_x$/SBA-15 SAA catalysts.[808] (a) Cu 3p (left) and Cu 2p + Pt 4f (right) XPS data showing the presence of a layer of CuO_x in these catalysts, especially after use. The detection of Pt was marginal, perhaps because of the low concentrations but also possibly because those atoms may be located in the NP subsurface. (b) IR spectra of carbon monoxide adsorbed on these catalysts at 125 K as a function of composition (Pt molar fraction x). Only a peak at 2125 cm^{-1}, associated with Cu, is seen with all samples but that made out of pure Pt; no evidence for surface Pt could be identified in any of the SAA. Adapted with permission from ref 808. Copyright 2019 American Chemical Society.

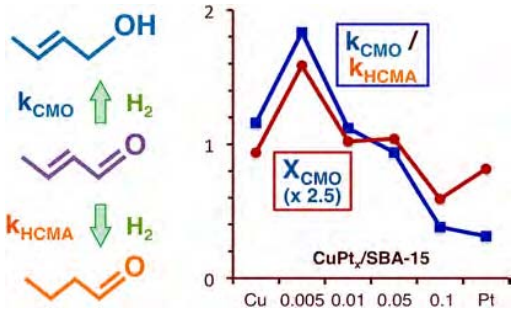

Figure 68. Kinetic trends for the hydrogenation of unsaturated aldehydes promoted by $CuPt_x$/SBA-15 SAA catalysts as a function of composition.[822] After a rapid increase in the ratio of reaction constants for the formation of the unsaturated alcohol (k_{CMO}) versus the hydrogenated aldehyde (k_{HCMA}) with the addition of a small fraction of Pt (0.5 mol %) to supported Cu catalysts, that ratio, which correlates with the selectivity toward the production of the desired product (X_{CMO}), decreases monotonically with increasing Pt content. Clearly, Pt not only helps with H_2 activation but also affects selectivity. Reproduced with permission from ref 822. Copyright 2020 American Chemical Society.

fraction of Pt in the bimetallic NPs), indicating that the addition of even small amounts of Pt to these Cu SAA catalysts affects the intrinsic performance of the hydrogenation catalytic sites. A possible explanation for these observations can be suggested on the basis of a recent alternative theory for the behavior of SAA catalysts put forward by the Sykes group where the electronic properties of the active metal atom (Rh in the case of that report) is modified, by virtue of its isolation in a matrix of the second element (Cu), to such an extent that they can promote organic conversions selectively in a way that they cannot when in bulk solid form.[850] In this scenario, it may be that it is the active metal (Pt, Pd, Rh) in its isolated form that carries out all catalytic steps. For all these reasons, the model for functioning SAA catalysts obtained from studies under UHV still await validation or reconsideration based on testing *in situ* under catalytic conditions.

On the whole, the potential of SAA catalysts in applications where catalytic selectivity needs to be improved is still been tested. The range of reactions for which they may be useful is somewhat narrow, at least at the present time, and issues of stability still need to be worked out. As mentioned above, even the simple bifunctional model used to describe their mode of operation is in question. It is convenient to envision the minority element in these SAAs as an isolated atom in a sea of the main metal, but it is clear that the components of metal alloys interact strongly with each other: the prevalent picture of bimetallic catalysts typically involves extensive electron mixing and charge transfer across the constituent metals leading to an average metallic behavior which can be described, to a first approximation, by the position of the center of the *d* band.[851−853] There is also the issue of the diffusion of metal atoms in and out of the bulk and onto the surface, a behavior that is quite dynamic and affected by the chemical environment above the surface.[854] It is not clear what the actual composition of the surface of the catalyst may be during reaction, or how far the influence of the minority element extends in terms of depth (distance from the surface). There is no doubt that these SAAs exhibit unique behavior that in several instances lead to improvements in catalytic selectivity, but generalization of this approach requires a better understanding of how they work.

4.4. Non-Metallic Sites

The design of single-site catalysts has mainly focused on isolated metal atoms, but other non-metallic centers can be conceived as well. In previous sections we have addressed the idea of adding molecular single sites to surfaces by, for instance, tethering, grafting, or immobilizing discrete molecules or moieties (Section 2). Here the focus is on single sites intrinsic to the surface of the solid used as catalyst.

The most obvious example of this is the Brønsted-acid sites associated with the terminal hydroxyl groups present on the

https://doi.org/10.1021/acs.chemrev.1c00905
Chem. Rev. XXXX, XXX, XXX−XXX

surface of many oxides; this is a well established type of catalytic site that has been studied in great detail for a number of decades.[855,856] Because many oxides in high-surface-area form (as often required in catalysis) are amorphous and display widely heterogeneous structures, surface hydroxyl groups can be found in a variety of local environments. One piece of evidence for this comes from IR absorption spectroscopy data: the signal for the O−H stretching mode of surface hydroxyl groups in oxides such as silica extends from approximately 2800 to 3800 cm^{-1}.[855,857−859] However, better defined sites can be isolated in crystalline oxides, in particular in zeolites.[860] Brønsted-acid sites in such crystalline aluminosilicates have been thoroughly characterized by multinuclear solid-state NMR spectroscopy,[861] and also titrated using appropriate molecules such as pyridines,[862,863] acetonitrile,[864] or carbon monoxide.[865,866] The role of those sites has been investigated in detail by Zecchina and coworkers in connection with the adsorption of small molecules such as H_2, CO and NO, and also in reference to the polymerization of ethylene.[867] Many correlations between the nature of the Brønsted-acid sites and catalytic activity have been reported.[686,866,868] In one report, different zeolites were shown to exhibit different distributions of Brønsted-acid sites on the basis of the different features detected in IR spectra in the O−H stretching region (Figure 69). Several surface species were evident: (1) a main band with

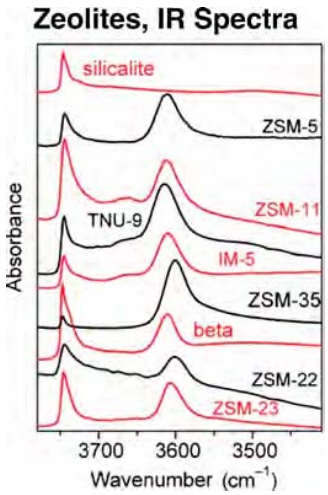

Figure 69. IR absorption spectra in the O−H stretching mode region for a family of zeolites.[869] These data illustrate the presence of several well-defined and distinct Brønsted-acid sites on the surfaces of these solids. Reproduced with permission from ref 869. Copyright 2012 Wiley-VCH Verlag GmbH & Co. KGaA, Weinheim.

a maximum at 3745 cm^{-1} with a tail extending to 3700 cm^{-1} associated with the ν(OH) stretching mode of free or very weakly perturbed silanol groups; (2) a feature in the 3616−3605 cm^{-1} range attributed to the ν(OH) mode of Si(OH)Al Brønsted sites; (3) a weak band at 3665 cm^{-1} due to extra-framework Al species (seen only in a few of the zeolites); and (4) a broad tail extending below 3500 cm^{-1} associated with interacting silanol groups from internal defects.[869] Each of these sites may play different and unique roles in catalysis.

The surfaces of many oxides expose Lewis-acid sites as well. Typical examples here are aluminas and aluminosilicates.[870−872] It is also common to create additional Lewis-acid sites on crystalline zeolites via substitutional exchange of some of the original cations with elements such as Mg, Ti, Zr, V, Nb, Ta, Mo, Ga, Sn, and other metal ions.[873−879] The acidity of those sites is centered at the metal ion, which can be found in a variety of environments on the surface, surrounded by structurally different ensembles of oxygen atoms.[695,870] For this reason, Lewis-acid sites in oxides may be less well-defined than their Brønsted counterparts. Nevertheless, they are capable of promoting a number of complex reactions selectively, especially in applications where hydrocarbon conversions are central such as in oil refining and the processing of biofuels and chemicals.[880−886] For instance, in aluminosilicates, the Busca research group established that Lewis-acid sites with alumina-like acid−base neighbors are more selective for the promotion of the dehydrogenation of ethanol to ethylene, whereas Lewis-acid sites with silica-like covalent neighbors catalyze the production of diethyl ether instead.[887,888] In another example, *operando* time-resolved IR spectroscopy was used to determine that in the selective catalytic reduction (SCR) of nitric oxide, the key step is a reaction with ammonia coordinated to the vanadia Lewis-acid sites present on vanadia-tungsta-titania mixed oxides (Figure 70).[889]

Brønsted- and Lewis-acid sites, intrinsic to many oxide supports, are often combined with other added atoms or moieties to create a more complex and selective catalytic site. This approach is common in the design of catalysts, but both making well-defined dual sites on support surfaces and obtaining direct proof that these sites act synergistically and are responsible for the catalysis is difficult. The key is to produce a final site where two or more components work cooperatively to facilitate the adsorption and/or surface conversion of the reactants; we make a distinction here between this type of cooperative effect to stabilize a single transition state during reaction and other types of bifunctionalities, some of which are mentioned in other places within this review (see, for instance, Section 2.5).[250] One example of the synergy addressed in this paragraph is that seen in the interface sites between metal NPs and their oxide supports. Much has been made, for instance, of the role of those in oxidation and photocatalytic reactions promoted by Au NPs dispersed on certain oxides such as titania or ceria;[890,891] in addition to quantum mechanics and molecular dynamics calculations,[892,893] the role of the interface sites has been nicely demonstrated experimentally by a series of experiments with model so-called inverse catalysts, in which submonolayer coverages of the oxide are deposited on a Au surface to maximize the number of mixed metal-oxide sites.[894,895] However, although the metal/oxide interface sites may be unique and contribute to catalysis, only limited progress has been made to create those in a controlled manner, as single sites. Similar arguments have been made in studies on the selective hydrogenation of unsaturated aldehydes with Pt-based catalysts.[896] A better example for our discussion is that of the conversion of organic compounds on surface-derivatized catalysts aided by adjacent acid sites. Take, for instance, the case reported by the Iwasawa group where C−C bond-forming conversions such as cyano-ethoxycarbonylation, the Michael reaction, and nitro-aldol condensation were promoted using a catalyst with silica-alumina-supported amine groups (Figure 71, top);[897,898] the presence of adjacent Brønsted-acid sites on the support was invoked to explain the stabilization of the reaction intermediate (Figure 71, bottom). It should be said, though, that the evidence for this is quite indirect. Similar

https://doi.org/10.1021/acs.chemrev.1c00905
Chem. Rev. XXXX, XXX, XXX−XXX

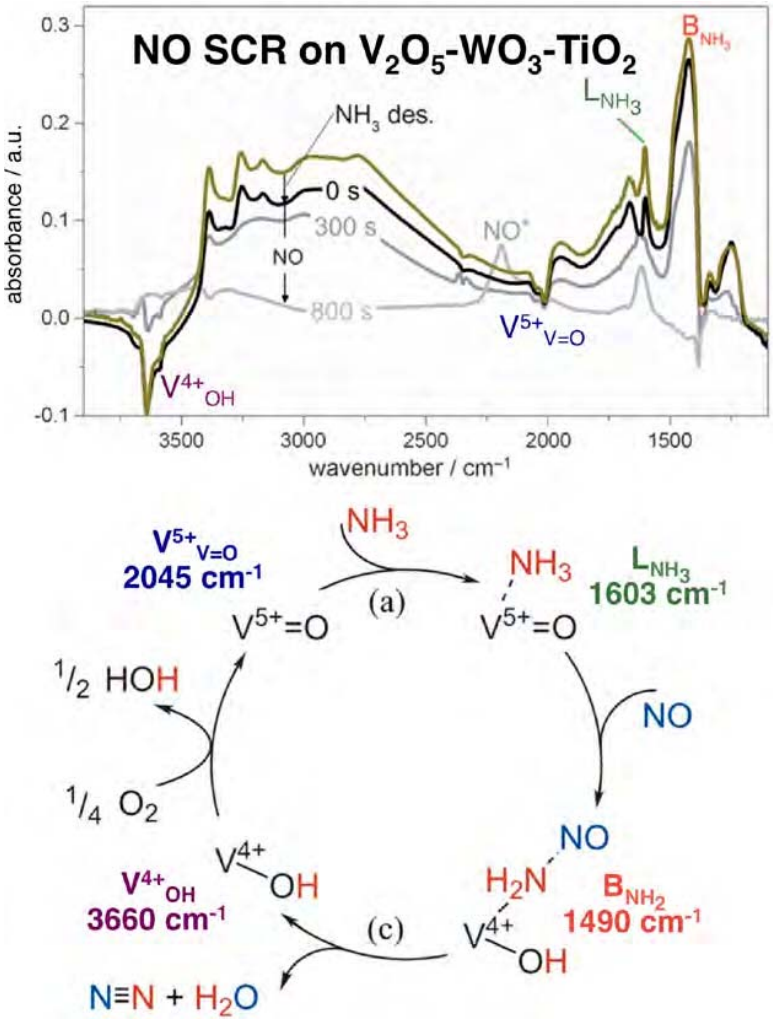

Figure 70. Example of the critical role of Lewis-acid sites in catalysis, in this case for the SCR of NO on V_2O_5–WO_3–TiO_2 mixed oxides.[889] Top: *Operando* transient diffuse-reflectance IR Fourier transform spectroscopy (DRIFTS) data versus time, highlighting the features of key intermediates. Bottom: Reaction mechanism proposed on the basis of the DRIFTS data. Notice in particular the central role played by the Lewis-acid site (L_{NH3}, 1603 cm^{-1}), which helps with ammonia adsorption; by contrast, the Brønsted-acid site (B_{NH2}, 1490 cm^{-1}) is believed to be an spectator. Reproduced with permission from Ref 889. Copyright 2016 Wiley-VCH Verlag GmbH & Co. KGaA, Weinheim.

examples of cooperative acid–base dual sites for catalysis have been reported by others.[180,290,899,900]

Oxide single sites can also be prepared via the controlled deposition of the oxide of a metal on a support made out of a different oxide, to create an active phase not present in the original support.[901] One good example of this approach is the case of catalysts made for the oxidative dehydrogenation of small alkanes (ethane, propane), for which oxides of early transition metals that can exist in several oxidation states such as Cr or V are dispersed on a solid such as silica or alumina (the example in Figure 70 falls within this category).[902] These systems have been studied extensively by several research groups, yet some of the mechanistic details are still in dispute.[903] In particular, it is not clear if isolated MO_x units are more or less effective than small oxide cluster in promoting these reactions. Iglesia, Bell, and coworkers early on reported that vanadia dispersed as isolated monovanadate species are prevalent at low surface densities and are slightly more selective for alkane dehydrogenation reactions that more extended vanadium oxide structures,[904] but a more comprehensive study by Schlogel and Wachs highlighted constant catalytic specific activity (TOFs) as a function of surface vanadia coverage, from which it was concluded that surface VO_4 monomers and V_xO_y oligomers exhibit the same activity (Figure 72, main plot).[905] That group also found a strong effect exerted by the support, which they ascribed to the critical importance of bridging mixed-oxide sites such as Zr–O–V (Figure 72, inset).[905] In a related matter, the oxidation state of the metal in the supported oxide has been determined to affect catalytic behavior: low oxidation states such as V^{3+}, which can act as Lewis acids, have been found to be more active than higher (V^{5+}) oxidation states.[906,907] However, contradictory assignments of those sites to monomers versus oligomers have been given by different research groups. Ultimately, it is clear that specific mixed-oxide sites are required to promote alkane dehydrogenations efficiently and selectively, but that the exact nature of those sites or a way to produce them systematically awaits further research.

In general, oxide sites made out of single units or of small oxide clusters have proven quite useful in catalysis, yet their

https://doi.org/10.1021/acs.chemrev.1c00905
Chem. Rev. XXXX, XXX, XXX–XXX

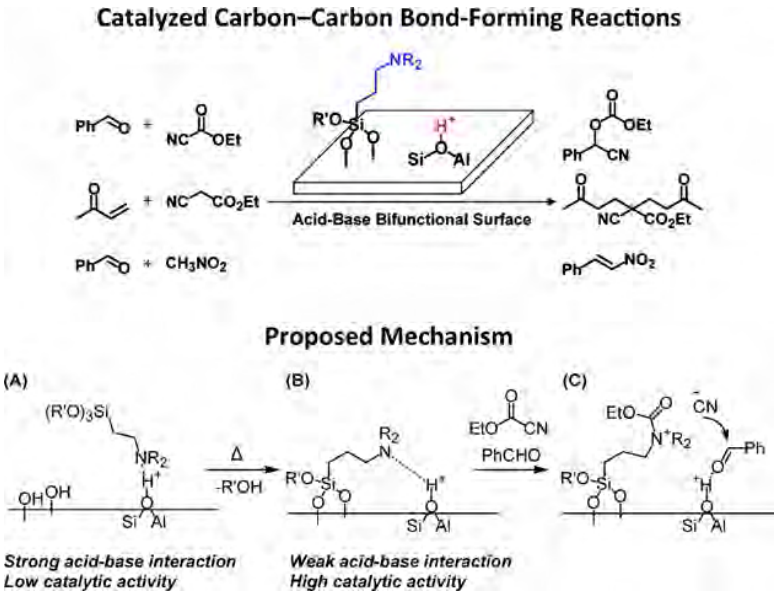

Figure 71. Example of a catalyst with acid and base cooperative sites.[897] This catalyst, which consists of silicoalumina-supported amine groups, was shown to be capable of promoting a number of organic C−C bond-forming reactions (top). The proposed mechanism involves the stabilization of the intermediate in the transition state by adjacent surface hydroxyl groups (bottom). Reproduced with permission from ref 897. Copyright 2007 American Chemical Society.

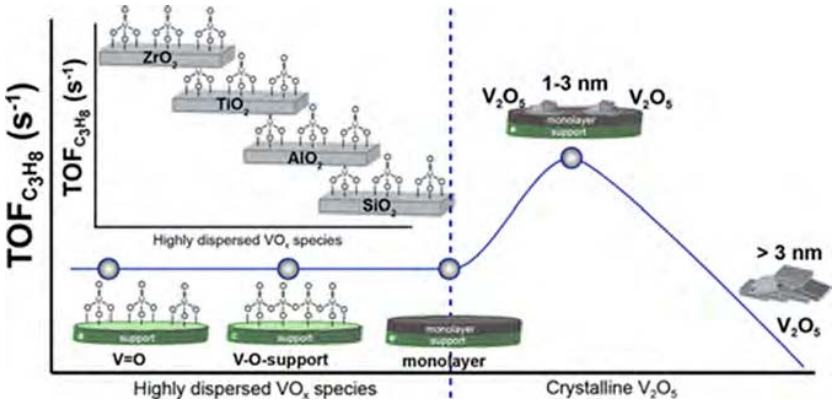

Figure 72. Trends in the behavior of supported vanadium oxide catalysts for the selective dehydrogenation of alkanes.[905] Main plot: Propane TOF versus VO_x surface coverage, showing a gradual transition from VO_4 monomers (with terminal V═O bonds) to V_xO_y small oligomers. Inset: TOFs versus the nature of the support. Reproduced with permission from ref 905. Copyright 2014 American Chemical Society.

synthesis in a controlled fashion is in general quite difficult. In most examples available to date the preparation of such catalysts has been done using conventional synthesis methods and has led to a distribution of sites; better control of what is made could potentially afford better selectivities, but that is still to be proven. Films made out of two-dimensional (2D) materials are also primed for the preparation of single sites on solid catalysts, and those can be made with better-designed surface sites.[908−911] A detailed discussion of these materials will be provided latter in this review (Section 6.4).

5. NOVEL NANOSTRUCTURES: METALS

Up to now, we have discussed different ways by which appropriate solids can be modified to alter or create specific surface sites to add selectivity in catalysis. Alternatively, such solids may be synthesized using sophisticated nanotechnologies to intrinsically display novel structures, exposing surfaces with atomic ensembles that may define useful catalytic sites. In the next sections, we review different ways by which this approach can be implemented. In this section, we focus on metal nanostructures, and in the next on nanostructures made out of other types of materials.

5.1. Colloidal Nanoparticles (NPs)

One established procedure for producing well-defined metal NPs is by using either colloidal or reverse micelle chemistry, a methodology by which organic surfactants are used to direct the growth of NPs via the slow and controlled incorporation of atoms from dissolved metal salts into initiating nuclei.[912−916] In its simplest version, colloidal chemistry can be used to synthesize monometallic NPs with narrow size distributions, but new methodology has also been advanced to control their shape.[917−919] The use of colloidal metal NPs in catalysis has in fact a long history[920] but has gained renewed interest thanks to new advances in synthetic methodology as well as in catalyst designs.

https://doi.org/10.1021/acs.chemrev.1c00905
Chem. Rev. XXXX, XXX, XXX−XXX

In the early reports of the use of metal colloidal NPs in catalysis, the reactions were often carried out in solution. This places those systems in a category in between homogeneous and heterogeneous catalysis.[915,921,922] Many examples have been provided by the El-Sayed group. In their study on the use of Pd NPs for the promotion of C−C bond-forming reactions (the Suzuki reaction in particular),[923] for instance, they identified and characterized a side process that leads to NP size growth as the catalytic reaction proceeds.[924] Such dynamic behavior in colloidal NPs, where changes not only in size but also in shape are intertwined with the catalytic chemistry, make it difficult to pinpoint the nature of the catalytic sites responsible for the promotion of reactions.[925] A more general argument is still ongoing on the homogeneous versus heterogeneous nature of the Pd catalyst in these coupling reactions,[926−931] with some reports claiming that the metal is in colloidal form,[932−935] and even citing NP size effects on catalytic performance.[914,936] Colloidal NPs suspended in solution have also been used to catalyze hydrogenation (and related) reactions,[937−943] and for the promotion of electron transfer processes.[944−946] A recent example of the latter is that of Quinson and coworkers, who tested the effect of particle size on the activity for the ORR by preparing four catalysts with average diameters varying from 1 to 5 nm using a surfactant-free synthesis in alkaline ethylene glycol and controlling and keeping constant all other parameters (Figure 73).[947] They showed that the intrinsic activity of the Pt sites is only weakly dependent on NP size.

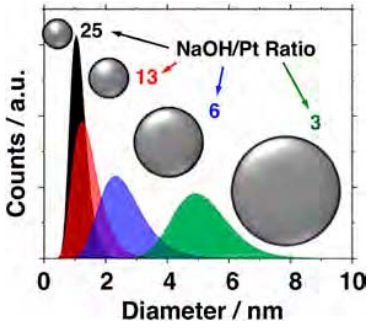

Figure 73. Size distribution of colloidal Pt NPs made using a surfactant-free polyol process in alkaline ethylene glycol.[947] The average size was controlled by varying the molar ratio of NaOH to the Pt precursor (H_2PtCl_6). Reproduced with permission from ref 947. Copyright 2018 American Chemical Society.

More common, and more relevant to this review, is the use of colloidal chemistry to synthesize metal NPs for dispersion on solid surfaces to produce high-surface-area heterogeneous catalysts.[51,948−951] In terms of tests of catalysts made by dispersing colloidal NPs on solid supports as a function of metal NP size, the Somorjai group has published a number of examples,[21] on the hydrogenation of cyclohexene and 1,4-cyclohexadiene,[952,953] of benzene and toluene,[954] and of crotonaldehyde,[955] on the hydrogenation and hydrogenolysis of pyrrole,[956] on the ring opening of methylcyclopentane,[957] and on the decarbonylation of furfural,[958] all on mesoporous-silica-supported Pt catalysts, as well as on the hydrogenation of CO_2 over Co/mesoporous silica[959] and on the oxidation of carbon monoxide over a Ru/Si(100)-wafer.[960] Various degrees of changes in activity and selectivity were identified for the different reactions as a function of metal NP size, which was varied between about 1 and 10 nm, and the observed trends were used to argue for the relative relevance of terrace versus edge (low-coordination) sites in catalysis. For instance, in the case of the conversion of 1,3-butadiene on Pt catalysts, selectivity was found to switch from a preference for full hydrogenation to butane with small NPs to a dominance for the production of half-hydrogenated 1-butene with NPs larger than ∼2 nm (Figure 74).[948,961] On the basis of vibrational

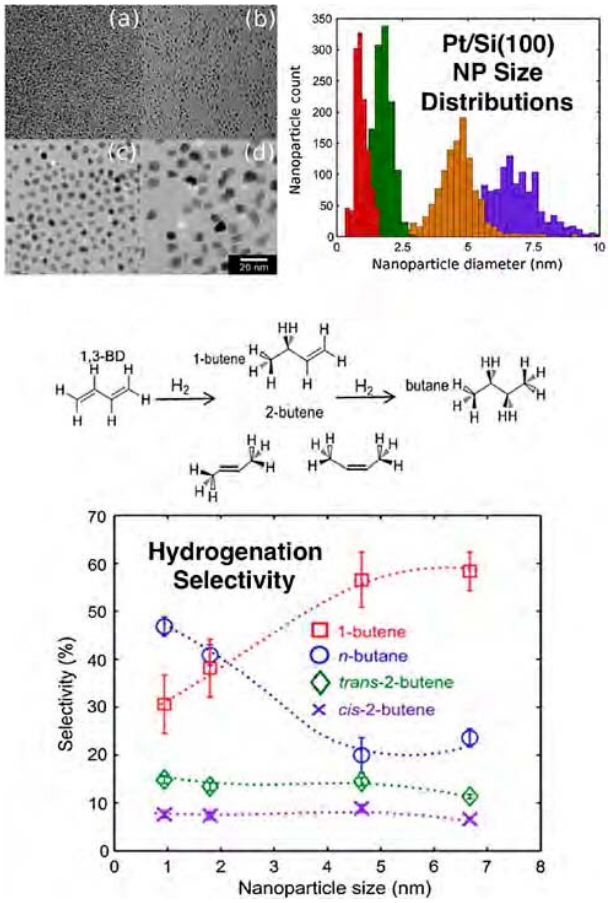

Figure 74. Results from the study of the effect of the size of the Pt NPs in Pt/Si(100) catalysts made by using colloidal chemistry on the selectivity of the hydrogenation of 1,3-butadiene.[948,961] Top: TEM images (left) and estimated NP size distributions (right) for four different catalysts. Middle: Reaction sequence. Bottom: Product selectivities as a function of Pt NP average size. Reproduced with permission from ref 948. Copyright 2015 Elsevier Inc.

spectra, this behavior was explained by a change in the regiochemistry of the pi adsorption mode of the first reaction intermediate, from a terminal to a central position of the remaining C═C double bond; presumably, the former favors full hydrogenation to the alkane whereas the latter stops at the formation of the alkene. The authors suggested that the prevalence of low-coordination sites in small Pt NPs promotes the insertion of hydrogen atoms at the internal carbon atoms, but provided no specific reasoning for why that should be so (other than possible steric and/or electronic effects). A few additional examples are available from other groups on this type of size-reactivity correlations with colloidal-made catalysts, including work on the hydrogenation (Fischer-Tropsh)[962−966] and oxidation[960,967] of carbon monoxide, but

https://doi.org/10.1021/acs.chemrev.1c00905
Chem. Rev. XXXX, XXX, XXX−XXX

well-controlled work in this area is still sparse.[51,54,968] Regardless, what is clear is that by varying the fraction of low-coordination sites in metal NPs via the systematic variations of their size it is possible to control selectivity in some catalytic reactions. The colloidal synthesis of NPs affords this control.

A particularly interesting case of catalytic performance dependence on metal NP size is with Au, because bulk Au is typically inert but in NP form (and dispersed on certain reducible supports) it has been shown to be quite good at promoting a variety of reactions.[969−973] There seems to be a "sweet spot" in terms of NP diameter for these catalysts to work,[974,975] and colloidal chemistry is ideal for the production of NPs with the desired sizes and with narrow distributions and a good degree of homogeneity.[916] A nice example of how catalytic performance can be optimized in complex reactions involving organic reactants by tuning the Au NP size using colloidal chemistry was provided recently by Fenger et al., who showed that the activity for the catalytic reduction of *p*-nitrophenol to *p*-aminophenol with sodium borohydride is maximized at Au NP average diameters around 13 nm; drops of about an order of magnitude in reaction rate were seen with either smaller or larger NPs (Figure 75).[976] Similar trends have

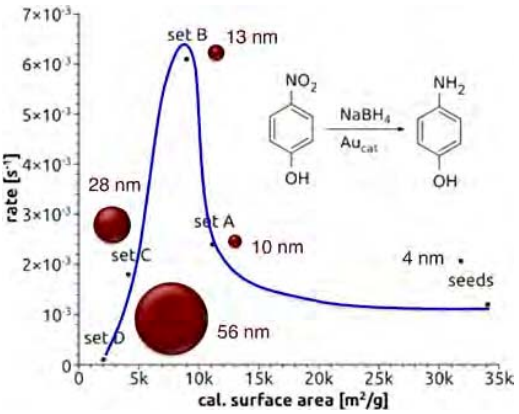

Figure 75. Dependence of catalytic activity for the hydrogenation of *p*-nitrophenol to *p*-aminophenol on Au NP size.[976]

been reported by others.[977,978] The reason for this "magic" size in the performance of Au NP catalysts is still being debated,[979,980] and several factors have been considered, including quantum effects due to the thickness of the NPs,[981,982] the density of low-coordination sites,[983] and interactions with the support leading to the formation of special metal/oxide interface sites,[890,984] but none have been definitively proven to be dominant. This question needs to be answered if the ability afforded by colloidal chemistry to produce metal NPs with specific sizes (and shapes) is to be fully exploited.

Recent developments in colloidal chemistry have added a new dimension to its use in catalysis, in that it is now possible to control not only the size but also the shape of the metal NPs. By using NPs with specific shapes, it is possible to design catalysts with only specific surface crystallographic planes exposed. The most common forms of colloidal NPs, beside spherical, are cubic and octahedral, which in fcc metals expose the most thermodynamically stable surfaces, mainly (111), (100), and (110) facets (Figure 76).[918,985−987] As discussed next, this can be used to control activity and selectivity in catalysis: much has been made over the years of the role of low-coordination metal sites in supported catalysts as particularly active sites (hence the differences in performance with varying NP size discussed above),[988−992] but modern surface-science experiments using model systems, mainly metal single crystals, have also indicated that many catalytic reactions are affected by the nature of the basal planes.[840,842,993−995] There have been interesting advances reported on the synthesis of colloidal NPs with less conventional shapes as well,[918,922,987,996−1000] some exposing high-Miller-index surfaces, but the incorporation of those in catalytic studies has to date been limited.

In solution, the use of colloidal metal NPs of specific shapes to demonstrate catalytic selectivity has been pioneered by the El Sayed group,[921,1001−1004] and advanced further by others.[991,1005−1009] Figure 77 provides an example of this shape selectivity in electrocatalysis, a dependence of formic acid oxidation on Pd NP shape.[1010] By smoothly transitioning from cubic to octahedral structures, the authors were able to tune the ratio of (100) (green in Figure 77) to (111) (yellow) surfaces exposed, and that way show that the former are several times more electrocatalytically active than the former. Most of this solution shape-sensitivity work has focused on electrocatalytic processes, but thermally activated reactions have been probed as well.[914,915,1011,1012] An example was provided by the Li group:[1013] they synthesized Ag NPs with three different shapes, namely, nanocubes, near-spherical NPs, and truncated triangular nanoplates (which again provide a way to transition from all (100) to all (111) exposed facets), and determined that the catalysts display decreasing activity during the oxidation of styrene with *tert*-butylhydroperoxide following that progression. In both cases, it appears that the less thermodynamic (100) surfaces are more active, although it is not clear yet how general this conclusion may be. No molecular-level explanation for the differences observed was provided in either report.

As in the case of NP with different sizes, the ability to synthesize colloidal metal NPs with specific shapes has been exploited in heterogeneous catalysis mainly as a way to premake those NPs before dispersing them onto high-surface-area supports. Several examples have been reported on the shape selectivity of catalytic reactions using this approach.[50,51,1014,1015] Metal-NP-promoted catalytic reactions that have shown shape selectivity include the hydrogenation of olefins, alkynes, and aromatics,[1016−1022] which is surprising given that traditionally these reactions have been considered to be structure insensitive.[8,1023] Nevertheless, variations in performance have been seen as the metal NP shapes are varied. The effect is not large, however, and although it appears that (100) planes are in general more active than (111) surfaces (with late transition metals such as Pt, Pd and Rh, at least), that conclusion is not universal.[51] A few examples are also available for the hydrogenation of unsaturated aldehydes[1024−1028] and of nitro compounds,[1029] and also for isomerization[1030,1031] and hydrogenolysis processes.[957,1032] In an example from our laboratory, catalysts prepared with tetrahedral[1033] and cubic[1020] Pt colloidal NPs were used to control selectivity during the isomerization of 2-butenes.[48,1034] Extensive surface-science experiments using model single-crystal surfaces,[1020,1034−1040] together with quantum mechanics calculations,[1034,1041−1043] had indicated that (111) planes have a particular preference for stabilizing the cis isomer (because the adsorption of the trans isomer induces an energy-costly

https://doi.org/10.1021/acs.chemrev.1c00905
Chem. Rev. XXXX, XXX, XXX−XXX

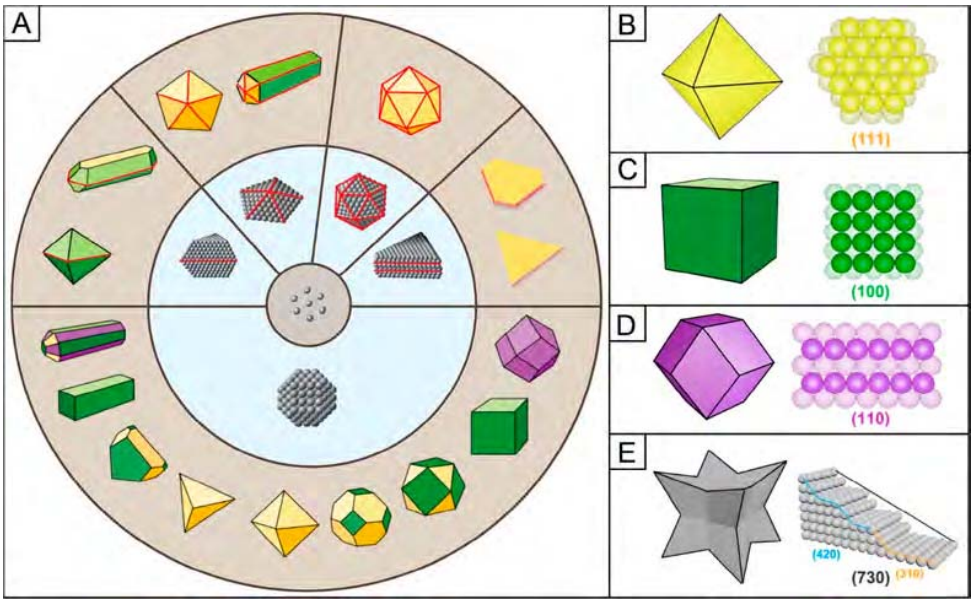

Figure 76. Correlation between NP shape and the type of facets exposed for fcc metals.[987] (A) Shapes (outer ring) and corresponding seeds used during growth (middle ring). (B–E) Main planes exposed in (B) octahedral, (C) cubic, (D) rhombic dodecahedral, and (E) star-like NPs. Reproduced with permission from ref 987. Copyright 2021 American Chemical Society.

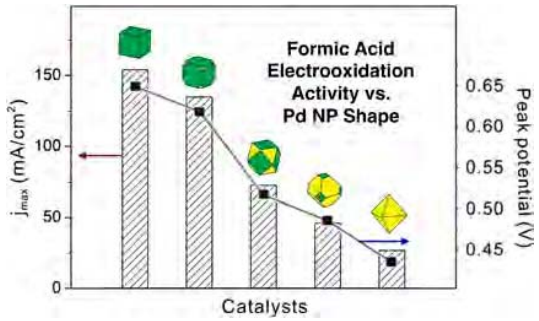

Figure 77. Dependence of catalytic activity for the electrooxidation of formic acid in solution on Pd NP shape.[1010] The green surfaces in the NP shape schematics represent (100) facets, the yellow color (111) ones. Adapted with permission from ref 51. Copyright 2013 Wiley-VCH Verlag GmbH& Co. KGaA, Weinheim.

reconstruction of the surface), and this was corroborated with the shape-selective dispersed Pt NPs: spherical Pt NPs promote the expected transformation of cis- to trans-2-butene, but tetrahedral NPs, which expose (111) facets, favor the conversion of trans-2-butene to its less thermodynamically stable but more desirable cis isomer (Figure 78).[1034]

Shape selectivity has also been tested for demanding reactions, oxidations in particular. On the basis of catalytic studies using supported colloidal Rh NPs with nanocube and different nanopolyhedra shapes, CO oxidation was initially reported to be surface insensitive,[1044] but later reports claim to have seen differences in catalytic activity with metal NPs of different shapes,[1045−1047] presumably because of higher activity on low-coordination sites and of self-poisoning on (111) facets (due to a higher CO adsorption energy). Pt(100) surfaces have also been shown recently to be more active than Pt(111) facets during the oxidation of glycerol,[1048] but Pd(111), not Pd(100), facets were reported to promote the oxidative coupling of CO to dimethyl oxalate[1049] as well as the production of hydrogen peroxide from $H_2 + O_2$ mixtures.[1050] Also, Pd and Pt edges were found to promote the oxidation of 2-propanol[1051] and 1-phenylethanol,[1048] but, curiously, not the oxidation of 2-butanol.[1052] For epoxidation reactions catalyzed by Ag, nanowires were shown to be highly selective, an observation that was ascribed to a lower activation barrier for the formation of surface oxametallacycle intermediates on the (100) facets.[1053−1056] Overall, no clear trends have been identified yet for the dependence of these oxidation reactions on surface structure. A word of cautions is also warranted in cases where the reactions are highly exothermic or require harsh temperature and pressure conditions, since the excess energy in those cases may induce a change the shape of the original NPs under reaction conditions.

5.2. Dendrimer Encapsulated Metal Nanoparticles

Another way to produce metal NPs with precise sizes is by using dendrimers as scaffolds. The use of these so-called dendrimer-encapsulated NPs (DENs) was pioneered by Crooks and coworkers.[1057−1060] In this methodology, dendrimers, which are repetitively-branched polymers, are used as templates and stabilizers, taking advantage of their monodispersity and spherical shape. It has been shown that metal ions can be complexed by interior functional groups such as amines in polyamidoamine (PAMAM) starburst dendrimers; by carefully titrating those groups, the number of complexed metal ions per dendrimer can be controlled with nearly atomic precision.[1061,1062] Further chemical reduction of theoe composites *in situ* leads to the formation of metal clusters encapsulated inside the dendritic structure (Figure 79, top).[1063] The size of the DENs can be predetermined by selecting the number of complexing groups in the organic structure, which can be tuned by choosing specific monomers and fixing the number of generations (layers) in the dendrimer, and/or by carefully selecting the ratio of metal ions added to each dendrimer structure. Excellent control in metal NP size, with very narrow distributions, can be obtained this way, in particular in the low (≤ 2 nm) size range (Figure 79,

https://doi.org/10.1021/acs.chemrev.1c00905
Chem. Rev. XXXX, XXX, XXX−XXX

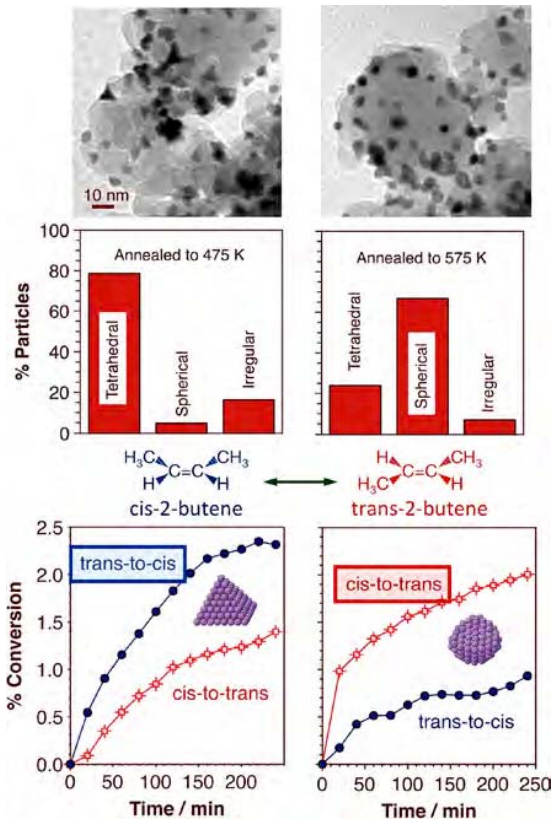

Figure 78. Example of shape selectivity.[1034,1038] Top: TEM images of catalysts made by dispersing colloidal tetrahedral Pt NPs on a silica support after cleaning and annealing to 475 (left) and 575 (right) K. The tetrahedral shape is preserved after the low temperature treatment, but lost to the formation of spherical NPs at higher temperatures. Middle: statistical analysis of the distribution of tetrahedral versus spherical NPs for both cases. Bottom: Catalytic activity, in the form of product accumulation versus time in a batch reactor, for the cis-to-trans (red) and trans-to-cis (blue) isomerization of 2-butene. Unique preferential cis-to-trans selectivity is only seen with the tetrahedral NPs, which expose (111) facets. Adapted with permission from ref 1038. Copyright 2011 the Owner Societies.

bottom).[1064] Following Crooks' early reports of DENs, others appeared in the literature shortly thereafter, and those helped further develop this methodology for controlling NP size.[1065−1067]

Crooks also pioneered the use of these DENs as catalysts. In solution-based catalytic applications, the dendrimer serves not only as a template for the preparation of the DENs but also as a nanoreactor and as an agent to stabilize the metal NP; it helps tune solubility, and enhances catalytic selectivity.[1063] Because of the high molecular weight of dendrimers, catalyst separation is also facilitated this way, and if magnetic NPs are added, even more separation options become available.[1068,1069] Already in their early reports of DENs, the Crooks group tested their newly developed nanostructures, (G4−OH(Pt_{60})/(Au electrode) in particular (where G4-OH stands for a 4th-generation hydroxyl-terminated PAMAM dendrimer), for the electrochemical reduction of O_2.[1057] Subsequent examples from the same group include the promotion of the hydrogenation of C=C double bonds,[1070,1071] and of various C−C coupling reactions.[1072] Other groups have provided additional cases of DEN-promoted reactions, hydrogenations and

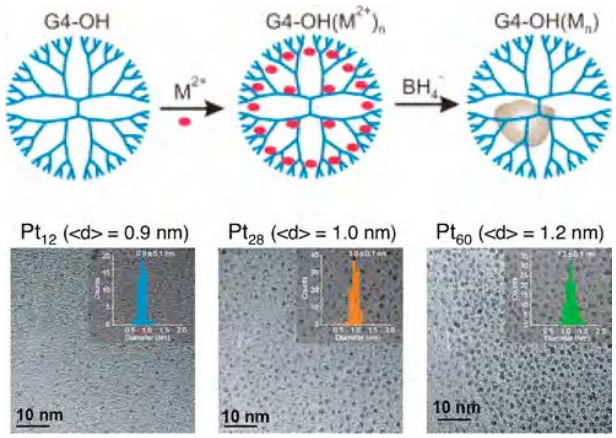

Figure 79. Top: Schematic representation of the synthesis of DENs.[1057,1063] Bottom: TEM images and size distributions for three Pt DENs obtained by controlling the ratio of Pt atoms to dendrimer structures; a phenylazomethine dendrimer with tetraphenylmethane was used as the core in this case.[1064] Reproduced with permission from ref 1064. Copyright 2014 American Chemical Society.

couplings[924,1073−1078] as well as other processes.[1011,1079−1085] The power of using DENs as catalysts is that, thanks to the precise synthetic control afforded by the dendrimer-based route, it is possible to test subtle trends in catalytic activity as a function of metal NP size with them. Several examples have been reported for this.[1071,1075,1082,1086−1090] In one case, the activity of Cu-PAMAM-DEN catalysts for the selective hydrogenation of carbonyl versus olefin groups in unsaturated aldehydes was found to drastically decrease with NPs containing 40 or more Cu atoms (Figure 80).[1091] The reasons for this were not explored by the authors.

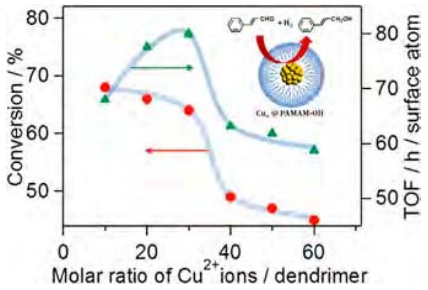

Figure 80. Total conversion and TOF for the hydrogenation of cinnamaldehyde promoted by Cu-PAMAM DEN catalysts as a function of the Cu^{2+} ion:PAMAM ratio used in the synthesis, which defines the final Cu NP size.[1091] A clear size effect is evident from the data. Adapted with permission from ref 1091. Copyright 2013 American Chemical Society.

The structure of the dendrimer may also be used to add selectivity to catalytic processes. In fact, dendrimers by themselves have been shown to act as catalysts for some conversions. Such dendrimers are often modified to retain metal ions in complexed form, thus displaying chemical properties akin to those of organometallic homogeneous catalysts.[1092−1094] Modification of the endings of dendrimers in DENs can also be used to add further flexibility to their synthesis. The pioneering work in this direction, in particular to add stereo- and enantio-selectivity to dendrimer-based catalysts, was published in the 90's by the Brunner group, who

https://doi.org/10.1021/acs.chemrev.1c00905
Chem. Rev. XXXX, XXX, XXX−XXX

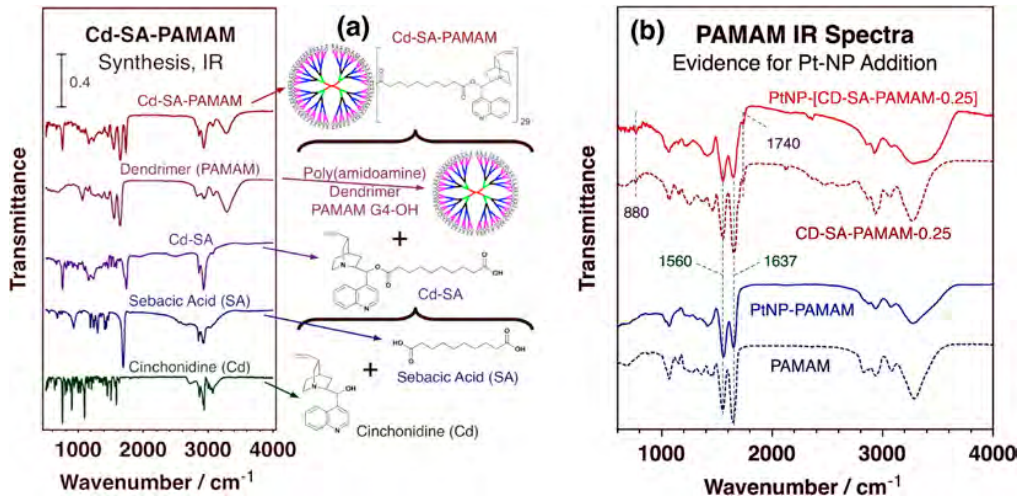

Figure 81. IR data obtained after each step during the synthesis of cinchonidine (Cd)-terminated G4-OH-based Pt DENs.[1105] (a) Evolution of the sample during the synthesis of the derivatized dendrimers, which was carried out by creating a carbamate link between the Cd and the terminal hydroxyl groups of the PAMAM using a sebatic acid (SA) linker, as shown by the scheme in the central part of the figure. (b) IR spectra for regular G4-OH and for the chirally-modified Cd-SA-PAMAM-0.25 (with only 25% of the PAMAM OH groups derivatized) sample before and after the addition of Pt NPs (to make the corresponding chiral DENs, which was evidenced by the change in relative intensities of the amide-II versus amide-I peaks at 1560 and 1637 cm^{-1}, respectively). In additional experiments, Cd was added to the PtNP-PAMAM sample afterward. Reproduced with permission from ref 1105. Copyright 2018 Springer Science+Business Media, LLC, part of Springer Nature.

attempted to add enantioselectivity to the cyclopropanation of styrene[1095] and to the hydrogenation of acetamidocinnamic acid.[1096] The enantioselectivity enhancement obtained then was minimal, but later trials by others have been more successful.[1097] Alternatively, a chiral center may be inserted at the core of the dendritic structure, an approach that has also been shown to add enantioselectivity.[1092,1098−1103] It is important to point out, though, that in that case the catalyst is a metal complex, a structure more akin to homogeneous than heterogeneous catalysts; the main difference is that, because of the large size of the dendrimers, separation after catalysis is easier. It is also potentially possible, although trickier, to use the dendrimer terminations as a way to control selectivity at the surface of the metal NP in DENs. Adding alkyl chains to the ends of dendrimers, for instance, has been recently shown to help grow larger metal NPs,[1104] but the usefulness of this type of modification to tune catalytic selectivity is still not fully realized. We have recently attempted to add enantioselectivity to hydrogenation reactions promoted with Pt/DENs by covalently attaching cinchonidine to the ends of the dendritic structure (Figure 81), but the final result was a suppression of catalytic activity, as the new ending groups appear to increase steric hindrance for the reactants to enter the inside of the DEN structure and access the surface of the metal; this proved to be the case even with only partial dendrimer derivatization.[1105] A different approach is to use chiral dendrimers to grow chiral metal NPs: the feasibility of this route was demonstrated by Pittelkow et al.,[1106] but no catalytic tests were carried out to assess the value of using such unique chiral DENs. More studies are needed to determine the viability of this idea of using chiral dendrimers or modifying the outside of the dendrimer structure to improve on catalytic performance.

One important aspect of DENs as catalysts is the degree of access that the reactants may have to reach the metal NPs, as they travel in solution through the dendritic structure.[1107] Dry DENs are likely to have the organic fragments collapsed, wrapping the metal NPs and blocking access to the metal surface. However, in solution, the organic structure can open up and create channels through which reactants and products can travel. Early on, Crooks showed that the catalytic performance of DENs is affected by the density of functional groups on the dendrimer periphery, specifically by demonstrating that the rate of hydrogenation of alcohols with Pd DENs decreases with increasing dendrimer size (Figure 82).[1070,1108]

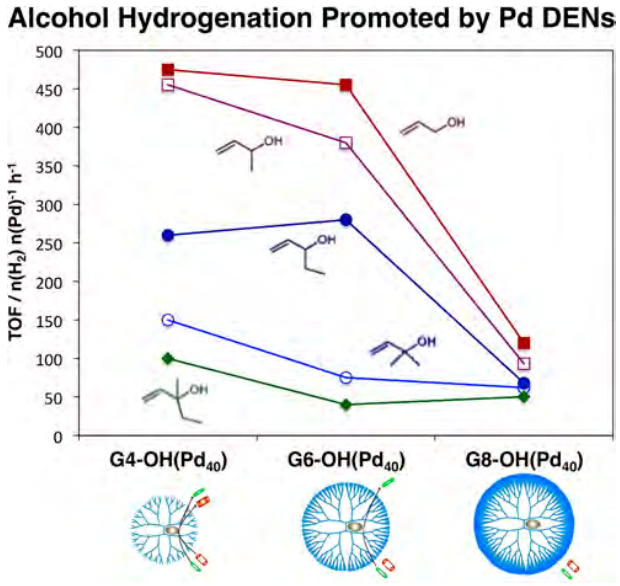

Figure 82. Catalytic activity of Pd DENs for the hydrogenation of several allyl alcohols as a function of the generation of dendrimer used (4th, 6th, and 8th generation hydroxyl-terminated PAMAM dendrimers).[1070] The data indicate that higher generations, which have larger organic structures, slow down the reaction. Adapted with permission from ref 1070. Copyright 2001 American Chemical Society.

https://doi.org/10.1021/acs.chemrev.1c00905
Chem. Rev. XXXX, XXX, XXX−XXX

They concluded that the dendrimer periphery acts as a size- and shape-selective "nanofilter". In a more complete study, Ooe et al. reported similar trends with dendrimer size for the case of the hydrogenation of dienes with Pd/(poly propyleneimine) DENs, and identified additional effects due to the polarity of the reactant.[1109] More recently, we offered more direct evidence of the accessibility of metal NPs in DENs by using *in situ* IR spectroscopy: the adsorption of carbon monoxide on Pt DENs was shown to be limited, weak, and reversible in the gas phase but extensive and stronger in the liquid phase.[1110] *In situ* electrochemical IR detection of CO adsorption on Pt-DENs tethered to carbon electrodes by the Crooks' group has also corroborated the accessibility of molecules to the surface of the metal NPs in solution.[1111]

DENs have also been dispersed onto high-surface-area solids to prepare metal-NP-based heterogeneous catalysts. As mentioned above, dendrimers collapse around the encapsulated NP upon drying, blocking the metal surface[1110,1112] and poisoning gas-phase catalytic reactions,[1113] and therefore need to be pretreated to expose the metal surfaces. This is discussed in more detail below, in Section 5.4. Once activated, however, the metal NPs may exhibit particular catalytic selectivity if the narrow size distribution of the original DEN is preserved. This has been proven in a number of cases. For instance, the Somorjai group has made DEN-based monodispersed Pt and Rh catalysts supported on silica solids for the promotion of the hydrogenation of olefins,[1114] aromatics,[954] and heterocycles[1115] as well as for facilitating C−C[1116] and C−N[1114,1117] bond activations. We have also reported the use of Pt-DEN/SiO_2 catalysts for the promotion of C=C cis−trans isomerization in olefins.[1118] Other reported examples include the catalytic hydrogenation of unreactive olefins,[1119] toluene,[1113,1120,1121] and citral,[1122] the reduction of NO_x by methane,[1123] the reductive amination of aldehydes,[1124] the oxidation of alcohols,[1125] inorganic (ferricyanide to ferrocyanide by thiosulfate) and organic (*p*-nitrophenol to *p*-aminophenol by sodium borohydride) electron transfer (redox) reactions,[1126] aldol condensations,[1127] and electrocatalysis.[1087,1128−1131] In some cases metal NPs have been grown on tethered dendrimers rather than separately (in solution) before dispersion on the solid support,[1132−1135] and a third synthetic approach has been to polymerize DEN monomers (or their metal-complexed dendrimers before reduction) to create a solid catalyst.[1136] In most cases, the main impetus behind the choice of DENs has been the need to control metal NP size in the low-size range. A nice example of how DEN-based supported catalysts can be used to test structure sensitivity in catalysis was provided recently by Huda et al. for the case of the selective oxidation of toluene on carbon-supported metal catalysts; as shown in Figure 83, the activity of this catalysis is dramatically affected by the size of the metal NPs within a very narrow range (in the sub-1 nm regime).[1137] Additional catalytic selectivity was achieved by selecting the appropriate metal (Cu being the best for the mild oxidation to benzyl alcohol, Pt for deep oxidation to benzoic acid).[1137]

The collaborative work of the Toste and Somorjai groups have advanced an interesting twist to the use of supported DENs, in that they exploited the reversibility of the reduction/oxidation of the metal to switch between encapsulated metal NPs and their precursors, the metal ions complexed on the functional groups of the dendrimers.[1138,1139] This offers the option of transitioning from heterogeneous to pseudo-homogeneous catalysis depending on the requirements of the

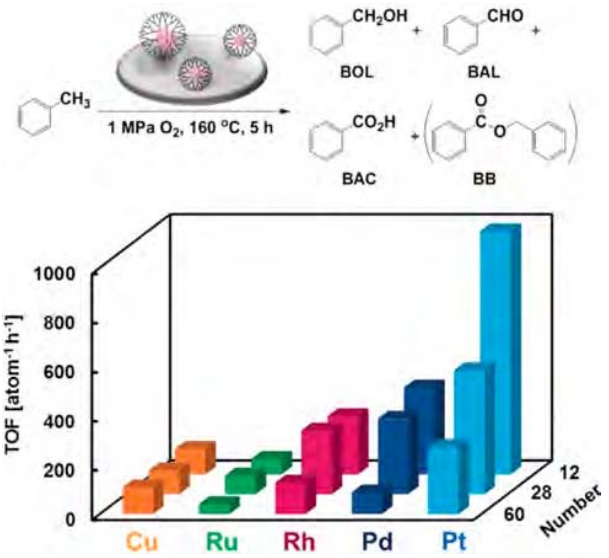

Figure 83. Catalytic activity of supported DEN-made catalysts for the oxidation of toluene as a function of both the nature of the metal and the NP size (number of metal atoms per NP).[1137] Reproduced with permission from ref 1137. Copyright 2019 Wiley-VCH Verlag GmbH & Co. KGaA, Weinheim.

reaction to be catalyzed. In addition of being excellent catalysts for typical heterogeneous reactions, including hydrogenations, alkane isomerizations and ring openings, the resulting supported DENs can also promote selective transformations that had been challenging in heterogeneous settings such as π-bond activation and aldol reactions (Figure 84).[1139] Selective catalysis has been shown, for instance, in the case of the reversible dehydrogenation/hydrogenation of indole (N-heterocycle) in solution, where Pt DENs proved to be excellent at promoting the direct arylation at the C-2 position (via C−H activation) of indole in water in the presence of a hypervalent iodine oxidant, and was used for the one-pot cascade dehydrogenation/arylation between indoline and an arylated agent.[1115] In another case, by combining size-selected DENs with well-defined mesoporous supports (and hydrophobic solvents), it was possible to direct diastereoselectivity in the Hayashi-Ito aldol reaction of methyl isocyanoacetate with benzaldehyde toward the trans diastereomer.[1127]

5.3. Bimetallics

We now revisit the idea of using bimetallics in catalysis. In Section 4.3 we discussed the use of bimetallic NPs in catalysis in the context of isolating single atoms of one metal to create unique sites in a matrix composed of a second metallic element, to produce so-called single-atom alloy (SAA) catalysts. Here we address the use of metal alloys in catalysis in a more conventional way, emphasizing the synthetic flexibility afforded by the colloidal and dendrimer-based approaches referred to above (Sections 5.1 and 5.2, respectively). We start by pointing out that the synthesis of bimetallic NPs using this type of self-assembly offers many of the same advantages in catalytic applications mentioned above in connection with monometallic NPs.[916,1067,1140] For instance, colloidal and dendrimer-based synthesis affords narrow size distributions and the potential of developing unique NP shapes with specific surfaces exposed. Also, the use of organic stabilizers sometimes helps with solubility issues in particular

https://doi.org/10.1021/acs.chemrev.1c00905
Chem. Rev. XXXX, XXX, XXX−XXX

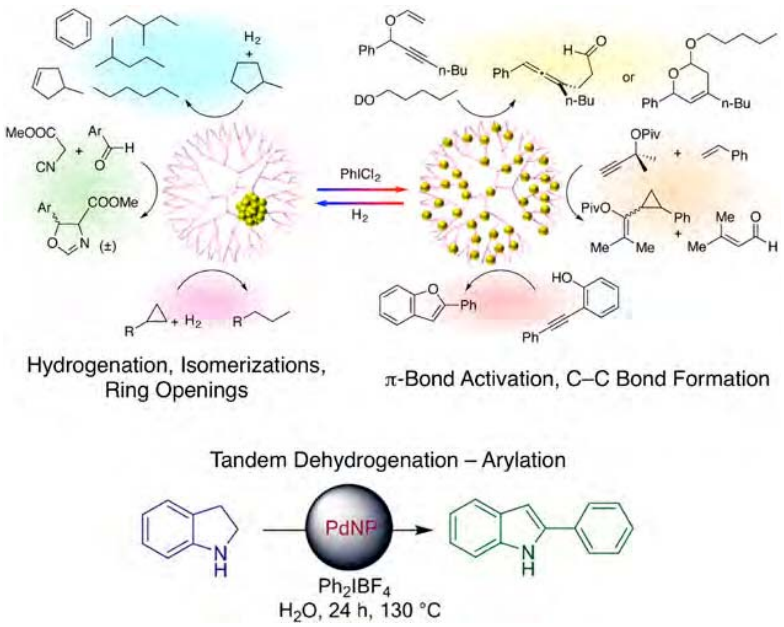

Figure 84. Examples of organic reactions that can be promoted by supported DENs in either reduced or oxidized states.[1139] Reproduced with permission from ref 1139. Copyright 2017 American Chemical Society.

solvents. The large size of the metal-organic combined structure makes separation of the catalyst easier than in homogeneous catalysis even if the process is carried out in solution, with the colloidal/DEN catalysts suspended in the liquid phase. Bimetallic colloidal NPs and DENs can also be used as precursors for the making of heterogeneous catalysts with metal NPs dispersed on solid supports.

One powerful aspect of bimetallic NP synthesis using colloidal- and dendrimer-based chemistry is that, because both the addition of the metal salt precursors and the reduction steps can be controlled in time (sequentially one at a time versus at the same time in a mixture), it is often possible to tune the spatial distribution of each metal component within the individual NPs.[1067] Other synthetic approaches such as underpotential deposition and galvanic replacement are available for the fine-tuning of bimetallic NP composition as well.[1141,1142] This affords the synthesis of bimetallic NPs in either of two extreme forms: fully mixed alloys, in which the elements are distributed evenly everywhere within the NPs according to the overall composition, and core−shell structures, where one component occupies the center of the NP as it is coated by an outside layer of the second.[1142] More complex structures are also possible, like, for instance, NPs with multiple alternating layers,[1143,1144] NPs with non-spherical shapes,[1145−1147] heterostructures with NPs of different metals coupled into one single unit (such as in a dumbbell configuration),[1148−1153] and even hollow structures if further processing such as etching is performed after the synthesis of the self-assembled layers.[1154,1155] Some three-component metallic NPs have been produced as well.[1143,1145,1156−1159] An example of the latter, a catalysts made out of three-layer Pd−Ni−Pt cubic NPs for electro-oxidations, is shown in Figure 85: it was claimed in that work that the higher specific initial activity seen with this material is explained by the structural strain imposed on the Pt outer layer by the introduction of the Ni intermediate layer.[1144] Complex

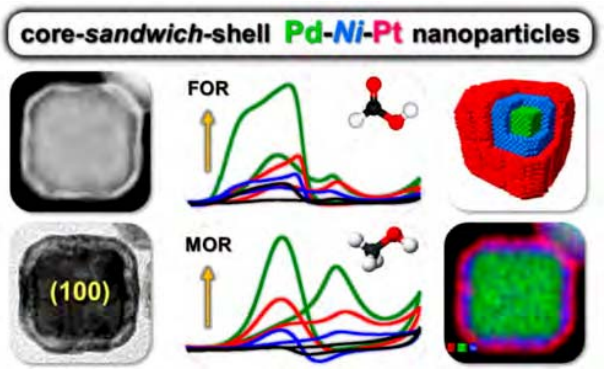

Figure 85. Cubic Pd−Ni−Pt layered NPs used for electro-oxidation catalysis.[1144] Left: HAADF (top) and regular TEM (bottom) images; Center: Cyclic voltammetry data for the electro-oxidation of formic acid (top) and of ethanol (bottom) (the different colors correspond to different NP sizes). Right: Recolored TEM image to highlight the distribution of the metals within each cubic NPs (bottom), illustrated schematically at the top. Reproduced with permission from ref 1144. Copyright 2014 American Chemical Society.

nanostructures such as these will be discussed in more detail later in this review (Section 7).

Well-mixed alloys are the default when the metals are miscible in bulk solids, and the preparation of alloyed colloidal NPs and their use in catalysis was already reported in the 90s[1160] but continues to advance to this day.[797,1140,1142,1161] Nevertheless, colloidal- and dendrimer-based synthesis also offers, in some instances, access to alloy compositions that are not thermodynamically stable in bulk solids. For example, well-mixed Au−Pt alloyed colloidal and dendrimer-based NPs covering a wide range (10 to 90 atAu%) of compositions, including the bulk miscibility gap for this binary system, have been made and used for catalytic applications such as CO oxidation[1162] and the electrocatalytic oxidation of methanol.[1163] The presence of both Au and Pt atoms were deemed

https://doi.org/10.1021/acs.chemrev.1c00905
Chem. Rev. XXXX, XXX, XXX−XXX

critical in the latter process, Pt to initially adsorb the methanol reactant and initiate its decomposition and Au to stabilize the intermediate CO-like species and/or to provide oxygenated species in the methanol oxidation process. In another case, Au was used to stabilize colloidal Rh NPs and thus enhance the catalytic selective hydrogenation of cinnamaldehyde; Rh-rich bimetallic catalysts (up to ~40 atAu%) exhibited enhanced activity and selectivity toward the desired hydrocinnamaldehyde product compared to pure Rh (increasing the Au concentration above 50 atAu% led to a loss of this beneficial effect).[1164,1165] The requirements in term of composition for optimum catalytic performance may depend on the particular reaction being considered. For instance, with Pd−Au bimetallic NPs, Pd-rich surfaces offer superior activity and selectivity for the hydrogenation of 2-chloronitrobenze to 2-chloroaniline, but an intermediate surface coverage of gold is required to optimize the production of hydrogen peroxide (Figure 86).[1166]

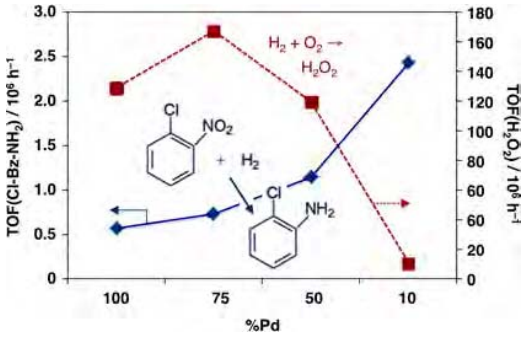

Figure 86. Reactivity of Pd−Au bimetallic NPs in electrocatalysis as a function of alloy composition, in the form of turnover frequencies for 2-chloronitrobenzene hydrogenation to 2-chloroaniline (blue) and for hydrogen peroxide synthesis (red) for four Pd:Au ratios.[1144]

It is wort mentioning that, in this latter example, the final NPs did not show the idealized homogeneous mixing expected in alloys but rather exhibited regions enriched in one or the other metal.[1166] Controlling the surface composition of bimetallic NPs is also critical to the optimization of electrocatalytic processes such as the ORR[1167] and other fuel-cell reactions.[1168] In general, the use of colloidal and dendrimer-based synthetic methods to grow bimetallic NPs and tune their electronic properties has in many instances mimicked similar approaches used in the past with more traditional alloy catalysts, but it has offered more control on size and composition.[1169−1178]

As already alluded to in the previous paragraph, homogeneous alloying of the metallic components within individual colloidal NPs may depend on the conditions to which they are exposed; the metals may segregate into two or more distinct phases after certain treatments. For instance, in studies on the selective hydrogenation of cinnamaldehyde with Rh−Au bimetallic catalysts, reduction of the NPs supported on a TiO_2 surface was shown to result in segregation into Janus NPs with decreased catalytic activity.[1164,1165] Segregation and phase separation in these bimetallic NPs is often driven by the formation of oxides.[1179] An example here is that of the two metals in Pd + 2nd-(promoter)-metal bimetallic NPs made by colloidal chemistry, which were shown to mix well initially but to separate upon heating in air into collocated metal oxide NPs; the new phases appear to add stability to the final catalysts (Figure 87).[1180] Similar phase segregation was

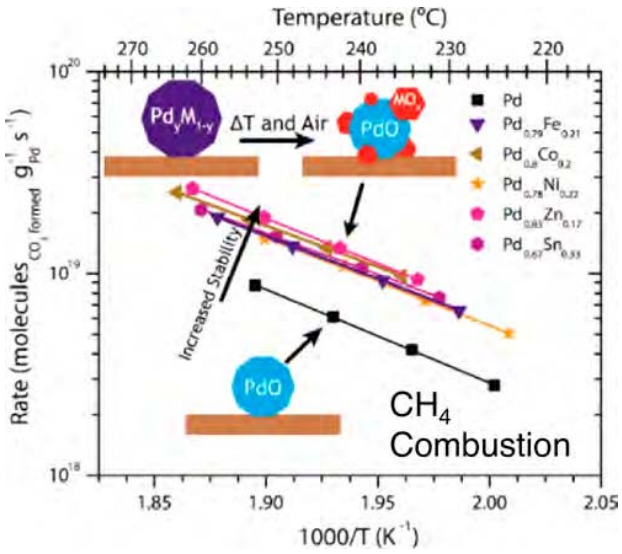

Figure 87. Stabilizing effect of the addition of a second metal to Pd NPs.[1180] Shown are data for the methane combustion activity of PdM_x/Al_2O_3 catalysts versus temperature (in Arrhenius form) after pre-oxidation in air at 850 °C, a process that leads to the formation of metal oxide NPs. Reproduced with permission from ref 1180. Copyright 2017 American Chemical Society.

reported with Ni−Fe NPs dispersed on Mg(Al)O supports, prepared to promote the dry reforming of methane: *operando* spectroscopic studies led to the observation of the formation of separate but adjacent metallic Ni and FeO NPs on the surface under reaction conditions, creating new coking-resistant catalytic sites.[1181] Other types of chemically induced segregations will be discussed in more detail in Section 5.4.

At the other end of the spectrum, in opposition to well-mixed alloys, the metals in colloidal or dendrimer-based bimetallic NPs may phase separate from the start, in which case the NPs may develop core−shell structures.[1140,1182,1183] As mentioned above, these can sometimes also be accessed via the sequential deposition of the metals. For instance, in a study of Au@Pd catalyst (where a Au NP core is covered by a Pd shell) for the promotion of trichloroethene hydrodechlorination, made by adding Pd to colloidal Au NPs of different sizes, the Pd dispersion and oxidation state were shown to transition from isolated atoms to metallic 2D Pd ensembles of varying sizes and then to partially oxidized 3D Pd ensembles as the Pd surface coverage was increased; those changes were seen to occur at different surface coverages with Au NP of different sizes.[1184] Catalytic performance was determined to correlate with all these changes, with metallic 2D Pd ensembles displaying optimum activity (Figure 88).[1184] These Au@Pd core−shell colloidal catalysts have also been shown to improve nitrite reduction performance, offering higher selectivity to N_2 in comparison to that of submonolayer Pd surface coverages or pure Pd NPs.[1185] Quantum mechanics calculations suggested that the optimum performance of catalysts with thin shells of the active metal (Pd) covering a core of a second (Au) may be due to an electron modification of the former by the latter, by Au increasing the occupation state of the Pd *d* orbitals in the particular cases cited above.[1186] Conversely, in the case of Au@Pt DEN catalysts, the increase in activity seen for the hydrogenation of nitrotoluenes to anilines and of 3-phenoxybenzaldehyde to 3-phenoxyphenyl

https://doi.org/10.1021/acs.chemrev.1c00905
Chem. Rev. XXXX, XXX, XXX−XXX

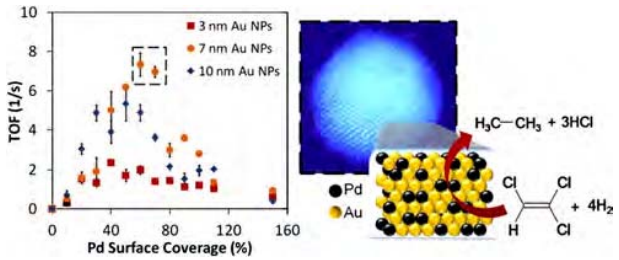

Figure 88. Activity of colloidal core−shell Au@Pd NPs for the catalytic hydrodechlorination of trichloroethene as a function of Au core size and of the amount of Pd added.[1184] Reproduced with permission from ref 1184. Copyright 2012 Elsevier Inc.

methanol was ascribed to electron transfer from the Pt shell to the Au core, which may lead to an enhancement in the adsorption of polar carboxyl groups.[1187] The surface modification of the active metal (Pd) with an electronic modifier (i.e., In) has been tested as well, taking advantage again of the possibility of performing colloidal chemistry in a sequential manner.[1188] In that case, optimum nitrate conversion was seen with submonolayer (40%) In surface coverages; metallic In was estimated to provide strong binding sites for nitrate adsorption and to lower the activation barrier for the nitrate-to-nitrite reduction step.

It is also interesting to note that in bimetallic systems with a tendency to phase segregate, the making of colloidal NPs consisting of diluted alloys can still lead to surfaces with good dispersion of the minority metal, which can thus be used for single-atom alloy catalysis (Section 4.3). An example of this has been recently provided by Duchesne et al., who made Au-based colloidal NPs with diluted amounts of Pt for the electrocatalytic oxidation of formic acid.[804] Both STEM/energy-dispersive X-ray spectroscopy (EDX) mapping and DFT calculations indicated that the Pt atoms sit on the surface of the NPs but are isolated from other Pt atoms if their overall concentration is kept low enough. An optimum performance was seen with Pt_4Au_{96} clusters, presumably because of the unique O-bonded adsorption configuration of the reactant on isolated Pt atoms. With analogous Pd−Au alloys, the same group determined that the ethanol electrooxidation reaction (EOR) in alkaline solution reaches peak specific activity and selectivity toward CO_2 production with Au-rich bimetallic NPs of $Pd_{34}Au_{66}$ composition (Figure 89).[1189] Similar observations were reported from a study on the use of colloid-made Au−Pd NPs to promote the aqueous-phase hydrodechlorination of trichloroethene.[1190] The researchers of the latter work found that the Pd atoms, which were added in submonolayer quantities, initially decorate the surface of the Au NPs in a random fashion, but intermix with the first couple of layers upon reduction in a H_2 atmosphere.

As discussed above, two main motivations for the use of core−shell NPs are to minimize the loading of expensive materials and to help tune the structural (strain) and/or electronic properties of the active phase. These nanostructures may display unique properties not seen in bulk bimetallics, offering new opportunities in catalysis.[1140,1142] For instance, colloidal NPs made out of Au cores covered with thin shells of a second transition metal (Pt, Pd, Rh, Ru) were shown to display optical plasmon resonances not seen in alloys of the same metals.[1191] This is particularly relevant to photocatalysis: the newly conceived NPs were shown to be active in a scheme for visible-light-induced hydrogen generation from water involving EDTA, tris(bpy)Ru(II), methyl viologen (MV), and the colloidal metal NPs, because the latter can act as electron mediator to accept electrons from the methyl viologen cation radical and donate those to protons, producing hydrogen molecules; this system performed much better than monometallic colloidal NPs made out of either of the constituent elements.[1191] Similar charge transfer between the elements of core−shell bimetallic NPs can assist thermal catalytic processes as well: witness, for instance, the use of Ag@Au NPs for the aerobic oxidation of glucose, a case where the increased activity (compared to that of regular Au NPs) was ascribed to the creation of negatively-charged Au atoms on the surface thanks to electron donation from the Ag core (Figure 90).[1192]

5.4. Removal of Organic Matter: Nanoparticle Stability

Supported catalysts made with colloids and dendrimers initially contain the surfactants or dendrimers used for their synthesis. Sometimes that organic matter can be exploited to gain selectivity in catalysis, as we discuss in the next paragraph, but more often they block access to the surface of the catalytic material and require their removal for more effective catalysis. This is particularly true with catalysts made by dispersing metal NPs on solid supports, in which case pretreatments are also common as a way to precondition the surface and assure that it has the appropriate oxidation state. Much has been written about this issue of the removal of the organic matter from

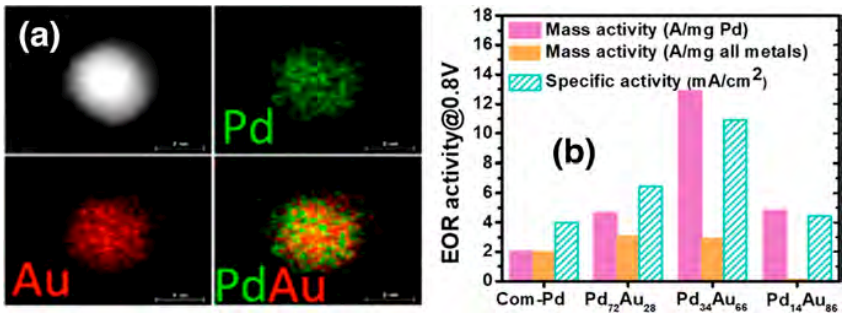

Figure 89. Example of the performance of colloid-made Pd−Au/C catalysts for the electrooxidation of ethanol.[1189] (a) HAADF-STEM image and elemental mapping of a $Pd_{34}Au_{66}$ NP, the composition that exhibit optimum electrocatalytic performance. The bottom-right image shows the well-dispersed nature of the Pd atoms. (b) EOR activity at 0.8 V, normalized to the mass of Pd (purple solid bars), the mass of all metals (gold solid bars), and the electrochemical surface area (dash bars). Reproduced with permission from ref 1189. Copyright 2019 American Chemical Society.

https://doi.org/10.1021/acs.chemrev.1c00905
Chem. Rev. XXXX, XXX, XXX−XXX

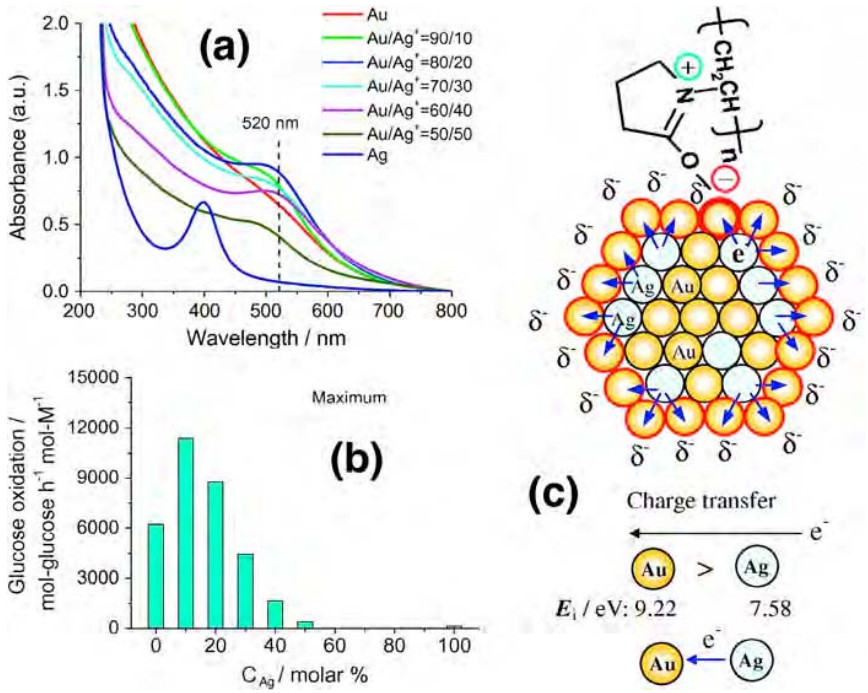

Figure 90. Use of plasmonic Ag@Au core−shell NPs for the promotion of oxidation reactions.[1192] (a) UV−Vis spectra of Ag@Au NPs of various compositions highlighting the development of a new plasmonic band at 520 nm with intermediate Ag:Au ratios. (b) Activity of the Ag@Au catalysts for glucose oxidation, showing a maximum at a composition of approximately 10% Ag. (c) Schematic illustration of the electronic charge transfer proposed to explain the increased catalytic activity. Reproduced with permission from ref 1192. Copyright 2013 Elsevier B.V.

colloidal and dendrimer-based NPs,[651,663,664,1193−1198] but no definitive conclusions have been reached yet.

First, we turn our attention to the possible influence that the added organics may have in catalysis. Beneficial effects are possible, mainly in catalysis carried out in liquid phase.[661,1199,1200] As already discussed in Section 5.2, the surfactants in colloidal NPs or the dendrimers in DENs can in principle restrain access to the metal surfaces. However, two issues also mentioned before contribute to the mitigation of this problem, or even to improvements in catalytic performance. First, it has been shown that in solution the organic matter around the NPs is flexible and adopts an open configuration with channels through which the reactants and products can travel, to diffuse in and out of the colloidal metal NPs or DENs.[1110] Second, the surfactants used in colloidal NPs and DENs can moderate the catalytic behavior of metal surfaces, and on occasion direct selectivity, in a way similar to that described in Section 3.3 when we discussed the use of SAMs to modify solid metal surfaces.[1201−1207] In many cases, selectivity is achieved by reducing the adsorption energy of some specific reactants/products or by blocking selected reaction pathways.[674,678,1208−1211] In Figure 91, for instance, a case is shown where phosphine ligands were used to block catalytic sites in PVP-stabilized Rh NPs in order to improve selectivity during the hydrogenation of phenylacetone to 1-cyclohexaneacetone. Unfortunately, as we already mentioned in Section 5.2, attempts to add selectivity to colloidal NPs or DENs via modifications of the organic surfactants or dendrimers have not always been successful because of the additional steric effects.[1105,1212−1216] In fact, most of the successful cases referenced here used small chiral molecules as colloidal stabilizers, not more traditional surfactants modified to add the desired selectivity. This limits the applicability of this approach.

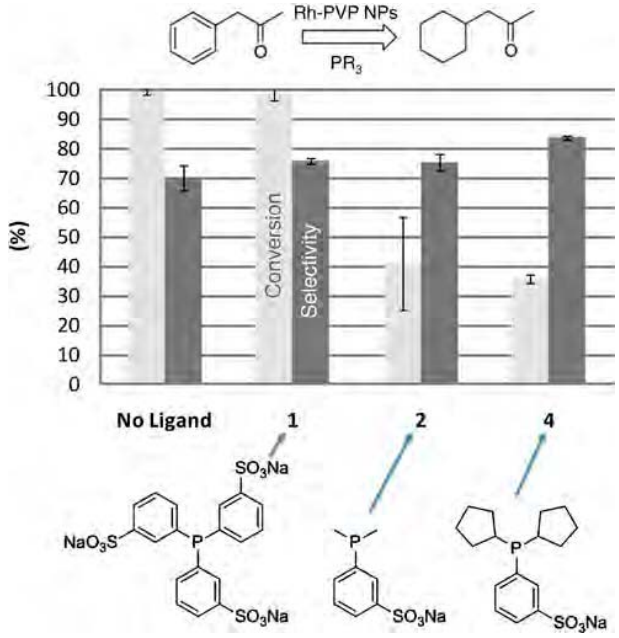

Figure 91. Control of chemoselectivity in the hydrogenation of phenylacetone promoted with PVP-stabilized Rh NPs via the addition of phosphine ligands.[1217] Small phosphines were shown to improve selectivity toward the hydrogenation of the aromatic ring via the blocking of the C═O hydrogenation pathway. Adapted with permission from ref 1217. Copyright 2012 American Chemical Society.

https://doi.org/10.1021/acs.chemrev.1c00905
Chem. Rev. XXXX, XXX, XXX−XXX

In heterogeneous catalysis, the benefits of organic matter around the metal NPs are much more limited. For one, given that many catalytic reactions promoted with heterogeneous catalysts are carried out in gas phase, they do not benefit from the presence of a solvent to help open up the organic structures. Instead, those tend to collapse and bock the metal surface, and need to be removed to activate the catalyst. Unfortunately, it has proven difficult to do this without affecting the final nature (size and shape) of the metal NPs. Typically, mild decomposition of the organic matter, by, for instance, using low-temperature thermal or calcination processes, occurs in a stepwise manner or is incomplete and leaves some organic residues on the surface, but if harsher treatments are used, the NPs are likely to loose their original shape, and/or may sinter.[1218] Several studies have aimed to identify the optimum conditions for supported metal NP activation, sometimes yielding contradictory reports. The groups of Amiridis and Chandler have shown that the decomposition of dendrimers in DENs starts are relatively low temperatures, as low as 50 °C, most likely at the mono-substituted amide groups.[1219−1222] However, they have also indicated that much harsher pretreatments such as oxidations at 300 °C or higher temperatures are required to fully clean the metal, and that sintering may take place in those instances. The removal of the organic matter is also affected by the nature of the support because of the contribution from specific interactions between the surfactants or dendrimers and the oxide.[1223] Other research groups have reported rosier outcomes, sometimes claiming complete metal cleaning while preserving NP size, shape, and catalytic activity, although in most cases there are nuances associated with those conclusions.[1033,1224,1225] This is illustrated by the mixed results reported by the group of Somorjai and coworkers.[663] In their system, based on PVP-stabilized Pt NPs, they showed that after the PVP is removed (via UV radiation or thermal oxidation), carbonaceous fragments remain on the surface that dynamically switch between being porous in H_2 and collapsing and closing in O_2. Consequently, the pre-treated NPs were shown to be effective catalysts for ethylene hydrogenation but not for methanol oxidation (Figure 92).[663]

Treatments based on a combination of ultraviolet radiation and ozonolysis (UV/O_3) have also been used for ligand removal (as in the example provided above, Figure 92).[1226−1228] This is a milder alternative to calcinations, but, again, the results are not always optimal, often leading to an incomplete removal of the organic matter.[663,1224,1226,1229−1232] On the other hand, controlled removal of the surfactants may sometimes be used to tune selectivity. In one example, in a study of the partial removal of the PVP stabilizers from silica-supported Au NPs by UV radiation/ozonolysis, it was shown that while retention of the surfactants on the surface benefits the selectivity of the hydrogenation of *p*-nitrochlorobenzene toward *p*-chloroaniline, possibly by forcing the reactant to adsorb in an on-end geometry, removal of the organic residues from the surface of the metal NPs is required to hydrogenate cinnamaldehyde (the extent of the C=C hydrogenation proved to be proportional to the area of the open surface; Figure 93).[1233]

Less disturbance of the properties of the metal NPs during organic-matter removal may be accomplished by using mild chemical treatments such as ligand exchange or solvent extraction.[1198,1234−1244] Successful treatments with $NaBH_4$ in particular, to remove thiol adsorbates, have been reported,[1245,1246] but, because of the reducing properties of that reactant, NP sintering may also occur in those cases.[1247] In more general terms, many of these chemical treatments can alter the surface of the NPs and with that their catalytic properties (Figure 94).[1248] Another alternative is to grow metal NPs without capping agents by using templating agents during metal deposition on solid surfaces instead.[1249,1250] Additional complications may appear, however. For instance, in one case, Br^- ions were used as surfactants to grow Pd NPs to take advantage of their easy subsequent removal via heating in water, but it was then found that such removal leads to the oxidation of the metal surface.[1251,1252] A definitive way to properly activate colloidal- or dendrimer-made metal NPs in supported catalysts is still not available.

As already alluded to, removal of the organic matter used in the synthesis of colloidal NPs or DENs risks modifying the structural and/or chemical properties of those metal NPs; again, witness the example provided in Figure 94. This is particularly critical because one of the main driving forces for choosing to prepare catalysts using these self-assembly procedures is the exquisite control they offer in terms of NP size and shape; if those are lost at the catalyst pre-treatment stage, the justification for using such complex and expensive synthetic routes is gone. One concern is the potential leaching of the metal during catalysis, a worry that applies mainly to reactions carried out in liquid phase.[1253] A particular set of

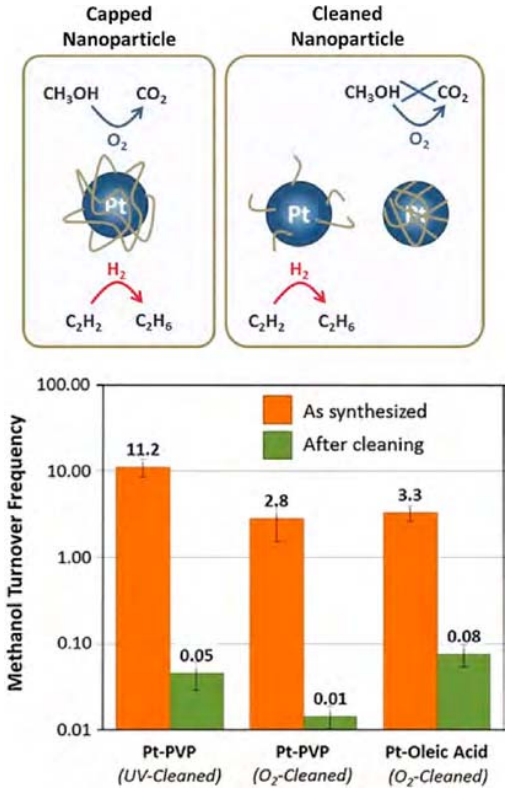

Figure 92. Effect of colloidal NP cleaning on catalytic performance. Reported are the rates of methanol oxidation relative to those of ethylene hydrogenation measured with three Pt colloidal catalysts following either radiation or thermal pre-treatments.[663] Some organic residues were detected on the surface using vibrational spectroscopy; they seem to aid hydrogenation processes but hinder oxidation reactions. Reproduced with permission from ref 56. Copyright 2021 The Author(s). Published by Elsevier B.V.

https://doi.org/10.1021/acs.chemrev.1c00905
Chem. Rev. XXXX, XXX, XXX−XXX

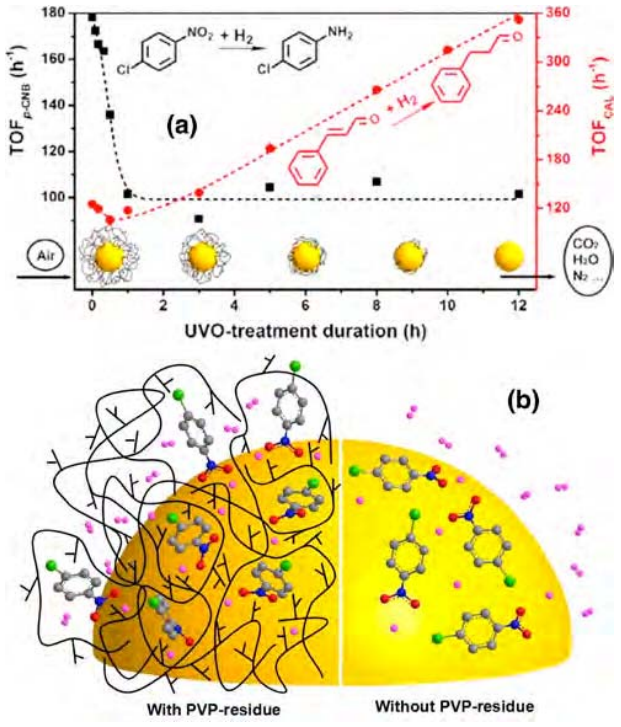

Figure 93. Effect of the presence of organic ligands on the performance of PVP-stabilized Au colloidal NPs dispersed on a silica support.[1233] (a) TOFs for the hydrogenation of *p*-nitrochlorobenzene (black squares) and cinnamaldehyde (red circles) as a function of the time the Au NPs were exposed to a combination of UV radiation and ozonolysis prior to reaction, to remove the organic matter. (b) Proposed model for the improved performance of the catalyst for the first reaction with increased organic ligand coverage, based on a change in adsorption mode for the reactant. Reproduced with permission from ref 1233. Copyright 2014 American Chemical Society.

reactions where this has become a hotly debated issue is C−C couplings such as the Suzuki and Heck reactions: some of the metal (typically Pd) atoms in the colloidal NPs or DENs may dissolved as ions, which may perhaps carry out the catalysis themselves.[312,927,931,1254] In an early study, the Crooks' group looked into the degree of metal leaching from G6−OH(Pd_{147}) DENs in aqueous solutions, and determined that the Pd NPs are fully stable for at least 36 h under reducing conditions but oxidize under N_2, a chemical change that is accompanied by partial leaching.[1255] Using a special membrane reactor, Thathagar et al. proved that, indeed, Pd atoms and ions do leach from Pd NPs in Heck and Suzuki coupling reactions (Figure 95),[928,1256] and experiments based on cross mixing of bimetallic NPs[1257] and direct X-ray absorption spectroscopies[1258] later confirmed this conclusion. Metal leaching has also been seen with other metals,[1259] and remains a concern to this date.

Metal NPs can also sinter. For instance, Au DENs were recently shown to grow in size during their use promoting the electrocatalytic reduction of CO_2.[1260] In these situations, the organic matter (surfactants or dendrimers) may actually help with stability: it was shown in that same study that higher generation (G8-OH PAMAM) dendrimers prevent metal NP sintering, presumably because of the compactness of the periphery of the organic framework (Figure 96).[1260] This is an interesting case of NPs growing in size in solution; much more common is metal NPs sintering in heterogeneous catalysts, because, once cleaned up, those catalysts are prone to the same effects well documented for catalysts made by other means.[1261−1263] Again, in the case of colloidal or dendrimer-based NPs, the organic matter may act as a retardant of metal mobility, improving on the stability and performance of the catalysts, but that is beneficial only if the metal surfaces remain accessible for reaction: there is a fine line between the positive role of these carbonaceous deposits as providers of additional structural stability versus the detrimental contribution as agents that block active sites. Less common but also possible in heterogeneous catalysts is the reverse dissolution of metal NPs into isolated atoms: this is what was recently reported in the case of Pd/Al_2O_3 catalysts used for methane combustion.[1264] It is worth mentioning that, because in that case rapid annealing at high temperatures was used to clean the colloidal metal NPs prior to their use, as in many of the other examples available on this subject, it is quite likely that the NP size redistribution observed during catalysis had nothing to do with the particular manner in which the catalysts were synthesized; these results do not provide meaningful insights into possible sintering or redispersion of colloidal NPs or DENs supported on solid surfaces. NPs size redistribution is nevertheless a concern here, as with all other catalysts.

The retention of the shape on metal NPs is a much subtler problem, because the NP shapes can easily vary and change under different conditions, even during their synthesis, given the dynamic nature of the capping process.[997,1198] Additional opportunities to affect NP shape in supported catalysts occur during catalyst pretreatments, as the organic matter is removed, and also during reaction.[1193] The structure of colloidal NPs is also likely to change with time due to possible reaction with chemical compounds from the surrounding environment such as solvents or gases.[1265] An obvious concern is oxidation. With Pd colloidal NPs, for instance, the higher rate seen for C−C coupling reactions on (100) (and other high Miller index planes) versus (111) facets has been ascribed to a higher oxygen-assisted leaching susceptibility.[1266,1267] These NP shape changes can even happen before catalysis; Figure 97 shows an example of such behavior for the case of PVP-capped Pd NPs dispersed on a carbon support.[1268] Nevertheless, the deterioration of NP shapes is often more pronounced under reaction conditions: examples of sructural changes have been reported for Pt colloidal NPs when used for the electron-transfer reaction between hexacyanoferrate (III) and thiosulfate ions in solution at room temperature[921,1003] as well as for Pt colloidal NPs dispersed on a carbon support employed for the promotion of the ORR in fuel cells.[1269]

Much has been made of the possibility of using the shape of metal NPs as a way to control catalytic selectivity, as discussed above (Section 5.1). Key to the success of that approach is the ability to preserve the NP shape during reaction. This is certainly possible for mild reactions carried out at relatively low temperatures and pressures. For instance, we have shown that the Pt NPs made using colloidal chemistry can retain their tetrahedral shape on silica supports during preconditioning as long as relatively mild oxidation-reduction conditions are used, but convert into their more thermodynamically stable spherical shape if calcination is carried out at higher temperatures (Figure 78).[1033,1034] In that work, we also showed that the NP shape is preserved during olefin isomerization reactions, which are carried out at temperature of about 375 K and under

https://doi.org/10.1021/acs.chemrev.1c00905
Chem. Rev. XXXX, XXX, XXX−XXX

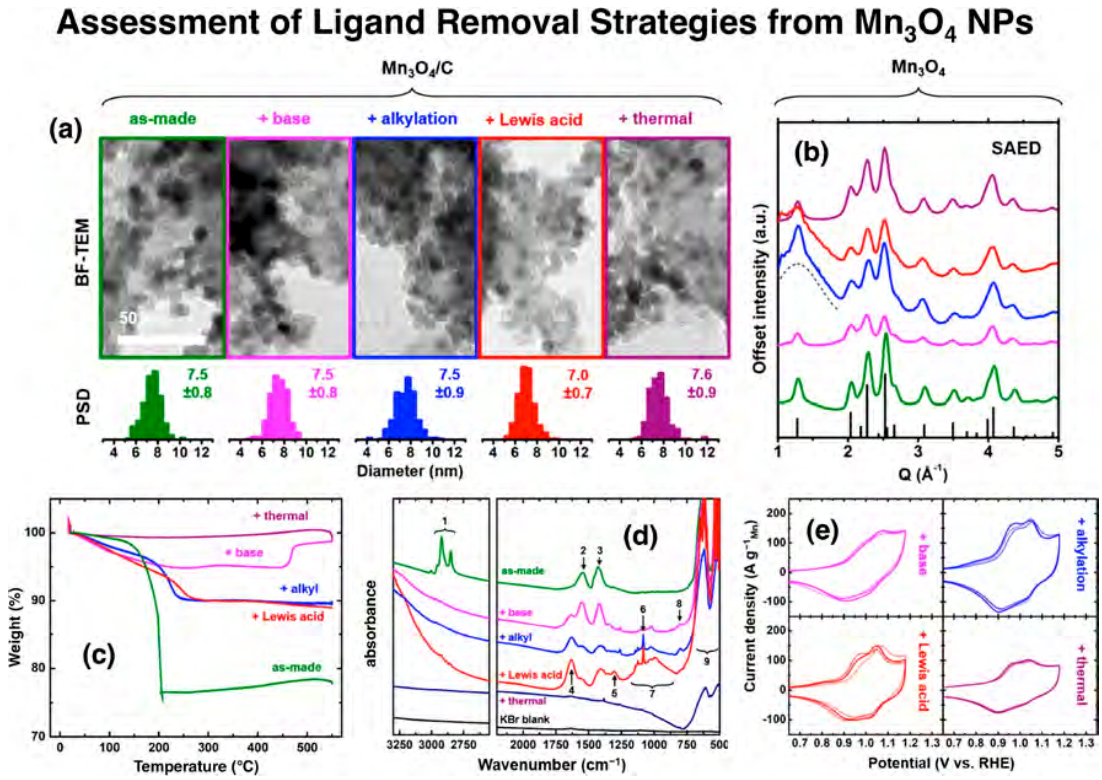

Figure 94. Comparative study of the effect of ligand removal treatment on the final properties of NPs.[1248] The example shown here corresponds to colloidal Mn_3O_4 NPs made using oleic acid as the surfactant. Four treatments were tested: thermal/combustion (data in magenta), and chemical treatments with a base (KOH, pink), an alkylating agent (triethyloxonium tetrafluoroborate, blue), and a Lewis acid (boron trifluoride-diethyl ether complex, red). (a) TEM images and NP size distributions. (b) Selected area electron diffraction (SAED) patterns. (c) Thermogravimetric analysis in air. (d) IR spectra. (e) Cyclic voltamograms. The structure of the final NPs appear to be the same after all treatments (a,b), but their physical and chemical properties are different, namely, they show different (c) final weights, (d) adsorbed species, and (e) redox behavior. Reproduced with permission from ref 1248. Copyright 2019 American Chemical Society.

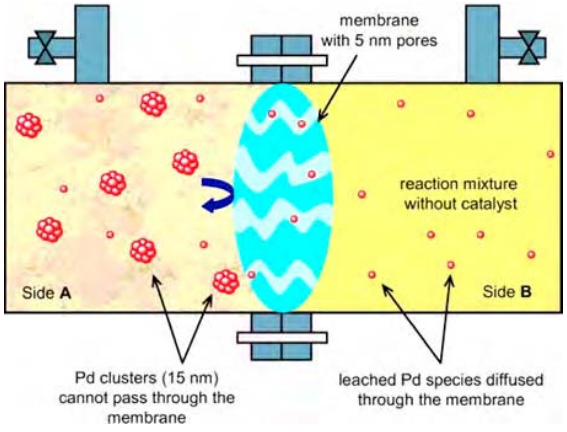

Figure 95. Experimental setup used to demonstrate the leaching of Pd atoms from Pd colloidal NPs during C−C coupling reactions.[928] Reproduced with permission from ref 928. Copyright 2006 Wiley-VCH Verlag GmbH & Co. KGaA, Weinheim.

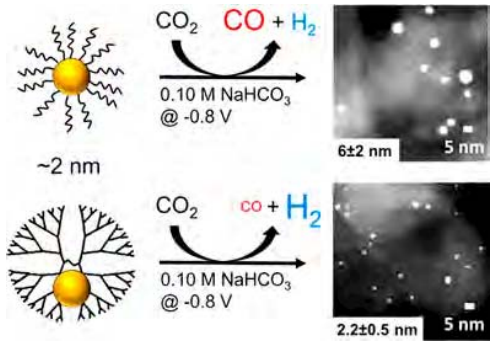

Figure 96. Evidence of the stabilizing effect exerted by large dendrimers on DENs, in this case the inhibition of the sintering of Au NPs in DENs by 8th-generation OH-terminated PAMAM dendrimers (G8-OH) during the electrocatalytic reduction of CO_2.[1260] Reproduced with permission from ref 1260. Copyright 2017 American Chemical Society.

atmospheric pressures.[1020,1034,1040] Success using this so-called shape selectivity has also been reported for other mild reactions such as hydrocarbon hydrogenations;[956,957,1014,1270−1272] an example of shape preservation in these processes is shown in Figure 98.[1017] Additional examples have been provided in the literature for shape selectivity in more demanding reactions such as the reduction of NO by CO[1273] or electrocatalytic oxidations,[1274] but even though differences in reactivity were observed when using NPs of different shapes, caution needs to be exerted before concluding that they are due to structural effects, since those reaction requires high temperatures and are often highly exothermic; the shape of the metal NPs is likely to change under those conditions (as we mentioned before, In Section 5.1),[1275−1277] and the differences observed there may be ascribed to other

https://doi.org/10.1021/acs.chemrev.1c00905
Chem. Rev. XXXX, XXX, XXX−XXX

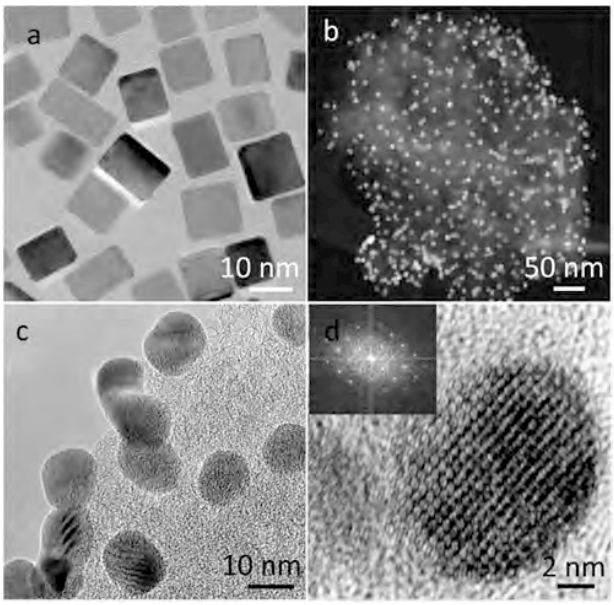

Figure 97. Example of the shape instability of colloidal metal NPs. Shown are STEM images of 10 nm PVP-capped cubic Pd NPs (a) as synthesized, (b) after deposition on activated carbon, (c) 6 months after deposition, and (d) aged for 12 months.[1268] The loss of the cubic structure, the sharp edges in particular, is evident. Reproduced with permission from ref 1268. Copyright 2014 American Chemical Society.

factors. Encapsulation of NPs with a thin protective layer has been attempted to help preserve NP shape, but although some success has been reported with this approach,[1278] some skepticism is again in order, as (1) roughening of NP surfaces requires minimum reconstruction difficult to stop by such protecting approach, and (2) covering of the surface leads to changes in its surface chemistry and likely blocks catalytic sites.

With bi- and multi-metallic NPs, an additional concern relates to the stability of the chemical composition of their surfaces. It has been long known that exposure of multi-component solids to thermal treatments or specific chemical environments often leads to the selective segregation of some of the components to the surface.[798,993,1279−1281] Bimetallic NPs are particularly susceptible to this effect, as their small sizes means that bulk atoms are only a few layers away from the surface, and also because NPs, with their highly-curved surfaces, obey somewhat different thermodynamic rules than those that apply to bulk solids. Of particular relevance to catalysis is the fact that the gases or liquids in the reaction mixture during catalysis can affect surface composition by driving particular metals in or out of the surface, often reversibly. We have in fact discussed some cases of bimetallic segregation due to the oxidation of one of the components already in Section 5.3. In reference to colloidal NPs, in a pioneering paper in 1995, Bradley et al., using IR spectroscopy to characterize the adsorption of CO on Pd−Cu catalysts, established a preference for room-temperature Pd segregation to the surface, a result that is in contrast with the more commonly observed surface enrichment in Cu seen with bulk alloys; further surface enrichment in Pd was shown to occur with long exposures (days) to CO atmospheres.[1282] More recently, Somorjai and coworkers used atmospheric-pressure XPS to follow the reversible segregation of Rh in Rh_xPd_{1-x} and Rh_xPt_{1-x} colloidal NPs (x = 0.2, 0.5, 0.8) with core−shell structures.[854,1283] They showed that the NPs undergo reversible changes in surface composition and chemical state as they are alternatively exposed to oxidizing and reducing conditions (Figure 99). These changes are particularly relevant in electrocatalysis, where the liquid phase interacting with the bimetallic NPs on the surface of the electrodes offers a strong driving force for surface composition changes, and where the

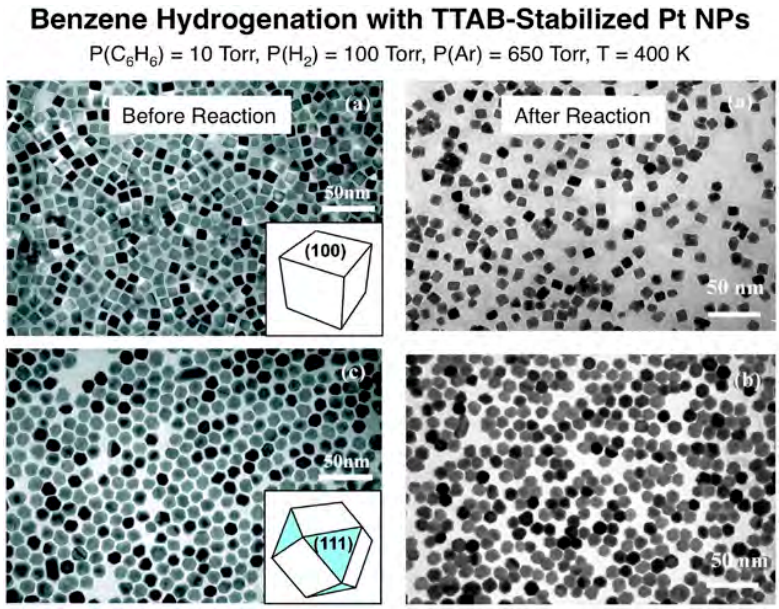

Figure 98. Electron microscopy proof of the stability of the shape of metal NPs during mild catalytic reactions. Shown are images for cubic (top row) and cubooctahedral (bottom) tetradecyltrimethylammonium bromide (TTAB)-stabilized Pt NPs before (left) and after (right) benzene hydrogenation catalysis.[1017] Reproduced with permission from ref 1017. Copyright 2007 American Chemical Society.

https://doi.org/10.1021/acs.chemrev.1c00905
Chem. Rev. XXXX, XXX, XXX−XXX

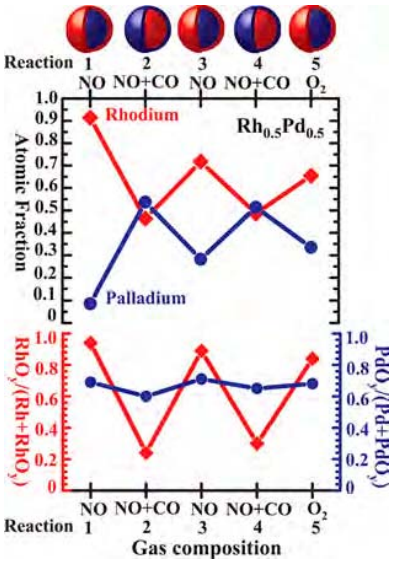

Figure 99. Evolution of the surface Rh and Pd atomic fractions (top) and of the fraction of both metals present in oxidized form (bottom) in colloidal $Rh_{0.5}Pd_{0.5}$ NPs at 300 °C under oxidizing conditions (100 mTorr NO or O_2) and catalytic conditions (100 mTorr NO and 100 mTorr CO).[854] The data highlight the dynamic nature of the distribution of the components in bimetallic colloidal NPs depending on the surrounding environment. Reproduced with permission from ref 854. Copyright 2008, American Association for the Advancement of Science.

presence of the second metal is imperative to temper the high reactivity of Pt, for instance.[1284] The relevance of the unique compositional structures afforded by using colloidal chemistry in the preparation of bimetallic NPs to catalysis may in many instances be brought into question because of the structural and compositional changes induced by the catalytic environment.

Mismatches in lattice constants between the core and shell metals in core−shell bimetallic NPs and other nanostructures can also cause changes in bond distances between atoms on the surface leading to changes in the chemical properties of the outer layer.[1285] Alternatively, they can create grain-boundary defects with particular chemical activity. Either way, these effects are likely to show up in the catalytic behavior of such NPs. To the best of our knowledge, there has not been a proper evaluation of this effect to date. Overall, it can be said that the ability to synthesize metal NPs with colloidal, dendrimer-based, and other self-assembly methodologies offer great control over their size, shape, and composition, parameters that can be then tuned to optimize catalytic behavior. Examples of the success of this approach are certainly available, as discussed above, but its use is somewhat limited to reactions that take place under mild conditions. In addition, special consideration needs to be given to the need to evaluate the role of the organic matter in the particular catalytic process of interest, to assess its beneficial or detrimental effects and to establish a reliable way to activate the metal NPs via their removal if necessary. Moreover, because the synthesis of colloidal NPs and DENs is expensive, their use in catalysis may have to be targeted to certain organic conversions difficult to promote by other means.

6. NOVEL NANOSTRUCTURES: OXIDES, OTHERS

Because of their ubiquity in catalysis, our focus in the previous section was on the synthesis of catalysts where the active phase is metallic. In heterogeneous catalysis, metals are commonly deposited in NP form on solid supports, preferably high-surface-area solids, to optimize dispersion and therefore minimize metal loading. In this traditional picture of catalysis, the support is inert; all the important catalytic chemistry takes place on the surface of the metal. However, it was learned very early on that this simplistic model is incomplete, and that the support itself can play additional roles in catalysis. For instance, it can modify the electronic or structural properties of the metal NPs. It can also interact strongly with the metal and create unique interface sites with new chemistry; the SMSI effect discussed in Section 4.2 is one example in this category. Finally, the so-called support can be a catalytic phase in its own right, acting by itself or in conjunction with metal NPs (in concerted or tandem fashion). In fact, much catalysis is carried out with non-metallic solids. Because of all of this, it is also important to develop an ability to control the structure and properties of non-metallic catalysts and supports. Some of the main ways by which nanotechnologies have been incorporated into the synthesis of novel non-metal structures, exposing surfaces with atomic ensembles that may define useful catalytic sites, will be discussed next. Because metal oxides are perhaps the most common supports and non-metallic promoters used in catalysis, most of our review will focus on those, but reference to other solids such as carbon-based materials, including polymers, will be made as well.

6.1. Zeolites

Zeolites, with their well-defined crystalline structures, are perhaps the oldest group of metal oxide materials used in catalysis where great control can be exerted on the structure of catalytic sites.[1286−1289] There are many types of zeolites found in nature, to which many more have been added by synthetic laboratories.[1290−1294] Most zeolites are aluminosilicates with basics unit consisting of 3D frameworks built by corner-sharing SiO_4 and AlO_4 units, which are organized to produced cavities and channels of different sizes (usually below 1 nm in diameter), shapes, and connectivities; these can involve rings with from 8 to 30 atoms.[1294,1295] The versatility in the way the basic units can be assembled to create well-defined diverse pore structures is one of the key properties that make zeolites such useful solids for catalysis.[1296] In addition, aluminosilicates exhibit both Lewis- and Brønsted-acid sites,[860] the strength and surface concentration of which can be controlled and tuned by adjusting the Si/Al ratio.[1297−1299] The literature on the use of zeolites as catalysts is quite extensive, and it is not our intention to cover it here; there are other excellent reviews[167,1286,1290,1299,1300] and books[1301−1304] that do better justice to the importance of these materials. Instead, below we highlight some of the key properties of zeolites that afford the design of catalysts with well-defined sites to control selectivity.

One of the main catalytic uses of zeolites is in the petroleum industry,[1294,1301,1305,1306] in fluid catalytic cracking refineries for gasoline production in particular.[1307−1309] Although this is a well established process, research continues in the search for ways to convert light and heavy crude oil fractions, and more recently biomass-based oxygenates, into specific products such as propylene and diesel-range fuels with high selectivity.[1300,1310,1311] One key aspect of this catalysis is the dependence of activity and selectivity on the nature of the

https://doi.org/10.1021/acs.chemrev.1c00905
Chem. Rev. XXXX, XXX, XXX−XXX

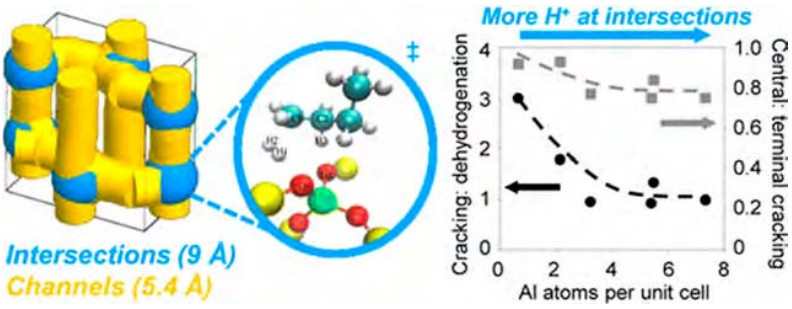

Figure 100. Left: Schematic structure of H-MFI zeolites highlighting the differences in diameter of the cavities at the channels versus at the intersections. Right: cracking-to-dehydrogenation and central-to-terminal cracking ratios as a function of the Al content of the H-MFI zeolite, which is associated with H^+ Brønsted-acid sites at the intersections. Higher Al content yields more of those sites, which preferentially promote more dehydrogenation and terminal cracking. Reproduced with permission from ref 1318. Copyright 2013, American Chemical Society.

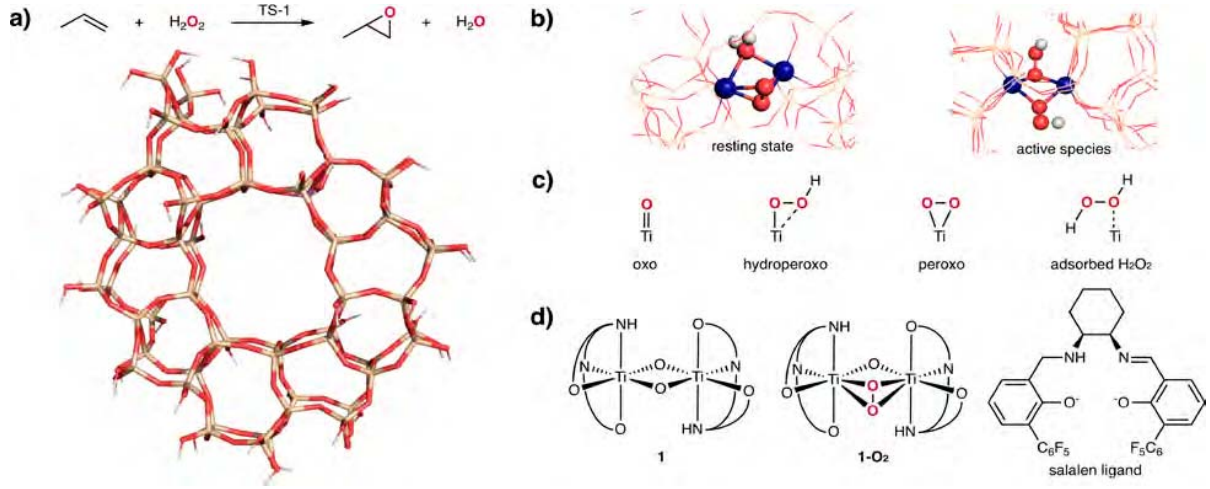

Figure 101. Dual-site TS-1 zeolite designed for the promotion of epoxidation reactions.[1332] (a) TS-1 structure. (b) Dinuclear site proposed for the epoxidation of propylene with TS-1 (blue spheres, Ti; red spheres, O; white spheres, H). (c) Proposed active species in the TS-1/H_2O_2 system. (d) Molecular dimeric Berkessel−Katsuki catalyst 1 (based on a salalen ligand) used to epoxidize olefins with H_2O_2, and corresponding peroxo species 1-O_2. Figure provided by Prof. Copéret.

acid sites, which not only relies on the Si/Al ratio, as mentioned above, but also on the distribution and specific placement of the Al ions within the zeolite framework,[1306,1309,1312,1313] a detail that has turned out to be difficult to characterize and control.[1298,1314,1315] In one example, related to the cracking of propane with Y zeolite, the intrinsic activity of the Brønsted-acid sites was deemed to be identical in all samples regardless of Si/Al ratios, and the enhanced activity seen with higher Si/Al values was attributed to the presence of more isolated Brønsted-acid sites.[1316] However, in another study, with HBEA zeolites, an increase in the Si/Al ratio was determined to lead to a reduction in the proportion of Lewis-acid sites relative to Brønsted-acid sites, undermining the protolysis of methylcyclohexane (which requires interaction of bridging OH groups with neighboring Lewis-acid sites).[1317] Moreover, Janda and Bell reported that, in H-MFI zeolites, the fraction of Brønsted protons located at channel intersections relative to those located in straight and sinusoidal channels increases with increasing Al content, and that this generally leads to increases in selectivity toward dehydrogenation versus cracking and toward terminal cracking versus central cracking (Figure 100).[1318] The authors explained these trends in terms of a confinement of the transition states of the reactions: the geometry of the transition state for dehydrogenation is bulkier than that for cracking, and therefore likely to be accessible only at the more spacious channel intersections (in comparison to the channels themselves).

Many zeolites are composed of aluminum and silicon oxide units exclusively, but some incorporate additional elements such as phosphorous or titanium.[167] Well-known examples are SAPOs (silicoaluminophosphates), specifically HSAPO-34, a zeolite used to promote methanol-to-olefin conversions.[1319−1322] A simpler HZSM-5 aluminosilicate zeolite had previously been used for such application, but secondary reactions with that material affect selectivity and lead to oligomerization and catalyst coking; the SAPO family, with smaller cages, minimizes chain growth and therefore shows better performance toward the production of lighter olefins (especially when synthesized as small crystallites or with a hierarchical pore structure).[1323−1326] The new elements added to zeolites may modify their overall properties, their acidity in particular, but may also create unique sites. A good example of the latter is TS-1, a titanium silicalite with a MFI structure often used for selective partial oxidation reactions.[1327−1330] The active site in that case is generally believed to be the isolated Ti ions that exist in the framework positions of hydrophobic zeolites, substituting Si atoms and forming

https://doi.org/10.1021/acs.chemrev.1c00905
Chem. Rev. XXXX, XXX, XXX−XXX

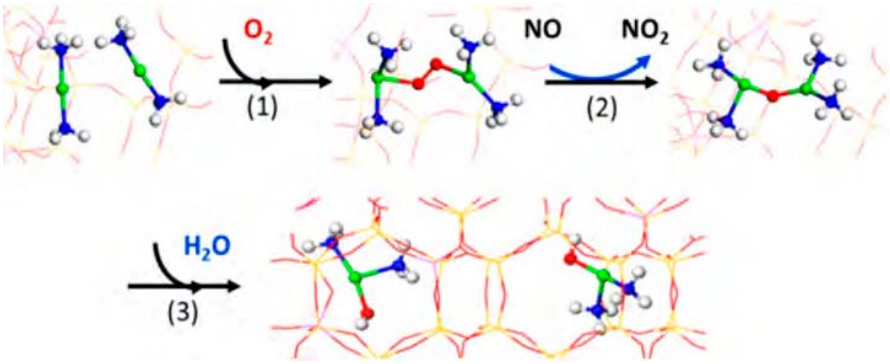

Figure 102. Schematic representation, based on DFT calculations, of the proposed restructuring of the Cu-ion-based site active in SCR reactions with ion-exchanged zeolites.[1360] Two isolated Cu(I) ions are believed to participate in the catalytic cycle via the formation of a transient $[Cu^{I}(NH_3)_2]^+-O_2-[Cu^{I}(NH_3)_2]^+$ intermediate. Color code: Cu (green), O (red), N (blue), H (light grey). Reproduced with permission from ref 1360. Copyright 2017 American Chemical Society.

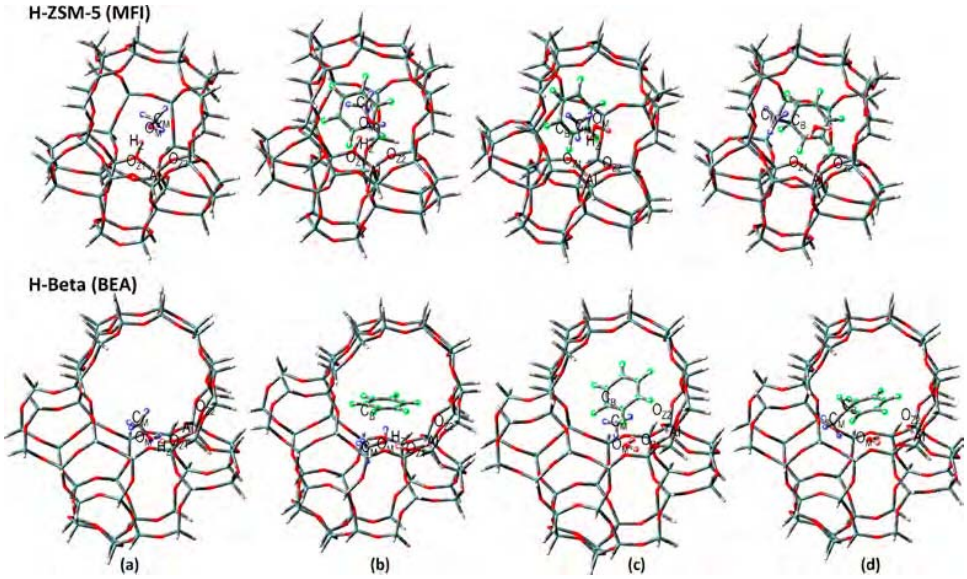

Figure 103. Example of the effect of confinement inside the pores of zeolites on the evolution of catalytic reactions throughout the reaction coordinate. This case relates to the promotion of the methylation of benzene by methanol in H-ZSM-5 (top row) versus H-Beta (bottom) zeolites.[1380] Shown are the DFT-calculated structures for (a) adsorbed methanol, (b) a coadsorbed benzene-methanol complex, (c) the transition state for methylation of benzene by methanol, and (d) an intermediate stage of conversion. Reproduced with permission from ref 1380. Copyright 2018 American Chemical Societyr.

tetrahedral TiO_4 units exposed at the inner surfaces of the pores of the zeolite.[1330,1331] Recently, a dinuclear alternative site has been proposed for the epoxidation of propylene, in a model that mimics to some extent the finesse that can be achieved for similar reactions with homogeneous catalysts (Figure 101).[1332] A third metal often used for ion substitutions in aluminosilicate zeolites is tin, employed for the conversion of biomass feedstocks.[1333] Other elements used to create Lewis-acid sites in zeolites include Zr, V, and Ta[1331]

In the examples cited in the previous paragraph the extra elements were incorporated into the zeolites during their synthesis, but metal ions can also be added afterward, via ion exchange with the protons of Brønsted-acid sites, for instance, to create new well-defined single sites.[1334−1336] Ion-exchanged zeolites have been used for the promotion of a number of processes, including the partial oxidation of methane to methanol,[1337−1342] the homologation of biomass-derived oxygenates to fuels,[1343,1344] and the SCR of nitrogen oxides in emission control.[1345−1352] Much research has gone into determining the nature of the active catalytic sites in these cases, in particular the oxidation state of the exchanged ions but also the number of ions involved, but full consensus has not yet been reached on the subject. For instance, bis(μ-oxo)dicopper,[1353] mono(μ-oxo)dicopper,[1337] μ-(η^2:η^2) peroxo dicopper,[1354] and tri-, tetra,- and penta-nuclear copper-oxo[1355−1357] surface ensembles have all been proposed as the key sites for the promotion of the direct oxidation of methane to methanol in Cu-based zeolite catalysts. Bimetallic sites have been advanced as a way to improve on catalytic performance for this reaction as well: with Fe−Cu-ZSM-5, for instance, Fe is believed to activate the C−H bonds whereas Cu is proposed to control selectivity toward methanol production.[1358] The ease with which the metal ion undergoes redox interconversion has been determined to be crucial for catalytic activity, a property that has been correlated with the Si/Al ratio.[1342,1359] Similar arguments have been playing out in the literature concerning

https://doi.org/10.1021/acs.chemrev.1c00905
Chem. Rev. XXXX, XXX, XXX−XXX

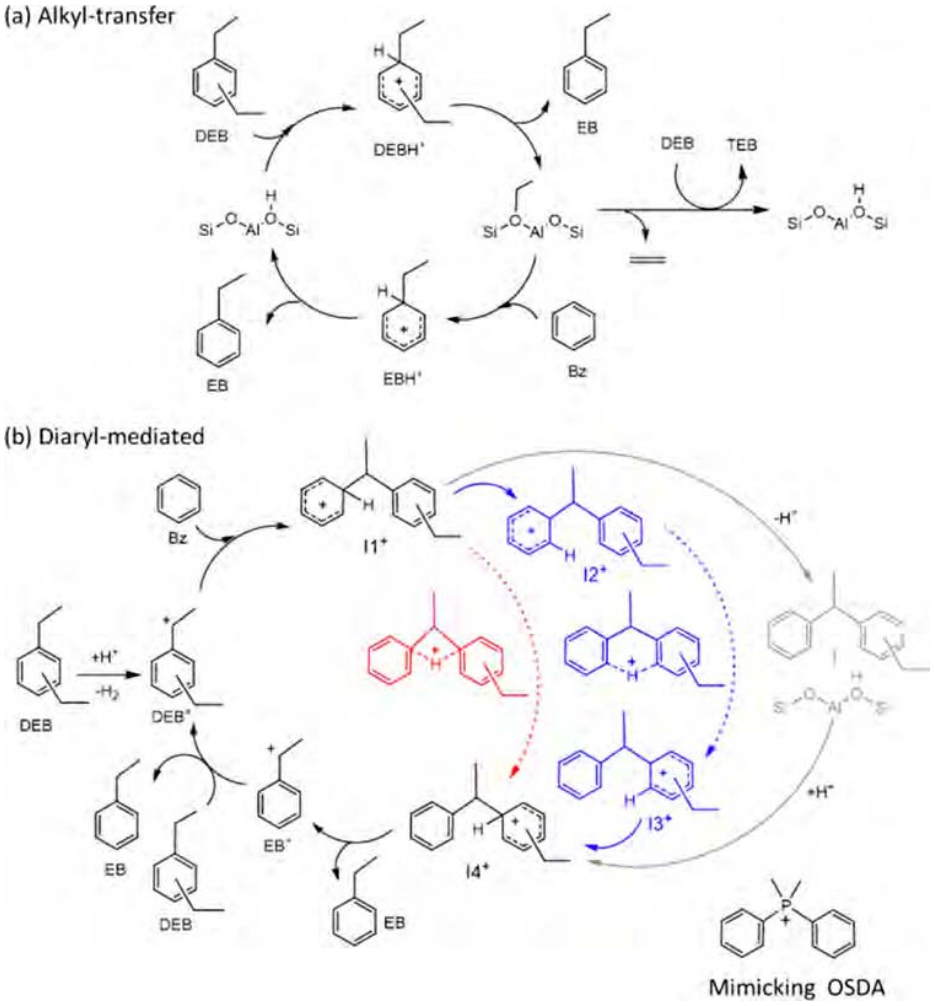

Figure 104. Use of diphenyldimethylphosphonium as an organic structure-directing agent that mimics the size, shape, and charge localization of the diaryl cation intermediate involved in the transalkylation between benzene and diethylbenzene.[1384] Shown are (a) the proposed mechanisms for the reaction; and (b) diaryl-mediated pathways and the proposed mimicking organic structure-directing agent. Reproduced with permission from ref 1384. Copyright 2021 American Chemical Society.

the details of the operative Cu-exchanged zeolites used for SCR. In that case, not only multinuclear sites have been invoked to describe the catalytic site, but a dynamic restructuring of such sites has been proposed during the Cu(II)−Cu(I)−Cu(II) reduction-oxidation cycle associated with the redox catalysis (Figure 102).[1360,1361]

In addition to the well-defined and tunable acidic properties of zeolites, their crystal structures with small pores of well-defined size and shape can be used to provide confined spaces for the conversion of reactants to products, thus directing selectivity via steric effects.[1362] The potential applicability of zeolites for so-called shape selectivity in catalysis was evidenced several decades ago in connection with the alkylation of toluene, which in zeolite Y was shown to significantly depart from the expected thermodynamic distribution of products and to strongly favor the formation of para- over meta- or ortho-xylene,[1363−1366] and was extended to other hydrocarbon conversions soon thereafter.[1286,1367−1370] Another well-known case of shape-selective catalysis involves the use of the 10-member-ring SAPO-11 zeolite to remove normal paraffins selectively from lubricating oils, leaving the branched paraffins behind.[1371,1372] A more recent system in this category is that of the selective acylation of toluene to para-methylacetophenone using the small-crystal-size zeolite beta.[1289] Examples in the fine-chemical industry include the production of diaminodiphenylmethane, a key intermediate in the production of polyurethanes,[1373] the ammoximation of cyclohexanone to produce ε-caprolactam, an intermediate for the production of Nylon-6,[1374] and the carbonylation of methanol for the production of acetic acid.[1375] Regarding the processing of biomass, it has been reported that the conversion of glucose to aromatic hydrocarbons can be enhanced by using zeolites such as ZSM-5 and ZSM-11, which have pore sizes in the intermediate range between 5.2 and 5.9 Å; smaller pores lead to much CO and CO_2 production, whereas larger cavities aid in the buildup of coke.[1376] Small-pore zeolites can also help with NO_x exhaust removal and with methanol conversion to light olefins by selectively providing access to small molecules (NO_x, methanol) while restricting entrance and departure of larger reactants and products.[1377,1378] Similarly, specific shapes can favor selected transition states, as in the case of hexamethylbenzene (HMB) methylation, where computational calculations showed that the linear O−C−C angle between the methyl group, a water molecule, and HMB required for the

https://doi.org/10.1021/acs.chemrev.1c00905
Chem. Rev. XXXX, XXX, XXX−XXX

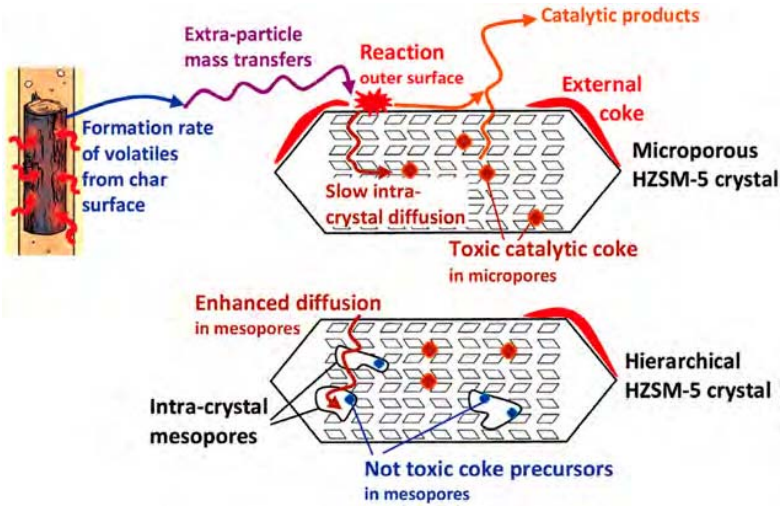

Figure 105. Schematic diagram of the mechanism of coke formation during the catalytic pyrolysis of biomass, highlighting the positive effect of hierarchical zeolite structures.[1421] Reproduced with permission from ref 1421 (open access article).

formation of the appropriate transition state is accessible in the AFX, CHA, ERI, LTA, RHO zeolites but not in the AEI, LEV and RTH counterparts, suggesting that the latter are not good catalysts for this reaction.[1379] In Figure 103, the DFT-calculated structures shown for the progression of the methylation of benzene with methanol in H-ZSM-5 and H-Beta zeolites indicate that the stability of the transition state is due to a stabilizing effect of the surrounding zeolite framework on the methyl cation via $H_2O\cdots CH_3^+\cdots C_B$ concerted bonds, which is higher in H-ZSM-5 than in H-Beta.[1380] In a recent example, cage effects in Fe-zeolites were exploited to control the mechanism of methane hydroxylation: by reducing the size of the pore apertures, the premature diffusion out of an individual zeolite cage is delayed, affording further reactivity of the methyl radical intermediate formed via H abstraction with the surface Fe(IV)−OH surface species formed in the same cavity to yield the desired methanol product.[1381]

Most zeolites exhibit pores with fairly symmetric geometries, a fact that limits their use in shape selectivity to discrimination based on molecular size only. However, more complex pore structures can in principle be conceived with well-defined single active sites and cavities or pockets where the reaction transition states may be stabilized by longer-range interactions. This is possible by, for instance, using mimics of the key molecular species involved in the reaction of interest in their synthesis; a discussion of this approach for the promotion of the conversion of methanol to olefins is provided in a recent article by Corma and coworkerss,[1382,1383] and another example, for the synthesis of the transalkylation between benzene and diethylbenzene, is illustrated in Figure 104.[1384] In fact, it is even possible, at least in principle, to promote stereo or enantioselective reactions by using chiral zeolites. There are some natural zeolites that can recognize enantiomers,[1385] but the custom-making of synthetic zeolites with desirable chiral sites remains quite challenging,[1386−1389] and in the few cases where this has been possible the enantioselective excesses (ee) measured in catalytic processes has been disappointingly low.[1390−1393] A couple of examples illustrate these limitations: the promotion of the acid conversion of t-stilbene oxide with polymorph-A slightly-enriched zeolite beta was found to yield (R,R)-diol with a ee of only 5%,[1290] and polymorph-A enriched Ti-beta was determined to bias the chirality of the product in the asymmetric epoxidation of β-methylstyrene by a similar value.[1394] Viable enantioselective catalytic processes using chiral zeolites are still to be developed.

Another recent approach to the enhancement of the use of the porous structure of zeolites to augment catalytic performance is by creating hierarchical pore networks displaying channels of different dimensions,[1395−1401] or by developing 2D layered solids.[1402,1403] These zeolites may not only improve catalytic kinetics by reducing mass transport limitations,[1404−1407] but also favor the preferential diffusion of reactants and products through different channel systems, allowing unique catalytic activities for specific chemical processes, from oil processing and fuel production to fine chemical synthesis and biomass conversion.[1401,1408−1424] A schematic illustration of how hierarchical zeoites can be used to minimize coke formation during the catalytic pyrolisis of biomass is provided in Figure 105.[1421] In the case of layered zeolites, adsorption and catalysis occur almost exclusively at the external surfaces, again minimizing mass transport bottlenecks and easing access of bulky molecules to the catalytic sites, and also providing higher tolerance against coking.[1425−1430] The structural details of zeolites can clearly affect their catalytic performance, their stability in particular (as reflected by catalytic lifetimes).[1416] Hierarchical pore structures can also afford the design of multifunctional catalysts where tandem reactions can be promoted in the appropriate sequence.[1431−1435] A recent report of this approach is that of the design of a porous zeolite framework with macropores functionalized with a sulfated zirconia solid-acid coating and mesopores functionalized with MgO solid-base NPs.[1436] This scheme was shown to be able to promote the two-step cascade deacetalization-Knoevenagel condensation of dimethyl acetals to cyanoates while preventing the poisoning of a base-catalyzed triacylglyceride transesterification process by free fatty acid impurities.

Overall, a multitude of zeolites have been successfully used in catalysis for many decades already, to take advantage of their acidic properties and well-defined pore shapes, yet newer ones continue to be developed. Zeolites are among the most versatile and most used oxides in catalysis, both by themselves

https://doi.org/10.1021/acs.chemrev.1c00905
Chem. Rev. XXXX, XXX, XXX−XXX

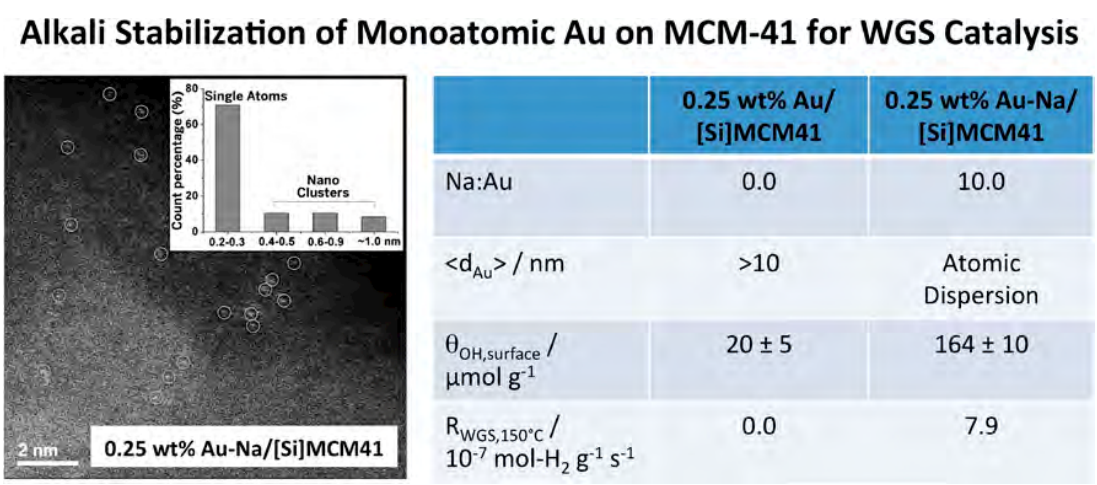

Figure 106. MCM-41-based catalysts for the promotion of the WGS reaction.[1483] Left: HAADF-STEM image indicating the atomic dispersion of Au on MCM-41 in a sample treated via Na^+ ion exchange. Right: Tabulated data showing the correlation between Au dispersion and OH surface coverage, parameters that can be modified via treatment with alkali metals, and WGS catalytic activity. Adapted with permission from ref 1483. Copyright 2014 American Association for the Advancement of Science.

and as support for other active catalytic phases such as metal NPs. On the negative side, because of the small size and symmetric shape of the pores in zeolites, their usefulness in shape selectivity is limited, although new synthetic methods using directing templating agents promise to expand the range of reactions where such selectivity may be incorporated.

6.2. Mesoporous Materials

The controlled and homogeneous structure of the pores in zeolites affords their use as shape-controlling agents. However, their dimensions, under 1 nm in diameter, limit their applicability to reactions involving relatively small reactants and products; bulky molecules cannot access the inside volume of their pores, and are able to react only on the external surfaces of most zeolites. Fortunately, a large variety of mesoporous materials has been developed over the past few decades to address this issue, with pore sizes between 2 and 50 nm in diameter, about one order of magnitude larger than those seen in zeolites.[1319,1437−1443] Indeed, the use of organic structure-directing agents as templates for the growth of solids with large porous structures has come a long way, and has helped in the design of new selective catalysts.[169,1444−1449] The first reported material within this category was MCM-41, a high-surface-area aluminosilicate molecular sieve that exhibits uniform one-dimension mesopores with tunable diameters between approximately 1.5 and 10 nm.[1386,1450] A second, very popular mesoporous material is SBA-15, a silicate with well-defined one-dimensional mesopores packed in the same hexagonal honeycomb arrangement as MCM-41 but with larger (5−15 nm) pore diameters.[1451] These solids are not crystalline, but do exhibit narrow pore size distributions and well-defined pore networks going from simple straight 1D cylindrical arrays, as in MCM-41 and SBA-15, to 3D networks and large spherical volumes connected by small windows.[1452] The wide pores of these solids afford their use with large reactants by reducing diffusional limitations. On the negative side, they tend to provide no particular advantage in terms of shape selectivity, and can be less stable than zeolites (although many have proven to be quite resistant to exposures to water[1453] or acids,[1454] and also to sintering upon heating to high temperatures).

Having chemical compositions similar to those of zeolites, typically aluminosilicates with or without other (P, Ti, etc.) added elements, the acidity of mesoporous materials can be tuned the same way,[1455] by adjusting the atomic ratio of the dopant (Al, Ti) to the silicon atoms, for instance,[871,1456] and used for the same acid−base reactions.[1438,1457−1460] Because of the larger size of the pores, however, acid−base catalysis with mesoporous materials can be expanded to complex feedstocks containing large molecules, as in the cases of, for instance, the hydrotreating of petroleum fractions[1457,1461,1462] and biofuels,[1463−1465] the cracking of polyolefins and plastics,[1466] the alkylation of organics,[1467−1469] and the processing of natural oils and fats.[1470] Another way to use mesoporous materials is for the control of the size of the products, ostensibly in polymerizations[1471,1472] and Fischer Tropsch synthesis.[1473−1476] Mesoporous materials can be made with other metal ions as well, incorporated during synthesis or via ion-exchange afterward, to use as redox catalysts.[1477−1482] Stabilization of catalytic sites within mesoporous materials is also possible, as in the case of the mononuclear gold catalyst that was stabilized by alkali ions in Au−O(OH)$_x$-(Na or K) ensembles on MCM-41 to optimize the promotion of the water−gas shift (WGS) reaction at low temperatures (Figure 106).[1483] It was determined that, in that case, the Au atoms create O linkages with more than eight alkali ions to establish an active monoatomic Au site on the silica-based irreducible support with intrinsic activity similar to that of reducible ceria, iron oxide, and titania supports.

Also similarly to the examples with zeolites, the shape and size of the inner volumes in mesoporous materials may be exploited to direct selectivity in catalytic conversions. Because of the large dimensions involved, on the order of several nanometers, this idea has in general not proven viable, but there are nevertheless some notable exceptions. For instance, a switch in selectivity has been reported, from the production of pyrimidine to enol lactones and δ-keto acids, when MCM-41 is used instead of other more conventional silica catalysts to promote the coupling of chromene with HCOOH.[1484] One particularly curious type of shape selectivity uses chiral mesoporous materials to introduce enantioselectivity in catalytic reactions. The synthesis of chiral mesoporous

https://doi.org/10.1021/acs.chemrev.1c00905
Chem. Rev. XXXX, XXX, XXX−XXX

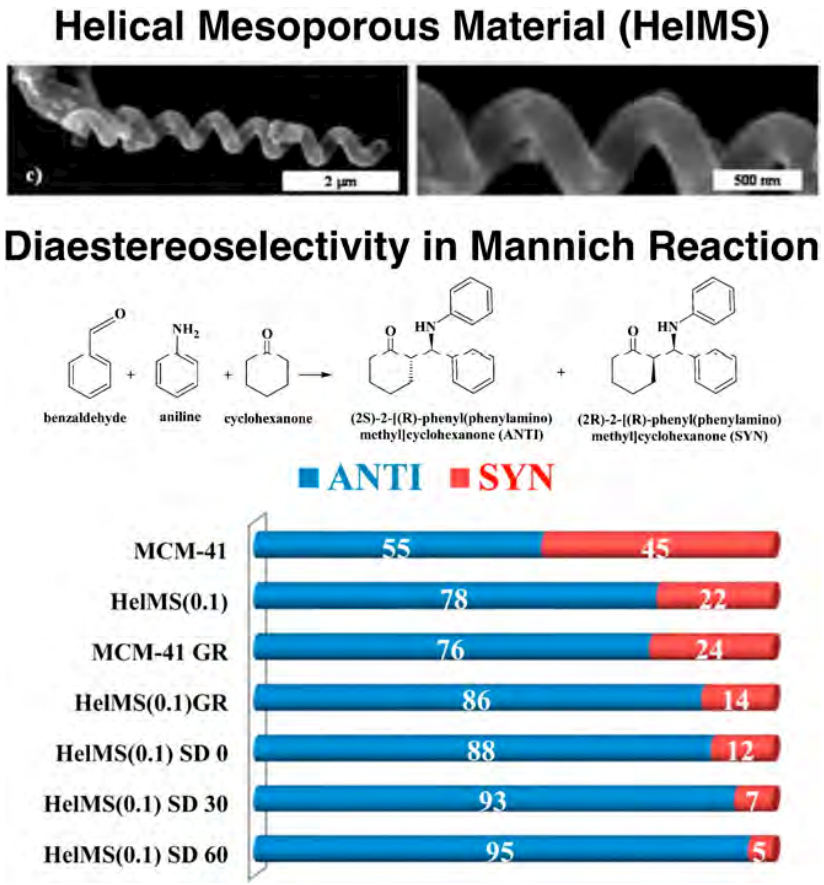

Figure 107. Use of chiral helical mesoporous materials (HeIMS), microscopy images of which are provided at the top, to direct diaestereoselectivity in the Mannich reaction (indicated in the center row).[1491] Data are provided for several HeIMSs, prepared following slightly different recipies, together with that for achiral MCM-41 for reference. Reproduced with permission from ref 1491. Copyright 2014 American Chemical Society.

materials has constituted a challenge in itself, and is a field still in its infancy.[1485−1489] Moreover, most of the few chiral mesoporous materials available to date are unstable, a fact that limits their application. Nevertheless, these materials have been successfully tested for the enantioselective resolution and adsorption of chiral compounds, for the delivery of chiral drugs, and for chromatographic separations.[1489] More relevant to this review, a helical mesoporous silica has been shown to, by virtue of the homohelicity of its structure, enantioselectively promote the asymmetric production of pyrimidyl alkanol from diisopropylzinc (i-Pr2Zn) and pyrimidine-5-carbaldehyde.[1490] In another case, similar materials were shown to add diaestereoselectivity to the Mannich reaction (Figure 107).[1491]

Although the large dimensions of the pores in mesoporous materials limits their ability to control shape selectivity, they do provide ample scope for the placement of active-phase catalytic sites within their inner volumes. Mesoporous materials are thus commonly used as supports for metal NPs, for instance.[167] The confined environment provided to active metal NPs by the cavities of mesoporous materials can be advantageous to help prevent, or at least minimize, coke formation during hydrocarbon conversions, in reactions such as methane dry reforming.[1492−1495] It may also affect selectivity in reactions promoted by active phases dispersed or tethered/anchored inside their pores: in spite of the relatively large radius of these pores, they still appear to exert an influence on the transition state of some promoted reactions. For instance, significant variations in enantioselectivity, both positive and negative, have been reported with chiral molecular catalysts immobilized inside the pores of mesoporous solid supports.[73,1496−1504] An example is provided in Figure 108, for a case where a chiral Mn salem complex grafted to the pores of MCM-41 was shown to improve enantioselectivity in olefin asymmetric epoxidation reactions.[1505] Heterogeneous catalysts made via the encapsulation of a Co-salen together with Ru-[N-2-(amino-κN)-1,2-diphenylethyl]-4-methylbenzenesulfonamidato-κN] inside the mesopores of SBA-16 were shown to perform as well as the free catalysts while affording their recycling without significant losses of catalytic performance.[1506] Other examples of reactions promoted by homogeneous catalysts encapsulated or tethered inside mesoporous materials include enantioselective hydrogenations,[1496,1507−1510] various C−C bond couplings[1511−1516] metathesis reactions,[1517] and alkane[1518] and sulfide oxidations.[1519] This confinement effect has been found to be the most pronounced within a specific range of pore sizes, depending on the reaction being promoted, and when the bonding between the tethered catalyst and the surface is more rigid.[1497] In some instances, the catalytic performance improvement, in terms of larger enantioselectivities in particular, has been ascribed to a kinetic resolution occurring inside the pores.[1520]

https://doi.org/10.1021/acs.chemrev.1c00905
Chem. Rev. XXXX, XXX, XXX−XXX

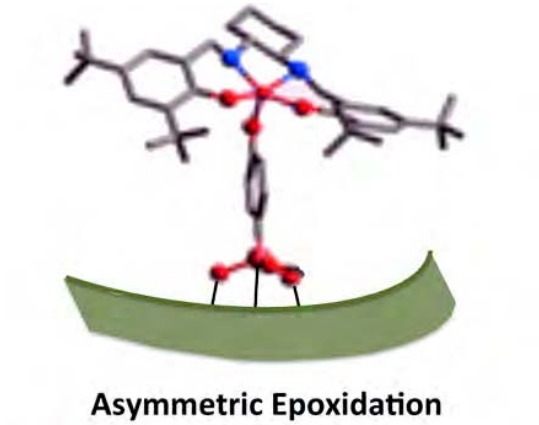

Catalyst	Mn(salen), Free	Mn(salen)/ MCM-41	Mn(salen)/ MCM-41
Solvent	CH_2Cl_2	CH_2Cl_2	EtOH
% Conversion	96	60	99
ee	56	72	70

Figure 108. Example of space confinement by mesoporous materials aiding enantioselectivity in catalysis, in this case for the asymmetric epoxidation of α-methylstyrene.[1505] Top: Chiral Mn salem complex grafted onto the inner surfaces of MCM-41. Bottom: Results from catalytic tests. First, it is clear that immobilization of the catalyst on the mesoporous support improves the ee of the reaction. Second, it can also be seen that the better ee is accompanied by a decrease in activity, which can be regained by selecting a better solvent; fortunately, the use of solid catalysts expands the range of solvents that can be used.

Trapping, encapsulation, or immobilization of large catalysts in mesoporous materials has become quite common,[167,1438] and has been even extended to enzymes.[202,208,1521−1526] In some instances, the surface of the mesoporous materials may assist in catalysis, via synergetic effects or after adding new functionalities on top of those of the primary phase,[259,1527−1530] and may also help with particular transition states or with multistep, tandem, or cascade reactions.[251,269,1436,1528,1531] Complex structures can be assembled inside the pores of mesoporous materials too. A nice example of this is provided by the work of Somorjai and coworkers, who prepared a catalyst based on Au clusters encapsulated in chiral SAMs inside the pores of MCF-17 to promote the asymmetric epoxidation of olefins (Figure 109).[1532]

Mesoporous materials can also be designed with hierarchical porous structures, although, because of their larger pore diameters, the advantages of doing so are not as obvious as with zeolites. On the other hand, mixed zeolites-mesoporous structures can be particularly useful to control the traffic of reactants and products through the porous structure, as discussed in Section 6.1.[1469] Overall, though, the most widespread application of mesoporous materials in catalysis may be as well-defined supports via the trapping or immobilization of NPs or homogeneous catalysts inside their cavities.

6.3. Metal-Organic Frameworks (MOFs)

Another type of porous crystalline materials that has gained prominence in catalysis in recent years is metal-organic frameworks (MOFs).[1533−1546] MOFs consist of ordered

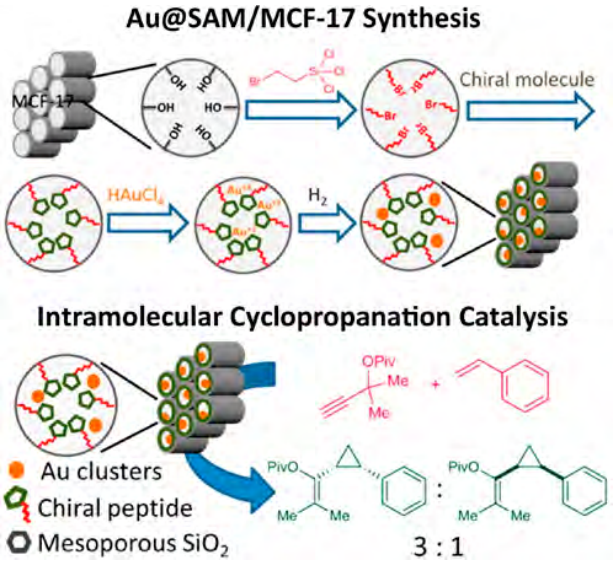

Figure 109. Top: Synthesis of catalysts based on Au NPs encapsulated inside a chiral-SAM/MCF-17 support.[1532] Bottom: Use for the enantioselective catalytic cyclopropanation of propargyl pivalate with styrene to preferentially produce the cis- (over trans-) substituted cyclopropane.[1532] Reproduced with permission from ref 1532. Copyright 2013 American Chemical Society.

structures made out of metal ions or clusters coordinated to organic ligands (which are sometimes referred to as "linkers" or "struts"). Given that metal ions are an integral part of the structure of MOFs, they may become interesting intrinsic catalytic sites analog to the ones seen in homogeneous catalysis. Moreover, because a diversity of metals (as well as organic functional groups) that can be incorporated in MOFs, much flexibility is available in catalysis design with these compounds. The organic struts can also exhibit catalytic activity, or, alternatively, can be used to tether other catalytic functionalities. Other advantages that MOFs have in common with zeolites and other mesoporous materials include high surface areas and tunable porosity, and also the fact that they can be used to direct shape selectivity. The structure of the framework imposes some limits on the nature of the ligands and on their number and geometry around the metal center, but many structures have been developed worth exploring for catalytic applications.[1547−1551] On the negative side, given that the scaffold of MOFs is based on organic molecules, those materials are in general less thermally stable than inorganic solids such as zeolites or mesoporous structures[1544,1546] This problem has nevertheless been successfully addressed in some cases in recent years.[1552−1554] Another limitation that many MOFs share with homogeneous catalysts include their poor chemical stability upon exposure to air, moisture, or other solvents.[1546,1552,1555,1556] Despite these limitations, the use of MOFs in catalysis has been expanding rapidly in recent years.

Much has been made of the ability of the metal ions in MOFs to coordinate to reactants and to promote conversion in a way similar to that seen with discrete metal molecular complexes. Perhaps the earliest report of this type of MOF-based catalysis was that of the promotion of the cyanosilylation of aldehydes by $[Cd(4,4'\text{-bpy})_2(NO_3)_2]_n$, a MOF with a 2D layered square-grid structure.[1557] Cyanosilylation, a reaction where nitrile and silyl groups are both added across double or triple bonds, is promoted by Lewis acids, and has been a

https://doi.org/10.1021/acs.chemrev.1c00905
Chem. Rev. XXXX, XXX, XXX−XXX

common application for MOFs. In the example above, the Cd-based MOF loses two water molecules upon activation to leave the metal centers unsaturated and with Lewis-acid character.[1557,1558] Other MOFs that can promote the cyanosilylation reaction include HKUST-1 ($[Cu_3$(benzene-1,3,5-tricarboxylate$)_2(H_2O)_3]_n$; HKUST = Hong Kong University of Science and Technology),[1559] Cr-MIL-101 ($[Cr_3(O)F$(benzene-1,4-dicarboxylate$)_3(H_2O)_2]_n$; MIL = matériaux de l'Institut Lavoisier),[1560] and $Mn_3[(Mn_4Cl)_3$(1,3,5-benzene-tristetrazol-5-yl$)_8(CH_3OH)_{10}]_n$,[1561] all materials that can easily release their coordinated water molecules to expose open Cu(II), Cr(III) or Mn(II) Lewis-acid sites, respectively. Given the greater Lewis acidity of Cr(III) versus Cu(II), Cr-MIL-101 has proven much more active in the promotion of cyanosilylation reactions than HKUST-1.[1562,1563] Studies with HKUST-1 have also highlighted some of the limitations common to MOFs cited in the previous paragraph, namely, the facts that the frameworks decompose with increasing reaction temperature due to the reduction of Cu(II) to Cu(I) by the reactant (the aldehyde), that they also decomposes in some organic solvents, and that electron donating solvents such as THF compete with aldehydes for coordination to the Cu(II) sites. One more recent and interesting example of MOFs catalysts is that of the homochiral Li(I) MOFs used to promote the asymmetric synthesis of cyanohydrin (Figure 110).[1564]

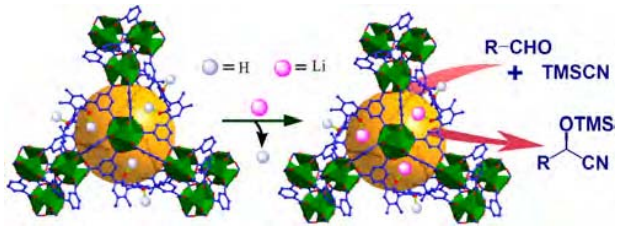

Figure 110. Homochiral MOF based on $[Zn_4(\mu 4\text{-}O)(L)_{3/2}]$ clusters used for the asymmetric synthesis of cyanohydrin (highlighted in green; the resulting cavity is indicated by the colored spheres).[1564] The catalyst was activated via ion exchange of protons with Li(I) ions prior to its use for the enantioselective promotion of the reaction of aldehydes (R−CHO) with trimethylsilyl cyanide (Me_3SiCN, TMSCN). Reproduced with permission from ref 1564. Copyright 2014 American Chemical Society.

The Lewis-acid sites in MOFs are also useful for the promotion of other reactions.[1565] An example is the Prins reaction, the electrophilic addition of aldehydes to alkenes or ketones followed by the capture of a nucleophile. In one study, it was reported that the activity for the addition of β-pinene to formaldehyde to produce nopol is proportional to the number of Lewis sites in the MOF use as catalyst, following the order ZIF-8 (M(methylimidazolate)$_2$, ZIF = zeolitic imidazolate framework) < Al-MIL-53 ($[Al(OH)$(benzene-1,4-dicarboxylate$)]_n$) < FeBTC ($[Fe$(1,3,5-benzenetricarboxylic acid$)]_n$, BTC = Basolite F300 or trimesic acid) < Cr-MIL-100 < Fe-MIL-100.[1566] Another example is that of the use of InPF-110 ($[In_3O(btb)_2(HCOO)(L)]_n$, ($H_3$btb = 1,3,5-tris(4-carboxyphenyl)benzene acid, L = methanol, water, or ethanol) to promote the Strecker reaction, that is, the condensation of aldehydes or ketones with amines in the presence of cyanides to form α-aminonitriles, which can be subsequently hydrolyzed to produce amino acids.[1567] Perhaps more common is the use of MOFs to promote Friedel-Crafts (alkylation or acylation) reactions, which proceed by electrophilic aromatic substitution assisted by a Lewis acid catalyst. It has been shown, for instance, that MOF-5 and other Zn-derived MOFs are efficient at promoting the *tert*-butylation of both toluene and biphenyl.[1568−1571] Interestingly, para-alkylation has been shown to be strongly favored over ortho-alkylation, forced by the shape of the cavity of the MOF.[1568] The Zn-based NU-601 MOF (NU = Northwestern University), with Zn paddlewheel dimers connected to a urea ligand and pillared with 4,4′-bipyridine (4,4′-bpy), has been reported as an active size-selective hydrogen-bond donor for Friedel-Crafts reactions between pyrroles and nitroalkenes (Figure 111).[1572] Other metal ions used in Lewis-acid MOFs for the promotion of Friedel Crafts coupling steps include Cu,[1573] Zr,[1574] and Fe.[1575] One final family of reactions that can be catalyzed by the Lewis-acid sites of MOFs is isomerizations, as in the case of the Fe MIL-based MOFs used to promote the α-pinene oxide rearrangement into camphonelal.[1576] Undercoordinated metals (i.e., defects) can serve as active Lewis-acid sites as well:[1561] Cu(I) defect sites in HKUST-1, for instance, can affect product selectivity and yield in cyclopropanation reactions.[1577]

MOFs that include transition metals able to sustain multiple oxidation states can also catalyze redox reactions.[1565,1578−1582] One common use of MOFs in this category is for the promotion of the aerobic oxidation of alcohols.[1583] For instance, a $[Pd$(2-hydroxypyrimidinolate$)_2]_n$ MOF has been shown to catalyze the selective oxidation of cinnamylalcohol to cinnamylaldehyde.[1584] It is curious that this is possible despite the initial coordinative saturation of the Pd ions. Also, at a minimum, these reactions require the redox interconversion of the metal nodes between Pd(II) and Pd(0) states, which is expected to be accompanied by changes in coordination number that should lead to the destabilization and potential destruction of the original framework. In another example, the Cu(II) ion in $[Cu_2$(trans-1,4-cyclohexanedicarboxylate$)]_n$ has been proven to promote the selective oxidation of 2-propanol, cyclohexanol, benzyl alcohol, 2-octanol, and 1-octanol with hydrogen peroxide.[1585] The oxidation of aromatic carbons to ketones using Fe-MIL-100 proved possible as well.[1586] In the example in Figure 112, isolated coordinatively-unsaturated metal sites were created in a HKUST-1 MOF via the incorporation of Pd ions into its framework to create an effective catalyst for the oxidation of benzyl alcohol to benzaldehyde.[1587] Other more-difficult-to-activate organic reactants can be oxidized using MOFs too. For example, the oxidation of cyclohexane to cyclohexanol and cyclohexanone have been reported to be promoted by Fe-based MOFs, in a case where the hydrophobicity of the pore environment was used to tune product selectivity.[1588] Even the more difficult oxidation of ethane to ethanol can be promoted using a coordinatively unsaturated Fe(II) MOF, $[Fe_2$(2,5-dioxido-1,4-benzenedicarboxylate$)]_n$.[1589] MOFs based on V_6O_{13} vanadium-oxo clusters as building blocks have proven active for the oxidation of thioether with O_2.[1590]

Redox reactions are an integral part of many photo- and electrochemical catalytic processes, and MOFs have been tested for those reactions as well.[1591,1592] Indeed, MOFs based on reducible ions such as Zr, Ti, and Ru have proven to be photoactive and viable for the promotion of photochemical reactions such as pollutant degradation[1593] and CO_2 reduction,[1594] even if this often requires a photosensitizer (which may or may not be incorporated in the MOF structure)[1595,1596] or a sacrificial agent.[1597] In the example in

https://doi.org/10.1021/acs.chemrev.1c00905
Chem. Rev. XXXX, XXX, XXX−XXX

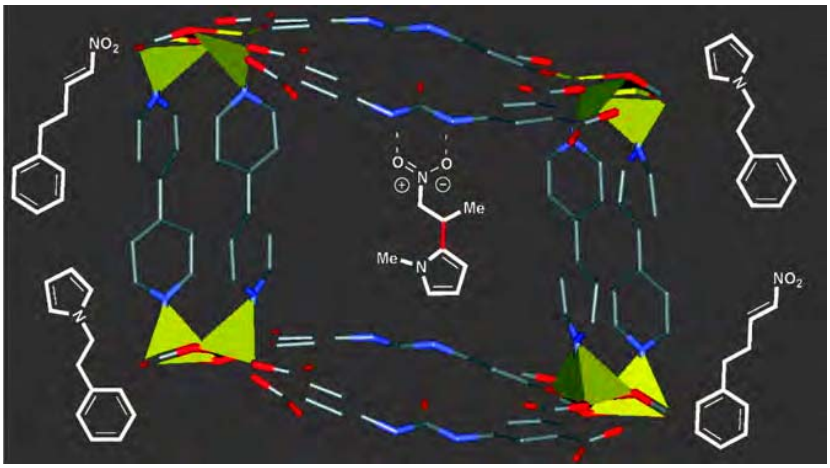

Figure 111. Structure of NU-601, a MOF made out of symmetrical urea tetracarboxylate struts, 4,4′-bpy, and $Zn(NO_3)_2{\cdot}6H_2O$ clusters.[1572] This material has been successfully used to promote Friedel−Crafts couplings between pyrroles and nitroalkenes (reactants shown on the outside, product in the inside of the MOF cavity). Reproduced with permission from ref 1572. Copyright 2012 American Chemical Society.

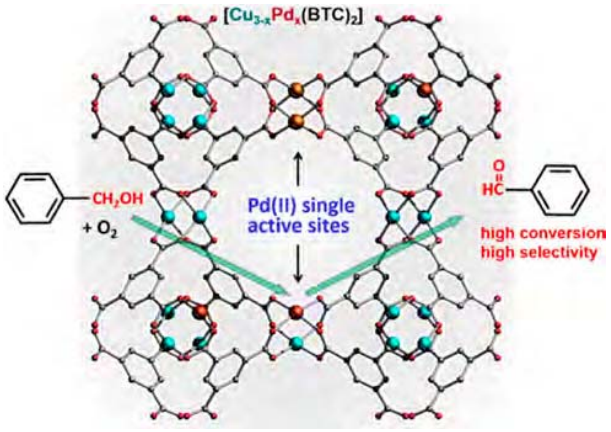

Figure 112. Pd-HKUST-1 MOF developed for the selective oxidation of benzyl alcohol to benzaldehyde.[1587] Reproduced with permission from ref 1587. Copyright 2018 American Chemical Society.

Figure 113. $[Zn_{0.986}$(meso-tetra(4-carboxyl-phenyl)porphyrin)-$(AlOH)_2]_n$ MOF as the photoactive component of a catalytic system to produce H_2 from water that also includes colloidal platinum NPs and sacrificial EDTA.[1598] Reproduced with permission from ref 1598. Copyright 2012 WILEY-VCH Verlag GmbH & Co. KGaA, Weinheim.

Figure 113, a Zn-based MOF, $[Zn_{0.986}$(meso-tetra(4-carboxyl-phenyl)porphyrin)$(AlOH)_2]_n$, was reported to aid in the visible-light photocatalytic evolution of hydrogen from water, in combination with colloidal platinum NPs and EDTA as a sacrificial agent.[1598] However, most MOFs can only reduce CO_2 to CO or formates.[1565] For instance, Ir, Re, and Ru H_2L_1−H_2L_6 complexes incorporated in $[Zr_6O_4(OH)_4$(para-biphenyldicarboxylic acid$)_6]_n$ (UiO-67; UiO = Universitetet i Oslo) selectively promote the production of CO,[1599] whereas $[Ti_8O_8(OH)_4$(benzene-1,4-dicarboxylate$)_6]_n$ (Ti-MIL-125) photocatalytically reduces CO_2 to formic acid.[1600] On the other hand, MOF/TiO_2 nanocomposites can be active for the reduction of CO_2 reduction to methane.[1601] Unfortunately, little discussion has been provided in the corresponding reports on what controls selectivity in these processes. The promotion of the electrochemical reduction of water[1602] or CO_2[1603] with MOFs is possible as well. In those cases, the initial electrochemistry relies on the electronic conductivity and activity of the reducible transition metal (Fe, Co, Mn) immobilized in the MOF framework. Many MOFs used for these applications are based on porphyrin frameworks, but, again, in the case of CO_2 reduction, MOFs tend to show high efficiency only toward the production of CO or methane,[1603−1605] like in the case of photocatalysis. To further produce alcohols, MOFs containing other metal centers, Cu in particular,[1606,1607] are required.

Other reactions promoted by the metal centers of MOFs include olefin hydrogenations, C−C couplings, and related reactions,[1565] although in the case of Pd-based MOFs it is difficult to rule out the possibility that catalysis takes place at the surface of MOF-encapsulated metal clusters or of NPs that may form from MOF decomposition.[1534,1584] A Zr-UiO MOFs functionalized with either Fe or Co complexes has been shown to be highly active for alkene hydrogenations.[1608] Salen-[1609] and porphyrin-[1610] based MOFs containing certain transition metals (Zn, Co, Ni), and MOFs with strong Lewis-acid sites,[1611−1613] have all been tested for CO_2 cyclizations to

https://doi.org/10.1021/acs.chemrev.1c00905
Chem. Rev. XXXX, XXX, XXX−XXX

produce cyclic carbonates. The structure used in the latter study, where sulfonate rather than carboxylate struts were used to increase polarity and bonding to CO_2 and to hence improve catalytic performance, is shown in Figure 114.[1613]

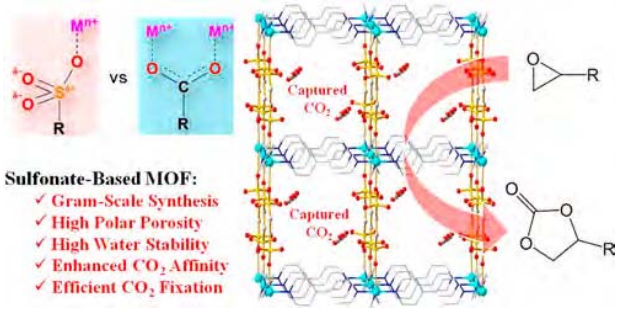

Figure 114. Cubic sulfonate-based MOF constructed with Jahn–Teller distorted Cu(II) centers and mixed organosulfonate/N-donor struts for the promotion of the CO_2 fixation with epoxides to produce cyclic carbonates.[1613] Reproduced with permission from ref 1613. Copyright 2016 American Chemical Society.

Much focus on the use of MOFs in catalysis has been placed on taking advantage of the chemistry of the metal centers, but in some cases catalytic promotion has been achieved by using functionality associated with the organic linkers, either in the coordinative groups that bind to the metal sites to hold the crystalline framework, or, more commonly, as reactive functional groups that remain uncoordinated and exposed inside the porous structure for reaction.[1614] An example of the latter is the amide functionalities of $[Cd(4\text{-}1,3,5\text{-benzene tricarboxylic acid tris}[N\text{-}(4\text{-pyridyl})amide)_2(NO_3)_2]\cdot 6H_2O\cdot 2DMF]_n$, which has been shown to catalyze the Knoevenagel condensation of benzaldehyde with malononitrile; limited activity with larger nitriles indicated that the catalysis takes place inside the pores of the MOF, and the fact that no catalysis was seen with the free struts in homogeneous solution pointed to the importance of intermolecular H-bonding between organic ligands in the final catalytic performance (Figure 115).[1615] In some cases, catalytic functionality can be added after the MOF synthesis. For instance, the post-synthetic addition of $Co(CO)_4^-$ to Cr-MIL-101 has been shown to result in a solid with catalytic performance comparable to homogenous catalysts for the ring-expansion carbonylation of epoxides; the observed behavior was explained on the basis of a synergy between the Cr(III) Lewis acid centers of the MOF and the added Co carbonyls.[1616] In another example, iodo-functionalized Al-based MOFs (MIL-53 and DUT-5; $[M_2(biphenyl\text{-}4,4'\text{-dicarboxylate})]_n$, DUT = Dresden University of Technology) and Zr-based MOFs (UiO-66 and UiO-67) were successfully tested for the catalytic oxidation of hydroquinones and diols.[1617,1618]

The ligands used in MOFs may be amenable to designs or modifications aimed at introducing Brønsted-acid sites. These have been employed to promote many reactions, including cyanosilylations of carbonyl compounds, Mukaiyama aldol condensations, Friedel–Crafts benzylations, α-pinene oxide isomerizations, and the conversion of citronellal to isopulegol, as well as oxidations of alcohols, sulfides, olefins, paraffins, and CO.[1619] For instance, modification of the interior of MIL-101 via Cr(III) coordination to only one of the two available

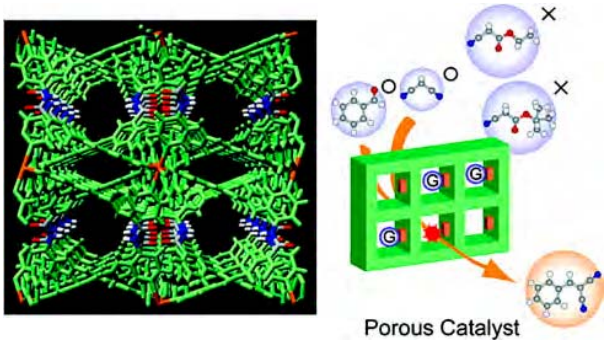

Figure 115. Left: Structure of a $[Cd(4\text{-}1,3,5\text{-benzene tricarboxylic acid tris}[N\text{-}(4\text{-pyridyl})amide)_2(NO_3)_2]\cdot 6H_2O\cdot 2DMF]_n$ MOF used for the promotion of the Knoevenagel condensation of benzaldehyde with nitriles.[1615] Right: Scheme highlighting the fact that the catalysis is successful only with small (malononitrile) nitriles, and not feasible with larger (ethyl cyanoacetate, cyano-acetic acid *tert*-butyl ester) reactants because of the limitations imposed by the MOF pore size. Reproduced with permission from ref 1615. Copyright 2007 American Chemical Society.

nitrogen atoms of the ethylenediamine ligands leaves free non-coordinated ends in those that can be used as Brønsted-base catalysts for the Knoevenagel condensation of benzaldehyde with nitriles.[1620,1621] Chirality can be added to the MOF-promoted chemistry as well, as in the case of $[Cu(L\text{-aspartate})(trans\text{-}1,2\text{-bis}(4\text{-pyridyl})ethylene)_{0.5}(HCl)(H_2O)]_n$, which has been selectively protonated at the carboxylic end of the amino acids (without protonating the amine groups) to create novel Brønsted-acid sites capable of facilitating the ring-opening methanolysis of small epoxides.[1622] In a perhaps more sophisticated application, a hybrid Cr-MIL-101-SO_3H MOF containing both Cr(III) strong Lewis-acid and $-SO_3H$ Brønsted-acid sites has been used to promote the dehydration of glucose to HMF: the first type of site helps with the isomerization of glucose to fructose, whereas the second is required for the dehydration of the new isomer (Figure 116).[1623]

MOFs can be used to encapsulate metal NPs, in which case the MOF can act simply as a support with a well-defined pore structure, or can also provide catalytic sites that may interact in

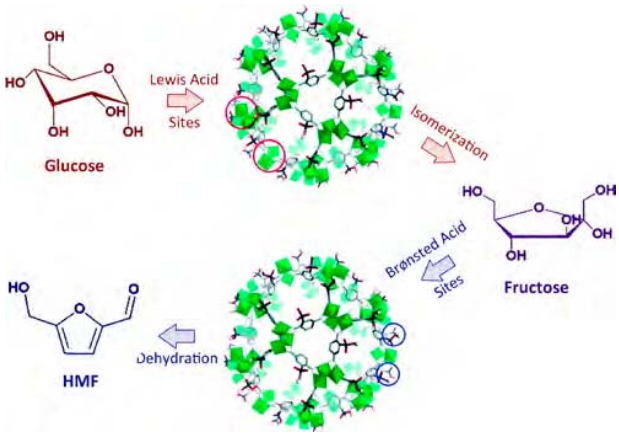

Figure 116. Lewis/Brønsted acid bifunctional catalysis based on Cr-MIL-101-SO_3H for the conversion of glucose to HMF.[1623] Adapted with permission from ref 1623. Copyright 2016 John Wiley and Sons.

https://doi.org/10.1021/acs.chemrev.1c00905
Chem. Rev. XXXX, XXX, XXX–XXX

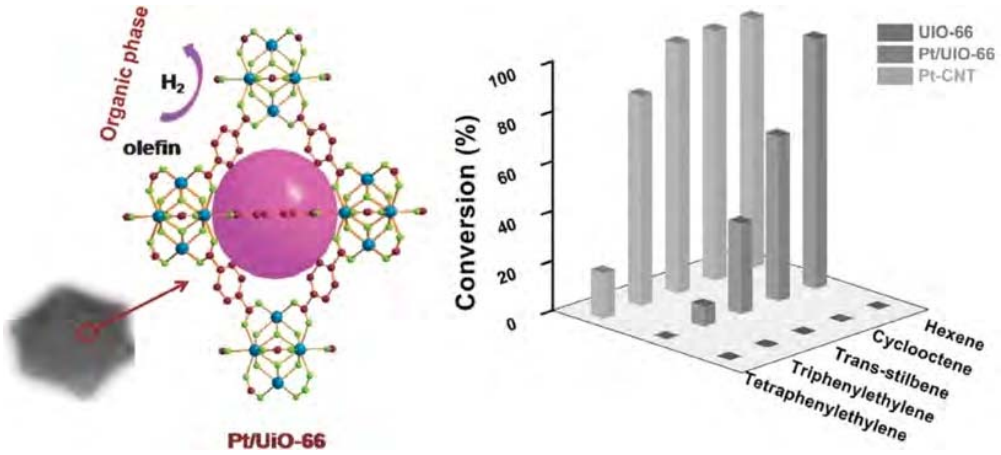

Figure 117. Performance of a (Pt NP)/UiO-66 catalyst, depicted on the left, in the hydrogenation of olefins.[1631] Right: Summary of the activity of this and of a more conventional Pt/CNT catalyst for the conversion of several reactants to highlight the size selectivity provided by the MOF structure, as the (Pt NP)/UiO-66 matches the performance of Pt/CNT with hexene but is virtually inactive for the hydrogenation of bulkier alkenes such as tri- and tetra-phenylethylenes. Reproduced with permission from ref 1631. Copyright 2014 WILEY-VCH Verlag GmbH & Co. KGaA, Weinheim.

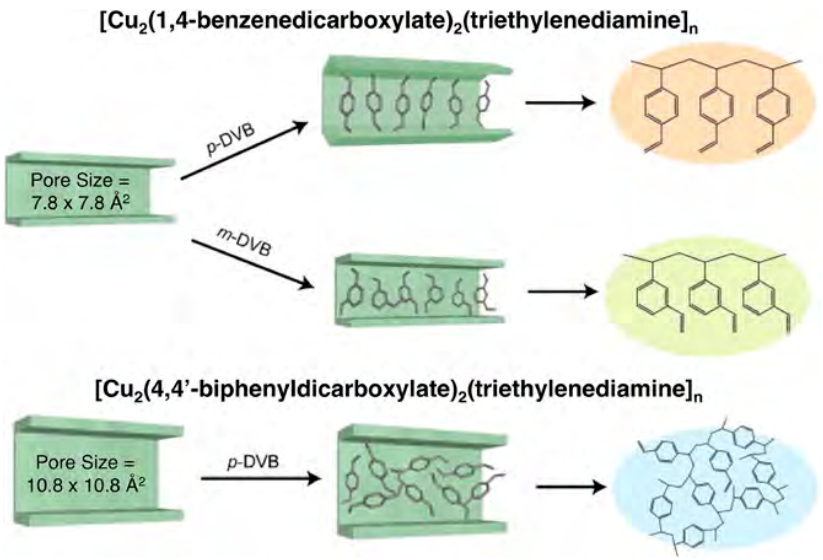

Figure 118. Effect of the pore size of Cu MOF catalysts on the selectivity of the tacticity of divinylbenzene (DVB) polymerization.[1640] Linearly extended topotactic polymerization without cross-linking is obtained with the small pores of the MOF made with benzenedicarboxylate struts but not with the larger pores of the biphenyldicarboxylate analog. Reproduced with permission from ref 1640. Copyright 2007 Wiley-VCH Verlag GmbH & Co. KGaA, Weinheim.

synergy with those provided by the NPs.[1624,1625] Because NPs are relatively large, introducing them into the MOF porous structure can be challenging. Nevertheless, this can be accomplished by assembling active species within the pores of the support (ship-in-bottle approach), by assembling the support around the active species (bottle-around-ship, or templated-synthesis, approach), or by growing the metal NPs *in situ* on functional groups grafted to MOFs. For instance, a catalyst consisting of Pd NP entrapped in Cr-MIL-101, made following the third synthetic methodology, was shown to exhibit similar catalytic activity as Pd NPs dispersed on a carbon support for the Heck reaction.[1621] Many hydrogenation reactions have been promoted with Lewis-acid sites of MOFs acting synergistically with metal NPs, helping with the coordination of the reactants; the metal NPs promote H_2 dissociation and H atom incorporation. In recent work from our group, for instance, Pt and Co intermetallic NPs were confined within the inside pores of Cr-MIL-101 to achieve enhanced selectivity for the hydrogenation of the carbonyl bond in α,β-unsaturated aldehydes; the catalytic performance improvement was ascribed to synergistic effects between electronically modified Pt sites (by the added Co) and Lewis (Cr) acid sites.[1626] In another example, Somorjai and co-workers have shown that the gas-phase hydrogenation of methylcyclopentane with UiO-66-encapsulated Pt NPs results in cyclohexane and benzene production at low temperatures, with selectivities dependent on pore size.[1627,1628] Modification of the MOFs to vary their hydrophobicity has been shown to stabilize Pd/MOF composite catalysts and hence improve their hydrogenation performance.[1629] The hydrogenation of CO_2 to

https://doi.org/10.1021/acs.chemrev.1c00905
Chem. Rev. XXXX, XXX, XXX−XXX

methanol with MOF-embedded metal NPs has been possible as well.[1630] MOFs can also be used to add shape selectivity to transition-metal-NP hydrogenation catalysis (Figure 117).[1631] In terms of oxidations, the case of Ru NPs entrapped in MOF-5 frameworks to catalyze the oxidation of benzyl alcohol to benzyaldehyde can be cited,[1632] and also that of Pd NPs embedded within defective HKUST-1 to promote stepwise benzyl alcohol oxidation.[1633] One shortcoming here is that the MOF can decompose under severe oxidation conditions. Other reactions catalyzed by metal-NP/MOF combinations include the acetalization or ketalization of carbonyl compounds, the rearrangement and ring opening of epoxides, the methylation of amines, aldol condensations, and cyanosilylations and heterocycle synthesis.[1634,1635] Even non-metallic clusters can be entrapped in MOFs and used as catalysts, as in the case of Cu-based polyoxometalate anionic clusters fitted inside the pores of HKUST-1 to catalyze the air-based oxidation of H_2S and other thiols and disulfides.[1636]

The crystalline nature of MOFs, with pores of well-defined size and shape, can also be exploited to add shape selectivity to catalytic reactions, as already alluded to in some of the examples cited above. Commonly, the pores of MOFs can be used to limit reactions to only small reactants, as in the example in Figure 117. In another case, the 10 Å pores in $[Mn_3[(Mn_4Cl)(1,3,5\text{-benzenetristetrazolate})_8(CH_3OH)_{10}]_2]_n$ were shown to limit cyanosilylation to small carbonyl substrates such as benzaldehyde; poor performance was seen with larger reactants such as biphenylmethyl ketone.[1561] Also, $[(Zn_4O)_3[(1,4\text{-benzenedicarboxylate-2-}C_6H_5N_2Pd(OAc)_2]_3\text{-}(4,4',4'\text{-benzene-1,3,5-triyl-tribenzoic acid})_4]_n$ has shown hydrogenation activities following a trans-chalcone < trans-stilbene ≪ cinnamyl acetate < styrene ordering.[1637] The range of sizes of molecules that can access the inside volume of the pores in MOFs is nevertheless significantly larger than that in zeolites, affording the use of MOFs for reactions such as the preferential photochemical decarbonylation of *o*-methyl dibenzyl ketone (with $[Co(biphenyldicarboxylate)_3(4,4'\text{-bpy})\cdot 4DMF\cdot H_2O]_n$).[1638] The pore size in $[Cu_2(L)_2\text{-}(triethylenediamine)]_n$ MOFs can also be tuned via the incorporating of L struts of different lengths to stabilize propagating radicals and suppress termination reactions in polymerization catalysis, to, for instance, convert divinylbenzenes into linearly extended topotactic polymers without cross-linking (Figure 118).[1639,1640]

Catalytic selectivity with MOFs can extend to regio-, stereo, and enantio-control when chiral MOFs are used.[484,1537,1641−1646] Several strategies can be followed for the making of homochiral MOFs, including the direct use of chiral ligands,[1509,1641,1647−1649] the chiral resolution of racemic linkers (using auxiliary chiral agents[1650,1651] or during crystallization[1652,1653]), and the addition of chiral functionality to achiral MOFs in post-synthesis steps.[1654−1657] Possibly, the first example of the synthesis and use of chiral MOFs in catalysis was that of a Zn based MOF made of tartaric-acid-derived chiral strut, which was shown to promote the transesterification of 2,4-dinitrophenyl acetate with racemic 1-phenyl-2-propanol with moderate enantioselectivity (ee ~8%).[1647] Many other examples have been reported since.[1658−1668] For instance, the protons on the biphenol strut in the $[(Cu_2(S)\text{-}2,2'\text{-dihydroxy-}6,6'\text{-dimethyl}(1,10\text{-biphenyl})\text{-}4,4'\text{-dicarboxylate})_2(H_2O)_2]_n$ chiral MOF (KUMOF-1; KU = Korea University) were replaced with Zn(II) cations to enantioselectively promote the cyclization of 3-methyl-geranial to the cyclic terpenoid analogue following a Lewis-acid-promoted carbonyl-ene reaction.[1669] In the case reported in Figure 119, a family of chiral MOFs with cubic network

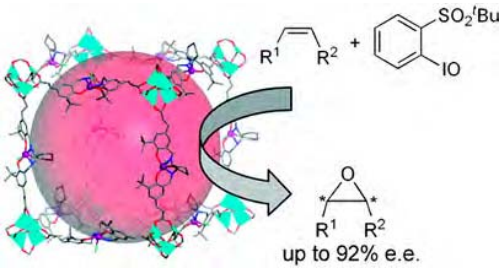

Figure 119. Isoreticular chiral MOF constructed from $[Zn_4(\mu_4\text{-}O)(O_2CR)_6]$ secondary building blocks linked by dicarboxylate struts derived from chiral Mn-Salen catalytic subunits, used for the asymmetric epoxidation unfunctionalized olefins.[1658] The pink sphere indicates the void space available. Reproduced with permission from ref 1658. Copyright 2010 American Chemical Society.

topologies was constructed using $[Zn_4(\mu_4\text{-}O)(O_2CR)_6]$ secondary units linked by dicarboxylate struts derived from chiral Mn-Salen subunits.[1658] The relative performance of the resulting catalysts indicated that, although diffusion of the alkene and the oxidant used in the asymmetric epoxidation of unfunctionalized olefins can be a rate-limiting factor, the catalytic activity of the MOFs with large open channels can also be limited by the intrinsic reactivity of the catalytic molecular building blocks.

If porous organic frameworks only involve organic constituents, without metals, they are denominated covalent organic frameworks (COFs), or, if they involve polymers, porous organic polymers (POFs).[1541] These highly crystalline porous solids were initially introduced by Yaghi and coworkers,[1670] and have been used in catalysis primarily as supports for molecular active phases, which can be covalently attached to specific sites within the organic framework.[1671−1673] Because of their well-defined porous structure, COFs have also been tested for shape-selective catalysis.[1674] Moreover, COFs are promising as promoters of chiral organic conversions,[1675−1677] and in photocatalysis.[1676,1678,1679] A recent example of COFs used in photocatalysis is the azine-linked N_2−COF photosensitizer, which, combined with chloro(pyridine)cobaloxime as a co-catalyst and triethanolamine as a sacrificial electron donor, was shown to efficiently promote the photocatalytic production of H_2; in this case, the catalytic mechanism was proposed to involve the initial transfer of an outer sphere electron from the COF to the co-catalyst.[1680] COFs can also themselves provide well-defined acid sites, as in the case of the sulfonated 2D 1,3,5-triformylphloroglucinol-2,5-diaminobenzenesulfonic acid COF tested for the selective dehydration of fructose to 5-HMF,[1681] or exhibit zwitterionic sites, useful for the reduction of CO_2.[1682] COFs containing π-electronic moieties such as anthracene have been shown to promote Diels-Alder reactions under ambient conditions.[1683] The use of COFs in catalysis is still in its early stages.

In conclusion, the incorporation of MOFs in catalysis is growing, and the new developments in this area are quite promising. Because of their intrinsic complex-like nature, MOFs offer the potential of high selectivities in sophisticated reactions, comparable to those seen with homogeneous

https://doi.org/10.1021/acs.chemrev.1c00905
Chem. Rev. XXXX, XXX, XXX−XXX

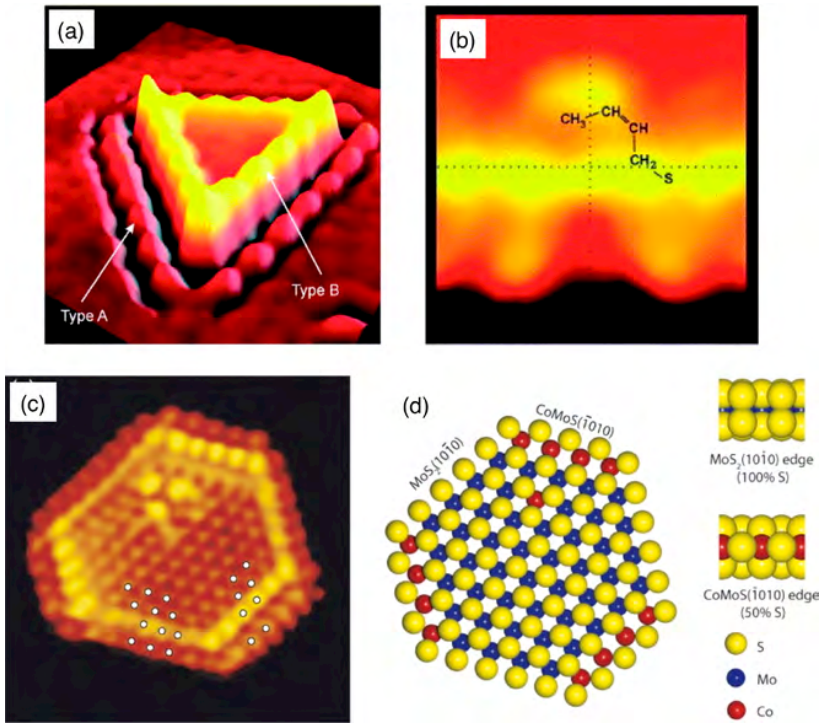

Figure 120. Characterization of a model MoS_2-based HDS catalytic surface. (a) 3D STM image of a triangular single-layer MoS_2 nanocluster after low-temperature exposure to thiophene. The molecularly adsorbed C_4H_4S was detected in two different configurations: decorating the perimeter of the cluster (Type A), and on top of the bright brim sites associated with an edge state (Type B).[1698] (b) STM image of a cis-but-2-ene-thiolate (C_4H_7S) molecule, a potential intermediate in HDS reactions, adsorbed on a metallic brim site.[1698] (c) STM image, and (d) ball model of a Co-treated MoS_2 nanocluster.[1702] Reproduced with permission from refs 1698 and 1702. Copyright 2004 and 2007 Elsevier Inc.

catalysts, while at the same time incorporating additional discriminating power driven by the size and shape of their pores. They also provide many of the advantages associated with other heterogeneous catalysts in terms of ease of separation, purification, recyclability, and viability in a variety of solvents in liquid phase. Nevertheless, the use of MOFs as catalysts does have some limitations. First and foremost, MOFs are less stable than other heterogeneous catalysts, as they usually cannot withstand high temperatures or be regenerated via calcination or other harsh treatments. They may also react easily with solvents, moisture, and other chemicals. The crystalline structures of the MOFs that have been used in catalysis up to date have been limited to only a handful of highly symmetric pore structures, a fact that limits their ability to direct selectivity. The options in coordination of reactants around the metal centers are also restricted, as that is mainly controlled by the ligands used to build the MOF structure, and catalytic reactions that require coordination changes (as is the case with many redox processes, for instance) may affect MOF stability and perhaps render the catalysts useless. Mass transport limitations may reduce reaction rates in some cases as well. Ultimately, though, even if MOFs may not be universally applicable to all problems of catalysis, they may be ideal for the promotion of certain families of reaction, in particular difficult organic conversions.

6.4. Two-Dimensional and Layered Materials

Two-dimensional (2D) materials have regained some notoriety recently in many applications because of their well-defined and unique characteristics,[1684,1685] and are increasingly being incorporated into heterogeneous catalysts.[908−911] It should be noted that some 2D materials have been used in catalytic processes for a long time already. In particular, MoS_2 and other transition metal dichalcogenides (TMDs) are well-known promoters of HDS and hydrotreatment reactions in petroleum processing,[1686−1691] and have also more recently been incorporated into the hydrotreating of bio-fuels.[1692,1693] Extensive fundamental studies on these systems have led to the conclusion that the basal planes of MoS_2 are inert, and that it is the special sites present at the edges of MoS_2 islands dispersed on solid supports that promote catalysis.[1694−1697] A major breakthrough in our molecular understanding of the functioning of these catalysts came from the extensive surface-science studies with model systems carried out by a Danish group.[1698,1699] By using STM in conjunction with DFT, they showed that monolayers of MoS_2 deposited on flat surfaces form triangular nanoclusters with fully sulfided edges and metallic character.[1698] Active sites in the form of S vacancies may be formed *in situ* via the reshaping of those MoS_2 2D islands within the reaction environment, following the removal of S atoms from the edges of the S-terminated islands.[1699] These so-called "brim" sites were showed to be capable of adsorbing thiophene (a prototypical molecule used to represent the S-containing impurities in crude oil; Figure 120a) and to promote its partial hydrogenation via C−S bond breaking and ring opening steps (Figure 120b).[1698] Presumably, a second C−S bond-scission step is to follow, to release a sulfur-free hydrocarbon molecule while the S atom, retained at the edge of the MoS_2 triangular structures, is then hydrogenated and removed as H_2S. With this knowledge in hand, methods were developed to produce similar brim sites on industrial-style nanocatalysts;[1696,1700] the end result from this

https://doi.org/10.1021/acs.chemrev.1c00905
Chem. Rev. XXXX, XXX, XXX−XXX

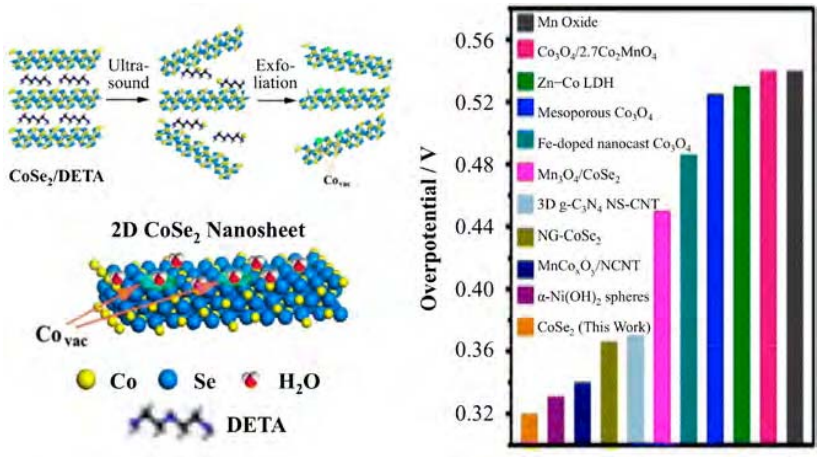

Figure 121. $CoSe_2$ catalyst for the promotion of OER.[1717] $CoSe_2$ nanosheets were prepared via exfoliation of the bulk material using diethylenetriamine (DETA, top-left). The resulting material displays many surface Co vacancies, which can act as sites for water adsorption and decomposition (bottom-left). The overpotential measured with these $CoSe_2$ nanosheets was approximately 0.32 V, lower than those seen with other reported OER catalysts (right). Adapted with permission from ref 1717. Copyright 2014 American Chemical Society.

effort has been the development of a number of TK-XXX BRIM commercial catalysts sold by the Haldor-Topsøe company. In many instances, metals such as Co or Ni are added as dopants to improve catalytic performance,[759,1701] and similar fundamental studies allowed the Danish researchers to locate the position of those adatoms; a particular Co−Mo−S edge structure was proposed as the catalytic site in those cases (Figure 120c,d).[1694,1702]

More recently, the catalytic use of TMDs has been extended to other reactions, in particular to the electrocatalytic HER and OER in aqueous solutions.[908,910,1703−1708] Because of their low onset overpotentials, low Tafel slopes (which provide estimates of how much the overpotential needs to be increased to increase the reaction rate by a factor ten), and large cathodic current densities, TMDs are good candidates for electrocatalysis. However, the challenge is to produce materials exhibiting abundant defect sites while still retaining good stability under electrocatalytic redox environments.[1709] Again, new synthetic protocols are being developed to accomplish this goal,[1710−1714] including the addition of dopants, as in the case of HDS.[1715] Critically, it has been shown that 2D (single-layer) versions of TMDs perform significantly better than bulk TMD materials.[1716] In one example, a $CoSe_2$ 2D nanosheet was made via exfoliation of bulk $CoSe_2$ to create surfaces with high density of defects; the resulting material proved to be quite effective for the promotion of OER, displaying a lower overpotential than many other materials used for this reaction (Figure 121).[1717] Amorphous materials, which have large number of defect sites, also display higher activities than their crystalline counterparts,[1718] even if less control can be exerted on their exact structure. TMDs can be used for photocatalysis as well.[1707,1708]

Another 2D material that has received increased attention in catalysis in recent years is graphene.[911,1719−1723] Carbon-based solids such as graphite and amorphous carbon have been long employed as catalyst supports; their electrical conductivity has made them particularly good candidates for electrocatalytic applications.[134,910,1724−1729] Graphene, a one-sheet-thick 2D layered material that consists of an hexagonal network of sp^2 carbon atoms and that when stacked makes graphite, has also become prevalent in catalysis and other application. Graphene can be synthesized via exfoliation of graphite, but can also be produced following alternative preparation procedures.[1719,1720,1730−1733] The basal planes of pure and defect-free graphene are mostly chemically inert (although they can act as pi ligands in metalorganic chemistry, for instance),[1734] and are therefore used primarily as supports.[1735] Nevertheless, graphene displays unique electronic, thermal, and mechanical properties that are sometimes useful in catalysis,[910,1721−1723,1736] in particular in electro-[910,911,1737−1739] and photo-[600,911,1708,1719,1740,1741] catalysis. In electrocatalysis, graphene has been tested for the promotion of ORR, OER, and HER.[910] In one recent example, Guo et. al. used highly-oriented N-doped pyrolytic graphite as a model catalysts to pin down the details of the ORR reaction, which they determined takes place via the initial adsorption of O_2 on a C atom adjacent to the pyridinic N followed by stepwise one-electron H^+ reduction and H addition steps (Figure 122).[1742] This example highlights the complexity of the sites required on graphene-type surfaces to effectively promote even simple catalytic reactions, and little effort have been spent to date to use graphene-based catalysts to control selectivity in more complex reactions. The promise is there, but more work is needed.

Graphene sheets can also display (or can be treated to develop) chemical point defects, typically the result of the removal of one or more C atoms from the hexagonal network to create vacancies in the form of localized organic moieties (alcohols, epoxides, or carboxylates in graphene oxide −GO−, for instance)[1743,1744] or substitutionally replaced atoms, and those can be used for surface derivatization and for functionality addition,[911,1745−1747] In many cases, these defects are used as nucleation sites for the creation of metal single-atom catalysts (an example of this was already provided in Figure 60).[134,1748−1750] Alternatively, defects can originate from dislocations in the graphene hexagonal carbon grid. Graphene can also be doped;[1722,1751−1755] typical dopants include N[910,1722,1742] and, less commonly, B,[1756−1758] Si,[1759] P,[1741,1760] S,[1761,1762] Se,[1761,1763] or I,[1764] and sometimes two or more elements are incorporated at once.[1753,1765,1766] Finally, graphene can be oxidized to produce GO, which tend to have more chemically active moieties and to be more chemically

https://doi.org/10.1021/acs.chemrev.1c00905
Chem. Rev. XXXX, XXX, XXX−XXX

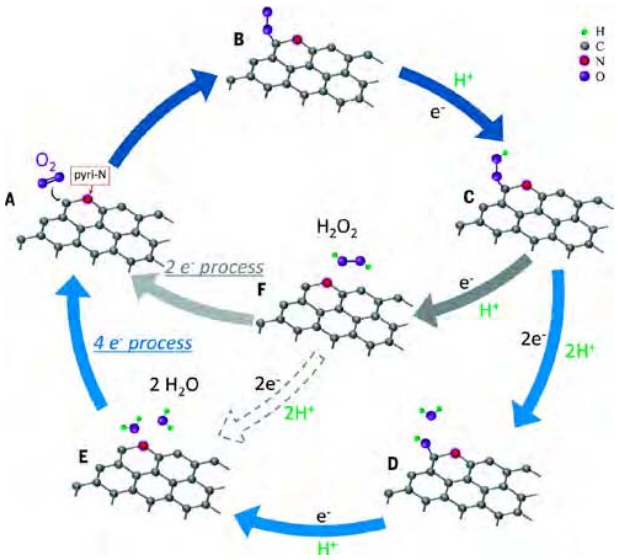

Figure 122. Proposed mechanism for the electrocatalytic ORR on a N-doped graphite electrode.[1742] Reproduced with permission from ref 1742. Copyright 2016 American Association for the Advancement of Science.

active.[1743] Figure 123 summarizes the most common types of active sites available in catalysts made out of graphene.[1723,1767]

As mentioned above, graphene and GO are often used as catalyst supports,[113,589,772] but they may also be employed as the active catalytic phase.[1719,1721,1744,1768] For instance, oxygen functionalities in GO can behave as green oxidants (Figure 124).[1769] In perhaps the first example of this type of application, Dreyer et al. showed in 2010 that GO is capable of promoting the mild oxidation of alcohols and the hydration of alkynes,[1770] work that they later extended to other reactions.[1768] On the basis of DFT calculations, the Dreyer group proposed that these reactions take place via an initial extraction of a H atoms from the organic molecule by an epoxide group within the GO surface followed by transfer of a second H to an adjacent hydroxyl, a step that results in the formation of water as a byproduct (Figure 125).[1771] The oxygenated elements of graphene can also act as solid acid/base sites (Figure 124, top-right),[1772−1774] as in the case of the promotion of Friedel-Crafts reactions with alkenes, which appears to follow a mechanism where the C═C double bond of an aromatic alcohol reactant is initially attacked by the oxygen atom in a hydroxyl surface group and then coupled with an arene adsorbed on an adjacent site.[1775] Interestingly, in the two specific cases mentioned in this paragraph there is a need for a cooperative behavior between two adjacent defect sites within the GO surface for the reaction to be fully promoted. This speaks to the level of complexity of the catalytic site required for such organic conversions as well as to the difficulty of producing those on GO surfaces in a

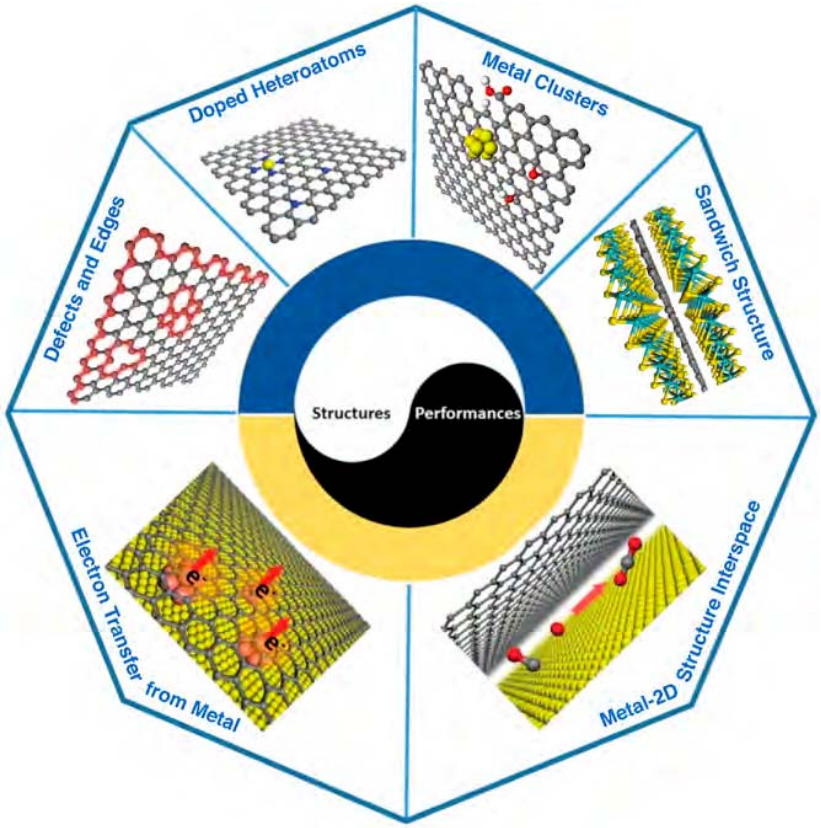

Figure 123. Types of catalytically active sites and catalysis-promotion mechanisms in graphene-based materials, which include defects and edges, doped heteroatoms, functional groups and metal clusters, electron transferring from metals, spacing between a metal surface and the outer layer of the 2D material, and the interstitial spacing in the sandwich structure of the 2D material.[1723,1767] Adapted with permission from ref 1767. Copyright 2019 WILEY-VCH Verlag GmbH & Co. KGaA, Weinheim.

https://doi.org/10.1021/acs.chemrev.1c00905
Chem. Rev. XXXX, XXX, XXX−XXX

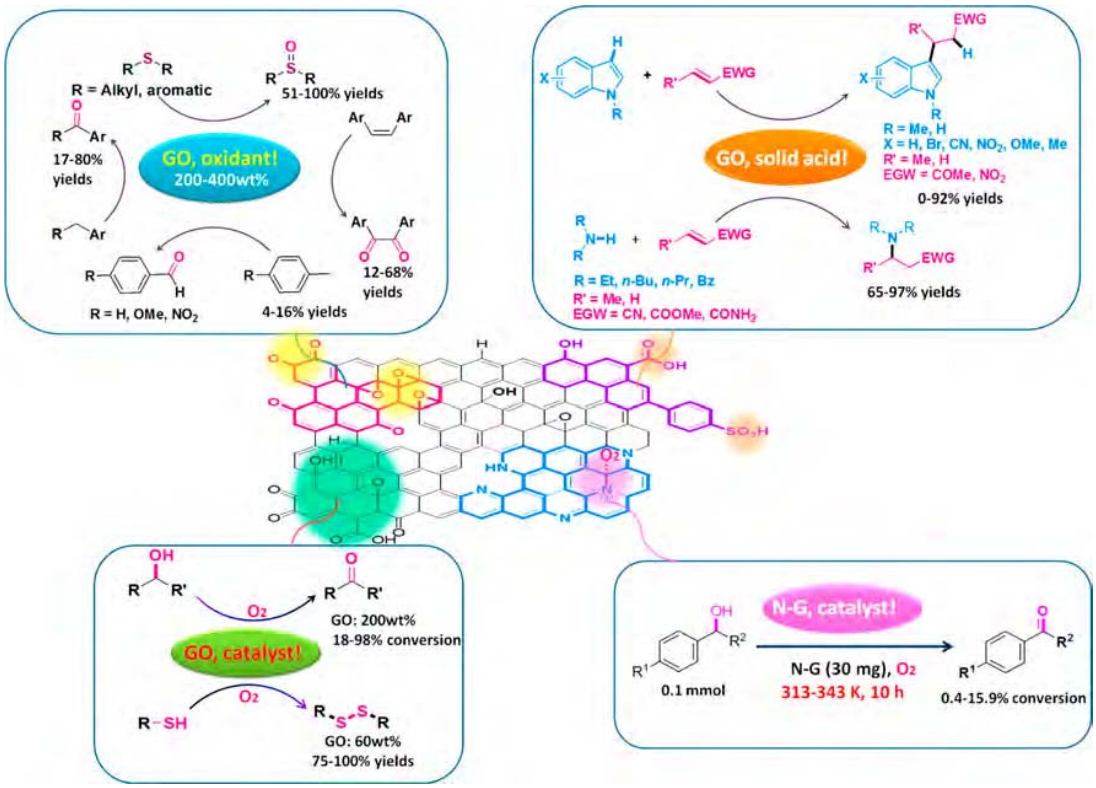

Figure 124. Examples of reactions catalyzed by GO, grouped by the type of catalytic site involved.[1744] Reproduced with permission from ref 1744. Copyright 2013 American Chemical Society.

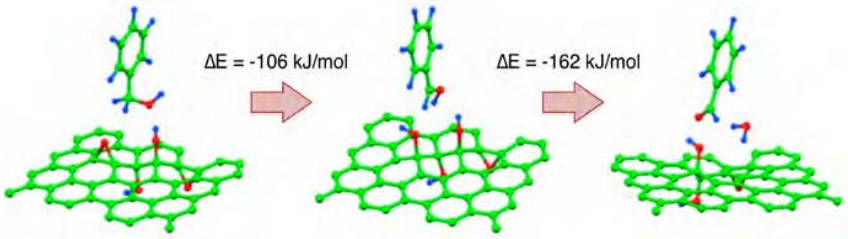

Figure 125. DFT calculations of the first steps in the mechanism of the dehydrogenation of benzyl alcohol on a GO surface.[1771] Green: C atoms; Red: O atoms; Blue: H atoms. Reproduced with permission from ref 1771. Copyright 2012 Wiley-VCH Verlag GmbH& Co. KGaA, Weinheim.

systematic way. Multiple other sites have been identified in GO and related graphene-based catalysts active for the promotion of specific catalytic conversions,[1747] but preparing catalysts displaying only the needed sites is still a challenge.

Other types of sites can be found at the edges or defects in GO, including carboxylic acids, diols, quinones, and aromatic C−H sites, and those have been shown to be active for oxygen-activation reactions.[1776] Moreover, the amphiphilic character of GO makes it useful as a phase-transfer catalyst in oil-water biphasic systems.[1777] Derivative materials such as graphene nitride have also been the focus of much research in catalysis, as the addition of heteroatoms can be used to modify the electronic properties of these carbon-based solids in a controlled manner.[1744,1778−1782] Finally, other graphene-related materials such as carbon nanotubes (CNTs, rolled-up sheets of graphene) and fullerenes (closed or partially closed meshes made out of fused carbon rings of five to seven atoms, sometimes referred to "buckyballs" −the best known being C_{60}) have also proven useful in catalysis, exhibiting similar sites as graphene but offering other advantages such as shape selectivity.[134,785,1727,1738,1783−1790]

Yet another family of compounds useful in catalysis relevant to this section of our review is the layered double hydroxides (LDHs) of general formula $[M^{2+}_{1-x}M'^{3+}_{x}(OH)_2]^{x+}(A^{n-})_{x/n} \cdot mH_2O$, anionic clays made out of positively charged 2D sheets (networks of brucite-like $M(OH)_6$ octahedra) held together by water and/or exchangeable charge-compensating anions (A) placed in between.[1791−1794] Examples of LDHs common in catalytic applications include hydrotalcite (HT, $Mg_6Al_2CO_3(OH)_{16}\cdot 4H_2O$) and kaolinite ($Al_2Si_2O_5(OH)_4$, or $Al_2O_3\cdot 2SiO_2\cdot 2H_2O$). Single-layer LDHs are often prepared via exfoliation of the bulk clays, but several direct synthetic approaches have been designed as well, with the aim of manipulating the active centers (crystal facets, defects, geometric and electronic states, macro-nano morphology) within their structure.[1792,1795−1797] Several properties of LDHs makes them attractive for catalysis, in particular their large number of uniformly distributed base sites and the ease with

https://doi.org/10.1021/acs.chemrev.1c00905
Chem. Rev. XXXX, XXX, XXX−XXX

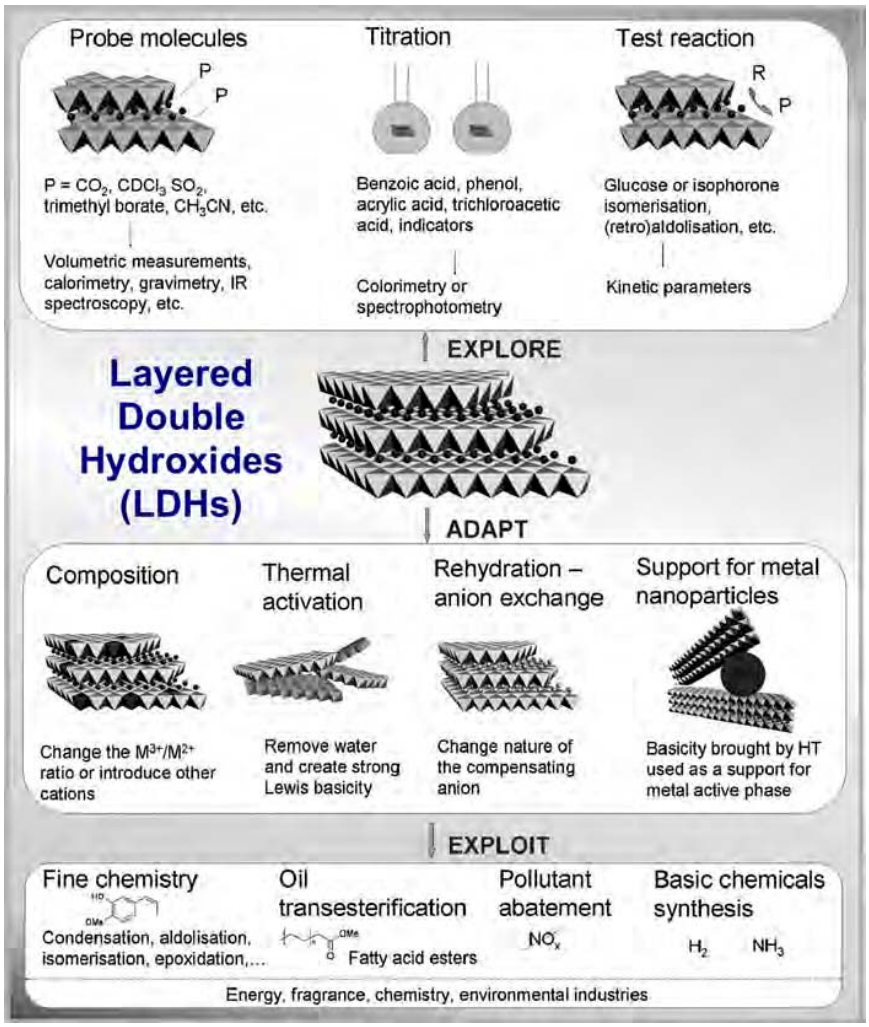

Figure 126. Overview of the role of LDHs in catalysis.[1799] The layered structure of LDHs is depicted schematically in the second row, the most common techniques used for their characterization illustrated in the top row, the synthetic approaches used for their chemical modification to tune their catalytic properties indicated in the third row, and a partial list of reactions promoted by them provided in the bottom row. Reproduced with permission from ref 1799. Copyright 2009 Wiley-VCH Verlag 3920 GmbH&Co. KGaA, Weinheim.

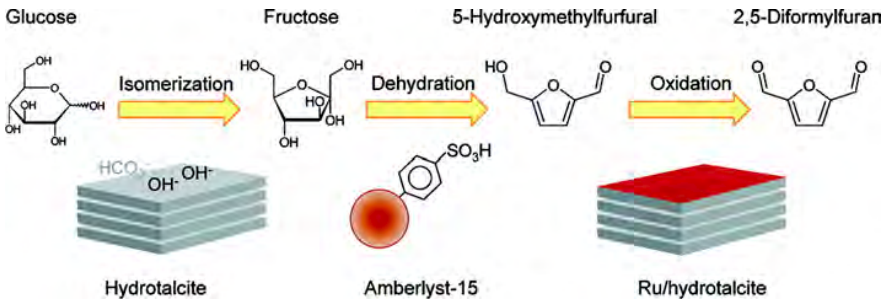

Figure 127. Use of a combination of three catalysts, two of them LDH-based, to promote a series of isomerization, dehydration, and selective oxidation reactions to convert glucose into 2,5-diformylfuran.[1809] Reproduced with permission from ref 1809. Copyright 2011 American Chemical Society.

which they can be modified to add acid sites.[1798−1800] Additional chemistry can also be incorporated to LDHs via cation exchange at the Brucite-like layer or anion exchange at the interlayer space (Figure 126).[1798,1799,1801] LDHs have large surface areas and therefore large adsorption capacity, are thermally stable, and have the ability to regain their original structure after catalysis via water treatments.[1802]

LDHs are excellent supports for many hydrocarbon-processing reactions catalyzed by metals.[1793,1800,1801] Specifically, they are increasingly being considered as supports for metal (typically Ni) active phases of catalysts used for CO and

https://doi.org/10.1021/acs.chemrev.1c00905
Chem. Rev. XXXX, XXX, XXX−XXX

methane reforming reactions as well as for the conversion of CO_2 to methane: in these, LDHs basicity helps minimize poisoning via coke formation.[1801−1806] They are equally useful supports for olefin polymerization catalysis.[1791] LDHs can nevertheless be active participants in acid−base catalysis, to promote, for instance, additions to C═O, C═C, C≡C, C≡N and other unsaturated bonds, alkylations, acylations, epoxidations, ring openings, and decarboxylations.[1791,1798,1807] Another popular application of LDHs is in the conversion of biomass feedstocks.[1800,1801,1808] In Figure 127, an example is shown where a combination of hydrotalcite, Amberlyst-15 (a polystyrene-based ion-exchange resin with strongly acidic sulfonic groups), and hydrotalcite-supported Ru catalysts successfully afforded the direct synthesis of 2,5-diformylfuran from glucose in one pot via successive isomerization, dehydration, and selective oxidation steps.[1809] It should be noted, however, that in most of these applications, LDHs provide large surface areas and high coverages of well-defined sites but rarely perform better than other more conventional catalysts.[1794]

Many reported applications of LDHs involve redox reactions, in which the LDH typically acts as a helpful support to enhance the activity of the added active functionality, often metal ions (which can be ion-exchanged on the surface of LDHs), complexes, or NPs.[1807,1810] One often cited case is the promotion of the Fenton reaction, a Fe^{2+}-catalyzed conversion of hydrogen peroxide to hydroxyl free radicals (OH·): the high density of surface ionic sites in LDHs can be used to disperse the active phase in the form of ions such as sulfonated iron phthalocyanine ($FePcSO_3^-$).[1811] Because they are highly reactive and oxidizing, the resulting OH· species can in turn be used to catalyze many organic conversions, for the degradation of pollutants in air and water and in organic synthesis.[1812−1814] Ion-exchanged LDHs have also proven to be good catalysts for the SCR of nitrogen oxides in environmental applications.[1815] LDHs offer a number of particular advantages for photocatalysis, including specific directional paths for charge mobility (to help with the separation of photogenerated electrons and holes), higher surface exposures compared to equivalent bulk materials, and tunability of electronic and optical properties such as band gaps via compositional adjustments and heterojunction formation.[1794,1816,1817] In one example, ZnAl-LDH 2D nanosheets were shown to exhibit high surface densities of coordinatively unsaturated Zn^+ centers and, accordingly, to be more efficient catalysts than bulk analogs for the photoreduction of CO_2 to CO with water (Figure 128).[1818] Similar tuning of electronic properties in LDHs, by, for instance, substituting some cations, replacing interlayer anions, creating vacancies, or preparing hybrid LDHs with conductive materials, can be used to design efficient electrocatalysts.[1816,1819−1823] The ORR has been a particular target here.

Overall, it is clear that 2D materials exhibit some unique properties that can be harvested to design unique well-performing catalysts. In particular, they display high surface areas with lots of interesting sites that can be tuned or modified to target specific reactants and reactions. They also exhibit specific electronic behavior sometimes desirable for electro- or photo-catalysis applications. For these reasons, 2D materials are increasingly been incorporated into the design of catalysts for a vast range or chemical processes. On the other hand, the basal planes of many 2D sheets are chemically inert, at least in the cases of metal chalcogenides and carbon-based

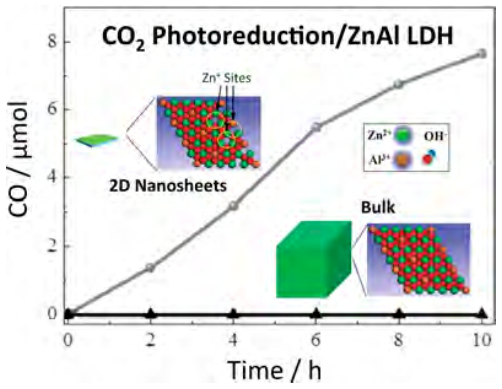

Figure 128. Photocatalytic conversion of CO_2 to CO promoted by ZnAl-based LDHs.[1818] 3D-bulk and 2D-nanosheet versions of the LDH were prepared via urea coprecipitation and either inverse microemulsion or controlled hydrolysis, respectively. The 2D catalyst was found to exhibit a high density of coordinatively unsaturated Zn^+ sites and, correspondingly, a much higher activity for CO_2 photoreduction. Adapted with permission from ref 1818. Copyright 2015 WILEY-VCH Verlag GmbH & Co. KGaA, Weinheim.

materials, and their modification to introduce active sites is not always easy to control. There is also the issue of cost, as in many instances other more conventional materials can offer comparable catalytic performance at lower prices. In spite of these limitations, 2D materials are likely to find commercial use in specific catalytic applications.

6.5. Metal-Oxide Clusters and Nanoparticles

Although less extensively than with metals, synthetic methodology has been developed for the making of NPs of metal oxides with controlled sizes and shapes as well, and those have been incorporated into catalytic designs.[51,843,1824] Because of their promise as promoters of important reactions, certain oxides have received special attention in this area, in particular oxides made out of metals such as Ce,[1825−1829] Ti,[1830,1831] Co,[1832−1838] and Cu,[1839−1844] but other materials such as MgO,[1845−1848] MnO_2,[1849−1853] Fe_2O_3,[1854−1857] and NiO[1858] have been investigated as well.[1859] Thanks to the great advances in the synthesis of metal-oxide NPs with well-defined characteristics seen in recent years,[986] it has been possible to study and exploit the dependence that catalytic performance may exhibit on oxide surface structural details.[1859,1860] Particularly useful has been the ability to design oxide NPs with different shapes, as those expose specific surface planes. For instance, in a recent example, it was shown that the hydrogenation of carbon monoxide with Co_3O_4 catalysts is optimized on so-called nanobelt-shaped NPs (CS-NB-20), which predominantly expose [110] surface planes; activity is somewhat lower with nanocubes (CS-NC-20), with their [100] surfaces, and reduced further with nanospheres (CS-NSP-20), which expose [112] facets (Figure 129).[1861] The authors of that work explained the observed trend in terms of the oxidation state of the metal ions on the surface, because while the [110] plane exposes large amounts of easily reducible Co^{3+}, the other planes mainly contain harder-to-reduce Co^{2+} instead (and less oxygen vacancies). It is important to note that in the most detailed studies of shape sensitivity in catalysis, like this one, an attempt has been made to identify the fundamental physical parameters that change with surface structure and affect catalysis, but, unfortunately, most publish work to date

https://doi.org/10.1021/acs.chemrev.1c00905
Chem. Rev. XXXX, XXX, XXX−XXX

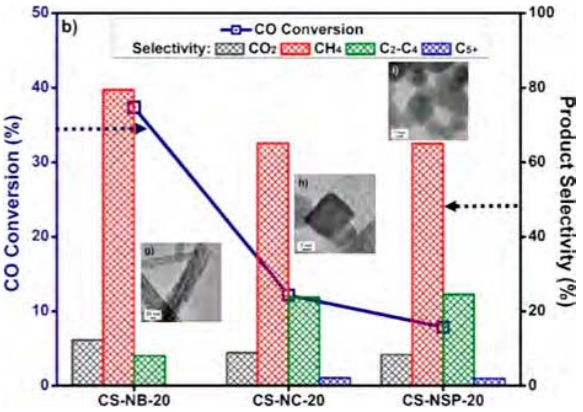

Figure 129. Steady-state activity and product distribution data for the hydrogenation of CO promoted by Co_3O_4 as a function of NP shape (electron microscopy images provided in the insets). Reproduced with permission from ref 1861. Copyright 2020 Elsevier B.V.

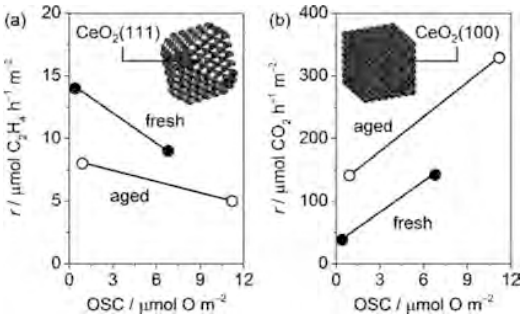

Figure 130. Reaction rates for C_2H_2 hydrogenation (left panel) and CO oxidation (right) as a function of the oxygen storage capacity (OSC) of fresh and aged ceria-NPs based catalysts. Data are shown for octahedron-like NPs, which expose [111] facets, and nanocubes, enclosed by [100] facets, the idealized structures of which are depicted in the insets. Correlations are seen between the NP shape and both OSC and catalytic reactivity, with the nanooctahedra displaying low OSC and particular preference for the promotion of hydrogenations and the nanocubes having higher OSC and better activity for oxidation catalysis. Reproduced with permission from ref 1867. Copyright 2016 Wiley-VCH Verlag GmbH & Co. KGaA, Weinheim.

has focused on the synthetic aspects of the research and only report empirical observations in terms of catalytic trends.

The example cited above is a hydrogenation conversion, where the reactant is reduced. It is well known that this and other redox reactions can be promoted using reducible oxides made out of metal ions that can exist in several oxidation states. Hydrogenations are more commonly carried out with metal-based catalysts, but in some instances can be promoted with oxides. Ceria, for instance, can be used to selectively hydrogenate alkynes in the presence of alkenes,[1862−1864] with optimum performance when polyhedral NPs exposing [111] facets are used. Interestingly, an opposite trend has been seen for the oxidation of CO, which is better served by ceria nanocubes and nanorods with predominantly [100] facets exposed.[1827,1865] The story is more complex for the WGS reaction, but there, again, the CO reactant is believed to reduce the ceria surface as it becomes oxidized and to be converted to CO_2, a step that is more favorable on the [100] planes of the ceria nanocubes.[1866] Even in hydrocarbon oxidations nanocubes seem to be the preferred form of ceria NPs.[1826] It appears that the oxygen vacancies seen in the [100] surface planes of nanocubes are required to catalyze oxidations, whereas oxygen sites in [111] surfaces seem to stabilize the adsorption of the reactants in hydrogenations (Figure 130).[1867] It has also been claimed that Ce^{3+} surface ions can act as Lewis-acid sites and that, together with adjacent neighboring surface lattice Lewis-base oxygen, they facilitate the activation of H_2 and with that reduction steps.[1868] With titania (anatase), oxidations appear to be favored on [111] facets, whereas reductions occur preferentially on [110] surfaces.[1869] Overall, the contrast reported here between hydrogenations and oxidations highlights that structure sensitivity in catalysis with metal oxides is specific to the reaction to be promoted.

An issue with oxides made out of metals with multiple oxidation states is the need to determine the nature of the active phase under catalytic conditions. In oxides such as titania the change in oxidation state manifest itself mainly via the formation of defects such as oxygen vacancies, which may act as catalytic sites and can be repopulated under oxidation conditions.[1870,1871] On the other hand, in other oxides, the oxidation state of the metal ion on the surface may be stable and may change the catalytic performance. For instance, tin oxide has been shown to have Sn^{2+}/Sn^{4+} ratios that depend on NP size, a behavior relevant to catalysis because it was also proven that it is the metastable Sn^{2+} sites the ones that appear to promote oxidation reactions.[1872] In another system, when Cu_2O is used as an oxidizing catalyst, a thin CuO film is usually formed, becoming the actual exposed surface for catalysis, as shown in the case of CO conversion. A structural dependence can still be operational, however: the CuO film formed on octahedral Cu_2O NPs proved to be more active than that grown on cubic Cu_2O NPs,[1839] a difference justified by the different CuO film structures estimated by quantum mechanics calculations (Figure 131).[1873] Synthetic approaches (using protective ligands, for instance) can be used to prevent the formation of such CuO films and to probe the structure sensitivity of catalysis on Cu_2O surfaces: structural dependences have been seen for the oxidation of CO[1874,1875] and propylene[1876] as well as for organic synthesis reactions[1840−1842,1877,1878] in those cases. A mechanistic explanation of why this is awaits further studies.

A particular class of redox reactions for which semiconductor oxides are well suited is photocatalysis. Titania in particular has been tested extensively for this purpose, by itself, doped, or after the addition of cocatalysts.[1879−1882] Early quantum mechanics calculations had suggested that photocatalysis with titania is affected by the structure of the surface, with the anatase [001] plane being particularly active for the adsorption of, and H_2 production from, water.[1883] Much research has therefore been directed toward the synthesis of titania NPs with maximum exposure of that surface, a challenge since the [101] facets are the most thermodynamically stable.[1884−1887] However, more recent work has indicated that it is the [101] (and [010]) planes that may be preferred for photocatalytic applications.[1888−1890] To complicate matters further, a surface heterojunction at the interface between [001] and [101] planes has been proposed to be necessary to inhibit charge recombination and thereby enhance photocatalytic activity; this appears to be true in both water splitting[1891] and the photocatalytic reduction of CO_2 to CO.[1892] When dealing with the photodegradation of organic molecules,[1893] reactivity has repeatedly been reported to correlate with the presence of

https://doi.org/10.1021/acs.chemrev.1c00905
Chem. Rev. XXXX, XXX, XXX−XXX

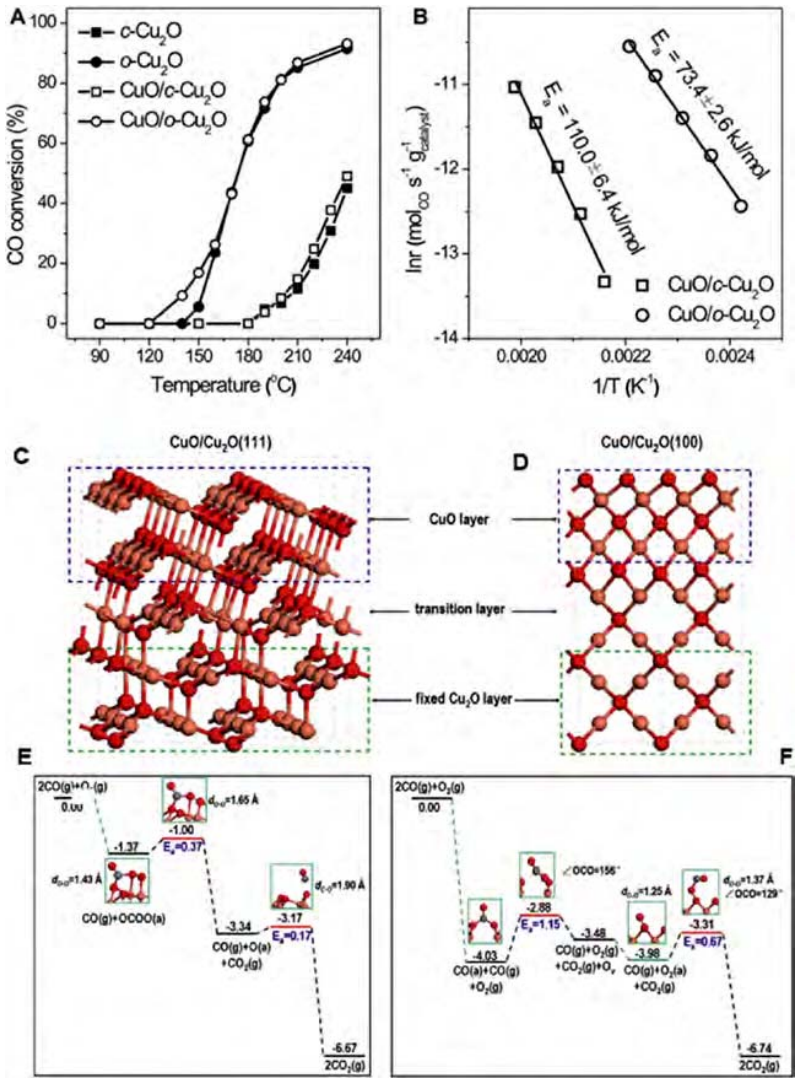

Figure 131. Dependence of activity on surface structure for the case of the catalytic oxidation of CO using Cu_2O NPs.[1873] The kinetic data in the top row show significantly higher activity with octahedral (o-Cu_2O) than with cubic (c-Cu_2O) NPs. This is explained by the differences in structure of the CuO film that forms on the surfaces of the two catalysts, as indicated by the DFT calculations shown in the middle row. The bottom row provides the energetics calculated for CO oxidation in both cases. Reproduced with permission from ref 843. Copyright 2019 Elsevier B.V.

hydroxyl radicals on the surface, which are in general more abundant in anatase [001] facets.[1894,1895] Nevertheless, other researchers have claimed that anatase [010] surfaces enhance adsorption and are more photocatalytic active.[1896] Yet a third opinion is that both reaction rates and selectivity in the promotion of the photocatalytic reduction of nitrobenzene using anatase titania, which follow the sequence [101] > [001] > [100], correlate with the magnitude of the bandgap of the semiconductor (Figure 132).[1897] Interestingly, oxidation reactions with the same catalysts were shown to be much more insensitive to surface structure. In terms of other oxides, several articles have reported efficient photodegradation of dyes with Cu_2O NPs.[1898−1904] Those studies, collectively, have suggested a preference for [110] planes, but most of this work has been empirical, and some discrepancies remain. It is clear that photocatalysis, like thermal catalysis, is affected by the structure of the surface of the oxides used, but the ordering of the surface planes in terms of catalytic activity and of the specific mechanism by which such changes occur is still being debated.

Other types of structure-sensitive reactions may be promoted with metal oxides, and their performance tuned by controlling the NP shape. In particular, the hydroxyl terminal groups in many oxide surfaces may act as Brønsted-acid sites, and the metal cations as Lewis acids or bases; the acid−base properties of these oxides depend on the coordination environments around the metal and oxygen surface sites, and vary with the morphology and exposed facets of the oxide NPs. For instance, the Ce surface ions in ceria NPs have been proven to act as weak Lewis-acid sites and to not show much variation in chemical performance versus surface structure, whereas the strength and amount of the hydroxyl groups and surface lattice-oxygen Lewis-base sites have been determined to be shape dependent, following the trend: rods > cubes > octahedra.[1905] Tests with ceria NPs of different shapes for the promotion of a Cannizzaro disproportionation into ethanol and acetate,[1906] for dimethyl carbonate synthesis from CO_2

https://doi.org/10.1021/acs.chemrev.1c00905
Chem. Rev. XXXX, XXX, XXX−XXX

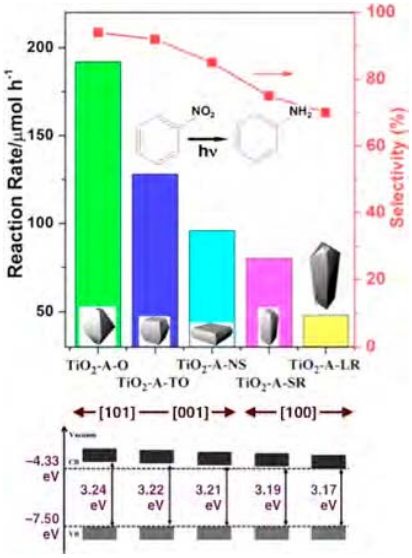

Figure 132. Top: Photocatalytic rates (left scale) and selectivities (right) for the reduction of nitrobenzene to aniline using TiO_2 NPs with different crystal forms and exposed facets.[1897] Bottom: Corresponding band structures, showing the variations in bandgap with NP structure. Reproduced with permission from ref 1897. Copyright 2013 American Chemical Society.

and methanol (Figure 133),[1907] and for the aerobic oxidative coupling of alcohols and amines to imines,[1908] all have shown

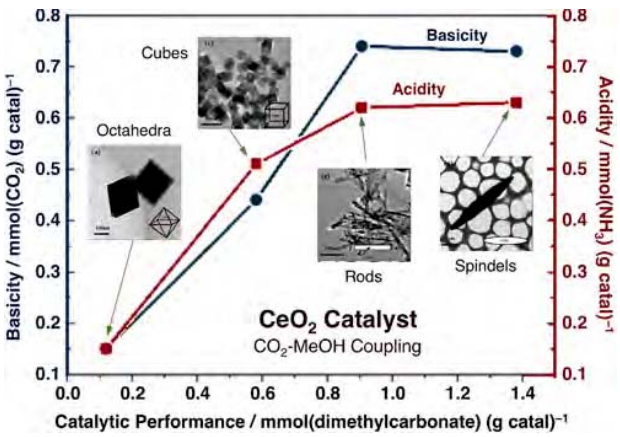

Figure 133. Correlation between acidity (right axis), basicity (left axis) and catalytic performance (bottom axis) for the coupling of CO_2 with methanol promoted by CeO_2 catalysts made out of NPs with different morphologies.[1907]

that CeO_2 nanorods/nanocubes are more active than ceria nanooctahedra. The trend was explained on the basis that the strong base sites found in the [100] facets of ceria help activate acetaldehyde to initiate the conversion. With TiO_2, NPs faceted along the [001] orientation proved to be quite active for the catalytic condensation of light oxygenated organic compounds, presumably because of an increase in stability of the Lewis-acid sites in the presence of organic acids under aqueous environments.[1909] Cr_2O_3 hexagonal-prism-shaped NPs proved more active and more stable than regular Cr_2O_3 catalysts for the dehydrofluorination of 1,1-difluoroethane, possibly because (at least in part) of a more abundant Lewis acidity due to a decrease in NP size.[1910] Finally, spiky-shaped Nb_2O_5 has been reported to be a highly stable and recoverable catalyst for the condensation of benzaldehyde with p-anisidine in the presence of trimethylsilyl cyanide to produce 2-((4-methoxyphenyl)amino)-2-phenylacetonitrile, presumably because of an increase in Lewis acidity thanks to the flexible Nb−O polyhedral structure of the individual [001]-oriented rods.[1911] Regarding basic oxides, a correlation has been identified between a decrease in density of surface base sites in MgO NPs, which follows the nanosheets > nanodisks > nanofibers order, a decrease in the percentage of [111] planes exposed, which mirrors the same order, and a decrease in activity for a Meerwein-Ponndorf-Verley reduction of benzaldehyde with ethanol; it was concluded that the base sites responsible for catalysis are primarily seen on the MgO[111] surfaces.[1912] All these examples point to some interesting aspects of the tunability of acidity and of acid−based catalysis in metal-oxide NPs by controlling NP shape, but further systematic studies of this type of correlations will be needed to add some predictability to catalyst design.

As already illustrated in some of the examples provided above, metal-oxide NPs have on occasion been used for organic conversions.[1908,1913] In one example, the promotion of the carbamoylation of aromatic amines was determined to be the most favored with CeO_2 NPs with nanooctahedra shapes (which expose [111] surfaces), followed by nanorods (with their [110] facets) and then nanocubes (and their [100] exposed faces); the trend was explained using results from quantum mechanics calculations as due to a combination of effects on the energetics of the individual elementary steps of the reaction (Figure 134).[1914] Another example involves the use of Cu_2O NPs for the reduction of 4-nitropheno to 4-aminophenol: it was concluded that the [111] facets are the most active for this reaction.[1915] Unfortunately, the data in this area of organic synthesis using well-shaped metal-oxide NPs are still sparse.

In the examples provided so far, the metal oxide constitutes the primary catalytic phase. More often, such materials are used as supports upon which the active element is deposited (as mentioned earlier in this review). Even in those cases, the control of surface structure afforded by the synthesis of metal-oxide NPs with specific shapes can be exploited to tune catalytic performance, by, for instance, controlling the growth of the metal NPs during their deposition.[1916,1917] In one example, Ru/CeO_2-nanorod catalysts were shown to exhibit high activity for the oxidative decomposition of chlorobenzene because of the formation of new Ru−O−Ce sites and the high oxygen mobility and high Ru^{4+} content favored by the associated [110] and [100] CeO_2 planes.[1918] In a second case, Au deposited on the [110] facets of ceria nanorods has been shown to display the highest activity for the WGS reaction (compared to analogous catalysts prepared on CeO_2 nanocubes and nanopolyhedra), presumably because of an enhancement in the fraction of Au atoms in ionic (Au^+ and Au^{3+}) states,[1919] or possibly because the abundance of OH species formed by activation of water on the oxygen vacancies present in the CeO_2[110] surfaces of ceria nanorods.[1920] In the case of formaldehyde removal, a similar preference for Au/CeO_2-nanorods was justified in terms of the relatively low energy required for oxygen vacancy formation and of the weakening of Ce−O bonds by Au on Ce[110] and Ce[100] planes.[1921] In the preferential oxidation of CO in a H_2-rich gas, by contrast, it is the formation of H-containing surface

https://doi.org/10.1021/acs.chemrev.1c00905
Chem. Rev. XXXX, XXX, XXX−XXX

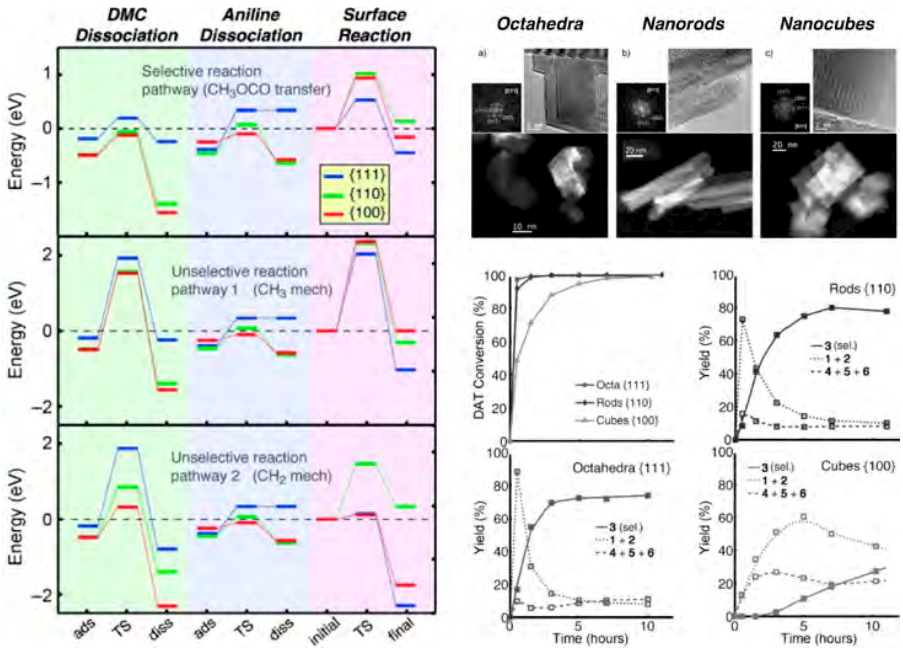

Figure 134. Shape dependence of the carbamoylation of aromatic amines promoted by CeO_2 NPs.[1914] Left: DFT calculations of the energetics of the selective (carbamoylation) and unselective (methylation) reaction pathways for the conversion of dimethylcarbonate (DMC) with aniline over the [111], [110], and [100] facets of CeO_2. Top-right: TEM images of CeO_2 nanooctahedra, nanorods, and nanocubes, which preferentially exhibit [111], [110], and [100] facets, respectively. Bottom-right: Catalytic data in the form of total conversion and yield for dicarbamoylated DAT (solid lines; DAT = diaminotoluene), monocarbamoylated DAT (dotted lines), and methylated products (dashed lines) versus time, obtained using the three CeO_2 nanostructures. Reproduced with permission from ref 1914. Copyright 2012 Wiley-VCH Verlag GmbH & Co. KGaA, Weinheim.

intermediates that is claimed to be responsible for the unique catalytic properties of the CeO_2 nanorods.[1922] Another dependence of the oxidation state of the metal phase on the structure of the surface of the metal-oxide support was found with Pd/CeO_2, in which case optimum CO, propane, and formaldehyde oxidations were obtained with the $Pd_xCe_{1-x}O_{2-\sigma}$ solid solutions that form on ceria nanorods, the PdO_x NPs favored on the [111] planes of ceria nanooctahedra, and the metallic Pd species that form on [100]-faceted nanocubes, respectively.[1923,1924] It should be indicated that some of the disagreements in the reported correlations between activity trends and physical properties can be traced back to differences in experimental results, as in the case of the XPS data shown in Figure 135 for the Pd/CeO_2 system. Finally, the stabilization of specific oxidation states on the active phases of the support may be even more critical with easy-to-oxidize metals such as copper.[1925−1927] Clearly, the structure of the metal oxide support affects many catalytic reactions, but a plethora of explanations have been offered to account for the experimental observations and no consensus seems to have been reached on this yet.

Certain facets of the metal-oxide NPs used as catalyst supports may also stabilize the catalytically active metal NPs, perhaps via a SMSI effect, as appears to be the case for Ni on the [110] and [100] surfaces of CeO_2: Ni/CeO_2 made with ceria nanorods and nanopolyhedra have proven more active and more resistant to cocking during the carbon dioxide reforming of methane than other more conventional catalysts.[1928] In other instances, either the support itself or the metal/oxide interface plays a more active role in catalytic reactions. As an example, Ru and Pt both appear to enhance the formation of oxygen vacancies, but follow opposite trends: Ru creates more oxygen vacancies on the [100] facets of CeO_2

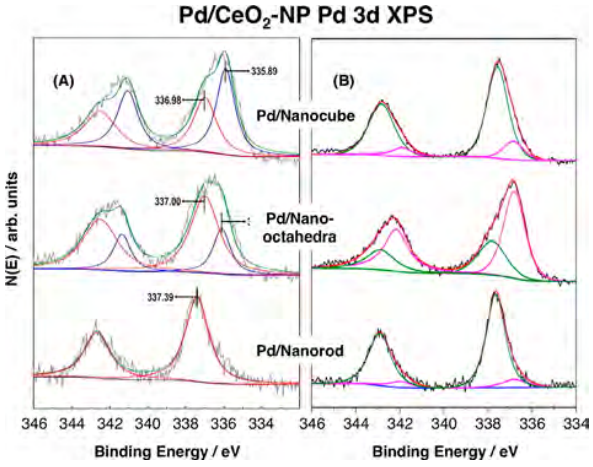

Figure 135. Pd 3d XPS data for Pd/CeO_2 catalysts made out of ceria NPs with different shapes. The panels correspond to spectra reported in Refs.[1923] (A, left) and[1924] (B, right), and highlight the different results that sometimes are obtained with what are seemingly the same samples. Adapted with permission from refs 1923 and 1924. Copyright 2015 and 2016, respectively, American Chemical Society.

nanocubes,[1929] whereas Pt shows higher reducibility on the [110] planes of CeO_2 nanorods.[1930] As a consequence, Ru/CeO_2-nanocubes have been shown to be the most active in CO_2 activation and methanation,[1929] whereas Pt/CeO_2-nanorods have been reported to be the ones that optimize toluene oxidation activity (Figure 136).[1930] In the case of Pd/CeO_2, it is presumably ceria microspheres that display enhanced reducibility, helping methane oxidation.[1931]

https://doi.org/10.1021/acs.chemrev.1c00905
Chem. Rev. XXXX, XXX, XXX−XXX

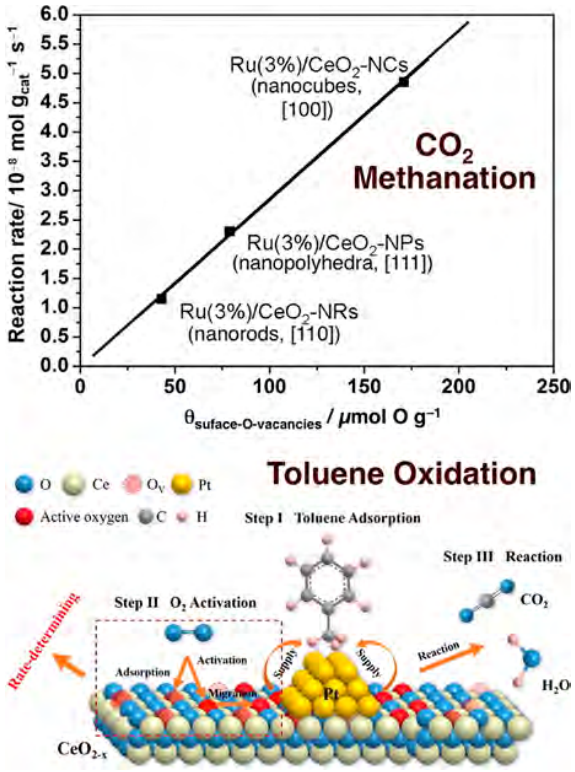

Figure 136. Top: Correlation between reaction rates for CO_2 methanation on Ru/CeO_2 catalysts and their concentration of surface oxygen vacancies, which depends on the shape of the ceria NPs.[1929] Bottom: Proposed mechanism for the oxidation of toluene on Pt/CeO_2-nanorods, with a limiting step involving the surface oxygen vacancies that in this case are maximized on the CeO_2[110] planes.[1930] Reproduced with permission from refs 1929 and 1930. Copyright 2015 Elsevier Inc. and 2016 Elsevier B.V.

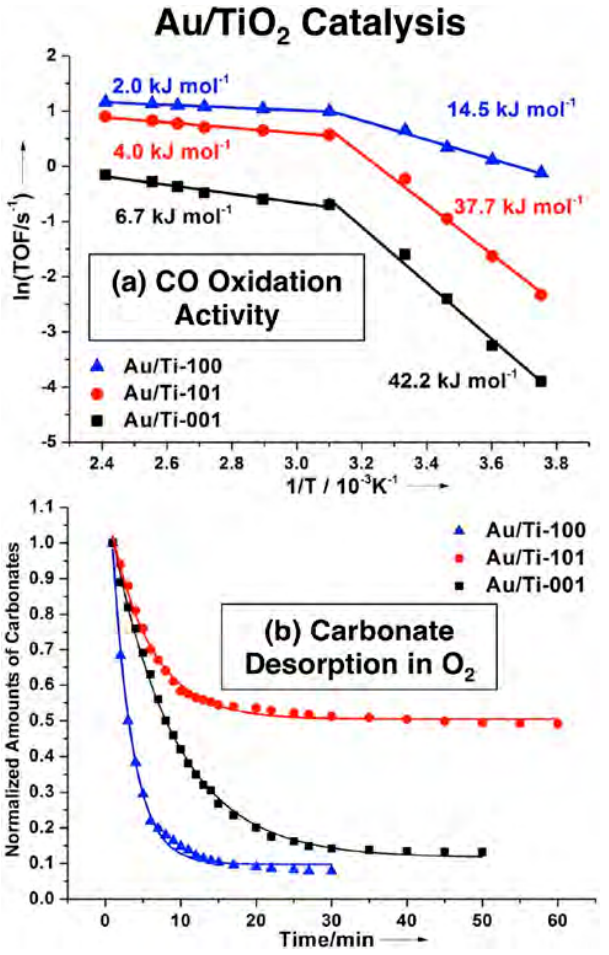

Figure 137. Effect of the oxide surface plane exposed on the activity of Au/TiO_2 catalysts for the promotion of CO oxidation.[1940] (a) Arrhenius plot of TOFs versus temperature with catalysts made with three different types of TiO_2 NPs, exposing different crystal planes. (b) Normalized desorption curves of carbonates in an O_2 atmosphere at 303 K. A correlation is seen between the ease with which carbonates desorb from the surface and CO oxidation activity. Reproduced with permission from ref 1940. Copyright 2013 American Chemical Society.

Particularly interesting are the cases where contributions by the metal/oxide interface to catalysis have been identified, like in some oxidations involving Au, Pt, and other transition metals together with reducible oxides such as TiO_2 or CeO_2.[54,949,1932−1937] For instance, by using catalysts with Pt deposited on TiO_2 NPs of different shapes, it was concluded that the activity for CO oxidation follows the order Pt/TiO_2[101] > Pt/TiO_2[100] > Pt/TiO_2[001] because the increasingly stronger metal-support interactions seen in this sequence afford better dispersion of the Pt atoms.[1938] Interestingly, the reverse order seems to be followed by the photocatalytic degradation of organic molecules.[1939] With Au/TiO_2, the activity for CO oxidation was found to follow a TiO_2[100] > TiO_2[101] > TiO_2[001] sequence, allegedly because of differences in the activation of O_2 and in the formation and desorption of carbonates on the different planes of the titania surface (Figure 137).[1940] An alternative explanation has been proposed for the trends seen with Au/TiO_2 catalysts based on the oxidation state of the Au atoms at the metal/oxide interface: allegedly, the $Au^{\delta+}$-rich interfaces that form on Au/TiO_2[100] justify the high activity for H_2 oxidation, whereas the $Au^{\delta-}$ species found on Au/TiO_2[001] favor selectivity toward H_2O_2 production and also toward propene epoxidation.[1941] It is clear from these and other examples in the literature that there are structural effects that affect performance in the catalysis promoted by metal/oxide systems. However, the physical chemistry underlying those is complex, involving several factors, and it is yet not possible to predict which metal/oxide interfaces are best for specific reactions.

In summary, it is clear that the surfaces of metal oxides, which are used as the active element in a number of catalytic processes, exhibit chemical properties that depend on the structure of the facets exposed. Specifically, redox properties, including the lability of lattice oxygen atoms and the consequential creation of surface vacancies as well as the ability of oxides of metals with multiple oxidation states to interconvert between those states, can be exploited to promote many catalytic processes, and tuned by using well-defined NPs with specific oriented surfaces. The strength and density of Brønsted and Lewis acid and base sites also depend on such structures, and can be relied upon to help with additional tuning of selectivity in catalytic conversions. Because of all of this, it is highly desirable to be able to synthesize catalysts out of metal-oxide NPs with well-defined sizes and shapes. Yet, the

https://doi.org/10.1021/acs.chemrev.1c00905
Chem. Rev. XXXX, XXX, XXX−XXX

preparation of shape-controlled metal-oxide NPs lags that of metals in terms of versatility: because of the ionic or covalent nature of most metal oxides, it is difficult to isolate non-thermodynamically-stable planes, as those may exhibit charged and therefore highly unstable surfaces. It is also typically the case that metal-oxide NPs tend to be large and non-porous, and therefore offer relatively low surface areas leading to low catalytic activities. Finally, within a number of notable exceptions (some of which were cited above), most work in this area has focused on NP synthesis and not on the physical chemistry of catalysis, and has yet to provide clear guidelines for the identification of specific NP targets to be made and used for specific catalytic conversions. These limitations are likely to be addressed in future research.

7. NOVEL NANOSTRUCTURES: LARGER ARCHITECTURES

7.1. Core–Shell and Yolk–Shell Nanostructures

Most of our discussion so far has focused on the creation of specific catalytic sites with well-defined characteristics at an atomic level. In addition, larger nanostructures can be used in catalysis to control other aspects of the kinetics of reactions, such as access to catalytic sites and/or control of mass transport rates and directionality. In this context, enclosed volumes can be used, for instance, as nanoreactors,[1942−1945] and multicomponent structures can be designed to hold different, complementary but possibly incompatible, catalytic functionalities. One now popular and relatively simple design for this is core–shell nanostructures, where NPs of one (core, A) component is fully covered by a second (shell, B); these are commonly referred to by using the nomenclature A@B.[647,1038,1946−1953] If a void space exists in between the inner and outer components, in a structure reminiscent of that of eggs (or rattles), the nanostructures are sometimes described as yolk–shell (often denoted as A@Void@B, although sometimes also written as A@B).[1948,1954−1956] Typically, the core NPs have diameters on the order of tens of nanometers, and the shells in the range of a few hundreds of nanometers, with thicknesses of a few tens of nanometers. The components can be both metals, as discussed already in Section 5.3, or a metal NP may be encased by a metal-oxide shell. Other materials such as carbon, in amorphous, graphene-like or nanotube form, have also been incorporated in these designs.

One of the main reasons why researchers have chosen to use core–shell and yolk–shell catalysts is to improve catalyst stability.[1957,1958] In the case of metal phases in particular, oxide layers may prevent NP sintering.[1959,1960] This is critical for reactions that are surface sensitive, where catalytic performance often depends on NP size distribution.[63,1961−1966] For instance, Au-based catalysis has been shown to be feasible only with small NPs,[978,1967,1968] and the initial activity in many of those systems is lost over time as the particles coalesce and grow in size.[1260,1969,1970] Zhang and coworkers showed that this problem may be minimized by encapsulating the Au NPs inside a porous silica shell: a clear increase in catalytic activity for CO oxidation was observed when the size of the Au NPs was decreased from 2.3 to 1.5 nm.[1971] Au@CeO_2,[1972] Pd@CeO_2,[1973] Pd@Void@CeO_2,[1974] and Au@SiO_2/TiO_2[1975] nanostructures have also been shown to enhance catalytic activity toward CO oxidation. In our work, the performance of a yolk–shell nanostructure (Au@Void@TiO_2) was contrasted with an equivalent catalyst made out by dispersing the same Au NPs on a conventional P25 titania powder (Au/TiO_2–P25): the initial activity for CO oxidation with the yolk–shell catalyst was about 50% higher than that with the regular catalyst, and significant sintering was observed in the Au/TiO_2–P25 sample but not in the Au@TiO_2 nanostructure upon calcination at 775 K (Figure 138).[1976] Sintering may also be a problem in

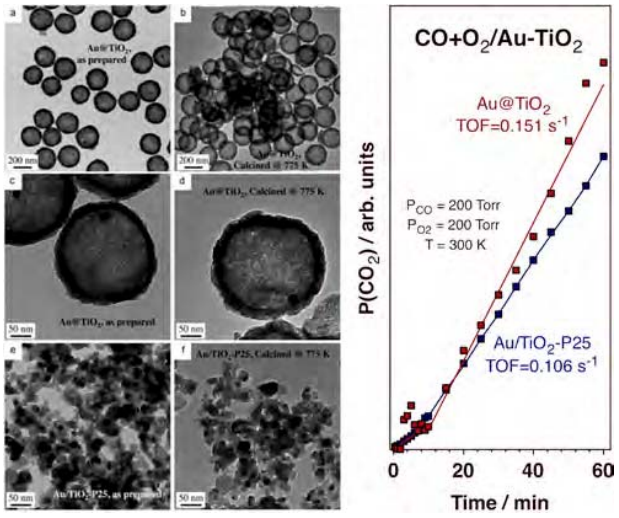

Figure 138. Performance comparison between Au@Void@TiO_2 (labeled Au@TiO_2 in this figure) and Au/TiO_2–P25 catalysts.[1976] Left: Low- (a, b) and high- (c, d) resolution TEM images of the Au@Void@TiO_2 catalyst, and TEM images of the Au/TiO_2–P25 reference sample (e, f), as prepared (left-hand column: a, c, e) and after calcination at 775 K for 2 h (right-hand column: b, d, f). Sintering of the Au NPs is only seen in panel f, for the reference catalyst. Right: Time dependence of the partial pressure of the carbon dioxide produced during the room-temperature oxidation of CO with O_2 in a batch reactor with both catalysts. Adapted with permission from ref 1976. Copyright 2011 Wiley-VCH Verlag GmbH & Co. KGaA, Weinheim.

reactions carried out at high temperatures or under reactive environments, and using oxide shells may help there as well. For instance, Pt@CeO_2 catalysts, used for the high-temperature oxidation of methane, were shown to be stable to temperatures as high as 1275 K.[1977−1982] In another case, a Pd@$Ce_{0.5}Zr_{0.5}O_2$/Al_2O_3 core–shell nanostructure was implemented to add hydrothermal stability to automotive three-way catalysts,[1983] and in a third group of examples, Pt@Void@TiO_2,[1984] Pd@CeO_2,[1985] and multishell-Pt/$Ce_{0.75}Zr_{0.25}O_2$[1986] nanoarchitectures were all shown to add stability during the WGS reaction. In yet another example, silica-encapsulated Pd NPs in a Pd@SiO_2 core–shell nanostructure proved quite stable in acetylene hydrogenation processes that included recycling via high-temperature oxidative coke removal.[1987] In fact, with many reactions involving carbon-containing reactants, the core–shell and yolk–shell nanoarchitectures may directly minimize the coking and/or deposition of other carbonaceous deposits that lead to catalyst poisoning, a problem particularly critical with Ni.[1988−1990] Accordingly, Ni NPs encapsulated inside a silica shell, in a Ni@Void@SiO_2 yolk–shell configuration, was shown to be quite stable at temperatures as high as 973 K and to be capable of high recyclability without loss of catalytic activity for methane reforming.[1991,1992] Similar resistance to coking was reported

https://doi.org/10.1021/acs.chemrev.1c00905
Chem. Rev. XXXX, XXX, XXX−XXX

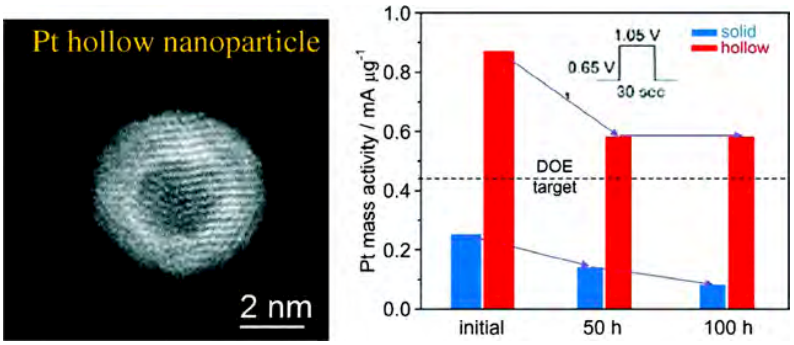

Figure 139. Left: High-resolution STEM image of a hollow Pt NP. Right: Comparison of ORR Pt mass activity as a function of potential cycling time with that measured with solid Pt NPs (red and blue, respectively).[2002] Reproduced with permission from ref 2002. Copyright 2011 American Chemical Society.

with $Ni@SiO_2$ core−shell catalysts during CO methanation.[1993]

The use of core−shell and yolk−shell nanostructures to improve catalyst stability is not limited to metals; it can be used with other active phases such as oxides as well. For instance, a $NiCeO_x@Void@SiO_2$ yolk−shell nanoarchitecture, developed for methane dry reforming, not only provided a way to minimize sintering, but also, thanks to the limited volume available within the confined NPs, Ni coking.[1994] A multiple core−shell $Ni-ZrO_2@SiO_2$ catalyst was also shown to display good sintering and coking resistance during the dry reforming of methane to syngas.[1995] A particularly clever idea is the use of magnetic materials, ferric oxide in particular, as the core of core−shell nanostructures to aid with catalyst separation.[1996−1998] Conversely, other materials such as 2D graphene or hexagonal-BN sheets can be used as shells, even if that may require more complex synthetic methods.[1999] In one case, Ni NPs were encapsulated within a thin hexagonal-BN shell to create a stable catalyst for syngas methanation.[2000] $Co-CoO_x@$ C(N-doped) capsules were also shown to be highly active and selective for the hydrogenation of nitrobenzene to aniline.[2001] Another alternative is to prepare monofunctional catalysts as hollow shells. For instance, Pt hollow shells were prepared using Ni NPs as templates and taking advantage of the Kirkendall effect to enhance and stabilize the activity of the metal toward the ORR in acid fuel cells (Figure 139).[2002] It should be noted that core−shell and yolk−shell nanostructures not always prevent sintering, and can also deactivate following other mechanisms. An example of this has been provided for the case of a $Pd@CeO_2$ catalysts developed for the promotion of the WGS reaction: a micro-emulsion synthesis led to a catalyst that was more stable than regular Pd/CeO_2 samples but that suffered condensation leading to low surface area and poor Pd accessibility.[2003]

In many of the examples provided so far, the catalytically active phase (usually a metal NP) is protected and prevented from sintering by encapsulating it inside an outer shell. This prevents the metal atoms from diffusing out and collecting elsewhere to create larger NPs, but can also block access of the reactants to the active surface.[2004−2007] Luckily, most of the materials used as shells are porous and afford easy diffusion of chemicals to the inside volume of the shells.[2008−2010] In particular, oxide (silica, titania) shells are often made by sol-gel methods, and those tend to grow low-density and open-structure solids. We[2011,2012] and others[2013] have shown, using IR, that molecules as large as porphyrins can diffuse in solution through the titania shells of $Pt@Void@TiO_2$ yolk−shell nanostructures and adsorb on the surface of the metal NPs trapped inside. Good diffusion-limited current densities were also obtained with CoFe@(N-doped graphene) nanostructures during ORR electrocatalysis.[2014] A particularly interesting additional development in this approach has been the ability to control the structure of the pores within the shells, as in the case of multifunctional yolk−shell NPs where a core of silica spheres was coated with an outer shell based on periodic mesoporous organosilica with perpendicularly-aligned mesoporous channels.[2015] Diffusion may even be controlled via the tuning of the reaction conditions: CO oxidation, for instance, can be blocked via capillary condensation of water vapor in the mesopores on the shells of $Au@Void@SiO_2$ catalysts.[2016] Furthermore, because of their porosity, shells can also act as sieves, preferentially allowing the diffusion of certain molecules and preventing access of others to the inside volume of the core−shell or yolk−shell nanostructure. This is what is claimed in the case of a $Pt/CeO_2@MOF$ core−shell catalyst used for the selective hydrogenation of furfural.[2017] Diffusion-induced shape selectivity was also reported in Suzuki coupling reactions promoted with $Pd@SiO_2$ catalysts.[2018] Another option is for the shells to provide excess surface area and microporous volume to adsorb reactants and products and to increase the number of active sites for catalytic reactions promoted by the shell material. For instance, Bi_2WO_6 hollow microspheres made using the Kirkendall effect were shown to display high efficiency in the promotion of the photoreduction of CO_2 to methanol, ostensibly thanks to the high CO_2 adsorption capacity of the microporous shell (Figure 140).[2019] It should be indicated, however, that in most cases the effect of mass transport on the kinetics of catalytic reactions promoted by core−shell and yolk−shell materials needs to be properly evaluated still.

Mass transport limitations can also be exploited to design tandem catalytic processes where two complementary catalytic steps can be arranged to take place on different phases at different sites within the inner and outer regions of the core−shell or yolk−shell nanostructures. In one example, $Ni/SiO_2@MOF-74$ nanostructures were tested for the promotion of a tandem imination of nitrobenzene with benzaldehyde.[2020] In this nanoarchitecture, the Ni phase promotes the hydrogenation of nitrobenzene to aniline and the MOF-74 the subsequent addition of the aldehyde, while the shell also contributes to the prevention of over-hydrogenation via molecular sieving. In fact, incompatible functionalities can be

https://doi.org/10.1021/acs.chemrev.1c00905
Chem. Rev. XXXX, XXX, XXX−XXX

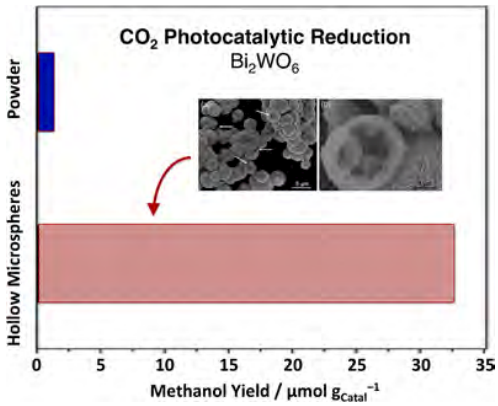

Figure 140. Methanol yields from CO_2 reduction on Bi_2WO_6 photocatalysts after 2 h of reaction under visible light irradiation.[2019] The activity of a regular powder (right) is contrasted with that of the Bi_2WO_6 hollow microspheres shown in the inset. Clearly, the latter is much more active than the former, presumably because of the much larger surface area of its porous structure.

kept apart in core−shell nanostructures this way,[2021] as in the example of the SiO_2−SO_3H@SiO_2@SiO_2−NH_2 tested for a one-pot acetal hydrolysis-Knoevenagel cascade reaction sequence.[2022] Another way to accomplish such functionality separation is by tethering acid groups on the outer surface and amine functionality on the inside of the shell (or vice versa).[293] Core−shell and yolk−shell nanostructures also provide a nice way to design different interfaces, aiming to promote specific catalytic steps that can be combined for the design of more complex reaction sequences. A nice example here is that of the Pt/CeO_2@SiO_2 nanostructure designed for the selective conversion of ethylene to propanal via tandem hydroformylation: the Pt/CeO_2 interface was shown to be active for the production of CO and H_2 from methanol decomposition, whereas the Pt/SiO_2 interface could catalyze the hydroformylation of ethylene with that resulting CO plus H_2 mixture (Figure 141).[2023] A similar Pt/CeO_2@Co/SiO_2

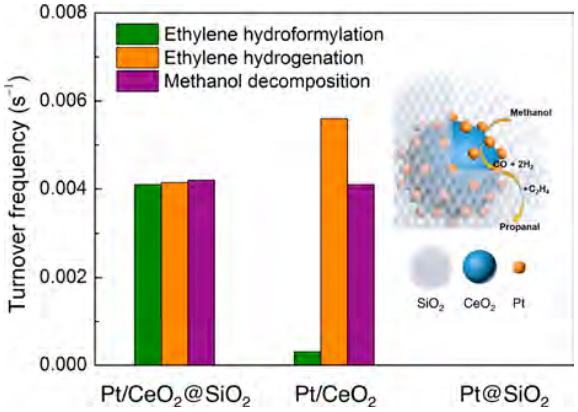

Figure 141. Comparison of the catalytic activity for the hydroformylation of ethylene with methanol between dual-interface Pt/CeO_2@SiO_2 and single-interface Pt/CeO_2 and Pt@SiO_2 catalysts.[2023] The Pt/CeO_2 catalyst is capable of carrying out both ethylene hydrogenation and methanol decomposition steps, but the Pt/SiO_2 interface is needed to promote the final hydroformylation. Reproduced with permission from ref 2023. Copyright 2016 American Chemical Society.

design was used to promote the hydrogenation of CO_2 to C_2−C_4 hydrocarbons: allegedly, the Pt/CeO_2 interface converts CO_2 and H_2 to CO, and the neighboring Co/SiO_2 interface promotes hydrocarbon chain growth via a Fischer-Tropsch process.[2024]

The idea of designing novel interfaces with unique catalytic performance within core−shell and yolk−shell nanostructures has been explored as well. For instance, the use of the boundaries between metals and reducible oxides such as TiO_2 and CeO_2 has become popular in the design of redox catalysts, and core−shell nanostructures offer a way to maximize the formation of such interfaces;[1951] witness, for instance, the improved performance of Pd@CeO_2 catalysts in enhancing methane oxidation.[1977] Interfaces can also help induce reconstructions. This behavior has been reported and exploited in the case of Pd@CeO_2 and Pd@SiO_2 NPs to enhance low-temperature CO conversion in three-way catalysts.[2025] A third way in which core−shell nanostructures can be used to create new interfaces and catalytic sites is by having the core element modify the electronic properties of the shell and this way affect its catalytic performance. This has become a often used approach with bimetallic systems.[1140,1168] although it is important to keep in mind that the initial core−shell composition profile may not be preserved once the catalyst is exposed to the reaction conditions because metals have the tendency to diffuse in and out of the bulk depending on temperature and chemical environment (Section 5.3).[1164,1283] Electron transfer from encapsulated metals in (Fe,Ni)@C nanostructures have also been used to tune the work function of the outer graphene layer and hence improve OER activity.[2026,2027] Regarding changes in electronic states on surface sites, one seldom discussed problem with core−shell and yolk−shell nanostructures is the fact that these are made by following multiple synthetic steps, often using sacrificial layers that are later removed by chemical means, and that such synthetic complexity often leads to the incorporation of impurities in the core and/or shell materials. One example from our laboratory illustrates how such changes may affect catalysis and how they may be tuned. In our case, the discovery that Au@Void@TiO_2 yolk−shell catalysts are capable of promoting the oxidation of carbon monoxide at cryogenic temperatures was traced back, at least in part, to the addition of Na^+ ions and the formation of a new sodium titanate phase in the titania shells during the etching step of the silica sacrificial layer;[2028−2030] removal of those ions via treatment with HCl resulted in the suppression of any catalytic activity below 300 K (Figure 142).[2028,2031] Unfortunately, it is not always possible to identify the source of the changes in catalytic performance between core−shell or yolk−shell nanostructures and more standard catalyst, let alone control and tune those changes.

Thanks to the variety of synthetic routes available for the preparation of core−shell and yolk−shell nanoarchitectures, it is possible to exert great control on their main structural and electronic parameters, including the core diameter and the shell diameter and thickness as well as the degree of intermixing (in multi-metallic cores) and the oxidation state. We have nicely illustrated this for the case of the photocatalytic production of hydrogen from water using Au@Void@TiO_2 and Pt@Void@TiO_2 materials.[1947,2029,2032] In previous work, we had challenged the conventional explanation given in the literature for the role of the metal (Au or Pt in this case) in these photocatalysts as electron scavengers following photon excitation at the semiconductor phase (titania), and had

https://doi.org/10.1021/acs.chemrev.1c00905
Chem. Rev. XXXX, XXX, XXX−XXX

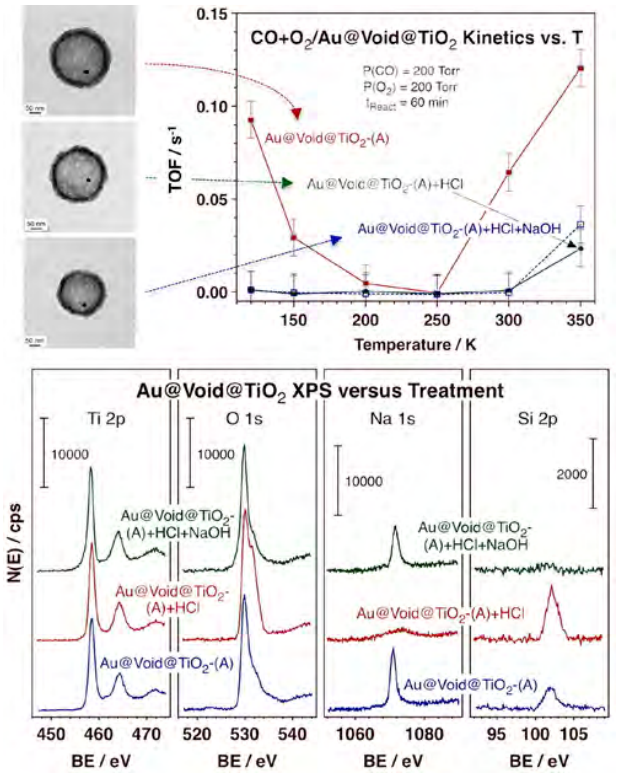

Figure 142. Au-titania yolk–shell catalysts for CO oxidation at cryogenic temperatures.[2028] Top-left: TEM images of the three catalysts contrasted here, namely, the original Au@Void@TiO_2-(A) yolk–shell sample as prepared and after treatments with HCl (Au@Void@TiO_2-(A)+HCl) and sequentially with HCl plus NaOH (Au@Void@TiO_2-(A)+HCl+NaOH). Top-right: Catalytic activities in terms of initial TOFs versus reaction temperature. Bottom: Ti 2p, O 1s, Na 1s, and Si 2p XPS. Reproduced with permission from ref 2028. Copyright 2016 Elsevier B.V.

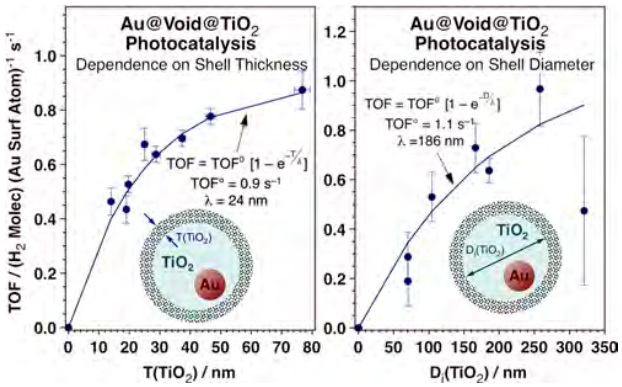

Figure 143. Use of the control of the structural parameters in Au@Void@TiO_2 yolk–shell nanostructures to test the mechanism of hydrogen photocatalytic production from water.[2029,2034] TOFs are plotted as a function of the thickness T(TiO_2) (left panel) and diameter D_i(TiO_2) (right) of the titania shells to highlight the different characteristic distances associated with the two parameters and to identify the latter with atomic hydrogen diffusion from the titania surface to the Au NP. Reproduced with permission from refs 56 and 2034. Copyright 2021, The Author(s). Published by Elsevier B.V.

suggested that its key participation is to catalytically promote the recombination of hydrogen atoms to form H_2 instead.[2033] By carrying out systematic measurements of catalytic photoactivity as a function of shell thickness and shell diameter, it was possible to identify two different characteristic lengths associated with the effects of the depth of the photoexcitation (needed for the reduction of H^+ on the titania surface) and the diffusion of hydrogen atoms on the surface (to reach the metal NP, where hydrogen recombination takes place), respectively (Figure 143).[2034] Shells can also be used to protect, constrain, and preserve the structure of core NPs, which can then be treated (thermally, for instance) with the aim of changing their properties in a controlled manner. A nice recent example here is that of a three-component Au@Pd@SiO_2 core–shell catalyst, where the effect of a transition from a Au@Pd core–shell metallic structure to a well-mixed alloy (induced by heating of the solid) was tested for the selective hydrogenation of butadiene: the core–shell bimetallic clearly outperformed the alloy, displaying much higher activity with comparable selectivity.[2035] In another study, a SiO_2 layer was added to Al_2O_3@Co/Al catalysts to minimize metal-support interactions and thus optimize their performance in Fischer-Tropsch conversions.[2036] The protected NPs can also be reduced in a controlled manner once protected by the added shells, a procedure that can improve catalytic selectivity.[2037−2039]

It is clear that core–shell and yolk–shell nanostructures offer unique features that can be beneficial for the design of catalysts. The potential of isolating active phases inside shells, together with the ability of controlling the volume available within the resulting individual nanoreactors. provides for a way to improve catalyst stability. The need for reactants and products to diffuse in and out of such nanoreactors can be exploited to add selectivity based on molecular size or shape. The possibility of controlling the structural parameters of these nanostructures offers additional tunability and affords the creation of new interfaces. On the other hand, the complexity of the synthetic procedures required to prepare core–shell and yolk–shell nanostructures may introduce impurities that can affect catalytic performance, and makes them quite expensive, limiting their potential commercial use. Ultimately, the use of these nanostructures in specific catalytic processes will need to be justified, a consideration that not always enters in the discussion of the published reports in this area. Nevertheless, nanosynthesis like these do add to the catalyst development toolbox, and can potentially help resolved specific catalytic problems.

7.2. Janus and Other Multicomponent Nanostructures

In addition to core–shell and yolk–shell materials, new nanotechnologies afford the synthesis of other nanoarchitectures with potential applications to catalysis. Among those, Janus nanostructures, with NPs exhibiting two or more separate phases, have become a popular way to add multiple functionalities to a single catalytic particle.[1153,2040,2041] Janus nanostructures are anisotropic and made out of combinations of two or more distinct sides with differences in polarity and/or chemical nature.[2042] The simplest and most common version of these catalysts is in the form of nanodumbbells, but other more complex multicomponent structures have been developed and tested as well.

Like with the core–shell and yolk–shell nanostructures, the use of nanodumbbells and similar nanoarchitectures in catalysis has in many instances been driven by the desire to control the properties of interfaces. With bimetallics, for

https://doi.org/10.1021/acs.chemrev.1c00905
Chem. Rev. XXXX, XXX, XXX−XXX

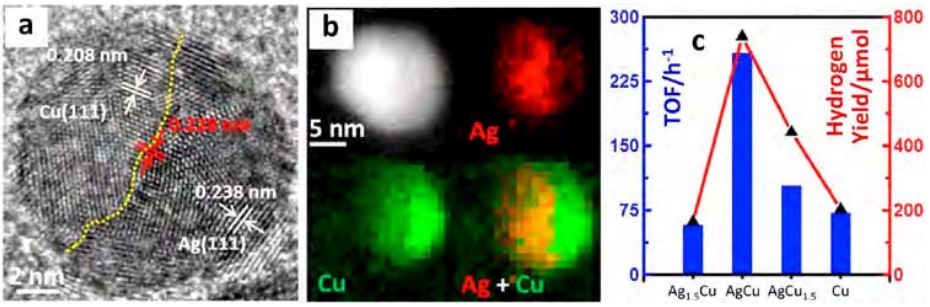

Figure 144. Characterization and testing of a Cu−Ag nanodumbbell catalyst used to promote the WGS reaction.[2044] The Janus nature of the NPs is evidenced by the sharp boundary seen in HRTEM images (a) and in HAADF-STEM element mappings (b). Optimum TOFs (blue bars) and hydrogen yields (red trace) were obtained with the 1:1 Cu:Ag composition that optimizes the interface area (c). Reproduced with permission from ref 2044. Copyright 2018 Wiley-VCH Verlag GmbH & Co. KGaA, Weinheim.

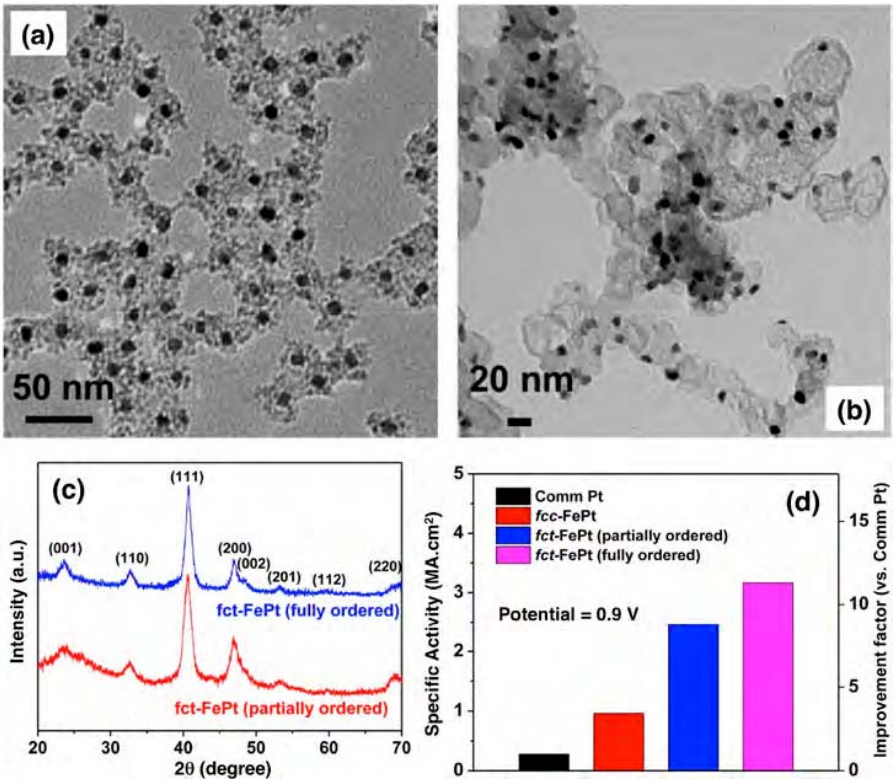

Figure 145. FePt−Fe_2O_3/MgO Janus nanostructures developed for the promotion of electrocatalytic reactions.[2048] The top row offers TEM images obtained right after synthesis (a) and following thermal annealing at 700 °C in a hydrogen atmosphere (b). XRD data (c) identified a transition from a fcc structure to fct ordering, leading to a clear increase in specific activity for the ORR (d). Reproduced with permission from ref 2048. Copyright 2015 American Chemical Society.

instance, Janus NPs offer a way to tune the electronic properties of the catalytically active phase. In one case, Au−Pt bimetallic nanorods have been shown to enhance the reduction of 4-nitrophenol, presumably because of a synergistic effect between the two metals.[1149] A similar argument was made to explain the high selectivity toward long-chain hydrocarbons in Fischer-Tropsch processes with bimetallic Janus Co−Fe NPs dispersed on carbon nanotubes.[2043] In an example with Cu−Ag nanodumbbells, used to promote the WGS reaction, the superior performance observed was attributed to the enhanced antioxidant properties of the metal−metal interface, which affords the preservation of a large ratio of the Cu atoms in their metallic state (Figure 144).[2044]

Janus NPs made out of combinations of metals and metal oxides are often used in catalysis to increase stability. In terms of structural effects, iron oxide has been a popular material. For instance, Au−Fe_2O_3 Janus NPs were shown to possess a unique interface with an intrinsic epitaxial linkage between the metal and the oxide that prevents metal sintering and thus sustains the initial high CO oxidation activity.[1148,2045] Curiously, in one study it was shown that, due to a strong SMSI effect, the metal (Au) could wet the iron oxide NPs upon vacuum annealing and transition from a dumbbell shape to a core−shell nanostructure.[2046] In the case of Pt−Fe_3O_4, used for the ORR, the ability to independently tune the sizes of the Pt and Fe_3O_4 NP components afforded the optimization of

https://doi.org/10.1021/acs.chemrev.1c00905
Chem. Rev. XXXX, XXX, XXX−XXX

the size and nature of the interface, and with that the electrocatalytic activity.[2047] A third case is that of the FePt–Fe_3O_4 nanodumbbells that have been developed to stabilize the face-centered tetragonal (fct) form of FePt, which was shown to exhibit enhanced electrocatalytic activity in acid media compared to the original face-centered cubic (fcc) structure (Figure 145).[2048] The metal–metal-oxide interfaces in Janus NPs can also introduce unique electronic properties. For example, the superior performance seen in the electrochemical reduction of H_2O_2 with Au–Fe_2O_3 nanodumbbell catalysts was ascribed to changes in the polarizability of the Au phase induced by the iron oxide side.[2049] Similar enhancement in reactivity was reported with dumbbell-like PtPd–Fe_3O_4 NPs designed for H_2O_2 detection in biological systems.[2050] An interesting example where both structural and electronic effects are at play is that of the room-temperature CO oxidation catalyst made by dispersing Au–Fe_3O_4 nanodumbbells on a TiO_2 support: in that case it was proposed that the Fe_3O_4 may structurally stabilize the Au NPs by preventing sintering while the Au/titania interface may provide the unique electronic properties required to promote catalysis.[2051]

Janus NPs can also offer the same advantages reported with the core–shell and yolk–shell nanostructures discussed in the previous section (Section 7.1), although the examples in this area are still limited. For instance, magnetite can be combined with an active phase to design a magnetism-based recycling process for the catalyst: bifunctional Au–Fe_3O_4 heterostructures have been tested for the catalytic reduction of nitrophenol,[1150] and MnO–Fe_3O_4 dumbbell nanostructures have been designed for the cyanosilylation of aromatic aldehydes in a size selective manner.[2052] In terms of tandem catalysis, a unique asymmetric (immobilized glucose oxidase/SiO_2)–γFe_2O_3 Janus NP design was developed as a multifunctional biosensing platform for the colorimetric detection of glucose: the enzyme tethered on the silica side converts glucose into gluconic acid and hydrogen peroxide, after which the hematite side consumes the H_2O_2 in a reaction to oxidize 3,3′,5,5′-tetramethylbenzidine (TMB) and yield the colored 3,3′,5,5′-tetramethylbenzidine diimine (oxTMB) product (Figure 146).[2053]

Janus nanostructures expose interfaces with unique electronic properties that may be particularly useful to improve the promotion of electrocatalytic reactions. For instance, Pt–FeNC dumbbell NPs were shown to perform better than conventional catalysts in the promotion of the ORR because of the electronic changes that occur at the interface.[2054] In another example, the electrochemical splitting of water was shown to be enhanced at the Ni–O–Fe bridging structures of the interface of Ni–Fe_2O_3 Janus NPs.[2055] In some cases, the value of the interface in Janus NPs is in creating unique electronic barriers, as in the example of the of Co–CoP Janus NPs with an interface that was shown to act as Mott-Schottky electrocatalysts for the promotion of water splitting (Figure 147, top).[2056] At the other end, PtFe–Fe_2C Janus-like NPs were shown to exhibit barrier-free electron transfer, thus enhancing the electrocatalytic ORR.[2057] Similar arguments apply to the use of Janus NP interfaces for photocatalysis. For instance, the rectifying effect of the Schottky junction in Co–Ti_3C_2 Janus NP photoanodes, which can be tuned by controlling the Co loading, facilitates the injection and separation of photogenerated carriers, thus enhancing the photoelectrochemical oxidation of water (Figure 147, bottom).[2058] With Au–TiO_2 nanodumbbells, the transfer of electrons from the Au nanorods to the TiO_2 nanoparticles under visible light irradiation leads to a directed spatial charge separation that enhances photocatalytic efficiency.[2059]

The asymmetry of Janus nanostructures also offers the possibility of designing catalysts with specific properties not easily accessible by other means. In particular, paired hydrophobic–hydrophilic NPs can be used to sit at the interface of water-oil biphasic systems such as emulsions and to selectively promote catalytic reactions in one of the two phases.[2060] In an early example, (Pd/CNT)–SiO_2 Janus NPs were synthesized for the selective hydrogenation of organic reactants in an oily phase, avoiding the competitive hydrogenation of water-soluble reactants.[2061] In another case, thanks to Pickering (particle) emulsion stabilization, and owing to an increase in reaction interface area, a (Pt/C)–SiO_2 dumbbell catalyst was shown to exhibit a more than three-fold increase in nitroarene reduction efficiency compared to a regular Pt/C catalyst used in an aqueous phase.[2062] A (Au/SiO_2)–polydivinylbenzene (PVDB)/polystyrene (PS) Janus-type catalyst has also been used to promote the reduction of 4-nitrophenol by Au in an organic phase with $NaBH_4$ dissolved in aqueous solution (Figure 148).[2063] Similarly, Pd clusters dispersed on the hydrophobic poly(tetradecyl acrylate) side of Janus NPs were shown to promote the oxidation of organic reactants in organic solvents while the Fe_2O_3 magnetic clusters dispersed on the hydrophilic poly(styrene-*co*-vinyl alcohol) side afforded easy separation for catalyst recycling.[2064] Although the catalysis applications of these biphasic Janus NPs may be limited, they can certainly help resolve the solubility problems often encounter in organic reactions.[2065] It is also promising that the systems considered here often involved complex reactions requiring high selectivity to make speciality or fine chemicals. Although a niche application, this is a promising route to the production of high value-added chemicals.

Another particularly interesting application of catalytic Janus nanostructures is for the development of self-propelled nanodevices. The asymmetry of the Janus design affords the creation of gradients in the surrounding solution that can induce NP motion.[2066−2068] This was first demonstrate with Au–Pt bimetallic nanorods, which were shown capable of autonomous self-propulsion in aqueous H_2O_2 because of a force generated along the rod axis by the oxygen concentration gradient created by the decomposition of the peroxide on the

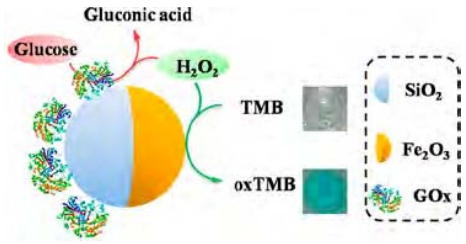

Figure 146. Schematic representation of the operational mechanism of a peroxidase-like Janus nanostructure designed for the colorimetric detection of glucose in blood.[2053] The glucose oxidase (GO_x) tethered to the silica side of SiO_2–γFe_2O_3 Janus NPs converts glucose into gluconic acid + H_2O_2, a reaction followed by the oxidation of 3,3′,5,5′-tetramethylbenzidine (TMB) to the colored 3,3′,5,5′-tetramethylbenzidine diimine (oxTMB) on the hematite side. Reproduced with permission from ref 2053. Copyright 2015 American Chemical Society.

https://doi.org/10.1021/acs.chemrev.1c00905
Chem. Rev. XXXX, XXX, XXX–XXX

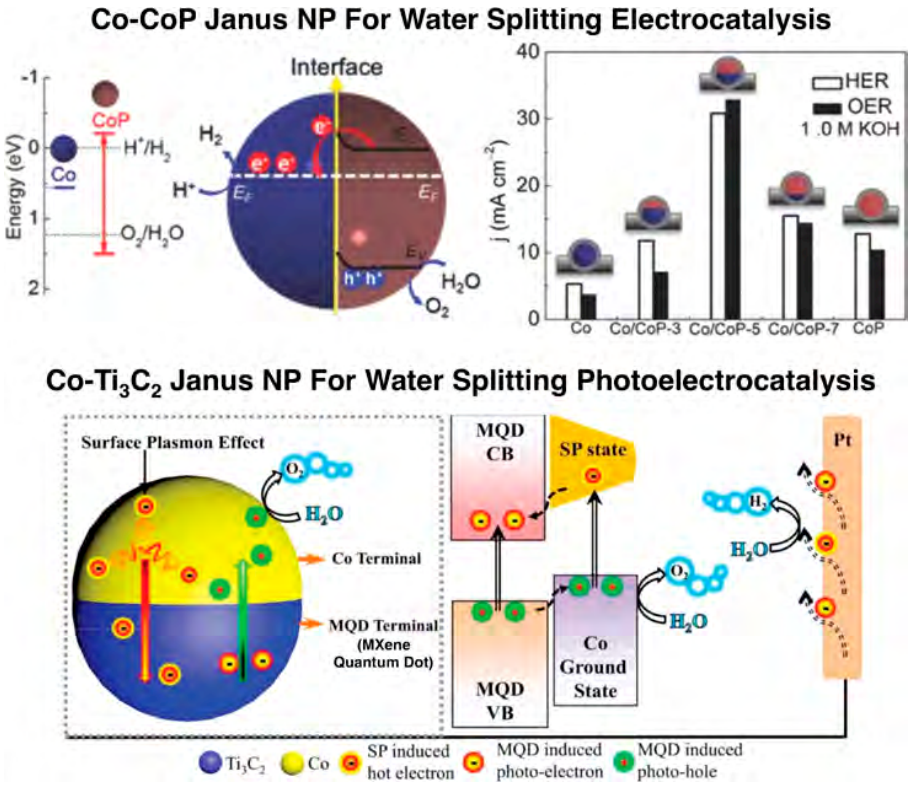

Figure 147. Examples of Co-based Janus nanostructures for electro- and photo-catalysis. Top: Electronic structure of the Co−CoP NPs used for the electrocatalytic splitting of water, highlighting the Mott-Schottky contact (left), and current densities measured for the HER and ORR reactions as a function of the ratio of the Co to Co−P phases.[2056] Reproduced with permission from ref 2056. Copyright 2017 Wiley-VCH Verlag GmbH & Co. KGaA, Weinheim. Bottom: Schematic illustration of the light harvesting and carrier separation mechanism of a Janus-structured Co−Ti_3C_2 NP material used for the photoeletrocatalytic splitting of water. Under illumination, due to the unique Schottky junction at the Co/interface, the hot electrons generated at the Co end are immediately injected into the carbide phase while the photoholes produced via Ti_3C_2 photoexcitation go through the Co terminal and oxidize OH^- ions (from water) into O_2.[2058] Reproduced with permission from ref 2058. Copyright 2020 Wiley-VCH Verlag GmbH & Co. KGaA, Weinheim.

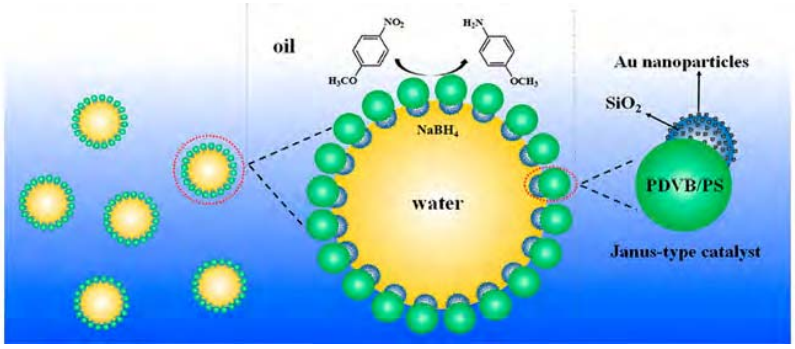

Figure 148. Schematic illustration of the way a Au/SiO_2−polydivinylbenzene (PVDB)/polystyrene (PS) dumbbell catalyst is proposed to promote the hydrogenation of 4-nitrophenol.[2063] The NPs are preferentially located at the oil-water interface, with the silica hydrophobic side containing the Au NPs that react with the $NaBH_4$ reducing agent and the polymeric end sticking out into the oily phase. Reproduced with permission from ref 2063. Copyright 2016 Elsevier Inc.

Pt side.[2069] In an recent application, Fe−Pt Janus NPs were shown capable of completely degrade methylene blue (on the iron side) in the presence of H_2O_2 in solution (which gets decomposed on the Pt side); the end result is a self propelling catalyst capable, at least in principle, of decontaminating water by removing toxic organic contaminants.[2070] The explanation for how the O_2 generation results in NP motion is still being debated, and several possible mechanisms have been advanced, including bubble recoiling, bubble implosion, Brownian ratcheting, thermal gradient formation, interfacial tension, and bipolar electrophoresis.[2071−2073] Moreover, the motion of these Janus NPs is random, but several ideas have been put forward to add control to their directionality. For instance, by anchoring Ni−Au nanorods to a silicon surface, it has been possible to induce a stationary rotary motion.[2074] There are also several groups exploring self-assembly designs to harvest

https://doi.org/10.1021/acs.chemrev.1c00905
Chem. Rev. XXXX, XXX, XXX−XXX

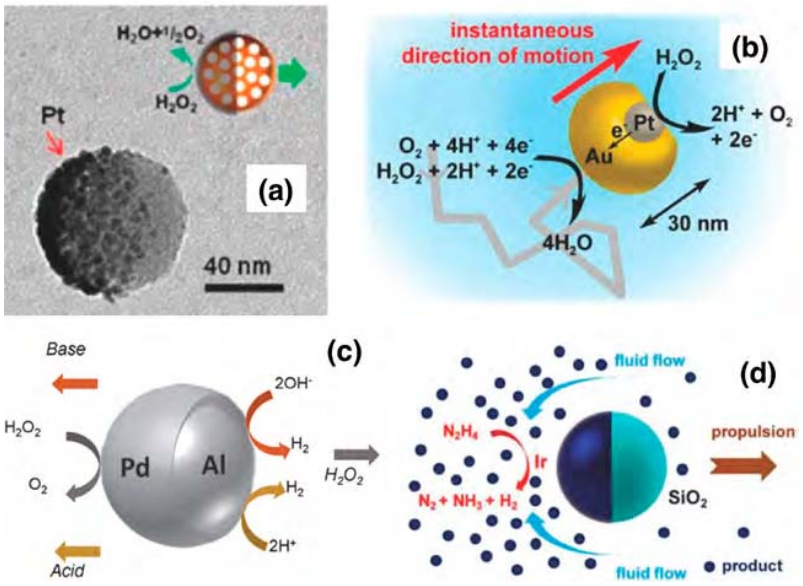

Figure 149. Examples of the use of catalysis in Janus nanoarchitectures to facilitate self-propulsion. (a) SiO_2−Pt/SiO_2 Janus nanomotor propelled by the O_2 bubbles generated via the Pt-catalyzed decomposition of H_2O_2.[2079] (b) Pt−Au anisotropic nanostructure, the motion of which is governed by self-electrophoresis in the presence of H_2O_2.[2083] (c) Pd−Al Janus micromotor propelled by a combination of two mechanisms, namely, the thrusts from H_2 bubbles generated from water reduction on the Al side and from O_2 production via H_2O_2 decomposition occurring on the Pt surface.[2084] (d) Ir−SiO_2 Janus NPs propelled by the N_2 and H_2 bubbles generated by the Ir-catalyzed decomposition of hydrazine[2085] Adapted with permission from ref 2081. Copyright 2018 Wiley-VCH Verlag GmbH & Co. KGaA, Weinheim.

the individual motions into collective directional displacements.[2075−2078] Most studies with self-propelled NPs rely on the generation of O_2 from catalytic decomposition of H_2O_2, like in the case of the Pt/SiO_2−SiO_2 NPs where the Pt is embedded within the interior of the mesoporous silica-based hollow particles to trigger the decomposition of H_2O_2 (Figure 149a).[2079] However, other fuels have been advanced as well, examples of which are provided in Figure 149,[2080,2081] and additional future candidates include organic peroxides, methanol, formic acid, diazomethane, azides, and hydrides. A unique design in this category is that of a Au−(Grubbs' catalyst/SiO_2) Janus NP where the silica side was derivatized with a [−C_3H_6−dihydroimidazole]$RuCl_2$[PCy_3][=CPh] ring-opening methatesis catalyst to promote fuel propulsion via the polymerization of norborene and the creation of a concentration gradient in solution leading to osmophoresis.[2082]

So far we have discussed the development of catalysts based on simple core−shell, yolk−shell, and dumbbell Janus nanoconstructions, but more complex combinations are also possible. For instance, it has become popular to conceive NPs, nanorods, or hollow nanoshells to which two or more different catalytically active phases are added (at the two ends in the nanorods, or to the inner and outer surfaces in the shells) to promote photocatalytic processes (Figure 150).[1153,2086−2088] For instance, the selective photodeposition of Rh/Cr_2O_3 and CoOOH co-catalysts on different crystal facets of $SrTiO_3$ semiconductor NPs has been used to promote hydrogen production and the OER separately, an approach that has achieved photocatalytic water splitting quantum efficiencies close to unity.[2089] In another example, spatially separating two redox co-catalysts, atomically dispersed cobalt to improve oxidation activity and anthraquinone to enhance reduction selectivity, onto 2D graphitic carbon nitride (C_3N_4) nanosheets was shown to increase photocatalytic H_2O_2 production from O_2 dissolved in an aqueous solution.[2090] Cases where the

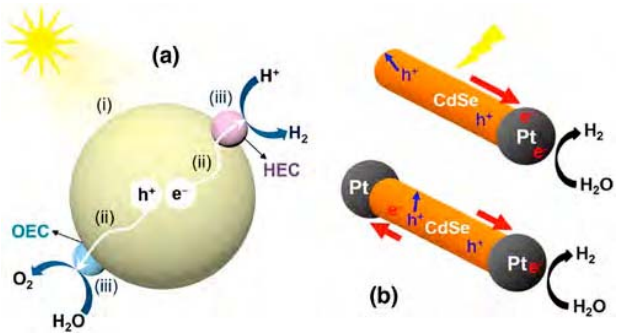

Figure 150. Examples of three-component nanostructured designs for the photocatalytic production of hydrogen from water. Shown are two cases, a supporting semiconductor NP modified with two different smaller NPs capable of promoting oxidation and reduction reactions (a),[2088] and a semiconductor nanorod terminated with metallic NPs at either one or the two ends (b).[1153] Reproduced with permission from refs 2088 and 1153. Copyright 2020 and 2015 American Chemical Society.

three-phase design has been implemented in shell nanostructures include the Co_3O_4(outside)/CNT(hollow shell)/Pt(inside) composite for photocatalytic water splitting[2091] and a NiN_4(inner)/graphene(shell)/FeN_4(outer) catalyst made to promote the OER and ORR, respectively.[2092] More complex nanostructures have been implemented to promote thermal catalysis as well. These include alternating layers[1143,1144] and other 3-component designs,[1143,1145,1156−1159] NPs with non-spherical shapes,[1145−1147] heterostructures with NPs of different metals coupled into a dumbbell configuration,[1148−1153] dumbbell-like NPs with splitting ends,[2093] cross-double dumbbell-like nanostructures,[2094] dumbbell-like NPs encapsulated inside hollow nanoshells,[2095] and etched hollow structures.[1154,1155] An example of an application of a complex

https://doi.org/10.1021/acs.chemrev.1c00905
Chem. Rev. XXXX, XXX, XXX−XXX

design for the promotion of tandem catalytic processes is that of a branched multi-arm Janus mesoporous silica nanostructure with organic-inorganic hybrid components to promote the deacetalization-Henry cascade conversion.[2096]

Overall, it is clear that the advances in the synthesis of complex nanostructures have opened new avenues for the construction of catalysts capable of addressing specific problems difficult to tackle in other ways. Both core−shell and Janus-type nanoarchitectures provide the means to develop interfaces in a controlled manner and to provide unique arrangements for different catalytic phases to operate and interact with each other. The uses of Janus nanostructures in biphasic catalysis and to produce self-propelling NPs are striking examples of the potential of this approach. On the other hand, these nanostructures are expensive to make, and may end up incorporating impurities that may modify the catalytic behavior of the constituent elements. They may only be justified if no easier alternatives are available, and if the cost cannot be avoided. This area of research is at the present time in an early exploratory phase, but consideration of the ultimate potential application and of its feasibility is still warranted. Another shortcoming of much of the current published research in this area is that catalytic tests are often not been properly carried out, in that they do not include direct comparisons with state-of-the-art equivalent catalysts or good estimates of kinetic parameters such as TOFs. Most reports focus on the synthesis of the materials and add catalytic results as an afterthought. Although understandable when trying to develop novel preparation protocols, this is not a good long-term strategy for catalysis. It would be desirable for future nanocatalysis research to be hypothesis driven, directed at addressing a particular problem in a catalytic process.

8. SURFACE MODIFICATION

Another way to improve catalytic performance and to add different functionalities as needed is to modify the original material used as the basis for the catalyst after being synthesized. In a sense, this is how most catalysts are made: for instance, metal-supported catalysts are often prepared via metal addition following different chemical methods such as impregnation or incipent wetness. In those procedures, however, the initial material is not catalytic; it is the metal (or any other phase) added afterwards that carries out the promotion of the desired reaction. Here we consider some methods where an already active catalyst is further modified to either improve its performance or add new functionality.

8.1. Silylation, Sol-Gel, Site Imprinting

One of the simplest and oldest procedures for post-modification of catalytic surfaces is silylation. This is a procedure by which terminal hydroxyl groups on surfaces (silanols in silica) are modified and capped with alkyl-terminated groups. The chemistry is typically used on metal oxides, primarily on silica, and the silylation agents added are mainly alkyl-substituted silanes (R_3SiX);[120,2097,2098] common silylation agents include silyl halides such as trimethyl-chlorosilane (TMCS) and octadecyltrichlorosilane (ODTS), silyl amines such as hexamethyldisilazane (HMDS), and trimethylsilyl ether (TMS).[2099] The chemistry involved in surface silylation is akin, but perhaps simpler, than that mentioned before in connection with the tethering of molecular functionalities to oxide surfaces (Section 2), and is also well known in organic synthesis, where silyl moieties are often used as protective groups.[2100,2101]

The main use of silylation is to treat hydrophilic surfaces in order to make them hydrophobic,[2102−2111] For instance, it has been shown that silylation of the metal oxide support in Pd-based Suzuki catalysts increases activity to values comparable to those seen on hydrophobic supports such as carbon.[2112] In the case of the use of a mixed organic-inorganic mesoporous matrix (made out of a perfluorosulfonic acid Nafion resin and SBA-15) as a strong acid catalyst for the promotion of isobutane/1-butene alkylation, silylation of the silica surface to make it hydrophobic resulted in a large enhancement in activity.[2113] Making the surface of a Schiff-base-functionalized Cu(II)/SBA-15 hydrophobic via silylation was shown to improve activity and selectivity for the epoxidation of styrene.[2114] Methyl modification of a Fe_2O_3@SiO_2 catalyst was used to render the silica surface hydrophobic so to prevent the readsorption of water during CO hydrogenation, inhibiting the undesirable WGS side reaction that produces CO_2 (Figure 151).[2115] A similar approach was reported with Co/SiO_2 Fischer−Tropsch catalysts.[2116]

The silylation process is also useful to block the Brønsted acidity of the surface OH groups.[2117] Even Lewis-acid sites may be poisoned by silylation.[2118] Blocking of the surface silanol groups of silica materials, which suppresses its acidic, is often desirable to prevent side reactions.[2119] For example, silylation of a Mo/HZSM-5 catalyst used for the non-oxidative aromatization of methane to benzene was shown to slow down the undesirable coke formation typical in this type of processes.[2120,2121] A similar effect was reported with pure ZSM-5 when used for the conversion of methanol to olefins.[2122] In the case of the promotion of the etherification of HMF with ethanol using Silicate-1, controlled silylation was employed to evaluate the relative activities of the weak versus strong acid sites present on the surface (Figure 152).[2123,2124] The advantage of blocking acid surface sites can be indirect as well. For instance, in the case of the hybrid Cu-ZnO-Al_2O_3/ZSM-5 catalysts used for the direct synthesis of dimethyl ether from syngas, selective neutralization of the acid sites on the zeolite outer surface by silylation was shown to prevent Cu sintering, thus improving catalyst stability.[2125]

Silylation can also be combined with the tethering of molecular functionalities to improve catalytic performance.[2126,2127] In an example from our group, it was found that the acidic silanol sites on the silica surface can add nonselective conversion to the enantioselective promotion of the addition of aromatic thiols to conjugated cyclohexanones by heterogenized cinchonidine, degrading the overall performance.[179] A combination of surface silylation and the use of non-protic solvents during reaction was found to solve this problem (Figure 153). A second example is that of the grafting of propylsulfonic groups on MCM-41; that catalyst was proven to be more effective promoting esterification reactions if the surface was further derivatized with octyltrimethoxysilane afterwards to cap the remaining bare silanol sites, a process also used to tune the hydrophobicity of the support.[2128] In a third recent study, several strategies were successfully explored to tether sulfonic acid and hydrophobic decyl hydrocarbon chains either simultaneously or sequentially on an azide-functionalized mesoporous silica platform in order to create a hydrophobic catalyst for the promotion of the esterification of octanol with acetic acid; the paired catalyst in the same organofunctionalized moiety showed the highest activity.[2129]

https://doi.org/10.1021/acs.chemrev.1c00905
Chem. Rev. XXXX, XXX, XXX−XXX

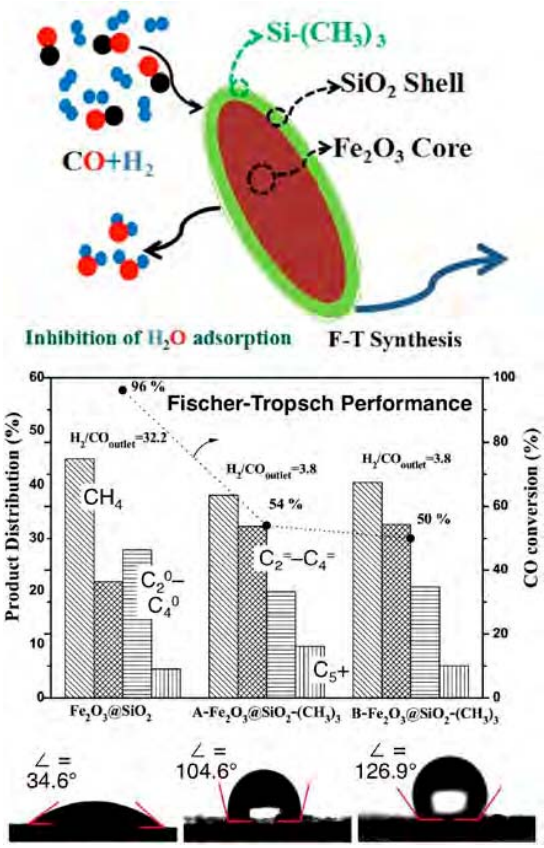

Figure 151. Use of silylation to control hydrophobicity in a Fe_2O_3@SiO_2 Fischer-Tropsch catalyst.[2115] Top: schematic representation of the core–shell NPs, with the iron oxide core (brown) surrounded by a silica layer (green) that has been subsequently silylated. Bottom: Contact angle measurements for three samples, as prepared (left) and after two silylation processes (A & B, the second using twice the amount of the silylation agent) to indicate that the silylation treatment leads to a transformation of the catalyst from hydrophilic to hydrophobic. Center: catalytic performance results showing that although the total conversion diminishes with increasing silylation, the selectivity improves, with more olefins and less CH_4 (and CO_2, not shown) being produced. Reproduced with permission from ref 2115. Copyright 2018 Elsevier B.V.

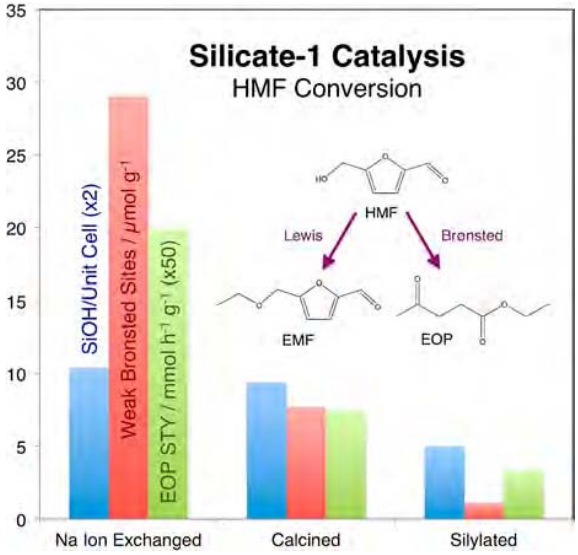

Figure 152. Example of the use of silylation as a way to block Brønsted-acid sites (in Silicate-1), in this case to selectively block the etherification of HMF to 5-(ethoxymethyl)furfan-2-carbaldehyde (EMF) and thus favor the promotion of the competing product, ethyl-4-oxopentanoate (EOP), via ring opening.[2123] The data indicate that silylation blocks about half of the silanol groups (blue bars), greatly reducing the coverage of weak Brønsted-acid sites on the surface (red), and with that lowering the activity for EOP production (green).

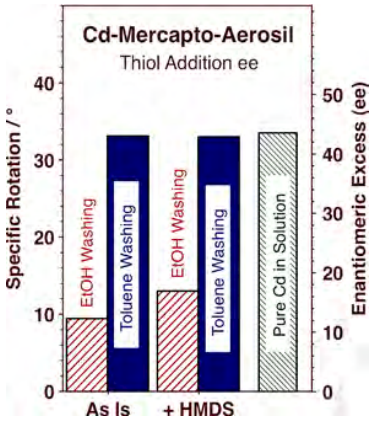

Figure 153. Effect of silylation on the performance of cinchonidine (Cd) mercapto-tethered to silica surfaces in terms of enantioselectivity during the addition of *p*-tertbutylbenzenethiol to 2-cyclohexene-1-one.[179] Silylation of the catalyst with HMDS, in conjunction with the use of toluene as a washing agent, affords reaction enantioselectivities comparable to that measured with free Cd in solution. Reproduced with permission from ref 179. Copyright 2012 American Chemical Society.

Although not as common, silylation can be carried out on materials other than silica.[2130] In one case, the silylation of an anatase TiO_2 catalyst used for the selective photooxidation of cyclohexane was seen to cause two competing changes, the blocking of OH surface sites at low silylation coverages, which reduces catalytic activity, and an enhancement in the desorption rate of the cyclohexanone product, which dominates at high silylation coverages and results in higher catalytic activity.[2131] In a study on the aldol condensation of cyclopentanone on a MgO catalyst, it was found that water affects the reaction in a way that depends on the degree of silylation of the surface: on non-functionalized (hydrophilic) MgO the rate decreases with the addition of water, but on hydrophobized MgO (via silylation with octadecyltrichlorosilane), the rate actually increases.[2132] It was argued that silylation alters the reaction mechanism by reducing the proximity between active sites and thus the rate of C–C coupling, and that water helps that step by bringing the reacting molecules closer together via chains of hydrogen bonds. One interesting example of silylation of non-oxide catalysts, where silylation was used to add functionality to catalytic surfaces, is that of the amine-group addition to GO to be use as an acid–base bifunctional catalyst for the conversion of diacetals, to promote a sequential hydrolysis step (on the acid sites of GO) followed by a Knoevenagel condensation (on the added amine moieties; Figure 154).[2133]

The hydrolysis of organosilanes such as tetraethyl orthosilicate (TEOS) has been used to grow protective silica

https://doi.org/10.1021/acs.chemrev.1c00905
Chem. Rev. XXXX, XXX, XXX–XXX

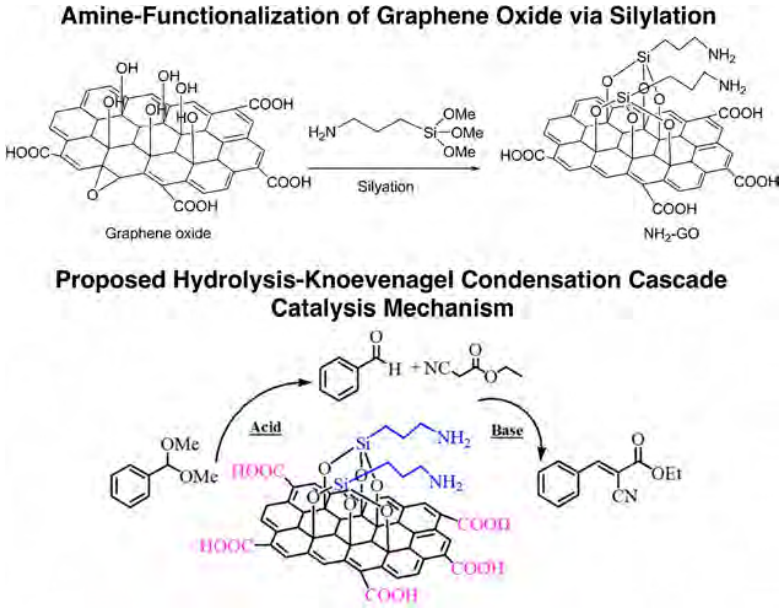

Figure 154. Preparation of (top), and proposed two-step cascade process (bottom) catalyzed by, amine-derivatized GO via silylation.[2133] Reproduced with permission from ref 2133. Copyright 2013 American Chemical Society.

thin layers on supported metal NPs with the aim to prevent their sintering and improve their stability.[2134−2136] For instance, thin silica films have been grown on carbon nanofibers (CNFs) using a combination of APTES and TEOS to facilitate Pt deposition and electrocatalytic oxidation performance, in particular to increase stability during multiple potential cycling (Figure 155).[2137] Thicker oxide layers can also be deposited on catalysts using related sol-gel chemistry, in a processes based on a two-step solid growth mechanism where the hydrolysis of the molecular precursor (i.e., TEOS and analogous compounds) in water leads first to the polymerization of individual units to form colloidal particles and then to their aggregation to form a solid gel.[1441,2138−2141] Solvent removal and gel aging can be attained subsequently via heat treatments. The characteristics of the final product, in particular its porosity, may be controlled by adjusting a number of parameters during synthesis, including the pH of the solution, the stoichiometry of the reactants (in particular if mixed oxides are to be grown), the gelation temperature and time, and the choice of solvent.[2142]

Sol-gel is more often used to prepare the catalytic materials themselves, but can be adapted to modify existing solids as well. One application is for the deposition and dispersion of catalytic active oxide phases on high-surface-area supports. A popular example here is the sol-gel dispersion of TiO_2 NPs for the photodecomposition of contaminants in wastewater.[2143,2144] Sol-gel synthesis is sometimes preferred because it can be carried out at low temperatures, but unfortunately the resulting films are typically amorphous and therefore perform poorly as photoactivators (which requires crystallinity to minimize excitation-trapping defects); thermal treatment at relatively high temperatures is required after the coating process, defeating the initial benefit of using this technique. Sol-gel-deposited titania NPs can nevertheless be used in other applications where this is not a problem, such as in lithium ion batteries.[2145] Alternatively, sol-gel-grown films can be used to cover and protect catalytically active NPs, typically metal phases. There are several examples in the literature where Pt NPs have been covered with silica layers this way to prevent sintering[2146−2149] and/or poisoning.[2150] Similar silica protection has also been used to protect Au NPs, which are particularly prone to the loss of their catalytic activity because of metal agglomeration.[2151,2152] Silica has been the material of choice in most cases, but films of other oxides such as alumina have been grown too.[2153] In an interesting example, sol-gel TiO_2 decoration of Au/SiO_2 oxidation catalysts was shown to serve the dual purpose of improving metal NP stability and creating new catalytically active interfaces.[2154] Two schemes were tested where the Au colloidal NPs were sol-gel-coated either before or after dispersion on the silica support (Figure 156): similar activity for CO oxidation was seen in both cases.

One limitation with this approach is that although sol-gel films tend to be amorphous and highly porous, they can still limit access of the reactants to the active phase.[1038,1942,2155] The problem may be aggravated by the slow evolution of sol-gel materials into denser and less porous materials with time. Organic growth-directing agents may potentially be used to define the directionality and/or shape of the pores in the newly deposited mesoporous material, to create radially oriented pores, for instance,[2156−2159] but examples of the use of this approach in the post-modification of catalysts are hard to come by. Alternatively, directional etching may be designed to open well-oriented channels after sol-gel deposition. In an example from our laboratory, after protecting Pt/SiO_2 NPs with a layer of sol-gel-grown mesoporous SiO_2, a surfactant was used to inhibit silica etching at the outside surface and promote selective Pt surface exposure.[49,1038,1942,2155] Significant thermal stability of the Pt NPs was obtained this way without sacrificing catalytic performance (Figure 157).

Organic templates can also be used to imprint catalytic cavities with specific shapes to increase selectivity in catalysis.[2160−2164] Most experiments in this category have focused on using the sacrificial templating agent during the synthesis of the catalyst.[334,2165−2175] but there are some examples of imprinting performed via the addition of polymer or sol-gel silica layers to existing catalysts. In one example, an

https://doi.org/10.1021/acs.chemrev.1c00905
Chem. Rev. XXXX, XXX, XXX−XXX

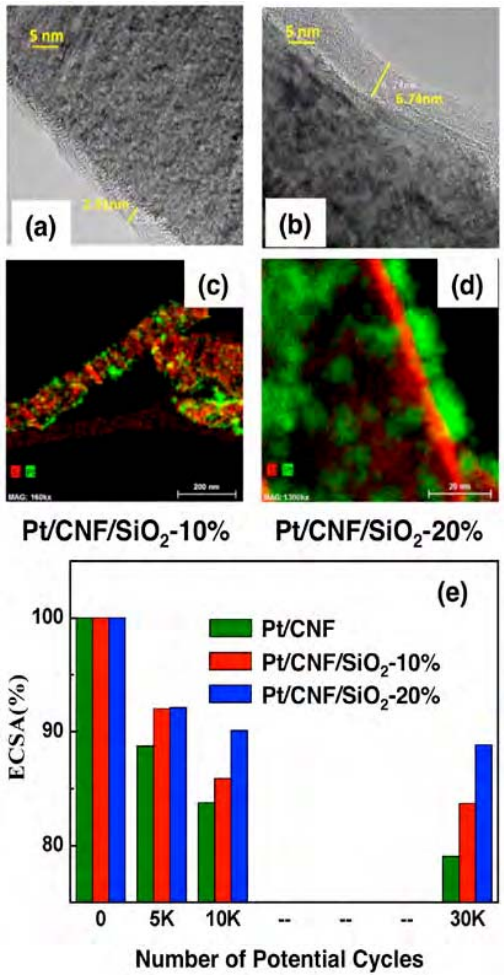

Figure 155. $Pt/SiO_2/CNF$ catalysts for the electrochemical ORR.[2137] Top: TEM images of catalysts with 10 wt % ($Pt/CNF/SiO_2$-10%, (a)) and 20 wt % ($Pt/CNF/SiO_2$-20%, (b)) SiO_2, respectively, deposited on the carbon nanofibers prior to the Pt addition. The thickness of the silica layers is indicated in yellow. Center: Corresponding EDX images indicating the distribution of the elements, Pt (green) and Si (red) in particular. Uniform SiO_2 and Pt dispersion was obtained on the 20 wt % SiO_2 (d) but not on the 10 wt % SiO_2 (c) sample. Bottom (e): Electrochemical active surface area (ECSA) measured for both catalysts as a function of the number of electrical potential cyclings performed. Data are also provided for a catalyst without silica (Pt/CNF) for reference. Clearly, the addition of the silica layer increases catalyst stability. Reproduced with permission from ref 2137. Copyright 2019 Hydrogen Energy Publications LLC. Published by Elsevier Ltd.

imprinted mesoporous La-doped titania film was prepared to selectively promote the hydrolysis of the pesticide paraoxon: mesoporosity was achieved by using a tri-block copolymer (Pluronic F127) as a micellar template, and molecular imprinting of catalytic cavities by adding a La(III)-(bis-4-nitro-phenyl-phosphate) complex.[2176] In another case, Fe_3O_4 NPs were covered with polymers imprinted with either 3,3′,5,5′-tetramethylbenzidine (TMB) or 2,2′-azino-bis(3-ethylbenzothiazoline-6-sulfonic acid (ABTS) to mimic the selectivity of peroxidase under near-physiological conditions.[2177] A third study focused on the construction of a novel glucose oxidase mimic based on AuPt NPs dispersed on magnetite (for ease of separation) and covered with a polymer-based shell imprinted with aminophenylboronic acid-glucose complexes; the glucose was eluted in a subsequent step to open up the catalytic sites for glucose oxidation.[2178] The Japanese team of Tada and coworkers has developed a number of silica-based enantioselective catalysts via site imprinting using organometallic complexes.[2164,2179,2180] They have made Rh-based catalysts for the promotion of α-methylstyrene hydrogenation,[2181] the asymmetric transfer hydrogenation of *o*-fluoroacetophenone in water media,[2182] and the selective reduction of acetophenones,[2183] and another based on a Pd complex to catalyze Suzuki cross-coupling reactions.[2184] Figure 158 shows the reported synthetic route to a doubly-imprinted catalyst developed to promote the hydrolysis of paraoxon: paraoxon (reactant; outside shell) and p-nitrophenol (product; inside shell) were used as templating agents in concentric catalytically-active polymer shells made out of DVB and a zinc dimethacrylate complex and built on top of a sacrificial vinyl-functionalized silica core.[2185] The resulting catalytic capsules were shown to promote the degradation of the reactant and the elimination of its product simultaneously.

In summary, in this section, we have introduced a number of synthetic tools to modify catalysts in specific ways. Simple silylation reactions are easy to carry out, and afford important surface modifications in terms of the affinity of the catalyst to water and of the control of surface acidity. Sol-gel procedures are also well established as a way to add specific materials to surfaces, although not in a particularly controlled fashion. Imprinting offers an exquisite way to carve catalytic sites and thus add refined selectivity to catalyst, although the sturdiness of those sites may be limited. All of these methods produce layers that may not survive exposures to high temperatures, and are therefore better suited for catalyst that operate under mild conditions. It may also be finicky to make the imprinting method work; only a handful of examples are available in the literature to attest to the feasibility of this approach. Within those constrains, however, these are procedures worth considering in particular circumstances, for the design of specific catalysts.

8.2. Atomic Layer Deposition

A catalyst post-modification procedure that has garnered great attention in recent years is atomic layer deposition (ALD).[763,764,2186−2194] ALD has mainly been developed in connection with the microelectronics and semiconductor industries,[2195−2199] but has now been extended to many other uses.[2200−2204] The central idea behind ALD, a particular implementation of chemical procedures for the deposition of thin films using gas-phase precursors, is that by separating the associated surface chemistry into two self-limiting and complementary half-reactions, which are carried out in an alternating fashion,[2197,2205−2207] only sub-monolayer coverages of the desired material are deposited in each ALD cycle.[763,764,2193,2208] The chemical nature of the process also helps with film conformality, especially when dealing with complex topographies or, as is often the case in catalysis, with powders or porous materials, although deposition on the inner surfaces of the latter requires additional considerations regarding mass transport.[2208,2209] A study from our group showed that either low or high precursor exposures (without proper pumping in between during the ALD cycles) can result in non-uniform pore coverage (Figure 159).[2210] Moreover, ALD is often carried out at relatively low temperatures, an advantage in some catalyst preparations but a condition that

https://doi.org/10.1021/acs.chemrev.1c00905
Chem. Rev. XXXX, XXX, XXX−XXX

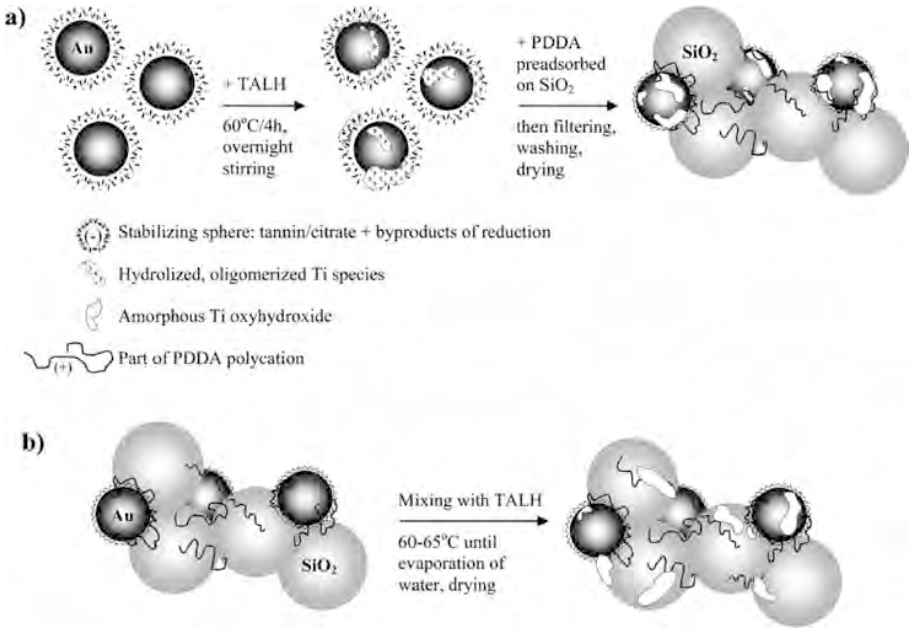

Figure 156. Synthetic procedures for the production of titania-protected Au NPs catalysts dispersed on silica beads.[2154] The TiO_2 layer was deposited, using a sol-gel method, either (a) before or (b) after metal dispersion on the support. Both procedures led to stable catalysts with comparable activities for the promotion of CO oxidation. Reproduced with permission from ref 2154. Copyright 2006 American Chemical Society.

leads to the growth of amorphous films, desirable in some cases but not others; if crystallinity is required, further annealing at higher temperatures may be required.[2211−2215] On the other hand, if the process parameters are properly tuned, ALD can be used to systematically reduce the pore diameters of high-surface-area materials, especially of ordered mesoporous materials such as SBA-15 or MCM-41.[2210,2216,2217] Another issue to consider is that, like with other chemically-based deposition methodology, ALD films are prone to contain impurities from decomposition of the precursors used.[2218−2220] Finally, ALD films are often smooth, but can in some instances become rough depending on the characteristics and distribution of nucleation sites (that is, the surface points at which the ALD chemistry is initiated) within the surface of the substrate.[2221]

One common use of ALD in catalysis is to deposit thin protective films around a catalytically active phase, to prevent sintering or chemical attack. ALD is ideal for this application because of the ability to control the thickness of the film down to only a few layers, and because of the conformality (which affords full surface protection without pinholes or other openings) and amorphous and porous nature (which allows easy access of the reactants and products to the catalytic surface) of the resulting films. The use of ALD to prevent metal sintering is exemplified by the case of the addition of an alumina layer to a Pd/Al_2O_3 catalyst used for the decomposition of methanol, where the layer-by-layer ALD of a protective alumina overlayer was shown to initially lead to the preservation of (in fact, to a slight increase in) the catalytic activity while preventing sintering of the Pd NPs (Figure 160).[2222] Also to note from the results of this study is the observation that the deposition of thicker layers (obtained after 20 ALD cycles or more) resulted in the gradual inactivation of the catalyst, a fact that highlights the advantage of using ALD as the technique that offers the best control of film thickness. Other examples include the ALD of a protective oxide (Al_2O_3, TiO_2, or Ce_2O_3) layer on a Pt/Al_2O_3 liquid-phase alcohol reforming catalyst,[2223] the Al_2O_3 stabilization of Cu/Al_2O_3, used for liquid-phase furfural hydrogenation catalysis,[2224] the SiO_2 ALD on a $PdCoNi/TiO_2$ formic acid dehydrogenation catalyst,[2225] the $LaFeO_3$ ALD stabilization of a $Pd/MgAl_2O_4$ catalyst used for CH_4 and CO oxidation,[2226] and the addition of a MO_x porous film to a Pt/C catalyst used for the decarboxylation of oleic acid.[2227] In all of those cases, much enhanced catalyst stability was reported while still retaining catalytic activities comparable to, some times even better than, those of the unprotected catalysts. Nevertheless, most often there is a trade-off between increase stability and decrease activity.[2228] Also, the structure and crystallinity of the film may matter (as mentioned above), so the catalyst may need to be annealed to achieve optimum performance; this is what was required, for instance, in the case of the ZrO_2 ALD on a Pd/Al_2O_3 methane oxidation catalyst.[2229,2230] The material used as the protective layer can make a difference too: it has been reported, for instance, that a thin ALD TiO_2 film stabilizes a Co/TiO_2 catalyst used for aqueous-phase hydrogenation reactions by preventing leaching and sintering, but that using Al_2O_3 instead causes the formation of an irreducible cobalt aluminate phase with no catalytic activity.[2231] Related to that observation, it should be indicated that the initiation of ALD requires specific nucleation sites not always available on metals. Interestingly, in an experiment in which Al_2O_3 ALD was performed to protect supported Pd NPs, film growth was shown to start preferentially at the defect sites of the metal, leaving catalytically active Pd(111) facets exposed.[2232,2233] This offers a potential additional approach to shape selectivity through the selective blocking of specific surface planes within the active catalyst.

A particularly interesting application of ALD to protect active phases is in electrocatalysis, since the electrodes in such cases may not require the degree of porosity associated with most catalysts; the ALD modification of electrodes can

https://doi.org/10.1021/acs.chemrev.1c00905
Chem. Rev. XXXX, XXX, XXX−XXX

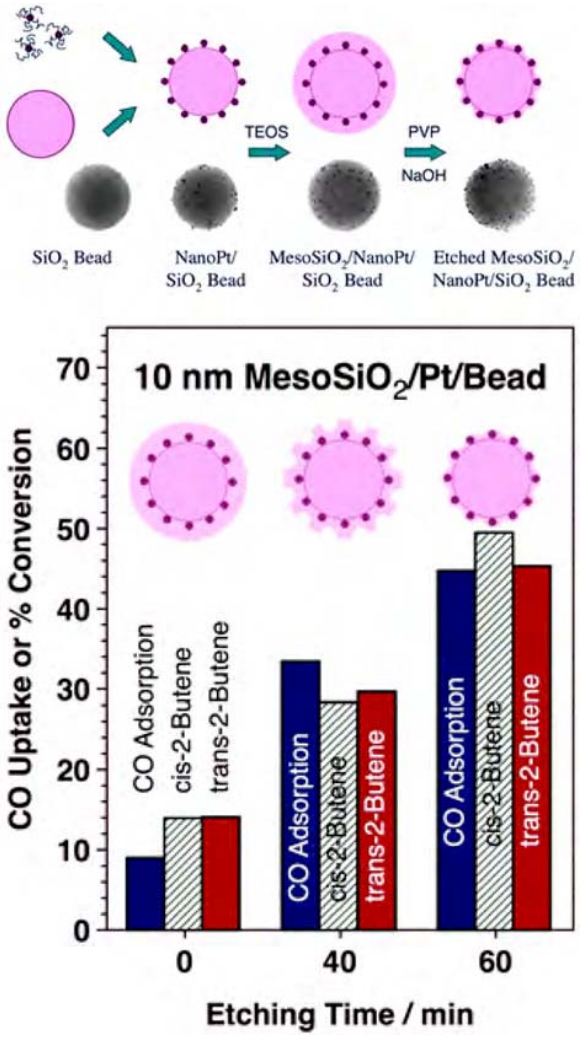

Figure 157. Demonstration of an etching protocol aimed to reopen access to the surface of the metal in sol-gel-protected Pt/SiO_2 catalysts.[49,1038,1942,2155] Top: Synthetic procedure for the preparation of the catalyst, highlighting the sol-gel protection and subsequent etching steps. TEM images are also provided for typical samples obtained after each step. Bottom: Results from tests to probe the accessibility to the surface of the Pt NPs right after silica protection and following two etching procedures. The data correspond to the extent of the uptake of carbon monoxide at 200 K (blue bars) and the activity toward the conversion of cis- and trans-2-butene in the presence of hydrogen gas (hatched-green and solid red bars, respectively). Reproduced with permission from ref 1038. Copyright 2011 the Owner Societies.

therefore be more easily implemented. On the other hand, the challenge here is to deposit appropriate layers capable of structurally and chemically protecting the surface of the electrodes while still allowing for electron transfer, chemical electroconversion, and favorable electronic band alignment. The feasibility of using ALD in electrocatalysis was proven in the case of a Si electrode ALD-protected with a thin TiO_2 layer placed in between the native SiO_2 layer that forms on the Si wafer and an Ir photocatalytic film: ALD guarantied the uniform and pinhole-free nature of the film, which was still thin enough to allow the tunneling of photoelectrons.[2234] More recent studies in this area include the ALD of a submonolayer $Co(OH)_2/Co_3O_4$ catalytic film on hematite for the enhancement of the photoelectrochemical oxidation of water,[2235] the covering of Si, GaAs, and GaP photoanodes with 100 nm ALD-grown TiO_2 (after which the NiO photoactive element was added) to promote the photooxidation of water (Figure 161),[2236] the passivation of surface states on water-splitting hematite photoanodes with ALD-grown Al_2O_3 overlayers to avoid electron-hole recombination at defects,[2237] and the implementation of a Cu_2O/Ga_2O_3-buried p−n junction coaxial nanowire structure for unassisted solar water splitting (ALD affords conformality).[2238] Once again, film crystallinity has proven important in many of these electrocatalytic applications of ALD. In the example of the ALD of MnO_x conformal thin films on glassy carbon electrocatalysts for OER and ORR, it was found that while the former could be promoted by the film as deposited, the latter required film annealing until Mn_2O_3 was formed.[2239] In the case of the sequential ALD deposition of Cu_2O(absorber)/Al:ZnO(n-type oxide)/TiO_2(protector)/Pt films to be used as photocathodes for water splitting, it was found that even without complete crystallization of the film, high-temperature deposition improved the film's chemical stability by removing residual excitation-trapping surface hydroxyl groups.[2214]

ALD can be used to deposit the active phase of a catalyst in a controlled manner as well. Many examples are available of ALD used for the growth of well-defined films of materials such as metal chalcogenides[2240] or metal oxides[2192,2241,2242] in catalysis. For instance, ALD can afford the preparation of catalysts with highly-dispersed tetracoordinated vanadia species; those were shown to display excellent catalytic performance for the dehydration of propane.[2243] In other studies, the ALD growth of tungsten[2244] and niobium[2216] oxides on the pores of SBA-15 has been shown to produce alcohol dehydration catalysts with better dispersion and better thermal stability than those prepared by conventional impregnation methods.[2244] In the first case, activity was also shown to be highly dependent on the density of WO_x species on the surface (Figure 162).[2244] In addition, because multiple materials can be added by ALD in alternating cycles, to make layered films, new mixed interfaces can be created. For example, ALD has been used for the controlled synthesis of bilayered vanadia/titania/silica catalysts: the improved activity seen in both ammonia conversion[2243] and o-xylene oxidation[2245] with that catalyst compared to what is observed with conventional silica and titania supported samples was ascribed to the formation of new −V−O−Ti− bonds on the surface. The selectivity of more complex Mo−V−Te−Nb intermixed oxides for propane ammoxidation could also be improved via the selective ALD of specific planes.[2246]

An alternative method to create mixed-oxide sites relies on the fact that in ALD the film growth starts at specific so-called nucleation sites, which on most oxides are surface hydroxyl groups;[2247−2249] since the density of those may be low (it is typically 1-2 OH groups per nm^2 in silica),[2250,2251] the first ALD cycles often result in the formation of new support/film interface sites with unique structural details and catalytic properties.[2244,2246,2252−2255] For instance, the limited ALD of titanium and vanadium oxide layers on SBA-15 and FDU-15 (a carbon-based mesoporous material) has been shown to afford the creation of new support−oxygen−metal sites with unique performance for the liquid-phase epoxidation of cyclohexene.[2256] The idea of creating mixed-oxide new sites via ALD has been explored in detail in our labora-

https://doi.org/10.1021/acs.chemrev.1c00905
Chem. Rev. XXXX, XXX, XXX−XXX

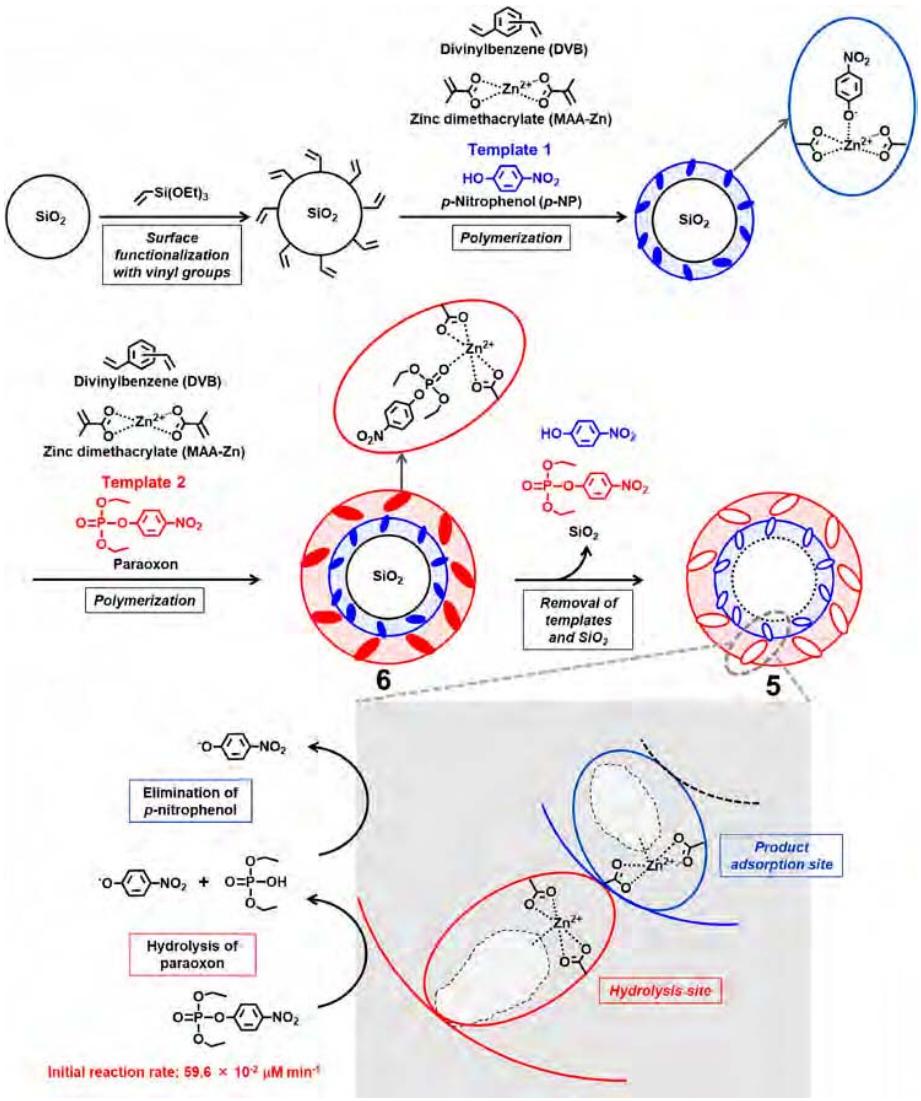

Figure 158. Reported synthetic route for the production of a doubly imprinted catalyst designed to promote the hydrolysis of paraoxon.[2185] A vinyl-derivatized silica bead was sequentially covered with two Zn-based polymer layers templated with *p*-nitrophenol and paraoxon, respectively, after which both the silica beads and the templating molecules were removed. The proposed mechanism by which this catalyst works is provided at the bottom. Reproduced with permission from ref 2164. Copyright 2020, Elsevier Ltd.

tory.[2210,2217,2255,2257] In one example, mixed −Al−O−Si− oxide sites with Brønsted-acid properties were created by adding submonolayer coverages of silica to Pt/Al_2O_3 catalysts, as identified by IR titration experiments using pyridine as the probe molecule (Figure 163, left panel).[2257] These new sites proved to help increase selectivity during the hydrogenation of unsaturated aldehydes (cinnamaldehyde, CMA) toward the desired unsaturated alcohol product (cinnamyl alcohol, CMO), as shown in the right panel of Figure 163. New redox sites can also be made via the ALD of reducible oxide films such as titania or ceria.[2255] The fact that it is the mixed-oxide interface the responsible for the new chemistry is suggested by the fact that in many cases optimum selectivity is seen at coverages of approximately half a monolayer of the new oxide film.[2217,2255,2257]

With metals, the deposition of smooth and uniform films is difficult, and, because of their low surface tension, those are unstable toward sintering and NP formation. An exception to this may be seen in the making of certain electrodes for electrocatalysis, where the ALD of thin metal films on top of other metals or on other wettable substrates can be implemented to save on cost: this was the case, for instance, of the (ALD-Pt)/WC-NP electrode made for the promotion of the HER.[2258] Nevertheless, even when sintering occurs, it is still useful to use ALD for the synthesis of metal-based catalysts as a way to tune the rate of metal deposition,[2259−2263] and also to improve on dispersion.[763,2264−2269] Examples of catalysts with highly dispersed metals made by ALD include that of Pt NPs grown on $Si@TiO_2$ core−shell nanowires for the photochemical reduction of water, where the NP size could be tuned between 0.5 and 3 nm (using different numbers of ALD cycles).[2270] $(ALD\text{-}PtNi)/Al_2O_3$ bimetallic catalysts made by ALD for the dry reforming of methane also afforded small enough NPs to prevent the growth of poisonous carbon whiskers during reaction, as seen with conventional catalysts.[2263] In fact, ALD has also been used to produce single-

https://doi.org/10.1021/acs.chemrev.1c00905
Chem. Rev. XXXX, XXX, XXX−XXX

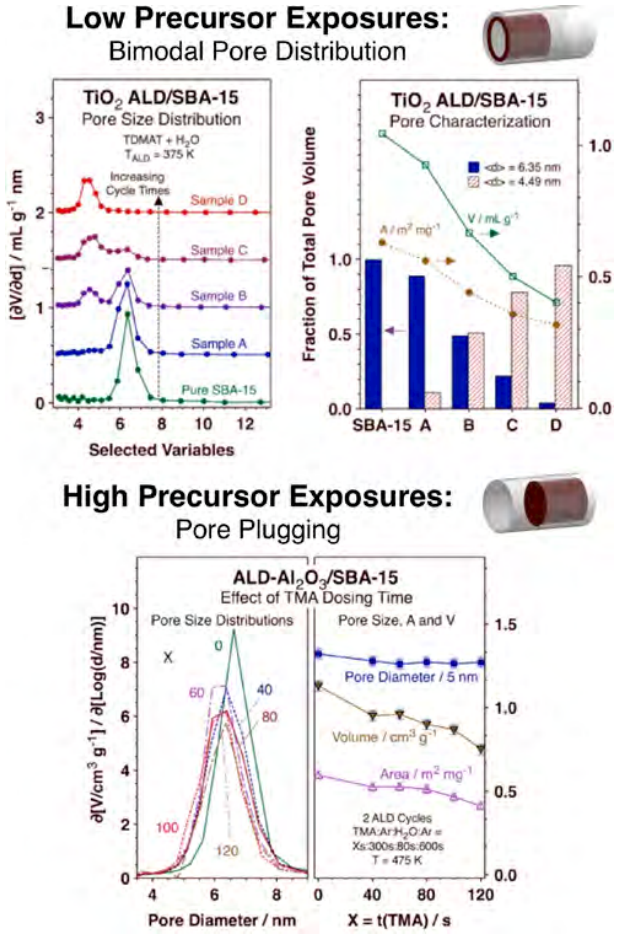

Figure 159. Results from studies of the quality of the films obtained inside the pores of SBA-15 by ALD.[2210] Top: Pore size distributions (left) and calculated fractions of uncovered (blue bars) and TiO_2-covered (hatched red bars) surfaces, total pore volumes, and total surface areas, after 8 TiO_2 ALD cycles as a function of increasing precursor exposures during each cycle (right). Short exposures lead to bimodal pore size distributions indicative of incomplete pore coverage. Bottom: Pore size distributions (left panel) and average pore diameters, total pore volumes, and total surface areas (right) after two Al_2O_3 ALD cycles as a function of precursor exposure time; long exposures lead to lower volumes and lower areas without changing the pore diameters, a result that suggests pore plugging. Reproduced with permission from ref 2210. Copyright 2018 The Royal Society of Chemistry.

atom (SA) catalysts: for instance, (ALD-SA-Pt)/graphene and (ALD-cluster-Pt)/graphene catalysts have been made for the HER,[1749] a (ALD-SA-Pd)/graphene catalyst was designed for the selective hydrogenation of 1,3-butadiene,[766] and a (ALD-SA-Co)/SiO_2 catalyst was synthesized to promote the dehydrogenation of ethane.[2271] Ultimate cluster size control was shown in the case of the making of a (ALD-dimer-Pt_2)/graphene catalyst via the sequential nucleation of Pt atoms on phenol-related oxygen anchor sites followed by the addition of a secondary Pt atom selectively at the newly-created metal sites (Figure 164).[2272] In the end, though, control of ALD-made metal catalyst surface morphology is difficult to attain at the same level as that described before using other methods such as colloidal and other self-assembly synthesis.[2260,2264,2265,2270]

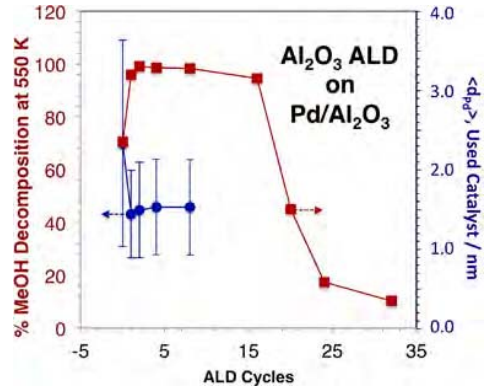

Figure 160. Modification of a Pd/Al_2O_3 catalyst via Al_2O_3 ALD to increase stability.[2222] Shown are the activity data for the catalytic decomposition of methanol at 550 K (red) and the average Pd NP size of the catalysts after use, both as a function of the number of ALD cycles used (which correlates to the thickness of the added layer). The retention of the original NP size is an indication that the ALD film prevents metal sintering.

The final nature of the catalysts made by ALD may depend on parameters associated with the ALD process itself. For instance, the effect of the co-reactant was made evident in the case of the making of (ALD-Pt)/Al_2O_3 with O_2 versus H_2: the use of the latter leads to the formation of smaller metal NPs, presumably because of an increase in the availability of surface hydroxyl nucleation sites.[2273] Unique nucleation sites can also be exploited to make well-dispersed catalysts: for instance, a highly active sintering-resistant single-site Ni catalyst supported on a Zr-based MOF (Ni/AIM) for gas-phase ethylene hydrogenation and oligomerization was made by Ni ALD on the Zr nodes.[2274] The composition of alloy-based catalysts can be tuned by controlling the ratio of metal ALD cycles: a (ALD-RuPt)/Al_2O_3 catalyst, for instance, was optimized this way to enhance methanol decomposition.[2275] In fact, bimetallics can be made via sequential ALD processes, as in the case of the Pd ALD on a Au/SiO_2 material to make (Au@Pd)/SiO_2 catalysts for the selective oxidation of benzyl alcohol: volcano-like behavior was seen in plots of initial activity as a function of Pd shell thickness, with optimum performance obtained with approximately three monolayers of Pd (8 ALD cycles).[2276] In a study on the promotion of the electrocatalytic oxidation of methanol, ALD-codeposited Pt−Ru films showed optimum activity at 1:1 stoichiometry (and the same behavior and activity as films made by sputtering); Pt thin ALD films were shown to enhance Ru performance but to never reach the activity level of the alloy.[2277] Finally, ALD is ideally suited for the buildup of complex nanostructures:[2278] witness, for instance, the porous TiO_2 nanotubes with spatially separated Pt and CoO_x cocatalysts (CoO_x/TiO_2/Pt) made using multiple ALD processes, as indicated in Figure 165, for the photocatalytic production of hydrogen from water.[2279] An even more elaborate concentric-nanotube Al_2O_3(first hollow nanotube)/Ni(1st outer)/Pt(2nd inner)/TiO_2(second nanotube) nanoarchitecture has been constructed involving 5 ALD steps to produce a catalyst capable of promoting nitrobenzene hydrogenation (over the Pt/TiO_2 interface) with hydrogen formed *in situ* by the decomposition of hydrazine hydrate (over Ni/Al_2O_3 interface).[2280]

ALD certainly adds great flexibility to the modification of existing catalysts in order to improve their performance. The

https://doi.org/10.1021/acs.chemrev.1c00905
Chem. Rev. XXXX, XXX, XXX−XXX

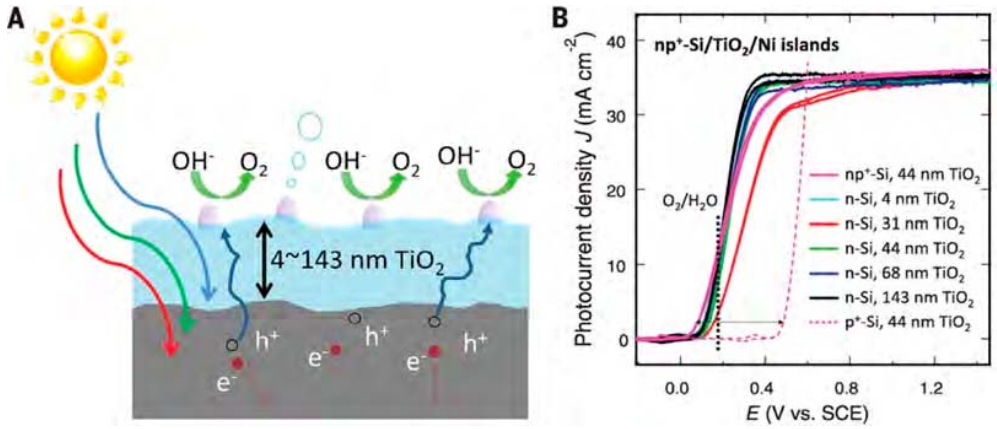

Figure 161. Use of ALD to protect electrode surfaces against corrosion during the photodriven oxidation of water.[2236] (A) Cross-sectional schematic of the ALD-film-protected photoanodes. Although the grown TiO_2 layer is amorphous and therefore electronically defective, the photogenerated holes are nevertheless conducted through the TiO_2 to the Ni electrocatalysts, where they oxidize water to O_2. (B) Photoelectrochemical behavior (in the form of photocurrent density versus applied potential) of TiO_2-coated n-Si photoanodes in 1.0 M KOH(aq) as a function of TiO_2 layer thickness (data for np^+-Si and p^+-Si are also provided for reference). Similar activity was seen with all the electrodes, even after depositing TiO_2 protective layers as thick as 143 nm. Reproduced with permission from ref 2236. Copyright 2014, American Association for the Advancement of Science.

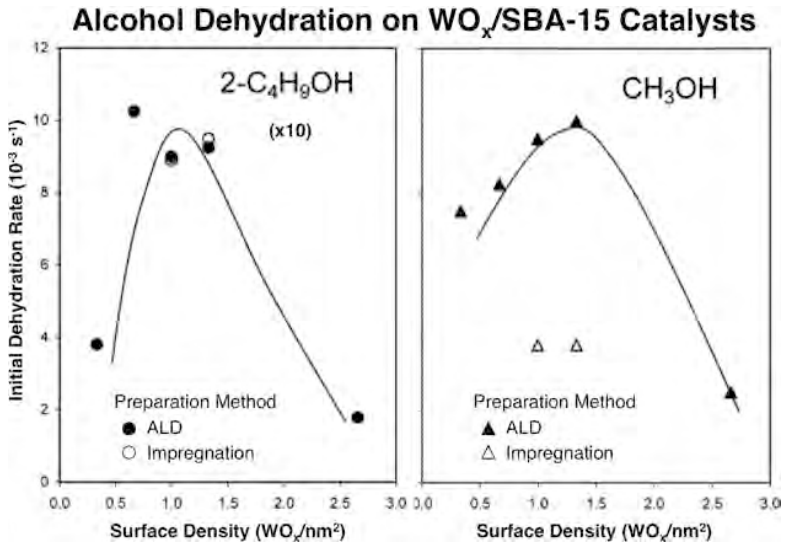

Figure 162. Use of ALD for the preparation of WO_x supported catalysts (on SBA-15).[2244] Shown are the values for 2-butanol (left) and methanol (right) dehydration initial rates as a function of WO_x surface density with catalysts prepared by both ALD (filled symbols) and a more traditional impregnation method (open symbols). Not only there is a strong dependence of activity on surface density, but the ALD catalysts also proved to be better performing, presumable because of an enhanced resistance against sintering. Reproduced with Permission from ref 2244. Copyright 2006 Elsevier Inc.

addition of protective layers to avoid sintering or chemical alteration of catalytic active phases is useful, but does need to be balanced against the accompanying reduction in surface accessibility. The deposition of new layers may also modify the behavior of the original catalytic surface, and even create new interfaces: this may in fact be beneficial for catalytic performance if properly engineered, but needs to be evaluated in each individual case. In terms of metal deposition, the benefit of using ALD is less obvious as the initial deposited films tend to sinter in ways not fully controllable. Perhaps the most promising use of ALD is for the deposition of catalytically active thin oxide films, which can be tuned to optimize the creation of mixed oxide sites. Metal ALD can also be used on wettable surface to minimize the use of expensive catalytic materials. On the other hand, cost is also a consideration with ALD, as it is a time consuming process that requires the use of costly chemicals. Keeping these limitations in mind, it is still worth adding ALD to the catalyst preparation toolbox.

9. CONCLUDING REMARKS

Thanks to recent advances in materials synthesis and nanotechnology, a variety of approaches have become available to the catalysis community to prepare catalysts in a controlled fashion and to design catalytic sites within solid structures for the selective promotion of complex reactions. In this review we have discussed some of the most prominent directions of research that have developed in this area in recent years. The review was organized to roughly follow the transition from

https://doi.org/10.1021/acs.chemrev.1c00905
Chem. Rev. XXXX, XXX, XXX−XXX

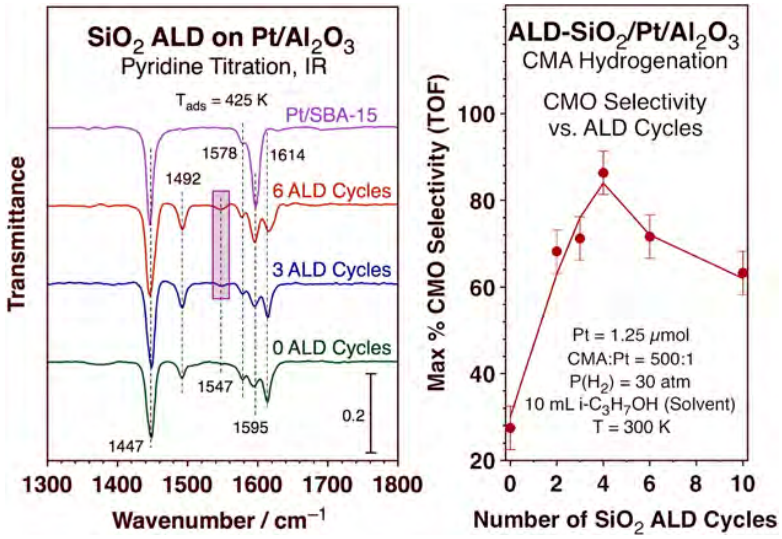

Figure 163. Example of catalysts with mixed-oxide sites made by limited ALD, in this case by depositing submonolayer SiO_2 films on a Pt/Al_2O_3 catalyst.[2257] Left: Pyridine-IR titration of acid sites indicating the formation of new strong Brønsted (1547 cm^{-1}, highlighted) and Lewis (1620 cm^{-1}) sites on the surface. Right: Maximum selectivity for the production of cinnamyl alcohol (CMO) from cinnamaldehyde (CMA) hydrogenation as a function of the number of SiO_2 ALD cycles used. Optimum performance was seen after 4 SiO_2 ALD cycles, which was estimated to correspond to a SiO_2 coverage of approximately half a monolayer. Reproduced with permission from ref 56. Copyright 2021 Elsevier B.V.

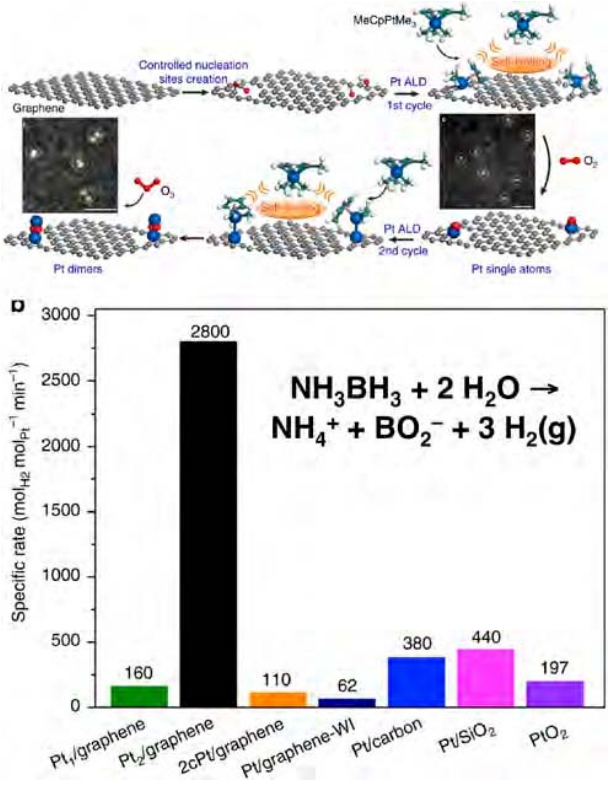

Figure 164. Pt_2/graphene catalyst prepared via metal ALD for the hydrolysis of ammonia borane. Top: synthetic route, based on two ALD cycles, together with TEM images of the Pt_1/graphene and Pt_2/graphene resulting samples. Bottom: Specific rates measured with the Pt_1/graphene and Pt_2/graphene catalysts as well as with several reference materials. High activity was seen only with the Pt_2 dimers. Adapted with permission from ref 2272. Creative Commons Attribution 4.0 International License.

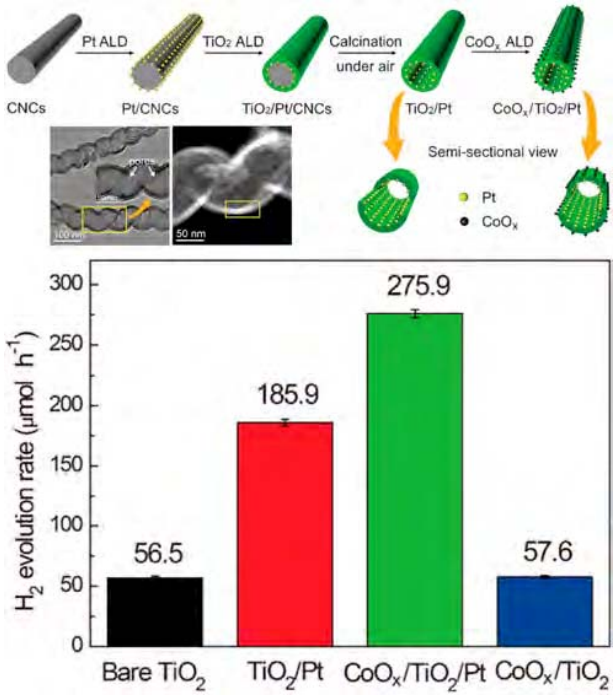

Figure 165. CoO_x(outer surface)/TiO_2(hollow nanotube)/Pt(inner surface) photocatalyst for water splitting and hydrogen production.[2279] Top: Synthetic route, emphasizing the use of ALD for the deposition of all three materials (on a sacrificial carbon nanocoil −CNC). Bottom: H_2 evolution rates measured using the relevant catalysts, highlighting the fact that all three phases are required for optimum performance. Reproduced with permission from ref 2279. Copyright 2017 Wiley-VCH Verlag GmbH & Co. KGaA, Weinheim.

homogeneous to heterogeneous catalysis, starting from the modification of solid surfaces with molecular agents, added to the reaction mixture or adsorbed on/immobilized on/tethered

https://doi.org/10.1021/acs.chemrev.1c00905
Chem. Rev. XXXX, XXX, XXX−XXX

to the surface, and ending with the synthesis of complex nanostructures and the post-modification of solids.

It was first shown that molecular modifiers offer exquisite selectivity, close to that seen in homogeneous catalysis, but may need to be added to reaction mixtures, and therefore to be separated from that mixture after reaction (thus defeating the value of using heterogeneous catalysts). The immobilization or tethering of such modifiers, or indeed of complete homogeneous catalysts, to the surfaces of solids partially solves that problem, but the resulting catalytically active phases are usually not very stable, as they may leach or decompose. Catalyst recyclability is a problem here too. Alternatively, single-atom catalysis provides a way to use fully heterogeneous catalysts with well-defined sites. On the negative side, the nature of single-atom sites are relatively simple, a fact that limits the scope of the attainable selectivity, and the catalysts may be unstable and undergo sintering, reconstruction, or other chemical change. More complex solid nanostructures can now be constructed, many stable under demanding catalytic conditions, but the best of those may be crystalline or otherwise ordered, and therefore offer relatively simple atomic ensembles on their surfaces as catalytic sites. Also, in this field the materials and nanotechnology synthesis communities seem to be ahead of those focusing on catalytic processes, and, as a consequence, advances in nanostructure complexity not always have translated into improvements in catalysis. Much of the synthetic work is not guided by catalysis-oriented hypotheses, and the resulting materials are therefore often tested perfunctorily, without rigorous kinetic measurements or comparisons with proper reference catalysts. A common limitation to most of these methodologies is cost, as the associated synthesis is complex, involves multiple steps, and may require expensive chemicals.

Each of these approaches offers advantages as well as disadvantages and is optimal for unique specific applications. In fact, these sub-areas of catalysis have by and large developed independently, with separate groups of researchers addressing each, perhaps unaware of advances by the others. More cross-collaborations among these groups is highly desirable, as that could offer new opportunities thanks to the meshing of different perspectives, and even the combination of synthetic schemes. Another important point to make is that it would be beneficial to implement an hypothesis driven approach to the use of these nanotechnologies in catalysis, that is, it is perhaps best to first enunciate the catalytic problem to be addressed, possibly with the help of fundamental mechanistic studies (using modern surface science techniques and/or quantum mechanics calculations), and to identify the specific characteristics demanded of catalytic sites before embarking on the synthesis of the catalysts. There is no doubt that the field of nanotechnology has provided a number of very useful synthetic methods to make structurally complex materials in recent years, but this not always leads to the development of truly superior catalysts.

Having highlighted some of the limitations of the catalyst synthesis approaches discussed in this review, we would like to end on a more positive note. Although progress in defining and synthesizing sophisticated catalytic sites may at times seem haphazard, it is real nevertheless. There have been some impressive advances in this direction in recent years. The synthetic skills are also improving all the time, which means that there is much that the catalysis community can borrow and adopt in terms of catalyst preparation once the catalytic problem is properly defined. Moreover, many of these fields are in their infancy; more advances are expected in the upcoming years. It would be useful to better coordinate synthesis with surface-science and reactivity studies to better target the development of materials of particular value to catalytic processes, and a better synergy between the two groups of researchers could make progress in selective catalysis even faster.

AUTHOR INFORMATION

Corresponding Author

Francisco Zaera − *Department of Chemistry and UCR Center for Catalysis, University of California, Riverside, California 92521, United States;* orcid.org/0000-0002-0128-7221; Email: zaera@ucr.edu

Complete contact information is available at: https://pubs.acs.org/10.1021/acs.chemrev.1c00905

Notes

The author declares no competing financial interest.

Biography

Francisco Zaera received his Licentiate degree in Chemistry from the Simón Bolívar University in Caracas, Venezuela (1979), and his Ph.D. from the University of California, Berkeley (1984). He held an Assistant Chemist position at the National Synchrotron Light Source of Brookhaven National Laboratory, in a joint appointment with Exxon Research Laboratories, until 1986, after which he became a faculty member at the University of California, Riverside. Presently, he is a Distinguished Professor, the Hartland H. Schmidt Founder's Chair in Chemistry, and the Director of the UCR Center for Catalysis. Prof. Zaera has been awarded the 1994 and 1995 Union Carbide Innovation Recognition Program Award, the 2001 ACS George A. Olah Award in Hydrocarbon or Petroleum Chemistry, the 2003 Paul H. Emmett Award of the North American Catalysis Society, a 2004 Humboldt Research Award for Senior U.S. Scientist, the 2008 ACS Arthur W. Adamson Award for Distinguished Service in the Advancement of Surface Chemistry, the Inaugural ACS CATL Exceptional Achievements in Catalysis Award in 2019, and the UCR Faculty Research Lecturer in 2021. He is a Fellow of the American Vacuum Society, the American Association for the Advancement of Science, and the American Chemical Society. Prof. Zaera has held several editorial positions, including his recent stint as Senior Editor of *The Journal of Physical Chemistry* and of *The Journal of Physical Chemistry Letters*. He has also held several professional offices, including those of Treasurer (1997, 1998), Vice Chair (2005), Chair-Elect (2006), and Chair (2007) of the Colloids and Surface Chemistry Division of the American Chemical Society, Treasurer-Secretary and President of the California Catalysis Society (1990−1992), and Member & Nominating Chair of the Executive Committee of the Surface Science Division of the American Vacuum Society. Prof. Zaera has published over 420 publications in scientific journals. His research interests are in surface and materials chemistry and in heterogeneous catalysis. More information about Prof. Zaera can be found at his web site, https://zaeralab.ucr.edu.

ACKNOWLEDGMENTS

Financial assistance was provided by the U. S. National Science Foundation under Grants Nos. 1953843 and 1854439 and by the U. S. Department of Energy under Grant No. DE-SC0001839.

REFERENCES

(1) Zaera, F. Outstanding mechanistic questions in heterogeneous catalysis. *J. Phys. Chem. B* **2002**, *106*, 4043−4052.
(2) Somorjai, G.; Kliewer, C. Reaction selectivity in heterogeneous catalysis: An invited review. *React. Kinet. Catal. Lett.* **2009**, *96*, 191−208.
(3) Zaera, F. Regio, Stereo, and Enantio Selectivity in Hydrocarbon Conversion on Metal Surfaces. *Acc. Chem. Res.* **2009**, *42*, 1152−1160.
(4) Berzelius, J. *Jahres-Bericht über die Fortschritte der Physichen Wissenschaften*; H. Laupp: Tübingen, 1836.
(5) *Catalysis: From Principles to Applications*; Beller, M., Renken, A., van Santen, R. A., Eds.; Wiley: Weinheim, Germany, 2012.
(6) Hagen, J. *Industrial Catalysis: A Practical Approach*; 3rd ed.; Wiley: Weinheim, Germany, 2015.
(7) Vilé, G.; Albani, D.; Almora-Barrios, N.; López, N.; Pérez-Ramírez, J. Advances in the Design of Nanostructured Catalysts for Selective Hydrogenation. *ChemCatChem.* **2016**, *8*, 21−33.
(8) Zaera, F. The Surface Chemistry of Metal-Based Hydrogenation Catalysis. *ACS Catal.* **2017**, *7*, 4947−4967.
(9) Zhang, L.; Zhou, M.; Wang, A.; Zhang, T. Selective Hydrogenation over Supported Metal Catalysts: From Nanoparticles to Single Atoms. *Chem. Rev.* **2020**, *120*, 683−733.
(10) Cavani, F.; Teles, J. H. Sustainability in Catalytic Oxidation: An Alternative Approach or a Structural Evolution? *ChemSusChem* **2009**, *2*, 508−534.
(11) Dimitratos, N.; Lopez-Sanchez, J. A.; Hutchings, G. J. Selective liquid phase oxidation with supported metal nanoparticles. *Chem. Sci.* **2012**, *3*, 20−44.
(12) Guo, Z.; Liu, B.; Zhang, Q.; Deng, W.; Wang, Y.; Yang, Y. Recent advances in heterogeneous selective oxidation catalysis for sustainable chemistry. *Chem. Soc. Rev.* **2014**, *43*, 3480−3524.
(13) Védrine, J. C.; Fechete, I. Heterogeneous partial oxidation catalysis on metal oxides. *Comptes Rendus Chim.* **2016**, *19*, 1203−1225.
(14) Blaser, H.-U.; Pugin, B.; Spindler, F. *Organometallics as Catalysts in the Fine Chemical Industry*; Beller, M., Blaser, H.-U., Eds.; Springer Berlin Heidelberg: Berlin, Heidelberg, 2012. DOI: 10.1007/3418_2011_27.
(15) *Strategies in asymmetric catalysis, a Beilstein Journal of Organic Chemistry Thematic series*; Yoon, T. P., Ed.; Beilstein-Institut zur Förderung der Chemischen Wissenschaften: Frankfurt am Main, Germany, 2016; Vol. *12*.
(16) Meemken, F.; Baiker, A. Recent Progress in Heterogeneous Asymmetric Hydrogenation of C=O and C=C Bonds on Supported Noble Metal Catalysts. *Chem. Rev.* **2017**, *117*, 11522−11569.
(17) Zaera, F. Chirality in adsorption on solid surfaces. *Chem. Soc. Rev.* **2017**, *46*, 7374−7398.
(18) Zaera, F. Mechanistic requirements for catalytic active sites. *J. Phys.: Condens. Matter* **2004**, *16*, S2299−S2310.
(19) Zaera, F. The surface chemistry of heterogeneous catalysis: Mechanisms, selectivity, and active sites. *Chem. Rec.* **2005**, *5*, 133−144.
(20) Somorjai, G. A.; Frei, H.; Park, J. Y. Advancing the frontiers in nanocatalysis, biointerfaces, and renewable energy conversion by innovations of surface techniques. *J. Am. Chem. Soc.* **2009**, *131*, 16589−16605.
(21) Ye, R.; Hurlburt, T. J.; Sabyrov, K.; Alayoglu, S.; Somorjai, G. A. Molecular catalysis science: Perspective on unifying the fields of catalysis. *Proc. Natl. Acad. Sci. U. S. A.* **2016**, *113*, 5159−5166.
(22) Pelletier, J. D. A.; Basset, J.-M. Catalysis by Design: Well-Defined Single-Site Heterogeneous Catalysts. *Acc. Chem. Res.* **2016**, *49*, 664−677.
(23) Zhao, Y.; Fu, G.; Zheng, N. Shaping the selectivity in heterogeneous hydrogenation by using molecular modification strategies: Experiment and theory. *Catal. Today* **2017**, *279*, 36−44.
(24) Kumar, G.; Nikolla, E.; Linic, S.; Medlin, J. W.; Janik, M. J. Multicomponent Catalysts: Limitations and Prospects. *ACS Catal.* **2018**, *8*, 3202−3208.
(25) Khersonsky, O.; Tawfik, D. S. *Comprehensive Natural Products III* **2010**, *79*, 705.
(26) de Carvalho, C. C. C. R. Enzymatic and whole cell catalysis: Finding new strategies for old processes. *Biotechnology Advances* **2011**, *29*, 75−83.
(27) Raynal, M.; Ballester, P.; Vidal-Ferran, A.; van Leeuwen, P. W. N. M. Supramolecular catalysis. Part 2: artificial enzyme mimics. *Chem. Soc. Rev.* **2014**, *43*, 1734−1787.
(28) Callender, R.; Dyer, R. B. The Dynamical Nature of Enzymatic Catalysis. *Acc. Chem. Res.* **2015**, *48*, 407−413.
(29) Palmer, T.; Bonner, P. L. R. *Enzymes: Biochemistry, Biotechnology, Clinical Chemistry*; 2nd ed.; Oxford Woodhead Publishing: Oxford, UK, 2011.
(30) Christopher, L. P.; Hemanathan, K.; Zambare, V. P. Enzymatic biodiesel: Challenges and opportunities. *Applied Energy* **2014**, *119*, 497−520.
(31) Brahmachari, G. *Biotechnology of Microbial Enzymes: Production, Biocatalysis and Industrial Applications*; 1st ed.; Academic Press, 2017.
(32) Sheldon, R. A.; Woodley, J. M. Role of Biocatalysis in Sustainable Chemistry. *Chem. Rev.* **2018**, *118*, 801−838.
(33) Huang, Y.; Ren, J.; Qu, X. Nanozymes: Classification, Catalytic Mechanisms, Activity Regulation, and Applications. *Chem. Rev.* **2019**, *119*, 4357−4412.
(34) *Metal-catalysis in Industrial Organic Processes*; Chiusoli, G. P., Maitlis, P. M., Eds.; Royal Society of Chemistry Publishing: Cambridge, UK, 2008.
(35) Palmer, A. M.; Zanotti-Gerosa, A. Homogenous asymmetric hydrogenation: Recent trends and industrial applications. *Current Opinion in Drug Discovery and Development* **2010**, *13*, 698−716.
(36) Bender, T. A.; Dabrowski, J. A.; Gagné, M. R. Homogeneous catalysis for the production of low-volume, high-value chemicals from biomass. *Nat. Rev. Chem.* **2018**, *2*, 35−46.
(37) *Applied Homogeneous Catalysis with Organometallic Compounds: A Comprehensive Handbook in Four Vol.s*; 3rd ed.; Cornils, B., Herrmann, W. A., Belle, M., Paciello, R., Eds.; Wiley-VCH: Weinheim, Germany, 2018.
(38) Bhaduri, S.; Mukesh, D. *Homogeneous Catalysis: Mechanisms and Industrial Applications*; 2nd ed.; Wiley: Weinheim, Germany, 2014.
(39) Cole-Hamilton, D. J. Homogeneous Catalysis-New Approaches to Catalyst Separation, Recovery, and Recycling. *Science* **2003**, *299*, 1702.
(40) Shende, V. S.; Saptal, V. B.; Bhanage, B. M. Recent Advances Utilized in the Recycling of Homogeneous Catalysis. *Chem. Rec.* **2019**, *19*, 2022−2043.
(41) Chadwick, J. C.; Duchateau, R.; Freixa, Z.; van Leeuwen, P. W. N. M. *Homogeneous Catalysts: Activity - Stability - Deactivation*; 1st ed.; Wiley-VCH: Weinheim, Germany, 2011.
(42) Ma, Z.; Zaera, F. In *Encyclopedia of Inorganic and Bioinorganic Chemistry*; Scott, R. A., Ed.; John Wiley & Sons, Ltd: Chichester, 2014. DOI: 10.1002/9781119951438.eibc0079.pub2.
(43) Hagen, J. *Industrial Catalysis: A Practical Approach*; 3rd ed.; Wiley-VCH: Weinheim, Germany, 2015.
(44) Heck, R. M.; Farrauto, R. J. Automobile exhaust catalysts. *Appl. Catal. A* **2001**, *221*, 443−457.
(45) Burch, R. Knowledge and know-how in emission control for mobile applications. *Catal. Rev.; Sci. Eng.* **2004**, *46*, 271−333.
(46) Sheldon, R. A.; van Bekkum, H. *Fine Chemicals through Heterogeneous Catalysis*; Wiley-VCH: Weinheim, Germany, 2001.
(47) Shiju, N. R.; Guliants, V. V. Recent developments in catalysis using nanostructured materials. *Appl. Catal. A* **2009**, *356*, 1−17.
(48) Zaera, F. The New Materials Science of Catalysis: Toward Controlling Selectivity by Designing the Structure of the Active Site. *J. Phys. Chem. Lett.* **2010**, *1*, 621−627.
(49) Zaera, F. New Challenges in Heterogeneous Catalysis for the 21st Century. *Catal. Lett.* **2012**, *142*, 501−516.
(50) Zaera, F. Nanostructured Materials for Applications in Heterogeneous Catalysis. *Chem. Soc. Rev.* **2013**, *42*, 2746−2762.

https://doi.org/10.1021/acs.chemrev.1c00905
Chem. Rev. XXXX, XXX, XXX−XXX

(51) Zaera, F. Shape-Controlled Nanostructures in Heterogeneous Catalysis. *ChemSusChem* **2013**, *6*, 1797−1820.
(52) Liu, L.; Corma, A. Metal Catalysts for Heterogeneous Catalysis: From Single Atoms to Nanoclusters and Nanoparticles. *Chem. Rev.* **2018**, *118*, 4981−5079.
(53) Hurlburt, T. J.; Liu, W.-C.; Ye, R.; Somorjai, G. A. Surface Science Approach to the Molecular Level Integration of the Principles in Heterogeneous, Homogeneous, and Enzymatic Catalysis. *Top. Catal.* **2018**, *61*, 1210−1217.
(54) Li, Z.; Ji, S.; Liu, Y.; Cao, X.; Tian, S.; Chen, Y.; Niu, Z.; Li, Y. Well-Defined Materials for Heterogeneous Catalysis: From Nanoparticles to Isolated Single-Atom Sites. *Chem. Rev.* **2020**, *120*, 623−682.
(55) Qi, Z.; Chen, L.; Zhang, S.; Su, J.; Somorjai, G. A. Integrating the Fields of Catalysis: Active Site Engineering in Metal Cluster, Metal Organic Framework and Metal Single Site. *Top. Catal.* **2020**, *63*, 628−634.
(56) Zaera, F. Molecular approaches to heterogeneous catalysis. *Coord. Chem. Rev.* **2021**, *448*, 214179.
(57) Tada, M.; Iwasawa, Y. Advanced design of catalytically active reaction space at surfaces for selective catalysis. *Coord. Chem. Rev.* **2007**, *251*, 2702−2716.
(58) Pugin, B.; Blaser, H. U. Immobilized complexes for enantioselective catalysis: When will they be used in industry? *Top. Catal.* **2010**, *53*, 953−962.
(59) Maurya, M. R.; Kumar, A.; Costa Pessoa, J. Vanadium complexes immobilized on solid supports and their use as catalysts for oxidation and functionalization of alkanes and alkenes. *Coord. Chem. Rev.* **2011**, *255*, 2315−2344.
(60) Wegener, S. L.; Marks, T. J.; Stair, P. C. Design Strategies for the Molecular Level Synthesis of Supported Catalysts. *Acc. Chem. Res.* **2012**, *45*, 206−214.
(61) Fukuzumi, S.; Lee, Y.-M.; Nam, W. Immobilization of Molecular Catalysts for Enhanced Redox Catalysis. *ChemCatChem.* **2018**, *10*, 1686−1702.
(62) Nodzewska, A.; Wadolowska, A.; Watkinson, M. Recent advances in the catalytic oxidation of alkene and alkane substrates using immobilized manganese complexes with nitrogen containing ligands. *Coord. Chem. Rev.* **2019**, *382*, 181−216.
(63) Gates, B. C. Supported metal clusters: Synthesis, structure, and catalysis. *Chem. Rev.* **1995**, *95*, 511−522.
(64) Copéret, C.; Chabanas, M.; Saint-Arroman, R. P.; Basset, J.-M. Homogeneous and Heterogeneous Catalysis: Bridging the Gap through Surface Organometallic Chemistry. *Angew. Chem., Int. Ed.* **2003**, *42*, 156−181.
(65) Samantaray, M. K.; Pump, E.; Bendjeriou-Sedjerari, A.; D'Elia, V.; Pelletier, J. D. A.; Guidotti, M.; Psaro, R.; Basset, J.-M. Surface organometallic chemistry in heterogeneous catalysis. *Chem. Soc. Rev.* **2018**, *47*, 8403−8437.
(66) Holbach, M.; Weck, M. Modular Approach for the Development of Supported, Monofunctionalized, Salen Catalysts. *J. Org. Chem.* **2006**, *71*, 1825−1836.
(67) Madhavan, N.; Jones, C. W.; Weck, M. Rational Approach to Polymer-Supported Catalysts: Synergy between Catalytic Reaction Mechanism and Polymer Design. *Acc. Chem. Res.* **2008**, *41*, 1153−1165.
(68) Blakemore, J. D.; Gupta, A.; Warren, J. J.; Brunschwig, B. S.; Gray, H. B. Noncovalent Immobilization of Electrocatalysts on Carbon Electrodes for Fuel Production. *J. Am. Chem. Soc.* **2013**, *135*, 18288−18291.
(69) Anwander, R.; SOMC@PMS. Surface Organometallic Chemistry at Periodic Mesoporous Silica. *Chem. Mater.* **2001**, *13*, 4419−4438.
(70) Lamb, H. H.; Gates, B. C.; Knözinger, H. Molecular Organometallic Chemistry on Surfaces: Reactivity of Metal Carbonyls on Metal Oxides. *Angew. Chem., Int. Ed.* **1988**, *27*, 1127−1144.
(71) Candy, J.-P.; Didillon, B.; Smith, E. L.; Shay, T. B.; Basset, J.-M. Surface organometallic chemistry on metals: a novel and effective route to custom-designed bimetallic catalysts. *J. Mol. Catal.* **1994**, *86*, 179−204.
(72) Guzman, J.; Gates, B. C. Supported molecular catalysts: metal complexes and clusters on oxides and zeolites. *Dalton Trans.* **2003**, 3303−3318.
(73) Thomas, J. M.; Raja, R. Catalytic significance of organometallic compounds immobilized on mesoporous silica: economically and environmentally important examples. *J. Organomet. Chem.* **2004**, *689*, 4110−4124.
(74) Dal Santo, V.; Liguori, F.; Pirovano, C.; Guidotti, M. Design and Use of Nanostructured Single-Site Heterogeneous Catalysts for the Selective Transformation of Fine Chemicals. *Molecules* **2010**, *15*, 3829.
(75) Rimoldi, M.; Mezzetti, A. Site isolated complexes of late transition metals grafted on silica: challenges and chances for synthesis and catalysis. *Catal. Sci. Technol.* **2014**, *4*, 2724−2740.
(76) Serna, P.; Gates, B. C. Molecular Metal Catalysts on Supports: Organometallic Chemistry Meets Surface Science. *Acc. Chem. Res.* **2014**, *47*, 2612−2620.
(77) Copéret, C.; Comas-Vives, A.; Conley, M. P.; Estes, D. P.; Fedorov, A.; Mougel, V.; Nagae, H.; Núñez-Zarur, F.; Zhizhko, P. A. Surface Organometallic and Coordination Chemistry toward Single-Site Heterogeneous Catalysts: Strategies, Methods, Structures, and Activities. *Chem. Rev.* **2016**, *116*, 323−421.
(78) Thornburg, N. E.; Nauert, S. L.; Thompson, A. B.; Notestein, J. M. Synthesis-Structure-Function Relationships of Silica-Supported Niobium(V) Catalysts for Alkene Epoxidation with H_2O_2. *ACS Catal.* **2016**, *6*, 6124−6134.
(79) Copéret, C.; Fedorov, A.; Zhizhko, P. A. Surface Organometallic Chemistry: Paving the Way Beyond Well-Defined Supported Organometallics and Single-Site Catalysis. *Catal. Lett.* **2017**, *147*, 2247−2259.
(80) Zhao, Y.; Sohn, H.; Hu, B.; Niklas, J.; Poluektov, O. G.; Tian, J.; Delferro, M.; Hock, A. S. Zirconium Modification Promotes Catalytic Activity of a Single-Site Cobalt Heterogeneous Catalyst for Propane Dehydrogenation. *ACS Omega* **2018**, *3*, 11117−11127.
(81) Grosso-Giordano, N. A.; Hoffman, A. S.; Boubnov, A.; Small, D. W.; Bare, S. R.; Zones, S. I.; Katz, A. Dynamic Reorganization and Confinement of TiIV Active Sites Controls Olefin Epoxidation Catalysis on Two-Dimensional Zeotypes. *J. Am. Chem. Soc.* **2019**, *141*, 7090−7106.
(82) Rimoldi, M.; Fodor, D.; van Bokhoven, J. A.; Mezzetti, A. A stable 16-electron iridium(iii) hydride complex grafted on SBA-15: a single-site catalyst for alkene hydrogenation. *Chem. Commun.* **2013**, *49*, 11314−11316.
(83) Rimoldi, M.; Mezzetti, A. Silica-Grafted 16-Electron Hydride Pincer Complexes of Iridium(III) and Their Soluble Analogues: Synthesis and Reactivity with CO. *Inorg. Chem.* **2014**, *53*, 11974−11984.
(84) Choi, Y. S.; Moschetta, E. G.; Miller, J. T.; Fasulo, M.; McMurdo, M. J.; Rioux, R. M.; Tilley, T. D. Highly Dispersed Pd-SBA15 Materials from Tris(tert-butoxy)siloxy Complexes of Pd(II). *ACS Catal.* **2011**, *1*, 1166−1177.
(85) Cao, R.; Thapa, R.; Kim, H.; Xu, X.; Gyu Kim, M.; Li, Q.; Park, N.; Liu, M.; Cho, J. Promotion of oxygen reduction by a bio-inspired tethered iron phthalocyanine carbon nanotube-based catalyst. *Nat. Commun.* **2013**, *4*, 2076.
(86) Artero, V.; Chavarot-Kerlidou, M.; Fontecave, M. Splitting Water with Cobalt. *Angew. Chem., Int. Ed.* **2011**, *50*, 7238−7266.
(87) Silva, M.; Calvete, M. J. F.; Gonçalves, N. P. F.; Burrows, H. D.; Sarakha, M.; Fernandes, A.; Ribeiro, M. F.; Azenha, M. E.; Pereira, M. M. Zinc(II) phthalocyanines immobilized in mesoporous silica Al-MCM-41 and their applications in photocatalytic degradation of pesticides. *J. Hazard. Mater.* **2012**, *233-234*, 79−88.
(88) Tian, H. Molecular Catalyst Immobilized Photocathodes for Water/Proton and Carbon Dioxide Reduction. *ChemSusChem* **2015**, *8*, 3746−3759.
(89) Wang, X.; Wisser, F. M.; Canivet, J.; Fontecave, M.; Mellot-Draznieks, C. Immobilization of a Full Photosystem in the Large-Pore

https://doi.org/10.1021/acs.chemrev.1c00905
Chem. Rev. XXXX, XXX, XXX−XXX

MIL-101 Metal-Organic Framework for CO_2 reduction. *ChemSusChem* **2018**, *11*, 3315−3322.
(90) Waki, M.; Yamanaka, K.-i.; Shirai, S.; Maegawa, Y.; Goto, Y.; Yamada, Y.; Inagaki, S. Re(bpy)$(CO)_3$Cl Immobilized on Bipyridine-Periodic Mesoporous Organosilica for Photocatalytic CO_2 Reduction. *Chem.-Eur. J.* **2018**, *24*, 3846−3853.
(91) Gao, Y.; Ding, X.; Liu, J.; Wang, L.; Lu, Z.; Li, L.; Sun, L. Visible Light Driven Water Splitting in a Molecular Device with Unprecedentedly High Photocurrent Density. *J. Am. Chem. Soc.* **2013**, *135*, 4219−4222.
(92) Fan, K.; Li, F.; Wang, L.; Daniel, Q.; Gabrielsson, E.; Sun, L. Pt-free tandem molecular photoelectrochemical cells for water splitting driven by visible light. *Phys. Chem. Chem. Phys.* **2014**, *16*, 25234−25240.
(93) Li, F.; Fan, K.; Xu, B.; Gabrielsson, E.; Daniel, Q.; Li, L.; Sun, L. Organic Dye-Sensitized Tandem Photoelectrochemical Cell for Light Driven Total Water Splitting. *J. Am. Chem. Soc.* **2015**, *137*, 9153−9159.
(94) Paille, G.; Gomez-Mingot, M.; Roch-Marchal, C.; Lassalle-Kaiser, B.; Mialane, P.; Fontecave, M.; Mellot-Draznieks, C.; Dolbecq, A. A Fully Noble Metal-Free Photosystem Based on Cobalt-Polyoxometalates Immobilized in a Porphyrinic Metal-Organic Framework for Water Oxidation. *J. Am. Chem. Soc.* **2018**, *140*, 3613−3618.
(95) Bachmeier, A.; Hall, S.; Ragsdale, S. W.; Armstrong, F. A. Selective Visible-Light-Driven CO_2 Reduction on a p-Type Dye-Sensitized NiO Photocathode. *J. Am. Chem. Soc.* **2014**, *136*, 13518−13521.
(96) Fierro-Gonzalez, J. C.; Kuba, S.; Hao, Y.; Gates, B. C. Oxide- and Zeolite-Supported Molecular Metal Complexes and Clusters: Physical Characterization and Determination of Structure, Bonding, and Metal Oxidation State. *J. Phys. Chem. B* **2006**, *110*, 13326−13351.
(97) Zacchini, S. Using Metal Carbonyl Clusters To Develop a Molecular Approach towards Metal Nanoparticles. *Eur. J. Inorg. Chem.* **2011**, *2011*, 4125−4145.
(98) Gates, B. C.; Flytzani-Stephanopoulos, M.; Dixon, D. A.; Katz, A. Atomically dispersed supported metal catalysts: perspectives and suggestions for future research. *Catal. Sci. Technol.* **2017**, *7*, 4259−4275.
(99) Kulkarni, A.; Lobo-Lapidus, R. J.; Gates, B. C. Metal clusters on supports: synthesis, structure, reactivity, and catalytic properties. *Chem. Commun.* **2010**, *46*, 5997−6015.
(100) Roukoss, C.; Basset, J.-M.; Copéret, C.; Lucas, C.; Kuntz, E. Effect of the nuclearity of perhydrocarbyl Fe(II) complexes on the grafting on oxide supports. *Comptes Rendus Chim.* **2008**, *11*, 620−627.
(101) Deschner, T.; Törnroos, K. W.; Anwander, R. Iron Silylamide-Grafted Periodic Mesoporous Silica. *Inorg. Chem.* **2011**, *50*, 7217−7228.
(102) Anderson, D. P.; Alvino, J. F.; Gentleman, A.; Qahtani, H. A.; Thomsen, L.; Polson, M. I. J.; Metha, G. F.; Golovko, V. B.; Andersson, G. G. Chemically-synthesised, atomically-precise gold clusters deposited and activated on titania. *Phys. Chem. Chem. Phys.* **2013**, *15*, 3917−3929.
(103) Alexeev, O. S.; Panjabi, G.; Phillips, B. L.; Gates, B. C. Carbonylation and Decarbonylation of γ-Al_2O_3-Supported Hexarhodium Clusters: Characterization by Infrared, ^{13}C NMR, and Extended X-ray Absorption Fine Structure Spectroscopies. *Langmuir* **2003**, *19*, 9494−9503.
(104) Bhirud, V. A.; Iddir, H.; Browning, N. D.; Gates, B. C. Intact and Fragmented Triosmium Clusters on MgO: Characterization by X-ray Absorption Spectroscopy and High-Resolution Transmission Electron Microscopy. *J. Phys. Chem. B* **2005**, *109*, 12738−12741.
(105) Uzun, A.; Gates, B. C. Real-Time Characterization of Formation and Breakup of Iridium Clusters in Highly Dealuminated Zeolite Y. *Angew. Chem., Int. Ed.* **2008**, *47*, 9245−9248.
(106) Li, F.; Gates, B. C. Size-dependent catalytic activity of zeolite-supported iridium clusters. *J. Phys. Chem. C* **2007**, *111*, 262−267.
(107) Oakton, E.; Vilé, G. S.; Levine, D.; Zocher, E.; Baudouin, D.; Pérez-Ramírez, J.; Copéret, C. Silver nanoparticles supported on passivated silica: preparation and catalytic performance in alkyne semi-hydrogenation. *Dalton Trans.* **2014**, *43*, 15138−15142.
(108) Fujdala, K. L.; Drake, I. J.; Bell, A. T.; Tilley, T. D. Atomic Level Control over Surface Species via a Molecular Precursor Approach: Isolated Cu(I) Sites and Cu Nanoparticles Supported on Mesoporous Silica. *J. Am. Chem. Soc.* **2004**, *126*, 10864−10866.
(109) Drake, I. J.; Fujdala, K. L.; Baxamusa, S.; Bell, A. T.; Tilley, T. D. Effects of Precursor Composition on the Local Structure of Cu Dispersed on Mesoporous Silica: A Detailed X-ray Absorption Spectroscopy Study. *J. Phys. Chem. B* **2004**, *108*, 18421−18434.
(110) Blümel, J. Linkers and catalysts immobilized on oxide supports: New insights by solid-state NMR spectroscopy. *Coord. Chem. Rev.* **2008**, *252*, 2410−2423.
(111) Sheet, D.; Halder, P.; Paine, T. K. Enhanced Reactivity of a Biomimetic Iron(II) α-Keto Acid Complex through Immobilization on Functionalized Gold Nanoparticles. *Angew. Chem., Int. Ed.* **2013**, *52*, 13314−13318.
(112) Sharma, R. K.; Sharma, S. Silica nanosphere-supported palladium(ii) furfural complex as a highly efficient and recyclable catalyst for oxidative amination of aldehydes. *Dalton Trans.* **2014**, *43*, 1292−1304.
(113) Su, H.; Li, Z.; Huo, Q.; Guan, J.; Kan, Q. Immobilization of transition metal (Fe^{2+}, Co^{2+}, VO^{2+} or Cu^{2+}) Schiff base complexes onto graphene oxide as efficient and recyclable catalysts for epoxidation of styrene. *RSC Adv.* **2014**, *4*, 9990−9996.
(114) Cheng, T.; Zhao, Q.; Zhang, D.; Liu, G. Transition-metal-functionalized ordered mesoporous silicas: an overview of sustainable chiral catalysts for enantioselective transformations. *Green Chem.* **2015**, *17*, 2100−2122.
(115) Rosser, T. E.; Reisner, E. Understanding Immobilized Molecular Catalysts for Fuel-Forming Reactions through UV/Vis Spectroelectrochemistry. *ACS Catal.* **2017**, *7*, 3131−3141.
(116) Sadjadi, S.; Heravi, M. M. Current advances in the utility of functionalized SBA mesoporous silica for developing encapsulated nanocatalysts: state of the art. *RSC Adv.* **2017**, *7*, 30815−30838.
(117) Peris, E.; Crabtree, R. H. Key factors in pincer ligand design. *Chem. Soc. Rev.* **2018**, *47*, 1959−1968.
(118) Sheet, D.; Bera, A.; Jana, R. D.; Paine, T. K. Oxidizing Ability of a Dioxygen-Activating Nonheme Iron(II)-Benzilate Complex Immobilized on Gold Nanoparticles. *Inorg. Chem.* **2019**, *58*, 4828−4841.
(119) Vinu, A.; Hossain, K. Z.; Ariga, K. Recent advances in functionalization of mesoporous silica. *J. Nanosci. Nanotechnol.* **2005**, *5*, 347−371.
(120) Pujari, S. P.; Scheres, L.; Marcelis, A. T. M.; Zuilhof, H. Covalent Surface Modification of Oxide Surfaces. *Angew. Chem., Int. Ed.* **2014**, *53*, 2−36.
(121) Fernandes, A. E.; Jonas, A. M.; Riant, O. Application of CuAAC for the covalent immobilization of homogeneous catalysts. *Tetrahedron* **2014**, *70*, 1709−1731.
(122) Ghosh, D.; Febriansyah, B.; Gupta, D.; Ng, L. K.-S.; Xi, S.; Du, Y.; Baikie, T.; Dong, Z.; Soo, H. S. Hybrid Nanomaterials with Single-Site Catalysts by Spatially Controllable Immobilization of Nickel Complexes via Photoclick Chemistry for Alkene Epoxidation. *ACS Nano* **2018**, *12*, 5903−5912.
(123) del Pozo, C.; Corma, A.; Iglesias, M.; Sánchez, F. Immobilization of (NHC)NN-Pincer Complexes on Mesoporous MCM-41 Support. *Organometallics* **2010**, *29*, 4491−4498.
(124) Kolb, H. C.; Finn, M. G.; Sharpless, K. B. Click Chemistry: Diverse Chemical Function from a Few Good Reactions. *Angew. Chem., Int. Ed.* **2001**, *40*, 2004−2021.
(125) Liang, L.; Astruc, D. The copper(I)-catalyzed alkyne-azide cycloaddition (CuAAC) "click" reaction and its applications. An overview. *Coord. Chem. Rev.* **2011**, *255*, 2933−2945.
(126) Nakazawa, J.; Smith, B. J.; Stack, T. D. P. Discrete Complexes Immobilized onto Click-SBA-15 Silica: Controllable Loadings and the Impact of Surface Coverage on Catalysis. *J. Am. Chem. Soc.* **2012**, *134*, 2750−2759.

https://doi.org/10.1021/acs.chemrev.1c00905
Chem. Rev. XXXX, XXX, XXX−XXX

(127) Malvi, B.; Panda, C.; Dhar, B. B.; Gupta, S. S. One pot glucose detection by [Fe^{III}(biuret-amide)] immobilized on mesoporous silica nanoparticles: an efficient HRP mimic. *Chem. Commun.* **2012**, *48*, 5289−5291.
(128) Nakazawa, J.; Hori, T.; Stack, T. D. P.; Hikichi, S. Alkane Oxidation by an Immobilized Nickel Complex Catalyst: Structural and Reactivity Differences Induced by Surface-Ligand Density on Mesoporous Silica. *Chem.-Asian J.* **2013**, *8*, 1191−1199.
(129) Martínez-Vargas, D. X.; Rivera De La Rosa, J.; Sandoval-Rangel, L.; Guzmán-Mar, J. L.; Garza-Navarro, M. A.; Lucio-Ortiz, C. J.; De Haro-Del Río, D. A. 5-Hydroxymethylfurfural catalytic oxidation under mild conditions by Co (II), Fe (III) and Cu (II) Salen complexes supported on SBA-15: Synthesis, characterization and activity. *Appl. Catal. A* **2017**, *547*, 132−145.
(130) Yao, S. A.; Ruther, R. E.; Zhang, L.; Franking, R. A.; Hamers, R. J.; Berry, J. F. Covalent Attachment of Catalyst Molecules to Conductive Diamond: CO_2 Reduction Using "Smart" Electrodes. *J. Am. Chem. Soc.* **2012**, *134*, 15632−15635.
(131) Zhao, Q.; Li, Y.; Liu, R.; Chen, A.; Zhang, G.; Zhang, F.; Fan, X. Enhanced hydrogenation of olefins and ketones with a ruthenium complex covalently anchored on graphene oxide. *J. Mater. Chem. A* **2013**, *1*, 15039−15045.
(132) Zhao, Q.; Bai, C.; Zhang, W.; Li, Y.; Zhang, G.; Zhang, F.; Fan, X. Catalytic Epoxidation of Olefins with Graphene Oxide Supported Copper (Salen) Complex. *Ind. Eng. Chem. Res.* **2014**, *53*, 4232−4238.
(133) Navalón, S.; Herance, J. R.; Álvaro, M.; García, H. Covalently Modified Graphenes in Catalysis, Electrocatalysis and Photoresponsive Materials. *Chem.-Eur. J.* **2017**, *23*, 15244−15275.
(134) Campisciano, V.; Gruttadauria, M.; Giacalone, F. Modified Nanocarbons for Catalysis. *ChemCatChem.* **2019**, *11*, 90−133.
(135) Axet, M. R.; Durand, J.; Gouygou, M.; Serp, P. In *Advances in Organometallic Chemistry*; Pérez, P. J., Ed.; Academic Press, 2019; Vol. *71*.
(136) Feng, Y.; Moschetta, E. G.; Jones, C. W. Polymer- and Silica-Supported Iron BPMEN-Inspired Catalysts for C-H Bond Functionalization Reactions. *Chem.-Asian J.* **2014**, *9*, 3142−3152.
(137) Fan, W.; Shi, D.; Feng, B. Immobilizing of oxo-molybdenum complex on cross-linked copolymer and its catalytic activity for epoxidation reactions. *Catal. Commun.* **2016**, *74*, 1−4.
(138) Huang, J.; Liu, S.; Ma, Y.; Cai, J. Chiral salen Mn (III) immobilized on ZnPS-PVPA through alkoxyl-triazole for superior performance catalyst in asymmetric epoxidation of unfunctionalized olefins. *Journal of Organometallic Chemistry* **2019**, *886*, 27−33.
(139) Lu, J.; Toy, P. H. Organic Polymer Supports for Synthesis and for Reagent and Catalyst Immobilization. *Chem. Rev.* **2009**, *109*, 815−838.
(140) Takamura, M.; Funabashi, K.; Kanai, M.; Shibasaki, M. Catalytic Enantioselective Reissert-Type Reaction: Development and Application to the Synthesis of a Potent NMDA Receptor Antagonist (−)-L-689,560 Using a Solid-Supported Catalyst. *J. Am. Chem. Soc.* **2001**, *123*, 6801−6808.
(141) Song, C. E.; Yang, J. W.; Roh, E. J.; Lee, S.-g.; Ahn, J. H.; Han, H. Heterogeneous Pd-Catalyzed Asymmetric Allylic Substitution Using Resin-Supported Trost-Type Bisphosphane Ligands. *Angew. Chem., Int. Ed.* **2002**, *41*, 3852−3854.
(142) Årstad, E.; Barrett, A. G. M.; Tedeschi, L. ROMPgel-supported tris(triphenylphosphine)rhodium(I) chloride: a selective hydrogenation catalyst for parallel synthesis. *Tetrahedron Lett.* **2003**, *44*, 2703−2707.
(143) Kobayashi, J.; Mori, Y.; Kobayashi, S. Novel immobilization method of enzymes using a hydrophilic polymer support. *Chem. Commun.* **2006**, 4227−4229.
(144) Altava, B.; Burguete, M. I.; García-Verdugo, E.; Luis, S. V. Chiral catalysts immobilized on achiral polymers: effect of the polymer support on the performance of the catalyst. *Chem. Soc. Rev.* **2018**, *47*, 2722−2771.
(145) Hong, J.; Djernes, K. E.; Lee, I.; Hooley, R. J.; Zaera, F. Heterogeneous Catalyst for the Selective Oxidation of Unactivated Hydrocarbons Based on a Tethered Metal-Coordinated Cavitand. *ACS Catal.* **2013**, *3*, 2154−2157.
(146) Sheet, D.; Bera, A.; Fu, Y.; Desmecht, A.; Riant, O.; Hermans, S. Carbon-Nanotube-Appended PAMAM Dendrimers Bearing Iron-(II) α-Keto Acid Complexes: Catalytic Non-Heme Oxygenase Models. *Chem.-Eur. J.* **2019**, *25*, 9191−9196.
(147) Notestein, J. M.; Iglesia, E.; Katz, A. Grafted metal-localixarenes as single-site surface organometallic catalysts. *J. Am. Chem. Soc.* **2004**, *126*, 16478−16486.
(148) De Silva, N.; Ha, J. M.; Solovyov, A.; Nigra, M. M.; Ogino, I.; Yeh, S. W.; Durkin, K. A.; Katz, A. A bioinspired approach for controlling accessibility in calix[4]arene-bound metal cluster catalysts. *Nat. Chem.* **2010**, *2*, 1062−1068.
(149) Thornburg, N. E.; Thompson, A. B.; Notestein, J. M. Periodic Trends in Highly Dispersed Groups IV and V Supported Metal Oxide Catalysts for Alkene Epoxidation with H_2O_2. *ACS Catal.* **2015**, *5*, 5077−5088.
(150) Solovyov, A.; Notestein, J. M.; Durkin, K. A.; Katz, A. Graftable chiral ligands for surface organometallic materials: Calixarenes bearing asymmetric centers directly attached to the lower rim. *New J. Chem.* **2008**, *32*, 1314−1325.
(151) Bartók, M. Advances in Immobilized Organocatalysts for the Heterogeneous Asymmetric Direct Aldol Reactions. *Catal. Rev.* **2015**, *57*, 192−255.
(152) Szollosi, G. Asymmetric one-pot reactions using heterogeneous chemical catalysis: recent steps towards sustainable processes. *Catal. Sci. Technol.* **2018**, *8*, 389−422.
(153) Blaser, H. U.; Spindler, F. *Comprehensive Organic Synthesis*, 2nd ed.; Knochel, P., Ed.; Elsevier: Amsterdam, 2014. DOI: 10.1016/B978-0-08-097742-3.00807-7.
(154) Chepiga, K. M.; Feng, Y.; Brunelli, N. A.; Jones, C. W.; Davies, H. M. L. Silica-Immobilized Chiral Dirhodium(II) Catalyst for Enantioselective Carbenoid Reactions. *Organic Letters* **2013**, *15*, 6136−6139.
(155) Lee, J.-M.; Kim, J.; Shin, Y.; Yeom, C.-E.; Lee, J. E.; Hyeon, T.; Moon Kim, B. Heterogeneous asymmetric Henry reaction using a chiral bis(oxazoline)-copper complex immobilized on magnetically separable mesocellular mesoporous silica support. *Tetrahedron: Asymmetry* **2010**, *21*, 285−291.
(156) Larionov, V. A.; Cruchter, T.; Mietke, T.; Meggers, E. Polymer-Supported Chiral-at-Metal Lewis Acid Catalysts. *Organometallics* **2017**, *36*, 1457−1460.
(157) Aranda, C.; Cornejo, A.; Fraile, J. M.; García-Verdugo, E.; Gil, M. J.; Luis, S. V.; Mayoral, J. A.; Martinez-Merino, V.; Ochoa, Z. Efficient enhancement of copper-pyridineoxazoline catalysts through immobilization and process design. *Green Chem.* **2011**, *13*, 983−990.
(158) Itsuno, S.; Hassan, M. M. Polymer-immobilized chiral catalysts. *RSC Adv.* **2014**, *4*, 52023−52043.
(159) Wight, A. P.; Davis, M. E. Design and Preparation of Organic-Inorganic Hybrid Catalysts. *Chem. Rev.* **2002**, *102*, 3589−3614.
(160) Valkenberg, M. H.; Hölderich, W. F. Preparation and use of hybrid organic-inorganic catalysts. *Catalysis Reviews* **2002**, *44*, 321−374.
(161) Corma, A.; Garcia, H. Silica-bound homogenous catalysts as recoverable and reusable catalysts in organic synthesis. *Adv. Synth. Catal.* **2006**, *348*, 1391−1412.
(162) Rostamnia, S.; Doustkhah, E. Nanoporous silica-supported organocatalyst: a heterogeneous and green hybrid catalyst for organic transformations. *RSC Adv.* **2014**, *4*, 28238−28248.
(163) Ferré, M.; Pleixats, R.; Wong Chi Man, M.; Cattoën, X. Recyclable organocatalysts based on hybrid silicas. *Green Chem.* **2016**, *18*, 881−922.
(164) Busca, G. Acid Catalysts in Industrial Hydrocarbon Chemistry. *Chem. Rev.* **2007**, *107*, 5366−5410.
(165) Derouane, E. G.; Védrine, J. C.; Pinto, R. R.; Borges, P. M.; Costa, L.; Lemos, M. A. N. D. A.; Lemos, F.; Ribeiro, F. R. The Acidity of Zeolites: Concepts, Measurements and Relation to Catalysis: A Review on Experimental and Theoretical Methods for the Study of Zeolite Acidity. *Catal. Rev.* **2013**, *55*, 454−515.

https://doi.org/10.1021/acs.chemrev.1c00905
Chem. Rev. XXXX, XXX, XXX−XXX

(166) Caillot, M.; Chaumonnot, A.; Digne, M.; van Bokhoven, J. A. The variety of Brønsted acid sites in amorphous aluminosilicates and zeolites. *J. Catal.* **2014**, *316*, 47−56.
(167) Liang, J.; Liang, Z.; Zou, R.; Zhao, Y. Heterogeneous Catalysis in Zeolites, Mesoporous Silica, and Metal-Organic Frameworks. *Adv. Mater.* **2017**, *29*, 1701139.
(168) Tamura, M.; Shimizu, K.-i.; Satsuma, A. Comprehensive IR study on acid/base properties of metal oxides. *Appl. Catal. A* **2012**, *433-434*, 135−145.
(169) Hoffmann, F.; Cornelius, M.; Morell, J.; Fröba, M. Silica-Based Mesoporous Organic-Inorganic Hybrid Materials. *Angew. Chem., Int. Ed.* **2006**, *45*, 3216−3251.
(170) Margolese, D.; Melero, J. A.; Christiansen, S. C.; Chmelka, B. F.; Stucky, G. D. Direct Syntheses of Ordered SBA-15 Mesoporous Silica Containing Sulfonic Acid Groups. *Chem. Mater.* **2000**, *12*, 2448−2459.
(171) Van Rhijn, W. M.; De Vos, D. E.; Sels, B. F.; Bossaert, W. D. Sulfonic acid functionalised ordered mesoporous materials as catalysts for condensation and esterification reactions. *Chem. Commun.* **1998**, 317−318.
(172) Fujita, S.; Inagaki, S. Self-Organization of Organosilica Solids with Molecular-Scale and Mesoscale Periodicities. *Chem. Mater.* **2008**, *20*, 891−908.
(173) Wang, X.; Liu, R.; Waje, M. M.; Chen, Z.; Yan, Y.; Bozhilov, K. N.; Feng, P. Sulfonated Ordered Mesoporous Carbon as a Stable and Highly Active Protonic Acid Catalyst. *Chem. Mater.* **2007**, *19*, 2395−2397.
(174) Gill, C. S.; Price, B. A.; Jones, C. W. Sulfonic acid-functionalized silica-coated magnetic nanoparticle catalysts. *J. Catal.* **2007**, *251*, 145−152.
(175) Kassaee, M. Z.; Masrouri, H.; Movahedi, F. Sulfamic acid-functionalized magnetic Fe_3O_4 nanoparticles as an efficient and reusable catalyst for one-pot synthesis of α-amino nitriles in water. *Appl. Catal. A* **2011**, *395*, 28−33.
(176) Wang, Q.; Shantz, D. F. Nitroaldol reactions catalyzed by amine-MCM-41 hybrids. *J. Catal.* **2010**, *271*, 170−177.
(177) Zailan, Z.; Tahir, M.; Jusoh, M.; Zakaria, Z. Y. A review of sulfonic group bearing porous carbon catalyst for biodiesel production. *Renewable Energy* **2021**, *175*, 430−452.
(178) Hong, J.; Lee, I.; Zaera, F. Cinchona Alkaloids Tethered on Porous Silica as Enantioselective Heterogeneous Catalysts. *Top. Catal.* **2011**, *54*, 1340−1347.
(179) Hong, J.; Zaera, F. Interference of the Surface of the Solid on the Performance of Tethered Molecular Catalysts. *J. Am. Chem. Soc.* **2012**, *134*, 13056−13065.
(180) Brunelli, N. A.; Jones, C. W. Tuning acid-base cooperativity to create next generation silica-supported organocatalysts. *J. Catal.* **2013**, *308*, 60−72.
(181) Collier, V. E.; Ellebracht, N. C.; Lindy, G. I.; Moschetta, E. G.; Jones, C. W. Kinetic and Mechanistic Examination of Acid-Base Bifunctional Aminosilica Catalysts in Aldol and Nitroaldol Condensations. *ACS Catal.* **2016**, *6*, 460−468.
(182) Moschetta, E. G.; Sakwa-Novak, M. A.; Greenfield, J. L.; Jones, C. W. Post-Grafting Amination of Alkyl Halide-Functionalized Silica for Applications in Catalysis, Adsorption, and ^{15}N NMR Spectroscopy. *Langmuir* **2015**, *31*, 2218−2227.
(183) Zhao, Y.-B.; Zhang, L.-W.; Wu, L.-Y.; Zhong, X.; Li, R.; Ma, J.-T. Silica-supported pyrrolidine-triazole, an insoluble, recyclable organocatalyst for the enantioselective Michael addition of ketones to nitroalkenes. *Tetrahedron: Asymmetry* **2008**, *19*, 1352−1355.
(184) Rajabi, F.; Fayyaz, F.; Luque, R. Cytosine-functionalized SBA-15 mesoporous nanomaterials: Synthesis, characterization and catalytic applications. *Microporous Mesoporous Mater.* **2017**, *253*, 64−70.
(185) Clot-Almenara, L.; Rodríguez-Escrich, C.; Osorio-Planes, L.; Pericàs, M. A. Polystyrene-Supported TRIP: A Highly Recyclable Catalyst for Batch and Flow Enantioselective Allylation of Aldehydes. *ACS Catal.* **2016**, *6*, 7647−7651.
(186) Akagawa, K.; Hirata, T.; Kudo, K. Asymmetric Epoxidation of Enones by Peptide-Based Catalyst: A Strategy Inverting Juliá-Colonna Stereoselectivity. *Synlett* **2016**, *27*, 1217−1222.
(187) Bourda, L.; Jena, H. S.; Van Deun, R.; Kaczmarek, A. M.; Van Der Voort, P. Functionalized periodic mesoporous organosilicas: from metal free catalysis to sensing. *Journal of Materials Chemistry A* **2019**, *7*, 14060−14069.
(188) Haghighat, M.; Leus, K.; Shirini, F.; Van Der Voort, P. Salen-decorated Periodic Mesoporous Organosilica: From Metal-assisted Epoxidation to Metal-free CO2 Insertion. *Chem.-Asian J.* **2021**, *16*, 2126−2135.
(189) Cheng, X.; Zhao, P.; Zhang, M.; Wang, S.; Liu, M.; Liu, F. Fabrication of robust and bifunctional cyclotriphosphazene-based periodic mesoporous organosilicas for efficient CO_2 adsorption and catalytic conversion. *Chem. Eng. J.* **2021**, *418*, 129360.
(190) Tuma, J.; Kohout, M. Silica gel-immobilized multidisciplinary materials applicable in stereoselective organocatalysis and HPLC separation. *RSC Adv.* **2018**, *8*, 1174−1181.
(191) Ayats, C.; Henseler, A. H.; Pericàs, M. A. A Solid-Supported Organocatalyst for Continuous-Flow Enantioselective Aldol Reactions. *ChemSusChem* **2012**, *5*, 320−325.
(192) Hajipour, A. R.; Khorsandi, Z. Application of Immobilized Proline on CNTs and Proline Ionic Liquid as Novel Organocatalysts in the Synthesis of 2-Amino-4H-pyran Derivatives: A Comparative Study between Their Catalytic Activities. *ChemistrySelect* **2017**, *2*, 8976−8982.
(193) Al Dine, W. N.; Mehdi, A.; BouMalham, I.; Herro, Z.; Vioux, A.; Brun, N.; Fontaine, O. Self-Limited Grafting of Sub-Monolayers via Diels-Alder Reaction on Glassy Carbon Electrodes: An Electrochemical Insight. *ACS Omega* **2019**, *4*, 20540−20546.
(194) Campisciano, V.; Gruttadauria, M.; Giacalone, F. *Catalyst Immobilization*, 2020. DOI: 10.1002/9783527817290.ch3.
(195) He, Y.; Itta, A. K.; Alwakwak, A.-a.; Huang, M.; Rezaei, F.; Rownaghi, A. A. Aminosilane-Grafted SiO_2-ZrO_2 Polymer Hollow Fibers as Bifunctional Microfluidic Reactor for Tandem Reaction of Glucose and Fructose to 5-Hydroxymethylfurfural. *ACS Sustainable Chem. Eng.* **2018**, *6*, 17211−17219.
(196) Mateo, C.; Palomo, J. M.; Fernandez-Lorente, G.; Guisan, J. M.; Fernandez-Lafuente, R. Improvement of enzyme activity, stability and selectivity via immobilization techniques. *Enzyme Microb. Technol.* **2007**, *40*, 1451−1463.
(197) Hartmann, M.; Jung, D. Biocatalysis with enzymes immobilized on mesoporous hosts: the status quo and future trends. *J. Mater. Chem.* **2010**, *20*, 844−857.
(198) Cowan, D. A.; Fernandez-Lafuente, R. Enhancing the functional properties of thermophilic enzymes by chemical modification and immobilization. *Enzyme Microb. Technol.* **2011**, *49*, 326−346.
(199) Li, H.; Moncecchi, J.; Truppo, M. D. Development of an Immobilized Ketoreductase for Enzymatic (R)-1-(3,5-Bis-(trifluoromethyl)phenyl)ethanol Production. *Org. Process Res. Dev.* **2015**, *19*, 695−700.
(200) Basso, A.; Serban, S. Industrial applications of immobilized enzymes—A review. *Molecular Catalysis* **2019**, *479*, 110607.
(201) Cao, L. *Carrier-bound Immobilized Enzymes: Principles, Application and Design*; 1st ed.; Wiley-VCH: Weinheim, 2005.
(202) Ansari, S. A.; Husain, Q. Potential applications of enzymes immobilized on/in nano materials: A review. *Biotechnology Advances* **2012**, *30*, 512−523.
(203) Singh, R. K.; Tiwari, M. K.; Singh, R.; Lee, J. K. From protein engineering to immobilization: Promising strategies for the upgrade of industrial enzymes. *International Journal of Molecular Sciences* **2013**, *14*, 1232−1277.
(204) Mohamad, N. R.; Marzuki, N. H. C.; Buang, N. A.; Huyop, F.; Wahab, R. A. An overview of technologies for immobilization of enzymes and surface analysis techniques for immobilized enzymes. *Biotechnology & Biotechnological Equipment* **2015**, *29*, 205−220.
(205) Sheldon, R. A.; Brady, D. The limits to biocatalysis: pushing the envelope. *Chem. Commun.* **2018**, *54*, 6088−6104.

https://doi.org/10.1021/acs.chemrev.1c00905
Chem. Rev. XXXX, XXX, XXX−XXX

(206) Wahab, R. A.; Elias, N.; Abdullah, F.; Ghoshal, S. K. On the taught new tricks of enzymes immobilization: An all-inclusive overview. *React. Funct. Polym.* **2020**, *152*, 104613.
(207) Zhao, X. S.; Bao, X. Y.; Guo, W.; Lee, F. Y. Immobilizing catalysts on porous materials. *Mater. Today* **2006**, *9*, 32−39.
(208) Lee, C.-H.; Lin, T.-S.; Mou, C.-Y. Mesoporous materials for encapsulating enzymes. *Nano Today* **2009**, *4*, 165−179.
(209) Hwang, E. T.; Gu, M. B. Enzyme stabilization by nano/microsized hybrid materials. *Engineering in Life Sciences* **2013**, *13*, 49−61.
(210) Santos, J. C. S. d.; Barbosa, O.; Ortiz, C.; Berenguer-Murcia, A.; Rodrigues, R. C.; Fernandez-Lafuente, R. Importance of the Support Properties for Immobilization or Purification of Enzymes. *ChemCatChem.* **2015**, *7*, 2413−2432.
(211) Reetz, M. T. *Immobilization of Enzymes and Cells*; 3rd ed.; Guisan, J. M., Ed.; Humana Press: Totowa, NJ, 2013. DOI: 10.1007/978-1-62703-550-7.
(212) Cantone, S.; Ferrario, V.; Corici, L.; Ebert, C.; Fattor, D.; Spizzo, P.; Gardossi, L. Efficient immobilisation of industrial biocatalysts: criteria and constraints for the selection of organic polymeric carriers and immobilisation methods. *Chem. Soc. Rev.* **2013**, *42*, 6262−6276.
(213) Hartmann, M.; Kostrov, X. Immobilization of enzymes on porous silicas - benefits and challenges. *Chem. Soc. Rev.* **2013**, *42*, 6277−6289.
(214) Magner, E. Immobilisation of enzymes on mesoporous silicate materials. *Chem. Soc. Rev.* **2013**, *42*, 6213−6222.
(215) Rodrigues, R. C.; Ortiz, C.; Berenguer-Murcia, Á.; Torres, R.; Fernández-Lafuente, R. Modifying enzyme activity and selectivity by immobilization. *Chem. Soc. Rev.* **2013**, *42*, 6290−6307.
(216) Zhang, Y.; Ge, J.; Liu, Z. Enhanced Activity of Immobilized or Chemically Modified Enzymes. *ACS Catal.* **2015**, *5*, 4503−4513.
(217) Ding, S.; Cargill, A. A.; Medintz, I. L.; Claussen, J. C. Increasing the activity of immobilized enzymes with nanoparticle conjugation. *Curr. Opin. Biotechnol.* **2015**, *34*, 242−250.
(218) Cao, S.-L.; Huang, Y.-M.; Li, X.-H.; Xu, P.; Wu, H.; Li, N.; Lou, W.-Y.; Zong, M.-H. Preparation and Characterization of Immobilized Lipase from Pseudomonas Cepacia onto Magnetic Cellulose Nanocrystals. *Sci. Rep.* **2016**, *6*, 20420.
(219) Abdul Manan, F. M.; Attan, N.; Widodo, N.; Aboul-Enein, H. Y.; Wahab, R. A. Rhizomucor miehei lipase immobilized on reinforced chitosan-chitin nanowhiskers support for synthesis of eugenyl benzoate. *Preparative Biochemistry & Biotechnology* **2018**, *48*, 92−102.
(220) Hudson, E. P.; Eppler, R. K.; Clark, D. S. Biocatalysis in semi-aqueous and nearly anhydrous conditions. *Curr. Opin. Biotechnol.* **2005**, *16*, 637−643.
(221) Elias, N.; Wahab, R. A.; Chandren, S.; Abdul Razak, F. I.; Jamalis, J. Effect of operative variables and kinetic study of butyl butyrate synthesis by Candida rugosa lipase activated by chitosan-reinforced nanocellulose derived from raw oil palm leaves. *Enzyme Microb. Technol.* **2019**, *130*, 109367.
(222) Cowan, D. A.; Daniel, R. M.; Morgan, H. W. Some observations on the inhibition and activation of a thermophilic protease. *Int. J. Biochem.* **1987**, *19*, 483−486.
(223) Aissaoui, N.; Landoulsi, J.; Bergaoui, L.; Boujday, S.; Lambert, J.-F. Catalytic activity and thermostability of enzymes immobilized on silanized surface: Influence of the crosslinking agent. *Enzyme Microb. Technol.* **2013**, *52*, 336−343.
(224) Guzik, U.; Hupert-Kocurek, K.; Wojcieszyńska, D. Immobilization as a Strategy for Improving Enzyme Properties-Application to Oxidoreductases. *Molecules* **2014**, *19*, 8995.
(225) Orrego, A. H.; Romero-Fernández, M.; Millán-Linares, M. D. C.; Yust, M. D. M.; Guisán, J. M.; Rocha-Martin, J. Stabilization of Enzymes by Multipoint Covalent Attachment on Aldehyde-Supports: 2-Picoline Borane as an Alternative Reducing Agent. *Catalysts* **2018**, *8*, 333.
(226) Guauque Torres, M. P.; Foresti, M. L.; Ferreira, M. L. CLEAs of Candida antarctica lipase B (CALB) with a bovine serum albumin (BSA) cofeeder core: Study of their catalytic activity. *Biochemical Engineering Journal* **2014**, *90*, 36−43.
(227) Quilles, J. C. J.; Brito, R. R.; Borges, J. P.; Aragon, C. C.; Fernandez-Lorente, G.; Bocchini-Martins, D. A.; Gomes, E.; da Silva, R.; Boscolo, M.; Guisan, J. M. Modulation of the activity and selectivity of the immobilized lipases by surfactants and solvents. *Biochemical Engineering Journal* **2015**, *93*, 274−280.
(228) Vescovi, V.; Giordano, R. L. C.; Mendes, A. A.; Tardioli, P. W. Immobilized Lipases on Functionalized Silica Particles as Potential Biocatalysts for the Synthesis of Fructose Oleate in an Organic Solvent/Water System. *Molecules* **2017**, *22*, 212.
(229) Yang, H.; Zhang, W. Surfactant Imprinting Hyperactivated Immobilized Lipase as Efficient Biocatalyst for Biodiesel Production from Waste Cooking Oil. *Catalysts* **2019**, *9*, 914.
(230) Jin, Q.; Jia, G.; Zhang, Y.; Yang, Q.; Li, C. Hydrophobic Surface Induced Activation of Pseudomonas cepacia Lipase Immobilized into Mesoporous Silica. *Langmuir* **2011**, *27*, 12016−12024.
(231) Campbell, A. S.; Dong, C.; Meng, F.; Hardinger, J.; Perhinschi, G.; Wu, N.; Dinu, C. Z. Enzyme Catalytic Efficiency: A Function of Bio-Nano Interface Reactions. *ACS Appl. Mater. Interfaces* **2014**, *6*, 5393−5403.
(232) Zhang, C.; Chen, S.; Alvarez, P. J. J.; Chen, W. Reduced graphene oxide enhances horseradish peroxidase stability by serving as radical scavenger and redox mediator. *Carbon* **2015**, *94*, 531−538.
(233) Dehkordi, A. M.; Tehrany, M. S.; Safari, I. Kinetics of Glucose Isomerization to Fructose by Immobilized Glucose Isomerase (Sweetzyme IT). *Ind. Eng. Chem. Res.* **2009**, *48*, 3271−3278.
(234) Karinen, R.; Vilonen, K.; Niemelä, M. Biorefining: Heterogeneously Catalyzed Reactions of Carbohydrates for the Production of Furfural and Hydroxymethylfurfural. *ChemSusChem* **2011**, *4*, 1002−1016.
(235) Franssen, M. C. R.; Steunenberg, P.; Scott, E. L.; Zuilhof, H.; Sanders, J. P. M. Immobilised enzymes in biorenewables production. *Chem. Soc. Rev.* **2013**, *42*, 6491−6533.
(236) Pellis, A.; Cantone, S.; Ebert, C.; Gardossi, L. Evolving biocatalysis to meet bioeconomy challenges and opportunities. *New Biotechnology* **2018**, *40*, 154−169.
(237) DiCosimo, R.; McAuliffe, J.; Poulose, A. J.; Bohlmann, G. Industrial use of immobilized enzymes. *Chem. Soc. Rev.* **2013**, *42*, 6437−6474.
(238) Bommarius, A. S.; Paye, M. F. Stabilizing biocatalysts. *Chem. Soc. Rev.* **2013**, *42*, 6534−6565.
(239) Rehm, F. B. H.; Chen, S.; Rehm, B. H. A. Enzyme Engineering for In Situ Immobilization. *Molecules* **2016**, *21*, 1370.
(240) Bernal, C.; Rodríguez, K.; Martínez, R. Integrating enzyme immobilization and protein engineering: An alternative path for the development of novel and improved industrial biocatalysts. *Biotechnology Advances* **2018**, *36*, 1470−1480.
(241) Cecchini, D. A.; Pavesi, R.; Sanna, S.; Daly, S.; Xaiz, R.; Pregnolato, M.; Terreni, M. Efficient biocatalyst for large-scale synthesis of cephalosporins, obtained by combining immobilization and site-directed mutagenesis of penicillin acylase. *Appl. Microbiol. Biotechnol.* **2012**, *95*, 1491−1500.
(242) Butterfield, D. A.; Bhattacharyya, D.; Daunert, S.; Bachas, L. Catalytic biofunctional membranes containing site-specifically immobilized enzyme arrays: a review. *J. Membr. Sci.* **2001**, *181*, 29−37.
(243) Campàs, M.; Prieto-Simón, B.; Marty, J.-L. A review of the use of genetically engineered enzymes in electrochemical biosensors. *Seminars in Cell & Developmental Biology* **2009**, *20*, 3−9.
(244) Hernandez, K.; Fernandez-Lafuente, R. Control of protein immobilization: Coupling immobilization and site-directed mutagenesis to improve biocatalyst or biosensor performance. *Enzyme Microb. Technol.* **2011**, *48*, 107−122.
(245) Madoz-Gúrpide, J.; Abad, J. M.; Fernández-Recio, J.; Vélez, M.; Vázquez, L.; Gómez-Moreno, C.; Fernández, V. M. Modulation of Electroenzymatic NADPH Oxidation through Oriented Immobilization of Ferredoxin:NADP$^+$ Reductase onto Modified Gold Electrodes. *J. Am. Chem. Soc.* **2000**, *122*, 9808−9817.

https://doi.org/10.1021/acs.chemrev.1c00905
Chem. Rev. XXXX, XXX, XXX−XXX

(246) Abian, O.; Grazú, V.; Hermoso, J.; González, R.; García, J. L.; Fernández-Lafuente, R.; Guisán, J. M. Stabilization of Penicillin G Acylase from Escherichia coli: Site-Directed Mutagenesis of the Protein Surface to Increase Multipoint Covalent Attachment. *Appl. Environ. Microbiol.* **2004**, *70*, 1249−1251.
(247) Liu, F.; Wang, L.; Wang, H.; Yuan, L.; Li, J.; Brash, J. L.; Chen, H. Modulating the Activity of Protein Conjugated to Gold Nanoparticles by Site-Directed Orientation and Surface Density of Bound Protein. *ACS Appl. Mater. Interfaces* **2015**, *7*, 3717−3724.
(248) Ginet, N.; Pardoux, R.; Adryanczyk, G.; Garcia, D.; Brutesco, C.; Pignol, D. Single-Step Production of a Recyclable Nanobiocatalyst for Organophosphate Pesticides Biodegradation Using Functionalized Bacterial Magnetosomes. *PLoS One* **2011**, *6*, No. e21442.
(249) Lohr, T. L.; Marks, T. J. Orthogonal tandem catalysis. *Nat. Chem.* **2015**, *7*, 477−482.
(250) Margelefsky, E. L.; Zeidan, R. K.; Davis, M. E. Cooperative catalysis by silica-supported organic functional groups. *Chem. Soc. Rev.* **2008**, *37*, 1118−1126.
(251) Climent, M. J.; Corma, A.; Iborra, S. Heterogeneous Catalysts for the One-Pot Synthesis of Chemicals and Fine Chemicals. *Chem. Rev.* **2011**, *111*, 1072−1133.
(252) Kung, H.; Kung, M. Inspiration from Nature for Heterogeneous Catalysis. *Catal. Lett.* **2014**, *144*, 1643−1652.
(253) Jagadeesan, D. Multifunctional nanocatalysts for tandem reactions: A leap toward sustainability. *Appl. Catal. A* **2016**, *511*, 59−77.
(254) Jin, R.; Zheng, D.; Liu, R.; Liu, G. Silica-Supported Molecular Catalysts for Tandem Reactions. *ChemCatChem.* **2018**, *10*, 1739−1752.
(255) Fogg, D. E.; dos Santos, E. N. Tandem catalysis: a taxonomy and illustrative review. *Coord. Chem. Rev.* **2004**, *248*, 2365−2379.
(256) Patil, N. T.; Shinde, V. S.; Gajula, B. A one-pot catalysis: the strategic classification with some recent examples. *Organic & Biomolecular Chemistry* **2012**, *10*, 211−224.
(257) Climent, M. J.; Corma, A.; Iborra, S.; Sabater, M. J. Heterogeneous Catalysis for Tandem Reactions. *ACS Catal.* **2014**, *4*, 870−891.
(258) Barber, D. M.; Duriš, A.; Thompson, A. L.; Sanganee, H. J.; Dixon, D. J. One-Pot Asymmetric Nitro-Mannich/Hydroamination Cascades for the Synthesis of Pyrrolidine Derivatives: Combining Organocatalysis and Gold Catalysis. *ACS Catal.* **2014**, *4*, 634−638.
(259) Motokura, K. Synergistic Catalysis by Multifunctionalized Solid Surfaces for Nucleophilic Addition Reactions. *Journal of the Japan Petroleum Institute* **2014**, *57*, 95−108.
(260) Bass, J. D.; Anderson, S. L.; Katz, A. The Effect of Outer-Sphere Acidity on Chemical Reactivity in a Synthetic Heterogeneous Base Catalyst. *Angew. Chem., Int. Ed.* **2003**, *42*, 5219−5222.
(261) Lauwaert, J.; De Canck, E.; Esquivel, D.; Van Der Voort, P.; Thybaut, J. W.; Marin, G. B. Effects of amine structure and base strength on acid-base cooperative aldol condensation. *Catal. Today* **2015**, *246*, 35−45.
(262) Motokura, K.; Tomita, M.; Tada, M.; Iwasawa, Y. Michael Reactions Catalyzed by Basic Alkylamines and Dialkylaminopyridine Immobilized on Acidic Silica-Alumina Surfaces. *Top. Catal.* **2009**, *52*, 579−585.
(263) Sharma, K. K.; Biradar, A. V.; Das, S.; Asefa, T. Bifunctional Mesoporous Silica Catalyst for C-C Bond Forming Tandem Reactions. *Eur. J. Inorg. Chem.* **2011**, *2011*, 3174−3182.
(264) Hong, J.; Lee, I.; Zaera, F. Correlated Bifunctionality in Heterogeneous Catalysts: Selective Tethering of Cinchonidine Next to Supported Pt Nanoparticles. *Catal. Sci. Technol.* **2015**, *5*, 680−689.
(265) Mäki-Arvela, P.; Sahin, S.; Kumar, N.; Heikkilä, T.; Lehto, V.-P.; Salmi, T.; Murzin, D. Y. Cascade approach for synthesis of R-1-phenyl ethyl acetate from acetophenone: Effect of support. *J. Mol. Catal. A* **2008**, *285*, 132−141.
(266) Ganai, A. K.; Shinde, P.; Dhar, B. B.; Sen Gupta, S.; Prasad, B. L. V. Development of a multifunctional catalyst for a "relay" reaction. *RSC Adv.* **2013**, *3*, 2186−2191.
(267) Zhang, D.; Xu, J.; Zhao, Q.; Cheng, T.; Liu, G. A Site-Isolated Organoruthenium-/Organopalladium-Bifunctionalized Periodic Mesoporous Organosilica Catalyzes Cascade Asymmetric Transfer Hydrogenation and Suzuki Cross-Coupling. *ChemCatChem.* **2014**, *6*, 2998−3003.
(268) Dwulet, G. E.; Coscia, B. J.; Shirts, M. R.; Gin, D. L. A nanostructured bifunctional acid-base catalyst resin formed by lyotropic liquid crystal monomers. *Canadian Journal of Chemistry* **2020**, *98*, 332−336.
(269) Shylesh, S.; Wagener, A.; Seifert, A.; Ernst, S.; Thiel, W. R. Mesoporous Organosilicas with Acidic Frameworks and Basic Sites in the Pores: An Approach to Cooperative Catalytic Reactions. *Angew. Chem., Int. Ed.* **2010**, *49*, 184−187.
(270) Shang, F.; Sun, J.; Liu, H.; Wang, C.; Guan, J.; Kan, Q. One-pot cascade reactions catalyzed by acid-base mesoporous MCM-41 materials. *Mater. Res. Bull.* **2012**, *47*, 801−806.
(271) Gianotti, E.; Diaz, U.; Velty, A.; Corma, A. Designing bifunctional acid-base mesoporous hybrid catalysts for cascade reactions. *Catal. Sci. Technol.* **2013**, *3*, 2677−2688.
(272) Zeidan, R. K.; Hwang, S.-J.; Davis, M. E. Multifunctional Heterogeneous Catalysts: SBA-15-Containing Primary Amines and Sulfonic Acids. *Angew. Chem., Int. Ed.* **2006**, *45*, 6332−6335.
(273) Zeidan, R. K.; Davis, M. E. The effect of acid-base pairing on catalysis: An efficient acid-base functionalized catalyst for aldol condensation. *J. Catal.* **2007**, *247*, 379−382.
(274) Shiju, N. R.; Alberts, A. H.; Khalid, S.; Brown, D. R.; Rothenberg, G. Mesoporous Silica with Site-Isolated Amine and Phosphotungstic Acid Groups: A Solid Catalyst with Tunable Antagonistic Functions for One-Pot Tandem Reactions. *Angew. Chem., Int. Ed.* **2011**, *50*, 9615−9619.
(275) Peng, W.-H.; Lee, Y.-Y.; Wu, C.; Wu, K. C. W. Acid-base bifunctionalized, large-pored mesoporous silica nanoparticles for cooperative catalysis of one-pot cellulose-to-HMF conversion. *J. Mater. Chem.* **2012**, *22*, 23181−23185.
(276) Huang, H.; Denard, C. A.; Alamillo, R.; Crisci, A. J.; Miao, Y.; Dumesic, J. A.; Scott, S. L.; Zhao, H. Tandem Catalytic Conversion of Glucose to 5-Hydroxymethylfurfural with an Immobilized Enzyme and a Solid Acid. *ACS Catal.* **2014**, *4*, 2165−2168.
(277) Wang, T.; Xu, Y.; He, Z.; Zhang, H.; Xiong, L.; Zhou, M.; Yu, W.; Shi, B.; Huang, K. Acid-Base Bifunctional Microporous Organic Nanotube Networks for Cascade Reactions. *Macromolecular Chemistry and Physics* **2017**, *218*, 1600431.
(278) Fernandes, A. E.; Riant, O.; Jensen, K. F.; Jonas, A. M. Molecular Engineering of Trifunctional Supported Catalysts for the Aerobic Oxidation of Alcohols. *Angew. Chem., Int. Ed.* **2016**, *55*, 11044−11048.
(279) Chandra, P.; Jonas, A. M.; Fernandes, A. E. Spatial Coordination of Cooperativity in Silica-Supported Cu/TEMPO/Imidazole Catalytic Triad. *ACS Catal.* **2018**, *8*, 6006−6011.
(280) Fernandes, A. E.; Jonas, A. M. Design and engineering of multifunctional silica-supported cooperative catalysts. *Catal. Today* **2019**, *334*, 173−186.
(281) Brunelli, N. A.; Didas, S. A.; Venkatasubbaiah, K.; Jones, C. W. Tuning Cooperativity by Controlling the Linker Length of Silica-Supported Amines in Catalysis and CO2 Capture. *J. Am. Chem. Soc.* **2012**, *134*, 13950−13953.
(282) Galloway, J. M.; Kung, M.; Kung, H. H. Synthesis and characterization of bifunctional surfaces with tunable functional group pairs. *Surf. Sci.* **2016**, *648*, 284−290.
(283) Lofgreen, J. E.; Ozin, G. A. Controlling morphology and porosity to improve performance of molecularly imprinted sol-gel silica. *Chem. Soc. Rev.* **2014**, *43*, 911−933.
(284) Katz, A.; Davis, M. E. Molecular imprinting of bulk, microporous silica. *Nature* **2000**, *403*, 286−289.
(285) Dufaud, V.; Davis, M. E. Design of Heterogeneous Catalysts via Multiple Active Site Positioning in Organic-Inorganic Hybrid Materials. *J. Am. Chem. Soc.* **2003**, *125*, 9403−9413.

https://doi.org/10.1021/acs.chemrev.1c00905
Chem. Rev. XXXX, XXX, XXX−XXX

(286) Mbaraka, I. K.; Shanks, B. H. Acid strength variation due to spatial location of organosulfonic acid groups on mesoporous silica. *J. Catal.* **2006**, *244*, 78−85.
(287) Margelefsky, E. L.; Zeidan, R. K.; Dufaud, V.; Davis, M. E. Organized Surface Functional Groups: Cooperative Catalysis via Thiol/Sulfonic Acid Pairing. *J. Am. Chem. Soc.* **2007**, *129*, 13691−13697.
(288) Ouwehand, J.; Lauwaert, J.; Esquivel, D.; Hendrickx, K.; Van Speybroeck, V.; Thybaut, J. W.; Van Der Voort, P. Facile Synthesis of Cooperative Acid-Base Catalysts by Clicking Cysteine and Cysteamine on an Ethylene-Bridged Periodic Mesoporous Organosilica. *Eur. J. Inorg. Chem.* **2016**, *2016*, 2144−2151.
(289) Zhong, L.; Xiao, J.; Li, C. Direct Asymmetric Aldol Reactions on Heterogeneous Bifunctional Catalyst. *Chinese Journal of Catalysis* **2011**, *28*, 673−675.
(290) Lauwaert, J.; Moschetta, E. G.; Van Der Voort, P.; Thybaut, J. W.; Jones, C. W.; Marin, G. B. Spatial arrangement and acid strength effects on acid-base cooperatively catalyzed aldol condensation on aminosilica materials. *J. Catal.* **2015**, *325*, 19−25.
(291) Weng, Z.; Yu, T.; Zaera, F. Synthesis of Solid Catalysts with Spatially Resolved Acidic and Basic Molecular Functionalities. *ACS Catal.* **2018**, *8*, 2870−2879.
(292) Huang, Y.; Xu, S.; Lin, V. S. Y. Bifunctionalized Mesoporous Materials with Site-Separated Brønsted Acids and Bases: Catalyst for a Two-Step Reaction Sequence. *Angew. Chem., Int. Ed.* **2011**, *50*, 661−664.
(293) Gao, J.; Zhang, X.; Lu, Y.; Liu, S.; Liu, J. Selective Functionalization of Hollow Nanospheres with Acid and Base Groups for Cascade Reactions. *Chem.-Eur. J.* **2015**, *21*, 7403−7407.
(294) Cleveland, J. W.; Kumar, D. R.; Cho, J.; Jang, S. S.; Jones, C. W. Creation of discrete active site domains via mesoporous silica poly(styrene) composite materials for incompatible acid-base cascade reactions. *Catal. Sci. Technol.* **2021**, *11*, 1311−1322.
(295) Lee, L.-C.; Lu, J.; Weck, M.; Jones, C. W. Acid-Base Bifunctional Shell Cross-Linked Micelle Nanoreactor for One-Pot Tandem Reaction. *ACS Catal.* **2016**, *6*, 784−787.
(296) Jia, Z.; Wang, K.; Tan, B.; Gu, Y. Hollow Hyper-Cross-Linked Nanospheres with Acid and Base Sites as Efficient and Water-Stable Catalysts for One-Pot Tandem Reactions. *ACS Catal.* **2017**, *7*, 3693−3702.
(297) Lu, J.; Dimroth, J.; Weck, M. Compartmentalization of Incompatible Catalytic Transformations for Tandem Catalysis. *J. Am. Chem. Soc.* **2015**, *137*, 12984−12989.
(298) Qu, P.; Kuepfert, M.; Jockusch, S.; Weck, M. Compartmentalized Nanoreactors for One-Pot Redox-Driven Transformations. *ACS Catal.* **2019**, *9*, 2701−2706.
(299) Kandel, K.; Althaus, S. M.; Pruski, M.; Slowing, I. I. *Novel Materials for Catalysis and Fuels*; Bravo-Suárez, J. J., Kidder, M. K., Schwartz, V., Eds.; American Chemical Society: Washington, DC, 2013; Vol. *1132*.
(300) Liu, Y.; Liu, P.; Gao, S.; Wang, Z.; Luan, P.; González-Sabín, J.; Jiang, Y. Construction of chemoenzymatic cascade reactions for bridging chemocatalysis and Biocatalysis: Principles, strategies and prospective. *Chem. Eng. J.* **2021**, *420*, 127659.
(301) Barrett, C. J.; Chheda, J. N.; Huber, G. W.; Dumesic, J. A. Single-reactor process for sequential aldol-condensation and hydrogenation of biomass-derived compounds in water. *Appl. Catal. B* **2006**, *66*, 111−118.
(302) Chheda, J. N.; Dumesic, J. A. An overview of dehydration, aldol-condensation and hydrogenation processes for production of liquid alkanes from biomass-derived carbohydrates. *Catal. Today* **2007**, *123*, 59−70.
(303) Faba, L.; Díaz, E.; Ordóñez, S. One-pot Aldol Condensation and Hydrodeoxygenation of Biomass-derived Carbonyl Compounds for Biodiesel Synthesis. *ChemSusChem* **2014**, *7*, 2816−2820.
(304) Hübner, S.; de Vries, J. G.; Farina, V. Why Does Industry Not Use Immobilized Transition Metal Complexes as Catalysts? *Adv. Synth. Catal.* **2016**, *358*, 3−25.
(305) Gutmann, T.; Ratajczyk, T.; Xu, Y.; Breitzke, H.; Grünberg, A.; Dillenberger, S.; Bommerich, U.; Trantzschel, T.; Bernarding, J.; Buntkowsky, G. Understanding the leaching properties of heterogenized catalysts: A combined solid-state and PHIP NMR study. *Solid State Nuclear Magnetic Resonance* **2010**, *38*, 90−96.
(306) Tregubov, A. A.; Walker, D. B.; Vuong, K. Q.; Gooding, J. J.; Messerle, B. A. The advantages of covalently attaching organometallic catalysts to a carbon black support: recyclable Rh(i) complexes that deliver enhanced conversion and product selectivity. *Dalton Trans.* **2015**, *44*, 7917−7926.
(307) Li, X.; Ding, Y.; Jiao, G.; Li, J.; Ya, L.; Zhu, H. Hydroformylation of methyl-3-pentenoate over a phosphite ligand modified Rh/SiO_2 catalyst. *Journal of Natural Gas Chemistry* **2008**, *17*, 351−354.
(308) Sudheesh, N.; Chaturvedi, A. K.; Shukla, R. S. $RhCl(TPPTS)_3$ encapsulated into the hexagonal mesoporous silica as an efficient heterogeneous catalyst for hydroformylation of vinyl esters. *Appl. Catal. A* **2011**, *409-410*, 99−105.
(309) Li, C.; Wang, W.; Yan, L.; Ding, Y. A mini review on strategies for heterogenization of rhodium-based hydroformylation catalysts. *Front. Chem. Sci. Eng.* **2018**, *12*, 113−123.
(310) Cypryk, M.; Pospiech, P.; Strzelec, K.; Wasikowska, K.; Sobczak, J. W. Soluble polysiloxane-supported palladium catalysts for the Mizoroki-Heck reaction. *J. Mol. Catal. A: Chem.* **2010**, *319*, 30−38.
(311) Lamblin, M.; Nassar-Hardy, L.; Hierso, J.-C.; Fouquet, E.; Felpin, F.-X. Recyclable Heterogeneous Palladium Catalysts in Pure Water: Sustainable Developments in Suzuki, Heck, Sonogashira and Tsuji-Trost Reactions. *Adv. Synth. Catal.* **2010**, *352*, 33−79.
(312) Cantillo, D.; Kappe, C. O. Immobilized Transition Metals as Catalysts for Cross-Couplings in Continuous Flow—A Critical Assessment of the Reaction Mechanism and Metal Leaching. *ChemCatChem.* **2014**, *6*, 3286−3305.
(313) Nunes, C. D.; Valente, A. A.; Pillinger, M.; Fernandes, A. C.; Romão, C. C.; Rocha, J.; Gonçalves, I. S. MCM-41 functionalized with bipyridyl groups and its use as a support for oxomolybdenum(vi) catalysts. *J. Mater. Chem.* **2002**, *12*, 1735−1742.
(314) Kuzniarska-Biernacka, I.; Silva, A. R.; Carvalho, A. P.; Pires, J.; Freire, C. Anchoring of Chiral Manganese(III) Salen Complex onto Organo Clay and Porous Clay Heterostructure and Catalytic Activity in Alkene Epoxidation. *Catal. Lett.* **2010**, *134*, 63−71.
(315) Balcar, H.; Shinde, T.; Žilková, N.; Bastl, Z. Hoveyda-Grubbs type metathesis catalyst immobilized on mesoporous molecular sieves MCM-41 and SBA-15. *Beilstein Journal of Organic Chemistry* **2011**, *7*, 22−28.
(316) Bek, D.; Balcar, H.; Žilková, N.; Zukal, A.; Horáček, M.; Cejka, J. Grubbs Catalysts Immobilized on Mesoporous Molecular Sieves via Phosphine and Pyridine Linkers. *ACS Catal.* **2011**, *1*, 709−718.
(317) Khatri, P. K.; Choudhary, S.; Singh, R.; Jain, S. L.; Khatri, O. P. Grafting of a rhenium-oxo complex on Schiff base functionalized graphene oxide: an efficient catalyst for the oxidation of amines. *Dalton Trans.* **2014**, *43*, 8054−8061.
(318) Savini, A.; Bucci, A.; Nocchetti, M.; Vivani, R.; Idriss, H.; Macchioni, A. Activity and Recyclability of an Iridium-EDTA Water Oxidation Catalyst Immobilized onto Rutile TiO_2. *ACS Catal.* **2015**, *5*, 264−271.
(319) Guenther, J.; Reibenspies, J.; Blümel, J. Synthesis, Immobilization, MAS and HR-MAS NMR of a New Chelate Phosphine Linker System, and Catalysis by Rhodium Adducts Thereof. *Adv. Synth. Catal.* **2011**, *353*, 443−460.
(320) Srour, M.; Hadjiali, S.; Brunnengräber, K.; Weidler, H.; Xu, Y.; Breitzke, H.; Gutmann, T.; Buntkowsky, G. A Novel Wilkinson's Type Silica Supported Polymer Catalyst: Insights from Solid-State NMR and Hyperpolarization Techniques. *J. Phys. Chem. C* **2021**, *125*, 7178−7187.
(321) Choi, S.; Gray, M. L.; Jones, C. W. Amine-Tethered Solid Adsorbents Coupling High Adsorption Capacity and Regenerability

https://doi.org/10.1021/acs.chemrev.1c00905
Chem. Rev. XXXX, XXX, XXX−XXX

for CO_2 Capture From Ambient Air. *ChemSusChem* **2011**, *4*, 628−635.
(322) Marciniec, B.; Maciejewski, H. Transition metal-siloxide complexes; synthesis, structure and application to catalysis. *Coord. Chem. Rev.* **2001**, *223*, 301−335.
(323) Scott, S. L.; Mills, A.; Chao, C.; Basset, J.-M.; Millot, N.; Santini, C. C. Silica-supported rhodium hydrides stabilized by triisopropylphosphine. *J. Mol. Catal. A* **2003**, *204-205*, 457−463.
(324) Kelly, M. J.; Barthel, A.; Maheu, C.; Sodpiban, O.; Dega, F.-B.; Vummaleti, S. V. C.; Abou-Hamad, E.; Pelletier, J. D. A.; Cavallo, L.; D'Elia, V.; et al. Conversion of actual flue gas CO_2 via cycloaddition to propylene oxide catalyzed by a single-site, recyclable zirconium catalyst. *Journal of CO2 Utilization* **2017**, *20*, 243−252.
(325) Grekov, D.; Bouhoute, Y.; Szeto, K. C.; Merle, N.; De Mallmann, A.; Lefebvre, F.; Lucas, C.; Del Rosal, I.; Maron, L.; Gauvin, R. M.; et al. Silica-Supported Tungsten Neosilyl Oxo Precatalysts: Impact of the Podality on Activity and Stability in Olefin Metathesis. *Organometallics* **2016**, *35*, 2188−2196.
(326) Liu, J.; Groszewicz, P. B.; Wen, Q.; Thankamony, A. S. L.; Zhang, B.; Kunz, U.; Sauer, G.; Xu, Y.; Gutmann, T.; Buntkowsky, G. Revealing Structure Reactivity Relationships in Heterogenized Dirhodium Catalysts by Solid-State NMR Techniques. *J. Phys. Chem. C* **2017**, *121*, 17409−17416.
(327) Hatridge, T. A.; Liu, W.; Yoo, C.-J.; Davies, H. M. L.; Jones, C. W. Optimized Immobilization Strategy for Dirhodium(II) Carboxylate Catalysts for C-H Functionalization and Their Implementation in a Packed Bed Flow Reactor. *Angew. Chem., Int. Ed.* **2020**, *132*, 19693.
(328) Doyle, M. P.; Yan, M.; Gau, H.-M.; Blossey, E. C. Catalysts with Mixed Ligands on Immobilized Supports. Electronic and Steric Advantages. *Organic Letters* **2003**, *5*, 561−563.
(329) Davies, H. M. L.; Walji, A. M. Universal Strategy for the Immobilization of Chiral Dirhodium Catalysts. *Organic Letters* **2005**, *7*, 2941−2944.
(330) Sharma, N.; Dhankhar, S. S.; Nagaraja, C. M. Environment-friendly, co-catalyst- and solvent-free fixation of CO_2 using an ionic zinc(ii)-porphyrin complex immobilized in porous metal-organic frameworks. *Sustainable Energy & Fuels* **2019**, *3*, 2977−2982.
(331) Pan, Y.; Li, H.; Farmakes, J.; Xiao, F.; Chen, B.; Ma, S.; Yang, Z. How Do Enzymes Orient When Trapped on Metal-Organic Framework (MOF) Surfaces? *J. Am. Chem. Soc.* **2018**, *140*, 16032−16036.
(332) Yamaguchi, A.; Saiga, M.; Inaba, D.; Aizawa, M.; Shibuya, Y.; Itoh, T. Structural Characterization of Proteins Adsorbed at Nanoporous Materials. *Analytical Sciences* **2021**, *37*, 49−59.
(333) Kaposi, M.; Cokoja, M.; Hutterer, C. H.; Hauser, S. A.; Kaposi, T.; Klappenberger, F.; Pöthig, A.; Barth, J. V.; Herrmann, W. A.; Kühn, F. E. Immobilisation of a molecular epoxidation catalyst on UiO-66 and -67: the effect of pore size on catalyst activity and recycling. *Dalton Trans.* **2015**, *44*, 15976−15983.
(334) Polborn, K.; Severin, K. Biomimetic Catalysis with Immobilised Organometallic Ruthenium Complexes: Substrate- and Regioselective Transfer Hydrogenation of Ketones. *Chem.-Eur. J.* **2000**, *6*, 4604−4611.
(335) Liu, H.; Tian, Y.; Deng, Z. Morphology-Dependent Electrochemistry and Electrocatalytical Activity of Cytochrome c. *Langmuir* **2007**, *23*, 9487−9494.
(336) Smith, S. W. Chiral Toxicology: It's the Same Thing. . .Only Different. *Toxicol. Sci.* **2009**, *110*, 4−30.
(337) Collins, A. N.; Sheldrake, G. N.; Crosby, J. *Chirality in Industry: The Commercial Manufacture and Applications of Optically Active Compounds*; John Wiley: New York, 1995.
(338) Kasprzyk-Hordern, B. Pharmacologically active compounds in the environment and their chirality. *Chem. Soc. Rev.* **2010**, *39*, 4466−4503.
(339) Blaser, H.-U. Chirality and its implications for the pharmaceutical industry. *Rendiconti Lincei* **2013**, *24*, 213−216.
(340) Bonner, W. A. Chirality and life. *Origins of Life and Evolution of the Biosphere* **1995**, *25*, 175−190.
(341) Podlech, J. Origin of organic molecules and biomolecular homochirality. *CMLS, Cell. Mol. Life Sci.* **2001**, *58*, 44−60.
(342) Hazen, R. M. Mineral surfaces and the prebiotic selection and organization of biomolecules. *Am. Mineral.* **2006**, *91*, 1715−1729.
(343) Sholl, D. S.; Asthagiri, A.; Power, T. D. Naturally chiral metal surfaces as enantiospecific adsorbents. *J. Phys. Chem. B* **2001**, *105*, 4771−4782.
(344) Ernst, K.-H. Molecular chirality at surfaces. *Phys. Status Solidi B* **2012**, *249*, 2057−2088.
(345) Dutta, S.; Gellman, A. J. Enantiomer surface chemistry: conglomerate versus racemate formation on surfaces. *Chem. Soc. Rev.* **2017**, *46*, 7787.
(346) Gellman, A. J.; Tysoe, W. T.; Zaera, F. Surface Chemistry for Enantioselective Catalysis. *Catal. Lett.* **2015**, *145*, 220−232.
(347) Webb, G.; Wells, P. B. Asymmetric hydrogenation. *Catal. Today* **1992**, *12*, 319−337.
(348) Studer, M.; Blaser, H. U.; Exner, C. Enantioselective hydrogenation using heterogeneous modified catalysts: An update [Review]. *Adv. Synth. Catal.* **2003**, *345*, 45−65.
(349) Akabori, S.; Sakurai, S.; Izumi, Y.; Fujii, Y. Asymmetric catalyst. *Nature* **1956**, *178*, 323−324.
(350) Osawa, T.; Harada, T.; Takayasu, O. Progress of enantio-differentiating hydrogenation of prochiral ketones over asymmetrically modified nickel catalysts and a newly proposed enantio-differentiation model. *Top. Catal.* **2000**, *13*, 155−168.
(351) Osawa, T.; Lee, I. Y. S.; Ikeda, S.; Kitamura, T.; Inoue, Y.; Borovkov, V. Simplified preparation of chirally modified nickel catalyst for enantioselective hydrogenation: A step forward to industrial use. *Appl. Catal. A* **2012**, *445-446*, 269−273.
(352) Osawa, T.; Tanabe, Y.; Fujiwara, M. Sodium Ion as the Most Essential and Effective Element for the Enantio-Differentiating Hydrogenation of Prochiral Ketones over Tartaric Acid Modified Ni Catalyst. *Catal. Lett.* **2017**, *147*, 686−692.
(353) López-Martínez, M.-A.; Shannon, I. J. Tartaric acid-Ni supported catalysts obtained from hydrotalcite-like compounds: Effects of catalyst preparation variables on enantioselectivity. *Appl. Catal. A* **2012**, *435-436*, 123−130.
(354) Osawa, T.; Wakasugi, M.; Kizawa, T.; Borovkov, V.; Inoue, Y. Enantio-differentiating hydrogenation of alkyl 3-oxobutanoates over tartaric acid-modified Ni catalyst: Enthalpy-entropy compensation effect as a tool for elucidating mechanistic features. *Molecular Catalysis* **2018**, *449*, 131−136.
(355) Choliq, A. A.; Murakami, E.; Yamamoto, S.; Misaki, T.; Fujita, M.; Okamoto, Y.; Sugimura, T. Enantioselective Hydrogenation of Ketones over a Tartaric Acid-Modified Raney Nickel Catalyst: Substrate-Modifier Interaction Strength and Enantioselectivity. *Bull. Chem. Soc. Jpn.* **2018**, *91*, 1325−1332.
(356) Ernst, K. H. Supramolecular surface chirality. *Top. Curr. Chem.* **2006**, *265*, 209−252.
(357) Raval, R. Chiral expression from molecular assemblies at metal surfaces: Insights from surface science techniques. *Chem. Soc. Rev.* **2009**, *38*, 707−721.
(358) Schrader, I.; Neumann, S.; Šulce, A.; Schmidt, F.; Azov, V.; Kunz, S. Asymmetric Heterogeneous Catalysis: Transfer of Molecular Principles to Nanoparticles by Ligand Functionalization. *ACS Catal.* **2017**, *7*, 3979−3987.
(359) Ortega Lorenzo, M.; Baddeley, C. J.; Muryn, C.; Raval, R. Extended surface chirality from supramolecular assemblies of adsorbed chiral molecules. *Nature* **2000**, *404*, 376−379.
(360) Parschau, M.; Romer, S.; Ernst, K.-H. Induction of Homochirality in Achiral Enantiomorphous Monolayers. *J. Am. Chem. Soc.* **2004**, *126*, 15398−15399.
(361) Raval, R. Molecular assembly at surfaces: progress and challenges. *Faraday Disc.* **2017**, *204*, 9−33.
(362) Lee, I.; Ma, Z.; Kaneko, S.; Zaera, F. 1-(1-Naphthyl)-ethylamine adsorption on platinum surfaces: On the mechanism of chiral modification in catalysis. *J. Am. Chem. Soc.* **2008**, *130*, 14597−14604.

https://doi.org/10.1021/acs.chemrev.1c00905
Chem. Rev. XXXX, XXX, XXX−XXX

(363) Gordon, A. D.; Karakalos, S.; Zaera, F. Dependence of the adsorption of chiral compounds on their enantiomeric composition. *Surf. Sci.* **2014**, *629*, 3−10.
(364) Stacchiola, D.; Burkholder, L.; Tysoe, W. T. Enantioselective chemisorption on a chirally modified surface in ultrahigh vacuum: Adsorption of propylene oxide on 2-butoxide-covered palladium(111). *J. Am. Chem. Soc.* **2002**, *124*, 8984−8989.
(365) Lee, I.; Zaera, F. Enantioselectivity of adsorption sites created by chiral 2-butanol adsorbed on Pt(111) single-crystal surfaces. *J. Phys. Chem. B* **2005**, *109*, 12920−12926.
(366) Lee, I.; Zaera, F. Chiral Templating of Surfaces: Adsorption of 2-Methylbutanoic Acid on Pt(111) Single-Crystal Surfaces. *J. Am. Chem. Soc.* **2006**, *128*, 8890−8898.
(367) Stacchiola, D.; Burkholder, L.; Zheng, T.; Weinert, M.; Tysoe, W. T. Requirements for the formation of a chiral template. *J. Phys. Chem. B* **2005**, *109*, 851−856.
(368) Karakalos, S.; Lawton, T. J.; Lucci, F. R.; Sykes, E. C. H.; Zaera, F. Enantiospecific Kinetics in Surface Adsorption: Propylene Oxide on Pt(111) Surfaces. *J. Phys. Chem. C* **2013**, *117*, 18588−18594.
(369) Mahapatra, M.; Burkholder, L.; Devarajan, S. P.; Boscoboinik, A.; Garvey, M.; Bai, Y.; Tysoe, W. T. Formation of Induced-Fit Chiral Templates by Amino Acid-Functionalized Pd(111) Surfaces. *J. Phys. Chem. C* **2015**, *119*, 3556−3563.
(370) Therrien, A. J.; Lawton, T. J.; Mernoff, B.; Lucci, F. R.; Pushkarev, V. V.; Gellman, A. J.; Sykes, E. C. H. Chiral nanoscale pores created during the surface explosion of tartaric acid on Cu(111). *Chem. Commun.* **2016**, *52*, 14282−14285.
(371) Zaera, F. Chiral modification of solid surfaces: A molecular view. *J. Phys. Chem. C* **2008**, *112*, 16196−16203.
(372) Orito, Y.; Imai, S.; Niwa, S.; Nguyen, G. H. Asymmetric hydrogenation of methyl benzoylformate using platinum-carbon catalysts modified with cinchonidine. *J. Synth. Org. Chem. Jpn.* **1979**, *37*, 173−174.
(373) Orito, Y.; Imai, S.; Niwa, S. Asymmetric hydrogenation of a-keto esters using a platinum-alumina catalyst modified with cinchona alkaloid. *J. Chem. Soc. Jpn.* **1980**, 670−672.
(374) Wehrli, J. T.; Baiker, A.; Monti, D. M.; Blaser, H. U. Particle size effect on enantioselective hydrogenation of ethyl pyruvate over alumina-supported platinum catalyst. *J. Mol. Catal.* **1989**, *49*, 195−203.
(375) Wells, P. B.; Wilkinson, A. G. Platinum group metals as heterogeneous enantioselective catalysts. *Top. Catal.* **1998**, *5*, 39−50.
(376) LeBlond, C.; Wang, J.; Andrews, A. T.; Sun, Y.-K. Establishment and maintenance of an optimal chiral surface in cinchona-modified 1% Pt/Al_2O_3 for enantioselective hydrogenation of a-keto esters. *Top. Catal.* **2000**, *13*, 169−174.
(377) Bartók, M. Heterogeneous catalytic enantioselective hydrogenation of activated ketones. *Curr. Org. Chem.* **2006**, *10*, 1533−1567.
(378) Mallat, T.; Orglmeister, E.; Baiker, A. Asymmetric catalysis at chiral metal surfaces. *Chem. Rev.* **2007**, *107*, 4863−4890.
(379) Blaser, H.-U.; Studer, M. Cinchona-Modified Platinum Catalysts: From Ligand Acceleration to Technical Processes. *Acc. Chem. Res.* **2007**, *40*, 1348−1356.
(380) Kim, J.; Song, B.; Hwang, G.; Bang, Y.; Yun, Y. Platinum nanoparticles supported on mesocellular silica foams as highly efficient catalysts for enantioselective hydrogenation. *J. Catal.* **2019**, *373*, 306−313.
(381) LeBlond, C.; Wang, J.; Liu, J.; Andrews, A. T.; Sun, Y.-K. Highly enantioselective heterogeneously catalyzed hydrogenation of a-ketoesters under mild conditions. *J. Am. Chem. Soc.* **1999**, *121*, 4920−4921.
(382) Li, X.; Wells, R. P. K.; Wells, P. B.; Hutchings, G. J. New insights into the relationship between conversion and enantioselectivity for the asymmetric hydrogenation of alkyl pyruvate. *J. Catal.* **2004**, *221*, 653−656.
(383) Hutchings, G. J. Heterogeneous asymmetric catalysts: Strategies for achieving high enantioselection. *Annu. Rev. Mater. Res.* **2005**, *35*, 143−166.
(384) Mallat, T.; Szabo, S.; Schurch, M.; Gobel, U. W.; Baiker, A. Enantioselective hydrogenation of carbonyl compounds over Pd-Pt/alumina catalysts. *Catal. Lett.* **1997**, *47*, 221−227.
(385) Slipszenko, J. A.; Griffiths, S. P.; Johnston, P.; Simons, K. E.; Vermeer, W. A. H.; Wells, P. B. Enantioselective hydrogenation v. Hydrogenation of butane-2,3-dione and of 3-hydroxybutan-2-one catalyzed by cinchona-modified platinum. *J. Catal.* **1998**, *179*, 267−276.
(386) von Arx, M.; Mallat, T.; Baiker, A. Unprecedented selectivity behavior in the hydrogenation of an α,β-unsaturated ketone: hydrogenation of ketoisophorone over alumina-supported Pt and Pd. *J. Mol. Catal. A: Chem.* **1999**, *148*, 275−283.
(387) Szabo, A.; Kunzle, N.; Mallat, T.; Baiker, A. Enantioselective hydrogenation of pyrrolidine-2,3,5-triones over the Pt-cinchonidine system. *Tetrahedron: Asymmetry* **1999**, *10*, 61−76.
(388) Kim, B.; Nakatsuji, M.; Mameda, T.; Kubota, T.; Fujita, M.; Sugimura, T.; Okamoto, Y. Kinetic Analysis of Enantioselective Hydrogenation of 2,3-(E)-Diarylpropenoic Acids over a Chiral Cinchona Alkaloid-Modified Pd/C Catalyst. *Bull. Chem. Soc. Jpn.* **2020**, *93*, 163−175.
(389) Yasukawa, T.; Miyamura, H.; Kobayashi, S. Chiral metal nanoparticle-catalyzed asymmetric C-C bond formation reactions. *Chem. Soc. Rev.* **2014**, *43*, 1450−1461.
(390) Szori, K.; Szollosi, G.; Bartok, M. The enantioselective hydrogenation of 5,6-dihydro-2H-pyran-3-carboxylic acid over a cinchona alkaloid-modified palladium catalyst: asymmetric synthesis of a cockroach attractant. *New J. Chem.* **2008**, *32*, 1354−1358.
(391) Li, C.; Zhang, L.; Zheng, C.; Zheng, X.; Fu, H.; Chen, H.; Li, R. Heterogeneous asymmetric hydrogenation of heteroaromatic methyl ketones catalyzed by cinchona-modified iridium catalysts. *Tetrahedron: Asymmetry* **2014**, *25*, 821−824.
(392) Margitfalvi, J. L.; Marti, P.; Baiker, A.; Botz, L.; Sticher, O. Role of the modifier in the enantioselective hydrogenation of ethyl pyruvate over platinum/alumina catalyst. *Catal. Lett.* **1990**, *6*, 281−288.
(393) Wang, G.; Heinz, T.; Pfaltz, A.; Minder, B.; Mallat, T.; Baiker, A. New chiral modifiers for the enantioselective hydrogenation of ethyl pyruvate over Pt/Al_2O_3 catalyst. *J. Chem. Soc., Chem. Commun.* **1994**, 2047−2048.
(394) Minder, B.; Schürch, M.; Mallat, T.; Baiker, A. Chiral nitrogen compounds as new modifiers for the enantioselective hydrogenation of ethyl pyruvate. *Catal. Lett.* **1995**, *31*, 143−151.
(395) Schurch, M.; Heinz, T.; Aeschimann, R.; Mallat, T.; Pfaltz, A.; Baiker, A. Design of new modifiers for the enantioselective hydrogenation of ethyl pyruvate. *J. Catal.* **1998**, *173*, 187−195.
(396) Wells, P. B.; Simons, K. E.; Slipszenko, J. A.; Griffiths, S. P.; Ewing, D. F. Chiral environments at alkaloid-modified platinum surfaces. *J. Mol. Catal. A: Chem.* **1999**, *146*, 159−166.
(397) Colston, N. J.; Wells, R. P. K.; Wells, P. B.; Hutchings, G. J. Unexpected inversion in enantioselectivity in the hydrogenation N-acetyl dehydrophenylalanine methyl ester using cinchona-modified Pd/Al_2O_3 catalyst. *Catal. Lett.* **2005**, *103*, 117−120.
(398) Tálas, E.; Margitfalvi, J. L. Natural alkaloids and synthetic relatives as chiral templates of the Orito's reaction. *Chirality* **2010**, *22*, 3−15.
(399) Szollosi, G.; Balázsik, K.; Bucsi, I.; Bartók, T.; Bartók, M. Modifier-substrate interactions of various types in the Orito reaction: Reversal of the enantioselection in the hydrogenation of ketopantolactone on Pt modified by β-isocinchonine and O-phenylcinchonidine. *Catal. Commun.* **2013**, *32*, 81−85.
(400) Nakatsuji, M.; Fujita, M.; Okamoto, Y.; Sugimura, T. Kinetic analysis of the asymmetric hydrogenation of (E)-2,3-diphenylpropenoic acid over cinchonidine derivative-modified Pd/C: quinoline ring modification. *Catal. Sci. Technol.* **2020**, *10*, 6573−6582.
(401) Nakatsuji, M.; Kubota, T.; Fujita, M.; Okamoto, Y.; Sugimura, T. Effect of Methyl-substitution of the Quinoline Ring of Cinchona Alkaloids on the Performance as a Modifier for the Enantioselective Hydrogenation of (E)-2,3-di(4-methoxyphenyl)propenoic Acid Over Pd/C: Kinetic Analysis. *Catal. Lett.* **2021**, *151*, 863−874.

https://doi.org/10.1021/acs.chemrev.1c00905
Chem. Rev. XXXX, XXX, XXX−XXX

(402) Gyorffy, N.; Tungler, A.; Fodor, M. Stereodifferentiation in heterogeneous catalytic hydrogenation. Kinetic resolution and asymmetric hydrogenation in the presence of (S)-proline: Catalyst-dependent processes. *J. Catal.* **2010**, *270*, 2−8.
(403) Rodríguez-García, L.; Hungerbühler, K.; Baiker, A.; Meemken, F. Enantioselection on Heterogeneous Noble Metal Catalyst: Proline-Induced Asymmetry in the Hydrogenation of Isophorone on Pd Catalyst. *J. Am. Chem. Soc.* **2015**, *137*, 12121.
(404) Ruggera, J. F.; Merlo, A. B.; Diez, R. P.; Casella, M. L. Experimental and theoretical investigation of the enantioselective hydrogenation of ethyl pyruvate with a Pt catalyst with new non-cinchona chiral modifiers. *J. Mol. Catal. A: Chem.* **2016**, *423*, 233−239.
(405) Attard, G. A.; Ahmadi, A.; Jenkins, D. J.; Hazzazi, O. A.; Wells, P. B.; Griffin, K. G.; Johnston, P.; Gillies, J. E. The characterisation of supported platinum nanoparticles on carbon used for enantioselective hydrogenation: A combined electrochemical - STM approach. *ChemPhysChem* **2003**, *4*, 123−130.
(406) Wehrli, J. T.; Baiker, A.; Monti, D. M.; Blaser, H. U.; Jalett, H. P. Enantioselective hydrogenation of a-ketoesters: influence of reaction medium and conversion. *J. Mol. Catal.* **1989**, *57*, 245−257.
(407) Minder, B.; Mallat, T.; Pickel, K. H.; Steiner, K.; Baiker, A. Enantioselective hydrogenation of ethyl pyruvate in supercritical fluids. *Catal. Lett.* **1995**, *34*, 1−9.
(408) Bürgi, T.; Baiker, A. Conformational Behavior of Cinchonidine in Different Solvents: A Combined NMR and ab Initio Investigation. *J. Am. Chem. Soc.* **1998**, *120*, 12920−12926.
(409) Margitfalvi, J. L.; Tálas, E. Anomalous behavior of rigid cinchona alkaloids in the enantioselective hydrogenation of ethyl pyruvate in an aprotic solvent. *Appl. Catal. A* **2006**, *301*, 187−195.
(410) Meheux, P. A.; Ibbotson, A.; Wells, P. B. Enantioselective hydrogenation. II. Variation of activity and optical yield with experimental variables in methyl pyruvate hydrogenation catalyzed by cinchona-modified platinum/silica (EUROPT-1). *J. Catal.* **1991**, *128*, 387−396.
(411) Minder, B.; Mallat, T.; Skrabal, P.; Baiker, A. Enantioselective hydrogenation of ethyl pyruvate. Influence of oxidative treatment of cinchonidine-modified platinum catalyst and hemiketal formation in alcoholic solvents. *Catal. Lett.* **1994**, *29*, 115−124.
(412) Wang, J.; Leblond, C.; Orella, C. F.; Sun, Y.; Bradley, J. S.; Blackmond, D. G. *Heterogeneous Catalysis and Fine Chemicals IV: Proceedings of the 4th International Symposium on Heterogeneous Catalysis and Fine Chemicals, Basel, Switzerland, September 8-12, 1996*; Blaser, H. U., Baiker, A., Prins, R., Eds.; Elsevier: Amsterdam, 1997; Vol. *108*.
(413) Blaser, H. U.; Jalett, H. P.; Monti, D. M.; Baiker, A.; Wehrli, J. T. Enantioselective hydrogenation of ethyl pyruvate: effect of catalyst and modifier structure. *Stud. Surf. Sci. Catal.* **1991**, *67*, 147−155.
(414) Balázsik, K.; Cserényi, S.; Szollosi, G.; Fülöp, F.; Bartók, M. New Data on the Orito Reaction: Effect of Substrate Structure on Nonlinear Phenomenon. *Catal. Lett.* **2008**, *125*, 401−407.
(415) Schmidt, E.; Vargas, A.; Mallat, T.; Baiker, A. Shape-Selective Enantioselective Hydrogenation on Pt Nanoparticles. *J. Am. Chem. Soc.* **2009**, *131*, 12358−12367.
(416) Attard, G. A.; Alabdulrahman, A. M. S.; Jenkins, D. J.; Johnston, P.; Griffin, K. G.; Wells, P. B. Restructuring Effects in the Platinum-Catalysed Enantioselective Hydrogenation of Ethyl Pyruvate. *Top. Catal.* **2021**, *64*, 945.
(417) Reyes, P.; Campos, C.; Fierro, J. L. G. Preparation of chiral organic-inorganic solid hybrids. Use as support of catalysts in the enantioselective hydrogenation of ethyl pyruvate. *J. Chil. Chem. Soc.* **2007**, *52*, 1249−1253.
(418) Weng, Z.; Zaera, F. Increase in Activity and Selectivity in Catalysis via Surface Modification with Self-Assembled Monolayers. *J. Phys. Chem. C* **2014**, *118*, 3672−3679.
(419) Campos, C. H.; Torres, C. C.; Leyton, A.; Belmar, J.; Mella, C.; Osorio-Vargas, P.; Ruiz, D.; Fierro, J. L. G.; Reyes, P. A new non-cinchona chiral modifier immobilized on Pt/SiO_2 catalysts for enantioselective heterogeneous hydrogenation. *Appl. Catal. A* **2015**, *498*, 76−87.
(420) Dong, Y.; Goubert, G.; Groves, M. N.; Lemay, J.-C.; Hammer, B.; McBreen, P. H. Structure and Dynamics of Individual Diastereomeric Complexes on Platinum: Surface Studies Related to Heterogeneous Enantioselective Catalysis. *Acc. Chem. Res.* **2017**, *50*, 1163−1170.
(421) Rodríguez-García, L.; Hungerbühler, K.; Baiker, A.; Meemken, F. Discrimination of active species in liquid-phase hydrogenation on supported noble metal catalyst: An operando spectroscopic study on the asymmetric hydrogenation of ketopantolactone on Pt/Al2O3 and Pt/C modified by cinchonidine. *Catal. Today* **2017**, *283*, 66−73.
(422) Boscoboinik, J. A.; Bai, Y.; Burkholder, L.; Tysoe, W. T. Structure and distribution of S-α-(1-naphthyl)-ethylamine on Pd(111). *J. Phys. Chem. C* **2011**, *115*, 16488−16494.
(423) Demers-Carpentier, V.; Goubert, G.; Masini, F.; Lafleur-Lambert, R.; Dong, Y.; Lavoie, S.; Mahieu, G.; Boukouvalas, J.; Gao, H.; Rasmussen, A. M. H.; et al. Direct Observation of Molecular Preorganization for Chirality Transfer on a Catalyst Surface. *Science* **2011**, *334*, 776−780.
(424) Attia, S.; Spadafora, E. J.; Schmidt, M. C.; Schröder, C.; Baumann, A.-K.; Schauermann, S. Adsorption geometry and self-assembling of chiral modifier (R)-(+)-1-(1-naphthylethylamine) on Pt(111). *Phys. Chem. Chem. Phys.* **2020**, *22*, 15696−15706.
(425) Lavoie, S.; Laliberté, M.-A.; McBreen, P. H. Adsorption States and Modifier-Substrate Interactions on Pt(111) Relevant to the Enantioselective Hydrogenation of Alkyl Pyruvates in the Orito Reaction. *J. Am. Chem. Soc.* **2003**, *125*, 15756−15757.
(426) Burkholder, L.; Stacchiola, D.; Boscoboinik, J. A.; Tysoe, W. T. Enantioselective chemisorption on model chirally modified surfaces: 2-Butanol on α-(1-naphthyl)ethylamine/Pd(111). *J. Phys. Chem. C* **2009**, *113*, 13877−13885.
(427) Zeng, Y.; Masini, F.; Rasmussen, A. M. H.; Groves, M. N.; Albert, V.; Boukouvalas, J.; McBreen, P. H. The most stable adsorption geometries of two chiral modifiers on Pt(111). *Surf. Sci.* **2018**, *676*, 17−22.
(428) Bonello, J. M.; Sykes, E. C. H.; Lindsay, R.; Williams, F. J.; Santra, A. K.; Lambert, R. M. Fundamental aspects of enantioselective heterogeneous catalysis: a NEXAFS study of methyl pyruvate and (S)-(−)-1-(1-naphthyl) ethylamine on Pt{1 1 1}. *Surf. Sci.* **2001**, *482-485*, 207−214.
(429) Bonello, J. M.; Williams, F. J.; Lambert, R. M. Aspects of enantioselective heterogeneous catalysis: Structure and reactivity of (S)-(−)-1-(1-naphthyl)ethylamine on Pt{111}. *J. Am. Chem. Soc.* **2003**, *125*, 2723−2729.
(430) Dementyev, P.; Peter, M.; Adamovsky, S.; Schauermann, S. Chirally-modified metal surfaces: energetics of interaction with chiral molecules. *Phys. Chem. Chem. Phys.* **2015**, *17*, 22726−22735.
(431) Vargas, A.; Santarossa, G.; Iannuzzi, M.; Baiker, A. Chiral recognition on catalytic surfaces: Theoretical insight in a biomimetic heterogeneous catalytic system. *J. Phys. Chem. C* **2008**, *112*, 10200−10208.
(432) Simons, K. E.; Meheux, P. A.; Griffiths, S. P.; Sutherland, I. M.; Johnston, P.; Wells, P. B.; Carley, A. F.; Rajumon, M. K.; Roberts, M. W.; Ibbotson, A. A model for the enantioselective hydrogenation of pyruvate catalyzed by alkaloid-modified platinum. *Recl. Trav. Chim. Pays-Bas* **1994**, *113*, 465−474.
(433) Zaera, F.; Gellman, A. J.; Somorjai, G. A. Surface science studies of catalysis: classification of reactions. *Acc. Chem. Res.* **1986**, *19*, 24−31.
(434) Ferri, D.; Bürgi, T.; Baiker, A. Molecular Interaction between Cinchonidine and Acetic Acid Studied by NMR, FTIR and Ab Initio Methods. *J. Chem. Soc., Perkin Trans. 2* **1999**, 1305−1311.
(435) Balazs, L.; Mallat, T.; Baiker, A. Nonlinear phenomenon in heterogeneous enantioselective catalysis. *J. Catal.* **2005**, *233*, 327−332.
(436) Baiker, A. Progress in asymmetric heterogeneous catalysis: Design of novel chirally modified platinum metal catalysts. *J. Mol. Catal. A: Chem.* **1997**, *115*, 473−493.

https://doi.org/10.1021/acs.chemrev.1c00905
Chem. Rev. XXXX, XXX, XXX−XXX

(437) Burgi, T.; Baiker, A. Heterogeneous enantioselective hydrogenation over cinchona alkaloid modified platinum: mechanistic insights into a complex reaction. *Acc. Chem. Res.* **2004**, *37*, 909−917.
(438) Lavoie, S.; Laliberte, M. A.; Temprano, I.; McBreen, P. H. A generalized two-point H-bonding model for catalytic stereoselective hydrogenation of activated ketones on chirally modified platinum. *J. Am. Chem. Soc.* **2006**, *128*, 7588−7593.
(439) Booth, T. D.; Wahnon, D.; Wainer, I. W. Is Chiral Recognition a Three-Point Process. *Chirality* **1997**, *9*, 96−98.
(440) Mahapatra, M.; Burkholder, L.; Garvey, M.; Bai, Y.; Saldin, D. K.; Tysoe, W. T. Enhanced hydrogenation activity and diastereomeric interactions of methyl pyruvate co-adsorbed with R-1-(1-naphthyl)-ethylamine on Pd(111). *Nat. Commun.* **2016**, *7*, 12380.
(441) Lemay, J.-C.; Dong, Y.; Albert, V.; Inouye, M.; Groves, M. N.; Boukouvalas, J.; McBreen, P. H. Relative Abundances of Surface Diastereomeric Complexes Formed by Two Chiral Modifiers That Differ by a Methyl Group. *ACS Catal.* **2020**, *10*, 3034−3041.
(442) Groves, M. N.; Goubert, G.; Rasmussen, A. M. H.; Dong, Y.; Lemay, J. C.; Demers-Carpentier, V.; McBreen, P. H.; Hammer, B. Structure determination of chemisorbed chirality transfer complexes: Accelerated STM analysis and exchange-correlation functional sensitivity. *Surf. Sci.* **2014**, *629*, 48−56.
(443) Nitta, Y.; Kubota, T.; Okamoto, Y. Effect of palladium dispersion on the enantioselective hydrogenation of.alpha.,.beta.-unsaturated acids with modified Pd/TiO2 catalysts. *Bull. Chem. Soc. Jpn.* **2001**, *74*, 2161−2165.
(444) Jenkins, D. J.; Alabdulrahman, A. M. S.; Attard, G. A.; Griffin, K. G.; Johnston, P.; Wells, P. B. Enantioselectivity and catalyst morphology: Step and terrace site contributions to rate and enantiomeric excess in Pt-catalysed ethyl pyruvate hydrogenation. *J. Catal.* **2005**, *234*, 230−239.
(445) Attard, G. A.; Griffin, K. G.; Jenkins, D. J.; Johnston, P.; Wells, P. B. Enantioselective hydrogenation of ethyl pyruvate catalysed by Pt/graphite: Superior performance of sintered metal particles. *Catal. Today* **2006**, *114*, 346−352.
(446) Kubota, J.; Ma, Z.; Zaera, F. In-situ characterization of adsorbates in solid-liquid interfaces by reflection-absorption infrared spectroscopy. *Langmuir* **2003**, *19*, 3371−3376.
(447) Chu, W.; LeBlanc, R. J.; Williams, C. T.; Kubota, J.; Zaera, F. Vibrational band assignments for the chiral modifier cinchonidine: Implications for surface studies. *J. Phys. Chem. B* **2003**, *107*, 14365−14373.
(448) Ma, Z.; Lee, I.; Kubota, J.; Zaera, F. In-situ characterization of the adsorption of cinchona chiral modifiers on platinum surfaces. *J. Mol. Catal. A: Chem.* **2004**, *216*, 199−207.
(449) Ma, Z.; Lee, I.; Zaera, F. Factors controlling adsorption equilibria from solution onto solid surfaces: The uptake of cinchona alkaloids on platinum surfaces. *J. Am. Chem. Soc.* **2007**, *129*, 16083−16090.
(450) Zaera, F. Infrared absorption spectroscopy characterization of liquid-solid interfaces: The case of chiral modification of catalysts. *Surf. Sci.* **2018**, *669*, 16−24.
(451) Kubota, J.; Zaera, F. Adsorption geometry of modifiers as key in imparting chirality to platinum catalysts. *J. Am. Chem. Soc.* **2001**, *123*, 11115−11116.
(452) Rodríguez-García, L.; Hungerbühler, K.; Baiker, A.; Meemken, F. The Critical Role of Tilted Cinchona Surface Species for Enantioselective Hydrogenation. *ACS Catal.* **2017**, *7*, 3799−3809.
(453) Gordon, A. D.; Zaera, F. Adsorption of 1-(1-Naphthyl)-ethylamine from Solution onto Platinum Surfaces: Implications for the Chiral Modification of Heterogeneous Catalysts. *Angew. Chem., Int. Ed.* **2013**, *52*, 3453−3456.
(454) Ni, Y.; Gordon, A. D.; Tanicala, F.; Zaera, F. Correlation Between Chiral Modifier Adsorption and Enantioselectivity in Hydrogenation Catalysis. *Angew. Chem., Int. Ed.* **2017**, *56*, 7963−7966.
(455) Dijkstra, G. D. H.; Kellogg, R. M.; Wynberg, H.; Svendsen, J. S.; Marko, I.; Sharpless, K. B. Conformational study of cinchona alkaloids. A combined NMR, molecular mechanics and x-ray approach. *J. Am. Chem. Soc.* **1989**, *111*, 8069−8076.
(456) Oleksyn, B. J.; Suszko-Purzycka, A.; Dive, G.; Lamotte-Brasseur, J. Molecular properties of Cinchona alkaloids: A theoretical approach. *J. Pharm. Sci.* **1992**, *81*, 122−127.
(457) Mink, L.; Ma, Z.; Olsen, R. A.; James, J. N.; Sholl, D. S.; Mueller, L. J.; Zaera, F. The physico-chemical properties of cinchona alkaloids responsible for their unique performance in chiral catalysis. *Top. Catal.* **2008**, *48*, 120−127.
(458) Lai, J.; Ma, Z.; Mink, L.; Mueller, L. J.; Zaera, F. Influence of Peripheral Groups on the Physical and Chemical Behavior of Cinchona Alkaloids. *J. Phys. Chem. B* **2009**, *113*, 11696−11701.
(459) Taskinen, A.; Nieminen, V.; Hotokka, M.; Murzin, D. Y. The role of modifier structure in heterogeneous enantioselective hydrogenation: One-to-one interactions of 1-phenyl-1,2-propanedione and methyl pyruvate with modifiers on the Pt(111) surface. *J. Phys. Chem. C* **2007**, *111*, 5128−5140.
(460) Schmidt, E.; Ferri, D.; Vargas, A.; Baiker, A. Chiral modification of Rh and Pt surfaces: Effect of rotational flexibility of cinchona-type modifiers on their adsorption behavior. *J. Phys. Chem. C* **2008**, *112*, 3866−3874.
(461) Ma, Z.; Zaera, F. Role of the solvent in the adsorption-desorption equilibrium of cinchona alkaloids between solution and a platinum surface: Correlations among solvent polarity, cinchona solubility, and catalytic performance. *J. Phys. Chem. B* **2005**, *109*, 406−414.
(462) Ni, Y.; Wang, Z.; Lee, I.; Zaera, F. Adsorption of Chiral Modifiers from Solution onto Supported Platinum Catalysts: The Effect of the Solvent, Other Coadsorbates, and the Support. *J. Phys. Chem. C* **2020**, *124*, 7903−7913.
(463) Blaser, H. U.; Imhof, D.; Studer, M. Kinetic modeling of the ligand accelerated catalysis in the enantioselective hydrogenation of ethyl pyruvate: influence of solvents, catalysts and additives. *Stud. Surf. Sci. Catal.* **1997**, *108*, 175−182.
(464) Collier, P. J.; Hall, T. J.; Iggo, J. A.; Johnston, P.; Slipszenko, J. A.; Wells, P. B.; Whyman, R.; et al. Solvent and substituent effects on the sense of the enantioselective hydrogenation of pyruvate esters catalyzed by Pd and Pt in colloidal and supported forms. *Chem. Commun.* **1998**, 1451−1452.
(465) Gamez, A.; Köhler, J.; Bradley, J. Solvent Effects in the Kinetics of the Enantioselective Hydrogenation of Ethyl Pyruvate. *Catal. Lett.* **1998**, *55*, 73−77.
(466) Wells, R. P. K.; McGuire, N. R.; Li, X. B.; Jenkins, R. L.; Collier, P. J.; Whyman, R.; Hutchings, G. J. The effect of water on the enantioselective hydrogenation of ethyl pyruvate and butane-2,3-dione using cinchona-modified Pt/Al2O3. *Phys. Chem. Chem. Phys.* **2002**, *4*, 2839−2845.
(467) Martin, G.; Mäki-Arvela, P.; Murzin, D. Y.; Salmi, T. Solvent Effects in the Enantioselective Hydrogenation of Ethyl Benzoylformate. *Catal. Lett.* **2013**, *143*, 1051−1060.
(468) Meier, D. M.; Mallat, T.; Ferri, D.; Baiker, A. Competition of chiral modifiers on platinum: A transient catalytic and in situ ATR-IR study in continuous reactors. *J. Catal.* **2006**, *244*, 260−263.
(469) Ma, Z.; Zaera, F. Competitive chemisorption between pairs of cinchona alkaloids and related compounds from solution onto platinum surfaces. *J. Am. Chem. Soc.* **2006**, *128*, 16414−16415.
(470) Schmidt, E.; Bucher, C.; Santarossa, G.; Mallat, T.; Gilmour, R.; Baiker, A. Fundamental insights into the enantioselectivity of hydrogenations on cinchona-modified platinum and palladium. *J. Catal.* **2012**, *289*, 238−248.
(471) Bonalumi, N.; Vargas, A.; Ferri, D.; Bürgi, T.; Mallat, T.; Baiker, A. Competition at chiral metal surfaces: Fundamental aspects of the inversion of enantioselectivity in hydrogenations on platinum. *J. Am. Chem. Soc.* **2005**, *127*, 8467−8477.
(472) Bartók, M.; Sutyinszki, M.; Balázsik, K.; Szöllodblacsi, G. Enantioselective hydrogenation of ethyl pyruvate catalysed by cinchonine-modified Pt/Al_2O_3: tilted adsorption geometry of cinchonine. *Catal. Lett.* **2005**, *100*, 161−167.

https://doi.org/10.1021/acs.chemrev.1c00905
Chem. Rev. XXXX, XXX, XXX−XXX

(473) Balázsik, K.; Szöllosi, G.; Bartók, M. New Data of Nonlinear Phenomenon in the Heterogeneous Enantioselective Hydrogenation of Activated Ketones. *Catal. Lett.* **2008**, *124*, 46.
(474) Szori, K.; Balázsik, K.; Cserényi, S.; Szollosi, G.; Bartók, M. Inversion of enantioselectivity in the 2,2,2-trifluoroacetophenone hydrogenation over Pt-alumina catalyst modified by cinchona alkaloids. *Appl. Catal. A* **2009**, *362*, 178−184.
(475) Bartók, M. Unexpected Inversions in Asymmetric Reactions: Reactions with Chiral Metal Complexes, Chiral Organocatalysts, and Heterogeneous Chiral Catalysts. *Chem. Rev.* **2010**, *110*, 1663−1705.
(476) Diezi, S.; Mallat, T.; Szabo, A.; Baiker, A. Fine tuning the "chiral sites" on solid enantioselective catalysts. *J. Catal.* **2004**, *228*, 162−173.
(477) Li, C.; Zhang, L.; Liu, H.; Zheng, X.; Fu, H.; Chen, H.; Li, R. Heterogeneous asymmetric hydrogenation of aromatic ketones enhanced by silanols on highly monodispersed silica spheres. *Catal. Commun.* **2014**, *54*, 27−30.
(478) Ma, Z.; Kubota, J.; Zaera, F. The influence of dissolved gases on the adsorption of cinchonidine from solution onto a platinum surface: and in-situ infrared spectroscopy study. *J. Catal.* **2003**, *219*, 404−416.
(479) LeBlanc, R. J.; Chu, W.; Williams, C. T. Surface Raman characterization of cinchonidine-modified platinum in ethanol: effects of liquid-phase concentration and co-adsorbed hydrogen. *J. Mol. Catal. A: Chem.* **2004**, *212*, 277−289.
(480) Motobayashi, K.; Tomioka, R.; Uchida, T.; Osawa, M. Effect of Hydrogen on the Orientation of Cinchonidine Adsorbed on Platinum: An ATR-SEIRAS Study. *Chem. Lett.* **2015**, *44*, 770−772.
(481) Blaser, H. U.; Jalett, H. P.; Wiehl, J. Enantioselective hydrogenation of a-keto esters with cinchona-modified platinum catalysts: effect of acidic and basic solvents and additives. *J. Mol. Catal.* **1991**, *68*, 215−222.
(482) Vargas, A.; Ferri, D.; Baiker, A. DFT and ATR-IR insight into the conformational flexibility of cinchonidine adsorbed on platinum: Proton exchange with metal. *J. Catal.* **2005**, *236*, 1−8.
(483) Olsen, R. A.; Borchardt, D.; Mink, L.; Agarwal, A.; Mueller, L. J.; Zaera, F. Effect of protonation on the conformation of cinchonidine. *J. Am. Chem. Soc.* **2006**, *128*, 15594−15595.
(484) Heitbaum, M.; Glorius, F.; Escher, I. Asymmetric heterogeneous catalysis. *Angew. Chem., Int. Ed.* **2006**, *45*, 4732−4762.
(485) Lv, B.; Lei, C.; Ren, F.; Wang, M.; Hua, F.; Meng, S.; Yang, Y.; Yang, Z.; Lei, Z. Asymmetric Hydrogenation of Acetophenone Catalyzed by Chirally Modified Ruthenium Nanoparticles Supported on Carbon Nanotubes. *ChemistrySelect* **2020**, *5*, 11803−11810.
(486) Cui, H.-Z.; Zhang, Z.-M.; Zhang, H.; Reheman, A.; Hong, X.; Zhan, B.; Zhang, J.; Hou, X.-F. Mesocellular silica foams supported size-controlled Pd nanoparticles for racemic and asymmetric iodomethyl dihydrobenzofuran synthesis. *Microporous and Mesoporous Materials* **2021**, *322*, 111157.
(487) Cano, I.; Tschan, M. J. L.; Martínez-Prieto, L. M.; Philippot, K.; Chaudret, B.; van Leeuwen, P. W. N. M. Enantioselective hydrogenation of ketones by iridium nanoparticles ligated with chiral secondary phosphine oxides. *Catal. Sci. Technol.* **2016**, *6*, 3758−3766.
(488) Ranganath, K. V. S.; Kloesges, J.; Schäfer, A. H.; Glorius, F. Asymmetric Nanocatalysis: N-Heterocyclic Carbenes as Chiral Modifiers of Fe_3O_4/Pd nanoparticles. *Angew. Chem., Int. Ed.* **2010**, *49*, 7786−7789.
(489) Choudary, B. M.; Kantam, M. L.; Ranganath, K. V. S.; Mahendar, K.; Sreedhar, B. Bifunctional Nanocrystalline MgO for Chiral Epoxy Ketones via Claisen-Schmidt Condensation-Asymmetric Epoxidation Reactions. *J. Am. Chem. Soc.* **2004**, *126*, 3396−3397.
(490) Choudary, B. M.; Ranganath, K. V. S.; Pal, U.; Kantam, M. L.; Sreedhar, B. Nanocrystalline MgO for Asymmetric Henry and Michael Reactions. *J. Am. Chem. Soc.* **2005**, *127*, 13167−13171.
(491) Liu, H.; Bayat, N.; Iglesia, E. Site Titration with Organic Bases During Catalysis: Selectivity Modifier and Structural Probe in Methanol Oxidation on Keggin Clusters. *Angew. Chem., Int. Ed.* **2003**, *42*, 5072−5075.
(492) Moeller, K. D. Synthetic Applications of Anodic Electrochemistry. *Tetrahedron* **2000**, *56*, 9527−9554.
(493) Hammerich, O.; Speiser, B. *Organic electrochemistry, fifth ed.: Revised and expanded*; CRC Press, 2015.
(494) Möhle, S.; Zirbes, M.; Rodrigo, E.; Gieshoff, T.; Wiebe, A.; Waldvogel, S. R. Modern Electrochemical Aspects for the Synthesis of Value-Added Organic Products. *Angew. Chem., Int. Ed.* **2018**, *57*, 6018−6041.
(495) Yan, M.; Kawamata, Y.; Baran, P. S. Synthetic Organic Electrochemical Methods Since 2000: On the Verge of a Renaissance. *Chem. Rev.* **2017**, *117*, 13230−13319.
(496) Schäfer, H. J. Anodic and Cathodic CC-Bond Formation. *Angew. Chem., Int. Ed.* **1981**, *20*, 911−934.
(497) Nepomnyashchii, A. B.; Bröring, M.; Ahrens, J.; Bard, A. J. Chemical and Electrochemical Dimerization of BODIPY Compounds: Electrogenerated Chemiluminescent Detection of Dimer Formation. *J. Am. Chem. Soc.* **2011**, *133*, 19498−19504.
(498) Kirste, A.; Elsler, B.; Schnakenburg, G.; Waldvogel, S. R. Efficient Anodic and Direct Phenol-Arene C,C Cross-Coupling: The Benign Role of Water or Methanol. *J. Am. Chem. Soc.* **2012**, *134*, 3571−3576.
(499) Perkins, R. J.; Xu, H.-C.; Campbell, J. M.; Moeller, K. D. Anodic coupling of carboxylic acids to electron-rich double bonds: A surprising non-Kolbe pathway to lactones. *Beilstein Journal of Organic Chemistry* **2013**, *9*, 1630−1636.
(500) Stang, C.; Harnisch, F. The Dilemma of Supporting Electrolytes for Electroorganic Synthesis: A Case Study on Kolbe Electrolysis. *ChemSusChem* **2016**, *9*, 50−60.
(501) Waldvogel, S. R.; Lips, S.; Selt, M.; Riehl, B.; Kampf, C. J. Electrochemical Arylation Reaction. *Chem. Rev.* **2018**, *118*, 6706−6765.
(502) Mihelcic, J.; Moeller, K. D. Oxidative Cyclizations: The Asymmetric Synthesis of (−)-Alliacol A. *J. Am. Chem. Soc.* **2004**, *126*, 9106−9111.
(503) Fuchigami, T.; Inagi, S. *Organic Electrochemistry, Fifth ed.: Revised and Expanded*; Hammerich, O., Speiser, B., Eds.; CRC Press: Boca Raton, 2015.
(504) Wen, J.; Shi, W.; Zhang, F.; Liu, D.; Tang, S.; Wang, H.; Lin, X.-M.; Lei, A. Electrooxidative Tandem Cyclization of Activated Alkynes with Sulfinic Acids To Access Sulfonated Indenones. *Organic Letters* **2017**, *19*, 3131−3134.
(505) Jiang, Y.; Xu, K.; Zeng, C. Use of Electrochemistry in the Synthesis of Heterocyclic Structures. *Chem. Rev.* **2018**, *118*, 4485−4540.
(506) Francke, R.; Little, R. D. Redox catalysis in organic electrosynthesis: basic principles and recent developments. *Chem. Soc. Rev.* **2014**, *43*, 2492−2521.
(507) Cheung, K.-C.; Wong, W.-L.; Ma, D.-L.; Lai, T.-S.; Wong, K.-Y. Transition metal complexes as electrocatalysts—Development and applications in electro-oxidation reactions. *Coord. Chem. Rev.* **2007**, *251*, 2367−2385.
(508) Sauer, G. S.; Lin, S. An Electrocatalytic Approach to the Radical Difunctionalization of Alkenes. *ACS Catal.* **2018**, *8*, 5175−5187.
(509) Siu, J. C.; Fu, N.; Lin, S. Catalyzing Electrosynthesis: A Homogeneous Electrocatalytic Approach to Reaction Discovery. *Acc. Chem. Res.* **2020**, *53*, 547−560.
(510) Spendelow, J. S.; Wieckowski, A. Electrocatalysis of oxygen reduction and small alcohol oxidation in alkaline media. *Phys. Chem. Chem. Phys.* **2007**, *9*, 2654−2675.
(511) Rabis, A.; Rodriguez, P.; Schmidt, T. J. Electrocatalysis for Polymer Electrolyte Fuel Cells: Recent Achievements and Future Challenges. *ACS Catal.* **2012**, *2*, 864−890.
(512) Francke, R.; Schille, B.; Roemelt, M. Homogeneously Catalyzed Electroreduction of Carbon Dioxide—Methods, Mechanisms, and Catalysts. *Chem. Rev.* **2018**, *118*, 4631−4701.
(513) Nam, D.-H.; De Luna, P.; Rosas-Hernández, A.; Thevenon, A.; Li, F.; Agapie, T.; Peters, J. C.; Shekhah, O.; Eddaoudi, M.;

https://doi.org/10.1021/acs.chemrev.1c00905
Chem. Rev. XXXX, XXX, XXX−XXX

Sargent, E. H. Molecular enhancement of heterogeneous CO_2 reduction. *Nat. Mater.* **2020**, *19*, 266−276.
(514) Shen, Y.; Atobe, M.; Fuchigami, T. Electroorganic Synthesis Using a Fluoride Ion Mediator under Ultrasonic Irradiation:1 Synthesis of Oxindole and 3-Oxotetrahydroisoquinoline Derivatives. *Organic Letters* **2004**, *6*, 2441−2444.
(515) Du, P.; Brosmer, J. L.; Peters, D. G. Electrosynthesis of Substituted 1H-Indoles from o-Nitrostyrenes. *Organic Letters* **2011**, *13*, 4072−4075.
(516) Mitsudo, K.; Nakagawa, Y.; Mizukawa, J.-i.; Tanaka, H.; Akaba, R.; Okada, T.; Suga, S. Electro-reductive cyclization of aryl halides promoted by fluorene derivatives. *Electrochim. Acta* **2012**, *82*, 444−449.
(517) Ashikari, Y.; Nokami, T.; Yoshida, J.-i. Integration of electrooxidative cyclization and chemical oxidation via alkoxysulfonium ions. Synthesis of exocyclic ketones from alkenes with cyclization. *Organic & Biomolecular Chemistry* **2013**, *11*, 3322−3331.
(518) Francke, R.; Little, R. D. Optimizing Electron Transfer Mediators Based on Arylimidazoles by Ring Fusion: Synthesis, Electrochemistry, and Computational Analysis of 2-Aryl-1-methylphenanthro[9,10-d]imidazoles. *J. Am. Chem. Soc.* **2014**, *136*, 427−435.
(519) Zhu, L.; Xiong, P.; Mao, Z.-Y.; Wang, Y.-H.; Yan, X.; Lu, X.; Xu, H.-C. Electrocatalytic Generation of Amidyl Radicals for Olefin Hydroamidation: Use of Solvent Effects to Enable Anilide Oxidation. *Angew. Chem., Int. Ed.* **2016**, *55*, 2226−2229.
(520) Kang, L.-S.; Xiao, H.-l.; Zeng, C.-C.; Hu, L.-M.; Little, R. D. Electrochemical synthesis of benzoxazoles mediated by 2,3-dichloro-5,6-dicyano-p-hydroquinone (DDH) as a redox catalyst. *J. Electroanal. Chem.* **2016**, *767*, 13−17.
(521) Tang, S.; Gao, X.; Lei, A. Electrocatalytic intramolecular oxidative annulation of N-aryl enamines into substituted indoles mediated by iodides. *Chem. Commun.* **2017**, *53*, 3354−3356.
(522) Wu, Z.-J.; Xu, H.-C. Synthesis of C3-Fluorinated Oxindoles through Reagent-Free Cross-Dehydrogenative Coupling. *Angew. Chem., Int. Ed.* **2017**, *56*, 4734−4738.
(523) Xiong, P.; Xu, H.-H.; Xu, H.-C. Metal- and Reagent-Free Intramolecular Oxidative Amination of Tri- and Tetrasubstituted Alkenes. *J. Am. Chem. Soc.* **2017**, *139*, 2956−2959.
(524) Nguyen, B. H.; Redden, A.; Moeller, K. D. Sunlight, electrochemistry, and sustainable oxidation reactions. *Green Chem.* **2014**, *16*, 69−72.
(525) Jutand, A. *Organic Electrochemistry, Fifth ed.: Revised and Expanded*; Hammerich, O., Speiser, B., Eds.; CRC Press: Boca Raton, 2015.
(526) Luca, O. R.; Blakemore, J. D.; Konezny, S. J.; Praetorius, J. M.; Schmeier, T. J.; Hunsinger, G. B.; Batista, V. S.; Brudvig, G. W.; Hazari, N.; Crabtree, R. H. Organometallic Ni Pincer Complexes for the Electrocatalytic Production of Hydrogen. *Inorg. Chem.* **2012**, *51*, 8704−8709.
(527) Blakemore, J. D.; Crabtree, R. H.; Brudvig, G. W. Molecular Catalysts for Water Oxidation. *Chem. Rev.* **2015**, *115*, 12974−13005.
(528) Moyer, B. A.; Thompson, M. S.; Meyer, T. J. Chemically catalyzed net electrochemical oxidation of alcohols, aldehydes, and unsaturated hydrocarbons using the system $(trpy)(bpy)Ru(OH_2)_2^{+}$/$(trpy)(bpy)RuO_2^{+}$. *J. Am. Chem. Soc.* **1980**, *102*, 2310−2312.
(529) Chen, C.-Y.; Cheng, S.-H.; Su, Y. O. Electrocatalytic oxidation of styrene by a high valent ruthenium porphyrin cation radical. *J. Electroanal. Chem.* **2000**, *487*, 51−56.
(530) Groves, J. T.; Gilbert, J. A. Electrochemical generation of an iron(IV) porphyrin. *Inorg. Chem.* **1986**, *25*, 123−125.
(531) Liu, M.-h.; Su, Y. O. Selective electrocatalysis of alkene oxidations in aqueous media. Electrochemical and spectral characterization of oxo-ferryl porphyrin, oxo-ferryl porphyrin radical cation and their reaction products with alkenes at room temperature. *J. Electroanal. Chem.* **1998**, *452*, 113−125.
(532) Hickman, D. L.; Nanthakumar, A.; Goff, H. M. Identification of high-valent fluoroiron porphyrin intermediates associated with the electrocatalytic functionalization of hydrocarbons. *J. Am. Chem. Soc.* **1988**, *110*, 6384−6390.
(533) Creager, S. E.; Raybuck, S. A.; Murray, R. W. An efficient electrocatalytic model cytochrome P-450 epoxidation cycle. *J. Am. Chem. Soc.* **1986**, *108*, 4225−4227.
(534) Horwitz, C. P.; Creager, S. E.; Murray, R. W. Electrocatalytic olefin epoxidation using manganese Schiff-base complexes and dioxygen. *Inorg. Chem.* **1990**, *29*, 1006−1011.
(535) Bedioui, F.; Devynck, J.; Bied-Charreton, C. Electropolymerized manganese porphyrin films as catalytic electrode materials for biomimetic oxidations with molecular oxygen. *J. Mol. Catal. A: Chem.* **1996**, *113*, 3−11.
(536) Creager, S. E.; Murray, R. W. Electrochemical studies of oxo(meso-tetraphenylporphinato)chromium(IV). Direct evidence for epoxidation of olefins by an electrochemically generated formal Chromium(V) state. *Inorg. Chem.* **1985**, *24*, 3824−3828.
(537) He, G. X.; Arasasingham, R. D.; Zhang, G. H.; Bruice, T. C. The rate-limiting step in the one-electron oxidation of an alkene by oxo[meso-tetrakis(2,6-dibromophenyl)porphinato]chromium(V) is the formation of a charge-transfer complex. *J. Am. Chem. Soc.* **1991**, *113*, 9828−9833.
(538) Lu, Y.-H.; Oliver Su, Y. Unusual redox properties of a sterically hindered water-soluble chromium porphyrin. Electrochemical and spectral speciation. *Chem. Commun.* **1997**, 753−754.
(539) Phougat, N.; Vasudevan, P.; Jha, N. K.; Bandhopadhyay, D. K. Metal porphyrins as electrocatalysts for commercially important reactions. *Transition Metal Chemistry* **2003**, *28*, 838−847.
(540) Chanda, N.; Mondal, B.; Puranik, V. G.; Lahiri, G. K. Ruthenium monoterpyridine complexes incorporating α,α'-diimine based ancillary functions. Synthesis, crystal structure, spectroelectrochemical properties and catalytic aspect. *Polyhedron* **2002**, *21*, 2033−2043.
(541) Sens, C.; Rodríguez, M.; Romero, I.; Llobet, A.; Parella, T.; Benet-Buchholz, J. Synthesis, Structure, and Acid-Base and Redox Properties of a Family of New Ru(II) Isomeric Complexes Containing the Trpy and the Dinucleating Hbpp Ligands. *Inorg. Chem.* **2003**, *42*, 8385−8394.
(542) Kim, M. Y.; Seok, W. K.; Dong, Y.; Yun, H. Crystal structure and electrochemical behavior of Rh polypyridyl complexes. *Inorg. Chim. Acta* **2001**, *319*, 194−198.
(543) Sugimoto, H.; Tsukube, H.; Tanaka, K. Immobilization of a High-Valent Rhenium Complex on an Indium-Doped Tin-Oxide Electrode: Enhanced Catalytic Activity of a trans-Dioxorhenium(V) Complex in Electrochemical Oxidation of Alcohols. *Eur. J. Inorg. Chem.* **2004**, *2004*, 4550−4553.
(544) Ciszewski, A.; Milczarek, G.; Lewandowska, B.; Krutowski, K. Electrocatalytic Properties of Electropolymerized Ni(II)curcumin Complex. *Electroanalysis* **2003**, *15*, 518−523.
(545) Mohan, J.; Joshi, S.; Prakash, R.; Srivastava, R. C. Novel Ni(II) Mixed Ligand Complex Modified Electrode: Catalytic Effect on Anodic Oxidation of Phenol. *Electroanalysis* **2004**, *16*, 572−576.
(546) Oszajca, M.; Franke, A.; Brindell, M.; Stochel, G.; van Eldik, R. Redox cycling in the activation of peroxides by iron porphyrin and manganese complexes. 'Catching' catalytic active intermediates. *Coord. Chem. Rev.* **2016**, *306*, 483−509.
(547) Han, X.; Wang, K.; Zhang, G.; Gao, W.; Chen, J. Application of the Electrochemical Oxygen Reduction Reaction (ORR) in Organic Synthesis. *Adv. Synth. Catal.* **2019**, *361*, 2804−2824.
(548) Machan, C. W. Advances in the Molecular Catalysis of Dioxygen Reduction. *ACS Catal.* **2020**, *10*, 2640−2655.
(549) Tomboc, G. M.; Park, Y.; Lee, K.; Jin, K. Directing transition metal-based oxygen-functionalization catalysis. *Chem. Sci.* **2021**, *12*, 8967−8995.
(550) Deronzier, A.; Moutet, J. C. *Comprehensive Coordination Chemistry II*; McCleverty, J. A., Meyer, T. J., Eds.; Pergamon: Oxford, 2003. DOI: 10.1016/B0-08-043748-6/09008-3.
(551) Zagal, J. H.; Griveau, S.; Silva, J. F.; Nyokong, T.; Bedioui, F. Metallophthalocyanine-based molecular materials as catalysts for electrochemical reactions. *Coord. Chem. Rev.* **2010**, *254*, 2755−2791.

https://doi.org/10.1021/acs.chemrev.1c00905
Chem. Rev. XXXX, XXX, XXX−XXX

(552) Jutand, A. Contribution of Electrochemistry to Organometallic Catalysis. *Chem. Rev.* **2008**, *108*, 2300−2347.
(553) Sauermann, N.; Meyer, T. H.; Qiu, Y.; Ackermann, L. Electrocatalytic C-H Activation. *ACS Catal.* **2018**, *8*, 7086−7103.
(554) Yamamoto, K.; Kuriyama, M.; Onomura, O. Asymmetric electrosynthesis: Recent advances in catalytic transformations. *Current Opinion in Electrochemistry* **2021**, *28*, 100714.
(555) Gennaro, A.; Isse, A. A.; Maran, F. Nickel(I)(salen)-electrocatalyzed reduction of benzyl chlorides in the presence of carbon dioxide. *J. Electroanal. Chem.* **2001**, *507*, 124−134.
(556) Matthessen, R.; Fransaer, J.; Binnemans, K.; De Vos, D. E. Electrocarboxylation: towards sustainable and efficient synthesis of valuable carboxylic acids. *Beilstein Journal of Organic Chemistry* **2014**, *10*, 2484−2500.
(557) Bazzi, S.; Le Duc, G.; Schulz, E.; Gosmini, C.; Mellah, M. CO_2 activation by electrogenerated divalent samarium for aryl halide carboxylation. *Organic & Biomolecular Chemistry* **2019**, *17*, 8546−8550.
(558) Cannes, C.; Condon, S.; Durandetti, M.; Périchon, J.; Nédélec, J. Y. Nickel-Catalyzed Electrochemical Couplings of Vinyl Halides: Synthetic and Stereochemical Aspects. *J. Org. Chem.* **2000**, *65*, 4575−4583.
(559) Klein, A.; Budnikova, Y. H.; Sinyashin, O. G. Electron transfer in organonickel complexes of α-diimines: Versatile redox catalysts for C-C or C-P coupling reactions - A review. *J. Organomet. Chem.* **2007**, *692*, 3156−3166.
(560) Miranda, J. A.; Wade, C. J.; Little, R. D. Indirect Electroreductive Cyclization and Electrohydrocyclization Using Catalytic Reduced Nickel(II) Salen. *J. Org. Chem.* **2005**, *70*, 8017−8026.
(561) Li, C.; Kawamata, Y.; Nakamura, H.; Vantourout, J. C.; Liu, Z.; Hou, Q.; Bao, D.; Starr, J. T.; Chen, J.; Yan, M.; et al. Electrochemically Enabled, Nickel-Catalyzed Amination. *Angew. Chem., Int. Ed.* **2017**, *56*, 13088−13093.
(562) Perkins, R. J.; Pedro, D. J.; Hansen, E. C. Electrochemical Nickel Catalysis for Sp^2-Sp^3 Cross-Electrophile Coupling Reactions of Unactivated Alkyl Halides. *Organic Letters* **2017**, *19*, 3755−3758.
(563) Yang, Q.-L.; Li, Y.-Q.; Ma, C.; Fang, P.; Zhang, X.-J.; Mei, T.-S. Palladium-Catalyzed C(sp^3)—H Oxygenation via Electrochemical Oxidation. *J. Am. Chem. Soc.* **2017**, *139*, 3293−3298.
(564) Shrestha, A.; Lee, M.; Dunn, A. L.; Sanford, M. S. Palladium-Catalyzed C-H Bond Acetoxylation via Electrochemical Oxidation. *Organic Letters* **2018**, *20*, 204−207.
(565) Cao, Y.; Yuan, Y.; Lin, Y.; Jiang, X.; Weng, Y.; Wang, T.; Bu, F.; Zeng, L.; Lei, A. Cobalt catalyzed electrochemical [4 + 2] annulation for the synthesis of sultams. *Green Chem.* **2020**, *22*, 1548−1552.
(566) Tian, S.; Lv, S.; Jia, X.; Ma, L.; Li, B.; Zhang, G.; Gao, W.; Wei, Y.; Chen, J. CV-driven Optimization: Cobalt-Catalyzed Electrochemical Expedient Oxychlorination of Alkenes via ORR. *Adv. Synth. Catal.* **2019**, *361*, 5626−5633.
(567) Gao, P.-S.; Weng, X.-J.; Wang, Z.-H.; Zheng, C.; Sun, B.; Chen, Z.-H.; You, S.-L.; Mei, T.-S. CuII/TEMPO-Catalyzed Enantioselective C(sp^3)-H Alkynylation of Tertiary Cyclic Amines through Shono-Type Oxidation. *Angew. Chem., Int. Ed.* **2020**, *59*, 15254−15259.
(568) Li, H.; Xue, Y.-F.; Ge, Q.; Liu, M.; Cong, H.; Tao, Z. Chiral electroorganic chemistry: An interdisciplinary research across electrocatalysis and asymmetric synthesis. *Molecular Catalysis* **2021**, *499*, 111296.
(569) Gourley, R. N.; Grimshaw, J.; Millar, P. G. Electrochemical reactions. Part VIII. Asymmetric induction during the reduction of coumarins modified by the presence of tertiary amines. *Journal of the Chemical Society C: Organic* **1970**, 2318−2323.
(570) Zhang, K.; Wang, H.; Zhao, S.-F.; Niu, D.-F.; Lu, J.-X. Asymmetric electrochemical carboxylation of prochiral acetophenone: An efficient route to optically active atrolactic acid via selective fixation of carbon dioxide. *Journal of Electroanalytical Chemistry* **2009**, *630*, 35−41.
(571) Zhao, S.-F.; Zhu, M.-X.; Zhang, K.; Wang, H.; Lu, J.-X. Alkaloid induced asymmetric electrocarboxylation of 4-methylpropiophenone. *Tetrahedron Lett.* **2011**, *52*, 2702−2705.
(572) Chen, B.-L.; Xiao, Y.; Xu, X.-M.; Yang, H.-P.; Wang, H.; Lu, J.-X. Alkaloid induced enantioselective electroreduction of acetophenone. *Electrochim. Acta* **2013**, *107*, 320−326.
(573) Wang, S.; Shi, Y.; Hou, Y.; Shan, S.-L.; Wang, H.; Lu, J.-X. Electrocatalytic asymmetric reduction of ethyl benzoylformate on bimetallic Ag-Cu cathodes. *Journal of Applied Electrochemistry* **2020**, *50*, 973.
(574) Ghosh, M.; Shinde, V. S.; Rueping, M. A review of asymmetric synthetic organic electrochemistry and electrocatalysis: concepts, applications, recent developments and future directions. *Beilstein Journal of Organic Chemistry* **2019**, *15*, 2710−2746.
(575) Lin, Q.; Li, L.; Luo, S. Asymmetric Electrochemical Catalysis. *Chem.-Eur. J.* **2019**, *25*, 10033−10044.
(576) Ho, X.-H.; Mho, S.-i.; Kang, H.; Jang, H.-Y. Electro-Organocatalysis: Enantioselective α-Alkylation of Aldehydes. *Eur. J. Org. Chem.* **2010**, *2010*, 4436−4441.
(577) Zhang, Q.; Chang, X.; Peng, L.; Guo, C. Asymmetric Lewis Acid Catalyzed Electrochemical Alkylation. *Angew. Chem., Int. Ed.* **2019**, *58*, 6999−7003.
(578) Huang, X.; Zhang, Q.; Lin, J.; Harms, K.; Meggers, E. Electricity-driven asymmetric Lewis acid catalysis. *Nat. Catal.* **2019**, *2*, 34−40.
(579) Jensen, K. L.; Franke, P. T.; Nielsen, L. T.; Daasbjerg, K.; Jørgensen, K. A. Anodic Oxidation and Organocatalysis: Direct Regio- and Stereoselective Access to meta-Substituted Anilines by α-Arylation of Aldehydes. *Angew. Chem., Int. Ed.* **2010**, *49*, 129−133.
(580) Jiao, K.-J.; Li, Z.-M.; Xu, X.-T.; Zhang, L.-P.; Li, Y.-Q.; Zhang, K.; Mei, T.-S. Palladium-catalyzed reductive electrocarboxylation of allyl esters with carbon dioxide. *Organic Chemistry Frontiers* **2018**, *5*, 2244−2248.
(581) Qiu, H.; Shuai, B.; Wang, Y.-Z.; Liu, D.; Chen, Y.-G.; Gao, P.-S.; Ma, H.-X.; Chen, S.; Mei, T.-S. Enantioselective Ni-Catalyzed Electrochemical Synthesis of Biaryl Atropisomers. *J. Am. Chem. Soc.* **2020**, *142*, 9872−9878.
(582) Fu, N.; Li, L.; Yang, Q.; Luo, S. Catalytic Asymmetric Electrochemical Oxidative Coupling of Tertiary Amines with Simple Ketones. *Organic Letters* **2017**, *19*, 2122−2125.
(583) Tanaka, H.; Kuroboshi, M.; Takeda, H.; Kanda, H.; Torii, S. Electrochemical asymmetric epoxidation of olefins by using an optically active Mn-salen complex. *J. Electroanal. Chem.* **2001**, *507*, 75−81.
(584) Fu, N.; Song, L.; Liu, J.; Shen, Y.; Siu, J. C.; Lin, S. New Bisoxazoline Ligands Enable Enantioselective Electrocatalytic Cyanofunctionalization of Vinylarenes. *J. Am. Chem. Soc.* **2019**, *141*, 14480−14485.
(585) Kohlmann, C.; Lütz, S. *Organic Electrochemistry, Fifth ed.: Revised and Expanded*; Hammerich, O., Speiser, B., Eds.; CRC Press: Boca Raton, 2015.
(586) Höllrigl, V.; Otto, K.; Schmid, A. Electroenzymatic Asymmetric Reduction of rac-3-Methylcyclohexanone to (1S,3S)-3-Methylcyclohexanol in Organic/Aqueous Media Catalyzed by a Thermophilic Alcohol Dehydrogenase. *Adv. Synth. Catal.* **2007**, *349*, 1337−1340.
(587) Hildebrand, F.; Lütz, S. Stable Electroenzymatic Processes by Catalyst Separation. *Chem.-Eur. J.* **2009**, *15*, 4998−5001.
(588) Lütz, S.; Vuorilehto, K.; Liese, A. Process development for the electroenzymatic synthesis of (R)-methylphenylsulfoxide by use of a 3-dimensional electrode. *Biotechnol. Bioeng.* **2007**, *98*, 525−534.
(589) Palanisamy, S.; Karuppiah, C.; Chen, S.-M. Direct electrochemistry and electrocatalysis of glucose oxidase immobilized on reduced graphene oxide and silver nanoparticles nanocomposite modified electrode. *Colloids Surf., B* **2014**, *114*, 164−169.
(590) Fang, L.; Liu, B.; Liu, L.; Li, Y.; Huang, K.; Zhang, Q. Direct electrochemistry of glucose oxidase immobilized on Au nanoparticles-functionalized 3D hierarchically ZnO nanostructures and its

application to bioelectrochemical glucose sensor. *Sens. Actuators, B* **2016**, *222*, 1096−1102.
(591) Kang, Z.; Jiao, K.; Yu, C.; Dong, J.; Peng, R.; Hu, Z.; Jiao, S. Direct electrochemistry and bioelectrocatalysis of glucose oxidase in CS/CNC film and its application in glucose biosensing and biofuel cells. *RSC Adv.* **2017**, *7*, 4572−4579.
(592) Hubig, S. M.; Rathore, R.; Kochi, J. K. Steric Control of Electron Transfer. Changeover from Outer-Sphere to Inner-Sphere Mechanisms in Arene/Quinone Redox Pairs. *J. Am. Chem. Soc.* **1999**, *121*, 617−626.
(593) Ohkubo, K.; Fujimoto, A.; Fukuzumi, S. Visible-Light-Induced Oxygenation of Benzene by the Triplet Excited State of 2,3-Dichloro-5,6-dicyano-p-benzoquinone. *J. Am. Chem. Soc.* **2013**, *135*, 5368−5371.
(594) Martindale, B. C. M.; Hutton, G. A. M.; Caputo, C. A.; Reisner, E. Solar Hydrogen Production Using Carbon Quantum Dots and a Molecular Nickel Catalyst. *J. Am. Chem. Soc.* **2015**, *137*, 6018−6025.
(595) Zhang, X.; Peng, T.; Song, S. Recent advances in dye-sensitized semiconductor systems for photocatalytic hydrogen production. *J. Mater. Chem. A* **2016**, *4*, 2365−2402.
(596) Li, K.; Peng, B.; Peng, T. Recent Advances in Heterogeneous Photocatalytic CO_2 Conversion to Solar Fuels. *ACS Catal.* **2016**, *6*, 7485−7527.
(597) Qin, J.; Wang, S.; Wang, X. Visible-light reduction CO_2 with dodecahedral zeolitic imidazolate framework ZIF-67 as an efficient co-catalyst. *Appl. Catal. B* **2017**, *209*, 476−482.
(598) Li, X.; Yu, J.; Jaroniec, M.; Chen, X. Cocatalysts for Selective Photoreduction of CO2 into Solar Fuels. *Chem. Rev.* **2019**, *119*, 3962−4179.
(599) DiSalle, B. F.; Bernhard, S. Orchestrated Photocatalytic Water Reduction Using Surface-Adsorbing Iridium Photosensitizers. *J. Am. Chem. Soc.* **2011**, *133*, 11819−11821.
(600) Wu, T.; Zou, L.; Han, D.; Li, F.; Zhang, Q.; Niu, L. A carbon-based photocatalyst efficiently converts CO_2 to CH_4 and C_2H_2 under visible light. *Green Chem.* **2014**, *16*, 2142−2146.
(601) Shen, J.; Kortlever, R.; Kas, R.; Birdja, Y. Y.; Diaz-Morales, O.; Kwon, Y.; Ledezma-Yanez, I.; Schouten, K. J. P.; Mul, G.; Koper, M. T. M. Electrocatalytic reduction of carbon dioxide to carbon monoxide and methane at an immobilized cobalt protoporphyrin. *Nat. Commun.* **2015**, *6*, 8177.
(602) Weng, Z.; Jiang, J.; Wu, Y.; Wu, Z.; Guo, X.; Materna, K. L.; Liu, W.; Batista, V. S.; Brudvig, G. W.; Wang, H. Electrochemical CO_2 Reduction to Hydrocarbons on a Heterogeneous Molecular Cu Catalyst in Aqueous Solution. *J. Am. Chem. Soc.* **2016**, *138*, 8076−8079.
(603) Liu, X.; Inagaki, S.; Gong, J. Heterogeneous Molecular Systems for Photocatalytic CO_2 Reduction with Water Oxidation. *Angew. Chem., Int. Ed.* **2016**, *55*, 14924−14950.
(604) Rao, H.; Schmidt, L. C.; Bonin, J.; Robert, M. Visible-light-driven methane formation from CO_2 with a molecular iron catalyst. *Nature* **2017**, *548*, 74−77.
(605) Shimakoshi, H.; Hisaeda, Y. B_{12}-TiO_2 Hybrid Catalyst for Light-Driven Hydrogen Production and Hydrogenation of C-C Multiple Bonds. *ChemPlusChem.* **2014**, *79*, 1250−1253.
(606) Bachmeier, A.; Murphy, B. J.; Armstrong, F. A. A Multi-Heme Flavoenzyme as a Solar Conversion Catalyst. *J. Am. Chem. Soc.* **2014**, *136*, 12876−12879.
(607) Hutton, G. A. M.; Reuillard, B.; Martindale, B. C. M.; Caputo, C. A.; Lockwood, C. W. J.; Butt, J. N.; Reisner, E. Carbon Dots as Versatile Photosensitizers for Solar-Driven Catalysis with Redox Enzymes. *J. Am. Chem. Soc.* **2016**, *138*, 16722−16730.
(608) Shimakoshi, H.; Nagami, Y.; Hisaeda, Y. Crystal Structure Dependence for Reactivities of B_{12}-TiO_2 Hybrid Catalysts with Anatase and Rutile Forms. *Rapid Communication in Photoscience* **2015**, *4*, 9−11.
(609) Shimakoshi, H.; Hisaeda, Y. A Hybrid Catalyst for Light-Driven Green Molecular Transformations. *ChemPlusChem.* **2017**, *82*, 18−29.
(610) Dalle, K. E.; Warnan, J.; Leung, J. J.; Reuillard, B.; Karmel, I. S.; Reisner, E. Electro- and Solar-Driven Fuel Synthesis with First Row Transition Metal Complexes. *Chem. Rev.* **2019**, *119*, 2752−2875.
(611) Brereton, K. R.; Bonn, A. G.; Miller, A. J. M. Molecular Photoelectrocatalysts for Light-Driven Hydrogen Production. *ACS Energy Letters* **2018**, *3*, 1128−1136.
(612) Anderson, L. A.; Redden, A.; Moeller, K. D. Connecting the dots: using sunlight to drive electrochemical oxidations. *Green Chem.* **2011**, *13*, 1652−1654.
(613) Kim, H.; Kim, H.; Lambert, T. H.; Lin, S. Reductive Electrophotocatalysis: Merging Electricity and Light To Achieve Extreme Reduction Potentials. *J. Am. Chem. Soc.* **2020**, *142*, 2087−2092.
(614) Hoek, A.; Sachtler, W. M. H. Enantioselectivity of Nickel Catalysts Modified with Tartaric Acid or Nickel Tartrate Complexes. *J. Catal.* **1979**, *58*, 276−286.
(615) Humblot, V.; Haq, S.; Muryn, C.; Hofer, W. A.; Raval, R. From Local Adsorption Stresses to Chiral Surfaces: (R,R)-Tartaric Acid on Ni(110). *J. Am. Chem. Soc.* **2002**, *124*, 503−510.
(616) Jones, T. E.; Baddeley, C. J. A RAIRS, STM and TPD study of the Ni{111}/R,R-tartaric acid system: Modelling the chiral modification of Ni nanoparticles. *Surf. Sci.* **2002**, *513*, 453−467.
(617) Hazzazi, O. A.; Attard, G. A.; Wells, P. B. Molecular recognition in adsorption and electro-oxidation at chiral platinum surfaces. *J. Mol. Catal. A: Chem.* **2004**, *216*, 247−255.
(618) Humblot, V.; Haq, S.; Muryn, C.; Raval, R. (R,R)-Tartaric acid on Ni(110): the dynamic nature of chiral adsorption motifs. *J. Catal.* **2004**, *228*, 130−140.
(619) Osawa, T.; Harada, T.; Takayasu, O. Asymmetrically modified nickel catalyst for the enantio-differentiating hydrogenation of prochiral ketones. *Curr. Org. Chem.* **2006**, *10*, 1513−1531.
(620) Watson, D. J.; Acharya, S.; Nicklin, R. E. J.; Held, G. Observing the in situ chiral modification of Ni nanoparticles using scanning transmission X-ray microspectroscopy. *Surf. Sci.* **2014**, *629*, 108−113.
(621) Arrigo, R.; Gallarati, S.; Schuster, M. E.; Seymour, J. M.; Gianolio, D.; da Silva, I.; Callison, J.; Feng, H.; Proctor, J. E.; Ferrer, P.; et al. Influence of Synthesis Conditions on the Structure of Nickel Nanoparticles and their Reactivity in Selective Asymmetric Hydrogenation. *ChemCatChem.* **2020**, *12*, 1491−1503.
(622) Gao, F.; Li, Z.; Wang, Y.; Burkholder, L.; Tysoe, W. T. Chemistry of Alanine on Pd(111): Temperature-programmed desorption and X-ray photoelectron spectroscopic study. *Surf. Sci.* **2007**, *601*, 3276−3288.
(623) Gao, F.; Wang, Y.; Burkholder, L.; Tysoe, W. T. Chemistry of l-proline on Pd(1 1 1): Temperature-programmed desorption and X-ray photoelectron spectroscopic study. *Surf. Sci.* **2007**, *601*, 3579−3588.
(624) Han, J. W.; James, J. N.; Sholl, D. S. Chemical speciation of adsorbed glycine on metal surfaces. *J. Chem. Phys.* **2011**, *135*, 034703.
(625) Fischer, S.; Papageorgiou, A. C.; Marschall, M.; Reichert, J.; Diller, K.; Klappenberger, F.; Allegretti, F.; Nefedov, A.; Wöll, C.; Barth, J. V. l-Cysteine on Ag(111): A Combined STM and X-ray Spectroscopy Study of Anchorage and Deprotonation. *J. Phys. Chem. C* **2012**, *116*, 20356−20362.
(626) Shavorskiy, A.; Eralp, T.; Schulte, K.; Bluhm, H.; Held, G. Surface chemistry of glycine on Pt{111} in different aqueous environments. *Surf. Sci.* **2013**, *607*, 10−19.
(627) Nicklin, R. E. J.; Cornish, A.; Shavorskiy, A.; Baldanza, S.; Schulte, K.; Liu, Z.; Bennett, R. A.; Held, G. Surface Chemistry of Alanine on Ni{111}. *J. Phys. Chem. C* **2015**, *119*, 26566−26574.
(628) Barlow, S. M.; Raval, R. Complex organic molecules at metal surfaces: Bonding, organisation and chirality. *Surf. Sci. Rep.* **2003**, *50*, 201−341.
(629) Barlow, S. M.; Raval, R. Nanoscale insights in the creation and transfer of chirality in amino acid monolayers at defined metal surfaces. *Curr. Opin. Coll. Interface Sci.* **2008**, *13*, 65−73.

https://doi.org/10.1021/acs.chemrev.1c00905
Chem. Rev. XXXX, XXX, XXX−XXX

(630) Cheong, W. Y.; Huang, Y.; Dangaria, N.; Gellman, A. J. Probing Enantioselectivity on Chirally Modified Cu(110), Cu(100), and Cu(111) Surfaces. *Langmuir* **2010**, *26*, 16412−16423.
(631) Clegg, M. L.; Morales de la Garza, L.; Karakatsani, S.; King, D. A.; Driver, S. M. Chirality in Amino Acid Overlayers on Cu Surfaces. *Top. Catal.* **2011**, *54*, 1429−1444.
(632) Song, H. S.; Han, J. W. Tuning the Surface Chemistry of Chiral Cu(531)S for Enhanced Enantiospecific Adsorption of Amino Acids. *J. Phys. Chem. C* **2015**, *119*, 15195−15203.
(633) Kunz, S.; Schreiber, P.; Ludwig, M.; Maturi, M. M.; Ackermann, O.; Tschurl, M.; Heiz, U. Rational design, characterization and catalytic application of metal clusters functionalized with hydrophilic, chiral ligands: a proof of principle study. *Phys. Chem. Chem. Phys.* **2013**, *15*, 19253−19261.
(634) Schrader, I.; Warneke, J.; Backenköhler, J.; Kunz, S. Functionalization of Platinum Nanoparticles with l-Proline: Simultaneous Enhancements of Catalytic Activity and Selectivity. *J. Am. Chem. Soc.* **2015**, *137*, 905−912.
(635) Holland, M. C.; Meemken, F.; Baiker, A.; Gilmour, R. Chiral imidazolidinone and proline-derived surface modifiers for the Pt-catalysed asymmetric hydrogenation of activated ketones. *J. Mol. Catal. A: Chem.* **2015**, *396*, 335−345.
(636) Luo, W.; Cheng, W.; Hu, M.; Wang, Q.; Cheng, X.; Zhang, Y.; Wang, Y.; Gao, D.; Bi, J.; Fan, G. Ultrahigh Catalytic Activity of l-Proline-Functionalized Rh Nanoparticles for Methanolysis of Ammonia Borane. *ChemSusChem* **2019**, *12*, 535−541.
(637) von Arx, M.; Dummer, N.; Willock, D. J.; Taylor, S. H.; Wells, R. P. K.; Wells, P. B.; Hutchings, G. J. Observation of high enantioselectivity for the gas phase hydrogenation of methyl pyruvate using supported Pt catalysts pre-modified with cinchonidine. *Chem. Commun.* **2003**, *9*, 1926−1927.
(638) Dummer, N. F.; Jenkins, R.; Li, X.; Bawaked, S. M.; McMorn, P.; Burrows, A.; Kiely, C. J.; Wells, R. P. K.; Willock, D. J.; Hutchings, G. J. Inversion of enantioselectivity for the hydrogenation of ethyl pyruvate in the gas-phase over Pt/SiO_2 modified with derivatives of hydroquinidine. *J. Catal.* **2006**, *243*, 165−170.
(639) Marshall, S. T.; O'Brien, M.; Oetter, B.; Corpuz, A.; Richards, R. M.; Schwartz, D. K.; Medlin, J. W. Controlled selectivity for palladium catalysts using self-assembled monolayers. *Nat. Mater.* **2010**, *9*, 853−858.
(640) Schoenbaum, C. A.; Schwartz, D. K.; Medlin, J. W. Controlling surface crowding on a Pd catalyst with thiolate self-assembled monolayers. *J. Catal.* **2013**, *303*, 92−99.
(641) Kahsar, K. R.; Schwartz, D. K.; Medlin, J. W. Control of Metal Catalyst Selectivity through Specific Noncovalent Molecular Interactions. *J. Am. Chem. Soc.* **2014**, *136*, 520−526.
(642) Pang, S. H.; Love, N. E.; Medlin, J. W. Synergistic Effects of Alloying and Thiolate Modification in Furfural Hydrogenation over Cu-Based Catalysts. *J. Phys. Chem. Lett.* **2014**, *5*, 4110−4114.
(643) Schoenbaum, C. A.; Schwartz, D. K.; Medlin, J. W. Controlling the Surface Environment of Heterogeneous Catalysts Using Self-Assembled Monolayers. *Acc. Chem. Res.* **2014**, *47*, 1438−1445.
(644) Pang, S. H.; Medlin, J. W. Controlling Catalytic Selectivity via Adsorbate Orientation on the Surface: From Furfural Deoxygenation to Reactions of Epoxides. *J. Phys. Chem. Lett.* **2015**, *6*, 1348−1356.
(645) Kumar, G.; Lien, C.-H.; Janik, M. J.; Medlin, J. W. Catalyst Site Selection via Control over Noncovalent Interactions in Self-Assembled Monolayers. *ACS Catal.* **2016**, *6*, 5086−5094.
(646) Pang, S. H.; Lien, C.-H.; Medlin, J. W. Control of surface alkyl catalysis with thiolate monolayers. *Catal. Sci. Technol.* **2016**, *6*, 2413−2418.
(647) Zhang, J.; Medlin, J. W. Catalyst design using an inverse strategy: From mechanistic studies on inverted model catalysts to applications of oxide-coated metal nanoparticles. *Surf. Sci. Rep.* **2018**, *73*, 117−152.
(648) Sá, J.; Medlin, J. W. On-the-fly Catalyst Modification: Strategy to Improve Catalytic Processes Selectivity and Understanding. *ChemCatChem.* **2019**, *11*, 3355−3365.
(649) Pang, S. H.; Schoenbaum, C. A.; Schwartz, D. K.; Medlin, J. W. Directing reaction pathways by catalyst active-site selection using self-assembled monolayers. *Nat. Commun.* **2013**, *4*, 2448.
(650) Kahsar, K. R.; Schwartz, D. K.; Medlin, J. W. Selective Hydrogenation of Polyunsaturated Fatty Acids Using Alkanethiol Self-Assembled Monolayer-Coated Pd/Al2O3 Catalysts. *ACS Catal.* **2013**, *3*, 2041−2044.
(651) Lu, L.; Zou, S.; Fang, B. The Critical Impacts of Ligands on Heterogeneous Nanocatalysis: A Review. *ACS Catal.* **2021**, *11*, 6020−6058.
(652) Fiorio, J. L.; López, N.; Rossi, L. M. Gold-Ligand-Catalyzed Selective Hydrogenation of Alkynes into cis-Alkenes via H2 Heterolytic Activation by Frustrated Lewis Pairs. *ACS Catal.* **2017**, *7*, 2973−2980.
(653) Zhao, X.; Zhou, L.; Zhang, W.; Hu, C.; Dai, L.; Ren, L.; Wu, B.; Fu, G.; Zheng, N. Thiol Treatment Creates Selective Palladium Catalysts for Semihydrogenation of Internal Alkynes. *Chem.* **2018**, *4*, 1080−1091.
(654) Yoshii, T.; Umemoto, D.; Kuwahara, Y.; Mori, K.; Yamashita, H. Engineering of Surface Environment of Pd Nanoparticle Catalysts on Carbon Support with Pyrene-Thiol Ligands for Semihydrogenation of Alkynes. *ACS Appl. Mater. Interfaces* **2019**, *11*, 37708−37719.
(655) Huang, L.; Subramanian, R.; Wang, J.; Kwon Oh, J.; Ye, Z. Ligand screening for palladium nanocatalysts towards selective hydrogenation of alkynes. *Molecular Catalysis* **2020**, *488*, 110923.
(656) Sadeghmoghaddam, E.; Gaïeb, K.; Shon, Y.-S. Catalytic isomerization of allyl alcohols to carbonyl compounds using poisoned Pd nanoparticles. *Appl. Catal. A* **2011**, *405*, 137−141.
(657) Campisi, S.; Ferri, D.; Villa, A.; Wang, W.; Wang, D.; Kröcher, O.; Prati, L. Selectivity Control in Palladium-Catalyzed Alcohol Oxidation through Selective Blocking of Active Sites. *J. Phys. Chem. C* **2016**, *120*, 14027−14033.
(658) Fan, X.; Zerebecki, S.; Du, R.; Hübner, R.; Marzum, G.; Jiang, G.; Hu, Y.; Barcikowki, S.; Reichenberger, S.; Eychmüller, A. Promoting the Electrocatalytic Performance of Noble Metal Aerogels by Ligand-Directed Modulation. *Angew. Chem., Int. Ed.* **2020**, *59*, 5706−5711.
(659) Gavia, D. J.; Shon, Y.-S. Controlling Surface Ligand Density and Core Size of Alkanethiolate-Capped Pd Nanoparticles and Their Effects on Catalysis. *Langmuir* **2012**, *28*, 14502−14508.
(660) Yoskamtorn, T.; Yamazoe, S.; Takahata, R.; Nishigaki, J.-i.; Thivasasith, A.; Limtrakul, J.; Tsukuda, T. Thiolate-Mediated Selectivity Control in Aerobic Alcohol Oxidation by Porous Carbon-Supported Au25 Clusters. *ACS Catal.* **2014**, *4*, 3696−3700.
(661) Chung, I.; Song, B.; Kim, J.; Yun, Y. Enhancing Effect of Residual Capping Agents in Heterogeneous Enantioselective Hydrogenation of α-keto Esters over Polymer-Capped Pt/Al_2O_3. *ACS Catal.* **2021**, *11*, 31−42.
(662) Nakanishi, T.; Matsunaga, M.; Nagasaka, M.; Ueno, T.; Osaka, T. Stereospecificity in redox reactions of catechins at gold electrodes modified with self-assembled monolayers of homocysteine. *Electrochim. Acta* **2008**, *53*, 6209−6214.
(663) Baker, L. R.; Kennedy, G.; Krier, J.; Spronsen, M.; Onorato, R.; Somorjai, G. The Role of an Organic Cap in Nanoparticle Catalysis: Reversible Restructuring of Carbonaceous Material Controls Catalytic Activity of Platinum Nanoparticles for Ethylene Hydrogenation and Methanol Oxidation. *Catal. Lett.* **2012**, *142*, 1286−1294.
(664) Niu, Z.; Li, Y. Removal and Utilization of Capping Agents in Nanocatalysis. *Chem. Mater.* **2014**, *26*, 72−83.
(665) Campisi, S.; Schiavoni, M.; Chan-Thaw, C. E.; Villa, A. Untangling the role of the capping agent in nanocatalysis: Recent advances and perspectives. *Catalysts* **2016**, *6*, 185.
(666) Wang, Y.; Wan, X.-K.; Ren, L.; Su, H.; Li, G.; Malola, S.; Lin, S.; Tang, Z.; Häkkinen, H.; Teo, B. K.; et al. Atomically Precise Alkynyl-Protected Metal Nanoclusters as a Model Catalyst: Observation of Promoting Effect of Surface Ligands on Catalysis by Metal Nanoparticles. *J. Am. Chem. Soc.* **2016**, *138*, 3278−3281.

https://doi.org/10.1021/acs.chemrev.1c00905
Chem. Rev. XXXX, XXX, XXX−XXX

(667) Rossi, L. M.; Fiorio, J. L.; Garcia, M. A. S.; Ferraz, C. P. The role and fate of capping ligands in colloidally prepared metal nanoparticle catalysts. *Dalton Trans.* **2018**, *47*, 5889−5915.
(668) Kunz, S. Supported, Ligand-Functionalized Nanoparticles: An Attempt to Rationalize the Application and Potential of Ligands in Heterogeneous Catalysis. *Top. Catal.* **2016**, *59*, 1671−1685.
(669) Jin, L.; Liu, B.; Duay, S. S.; He, J. Engineering surface ligands of noble metal nanocatalysts in tuning the product selectivity. *Catalysts* **2017**, *7*, 44.
(670) Zhong, R.-Y.; Yan, X.-H.; Gao, Z.-K.; Zhang, R.-J.; Xu, B.-Q. Stabilizer substitution and its effect on the hydrogenation catalysis by Au nanoparticles from colloidal synthesis. *Catal. Sci. Technol.* **2013**, *3*, 3013−3019.
(671) Udumula, V.; Tyler, J. H.; Davis, D. A.; Wang, H.; Linford, M. R.; Minson, P. S.; Michaelis, D. J. Dual Optimization Approach to Bimetallic Nanoparticle Catalysis: Impact of M_1/M_2 Ratio and Supporting Polymer Structure on Reactivity. *ACS Catal.* **2015**, *5*, 3457−3462.
(672) Liu, P.; Qin, R.; Fu, G.; Zheng, N. Surface Coordination Chemistry of Metal Nanomaterials. *J. Am. Chem. Soc.* **2017**, *139*, 2122−2131.
(673) Ghosh, A.; Basak, S.; Wunsch, B. H.; Kumar, R.; Stellacci, F. Effect of Composition on the Catalytic Properties of Mixed-Ligand-Coated Gold Nanoparticles. *Angew. Chem., Int. Ed.* **2011**, *50*, 7900−7905.
(674) Kwon, S. G.; Krylova, G.; Sumer, A.; Schwartz, M. M.; Bunel, E. E.; Marshall, C. L.; Chattopadhyay, S.; Lee, B.; Jellinek, J.; Shevchenko, E. V. Capping Ligands as Selectivity Switchers in Hydrogenation Reactions. *Nano Lett.* **2012**, *12*, 5382−5388.
(675) Fedorov, A.; Liu, H.-J.; Lo, H.-K.; Copéret, C. Silica-Supported Cu Nanoparticle Catalysts for Alkyne Semihydrogenation: Effect of Ligands on Rates and Selectivity. *J. Am. Chem. Soc.* **2016**, *138*, 16502−16507.
(676) You, J.-G.; Shanmugam, C.; Liu, Y.-W.; Yu, C.-J.; Tseng, W.-L. Boosting catalytic activity of metal nanoparticles for 4-nitrophenol reduction: Modification of metal naoparticles with poly-(diallyldimethylammonium chloride). *J. Hazard. Mater.* **2017**, *324*, 420−427.
(677) Chen, G.; Xu, C.; Huang, X.; Ye, J.; Gu, L.; Li, G.; Tang, Z.; Wu, B.; Yang, H.; Zhao, Z.; et al. Interfacial electronic effects control the reaction selectivity of platinum catalysts. *Nat. Mater.* **2016**, *15*, 564−569.
(678) Chen, K.; Wu, H.; Hua, Q.; Chang, S.; Huang, W. Enhancing catalytic selectivity of supported metal nanoparticles with capping ligands. *Phys. Chem. Chem. Phys.* **2013**, *15*, 2273−2277.
(679) Jeong, H.; Kim, C.; Yang, S.; Lee, H. Selective hydrogenation of furanic aldehydes using Ni nanoparticle catalysts capped with organic molecules. *J. Catal.* **2016**, *344*, 609−615.
(680) Šulce, A.; Flaherty, D. W.; Kunz, S. Kinetic analysis of the asymmetric hydrogenation of ß-keto esters over α-amino acid-functionalized Pt nanoparticles. *J. Catal.* **2019**, *374*, 82−92.
(681) Jia, X.; Ma, J.; Xia, F.; Xu, Y.; Gao, J.; Xu, J. Carboxylic acid-modified metal oxide catalyst for selectivity-tunable aerobic ammoxidation. *Nat. Commun.* **2018**, *9*, 933.
(682) Jia, X.; Ma, J.; Xia, F.; Gao, M.; Gao, J.; Xu, J. Switching acidity on manganese oxide catalyst with acetylacetones for selectivity-tunable amines oxidation. *Nat. Commun.* **2019**, *10*, 2338.
(683) Ballesteros-Soberanas, J.; Ellis, L. D.; Medlin, J. W. Effects of Phosphonic Acid Monolayers on the Dehydration Mechanism of Aliphatic Alcohols on TiO2. *ACS Catal.* **2019**, *9*, 7808−7816.
(684) Thomas, J. M.; Raja, R.; Lewis, D. W. Single-Site Heterogeneous Catalysts. *Angew. Chem., Int. Ed.* **2005**, *44*, 6456−6482.
(685) Gajan, D.; Copéret, C. Silica-supported single-site catalysts: to be or not to be? A conjecture on silica surfaces. *New J. Chem.* **2011**, *35*, 2403−2408.
(686) Thomas, J. M. The concept, reality and utility of single-site heterogeneous catalysts (SSHCs). *Phys. Chem. Chem. Phys.* **2014**, *16*, 7647−7661.
(687) Yang, X.-F.; Wang, A.; Qiao, B.; Li, J.; Liu, J.; Zhang, T. Single-Atom Catalysts: A New Frontier in Heterogeneous Catalysis. *Acc. Chem. Res.* **2013**, *46*, 1740−1748.
(688) Flytzani-Stephanopoulos, M. Supported metal catalysts at the single-atom limit - A viewpoint. *Chin. J. Catal.* **2017**, *38*, 1432−1442.
(689) Chen, Y.; Ji, S.; Chen, C.; Peng, Q.; Wang, D.; Li, Y. Single-Atom Catalysts: Synthetic Strategies and Electrochemical Applications. *Joule* **2018**, *2*, 1242−1264.
(690) Wang, A.; Li, J.; Zhang, T. Heterogeneous single-atom catalysis. *Nat. Rev. Chem.* **2018**, *2*, 65−81.
(691) Kaiser, S. K.; Chen, Z.; Faust Akl, D.; Mitchell, S.; Pérez-Ramírez, J. Single-Atom Catalysts across the Periodic Table. *Chem. Rev.* **2020**, *120*, 11703−11809.
(692) Singh, B.; Sharma, V.; Gaikwad, R. P.; Fornasiero, P.; Zboril, R.; Gawande, M. B. Single-Atom Catalysts: A Sustainable Pathway for the Advanced Catalytic Applications. *Small* **2021**, *17*, 2006473.
(693) Witzke, R. J.; Chapovetsky, A.; Conley, M. P.; Kaphan, D. M.; Delferro, M. Nontraditional Catalyst Supports in Surface Organometallic Chemistry. *ACS Catal.* **2020**, *10*, 11822−11840.
(694) Lefort, L.; Chabanas, M.; Maury, O.; Meunier, D.; Copéret, C.; Thivolle-Cazat, J.; Basset, J.-M. Versatility of silica used as a ligand: effect of thermal treatments of silica on the nature of silica-supported alkyl tantalum species. *J. Organomet. Chem.* **2000**, *593-594*, 96−100.
(695) Rascón, F.; Wischert, R.; Copéret, C. Molecular nature of support effects in single-site heterogeneous catalysts: silica vs. alumina. *Chem. Sci.* **2011**, *2*, 1449−1456.
(696) Trovitch, R. J.; Guo, N.; Janicke, M. T.; Li, H.; Marshall, C. L.; Miller, J. T.; Sattelberger, A. P.; John, K. D.; Baker, R. T. Spectroscopic Characterization of Alumina-Supported Bis(allyl) iridium Complexes: Site-Isolation, Reactivity, and Decomposition Studies. *Inorg. Chem.* **2010**, *49*, 2247−2258.
(697) Delgado, M.; Delbecq, F.; Santini, C. C.; Lefebvre, F.; Norsic, S.; Putaj, P.; Sautet, P.; Basset, J.-M. Evolution of Structure and of Grafting Properties of γ-Alumina with Pretreatment Temperature. *J. Phys. Chem. C* **2012**, *116*, 834−843.
(698) Bando, K. K.; Asakura, K.; Arakawa, H.; Isobe, K.; Iwasawa, Y. Surface Structures and Catalytic Hydroformylation Activities of Rh Dimers Attached on Various Inorganic Oxide Supports. *J. Phys. Chem.* **1996**, *100*, 13636−13645.
(699) Grasser, S.; Haeßner, C.; Köhler, K.; Lefebvre, F.; Basset, J.-M. Structures of paramagnetic V^{iv} amido complexes grafted onto metal oxide surfaces: Model systems for heterogeneous vanadium catalysts. *Phys. Chem. Chem. Phys.* **2003**, *5*, 1906−1911.
(700) Guzman, J.; Kuba, S.; Fierro-Gonzalez, J. C.; Gates, B. C. Formation of Gold Clusters on TiO_2 from Adsorbed Au-$(CH_3)_2(C_5H_7O_2)$: Characterization by X-ray Absorption Spectroscopy. *Catal. Lett.* **2004**, *95*, 77−86.
(701) Aguilar-Guerrero, V.; Gates, B. C. Genesis of a highly active cerium oxide-supported gold catalyst for CO oxidation. *Chem. Commun.* **2007**, 3210−3212.
(702) Khabuanchalad, S.; Wittayakun, J.; Lobo-Lapidus, R. J.; Stoll, S.; Britt, R. D.; Gates, B. C. Formation of MgO-Supported Manganese Carbonyl Complexes by Chemisorption of Mn(CO)5CH3. *Langmuir* **2013**, *29*, 6279−6286.
(703) Moses, A. W.; Raab, C.; Nelson, R. C.; Leifeste, H. D.; Ramsahye, N. A.; Chattopadhyay, S.; Eckert, J.; Chmelka, B. F.; Scott, S. L. Spectroscopically Distinct Sites Present in Methyltrioxorhenium Grafted onto Silica-Alumina, and Their Abilities to Initiate Olefin Metathesis. *J. Am. Chem. Soc.* **2007**, *129*, 8912−8920.
(704) Le Roux, E.; Taoufik, M.; Chabanas, M.; Alcor, D.; Baudouin, A.; Copéret, C.; Thivolle-Cazat, J.; Basset, J.-M.; Lesage, A.; Hediger, S.; et al. Well-Defined Surface Tungstenocarbyne Complexes through the Reaction of [W(⋮CtBu)(CH2tBu)3] with Silica. *Organometallics* **2005**, *24*, 4274−4279.
(705) Tosin, G.; Delgado, M.; Baudouin, A.; Santini, C. C.; Bayard, F.; Basset, J.-M. Surface Organometallic Chemistry of Hf(CH2tBu)4 on Silica and Silica-Alumina: Reaction of the Resulting Grafted

https://doi.org/10.1021/acs.chemrev.1c00905
Chem. Rev. XXXX, XXX, XXX−XXX

Hafnium Neopentyl with Dihydrogen. *Organometallics* **2010**, *29*, 1312−1322.
(706) Bonati, M. L. M.; Douglas, T. M.; Gaemers, S.; Guo, N. Synthesis, Characterization, and Catalytic Properties of Novel Single-Site and Nanosized Platinum Catalysts. *Organometallics* **2012**, *31*, 5243−5251.
(707) Samantaray, M. K.; Callens, E.; Abou-Hamad, E.; Rossini, A. J.; Widdifield, C. M.; Dey, R.; Emsley, L.; Basset, J.-M. WMe6 Tamed by Silica: ≡Si-O-WMe5 as an Efficient, Well-Defined Species for Alkane Metathesis, Leading to the Observation of a Supported W-Methyl/Methylidyne Species. *J. Am. Chem. Soc.* **2014**, *136*, 1054−1061.
(708) Le Roux, E.; Chabanas, M.; Baudouin, A.; de Mallmann, A.; Copéret, C.; Quadrelli, E. A.; Thivolle-Cazat, J.; Basset, J.-M.; Lukens, W.; Lesage, A.; et al. Detailed Structural Investigation of the Grafting of $[Ta(=CHtBu)(CH_2tBu)_3]$ and $[Cp^*TaMe_4]$ on Silica Partially Dehydroxylated at 700 °C and the Activity of the Grafted Complexes toward Alkane Metathesis. *J. Am. Chem. Soc.* **2004**, *126*, 13391−13399.
(709) Taoufik, M.; Roux, E. L.; Thivolle-Cazat, J.; Copéret, C.; Basset, J.-M.; Maunders, B.; Sunley, G. J. Alumina supported tungsten hydrides, new efficient catalysts for alkane metathesis. *Top. Catal.* **2006**, *40*, 65−70.
(710) Alphazan, T.; Bonduelle-Skrzypczak, A.; Legens, C.; Gay, A.-S.; Boudene, Z.; Girleanu, M.; Ersen, O.; Copéret, C.; Raybaud, P. Highly Active Nonpromoted Hydrotreating Catalysts through the Controlled Growth of a Supported Hexagonal WS_2 Phase. *ACS Catal.* **2014**, *4*, 4320−4331.
(711) Le Roux, E.; Taoufik, M.; Copéret, C.; de Mallmann, A.; Thivolle-Cazat, J.; Basset, J.-M.; Maunders, B. M.; Sunley, G. J. Development of Tungsten-Based Heterogeneous Alkane Metathesis Catalysts Through a Structure-Activity Relationship. *Angew. Chem., Int. Ed.* **2005**, *44*, 6755−6758.
(712) Ek, S.; Root, A.; Peussa, M.; Niinistö, L. Determination of the hydroxyl group content in silica by thermogravimetry and a comparison with 1H MAS NMR results. *Thermochim. Acta* **2001**, *379*, 201−212.
(713) Potapov, V. V.; Zhuravlev, L. T. Temperature Dependence of the Concentration of Silanol Groups in Silica Precipitated from a Hydrothermal Solution. *Glass Physics and Chemistry* **2005**, *31*, 661−670.
(714) Warring, S. L.; Beattie, D. A.; McQuillan, A. J. Surficial Siloxane-to-Silanol Interconversion during Room-Temperature Hydration/Dehydration of Amorphous Silica Films Observed by ATR-IR and TIR-Raman Spectroscopy. *Langmuir* **2016**, *32*, 1568−1576.
(715) Jarupatrakorn, J.; Tilley, T. D. Silica-Supported, Single-Site Titanium Catalysts for Olefin Epoxidation. A Molecular Precursor Strategy for Control of Catalyst Structure. *J. Am. Chem. Soc.* **2002**, *124*, 8380−8388.
(716) Héroguel, F.; Siddiqi, G.; Detwiler, M. D.; Zemlyanov, D. Y.; Safonova, O. V.; Copéret, C. Simultaneous generation of mild acidic functionalities and small supported Ir NPs from alumina-supported well-defined iridium siloxide. *J. Catal.* **2015**, *321*, 81−89.
(717) Ruddy, D. A.; Tilley, T. D. Highly selective olefin epoxidation with aqueous H_2O_2 over surface-modified TaSBA15 prepared via the TMP method. *Chem. Commun.* **2007**, 3350−3352.
(718) Delley, M. F.; Núñez-Zarur, F.; Conley, M. P.; Comas-Vives, A.; Siddiqi, G.; Norsic, S.; Monteil, V.; Safonova, O. V.; Copéret, C. Proton transfers are key elementary steps in ethylene polymerization on isolated chromium(III) silicates. *Proc. Natl. Acad. Sci. U. S. A.* **2014**, *111*, 11624.
(719) Marciniec, B.; Rogalski, S.; Potrzebowski, M. J.; Pietraszuk, C. Ruthenium Carbene Siloxide Complexes Immobilized on Silica: Synthesis and Catalytic Activity in Olefin Metathesis. *ChemCatChem.* **2011**, *3*, 904−910.
(720) Estes, D. P.; Bittner, C.; Àrias, Ò.; Casey, M.; Fedorov, A.; Tamm, M.; Copéret, C. Alkyne Metathesis with Silica-Supported and Molecular Catalysts at Parts-per-Million Loadings. *Angew. Chem., Int. Ed.* **2016**, *55*, 13960−13964.
(721) Pucino, M.; Mougel, V.; Schowner, R.; Fedorov, A.; Buchmeiser, M. R.; Copéret, C. Cationic Silica-Supported N-Heterocyclic Carbene Tungsten Oxo Alkylidene Sites: Highly Active and Stable Catalysts for Olefin Metathesis. *Angew. Chem., Int. Ed.* **2016**, *55*, 4300−4302.
(722) Bendjeriou-Sedjerari, A.; Sofack-Kreutzer, J.; Minenkov, Y.; Abou-Hamad, E.; Hamzaoui, B.; Werghi, B.; Anjum, D. H.; Cavallo, L.; Huang, K.-W.; Basset, J.-M. Tungsten(VI) Carbyne/Bis(carbene) Tautomerization Enabled by N-Donor SBA15 Surface Ligands: A Solid-State NMR and DFT Study. *Angew. Chem., Int. Ed.* **2016**, *55*, 11162−11166.
(723) Mazoyer, E.; Merle, N.; Mallmann, A. d.; Basset, J.-M.; Berrier, E.; Delevoye, L.; Paul, J.-F.; Nicholas, C. P.; Gauvin, R. M.; Taoufik, M. Development of the first well-defined tungsten oxo alkyl derivatives supported on silica by SOMC: towards a model of WO_3/SiO_2 olefin metathesis catalyst. *Chem. Commun.* **2010**, *46*, 8944−8946.
(724) Genelot, M.; Cheval, N. P.; Vitorino, M.; Berrier, E.; Weibel, J.-M.; Pale, P.; Mortreux, A.; Gauvin, R. M. Well-defined silica-supported molybdenum nitride species: silica grafting triggers alkyne metathesis activity. *Chem. Sci.* **2013**, *4*, 2680−2685.
(725) Estes, D. P.; Gordon, C. P.; Fedorov, A.; Liao, W.-C.; Ehrhorn, H.; Bittner, C.; Zier, M. L.; Bockfeld, D.; Chan, K. W.; Eisenstein, O.; et al. Molecular and Silica-Supported Molybdenum Alkyne Metathesis Catalysts: Influence of Electronics and Dynamics on Activity Revealed by Kinetics, Solid-State NMR, and Chemical Shift Analysis. *J. Am. Chem. Soc.* **2017**, *139*, 17597−17607.
(726) Lopez, L. P. H.; Schrock, R. R.; Müller, P. Dimers that Contain Unbridged W(IV)/W(IV) Double Bonds. *Organometallics* **2006**, *25*, 1978−1986.
(727) Mougel, V.; Copéret, C. Magnitude and consequences of OR ligand σ-donation on alkene metathesis activity in d0 silica supported (≡SiO)W(NAr)(=CHtBu)(OR) catalysts. *Chem. Sci.* **2014**, *5*, 2475−2481.
(728) Gauvin, R. M.; Mortreux, A. Silica-supported lanthanide silylamides for methyl methacrylate polymerisation: controlled grafting induces controlled reactivity. *Chem. Commun.* **2005**, 1146−1148.
(729) Ajellal, N.; Durieux, G.; Delevoye, L.; Tricot, G.; Dujardin, C.; Thomas, C. M.; Gauvin, R. M. Polymerization of racemic β-butyrolactone using supported catalysts: a simple access to isotactic polymers. *Chem. Commun.* **2010**, *46*, 1032−1034.
(730) Dötterl, M.; Alt, H. G. Silica Based Cocatalysts for Heterogeneous Olefin Dimerization and Ethene Polymerization Reactions with Nickel Complexes. *ChemCatChem.* **2012**, *4*, 660−667.
(731) Chen, Y.; Callens, E.; Abou-Hamad, E.; Merle, N.; White, A. J. P.; Taoufik, M.; Copéret, C.; Le Roux, E.; Basset, J.-M. $[(\equiv SiO)\text{-}Ta^{V}Cl_2Me_2]$: A Well-Defined Silica-Supported Tantalum(V) Surface Complex as Catalyst Precursor for the Selective Cocatalyst-Free Trimerization of Ethylene. *Angew. Chem., Int. Ed.* **2012**, *51*, 11886−11889.
(732) Le Roux, E.; Liang, Y.; Törnroos, K. W.; Nief, F.; Anwander, R. Heterogenization of Lanthanum and Neodymium Monophosphacyclopentadienyl Bis(tetramethylaluminate) Complexes onto Periodic Mesoporous Silica SBA-15. *Organometallics* **2012**, *31*, 6526−6537.
(733) Chen, E. Y.-X.; Marks, T. J. Cocatalysts for Metal-Catalyzed Olefin Polymerization: Activators, Activation Processes, and Structure-Activity Relationships. *Chem. Rev.* **2000**, *100*, 1391−1434.
(734) Amor Nait Ajjou, J.; Scott, S. L. A Kinetic Study of Ethylene and 1-Hexene Homo- and Copolymerization Catalyzed by a Silica-Supported Cr(IV) Complex: Evidence for Propagation by a Migratory Insertion Mechanism. *J. Am. Chem. Soc.* **2000**, *122*, 8968−8976.
(735) Jezequel, M.; Dufaud, V.; Ruiz-Garcia, M. J.; Carrillo-Hermosilla, F.; Neugebauer, U.; Niccolai, G. P.; Lefebvre, F.; Bayard, F.; Corker, J.; Fiddy, S.; et al. Supported Metallocene Catalysts by Surface Organometallic Chemistry. Synthesis, Characterization, and Reactivity in Ethylene Polymerization of Oxide-Supported Mono- and Biscyclopentadienyl Zirconium Alkyl Com-

https://doi.org/10.1021/acs.chemrev.1c00905
Chem. Rev. XXXX, XXX, XXX−XXX

plexes: Establishment of Structure/Reactivity Relationships. *J. Am. Chem. Soc.* **2001**, *123*, 3520−3540.
(736) Scott, S. L.; Church, T. L.; Nguyen, D. H.; Mader, E. A.; Moran, J. An investigation of catalyst/cocatalyst/support interactions in silica-supported olefin polymerization catalysts based on Cp*TiMe$_3$*. *Top. Catal.* **2005**, *34*, 109−120.
(737) Schweitzer, N. M.; Hu, B.; Das, U.; Kim, H.; Greeley, J.; Curtiss, L. A.; Stair, P. C.; Miller, J. T.; Hock, A. S. Propylene Hydrogenation and Propane Dehydrogenation by a Single-Site Zn^{2+} on Silica Catalyst. *ACS Catal.* **2014**, *4*, 1091−1098.
(738) Rimoldi, M.; Mezzetti, A. Batch and Continuous Flow Hydrogenation of Liquid and Gaseous Alkenes Catalyzed by a Silica-grafted Iridium(III) Hydride. *Helv. Chim. Acta* **2016**, *99*, 908−915.
(739) Gu, W.; Stalzer, M. M.; Nicholas, C. P.; Bhattacharyya, A.; Motta, A.; Gallagher, J. R.; Zhang, G.; Miller, J. T.; Kobayashi, T.; Pruski, M.; et al. Benzene Selectivity in Competitive Arene Hydrogenation: Effects of Single-Site Catalyst···Acidic Oxide Surface Binding Geometry. *J. Am. Chem. Soc.* **2015**, *137*, 6770−6780.
(740) Coperet, C. C-H Bond Activation and Organometallic Intermediates on Isolated Metal Centers on Oxide Surfaces. *Chem. Rev.* **2010**, *110*, 656−680.
(741) Copéret, C.; Allouche, F.; Chan, K. W.; Conley, M. P.; Delley, M. F.; Fedorov, A.; Moroz, I. B.; Mougel, V.; Pucino, M.; Searles, K.; et al. Bridging the Gap between Industrial and Well-Defined Supported Catalysts. *Angew. Chem., Int. Ed.* **2018**, *57*, 6398−6440.
(742) Qiao, B.; Wang, A.; Yang, X.; Allard, L. F.; Jiang, Z.; Cui, Y.; Liu, J.; Li, J.; Zhang, T. Single-atom catalysis of CO oxidation using Pt_1/FeO_x. *Nat. Chem.* **2011**, *3*, 634−641.
(743) Ji, S.; Chen, Y.; Wang, X.; Zhang, Z.; Wang, D.; Li, Y. Chemical Synthesis of Single Atomic Site Catalysts. *Chem. Rev.* **2020**, *120*, 11900.
(744) Nie, L.; Mei, D.; Xiong, H.; Peng, B.; Ren, Z.; Hernandez, X. I. P.; DeLaRiva, A.; Wang, M.; Engelhard, M. H.; Kovarik, L.; et al. Activation of surface lattice oxygen in single-atom Pt/CeO_2 for low-temperature CO oxidation. *Science* **2017**, *358*, 1419.
(745) Chen, J.; Wanyan, Y.; Zeng, J.; Fang, H.; Li, Z.; Dong, Y.; Qin, R.; Wu, C.; Liu, D.; Wang, M.; et al. Surface Engineering Protocol To Obtain an Atomically Dispersed Pt/CeO_2 Catalyst with High Activity and Stability for CO Oxidation. *ACS Sustainable Chem. Eng.* **2018**, *6*, 14054−14062.
(746) Chen, L.-N.; Hou, K.-P.; Liu, Y.-S.; Qi, Z.-Y.; Zheng, Q.; Lu, Y.-H.; Chen, J.-Y.; Chen, J.-L.; Pao, C.-W.; Wang, S.-B.; et al. Efficient Hydrogen Production from Methanol Using a Single-Site Pt_1/CeO_2 Catalyst. *J. Am. Chem. Soc.* **2019**, *141*, 17995−17999.
(747) DeRita, L.; Dai, S.; Lopez-Zepeda, K.; Pham, N.; Graham, G. W.; Pan, X.; Christopher, P. Catalyst Architecture for Stable Single Atom Dispersion Enables Site-Specific Spectroscopic and Reactivity Measurements of CO Adsorbed to Pt Atoms, Oxidized Pt Clusters, and Metallic Pt Clusters on TiO_2. *J. Am. Chem. Soc.* **2017**, *139*, 14150−14165.
(748) DeRita, L.; Resasco, J.; Dai, S.; Boubnov, A.; Thang, H. V.; Hoffman, A. S.; Ro, I.; Graham, G. W.; Bare, S. R.; Pacchioni, G.; et al. Structural evolution of atomically dispersed Pt catalysts dictates reactivity. *Nat. Mater.* **2019**, *18*, 746−751.
(749) Qi, J.; Christopher, P. Atomically Dispersed Rh Active Sites on Oxide Supports with Controlled Acidity for Gas-Phase Halide-Free Methanol Carbonylation to Acetic Acid. *Ind. Eng. Chem. Res.* **2019**, *58*, 12632−12641.
(750) Resasco, J.; DeRita, L.; Dai, S.; Chada, J. P.; Xu, M.; Yan, X.; Finzel, J.; Hanukovich, S.; Hoffman, A. S.; Graham, G. W.; et al. Uniformity Is Key in Defining Structure-Function Relationships for Atomically Dispersed Metal Catalysts: The Case of Pt/CeO_2. *J. Am. Chem. Soc.* **2020**, *142*, 169−184.
(751) Wei, H.; Liu, X.; Wang, A.; Zhang, L.; Qiao, B.; Yang, X.; Huang, Y.; Miao, S.; Liu, J.; Zhang, T. FeO_x-supported platinum single-atom and pseudo-single-atom catalysts for chemoselective hydrogenation of functionalized nitroarenes. *Nat. Commun.* **2014**, *5*, 5634.
(752) Li, T.; Liu, F.; Tang, Y.; Li, L.; Miao, S.; Su, Y.; Zhang, J.; Huang, J.; Sun, H.; Haruta, M.; et al. Maximizing the Number of Interfacial Sites in Single-Atom Catalysts for the Highly Selective, Solvent-Free Oxidation of Primary Alcohols. *Angew. Chem., Int. Ed.* **2018**, *57*, 7795−7799.
(753) Lu, Y.; Wang, J.; Yu, L.; Kovarik, L.; Zhang, X.; Hoffman, A. S.; Gallo, A.; Bare, S. R.; Sokaras, D.; Kroll, T.; et al. Identification of the active complex for CO oxidation over single-atom Ir-on-$MgAl_2O_4$ catalysts. *Nat. Catal.* **2019**, *2*, 149−156.
(754) Lin, L.; Yao, S.; Gao, R.; Liang, X.; Yu, Q.; Deng, Y.; Liu, J.; Peng, M.; Jiang, Z.; Li, S.; et al. A highly CO-tolerant atomically dispersed Pt catalyst for chemoselective hydrogenation. *Nat. Nanotechnol.* **2019**, *14*, 354−361.
(755) Wei, H.; Huang, K.; Wang, D.; Zhang, R.; Ge, B.; Ma, J.; Wen, B.; Zhang, S.; Li, Q.; Lei, M.; et al. Iced photochemical reduction to synthesize atomically dispersed metals by suppressing nanocrystal growth. *Nat. Commun.* **2017**, *8*, 1490.
(756) Huang, K.; Wang, R.; Wu, H.; Wang, H.; He, X.; Wei, H.; Wang, S.; Zhang, R.; Lei, M.; Guo, W.; et al. Direct immobilization of an atomically dispersed Pt catalyst by suppressing heterogeneous nucleation at -40 °C. *J. Mater. Chem. A* **2019**, *7*, 25779−25784.
(757) Zhou, S.; Shang, L.; Zhao, Y.; Shi, R.; Waterhouse, G. I. N.; Huang, Y.-C.; Zheng, L.; Zhang, T. Pd Single-Atom Catalysts on Nitrogen-Doped Graphene for the Highly Selective Photothermal Hydrogenation of Acetylene to Ethylene. *Adv. Mater.* **2019**, *31*, 1900509.
(758) Li, Y.; Hao, J.; Song, H.; Zhang, F.; Bai, X.; Meng, X.; Zhang, H.; Wang, S.; Hu, Y.; Ye, J. Selective light absorber-assisted single nickel atom catalysts for ambient sunlight-driven CO_2 methanation. *Nat. Commun.* **2019**, *10*, 2359.
(759) Liu, G.; Robertson, A. W.; Li, M. M.-J.; Kuo, W. C. H.; Darby, M. T.; Muhieddine, M. H.; Lin, Y.-C.; Suenaga, K.; Stamatakis, M.; Warner, J. H.; et al. MoS_2 monolayer catalyst doped with isolated Co atoms for the hydrodeoxygenation reaction. *Nat. Chem.* **2017**, *9*, 810−816.
(760) He, Q.; Tian, D.; Jiang, H.; Cao, D.; Wei, S.; Liu, D.; Song, P.; Lin, Y.; Song, L. Achieving Efficient Alkaline Hydrogen Evolution Reaction over a Ni5P4 Catalyst Incorporating Single-Atomic Ru Sites. *Adv. Mater.* **2020**, *32*, 1906972.
(761) Chen, Y.; Ji, S.; Sun, W.; Lei, Y.; Wang, Q.; Li, A.; Chen, W.; Zhou, G.; Zhang, Z.; Wang, Y.; et al. Engineering the Atomic Interface with Single Platinum Atoms for Enhanced Photocatalytic Hydrogen Production. *Angew. Chem., Int. Ed.* **2020**, *59*, 1295−1301.
(762) Sun, S.; Zhang, G.; Gauquelin, N.; Chen, N.; Zhou, J.; Yang, S.; Chen, W.; Meng, X.; Geng, D.; Banis, M. N.; et al. Single-atom Catalysis Using Pt/Graphene Achieved through Atomic Layer Deposition. *Sci. Rep.* **2013**, *3*, 1775.
(763) Lu, J.; Elam, J. W.; Stair, P. C. Atomic layer deposition—Sequential self-limiting surface reactions for advanced catalyst "bottom-up" synthesis. *Surf. Sci. Rep.* **2016**, *71*, 410−472.
(764) Singh, J. A.; Yang, N.; Bent, S. F. Nanoengineering Heterogeneous Catalysts by Atomic Layer Deposition. *Annu. Rev. Chem. Biomol. Eng.* **2017**, *8*, 41−62.
(765) Zhang, L.; Si, R.; Liu, H.; Chen, N.; Wang, Q.; Adair, K.; Wang, Z.; Chen, J.; Song, Z.; Li, J.; et al. Atomic layer deposited Pt-Ru dual-metal dimers and identifying their active sites for hydrogen evolution reaction. *Nat. Commun.* **2019**, *10*, 4936.
(766) Yan, H.; Cheng, H.; Yi, H.; Lin, Y.; Yao, T.; Wang, C.; Li, J.; Wei, S.; Lu, J. Single-Atom Pd1/Graphene Catalyst Achieved by Atomic Layer Deposition: Remarkable Performance in Selective Hydrogenation of 1,3-Butadiene. *J. Am. Chem. Soc.* **2015**, *137*, 10484−10487.
(767) Gawande, M. B.; Fornasiero, P.; Zbořil, R. Carbon-Based Single-Atom Catalysts for Advanced Applications. *ACS Catal.* **2020**, *10*, 2231−2259.
(768) Chen, Y.; Ji, S.; Sun, W.; Chen, W.; Dong, J.; Wen, J.; Zhang, J.; Li, Z.; Zheng, L.; Chen, C.; et al. Discovering Partially Charged Single-Atom Pt for Enhanced Anti-Markovnikov Alkene Hydrosilylation. *J. Am. Chem. Soc.* **2018**, *140*, 7407−7410.

https://doi.org/10.1021/acs.chemrev.1c00905
Chem. Rev. XXXX, XXX, XXX−XXX

(769) Qiu, H. J.; Ito, Y.; Cong, W.; Tan, Y.; Liu, P.; Hirata, A.; Fujita, T.; Tang, Z.; Chen, M. Nanoporous Graphene with Single-Atom Nickel Dopants: An Efficient and Stable Catalyst for Electrochemical Hydrogen Production. *Angew. Chem., Int. Ed.* **2015**, *54*, 14031−14035.
(770) Wang, B.; Wang, X.; Zou, J.; Yan, Y.; Xie, S.; Hu, G.; Li, Y.; Dong, A. Simple-Cubic Carbon Frameworks with Atomically Dispersed Iron Dopants toward High-Efficiency Oxygen Reduction. *Nano Lett.* **2017**, *17*, 2003−2009.
(771) Xue, Y.; Huang, B.; Yi, Y.; Guo, Y.; Zuo, Z.; Li, Y.; Jia, Z.; Liu, H.; Li, Y. Anchoring zero valence single atoms of nickel and iron on graphdiyne for hydrogen evolution. *Nat. Commun.* **2018**, *9*, 1460.
(772) Fei, H.; Dong, J.; Wan, C.; Zhao, Z.; Xu, X.; Lin, Z.; Wang, Y.; Liu, H.; Zang, K.; Luo, J.; et al. Microwave-Assisted Rapid Synthesis of Graphene-Supported Single Atomic Metals. *Adv. Mater.* **2018**, *30*, 1802146.
(773) Yao, Y.; Huang, Z.; Xie, P.; Wu, L.; Ma, L.; Li, T.; Pang, Z.; Jiao, M.; Liang, Z.; Gao, J.; et al. High temperature shockwave stabilized single atoms. *Nat. Nanotechnol.* **2019**, *14*, 851−857.
(774) Cui, X.; Xiao, J.; Wu, Y.; Du, P.; Si, R.; Yang, H.; Tian, H.; Li, J.; Zhang, W.-H.; Deng, D.; et al. A Graphene Composite Material with Single Cobalt Active Sites: A Highly Efficient Counter Electrode for Dye-Sensitized Solar Cells. *Angew. Chem., Int. Ed.* **2016**, *55*, 6708−6712.
(775) Chen, L.; Sterbinsky, G. E.; Tait, S. L. Synthesis of platinum single-site centers through metal-ligand self-assembly on powdered metal oxide supports. *J. Catal.* **2018**, *365*, 303−312.
(776) Ding, S.; Guo, Y.; Hülsey, M. J.; Zhang, B.; Asakura, H.; Liu, L.; Han, Y.; Gao, M.; Hasegawa, J.-y.; Qiao, B.; et al. Electrostatic Stabilization of Single-Atom Catalysts by Ionic Liquids. *Chem.* **2019**, *5*, 3207−3219.
(777) Tauster, S. J. Strong metal-support interactions. *Acc. Chem. Res.* **1987**, *20*, 389−394.
(778) Resasco, D. E.; Haller, G. L. A model of metal-oxide support interaction for Rh on TiO_2. *J. Catal.* **1983**, *82*, 279−288.
(779) de la Peña O'Shea, V. A.; Álvarez Galván, M. C.; Platero Prats, A. E.; Campos-Martin, J. M.; Fierro, J. L. G. Direct evidence of the SMSI decoration effect: The case of Co/TiO_2 catalyst. *Chem. Commun.* **2011**, *47*, 7131−7133.
(780) Liu, X. Y.; Wang, A.; Zhang, T.; Mou, C.-Y. Catalysis by gold: New insights into the support effect. *Nano Today* **2013**, *8*, 403−416.
(781) Han, B.; Guo, Y.; Huang, Y.; Xi, W.; Xu, J.; Luo, J.; Qi, H.; Ren, Y.; Liu, X.; Qiao, B.; et al. Strong Metal-Support Interactions between Pt Single Atoms and TiO_2. *Angew. Chem., Int. Ed.* **2020**, *59*, 11824−11829.
(782) Daelman, N.; Capdevila-Cortada, M.; López, N. Dynamic charge and oxidation state of Pt/CeO_2 single-atom catalysts. *Nat. Mater.* **2019**, *18*, 1215−1221.
(783) Vindigni, F.; Manzoli, M.; Chiorino, A.; Boccuzzi, F. Catalytically active gold sites: nanoparticles, borderline sites, clusters, cations, anions? FTIR spectra analysis of ^{12}CO and ^{12}CO-^{13}CO isotopic mixtures. *Gold Bulletin* **2009**, *42*, 106−112.
(784) Wang, C.; Gu, X.-K.; Yan, H.; Lin, Y.; Li, J.; Liu, D.; Li, W.-X.; Lu, J. Water-Mediated Mars-Van Krevelen Mechanism for CO Oxidation on Ceria-Supported Single-Atom Pt1 Catalyst. *ACS Catal.* **2017**, *7*, 887−891.
(785) Rivera-Cárcamo, C.; Serp, P. Single Atom Catalysts on Carbon-Based Materials. *ChemCatChem.* **2018**, *10*, 5058−5091.
(786) Parkinson, G. S. Single-Atom Catalysis: How Structure Influences Catalytic Performance. *Catal. Lett.* **2019**, *149*, 1137−1146.
(787) Wang, Q.; Huang, X.; Zhao, Z. L.; Wang, M.; Xiang, B.; Li, J.; Feng, Z.; Xu, H.; Gu, M. Ultrahigh-Loading of Ir Single Atoms on NiO Matrix to Dramatically Enhance Oxygen Evolution Reaction. *J. Am. Chem. Soc.* **2020**, *142*, 7425−7433.
(788) Gao, C.; Low, J.; Long, R.; Kong, T.; Zhu, J.; Xiong, Y. Heterogeneous Single-Atom Photocatalysts: Fundamentals and Applications. *Chem. Rev.* **2020**, *120*, 12175.
(789) Zhang, Z.; Zhu, Y.; Asakura, H.; Zhang, B.; Zhang, J.; Zhou, M.; Han, Y.; Tanaka, T.; Wang, A.; Zhang, T.; et al. Thermally stable single atom $Pt/m\text{-}Al_2O_3$ for selective hydrogenation and CO oxidation. *Nat. Commun.* **2017**, *8*, 16100.
(790) Huang, F.; Deng, Y.; Chen, Y.; Cai, X.; Peng, M.; Jia, Z.; Xie, J.; Xiao, D.; Wen, X.; Wang, N.; et al. Anchoring Cu_1 species over nanodiamond-graphene for semi-hydrogenation of acetylene. *Nat. Commun.* **2019**, *10*, 4431.
(791) Li, X.; Yang, X.; Huang, Y.; Zhang, T.; Liu, B. Supported Noble-Metal Single Atoms for Heterogeneous Catalysis. *Adv. Mater.* **2019**, *31*, 1902031.
(792) Liu, L.; Corma, A. Evolution of Isolated Atoms and Clusters in Catalysis. *Trends in Chemistry* **2020**, *2*, 383−400.
(793) Li, X.; Rong, H.; Zhang, J.; Wang, D.; Li, Y. Modulating the local coordination environment of single-atom catalysts for enhanced catalytic performance. *Nano Res.* **2020**, *13*, 1842−1855.
(794) Han, J.; Lu, J.; Wang, M.; Wang, Y.; Wang, F. Single Atom Alloy Preparation and Applications in Heterogeneous Catalysis. *Chin. J. Chem.* **2019**, *37*, 977−988.
(795) Hannagan, R. T.; Giannakakis, G.; Flytzani-Stephanopoulos, M.; Sykes, E. C. H. Single-Atom Alloy Catalysis. *Chem. Rev.* **2020**, *120*, 12044−12088.
(796) Sinfelt, J. H. *Bimetallic Catalysts: Discoveries, Concepts and Applications*; John Wiley and Sons: New York, 1983.
(797) Ferrando, R.; Jellinek, J.; Johnston, R. L. Nanoalloys: From Theory to Applications of Alloy Clusters and Nanoparticles. *Chem. Rev.* **2008**, *108*, 845−910.
(798) Yu, W.; Porosoff, M. D.; Chen, J. G. Review of Pt-Based Bimetallic Catalysis: From Model Surfaces to Supported Catalysts. *Chem. Rev.* **2012**, *112*, 5780−5817.
(799) Rodriguez, J. A. Physical and Chemical Properties of Bimetallic Surfaces. *Surf. Sci. Rep.* **1996**, *24*, 223−287.
(800) Wang, Y.; Balbuena, P. B. Design of Oxygen Reduction Bimetallic Catalysts: Ab-Initio-Derived Thermodynamic Guidelines. *J. Phys. Chem. B* **2005**, *109*, 18902−18906.
(801) Medford, A. J.; Vojvodic, A.; Hummelshøj, J. S.; Voss, J.; Abild-Pedersen, F.; Studt, F.; Bligaard, T.; Nilsson, A.; Nørskov, J. K. From the Sabatier principle to a predictive theory of transition-metal heterogeneous catalysis. *J. Catal.* **2015**, *328*, 36−42.
(802) Greiner, M. T.; Jones, T. E.; Beeg, S.; Zwiener, L.; Scherzer, M.; Girgsdies, F.; Piccinin, S.; Armbrüster, M.; Knop-Gericke, A.; Schlögl, R. Free-atom-like d states in single-atom alloy catalysts. *Nat. Chem.* **2018**, *10*, 1008−1015.
(803) Sarfraz, S.; Garcia-Esparza, A. T.; Jedidi, A.; Cavallo, L.; Takanabe, K. Cu-Sn Bimetallic Catalyst for Selective Aqueous Electroreduction of CO_2 to CO. *ACS Catal.* **2016**, *6*, 2842−2851.
(804) Duchesne, P. N.; Li, Z. Y.; Deming, C. P.; Fung, V.; Zhao, X.; Yuan, J.; Regier, T.; Aldalbahi, A.; Almarhoon, Z.; Chen, S.; et al. Golden single-atomic-site platinum electrocatalysts. *Nat. Mater.* **2018**, *17*, 1033−1039.
(805) *Metal-Support and Metal-Additive Effects in Catalysis*; Naccache, G., Coudurier, H., Praliaud, P., Meriaudeau, P., Gallezot, G. A., Martin, G. A., Vedrine, J. C., Eds.; Elsevier: New York, 1982; Vol. *11*.
(806) Osaki, T.; Mori, T. Role of Potassium in Carbon-Free CO_2 Reforming of Methane on K-Promoted Ni/Al_2O_3 Catalysts. *J. Catal.* **2001**, *204*, 89−97.
(807) Haneda, M.; Kintaichi, Y.; Bion, N.; Hamada, H. Alkali metal-doped cobalt oxide catalysts for NO decomposition. *Appl. Catal. B* **2003**, *46*, 473−482.
(808) Cao, Y.; Chen, B.; Guerrero-Sánchez, J.; Lee, I.; Zhou, X.; Takeuchi, N.; Zaera, F. Controlling Selectivity in Unsaturated Aldehyde Hydrogenation Using Single-Site Alloy Catalysts. *ACS Catal.* **2019**, *9*, 9150−9157.
(809) Aich, P.; Wei, H.; Basan, B.; Kropf, A. J.; Schweitzer, N. M.; Marshall, C. L.; Miller, J. T.; Meyer, R. Single-Atom Alloy Pd-Ag Catalyst for Selective Hydrogenation of Acrolein. *J. Phys. Chem. C* **2015**, *119*, 18140−18148.
(810) Pei, G. X.; Liu, X. Y.; Yang, X.; Zhang, L.; Wang, A.; Li, L.; Wang, H.; Wang, X.; Zhang, T. Performance of Cu-Alloyed Pd Single-

https://doi.org/10.1021/acs.chemrev.1c00905
Chem. Rev. XXXX, XXX, XXX−XXX

Atom Catalyst for Semihydrogenation of Acetylene under Simulated Front-End Conditions. *ACS Catal.* **2017**, *7*, 1491−1500.
(811) Xing, F.; Jeon, J.; Toyao, T.; Shimizu, K.-i.; Furukawa, S. A Cu-Pd single-atom alloy catalyst for highly efficient NO reduction. *Chem. Sci.* **2019**, *10*, 8292−8298.
(812) Giannakakis, G.; Trimpalis, A.; Shan, J.; Qi, Z.; Cao, S.; Liu, J.; Ye, J.; Biener, J.; Flytzani-Stephanopoulos, M. NiAu Single Atom Alloys for the Non-oxidative Dehydrogenation of Ethanol to Acetaldehyde and Hydrogen. *Top. Catal.* **2018**, *61*, 475−486.
(813) Boucher, M. B.; Zugic, B.; Cladaras, G.; Kammert, J.; Marcinkowski, M. D.; Lawton, T. J.; Sykes, E. C. H.; Flytzani-Stephanopoulos, M. Single atom alloy surface analogs in $Pd_{0.18}Cu_{15}$ nanoparticles for selective hydrogenation reactions. *Phys. Chem. Chem. Phys.* **2013**, *15*, 12187−12196.
(814) da Silva, A. G. M.; Rodrigues, T. S.; Haigh, S. J.; Camargo, P. H. C. Galvanic replacement reaction: recent developments for engineering metal nanostructures towards catalytic applications. *Chem. Commun.* **2017**, *53*, 7135−7148.
(815) Raman, N.; Maisel, S.; Grabau, M.; Taccardi, N.; Debuschewitz, J.; Wolf, M.; Wittkämper, H.; Bauer, T.; Wu, M.; Haumann, M.; et al. Highly Effective Propane Dehydrogenation Using Ga-Rh Supported Catalytically Active Liquid Metal Solutions. *ACS Catal.* **2019**, *9*, 9499−9507.
(816) Yao, Y.; Hu, S.; Chen, W.; Huang, Z.-Q.; Wei, W.; Yao, T.; Liu, R.; Zang, K.; Wang, X.; Wu, G.; et al. Engineering the electronic structure of single atom Ru sites via compressive strain boosts acidic water oxidation electrocatalysis. *Nat. Catal.* **2019**, *2*, 304−313.
(817) Therrien, A. J.; Hensley, A. J. R.; Marcinkowski, M. D.; Zhang, R.; Lucci, F. R.; Coughlin, B.; Schilling, A. C.; McEwen, J.-S.; Sykes, E. C. H. An atomic-scale view of single-site Pt catalysis for low-temperature CO oxidation. *Nat. Catal.* **2018**, *1*, 192−198.
(818) Lucci, F. R.; Liu, J.; Marcinkowski, M. D.; Yang, M.; Allard, L. F.; Flytzani-Stephanopoulos, M.; Sykes, E. C. H. Selective hydrogenation of 1,3-butadiene on platinum-copper alloys at the single-atom limit. *Nat. Commun.* **2015**, *6*, 8550.
(819) Lv, C.-Q.; Liu, J.-H.; Guo, Y.; Wang, G.-C. Selective hydrogenation of 1,3-butadiene over single Pt_1/Cu(111) model catalysts: A DFT study. *Appl. Surf. Sci.* **2019**, *466*, 946−955.
(820) Yang, K.; Yang, B. Identification of the Active and Selective Sites over a Single Pt Atom-Alloyed Cu Catalyst for the Hydrogenation of 1,3-Butadiene: A Combined DFT and Microkinetic Modeling Study. *J. Phys. Chem. C* **2018**, *122*, 10883−10891.
(821) Luneau, M.; Shirman, T.; Foucher, A. C.; Duanmu, K.; Verbart, D. M. A.; Sautet, P.; Stach, E. A.; Aizenberg, J.; Madix, R. J.; Friend, C. M. Achieving High Selectivity for Alkyne Hydrogenation at High Conversions with Compositionally Optimized PdAu Nanoparticle Catalysts in Raspberry Colloid-Templated SiO_2. *ACS Catal.* **2020**, *10*, 441−450.
(822) Cao, Y.; Guerrero-Sańchez, J.; Lee, I.; Zhou, X.; Takeuchi, N.; Zaera, F. Kinetic Study of the Hydrogenation of Unsaturated Aldehydes Promoted by $CuPt_x$/SBA-15 Single-Atom Alloy (SAA) Catalysts. *ACS Catal.* **2020**, *10*, 3431−3443.
(823) Meng, Y.; Xia, S.; Zhou, X.; Pan, G. Mechanism of selective hydrogenation of cinnamaldehyde on Ni-Pt(111) with different structures: A comparative study. *Chem. Phys. Lett.* **2020**, *740*, 137049.
(824) Wang, Z.-T.; Hoyt, R. A.; El-Soda, M.; Madix, R. J.; Kaxiras, E.; Sykes, E. C. H. Dry Dehydrogenation of Ethanol on Pt-Cu Single Atom Alloys. *Top. Catal.* **2018**, *61*, 328−335.
(825) Marcinkowski, M. D.; Liu, J.; Murphy, C. J.; Liriano, M. L.; Wasio, N. A.; Lucci, F. R.; Flytzani-Stephanopoulos, M.; Sykes, E. C. H. Selective Formic Acid Dehydrogenation on Pt-Cu Single-Atom Alloys. *ACS Catal.* **2017**, *7*, 413−420.
(826) Peng, Y.; Geng, Z.; Zhao, S.; Wang, L.; Li, H.; Wang, X.; Zheng, X.; Zhu, J.; Li, Z.; Si, R.; et al. Pt Single Atoms Embedded in the Surface of Ni Nanocrystals as Highly Active Catalysts for Selective Hydrogenation of Nitro Compounds. *Nano Lett.* **2018**, *18*, 3785−3791.
(827) Jirkovský, J. S.; Panas, I.; Ahlberg, E.; Halasa, M.; Romani, S.; Schiffrin, D. J. Single Atom Hot-Spots at Au-Pd Nanoalloys for Electrocatalytic H_2O_2 Production. *J. Am. Chem. Soc.* **2011**, *133*, 19432−19441.
(828) Zhou, L.; Martirez, J. M. P.; Finzel, J.; Zhang, C.; Swearer, D. F.; Tian, S.; Robatjazi, H.; Lou, M.; Dong, L.; Henderson, L.; et al. Light-driven methane dry reforming with single atomic site antenna-reactor plasmonic photocatalysts. *Nature Energy* **2020**, *5*, 61−70.
(829) Kyriakou, G.; Boucher, M. B.; Jewell, A. D.; Lewis, E. A.; Lawton, T. J.; Baber, A. E.; Tierney, H. L.; Flytzani-Stephanopoulos, M.; Sykes, E. C. H. Isolated Metal Atom Geometries as a Strategy for Selective Heterogeneous Hydrogenations. *Science* **2012**, *335*, 1209−1212.
(830) Lucci, F. R.; Marcinkowski, M. D.; Lawton, T. J.; Sykes, E. C. H. H_2 Activation and Spillover on Catalytically Relevant Pt-Cu Single Atom Alloys. *J. Phys. Chem. C* **2015**, *119*, 24351−24357.
(831) Darby, M. T.; Stamatakis, M.; Michaelides, A.; Sykes, E. C. H. Lonely Atoms with Special Gifts: Breaking Linear Scaling Relationships in Heterogeneous Catalysis with Single-Atom Alloys. *J. Phys. Chem. Lett.* **2018**, *9*, 5636−5646.
(832) Lucci, F. R.; Lawton, T. J.; Pronschinske, A.; Sykes, E. C. H. Atomic Scale Surface Structure of Pt/Cu(111) Surface Alloys. *J. Phys. Chem. C* **2014**, *118*, 3015−3022.
(833) Lucci, F. R.; Darby, M. T.; Mattera, M. F. G.; Ivimey, C. J.; Therrien, A. J.; Michaelides, A.; Stamatakis, M.; Sykes, E. C. H. Controlling Hydrogen Activation, Spillover, and Desorption with Pd-Au Single-Atom Alloys. *J. Phys. Chem. Lett.* **2016**, *7*, 480−485.
(834) Darby, M. T.; Réocreux, R.; Sykes, E. C. H.; Michaelides, A.; Stamatakis, M. Elucidating the Stability and Reactivity of Surface Intermediates on Single-Atom Alloy Catalysts. *ACS Catal.* **2018**, *8*, 5038−5050.
(835) Liu, J.; Lucci, F. R.; Yang, M.; Lee, S.; Marcinkowski, M. D.; Therrien, A. J.; Williams, C. T.; Sykes, E. C. H.; Flytzani-Stephanopoulos, M. Tackling CO Poisoning with Single-Atom Alloy Catalysts. *J. Am. Chem. Soc.* **2016**, *138*, 6396−6399.
(836) Marcinkowski, M. D.; Darby, M. T.; Liu, J.; Wimble, J. M.; Lucci, F. R.; Lee, S.; Michaelides, A.; Flytzani-Stephanopoulos, M.; Stamatakis, M.; Sykes, E. C. H. Pt/Cu single-atom alloys as coke-resistant catalysts for efficient C-H activation. *Nat. Chem.* **2018**, *10*, 325.
(837) Sun, G.; Zhao, Z.-J.; Mu, R.; Zha, S.; Li, L.; Chen, S.; Zang, K.; Luo, J.; Li, Z.; Purdy, S. C.; et al. Breaking the scaling relationship via thermally stable Pt/Cu single atom alloys for catalytic dehydrogenation. *Nat. Commun.* **2018**, *9*, 4454.
(838) Liu, D.; Chen, H. Y.; Zhang, J. Y.; Huang, J. Y.; Li, Y. M.; Peng, Q. M. Theoretical investigation of selective hydrogenation of 1,3-butadiene on Pt doping Cu nanoparticles. *Appl. Surf. Sci.* **2018**, *456*, 59−68.
(839) Freund, H. J.; Ernst, N.; Risse, T.; Hamann, H.; Rupprechter, G. Model in Heterogeneous Catalysis: Surface Science Quo Vadis? *Phys. Status Solidi* **2001**, *187*, 257−274.
(840) Zaera, F. Probing catalytic reactions at surfaces. *Prog. Surf. Sci.* **2001**, *69*, 1−98.
(841) Vattuone, L.; Savio, L.; Rocca, M. Bridging the structure gap: Chemistry of nanostructured surfaces at well-defined defects. *Surf. Sci. Rep.* **2008**, *63*, 101−168.
(842) Gao, F.; Goodman, D. W. Model Catalysts: Simulating the Complexities of Heterogeneous Catalysts. *Annu. Rev. Phys. Chem.* **2012**, *63*, 265−286.
(843) Chen, S.; Xiong, F.; Huang, W. Surface chemistry and catalysis of oxide model catalysts from single crystals to nanocrystals. *Surf. Sci. Rep.* **2019**, *74*, 100471.
(844) Rodriguez, J. A.; Goodman, D. W. High-Pressure Catalytic Reactions over Single-Crystal Metal Surfaces. *Surf. Sci. Rep.* **1991**, *14*, 1−107.
(845) Somorjai, G. A.; Park, J. Y. Concepts, instruments, and model systems that enabled the rapid evolution of surface science. *Surf. Sci.* **2009**, *603*, 1293−1300.
(846) Simonovis, J. P.; Hunt, A.; Palomino, R. M.; Senanayake, S. D.; Waluyo, I. Enhanced Stability of Pt-Cu Single-Atom Alloy

https://doi.org/10.1021/acs.chemrev.1c00905
Chem. Rev. XXXX, XXX, XXX−XXX

Catalysts: In Situ Characterization of the Pt/Cu(111) Surface in an Ambient Pressure of CO. *J. Phys. Chem. C* **2018**, *122*, 4488−4495.
(847) van Spronsen, M. A.; Daunmu, K.; O'Connor, C. R.; Egle, T.; Kersell, H.; Oliver-Meseguer, J.; Salmeron, M. B.; Madix, R. J.; Sautet, P.; Friend, C. M. Dynamics of Surface Alloys: Rearrangement of Pd/Ag(111) Induced by CO and O_2. *J. Phys. Chem. C* **2019**, *123*, 8312−8323.
(848) Simonovis, J. P.; Hunt, A.; Senanayake, S. D.; Waluyo, I. Subtle and reversible interactions of ambient pressure H_2 with Pt/Cu(111) single-atom alloy surfaces. *Surf. Sci.* **2019**, *679*, 207−213.
(849) Gumuslu, G.; Kondratyuk, P.; Boes, J. R.; Morreale, B.; Miller, J. B.; Kitchin, J. R.; Gellman, A. J. Correlation of Electronic Structure with Catalytic Activity: H_2-D_2 Exchange across Cu_xPd_{1-x} Composition Space. *ACS Catal.* **2015**, *5*, 3137−3147.
(850) Hannagan, R. T.; Giannakakis, G.; Réocreux, R.; Schumann, J.; Finzel, J.; Wang, Y.; Michaelides, A.; Deshlahra, P.; Christopher, P.; Flytzani-Stephanopoulos, M.; et al. First-principles design of a single-atom-alloy propane dehydrogenation catalyst. *Science* **2021**, *372*, 1444.
(851) Rodriguez, J. A.; Goodman, D. W. The nature of the metal-metal bond in bimetallic surfaces. *Science* **1992**, *257*, 897−903.
(852) Kitchin, J. R.; Nørskov, J. K.; Barteau, M. A.; Chen, J. G. Role of Strain and Ligand Effects in the Modification of the Electronic and Chemical Properties of Bimetallic Surfaces. *Phys. Rev. Lett.* **2004**, *93*, 156801.
(853) Xin, H.; Vojvodic, A.; Voss, J.; Nørskov, J. K.; Abild-Pedersen, F. Effects of *d*-band shape on the surface reactivity of transition-metal alloys. *Phys. Rev. B* **2014**, *89*, 115114.
(854) Tao, F.; Grass, M. E.; Zhang, Y.; Butcher, D. R.; Renzas, J. R.; Liu, Z.; Chung, J. Y.; Mun, B. S.; Salmeron, M.; Somorjai, G. A. Reaction-Driven Restructuring of Rh-Pd and Pt-Pd Core-Shell Nanoparticles. *Science* **2008**, *322*, 932−934.
(855) Xu, B.; Sievers, C.; Lercher, J. A.; van Veen, J. A. R.; Giltay, P.; Prins, R.; van Bokhoven, J. A. Strong Brønsted Acidity in Amorphous Silica-Aluminas. *J. Phys. Chem. C* **2007**, *111*, 12075−12079.
(856) Ardagh, M. A.; Bo, Z.; Nauert, S. L.; Notestein, J. M. Depositing SiO_2 on Al_2O_3: a Route to Tunable Brønsted Acid Catalysts. *ACS Catal.* **2016**, *6*, 6156−6164.
(857) McDonald, R. S. Surface Functionality of Amorphous Silica by Infrared Spectroscopy. *J. Phys. Chem.* **1958**, *62*, 1168−1178.
(858) Yates, D. J. C. Infrared Studies of The Surface Hydroxyl Groups on Titanium Dioxide, and of the Chemisorption of Carbon Monoxide and Carbon Dioxide. *J. Phys. Chem.* **1961**, *65*, 746−753.
(859) Crépeau, G.; Montouillout, V.; Vimont, A.; Mariey, L.; Cseri, T.; Maugé, F. Nature, Structure and Strength of the Acidic Sites of Amorphous Silica Alumina: An IR and NMR Study. *J. Phys. Chem. B* **2006**, *110*, 15172−15185.
(860) Busca, G. Acidity and basicity of zeolites: A fundamental approach. *Microporous Mesoporous Mater.* **2017**, *254*, 3−16.
(861) Hunger, M. Bronsted Acid Sites in Zeolites Characterized by Multinuclear Solid-State NMR Spectroscopy. *Catal. Rev.* **1997**, *39*, 345−393.
(862) Holm, M. S.; Svelle, S.; Joensen, F.; Beato, P.; Christensen, C. H.; Bordiga, S.; Bjørgen, M. Assessing the acid properties of desilicated ZSM-5 by FTIR using CO and 2,4,6-trimethylpyridine (collidine) as molecular probes. *Appl. Catal. A* **2009**, *356*, 23−30.
(863) Kondo, J. N.; Nishitani, R.; Yoda, E.; Yokoi, T.; Tatsumi, T.; Domen, K. A comparative IR characterization of acidic sites on HY zeolite by pyridine and CO probes with silica-alumina and [gamma]-alumina references. *Phys. Chem. Chem. Phys.* **2010**, *12*, 11576−11586.
(864) Pelmenschikov, A. G.; van Santen, R. A.; Janchen, J.; Meijer, E. Acetonitrile-d3 as a probe of Lewis and Broensted acidity of zeolites. *J. Phys. Chem.* **1993**, *97*, 11071−11074.
(865) Knözinger, H.; Huber, S. IR spectroscopy of small and weakly interacting molecular probes for acidic and basic zeolites. *J. Chem. Soc., Faraday Trans.* **1998**, *94*, 2047−2059.
(866) Cairon, O. Large heterogeneity of Bronsted acid sites in ASA and USY zeolites: evidencing a third acidic component. *Phys. Chem. Chem. Phys.* **2010**, *12*, 6333−6336.
(867) Lamberti, C.; Zecchina, A.; Groppo, E.; Bordiga, S. Probing the surfaces of heterogeneous catalysts by in situ IR spectroscopy. *Chem. Soc. Rev.* **2010**, *39*, 4951−5001.
(868) Xu, B.; Sievers, C.; Hong, S. B.; Prins, R.; van Bokhoven, J. A. Catalytic activity of Brønsted acid sites in zeolites: Intrinsic activity, rate-limiting step, and influence of the local structure of the acid sites. *J. Catal.* **2006**, *244*, 163−168.
(869) Olsbye, U.; Svelle, S.; Bjørgen, M.; Beato, P.; Janssens, T. V. W.; Joensen, F.; Bordiga, S.; Lillerud, K. P. Conversion of Methanol to Hydrocarbons: How Zeolite Cavity and Pore Size Controls Product Selectivity. *Angew. Chem., Int. Ed.* **2012**, *51*, 5810−5831.
(870) Hensen, E. J. M.; Poduval, D. G.; Degirmenci, V.; Ligthart, D. A. J. M.; Chen, W.; Maugé, F.; Rigutto, M. S.; van Veen, J. A. R. Acidity Characterization of Amorphous Silica-Alumina. *J. Phys. Chem. C* **2012**, *116*, 21416−21429.
(871) Ungureanu, A.; Dragoi, B.; Hulea, V.; Cacciaguerra, T.; Meloni, D.; Solinas, V.; Dumitriu, E. Effect of aluminium incorporation by the "pH-adjusting" method on the structural, acidic and catalytic properties of mesoporous SBA-15. *Microporous Mesoporous Mater.* **2012**, *163*, 51−64.
(872) Matsunaga, Y.; Yamazaki, H.; Yokoi, T.; Tatsumi, T.; Kondo, J. N. IR Characterization of Homogeneously Mixed Silica-Alumina Samples and Dealuminated Y Zeolites by Using Pyridine, CO, and Propene Probe Molecules. *J. Phys. Chem. C* **2013**, *117*, 14043−14050.
(873) Borry, R. W.; Kim, Y. H.; Huffsmith, A.; Reimer, J. A.; Iglesia, E. Structure and Density of Mo and Acid Sites in Mo-Exchanged H-ZSM5 Catalysts for Nonoxidative Methane Conversion. *J. Phys. Chem. B* **1999**, *103*, 5787−5796.
(874) Penzien, J.; Abraham, A.; van Bokhoven, J. A.; Jentys, A.; Müller, T. E.; Sievers, C.; Lercher, J. A. Generation and Characterization of Well-Defined Zn^{2+} Lewis Acid Sites in Ion Exchanged Zeolite BEA. *J. Phys. Chem. B* **2004**, *108*, 4116−4126.
(875) Rane, N.; Kersbulck, M.; van Santen, R. A.; Hensen, E. J. M. Cracking of n-heptane over Brønsted acid sites and Lewis acid Ga sites in ZSM-5 zeolite. *Microporous Mesoporous Mater.* **2008**, *110*, 279−291.
(876) Cruz-Cabeza, A. J.; Esquivel, D.; Jiménez-Sanchidrián, C.; Romero-Salguero, F. J. Metal-Exchanged β Zeolites as Catalysts for the Conversion of Acetone to Hydrocarbons. *Materials* **2012**, *5*, 121−134.
(877) Wang, S.; Guo, W.; Zhu, L.; Wang, H.; Qiu, K.; Cen, K. Methyl Acetate Synthesis from Dimethyl Ether Carbonylation over Mordenite Modified by Cation Exchange. *J. Phys. Chem. C* **2015**, *119*, 524−533.
(878) Veses, A.; Puértolas, B.; López, J. M.; Callén, M. S.; Solsona, B.; García, T. Promoting Deoxygenation of Bio-Oil by Metal-Loaded Hierarchical ZSM-5 Zeolites. *ACS Sustainable Chem. Eng.* **2016**, *4*, 1653−1660.
(879) Marianou, A. A.; Michailof, C. M.; Pineda, A.; Iliopoulou, E. F.; Triantafyllidis, K. S.; Lappas, A. A. Effect of Lewis and Brønsted acidity on glucose conversion to 5-HMF and lactic acid in aqueous and organic media. *Appl. Catal. A* **2018**, *555*, 75−87.
(880) Holm, M. S.; Saravanamurugan, S.; Taarning, E. Conversion of Sugars to Lactic Acid Derivatives Using Heterogeneous Zeotype Catalysts. *Science* **2010**, *328*, 602.
(881) Osmundsen, C. M.; Holm, M. S.; Dahl, S.; Taarning, E. Tin-containing silicates: structure-activity relations. *Proceedings of the Royal Society A: Mathematical, Physical and Engineering Sciences* **2012**, *468*, 2000−2016.
(882) Bermejo-Deval, R.; Assary, R. S.; Nikolla, E.; Moliner, M.; Román-Leshkov, Y.; Hwang, S.-J.; Palsdottir, A.; Silverman, D.; Lobo, R. F.; Curtiss, L. A.; et al. Metalloenzyme-like catalyzed isomerizations of sugars by Lewis acid zeolites. *Proc. Natl. Acad. Sci. U. S. A.* **2012**, *109*, 9727.
(883) Salavati-fard, T.; Vasiliadou, E. S.; Jenness, G. R.; Lobo, R. F.; Caratzoulas, S.; Doren, D. J. Lewis Acid Site and Hydrogen-Bond-Mediated Polarization Synergy in the Catalysis of Diels-Alder Cycloaddition by Band-Gap Transition-Metal Oxides. *ACS Catal.* **2019**, *9*, 701−715.

https://doi.org/10.1021/acs.chemrev.1c00905
Chem. Rev. XXXX, XXX, XXX−XXX

(884) Liang, M.; Zhu, X.; Ma, W. The Propylene Oxide Rearrangement Catalyzed by the Lewis Acid Sites of ZSM-5 Catalyst with Controllable Surface Acidity. *Catal. Lett.* **2019**, *149*, 942−949.
(885) Gundeboina, R.; Velisoju, V. K.; Gutta, N.; Medak, S.; Aytam, H. P. Influence of surface Lewis acid sites for the selective hydrogenation of levulinic acid to γ-valerolactone over Ni-Cu-Al mixed oxide catalyst. *React. Kinet., Mech. Catal.* **2019**, *127*, 601−616.
(886) Yang, J.; Hu, S.; Shi, L.; Hoang, S.; Yang, W.; Fang, Y.; Liang, Z.; Pan, C.; Zhu, Y.; Li, L.; et al. Oxygen Vacancies and Lewis Acid Sites Synergistically Promoted Catalytic Methane Combustion over Perovskite Oxides. *Environ. Sci. Technol.* **2021**, *55*, 9243−9254.
(887) Phung, T. K.; Lagazzo, A.; Rivero Crespo, M. Á.; Sánchez Escribano, V.; Busca, G. A study of commercial transition aluminas and of their catalytic activity in the dehydration of ethanol. *J. Catal.* **2014**, *311*, 102−113.
(888) Phung, T. K.; Busca, G. Ethanol dehydration on silica-aluminas: Active sites and ethylene/diethyl ether selectivities. *Catal. Commun.* **2015**, *68*, 110−115.
(889) Marberger, A.; Ferri, D.; Elsener, M.; Kröcher, O. The Significance of Lewis Acid Sites for the Selective Catalytic Reduction of Nitric Oxide on Vanadium-Based Catalysts. *Angew. Chem., Int. Ed.* **2016**, *55*, 11989−11994.
(890) Green, I. X.; Tang, W.; Neurock, M.; Yates, J. T., Jr Spectroscopic observation of dual catalytic sites during oxidation of CO on a Au/TiO_2 catalyst. *Science* **2011**, *333*, 736−739.
(891) Panayotov, D. A.; Morris, J. R. Surface chemistry of Au/TiO_2: Thermally and photolytically activated reactions. *Surf. Sci. Rep.* **2016**, *71*, 77−271.
(892) Wang, Y.-G.; Cantu, D. C.; Lee, M.-S.; Li, J.; Glezakou, V.-A.; Rousseau, R. CO Oxidation on Au/TiO_2: Condition-Dependent Active Sites and Mechanistic Pathways. *J. Am. Chem. Soc.* **2016**, *138*, 10467−10476.
(893) Puigdollers, A. R.; Pacchioni, G. CO Oxidation on Au Nanoparticles Supported on ZrO_2: Role of Metal/Oxide Interface and Oxide Reducibility. *ChemCatChem.* **2017**, *9*, 1119−1127.
(894) Rodriguez, J. A.; Ma, S.; Liu, P.; Hrbek, J.; Evans, J.; Pérez, M. Activity of CeO_x and TiO_x Nanoparticles Grown on Au(111) in the Water-Gas Shift Reaction. *Science* **2007**, *318*, 1757−1760.
(895) Senanayake, S. D.; Stacchiola, D.; Rodriguez, J. A. Unique Properties of Ceria Nanoparticles Supported on Metals: Novel Inverse Ceria/Copper Catalysts for CO Oxidation and the Water-Gas Shift Reaction. *Acc. Chem. Res.* **2013**, *46*, 1702−1711.
(896) Delbecq, F.; Li, Y.; Loffreda, D. Metal-support interaction effects on chemo-regioselectivity: Hydrogenation of crotonaldehyde on $Pt_{13}/CeO_2(111)$. *J. Catal.* **2016**, *334*, 68−78.
(897) Motokura, K.; Tada, M.; Iwasawa, Y. Heterogeneous Organic Base-Catalyzed Reactions Enhanced by Acid Supports. *J. Am. Chem. Soc.* **2007**, *129*, 9540−9541.
(898) Motokura, K.; Tomita, M.; Tada, M.; Iwasawa, Y. Acid-Base Bifunctional Catalysis of Silica-Alumina-Supported Organic Amines for Carbon-Carbon Bond-Forming Reactions. *Chem.-Eur. J.* **2008**, *14*, 4017−4027.
(899) Hruby, S. L.; Shanks, B. H. Acid-base cooperativity in condensation reactions with functionalized mesoporous silica catalysts. *J. Catal.* **2009**, *263*, 181−188.
(900) Zhang, J.-F.; Wang, Z.-M.; Lyu, Y.-J.; Xie, H.; Qi, T.; Si, Z.-B.; Liu, L.-J.; Yang, H.-Q.; Hu, C.-W. Synergistic Catalytic Mechanism of Acidic Silanol and Basic Alkylamine Bifunctional Groups Over SBA-15 Zeolite toward Aldol Condensation. *J. Phys. Chem. C* **2019**, *123*, 4903−4913.
(901) Stacchiola, D. J.; Senanayake, S. D.; Liu, P.; Rodriguez, J. A. Fundamental Studies of Well-Defined Surfaces of Mixed-Metal Oxides: Special Properties of $MO_x/TiO_2(110)$ {M = V, Ru, Ce, or W}. *Chem. Rev.* **2013**, *113*, 4373−4390.
(902) Hu, Z.-P.; Yang, D.; Wang, Z.; Yuan, Z.-Y. State-of-the-art catalysts for direct dehydrogenation of propane to propylene. *Chin. J. Catal.* **2019**, *40*, 1233−1254.
(903) Gärtner, C. A.; van Veen, A. C.; Lercher, J. A. Oxidative Dehydrogenation of Ethane: Common Principles and Mechanistic Aspects. *ChemCatChem.* **2013**, *5*, 3196−3217.
(904) Argyle, M. D.; Chen, K.; Bell, A. T.; Iglesia, E. Effect of Catalyst Structure on Oxidative Dehydrogenation of Ethane and Propane on Alumina-Supported Vanadia. *J. Catal.* **2002**, *208*, 139−149.
(905) Carrero, C. A.; Schloegl, R.; Wachs, I. E.; Schomaecker, R. Critical Literature Review of the Kinetics for the Oxidative Dehydrogenation of Propane over Well-Defined Supported Vanadium Oxide Catalysts. *ACS Catal.* **2014**, *4*, 3357−3380.
(906) Liu, G.; Zhao, Z.-J.; Wu, T.; Zeng, L.; Gong, J. Nature of the Active Sites of VO_x/Al_2O_3 Catalysts for Propane Dehydrogenation. *ACS Catal.* **2016**, *6*, 5207−5214.
(907) Rodemerck, U.; Stoyanova, M.; Kondratenko, E. V.; Linke, D. Influence of the kind of VO_x structures in VO_x/MCM-41 on activity, selectivity and stability in dehydrogenation of propane and isobutane. *J. Catal.* **2017**, *352*, 256−263.
(908) Kibsgaard, J.; Chen, Z.; Reinecke, B. N.; Jaramillo, T. F. Engineering the surface structure of MoS_2 to preferentially expose active edge sites for electrocatalysis. *Nat. Mater.* **2012**, *11*, 963−969.
(909) Chhowalla, M.; Shin, H. S.; Eda, G.; Li, L.-J.; Loh, K. P.; Zhang, H. The chemistry of two-dimensional layered transition metal dichalcogenide nanosheets. *Nat. Chem.* **2013**, *5*, 263−275.
(910) Jin, H.; Guo, C.; Liu, X.; Liu, J.; Vasileff, A.; Jiao, Y.; Zheng, Y.; Qiao, S.-Z. Emerging Two-Dimensional Nanomaterials for Electrocatalysis. *Chem. Rev.* **2018**, *118*, 6337−6408.
(911) Wang, Y.; Mao, J.; Meng, X.; Yu, L.; Deng, D.; Bao, X. Catalysis with Two-Dimensional Materials Confining Single Atoms: Concept, Design, and Applications. *Chem. Rev.* **2019**, *119*, 1806−1854.
(912) Bönnemann, H.; Richards, R. M. Nanoscopic metal particles - synthetic methods and potential applications. *Eur. J. Inorg. Chem.* **2001**, *2001*, 2455−2480.
(913) Lisiecki, I. Size, shape, and structural control of metallic nanocrystals. *J. Phys. Chem. B* **2005**, *109*, 12231−12244.
(914) Semagina, N.; Kiwi-Minsker, L. Recent advances in the liquid-phase synthesis of metal nanostructures with controlled shape and size for catalysis. *Catal. Rev. - Sci. Eng.* **2009**, *51*, 147−217.
(915) Jia, C.-J.; Schüth, F. Colloidal metal nanoparticles as a component of designed catalyst. *Phys. Chem. Chem. Phys.* **2011**, *13*, 2457−2487.
(916) Jin, R.; Zeng, C.; Zhou, M.; Chen, Y. Atomically Precise Colloidal Metal Nanoclusters and Nanoparticles: Fundamentals and Opportunities. *Chem. Rev.* **2016**, *116*, 10346−10413.
(917) Tao, A. R.; Habas, S.; Yang, P. Shape Control of Colloidal Metal Nanocrystals. *Small* **2008**, *4*, 310−325.
(918) Xia, Y.; Xiong, Y.; Lim, B.; Skrabalak, S. E. Shape-Controlled Synthesis of Metal Nanocrystals: Simple Chemistry Meets Complex Physics? *Angew. Chem., Int. Ed.* **2009**, *48*, 60−103.
(919) Muzzio, M.; Li, J.; Yin, Z.; Delahunty, I. M.; Xie, J.; Sun, S. Monodisperse nanoparticles for catalysis and nanomedicine. *Nanoscale* **2019**, *11*, 18946−18967.
(920) Lewis, L. N. Chemical catalysis by colloids and clusters. *Chem. Rev.* **1993**, *93*, 2693−2730.
(921) Narayanan, R.; El-Sayed, M. A. Catalysis with transition metal nanoparticles in colloidal solution: Nanoparticle shape dependence and stability. *J. Phys. Chem. B* **2005**, *109*, 12663−12676.
(922) Jin, R. The impacts of nanotechnology on catalysis by precious metal nanoparticles. *Nanotechnol. Rev.* **2012**, *1*, 31−56.
(923) Li, Y.; Hong, X. M.; Collard, D. M.; El-Sayed, M. A. Suzuki Cross-Coupling Reactions Catalyzed by Palladium Nanoparticles in Aqueous Solution. *Organic Letters* **2000**, *2*, 2385−2388.
(924) Narayanan, R.; El-Sayed, M. A. Effect of Colloidal Catalysis on the Nanoparticle Size Distribution: Dendrimer-Pd vs PVP-Pd Nanoparticles Catalyzing the Suzuki Coupling Reaction†. *J. Phys. Chem. B* **2004**, *108*, 8572−8580.
(925) Narayanan, R.; Tabor, C.; El-Sayed, M. Can the Observed Changes in the Size or Shape of a Colloidal Nanocatalyst Reveal the

https://doi.org/10.1021/acs.chemrev.1c00905
Chem. Rev. XXXX, XXX, XXX−XXX

Nanocatalysis Mechanism Type: Homogeneous or Heterogeneous? *Top. Catal.* **2008**, *48*, 60−74.
(926) Widegren, J. A.; Finke, R. G. A review of the problem of distinguishing true homogeneous catalysis from soluble or other metal-particle heterogeneous catalysis under reducing conditions. *J. Mol. Catal. A: Chem.* **2003**, *198*, 317−341.
(927) Phan, N. T. S.; Van Der Sluys, M.; Jones, C. W. On the Nature of the Active Species in Palladium Catalyzed Mizoroki-Heck and Suzuki-Miyaura Couplings - Homogeneous or Heterogeneous Catalysis, A Critical Review. *Adv. Synth. Catal.* **2006**, *348*, 609−679.
(928) Thathagar, M. B.; ten Elshof, J. E.; Rothenberg, G. Pd Nanoclusters in C-C Coupling Reactions: Proof of Leaching. *Angew. Chem., Int. Ed.* **2006**, *45*, 2886−2890.
(929) Astruc, D. Palladium Nanoparticles as Efficient Green Homogeneous and Heterogeneous Carbon-Carbon Coupling Precatalysts: A Unifying View. *Inorg. Chem.* **2007**, *46*, 1884−1894.
(930) Bej, A.; Ghosh, K.; Sarkar, A.; Knight, D. W. Palladium nanoparticles in the catalysis of coupling reactions. *RSC Adv.* **2016**, *6*, 11446−11453.
(931) Biffis, A.; Centomo, P.; Del Zotto, A.; Zecca, M. Pd Metal Catalysts for Cross-Couplings and Related Reactions in the 21st Century: A Critical Review. *Chem. Rev.* **2018**, *118*, 2249−2295.
(932) Moreno-Mañas, M.; Pleixats, R.; Villarroya, S. Fluorous Phase Soluble Palladium Nanoparticles as Recoverable Catalysts for Suzuki Cross-Coupling and Heck Reactions. *Organometallics* **2001**, *20*, 4524−4528.
(933) Thathagar, M. B.; Beckers, J.; Rothenberg, G. Copper-Catalyzed Suzuki Cross-Coupling Using Mixed Nanocluster Catalysts. *J. Am. Chem. Soc.* **2002**, *124*, 11858−11859.
(934) Na, Y.; Park, S.; Han, S. B.; Han, H.; Ko, S.; Chang, S. Ruthenium-Catalyzed Heck-Type Olefination and Suzuki Coupling Reactions: Studies on the Nature of Catalytic Species. *J. Am. Chem. Soc.* **2004**, *126*, 250−258.
(935) Gniewek, A.; Trzeciak, A. M.; Ziółkowski, J. J.; Kepiński, L.; Wrzyszcz, J.; Tylus, W. Pd-PVP colloid as catalyst for Heck and carbonylation reactions: TEM and XPS studies. *J. Catal.* **2005**, *229*, 332−343.
(936) Kashin, A. N.; Beletskaya, I. P. Suzuki-Miyaura reaction in water, catalyzed by palladium nanoparticles stabilized by Pluronic F68 triblock copolymer. *Russian Journal of Organic Chemistry* **2011**, *47*, 475−479.
(937) Fonseca, G. S.; Umpierre, A. P.; Fichtner, P. F. P.; Teixeira, S. R.; Dupont, J. The Use of Imidazolium Ionic Liquids for the Formation and Stabilization of Ir0 and Rh0 Nanoparticles: Efficient Catalysts for the Hydrogenation of Arenes. *Chem.-Eur. J.* **2003**, *9*, 3263−3269.
(938) Semagina, N. V.; Bykov, A. V.; Sulman, E. M.; Matveeva, V. G.; Sidorov, S. N.; Dubrovina, L. V.; Valetsky, P. M.; Kiselyova, O. I.; Khokhlov, A. R.; Stein, B.; et al. Selective dehydrolinalool hydrogenation with poly(ethylene oxide)-block-poly-2-vinylpyridine micelles filled with Pd nanoparticles. *J. Mol. Catal. A: Chem.* **2004**, *208*, 273−284.
(939) Semagina, N.; Renken, A.; Laub, D.; Kiwi-Minsker, L. Synthesis of monodispersed palladium nanoparticles to study structure sensitivity of solvent-free selective hydrogenation of 2-methyl-3-butyn-2-ol. *J. Catal.* **2007**, *246*, 308−314.
(940) Miyake, M.; Miyabayashi, K. Shape and Size Controlled Pt Nanocrystals as Novel Model Catalysts. *Catal. Surv. Asia* **2012**, *16*, 1−13.
(941) Baeza, J. A.; Calvo, L.; Gilarranz, M. A.; Mohedano, A. F.; Casas, J. A.; Rodriguez, J. J. Catalytic behavior of size-controlled palladium nanoparticles in the hydrodechlorination of 4-chlorophenol in aqueous phase. *J. Catal.* **2012**, *293*, 85−93.
(942) Chau, N. T. T.; Handjani, S.; Guegan, J.-P.; Guerrero, M.; Monflier, E.; Philippot, K.; Denicourt-Nowicki, A.; Roucoux, A. Methylated β-Cyclodextrin-Capped Ruthenium Nanoparticles: Synthesis Strategies, Characterization, and Application in Hydrogenation Reactions. *ChemCatChem.* **2013**, *5*, 1497−1503.
(943) Simakova, I. L.; Murzin, D. Y. *Advanced Nanomaterials for Catalysis and Energy*; Sadykov, V. A., Ed.; Elsevier, 2019, DOI: 10.1016/B978-0-12-814807-5.00004-8.
(944) Freund, P. L.; Spiro, M. Colloidal catalysis: the effect of sol size and concentration. *J. Phys. Chem.* **1985**, *89*, 1074−1077.
(945) Li, Y.; Petroski, J.; El-Sayed, M. A. Activation Energy of the Reaction between Hexacyanoferrate(III) and Thiosulfate Ions Catalyzed by Platinum Nanoparticles. *J. Phys. Chem. B* **2000**, *104*, 10956−10959.
(946) Sharma, R. K.; Sharma, P.; Maitra, A. Size-dependent catalytic behavior of platinum nanoparticles on the hexacyanoferrate(III)/thiosulfate redox reaction. *J. Colloid Interface Sci.* **2003**, *265*, 134−140.
(947) Quinson, J.; Inaba, M.; Neumann, S.; Swane, A. A.; Bucher, J.; Simonsen, S. B.; Theil Kuhn, L.; Kirkensgaard, J. J. K.; Jensen, K. M. Ø.; Oezaslan, M.; et al. Investigating Particle Size Effects in Catalysis by Applying a Size-Controlled and Surfactant-Free Synthesis of Colloidal Nanoparticles in Alkaline Ethylene Glycol: Case Study of the Oxygen Reduction Reaction on Pt. *ACS Catal.* **2018**, *8*, 6627−6635.
(948) Gross, E.; Somorjai, G. A. Molecular catalysis science: Nanoparticle synthesis and instrument development for studies under reaction conditions. *J. Catal.* **2015**, *328*, 91−101.
(949) Roldan Cuenya, B.; Behafarid, F. Nanocatalysis: size- and shape-dependent chemisorption and catalytic reactivity. *Surf. Sci. Rep.* **2015**, *70*, 135−187.
(950) Cao, S.; Tao, F.; Tang, Y.; Li, Y.; Yu, J. Size- and shape-dependent catalytic performances of oxidation and reduction reactions on nanocatalysts. *Chem. Soc. Rev.* **2016**, *45*, 4747−4765.
(951) Losch, P.; Huang, W.; Goodman, E. D.; Wrasman, C. J.; Holm, A.; Riscoe, A. R.; Schwalbe, J. A.; Cargnello, M. Colloidal nanocrystals for heterogeneous catalysis. *Nano Today* **2019**, *24*, 15−47.
(952) Rioux, R. M.; Hsu, B. B.; Grass, M. E.; Song, H.; Somorjai, G. A. Influence of particle size on reaction selectivity in cyclohexene hydrogenation and dehydrogenation over silica-supported monodisperse pt particles. *Catal. Lett.* **2008**, *126*, 10−19.
(953) Krier, J. M.; Komvopoulos, K.; Somorjai, G. A. Cyclohexene and 1,4-Cyclohexadiene Hydrogenation Occur through Mutually Exclusive Intermediate Pathways on Platinum Nanoparticles. *J. Phys. Chem. C* **2016**, *120*, 8246−8250.
(954) Pushkarev, V. V.; An, K.; Alayoglu, S.; Beaumont, S. K.; Somorjai, G. A. Hydrogenation of benzene and toluene over size controlled Pt/SBA-15 catalysts: Elucidation of the Pt particle size effect on reaction kinetics. *J. Catal.* **2012**, *292*, 64−72.
(955) Grass, M. E.; Rioux, R. M.; Somorjai, G. A. Dependence of gas-phase crotonaldehyde hydrogenation selectivity and activity on the size of Pt nanoparticles (1.7-7.1 nm) supported on SBA-15. *Catal. Lett.* **2009**, *128*, 1−8.
(956) Tsung, C.-K.; Kuhn, J. N.; Huang, W.; Aliaga, C.; Hung, L.-I.; Somorjai, G. A.; Yang, P. Sub-10 nm Platinum Nanocrystals with Size and Shape Control: Catalytic Study for Ethylene and Pyrrole Hydrogenation. *J. Am. Chem. Soc.* **2009**, *131*, 5816−5822.
(957) Alayoglu, S.; Aliaga, C.; Sprung, C.; Somorjai, G. Size and Shape Dependence on Pt Nanoparticles for the Methylcyclopentane/Hydrogen Ring Opening/Ring Enlargement Reaction. *Catal. Lett.* **2011**, *141*, 914−924.
(958) Pushkarev, V. V.; Musselwhite, N.; An, K.; Alayoglu, S.; Somorjai, G. A. High Structure Sensitivity of Vapor-Phase Furfural Decarbonylation/Hydrogenation Reaction Network as a Function of Size and Shape of Pt Nanoparticles. *Nano Lett.* **2012**, *12*, 5196−5201.
(959) Iablokov, V.; Beaumont, S. K.; Alayoglu, S.; Pushkarev, V. V.; Specht, C.; Gao, J.; Alivisatos, A. P.; Kruse, N.; Somorjai, G. A. Size-Controlled Model Co Nanoparticle Catalysts for CO_2 Hydrogenation: Synthesis, Characterization, and Catalytic Reactions. *Nano Lett.* **2012**, *12*, 3091−3096.
(960) Joo, S. H.; Park, J. Y.; Renzas, J. R.; Butcher, D. R.; Huang, W.; Somorjai, G. A. Size Effect of Ruthenium Nanoparticles in Catalytic Carbon Monoxide Oxidation. *Nano Lett.* **2010**, *10*, 2709−2713.

https://doi.org/10.1021/acs.chemrev.1c00905
Chem. Rev. XXXX, XXX, XXX−XXX

(961) Michalak, W. D.; Krier, J. M.; Komvopoulos, K.; Somorjai, G. A. Structure Sensitivity in Pt Nanoparticle Catalysts for Hydrogenation of 1,3-Butadiene: In Situ Study of Reaction Intermediates Using SFG Vibrational Spectroscopy. *J. Phys. Chem. C* **2013**, *117*, 1809−1817.
(962) Ojeda, M.; Rojas, S.; Boutonnet, M.; Pérez-Alonso, F. J.; Javier Garcıa-Garcıa, F.; Fierro, J. L. G. Synthesis of Rh nano-particles by the microemulsion technology: Particle size effect on the CO+H_2 reaction. *Appl. Catal. A* **2004**, *274*, 33−41.
(963) Trépanier, M.; Dalai, A. K.; Abatzoglou, N. Synthesis of CNT-supported cobalt nanoparticle catalysts using a microemulsion technique: Role of nanoparticle size on reducibility, activity and selectivity in Fischer-Tropsch reactions. *Appl. Catal. A* **2010**, *374*, 79−86.
(964) Pour, A. N.; Housaindokht, M. R.; Shahri, S. M. K.; Babakhani, E. G.; Irani, M. Size dependence on reduction kinetic of iron based Fischer-Tropsch catalyst. *Journal of Industrial and Engineering Chemistry* **2011**, *17*, 596−602.
(965) Nakhaei Pour, A.; Housaindokht, M. Fischer-Tropsch Synthesis Over CNT Supported Cobalt Catalysts: Role of Metal Nanoparticle Size on Catalyst Activity and Products Selectivity. *Catal. Lett.* **2013**, *143*, 1328−1338.
(966) Casavola, M.; Hermannsdörfer, J.; de Jonge, N.; Dugulan, A. I.; de Jong, K. P. Fabrication of Fischer-Tropsch Catalysts by Deposition of Iron Nanocrystals on Carbon Nanotubes. *Adv. Funct. Mater.* **2015**, *25*, 5309−5319.
(967) Jin, M.; Liu, H.; Zhang, H.; Xie, Z.; Liu, J.; Xia, Y. Synthesis of Pd nanocrystals enclosed by {100} facets and with sizes <10 nm for application in CO oxidation. *Nano Res.* **2011**, *4*, 83−91.
(968) Navlani-García, M.; Salinas-Torres, D.; Mori, K.; Kuwahara, Y.; Yamashita, H. Tailoring the Size and Shape of Colloidal Noble Metal Nanocrystals as a Valuable Tool in Catalysis. *Catal. Surv. Asia* **2019**, *23*, 127−148.
(969) Hutchings, G. J.; Haruta, M. A golden age of catalysis: A perspective. *Appl. Catal. A* **2005**, *291*, 2−5.
(970) Hashmi, A. S. K.; Hutchings, G. J. Gold Catalysis. *Angew. Chem., Int. Ed.* **2006**, *45*, 7896−7936.
(971) Corma, A.; Leyva-Pérez, A.; Sabater, M. J. Gold-Catalyzed Carbon-Heteroatom Bond-Forming Reactions. *Chem. Rev.* **2011**, *111*, 1657−1712.
(972) Takei, T.; Akita, T.; Nakamura, I.; Fujitani, T.; Okumura, M.; Okazaki, K.; Huang, J.; Ishida, T.; Haruta, M. Heterogeneous Catalysis by Gold. *Adv. Catal.* **2012**, *55*, 1−126.
(973) Haruta, M. Chance and Necessity: My Encounter with Gold Catalysts. *Angew. Chem., Int. Ed.* **2014**, *53*, 52−56.
(974) Choudhary, T. V.; Goodman, D. W. Catalytically active gold: The role of cluster morphology. *Appl. Catal. A* **2005**, *291*, 32.
(975) Tsunoyama, H.; Sakurai, H.; Tsukuda, T. Size effect on the catalysis of gold clusters dispersed in water for aerobic oxidation of alcohol. *Chem. Phys. Lett.* **2006**, *429*, 528−532.
(976) Fenger, R.; Fertitta, E.; Kirmse, H.; Thünemann, A. F.; Rademann, K. Size dependent catalysis with CTAB-stabilized gold nanoparticles. *Phys. Chem. Chem. Phys.* **2012**, *14*, 9343−9349.
(977) Biella, S.; Porta, F.; Prati, L.; Rossi, M. Surfactant-Protected Gold Particles: New Challenge for Gold-on-Carbon Catalysts. *Catal. Lett.* **2003**, *90*, 23−29.
(978) Suchomel, P.; Kvitek, L.; Prucek, R.; Panacek, A.; Halder, A.; Vajda, S.; Zboril, R. Simple size-controlled synthesis of Au nanoparticles and their size-dependent catalytic activity. *Sci. Rep.* **2018**, *8*, 4589.
(979) Liu, Y.; Jia, C.-J.; Yamasaki, J.; Terasaki, O.; Schüth, F. Highly Active Iron Oxide Supported Gold Catalysts for CO Oxidation: How Small Must the Gold Nanoparticles Be? *Angew. Chem., Int. Ed.* **2010**, *49*, 5771−5775.
(980) He, Y.; Liu, J.-C.; Luo, L.; Wang, Y.-G.; Zhu, J.; Du, Y.; Li, J.; Mao, S. X.; Wang, C. Size-dependent dynamic structures of supported gold nanoparticles in CO oxidation reaction condition. *Proc. Nat. Acad. Sci.* **2018**, *115*, 7700.
(981) Valden, M.; Lai, X.; Goodman, D. W. Onset of catalytic activity of gold clusters on titania with the appearance of nonmetallic properties. *Science* **1998**, *281*, 1647−1650.
(982) Herzing, A. A.; Kiely, C. J.; Carley, A. F.; Landon, P.; Hutchings, G. J. Identification of Active Gold Nanoclusters on Iron Oxide Supports for CO Oxidation. *Science* **2008**, *321*, 1331−1335.
(983) Janssens, T. V. W.; Clausen, B. S.; Hvolbæk, B.; Falsig, H.; Christensen, C. H.; Bligaard, T.; Nørskov, J. K. Insights into the reactivity of supported Au nanoparticles: Combining theory and experiments. *Top. Catal.* **2007**, *44*, 15−26.
(984) Cargnello, M.; Doan-Nguyen, V. V. T.; Gordon, T. R.; Diaz, R. E.; Stach, E. A.; Gorte, R. J.; Fornasiero, P.; Murray, C. B. Control of Metal Nanocrystal Size Reveals Metal-Support Interface Role for Ceria Catalysts. *Science* **2013**, *341*, 771.
(985) Sun, Y.; Xia, Y. Shape-Controlled Synthesis of Gold and Silver Nanoparticles. *Science* **2002**, *298*, 2176.
(986) Zhou, K.; Li, Y. Catalysis Based on Nanocrystals with Well-Defined Facets. *Angew. Chem., Int. Ed.* **2012**, *51*, 602−613.
(987) Shi, Y.; Lyu, Z.; Zhao, M.; Chen, R.; Nguyen, Q. N.; Xia, Y. Noble-Metal Nanocrystals with Controlled Shapes for Catalytic and Electrocatalytic Applications. *Chem. Rev.* **2021**, *121*, 649−735.
(988) Taylor, H. S. A theory of the catalytic surface. *Proc. R. Soc.* **1925**, *A108*, 105−111.
(989) Zaera, F.; Somorjai, G. A. Direct Determination of Blocking of Surface Defects by Carbonaceous Deposits during Hydrocarbon Reactions on Platinum Single Crystals. *Langmuir* **1986**, *2*, 686−688.
(990) Bartholomew, C. H.; Farrauto, R. J. *Fundamentals of Industrial Catalytic Processes*, 2nd ed.; John Wiley & Sons, 2010.
(991) Koper, M. T. M. Structure sensitivity and nanoscale effects in electrocatalysis. *Nanoscale* **2011**, *3*, 2054−2073.
(992) Thomas, J. M.; Thomas, W. J. *Principles and Practice of Heterogeneous Catalysis*, 2nd ed.; Wiley-VCH: Weinheim, Germany, 2015.
(993) Somorjai, G. A.; Li, Y. *Introduction to Surface Chemistry and Catalysis*; 2nd ed.; John Wiley & Sons: New York, 2010.
(994) Schauermann, S.; Nilius, N.; Shaikhutdinov, S.; Freund, H.-J. Nanoparticles for Heterogeneous Catalysis: New Mechanistic Insights. *Acc. Chem. Res.* **2013**, *46*, 1673−1681.
(995) Roldan Cuenya, B. Metal Nanoparticle Catalysts Beginning to Shape-up. *Acc. Chem. Res.* **2013**, *46*, 1682−1691.
(996) Wu, B.; Zheng, N. Surface and interface control of noble metal nanocrystals for catalytic and electrocatalytic applications. *Nano Today* **2013**, *8*, 168−197.
(997) Xie, S.; Choi, S.-I.; Xia, X.; Xia, Y. Catalysis on faceted noble-metal nanocrystals: both shape and size matter. *Current Opinion in Chemical Engineering* **2013**, *2*, 142−150.
(998) Huo, D.; Cao, Z.; Li, J.; Xie, M.; Tao, J.; Xia, Y. Seed-Mediated Growth of Au Nanospheres into Hexagonal Stars and the Emergence of a Hexagonal Close-Packed Phase. *Nano Lett.* **2019**, *19*, 3115−3121.
(999) Sow, C.; P, S.; Mettela, G.; Kulkarni, G. U. Noble Metal Nanomaterials with Nontraditional Crystal Structures. *Annu. Rev. Mater. Res.* **2020**, *50*, 345−370.
(1000) Huang, H.; Chen, R.; Liu, M.; Wang, J.; Kim, M. J.; Ye, Z.; Xia, Y. Aqueous Synthesis of Pd-M (M = Pd, Pt, and Au) Decahedra with Concave Facets for Catalytic Applications. *Top. Catal.* **2020**, *63*, 664−672.
(1001) Narayanan, R.; El-Sayed, M. A. Shape-dependent catalytic activity of platinum nanoparticles in colloidal solution. *Nano Lett.* **2004**, *4*, 1343−1348.
(1002) Narayanan, R.; El-Sayed, M. A. Changing catalytic activity during colloidal platinum nanocatalysis due to shape changes: Electron-transfer reaction. *J. Am. Chem. Soc.* **2004**, *126*, 7194−7195.
(1003) Narayanan, R.; El-Sayed, M. A. Effect of Nanocatalysis in Colloidal Solution on the Tetrahedral and Cubic Nanoparticle Shape: Electron-Transfer Reaction Catalyzed by Platinum Nanoparticles. *J. Phys. Chem. B* **2004**, *108*, 5726−5733.

https://doi.org/10.1021/acs.chemrev.1c00905
Chem. Rev. XXXX, XXX, XXX−XXX

(1004) Burda, C.; Chen, X.; Narayanan, R.; El-Sayed, M. A. Chemistry and properties of nanocrystals of different shapes. *Chem. Rev.* **2005**, *105*, 1025−1102.
(1005) Chen, J.; Lim, B.; Lee, E. P.; Xia, Y. Shape-controlled synthesis of platinum nanocrystals for catalytic and electrocatalytic applications. *Nano Today* **2009**, *4*, 81−95.
(1006) Guo, S.; Wang, E. Noble metal nanomaterials: Controllable synthesis and application in fuel cells and analytical sensors. *Nano Today* **2011**, *6*, 240−264.
(1007) Guo, S.; Zhang, S.; Sun, S. Tuning Nanoparticle Catalysis for the Oxygen Reduction Reaction. *Angew. Chem., Int. Ed.* **2013**, *52*, 8526−8544.
(1008) Zheng, W.; Qu, J.; Hong, X.; Tedsree, K.; Tsang, S. C. E. Probing the Size and Shape Effects of Cubic- and Spherical-Shaped Palladium Nanoparticles in the Electrooxidation of Formic Acid. *ChemCatChem.* **2015**, *7*, 3826−3831.
(1009) Rizo, R.; Roldan Cuenya, B. Shape-Controlled Nanoparticles as Anodic Catalysts in Low-Temperature Fuel Cells. *ACS Energy Letters* **2019**, *4*, 1484−1495.
(1010) Jin, M.; Zhang, H.; Xie, Z.; Xia, Y. Palladium nanocrystals enclosed by {100} and {111} facets in controlled proportions and their catalytic activities for formic acid oxidation. *Energy Environ. Sci.* **2012**, *5*, 6352−6357.
(1011) Zahmakıran, M.; Özkar, S. Metal nanoparticles in liquid phase catalysis; from recent advances to future goals. *Nanoscale* **2011**, *3*, 3462−3481.
(1012) Chanda, K.; Rej, S.; Liu, S.-Y.; Huang, M. H. Facet-Dependent Catalytic Activity of Palladium Nanocrystals in Tsuji-Trost Allylic Amination Reactions with Product Selectivity. *ChemCatChem.* **2015**, *7*, 1813−1817.
(1013) Xu, R.; Wang, D.; Zhang, J.; Li, Y. Shape-Dependent Catalytic Activity of Silver Nanoparticles for the Oxidation of Styrene. *Chem.-Asian J.* **2006**, *1*, 888−893.
(1014) An, K.; Somorjai, G. A. Size and Shape Control of Metal Nanoparticles for Reaction Selectivity in Catalysis. *ChemCatChem.* **2012**, *4*, 1512−1524.
(1015) Nishimura, S.; Ebitani, K. Recent Advances in Heterogeneous Catalysis with Controlled Nanostructured Precious Monometals. *ChemCatChem.* **2016**, *8*, 2303−2316.
(1016) Yoo, J. W.; Lee, S.-M.; Kim, H.-T.; El-Sayed, M. A. Propylene hydrogenation over cubic Pt nanoparticles deposited on alumina. *Bull. Korean Chem. Soc.* **2004**, *25*, 843−846.
(1017) Bratlie, K. M.; Lee, H.; Komvopoulos, K.; Yang, P.; Somorjai, G. A. Platinum Nanoparticle Shape Effects on Benzene Hydrogenation Selectivity. *Nano Lett.* **2007**, *7*, 3097−3101.
(1018) Park, K. H.; Jang, K.; Kim, H. J.; Son, S. U. Near-Monodisperse Tetrahedral Rhodium Nanoparticles on Charcoal: The Shape-Dependent Catalytic Hydrogenation of Arenes. *Angew. Chem., Int. Ed.* **2007**, *46*, 1152−1155.
(1019) Piccolo, L.; Valcarcel, A.; Bausach, M.; Thomazeau, C.; Uzio, D.; Berhault, G. Tuning the shape of nanoparticles to control their catalytic properties: selective hydrogenation of 1,3-butadiene on Pd/Al2O3. *Phys. Chem. Chem. Phys.* **2008**, *10*, 5504−5506.
(1020) Lee, I.; Zaera, F. Catalytic Conversion of Olefins on Supported Cubic Platinum Nanoparticles: Selectivity of (100) versus (111) Surfaces. *J. Catal.* **2010**, *269*, 359−366.
(1021) Hu, B.; Ding, K.; Wu, T.; Zhou, X.; Fan, H.; Jiang, T.; Wang, Q.; Han, B. Shape controlled synthesis of palladium nanocrystals by combination of oleylamine and alkylammonium alkylcarbamate and their catalytic activity. *Chem. Commun.* **2010**, *46*, 8552−8554.
(1022) Zang, W.; Li, G.; Wang, L.; Zhang, X. Catalytic hydrogenation by noble-metal nanocrystals with well-defined facets: a review. *Catal. Sci. Technol.* **2015**, *5*, 2532−2553.
(1023) Zaera, F. Key unanswered questions about the mechanism of olefin hydrogenation catalysis by transition-metal surfaces: a surface-science perspective. *Phys. Chem. Chem. Phys.* **2013**, *15*, 11988−12003.
(1024) Serrano-Ruiz, J. C.; López-Cudero, A.; Solla-Gullón, J.; Sepúlveda-Escribano, A.; Aldaz, A.; Rodríguez-Reinoso, F. Hydrogenation of α, β unsaturated aldehydes over polycrystalline, (111) and (100) preferentially oriented Pt nanoparticles supported on carbon. *J. Catal.* **2008**, *253*, 159−166.
(1025) Ramos-Fernández, E. V.; Ramos-Fernández, J. M.; Martínez-Escandell, M.; Sepúlveda-Escribano, A.; Rodríguez-Reinoso, F. Selective Hydrogenation of Cinnamaldehyde over (111) Preferentially Oriented Pt Particles Supported on Expanded Graphite. *Catal. Lett.* **2009**, *133*, 267−272.
(1026) Zhang, Z.-C.; Zhang, X.; Yu, Q.-Y.; Liu, Z.-C.; Xu, C.-M.; Gao, J.-S.; Zhuang, J.; Wang, X. Pd Cluster Nanowires as Highly Efficient Catalysts for Selective Hydrogenation Reactions. *Chem.-Eur. J.* **2012**, *18*, 2639−2645.
(1027) Yuan, Y.; Yao, S.; Wang, M.; Lou, S.; Yan, N. Recent progress in chemoselective hydrogenation of α,β-unsaturated aldehyde to unsaturated alcohol over nanomaterials. *Curr. Org. Chem.* **2013**, *17*, 400−413.
(1028) Kato, S.; Ohyama, J.; Machida, M.; Satsuma, A. Gas-phase synthesis of morphology-controlled Pt nanoparticles and their impact on cinnamaldehyde hydrogenation. *Catal. Sci. Technol.* **2019**, *9*, 2097−2102.
(1029) Navlani-García, M.; Verma, P.; Mori, K.; Kuwahara, Y.; Yamashita, H. Morphology-controlled Pd nanocrystals as catalysts in tandem dehydrogenation-hydrogenation reactions. *Journal of Chemical Sciences* **2017**, *129*, 1695−1703.
(1030) Wang, Y.; Tao, Z.; Wu, B.; Chen, H.; Xu, J.; Yang, Y.; Li, Y. Shape-controlled synthesis of Pt particles and their catalytic performances in the n-hexadecane hydroconversion. *Catal. Today* **2016**, *259*, 331−339.
(1031) Chen, H.; Liu, S.; Yin, J.; Gao, X.; Tao, Z.; Wu, B.; Xiang, H.; Yang, Y.; Li, Y. The Influence of Size and Shape of Pd Nanoparticles on the Performances of Pd/Beta Catalysts for n-Heptane Hydroisomerization. *ChemCatChem.* **2019**, *11*, 3542−3551.
(1032) Fukuoka, A.; Higashimoto, N.; Sakamoto, Y.; Inagaki, S.; Fukushima, Y.; Ichikawa, M. Preparation and catalysis of Pt and Rh nanowires and particles in FSM-16. *Microporous Mesoporous Mater.* **2001**, *48*, 171−179.
(1033) Lee, I.; Morales, R.; Albiter, M. A.; Zaera, F. Synthesis of heterogeneous catalysts with well-shaped platinum particles to control reaction selectivity. *Proc. Natl. Acad. Sci. U. S. A.* **2008**, *105*, 15241−15246.
(1034) Lee, I.; Delbecq, F.; Morales, R.; Albiter, M. A.; Zaera, F. Tuning selectivity in catalysis by controlling particle shape. *Nat. Mater.* **2009**, *8*, 132−138.
(1035) Lee, I.; Zaera, F. Thermal chemistry of C_4 hydrocarbons on Pt(111): Mechanism for double-bond isomerization. *J. Phys. Chem. B* **2005**, *109*, 2745−2753.
(1036) Lee, I.; Zaera, F. Selectivity in platinum-catalyzed cis-trans carbon-carbon double-bond isomerization. *J. Am. Chem. Soc.* **2005**, *127*, 12174−12175.
(1037) Lee, I.; Nguyen, M. K.; Morton, T. H.; Zaera, F. Thermal chemistry of 1,4-difluoro-2-butenes on Pt(111) single crystal surfaces. *J. Phys. Chem. C* **2008**, *112*, 14117−14123.
(1038) Lee, I.; Albiter, M. A.; Zhang, Q.; Ge, J.; Yin, Y.; Zaera, F. New Nanostructured Heterogeneous Catalysts with Increased Selectivity and Stability. *Phys. Chem. Chem. Phys.* **2011**, *13*, 2449−2456.
(1039) Lee, I.; Hong, J.; Zaera, F. The Stereoselectivity of the Dehydrogenation of Alkyl Groups on Pt(111) Single-Crystal Surfaces. *J. Phys. Chem. C* **2011**, *115*, 982−989.
(1040) Lee, I.; Zaera, F. Nanoparticle Shape Selectivity in Catalysis: Butene Isomerization and Hydrogenation on Platinum. *Top. Catal.* **2013**, *56*, 1284−1298.
(1041) Delbecq, F.; Zaera, F. Origin of trans-to-cis isomerization selectivity in 2-butene adsorbed on Pt(111) single crystal surfaces: A DFT study. *J. Am. Chem. Soc.* **2008**, *130*, 14924−14925.
(1042) Li, J.; Fleurat-Lessard, P.; Zaera, F.; Delbecq, F. Mechanistic Investigation of the cis/trans Isomerization of 2-butene on Pt(111): DFT Study of the Influence of the Hydrogen Coverage. *J. Catal.* **2014**, *311*, 190−198.

https://doi.org/10.1021/acs.chemrev.1c00905
Chem. Rev. XXXX, XXX, XXX−XXX

(1043) Li, J.; Fleurat-Lessard, P.; Zaera, F.; Delbecq, F. Switch in Relative Stability between cis and trans 2-Butene on Pt(111) as a Function of Experimental Conditions: A Density Functional Theory Study. *ACS Catal.* **2018**, *8*, 3067−3075.
(1044) Zhang, Y.; Grass, M. E.; Huang, W.; Somorjai, G. A. Seedless Polyol Synthesis and CO Oxidation Activity of Monodisperse (111)- and (100)-Oriented Rhodium Nanocrystals in Sub-10 nm Sizes. *Langmuir* **2010**, *26*, 16463−16468.
(1045) Wang, R.; He, H.; Liu, L.-C.; Dai, H.-X.; Zhao, Z. Shape-dependent catalytic activity of palladium nanocrystals for the oxidation of carbon monoxide. *Catal. Sci. Technol.* **2012**, *2*, 575−580.
(1046) Wang, R.; He, H.; Wang, J.; Liu, L.; Dai, H. Shape-regulation: An effective way to control CO oxidation activity over noble metal catalysts. *Catal. Today* **2013**, *201*, 68−78.
(1047) Sreedhala, S.; Sudheeshkumar, V.; Vinod, C. P. CO oxidation on large high-index faceted Pd nanostructures. *J. Catal.* **2016**, *337*, 138−144.
(1048) Zhou, J.; Hu, J.; Zhang, X.; Li, J.; Jiang, K.; Liu, Y.; Zhao, G.; Wang, X.; Chu, H. Facet effect of Pt nanocrystals on catalytical properties toward glycerol oxidation reaction. *J. Catal.* **2020**, *381*, 434−442.
(1049) Xu, Z.-N.; Sun, J.; Lin, C.-S.; Jiang, X.-M.; Chen, Q.-S.; Peng, S.-Y.; Wang, M.-S.; Guo, G.-C. High-Performance and Long-Lived Pd Nanocatalyst Directed by Shape Effect for CO Oxidative Coupling to Dimethyl Oxalate. *ACS Catal.* **2013**, *3*, 118−122.
(1050) Kim, S.; Lee, D.-W.; Lee, K.-Y. Shape-dependent catalytic activity of palladium nanoparticles for the direct synthesis of hydrogen peroxide from hydrogen and oxygen. *J. Mol. Catal. A* **2014**, *391*, 48−54.
(1051) Mostafa, S.; Behafarid, F.; Croy, J. R.; Ono, L. K.; Li, L.; Yang, J. C.; Frenkel, A. I.; Roldan Cuenya, B. Shape-Dependent Catalytic Properties of Pt Nanoparticles. *J. Am. Chem. Soc.* **2010**, *132*, 15714−15719.
(1052) Mistry, H.; Behafarid, F.; Zhou, E.; Ono, L. K.; Zhang, L.; Roldan Cuenya, B. Shape-Dependent Catalytic Oxidation of 2-Butanol over Pt Nanoparticles Supported on γ-Al2O3. *ACS Catal.* **2014**, *4*, 109−115.
(1053) Christopher, P.; Linic, S. Engineering Selectivity in Heterogeneous Catalysis: Ag Nanowires as Selective Ethylene Epoxidation Catalysts. *J. Am. Chem. Soc.* **2008**, *130*, 11264−11265.
(1054) Christopher, P.; Linic, S. Shape- and Size-Specific Chemistry of Ag Nanostructures in Catalytic Ethylene Epoxidation. *ChemCatChem.* **2010**, *2*, 78−83.
(1055) Linic, S.; Christopher, P. Overcoming Limitation in the Design of Selective Solid Catalysts by Manipulating Shape and Size of Catalytic Particles: Epoxidation Reactions on Silver. *ChemCatChem.* **2010**, *2*, 1061−1063.
(1056) Pulido, A.; Concepción, P.; Boronat, M.; Corma, A. Aerobic epoxidation of propene over silver (111) and (100) facet catalysts. *J. Catal.* **2012**, *292*, 138−147.
(1057) Zhao, M.; Crooks, R. M. Dendrimer-encapsulated Pt nanoparticles. Synthesis, characterization, and applications to catalysis. *Adv. Mater.* **1999**, *11*, 217−220.
(1058) Zhao, M.; Crooks, R. M. Homogeneous hydrogenation catalysis with monodisperse, dendrimer-encapsulated Pd and Pt nanoparticles. *Angew. Chem., Int. Ed.* **1999**, *38*, 364−366.
(1059) Crooks, R. M.; Lemon, B. I., III; Sun, L.; Yeung, L. K.; Zhao, M. Dendrimer-encapsulated metals and semiconductors: Synthesis, characterization, and applications. *Top. Curr. Chem.* **2001**, *212*, 81−135.
(1060) Myers, V. S.; Weir, M. G.; Carino, E. V.; Yancey, D. F.; Pande, S.; Crooks, R. M. Dendrimer-encapsulated nanoparticles: New synthetic and characterization methods and catalytic applications. *Chem. Sci.* **2011**, *2*, 1632−1646.
(1061) Gu, Y.; Sanders, P.; Ploehn, H. J. Quantitative analysis of Pt-PAMAM ligand exchange reactions: Time and concentration effects. *Colloids Surf., A* **2010**, *356*, 10−15.
(1062) Nazarpoor, Z.; Khivantsev, K.; Kyriakidou, E.; Kubicki, C.; Ma, S.; Fanson, P. T.; Alexeev, O. S.; Amiridis, M. D. Dendrimer-mediated synthesis of supported rhodium nanoparticles with controlled size: Effect of pH and dialysis. *J. Coll. Interface Sci.* **2013**, *398*, 22−32.
(1063) Niu, Y.; Crooks, R. M. Dendrimer-encapsulated metal nanoparticles and their applications to catalysis. *Comp. Rend. Chim.* **2003**, *6*, 1049−1059.
(1064) Yamamoto, K.; Imaoka, T. Precision Synthesis of Subnanoparticles Using Dendrimers as a Superatom Synthesizer. *Acc. Chem. Res.* **2014**, *47*, 1127−1136.
(1065) Balogh, L.; Tomalia, D. A. Poly(Amidoamine) Dendrimer-Templated Nanocomposites. 1. Synthesis of Zerovalent Copper Nanoclusters. *J. Am. Chem. Soc.* **1998**, *120*, 7355−7356.
(1066) Esumi, K.; Suzuki, A.; Aihara, N.; Usui, K.; Torigoe, K. Preparation of Gold Colloids with UV Irradiation Using Dendrimers as Stabilizer. *Langmuir* **1998**, *14*, 3157−3159.
(1067) Yamamoto, K.; Imaoka, T.; Tanabe, M.; Kambe, T. New Horizon of Nanoparticle and Cluster Catalysis with Dendrimers. *Chem. Rev.* **2020**, *120*, 1397−1437.
(1068) Shylesh, S.; Schünemann, V.; Thiel, W. R. Magnetically Separable Nanocatalysts: Bridges between Homogeneous and Heterogeneous Catalysis. *Angew. Chem., Int. Ed.* **2010**, *49*, 3428−3459.
(1069) Wang, D.; Deraedt, C.; Ruiz, J.; Astruc, D. Magnetic and Dendritic Catalysts. *Acc. Chem. Res.* **2015**, *48*, 1871−1880.
(1070) Niu, Y.; Yeung, L. K.; Crooks, R. M. Size-selective hydrogenation of olefins by Dendrimer-encapsulated palladium nanoparticles. *J. Am. Chem. Soc.* **2001**, *123*, 6840−6846.
(1071) Wilson, O. M.; Knecht, M. R.; Garcia-Martinez, J. C.; Crooks, R. M. Effect of Pd Nanoparticle Size on the Catalytic Hydrogenation of Allyl Alcohol. *J. Am. Chem. Soc.* **2006**, *128*, 4510−4511.
(1072) Yeung, L. K.; Crooks, R. M. Heck Heterocoupling within a Dendritic Nanoreactor. *Nano Lett.* **2001**, *1*, 14−17.
(1073) Lemo, J.; Heuzé, K.; Astruc, D. Synthesis and catalytic activity of DAB-dendrimer encapsulated Pd nanoparticles for the Suzuki coupling reaction. *Inorg. Chim. Acta* **2006**, *359*, 4909−4911.
(1074) Diallo, A. K.; Ornelas, C.; Salmon, L.; Ruiz Aranzaes, J.; Astruc, D. Homeopathic" Catalytic Activity and Atom-Leaching Mechanism in Miyaura-Suzuki Reactions under Ambient Conditions with Precise Dendrimer-Stabilized Pd Nanoparticles. *Angew. Chem., Int. Ed.* **2007**, *46*, 8644−8648.
(1075) Ornelas, C.; Aranzaes, J. R.; Salmon, L.; Astruc, D. Click" Dendrimers: Synthesis, Redox Sensing of $Pd(OAc)_2$, and Remarkable Catalytic Hydrogenation Activity of Precise Pd Nanoparticles Stabilized by 1,2,3-Triazole-Containing Dendrimers. *Chem.-Eur. J.* **2008**, *14*, 50−64.
(1076) Nakamula, I.; Yamanoi, Y.; Yonezawa, T.; Imaoka, T.; Yamamoto, K.; Nishihara, H. Nanocage catalysts - Rhodium nanoclusters encapsulated with dendrimers as accessible and stable catalysts for olefin and nitroarene hydrogenations. *Chem. Commun.* **2008**, 5716−5718.
(1077) Deraedt, C.; Salmon, L.; Astruc, D. Click" Dendrimer-Stabilized Palladium Nanoparticles as a Green Catalyst Down to Parts per Million for Efficient C-C Cross-Coupling Reactions and Reduction of 4-Nitrophenol. *Adv. Synth. Catal.* **2014**, *356*, 2525−2538.
(1078) Bernechea, M. a.; de Jesüs, E.; Löpez-Mardomingo, C.; Terreros, P. Dendrimer-Encapsulated Pd Nanoparticles versus Palladium Acetate as Catalytic Precursors in the Stille Reaction in Water. *Inorg. Chem.* **2009**, *48*, 4491−4496.
(1079) Esumi, K.; Isono, R.; Yoshimura, T. Preparation of PAMAM- and PPI-Metal (Silver, Platinum, and Palladium) Nanocomposites and Their Catalytic Activities for Reduction of 4-Nitrophenol. *Langmuir* **2004**, *20*, 237−243.
(1080) Kracke, P.; Haas, T.; Saltsburg, H.; Flytzani-Stephanopoulos, M. CO Oxidation on Unsupported Dendrimer-Encapsulated Gold Nanoparticles. *J. Phys. Chem. C* **2010**, *114*, 16401−16407.

https://doi.org/10.1021/acs.chemrev.1c00905
Chem. Rev. XXXX, XXX, XXX−XXX

(1081) Yu, T.; Wang, W.; Chen, J.; Zeng, Y.; Li, Y.; Yang, G.; Li, Y. Dendrimer-Encapsulated Pt Nanoparticles: An Artificial Enzyme for Hydrogen Production. *J. Phys. Chem. C* **2012**, *116*, 10516−10521.
(1082) Antonels, N. C.; Meijboom, R. Preparation of Well-Defined Dendrimer Encapsulated Ruthenium Nanoparticles and Their Evaluation in the Reduction of 4-Nitrophenol According to the Langmuir-Hinshelwood Approach. *Langmuir* **2013**, *29*, 13433−13442.
(1083) Noh, J.-H.; Meijboom, R. Synthesis and catalytic evaluation of dendrimer-templated and reverse microemulsion Pd and Pt nanoparticles in the reduction of 4-nitrophenol: The effect of size and synthetic methodologies. *Appl. Catal. A* **2015**, *497*, 107−120.
(1084) Ilunga, A. K.; Meijboom, R. A Review of Dendrimer-Encapsulated Metal Nanocatalysts Applied in the Fine Chemical Transformations. *Catal. Lett.* **2019**, *149*, 84−99.
(1085) Eghbali, P.; Gürbüz, M. U.; Ertürk, A. S.; Metin, Ö. In situ synthesis of dendrimer-encapsulated palladium(0) nanoparticles as catalysts for hydrogen production from the methanolysis of ammonia borane. *International Journal of Hydrogen Energy* **2020**, *45*, 26274−26285.
(1086) Esumi, K.; Houdatsu, H.; Yoshimura, T. Antioxidant Action by Gold-PAMAM Dendrimer Nanocomposites. *Langmuir* **2004**, *20*, 2536−2538.
(1087) Ye, H.; Crooks, J. A.; Crooks, R. M. Effect of particle size on the kinetics of the electrocatalytic oxygen reduction reaction catalyzed by Pt dendrimer-encapsulated nanoparticles. *Langmuir* **2007**, *23*, 11901−11906.
(1088) Johnson, J. A.; Makis, J. J.; Marvin, K. A.; Rodenbusch, S. E.; Stevenson, K. J. Size-Dependent Hydrogenation of p-Nitrophenol with Pd Nanoparticles Synthesized with Poly(amido)amine Dendrimer Templates. *J. Phys. Chem. C* **2013**, *117*, 22644−22651.
(1089) Kibata, T.; Mitsudome, T.; Mizugaki, T.; Jitsukawa, K.; Kaneda, K. Investigation of size-dependent properties of sub-nanometer palladium clusters encapsulated within a polyamine dendrimer. *Chem. Commun.* **2013**, *49*, 167−169.
(1090) Nemanashi, M.; Meijboom, R. Catalytic Behavior of Different Sizes of Dendrimer-Encapsulated Aun Nanoparticles in the Oxidative Degradation of Morin with H_2O_2. *Langmuir* **2015**, *31*, 9041−9053.
(1091) Maity, P.; Yamazoe, S.; Tsukuda, T. Dendrimer-Encapsulated Copper Cluster as a Chemoselective and Regenerable Hydrogenation Catalyst. *ACS Catal.* **2013**, *3*, 182−185.
(1092) Astruc, D.; Chardac, F. Dendritic catalysts and dendrimers in catalysis. *Chem. Rev.* **2001**, *101*, 2991−3023.
(1093) Wang, D.; Astruc, D. Dendritic catalysis—Basic concepts and recent trends. *Coord. Chem. Rev.* **2013**, *257*, 2317−2334.
(1094) Caminade, A.-M.; Ouali, A.; Laurent, R.; Turrin, C.-O.; Majoral, J.-P. Coordination chemistry with phosphorus dendrimers. Applications as catalysts, for materials, and in biology. *Coord. Chem. Rev.* **2016**, *308*, 478−497.
(1095) Brunner, H. Dendrizymes: Expanded ligands for enantioselective catalysis. *Journal of Organometallic Chemistry* **1995**, *500*, 39−46.
(1096) Brunner, H.; Janura, M.; Stefaniak, S. Enantioselective Catalysis: 123: Octaaldehyde Type Chelating Ligands - A Divergent Synthesis Approach to Easily Tunable Expanded Ligands for Enantioselective Catalysis. *Synthesis* **1998**, *1998*, 1742−1749.
(1097) Schneider, R.; Köllner, C.; Weber, I.; Togni, A. Dendrimers based on cyclophosphazene units and containing chiral ferrocenyl ligands for asymmetric catalysis†. *Chem. Commun.* **1999**, 2415−2416.
(1098) Yamago, S.; Furukawa, M.; Azuma, A.; Yoshida, J.-i. Synthesis of optically active dendritic binaphthols and their metal complexes for asymmetric catalysis. *Tetrahedron Lett.* **1998**, *39*, 3783−3786.
(1099) Bolm, C.; Derrien, N.; Seger, A. Hyperbranched chiral catalysts for the asymmetric reduction of ketones with borane. *Chem. Commun.* **1999**, 2087−2088.
(1100) Fan, Q.-H.; Chen, Y.-M.; Chen, X.-M.; Jiang, D.-Z.; Xi, F.; Chan, A. S. C. Highly effective and recyclable dendritic BINAP ligands for asymmetric hydrogenation. *Chem. Commun.* **2000**, 789−790.
(1101) Wang, Z.-J.; Deng, G.-J.; Li, Y.; He, Y.-M.; Tang, W.-J.; Fan, Q.-H. Enantioselective Hydrogenation of Quinolines Catalyzed by Ir(BINAP)-Cored Dendrimers: Dramatic Enhancement of Catalytic Activity. *Organic Letters* **2007**, *9*, 1243−1246.
(1102) Gissibl, A.; Padié, C.; Hager, M.; Jaroschik, F.; Rasappan, R.; Cuevas-Yañez, E.; Turrin, C.-O.; Caminade, A.-M.; Majoral, J.-P.; Reiser, O. Synthesis and Application of Phosphorus Dendrimer Immobilized Azabis(oxazolines). *Organic Letters* **2007**, *9*, 2895−2898.
(1103) Wang, W.; Wang, Q. A fluorinated dendritic TsDPEN-Ru(ii) catalyst for asymmetric transfer hydrogenation of prochiral ketones in aqueous media. *Chem. Commun.* **2010**, *46*, 4616−4618.
(1104) Chen, T.; Cheng, Z.; Yi, C.; Xu, Z. Synthesis of platinum nanoparticles templated by dendrimers terminated with alkyl chains. *Chem. Commun.* **2018**, *54*, 9143−9146.
(1105) Weng, Z.; Zaera, F. Synthesis of Chiral Dendrimer-Encapsulated Nanoparticle (DEN) Catalysts. *Top. Catal.* **2018**, *61*, 902−914.
(1106) Pittelkow, M.; Brock-Nannestad, T.; Moth-Poulsen, K.; Christensen, J. B. Chiral dendrimer encapsulated Pd and Rh nanoparticles. *Chem. Commun.* **2008**, 2358−2360.
(1107) Dumitrescu, I.; Crooks, R. M. Effect of mass transfer on the oxygen reduction reaction catalyzed by platinum dendrimer encapsulated nanoparticles. *Proc. Nat. Acad. Sci.* **2012**, *109*, 11493.
(1108) Scott, R. W. J.; Wilson, O. M.; Crooks, R. M. Synthesis, Characterization, and Applications of Dendrimer-Encapsulated Nanoparticles. *J. Phys. Chem. B* **2005**, *109*, 692−704.
(1109) Ooe, M.; Murata, M.; Mizugaki, T.; Ebitani, K.; Kaneda, K. Dendritic Nanoreactors Encapsulating Pd Particles for Substrate-Specific Hydrogenation of Olefins. *Nano Lett.* **2002**, *2*, 999−1002.
(1110) Albiter, M. A.; Crooks, R. M.; Zaera, F. Adsorption of Carbon Monoxide on Dendrimer-Encapsulated Platinum Nanoparticles: Liquid versus Gas Phase. *J. Phys. Chem. Lett.* **2010**, *1*, 38−40.
(1111) Anderson, R. M.; Zhang, L.; Wu, D.; Brankovic, S. R.; Henkelman, G.; Crooks, R. M. A Theoretical and Experimental In-Situ Electrochemical Infrared Spectroscopy Study of Adsorbed CO on Pt Dendrimer-Encapsulated Nanoparticles. *J. Electrochem. Soc.* **2016**, *163*, H3061−H3065.
(1112) Albiter, M. A.; Zaera, F. Adsorption Properties of Supported Platinum Catalysts Prepared using Dendrimers. *Langmuir* **2010**, *26*, 16204−16210.
(1113) Lang, H.; May, R. A.; Iversen, B. L.; Chandler, B. D. Dendrimer-Encapsulated Nanoparticle Precursors to Supported Platinum Catalysts. *J. Am. Chem. Soc.* **2003**, *125*, 14832−14836.
(1114) Huang, W.; Kuhn, J. N.; Tsung, C.-K.; Zhang, Y.; Habas, S. E.; Yang, P.; Somorjai, G. A. Dendrimer Templated Synthesis of One Nanometer Rh and Pt Particles Supported on Mesoporous Silica: Catalytic Activity for Ethylene and Pyrrole Hydrogenation. *Nano Lett.* **2008**, *8*, 2027−2034.
(1115) Deraedt, C.; Ye, R.; Ralston, W. T.; Toste, F. D.; Somorjai, G. A. Dendrimer-Stabilized Metal Nanoparticles as Efficient Catalysts for Reversible Dehydrogenation/Hydrogenation of N-Heterocycles. *J. Am. Chem. Soc.* **2017**, *139*, 18084−18092.
(1116) Ye, R.; Yuan, B.; Zhao, J.; Ralston, W. T.; Wu, C.-Y.; Unel Barin, E.; Toste, F. D.; Somorjai, G. A. Metal Nanoparticles Catalyzed Selective Carbon-Carbon Bond Activation in the Liquid Phase. *J. Am. Chem. Soc.* **2016**, *138*, 8533−8537.
(1117) Kuhn, J. N.; Huang, W.; Tsung, C.-K.; Zhang, Y.; Somorjai, G. A. Structure Sensitivity of Carbon-Nitrogen Ring Opening: Impact of Platinum Particle Size from below 1 to 5 nm upon Pyrrole Hydrogenation Product Selectivity over Monodisperse Platinum Nanoparticles Loaded onto Mesoporous Silica. *J. Am. Chem. Soc.* **2008**, *130*, 14026−14027.
(1118) Albiter, M. A.; Zaera, F.; et al. Dendrimer-Based Synthesis of Pt Catalysts for Hydrocarbon Conversion. *Appl. Catal. A* **2011**, *391*, 386−393.

https://doi.org/10.1021/acs.chemrev.1c00905
Chem. Rev. XXXX, XXX, XXX−XXX

(1119) Takahashi, M.; Imaoka, T.; Hongo, Y.; Yamamoto, K. Formation of a Pt_{12} Cluster by Single-Atom Control That Leads to Enhanced Reactivity: Hydrogenation of Unreactive Olefins. *Angew. Chem., Int. Ed.* **2013**, *52*, 7419−7421.
(1120) Beakley, L. W.; Yost, S. E.; Cheng, R.; Chandler, B. D. Nanocomposite catalysts: Dendrimer encapsulated nanoparticles immobilized in sol-gel silica. *Appl. Catal. A* **2005**, *292*, 124−129.
(1121) Antonels, N. C.; Benjamin Williams, M.; Meijboom, R.; Haumann, M. Well-defined dendrimer encapsulated ruthenium SCILL catalysts for partial hydrogenation of toluene in liquid-phase. *J. Mol. Catal. A* **2016**, *421*, 156−160.
(1122) Keshtiara, P.; Hadadzadeh, H.; Daryanavard, M.; Mousavi, N.; Dinari, M. New dendrimers containing ruthenium nanoparticles as catalysts for hydrogenation of citral to 3,7-dimethyloctanol. *Materials Chemistry and Physics* **2020**, *249*, 122962.
(1123) Kumar, P. A.; Ha, H. P. Synthesis and Dispersion of Dendrimer-Encapsulated Pt Nanoparticles on γ-Al_2O_3 for the Reduction of NO_x by Methane. *Catal. Lett.* **2010**, *136*, 177−184.
(1124) Takahashi, M.; Imaoka, T.; Hongo, Y.; Yamamoto, K. A highly-active and poison-tolerant Pt_{12} sub-nanocluster catalyst for the reductive amination of aldehydes with amines. *Dalton Trans.* **2013**, *42*, 15919−15921.
(1125) Takahashi, M.; Imaoka, T.; Yamamoto, K. Reactivities of platinum subnanocluster catalysts for the oxidation reaction of alcohols. *RSC Adv.* **2015**, *5*, 100693−100696.
(1126) Li, H.; Lü, J.; Zheng, Z.; Cao, R. An efficient and reusable silica/dendrimer supported platinum catalyst for electron transfer reactions. *J. Colloid Interface Sci.* **2011**, *353*, 149−155.
(1127) Ye, R.; Zhao, J.; Yuan, B.; Liu, W.-C.; Rodrigues De Araujo, J.; Faucher, F. F.; Chang, M.; Deraedt, C. V.; Toste, F. D.; Somorjai, G. A. New Insights into Aldol Reactions of Methyl Isocyanoacetate Catalyzed by Heterogenized Homogeneous Catalysts. *Nano Lett.* **2017**, *17*, 584−589.
(1128) Ye, H.; Crooks, R. M. Electrocatalytic O_2 Reduction at Glassy Carbon Electrodes Modified with Dendrimer-Encapsulated Pt Nanoparticles. *J. Am. Chem. Soc.* **2005**, *127*, 4930−4934.
(1129) Vijayaraghavan, G.; Stevenson, K. J. Synergistic Assembly of Dendrimer-Templated Platinum Catalysts on Nitrogen-Doped Carbon Nanotube Electrodes for Oxygen Reduction. *Langmuir* **2007**, *23*, 5279−5282.
(1130) Yamamoto, K.; Imaoka, T.; Chun, W.-J.; Enoki, O.; Katoh, H.; Takenaga, M.; Sonoi, A. Size-specific catalytic activity of platinum clusters enhances oxygen reduction reactions. *Nat. Chem.* **2009**, *1*, 397−402.
(1131) Shen, Y.; Xu, Q.; Gao, H.; Zhu, N. Dendrimer-encapsulated Pd nanoparticles anchored on carbon nanotubes for electro-catalytic hydrazine oxidation. *Electrochem. Commun.* **2009**, *11*, 1329−1332.
(1132) Jiang, Y.; Gao, Q. Heterogeneous Hydrogenation Catalyses over Recyclable Pd(0) Nanoparticle Catalysts Stabilized by PAMAM-SBA-15 Organic-Inorganic Hybrid Composites. *J. Am. Chem. Soc.* **2006**, *128*, 716−717.
(1133) Zheng, Z.; Li, H.; Liu, T.; Cao, R. Monodisperse noble metal nanoparticles stabilized in SBA-15: Synthesis, characterization and application in microwave-assisted Suzuki-Miyaura coupling reaction. *J. Catal.* **2010**, *270*, 268−274.
(1134) Karakhanov, E.; Maximov, A.; Kardasheva, Y.; Semernina, V.; Zolotukhina, A.; Ivanov, A.; Abbott, G.; Rosenberg, E.; Vinokurov, V. Pd Nanoparticles in Dendrimers Immobilized on Silica-Polyamine Composites as Catalysts for Selective Hydrogenation. *ACS Appl. Mater. Interfaces* **2014**, *6*, 8807−8816.
(1135) Giacalone, F.; Campisciano, V.; Calabrese, C.; La Parola, V.; Syrgiannis, Z.; Prato, M.; Gruttadauria, M. Single-Walled Carbon Nanotube-Polyamidoamine Dendrimer Hybrids for Heterogeneous Catalysis. *ACS Nano* **2016**, *10*, 4627−4636.
(1136) Ogasawara, S.; Kato, S. Palladium Nanoparticles Captured in Microporous Polymers: A Tailor-Made Catalyst for Heterogeneous Carbon Cross-Coupling Reactions. *J. Am. Chem. Soc.* **2010**, *132*, 4608−4613.
(1137) Huda, M.; Minamisawa, K.; Tsukamoto, T.; Tanabe, M.; Yamamoto, K. Aerobic Toluene Oxidation Catalyzed by Subnano Metal Particles. *Angew. Chem., Int. Ed.* **2019**, *58*, 1002−1006.
(1138) Gross, E.; Liu, J. H.-C.; Toste, F. D.; Somorjai, G. A. Control of selectivity in heterogeneous catalysis by tuning nanoparticle properties and reactor residence time. *Nat. Chem.* **2012**, *4*, 947.
(1139) Ye, R.; Zhukhovitskiy, A. V.; Deraedt, C. V.; Toste, F. D.; Somorjai, G. A. Supported Dendrimer-Encapsulated Metal Clusters: Toward Heterogenizing Homogeneous Catalysts. *Acc. Chem. Res.* **2017**, *50*, 1894−1901.
(1140) Zaleska-Medynska, A.; Marchelek, M.; Diak, M.; Grabowska, E. Noble metal-based bimetallic nanoparticles: the effect of the structure on the optical, catalytic and photocatalytic properties. *Adv. Colloid Interface Sci.* **2016**, *229*, 80−107.
(1141) Zhang, H.; Jin, M.; Xia, Y. Enhancing the catalytic and electrocatalytic properties of Pt-based catalysts by forming bimetallic nanocrystals with Pd. *Chem. Soc. Rev.* **2012**, *41*, 8035−8049.
(1142) Xu, Y.; Chen, L.; Wang, X.; Yao, W.; Zhang, Q. Recent advances in noble metal based composite nanocatalysts: colloidal synthesis, properties, and catalytic applications. *Nanoscale* **2015**, *7*, 10559−10583.
(1143) Wang, L.; Yamauchi, Y. Strategic Synthesis of Trimetallic Au@Pd@Pt Core-Shell Nanoparticles from Poly(vinylpyrrolidone)-Based Aqueous Solution toward Highly Active Electrocatalysts. *Chem. Mater.* **2011**, *23*, 2457−2465.
(1144) Sneed, B. T.; Young, A. P.; Jalalpoor, D.; Golden, M. C.; Mao, S.; Jiang, Y.; Wang, Y.; Tsung, C.-K. Shaped Pd-Ni-Pt Core-Sandwich-Shell Nanoparticles: Influence of Ni Sandwich Layers on Catalytic Electrooxidations. *ACS Nano* **2014**, *8*, 7239−7250.
(1145) Zhang, G.-R.; Wu, J.; Xu, B.-Q. Syntheses of Sub-30 nm Au@Pd Concave Nanocubes and Pt-on-(Au@Pd) Trimetallic Nanostructures as Highly Efficient Catalysts for Ethanol Oxidation. *J. Phys. Chem. C* **2012**, *116*, 20839−20847.
(1146) Zhang, L.; Choi, S.-I.; Tao, J.; Peng, H.-C.; Xie, S.; Zhu, Y.; Xie, Z.; Xia, Y. Pd-Cu Bimetallic Tripods: A Mechanistic Understanding of the Synthesis and Their Enhanced Electrocatalytic Activity for Formic Acid Oxidation. *Adv. Funct. Mater.* **2014**, *24*, 7520−7529.
(1147) Zhang, Z.-Q.; Huang, J.; Zhang, L.; Sun, M.; Wang, Y.-C.; Lin, Y.; Zeng, J. Facile synthesis of Cu-Pd bimetallic multipods for application in cyclohexane oxidation. *Nanotechnol.* **2014**, *25*, 435602.
(1148) Yin, H.; Wang, C.; Zhu, H.; Overbury, S. H.; Sun, S.; Dai, S. Colloidal deposition synthesis of supported gold nanocatalysts based on Au-Fe3O4 dumbbell nanoparticles. *Chem. Commun.* **2008**, 4357−4359.
(1149) Lu, Y.; Yuan, J.; Polzer, F.; Drechsler, M.; Preussner, J. In Situ Growth of Catalytic Active Au-Pt Bimetallic Nanorods in Thermoresponsive Core-Shell Microgels. *ACS Nano* **2010**, *4*, 7078−7086.
(1150) Lin, F.-h.; Doong, R.-a. Bifunctional Au-Fe_3O_4 Heterostructures for Magnetically Recyclable Catalysis of Nitrophenol Reduction. *J. Phys. Chem. C* **2011**, *115*, 6591−6598.
(1151) George, C.; Genovese, A.; Casu, A.; Prato, M.; Povia, M.; Manna, L.; Montanari, T. CO Oxidation on Colloidal Au0.80Pd0.20-FexOy Dumbbell Nanocrystals. *Nano Lett.* **2013**, *13*, 752−757.
(1152) Khi, N. T.; Yoon, J.; Kim, H.; Lee, S.; Kim, B.; Baik, H.; Kwon, S. J.; Lee, K. Axially twinned nanodumbbell with a Pt bar and two Rh@Pt balls designed for high catalytic activity. *Nanoscale* **2013**, *5*, 5738−5742.
(1153) Song, H. Metal Hybrid Nanoparticles for Catalytic Organic and Photochemical Transformations. *Acc. Chem. Res.* **2015**, *48*, 491−499.
(1154) Feng, Y.; Liu, H.; Wang, P.; Ye, F.; Tan, Q.; Yang, J. Enhancing the Electrocatalytic Property of Hollow Structured Platinum Nanoparticles for Methanol Oxidation Through A Hybrid Construction. *Sci. Rep.* **2015**, *4*, 6204.
(1155) Park, J.; Kwon, T.; Kim, J.; Jin, H.; Kim, H. Y.; Kim, B.; Joo, S. H.; Lee, K. Hollow nanoparticles as emerging electrocatalysts for

https://doi.org/10.1021/acs.chemrev.1c00905
Chem. Rev. XXXX, XXX, XXX−XXX

renewable energy conversion reactions. *Chem. Soc. Rev.* **2018**, *47*, 8173−8202.
(1156) Cochell, T.; Manthiram, A. Pt@PdxCuy/C Core-Shell Electrocatalysts for Oxygen Reduction Reaction in Fuel Cells. *Langmuir* **2012**, *28*, 1579−1587.
(1157) Wu, Y.; Wang, D.; Chen, X.; Zhou, G.; Yu, R.; Li, Y. Defect-Dominated Shape Recovery of Nanocrystals: A New Strategy for Trimetallic Catalysts. *J. Am. Chem. Soc.* **2013**, *135*, 12220−12223.
(1158) Choi, S.-I.; Shao, M.; Lu, N.; Ruditskiy, A.; Peng, H.-C.; Park, J.; Guerrero, S.; Wang, J.; Kim, M. J.; Xia, Y. Synthesis and Characterization of Pd@Pt-Ni Core-Shell Octahedra with High Activity toward Oxygen Reduction. *ACS Nano* **2014**, *8*, 10363−10371.
(1159) Guo, S.; Zhang, X.; Zhu, W.; He, K.; Su, D.; Mendoza-Garcia, A.; Ho, S. F.; Lu, G.; Sun, S. Nanocatalyst Superior to Pt for Oxygen Reduction Reactions: The Case of Core/Shell Ag(Au)/CuPd Nanoparticles. *J. Am. Chem. Soc.* **2014**, *136*, 15026−15033.
(1160) Bönnemann, H.; Braun, G.; Brijoux, W.; Brinkmann, R.; Tilling, A. S.; Seevogel, K.; Siepen, K. Nanoscale colloidal metals and alloys stabilized by solvents and surfactants Preparation and use as catalyst precursors. *Journal of Organometallic Chemistry* **1996**, *520*, 143−162.
(1161) Chandler, B.; Gilbertson, J. Dendrimer-Encapsulated Bimetallic Nanoparticles: Synthesis, Characterization, and Applications to Homogeneous and Heterogeneous Catalysis. *Top. Organomet. Chem.* **2006**, *20*, 97−120.
(1162) Lang, H.; Maldonado, S.; Stevenson, K. J.; Chandler, B. D. Synthesis and characterization of dendrimer templated supported bimetallic Pt-Au nanoparticles. *J. Am. Chem. Soc.* **2004**, *126*, 12949−12956.
(1163) Luo, J.; Njoki, P. N.; Lin, Y.; Mott, D.; Wang; Zhong, C.-J. Characterization of Carbon-Supported AuPt Nanoparticles for Electrocatalytic Methanol Oxidation Reaction. *Langmuir* **2006**, *22*, 2892−2898.
(1164) Piccolo, L.; Li, Z. Y.; Demiroglu, I.; Moyon, F.; Konuspayeva, Z.; Berhault, G.; Afanasiev, P.; Lefebvre, W.; Yuan, J.; Johnston, R. L. Understanding and controlling the structure and segregation behaviour of AuRh nanocatalysts. *Sci. Rep.* **2016**, *6*, 35226.
(1165) Konuspayeva, Z.; Berhault, G.; Afanasiev, P.; Nguyen, T.-S.; Giorgio, S.; Piccolo, L. Monitoring in situ the colloidal synthesis of AuRh/TiO_2 selective-hydrogenation nanocatalysts. *Journal of Materials Chemistry A* **2017**, *5*, 17360−17367.
(1166) Corbos, E. C.; Ellis, P. R.; Cookson, J.; Briois, V.; Hyde, T. I.; Sankar, G.; Bishop, P. T. Tuning the properties of PdAu bimetallic nanocatalysts for selective hydrogenation reactions. *Catal. Sci. Technol.* **2013**, *3*, 2934−2943.
(1167) Wang, C.; Markovic, N. M.; Stamenkovic, V. R. Advanced Platinum Alloy Electrocatalysts for the Oxygen Reduction Reaction. *ACS Catal.* **2012**, *2*, 891−898.
(1168) Long, N. V.; Yang, Y.; Minh Thi, C.; Minh, N. V.; Cao, Y.; Nogami, M. The development of mixture, alloy, and core-shell nanocatalysts with nanomaterial supports for energy conversion in low-temperature fuel cells. *Nano Energy* **2013**, *2*, 636−676.
(1169) Endo, T.; Yoshimura, T.; Esumi, K. Synthesis and catalytic activity of gold-silver binary nanoparticles stabilized by PAMAM dendrimer. *J. Coll. Interface Sci.* **2005**, *286*, 602−609.
(1170) Peng, X.; Pan, Q.; Lu, X. Regioselective catalyzed modification of poly(methylhydro)siloxane using RuRh and RuPt bimetallic dendrimer-encapsulated nanoparticles. *J. Appl. Polym. Sci.* **2011**, *122*, 334−341.
(1171) Nakamula, I.; Yamanoi, Y.; Imaoka, T.; Yamamoto, K.; Nishihara, H. A Uniform Bimetallic Rhodium/Iron Nanoparticle Catalyst for the Hydrogenation of Olefins and Nitroarenes. *Angew. Chem., Int. Ed.* **2011**, *50*, 5830−5833.
(1172) Wang, Y.; Peng, X. RuRh Bimetallic Nanoparticles Stabilized by 15-membered Macrocycles-terminated Poly(propylene imine) Dendrimer: Preparation and Catalytic Hydrogenation of Nitrile—Butadiene Rubber. *Nano-Micro Letters* **2014**, *6*, 55−62.
(1173) Hosseini, H.; Mahyari, M.; Bagheri, A.; Shaabani, A. Pd and PdCo alloy nanoparticles supported on polypropylenimine dendrimer-grafted graphene: A highly efficient anodic catalyst for direct formic acid fuel cells. *J. Power Sources* **2014**, *247*, 70−77.
(1174) Ricciardi, R.; Huskens, J.; Verboom, W. Influence of the Au/Ag Ratio on the Catalytic Activity of Dendrimer-Encapsulated Bimetallic Nanoparticles in Microreactors. *Journal of Flow Chemistry* **2015**, *5*, 228−233.
(1175) Karakhanov, E. A.; Maximov, A. L.; Zolotukhina, A. V.; Yatmanova, N.; Rosenberg, E. Alkyne hydrogenation using Pd-Ag hybrid nanocatalysts in surface-immobilized dendrimers. *Appl. Organomet. Chem.* **2015**, *29*, 777−784.
(1176) Chen, T.; Rodionov, V. O. Controllable Catalysis with Nanoparticles: Bimetallic Alloy Systems and Surface Adsorbates. *ACS Catal.* **2016**, *6*, 4025−4033.
(1177) Zhou, W.; Lu, X.; Jin, Z.; Peng, X. Preparation, characterization and catalytic application of PdPt bimetallic nanoparticles stabilized by 15-membered triolefinic macrocycle-terminated poly(propylene imine) dendrimer. *Appl. Organomet. Chem.* **2017**, *31*, No. e3586.
(1178) Wang, Q.; Fu, F.; Yang, S.; Martinez Moro, M.; Ramirez, M. d. l. A.; Moya, S.; Salmon, L.; Ruiz, J.; Astruc, D. Dramatic Synergy in CoPt Nanocatalysts Stabilized by "Click" Dendrimers for Evolution of Hydrogen from Hydrolysis of Ammonia Borane. *ACS Catal.* **2019**, *9*, 1110−1119.
(1179) Liu, X.; Ruiz, J.; Astruc, D. Prevention of aerobic oxidation of copper nanoparticles by anti-galvanic alloying: gold versus silver. *Chem. Commun.* **2017**, *53*, 11134−11137.
(1180) Willis, J. J.; Goodman, E. D.; Wu, L.; Riscoe, A. R.; Martins, P.; Tassone, C. J.; Cargnello, M. Systematic Identification of Promoters for Methane Oxidation Catalysts Using Size- and Composition-Controlled Pd-Based Bimetallic Nanocrystals. *J. Am. Chem. Soc.* **2017**, *139*, 11989−11997.
(1181) Margossian, T.; Larmier, K.; Kim, S. M.; Krumeich, F.; Müller, C.; Copéret, C. Supported Bimetallic NiFe Nanoparticles through Colloid Synthesis for Improved Dry Reforming Performance. *ACS Catal.* **2017**, *7*, 6942−6948.
(1182) Carino, E. V.; Crooks, R. M. Characterization of Pt@Cu Core@Shell Dendrimer-Encapsulated Nanoparticles Synthesized by Cu Underpotential Deposition. *Langmuir* **2011**, *27*, 4227−4235.
(1183) Choi, S.-I.; Young, A.; Lee, S. R.; Ma, C.; Luo, M.; Chi, M.; Tsung, C.-K.; Xia, Y. Pd@Rh core-shell nanocrystals with well-defined facets and their enhanced catalytic performance towards CO oxidation. *Nanoscale Horizons* **2019**, *4*, 1232−1238.
(1184) Pretzer, L. A.; Song, H. J.; Fang, Y.-L.; Zhao, Z.; Guo, N.; Wu, T.; Arslan, I.; Miller, J. T.; Wong, M. S. Hydrodechlorination catalysis of Pd-on-Au nanoparticles varies with particle size. *J. Catal.* **2013**, *298*, 206−217.
(1185) Li, H.; Guo, S.; Shin, K.; Wong, M. S.; Henkelman, G. Design of a Pd-Au Nitrite Reduction Catalyst by Identifying and Optimizing Active Ensembles. *ACS Catal.* **2019**, *9*, 7957−7966.
(1186) Liu, R.; Chen, H.-m.; Fang, L.-p.; Xu, C.; He, Z.; Lai, Y.; Zhao, H.; Bekana, D.; Liu, J.-f. Au@Pd Bimetallic Nanocatalyst for Carbon-Halogen Bond Cleavage: An Old Story with New Insight into How the Activity of Pd is Influenced by Au. *Environ. Sci. Technol.* **2018**, *52*, 4244−4255.
(1187) Zhang, W.; Li, L.; Du, Y.; Wang, X.; Yang, P. Gold/Platinum Bimetallic Core/Shell Nanoparticles Stabilized by a Fréchet-Type Dendrimer: Preparation and Catalytic Hydrogenations of Phenylaldehydes and Nitrobenzenes. *Catal. Lett.* **2009**, *127*, 429−436.
(1188) Guo, S.; Heck, K.; Kasiraju, S.; Qian, H.; Zhao, Z.; Grabow, L. C.; Miller, J. T.; Wong, M. S. Insights into Nitrate Reduction over Indium-Decorated Palladium Nanoparticle Catalysts. *ACS Catal.* **2018**, *8*, 503−515.
(1189) Lin, H.; Muzzio, M.; Wei, K.; Zhang, P.; Li, J.; Li, N.; Yin, Z.; Su, D.; Sun, S. PdAu Alloy Nanoparticles for Ethanol Oxidation in Alkaline Conditions: Enhanced Activity and C1 Pathway Selectivity. *ACS Applied Energy Materials* **2019**, *2*, 8701−8706.

https://doi.org/10.1021/acs.chemrev.1c00905
Chem. Rev. XXXX, XXX, XXX−XXX

(1190) Fang, Y.-L.; Miller, J. T.; Guo, N.; Heck, K. N.; Alvarez, P. J. J.; Wong, M. S. Structural analysis of palladium-decorated gold nanoparticles as colloidal bimetallic catalysts. *Catal. Today* **2011**, *160*, 96−102.
(1191) Toshima, N. Core/shell-structured bimetallic nanocluster catalysts for visible-light-induced electron transfer. *Pure Appl. Chem.* **2000**, *72*, 317−325.
(1192) Zhang, H.; Toshima, N.; Takasaki, K.; Okumura, M. Preparation of Agcore/Aushell bimetallic nanoparticles from physical mixtures of Au clusters and Ag ions under dark conditions and their catalytic activity for aerobic glucose oxidation. *Journal of Alloys and Compounds* **2014**, *586*, 462−468.
(1193) Lee, H. Utilization of shape-controlled nanoparticles as catalysts with enhanced activity and selectivity. *RSC Adv.* **2014**, *4*, 41017−41027.
(1194) Campisi, S.; Schiavoni, M.; Chan-Thaw, E. C.; Villa, A. Untangling the Role of the Capping Agent in Nanocatalysis: Recent Advances and Perspectives. *Catalysts* **2016**, *6*, 185.
(1195) Su, N.; Gao, X.; Chen, X.; Yue, B.; He, H. The enantioselective hydrogenation of acetophenone over Pd concave tetrahedron nanocrystals affected by the residual adsorbed capping agent polyvinylpyrrolidone (PVP). *J. Catal.* **2018**, *367*, 244−251.
(1196) Garcia-Cruz, L.; Montiel, V.; Solla-Gullon, J. Shape-controlled metal nanoparticles for electrocatalytic applications. *Physical Sciences Reviews* **2019**, *4*, 20170124.
(1197) Bryant, K.; West, C. W.; Saunders, S. R. Impacts of calcination on surface-clean supported nanoparticle catalysts. *Appl. Catal. A* **2019**, *579*, 58−64.
(1198) Yang, T.-H.; Shi, Y.; Janssen, A.; Xia, Y. Surface Capping Agents and Their Roles in Shape-Controlled Synthesis of Colloidal Metal Nanocrystals. *Angew. Chem., Int. Ed.* **2020**, *59*, 15378−15401.
(1199) Zuo, X.; Liu, H.; Yue, C. Enantioselective hydrogenation of methyl pyruvate over polymer-stabilized and supported iridium clusters. *J. Mol. Catal. A: Chem.* **1999**, *147*, 63−72.
(1200) Sonstrom, P.; Bäumer, M. Supported colloidal nanoparticles in heterogeneous gas phase catalysis: on the way to tailored catalysts. *Phys. Chem. Chem. Phys.* **2011**, *13*, 19270−19284.
(1201) Nasar, K.; Fache, F.; Lemaire, M.; Béziat, J.-C.; Besson, M.; Gallezot, P. Stereoselective reduction of disubstituted aromatics on colloidal rhodium. *J. Mol. Catal.* **1994**, *87*, 107−115.
(1202) Bönnemann, H.; Braun, G. A. Enantioselectivity Control with Metal Colloids as Catalysts. *Chem.-Eur. J.* **1997**, *3*, 1200−1202.
(1203) Tamura, M.; Fujihara, H. Chiral Bisphosphine BINAP-Stabilized Gold and Palladium Nanoparticles with Small Size and Their Palladium Nanoparticle-Catalyzed Asymmetric Reaction. *J. Am. Chem. Soc.* **2003**, *125*, 15742−15743.
(1204) Jansat, S.; Picurelli, D.; Pelzer, K.; Philippot, K.; Gómez, M.; Muller, G.; Lecante, P.; Chaudret, B. Synthesis, characterization and catalytic reactivity of ruthenium nanoparticles stabilized by chiral N-donor ligands. *New J. Chem.* **2006**, *30*, 115−122.
(1205) Takizawa, S.; Patil, M. L.; Marubayashi, K.; Sasai, H. Development of new methods toward efficient immobilization of chiral catalysts. *Tetrahedron* **2007**, *63*, 6512−6528.
(1206) Diéguez, M.; Pàmies, O.; Mata, Y.; Teuma, E.; Gómez, M.; Ribaudo, F.; van Leeuwen, P. W. N. M. Palladium Nanoparticles in Allylic Alkylations and Heck Reactions: The Molecular Nature of the Catalyst Studied in a Membrane Reactor. *Adv. Synth. Catal.* **2008**, *350*, 2583−2598.
(1207) Barbaro, P.; Santo, V. D.; Liguori, F. Emerging strategies in sustainable fine-chemical synthesis: asymmetric catalysis by metal nanoparticles. *Dalton Trans.* **2010**, *39*, 8391−8402.
(1208) Stowell, C. A.; Korgel, B. A. Iridium Nanocrystal Synthesis and Surface Coating-Dependent Catalytic Activity. *Nano Lett.* **2005**, *5*, 1203−1207.
(1209) Tsunoyama, H.; Ichikuni, N.; Sakurai, H.; Tsukuda, T. Effect of Electronic Structures of Au Clusters Stabilized by Poly(N-vinyl-2-pyrrolidone) on Aerobic Oxidation Catalysis. *J. Am. Chem. Soc.* **2009**, *131*, 7086−7093.
(1210) Sadeghmoghaddam, E.; Gu, H.; Shon, Y.-S. Pd Nanoparticle-Catalyzed Isomerization vs Hydrogenation of Allyl Alcohol: Solvent-Dependent Regioselectivity. *ACS Catal.* **2012**, *2*, 1838−1845.
(1211) Wu, B.; Huang, H.; Yang, J.; Zheng, N.; Fu, G. Selective Hydrogenation of α,β-Unsaturated Aldehydes Catalyzed by Amine-Capped Platinum-Cobalt Nanocrystals. *Angew. Chem., Int. Ed.* **2012**, *51*, 3440−3443.
(1212) Gómez, M.; Philippot, K.; Collière, V.; Lecante, P.; Muller, G.; Chaudret, B. Novel super-structures resulting from the coordination of chiral oxazolines on platinum nanoparticles. *New J. Chem.* **2003**, *27*, 114−120.
(1213) Kraynov, A.; Richards, R. Enantioselective hydrogenation of ethyl pyruvate over diop modified Pt nanoclusters. Determination of geometry of the ligand adsorption mode via DRIFTS. *Phys. Chem. Chem. Phys.* **2007**, *9*, 884−890.
(1214) Favier, I.; Gómez, M.; Muller, G.; Axet, M. R.; Castillón, S.; Claver, C.; Jansat, S.; Chaudret, B.; Philippot, K. Palladium Catalytic Species Containing Chiral Phosphites: Towards a Discrimination between Molecular and Colloidal Catalysts. *Adv. Synth. Catal.* **2007**, *349*, 2459−2469.
(1215) Axet, M. R.; Castillón, S.; Claver, C.; Philippot, K.; Lecante, P.; Chaudret, B. Chiral Diphosphite-Modified Rhodium(0) Nanoparticles: Catalyst Reservoir for Styrene Hydroformylation. *Eur. J. Inorg. Chem.* **2008**, *2008*, 3460−3466.
(1216) Gual, A.; Godard, C.; Philippot, K.; Chaudret, B.; Denicourt-Nowicki, A.; Roucoux, A.; Castillón, S.; Claver, C. Carbohydrate-Derived 1,3-Diphosphite Ligands as Chiral Nanoparticle Stabilizers: Promising Catalytic Systems for Asymmetric Hydrogenation. *ChemSusChem* **2009**, *2*, 769−779.
(1217) Snelders, D. J. M.; Yan, N.; Gan, W.; Laurenczy, G.; Dyson, P. J. Tuning the Chemoselectivity of Rh Nanoparticle Catalysts by Site-Selective Poisoning with Phosphine Ligands: The Hydrogenation of Functionalized Aromatic Compounds. *ACS Catal.* **2012**, *2*, 201−207.
(1218) Brimaud, S.; Coutanceau, C.; Garnier, E.; Léger, J. M.; Gérard, F.; Pronier, S.; Leoni, M. Influence of surfactant removal by chemical or thermal methods on structure and electroactivity of Pt/C catalysts prepared by water-in-oil microemulsion. *J. Electroanal. Chem.* **2007**, *602*, 226−236.
(1219) Deutsch, D. S.; Lafaye, G.; Liu, D.; Chandler, B.; Williams, C. T.; Amiridis, M. D. Decomposition and Activation of Pt-Dendrimer Nanocomposites on a Silica Support. *Catal. Lett.* **2004**, *97*, 139−143.
(1220) Lafaye, G.; Williams, C. T.; Amiridis, M. D. Synthesis and microscopic characterization of dendrimer-derived Ru/Al_2O_3 catalysts. *Catal. Lett.* **2004**, *96*, 43−47.
(1221) Singh, A.; Chandler, B. D. Low-temperature activation conditions for PAMAM dendrimer templated Pt nanoparticles. *Langmuir* **2005**, *21*, 10776−10782.
(1222) Lafaye, G.; Siani, A.; Marécot, P.; Amiridis, M. D.; Williams, C. T. Particle size control in dendrimer-derived supported ruthenium catalysts. *J. Phys. Chem. B* **2006**, *110*, 7725−7731.
(1223) Crump, C.; Gilbertson, J.; Chandler, B. CO Oxidation and Toluene Hydrogenation by Pt/TiO_2 Catalysts Prepared from Dendrimer Encapsulated Nanoparticle Precursors. *Top. Catal.* **2008**, *49*, 233−240.
(1224) Liu, Z.; Shamsuzzoha, M.; Ada, E. T.; Reichert, W. M.; Nikles, D. E. Synthesis and activation of Pt nanoparticles with controlled size for fuel cell electrocatalysts. *J. Power Sources* **2007**, *164*, 472−480.
(1225) Cargnello, M.; Chen, C.; Diroll, B. T.; Doan-Nguyen, V. V. T.; Gorte, R. J.; Murray, C. B. Efficient Removal of Organic Ligands from Supported Nanocrystals by Fast Thermal Annealing Enables Catalytic Studies on Well-Defined Active Phases. *J. Am. Chem. Soc.* **2015**, *137*, 6906−6911.
(1226) Aliaga, C.; Park, J. Y.; Yamada, Y.; Lee, H. S.; Tsung, C.-K.; Yang, P.; Somorjai, G. A. Sum Frequency Generation and Catalytic Reaction Studies of the Removal of Organic Capping Agents from Pt Nanoparticles by UV-Ozone Treatment. *J. Phys. Chem. C* **2009**, *113*, 6150−6155.

https://doi.org/10.1021/acs.chemrev.1c00905
Chem. Rev. XXXX, XXX, XXX−XXX

(1227) Zhong, R.-Y.; Yang, J.-W.; Hu, Z.; Xu, B.-Q. Removal of Residual Poly(vinylpyrrolidone) from Gold Nanoparticles Immobilized on SiO_2 by Ultraviolet-Ozone Treatment. *ACS Applied Nano Materials* **2019**, *2*, 5720−5729.
(1228) Johnson, N. J. J.; Lam, B.; Sherbo, R. S.; Fork, D. K.; Berlinguette, C. P. Ligands Affect Hydrogen Absorption and Desorption by Palladium Nanoparticles. *Chem. Mater.* **2019**, *31*, 8679−8684.
(1229) Pang, S.; Kurosawa, Y.; Kondo, T.; Kawai, T. Decomposition of Monolayer Coverage on Gold Nanoparticles by UV/ozone Treatment. *Chem. Lett.* **2005**, *34*, 544−545.
(1230) Mirsaleh-Kohan, N.; Bass, A. D.; Sanche, L. X-ray Photoelectron Spectroscopy Analysis of Gold Surfaces after Removal of Thiolated DNA Oligomers by Ultraviolet/Ozone Treatment. *Langmuir* **2010**, *26*, 6508−6514.
(1231) Crespo-Quesada, M.; Andanson, J.-M.; Yarulin, A.; Lim, B.; Xia, Y.; Kiwi-Minsker, L. UV-Ozone Cleaning of Supported Poly(vinylpyrrolidone)-Stabilized Palladium Nanocubes: Effect of Stabilizer Removal on Morphology and Catalytic Behavior. *Langmuir* **2011**, *27*, 7909−7916.
(1232) Zhang, L.; Guan, C.; Wang, Y.; Liao, J. Highly effective and uniform SERS substrates fabricated by etching multi-layered gold nanoparticle arrays. *Nanoscale* **2016**, *8*, 5928−5937.
(1233) Zhong, R.-Y.; Sun, K.-Q.; Hong, Y.-C.; Xu, B.-Q. Impacts of Organic Stabilizers on Catalysis of Au Nanoparticles from Colloidal Preparation. *ACS Catal.* **2014**, *4*, 3982−3993.
(1234) Mazumder, V.; Sun, S. Oleylamine-Mediated Synthesis of Pd Nanoparticles for Catalytic Formic Acid Oxidation. *J. Am. Chem. Soc.* **2009**, *131*, 4588−4589.
(1235) Lopez-Sanchez, J. A.; Dimitratos, N.; Hammond, C.; Brett, G. L.; Kesavan, L.; White, S.; Miedziak, P.; Tiruvalam, R.; Jenkins, R. L.; Carley, A. F.; et al. Facile removal of stabilizer-ligands from supported gold nanoparticles. *Nat. Chem.* **2011**, *3*, 551−556.
(1236) Monzó, J.; Koper, M. T. M.; Rodriguez, P. Removing Polyvinylpyrrolidone from Catalytic Pt Nanoparticles without Modification of Superficial Order. *ChemPhysChem* **2012**, *13*, 709−715.
(1237) Kilmartin, J.; Sarip, R.; Grau-Crespo, R.; Di Tommaso, D.; Hogarth, G.; Prestipino, C.; Sankar, G. Following the Creation of Active Gold Nanocatalysts from Phosphine-Stabilized Molecular Clusters. *ACS Catal.* **2012**, *2*, 957−963.
(1238) Li, D.; Wang, C.; Tripkovic, D.; Sun, S.; Markovic, N. M.; Stamenkovic, V. R. Surfactant Removal for Colloidal Nanoparticles from Solution Synthesis: The Effect on Catalytic Performance. *ACS Catal.* **2012**, *2*, 1358−1362.
(1239) Rosen, E. L.; Buonsanti, R.; Llordes, A.; Sawvel, A. M.; Milliron, D. J.; Helms, B. A. Exceptionally Mild Reactive Stripping of Native Ligands from Nanocrystal Surfaces by Using Meerwein's Salt. *Angew. Chem., Int. Ed.* **2012**, *51*, 684−689.
(1240) Naresh, N.; Wasim, F. G. S.; Ladewig, B. P.; Neergat, M. Removal of surfactant and capping agent from Pd nanocubes (Pd-NCs) using tert-butylamine: its effect on electrochemical characteristics. *Journal of Materials Chemistry A* **2013**, *1*, 8553−8559.
(1241) Luo, M.; Hong, Y.; Yao, W.; Huang, C.; Xu, Q.; Wu, Q. Facile removal of polyvinylpyrrolidone (PVP) adsorbates from Pt alloy nanoparticles. *Journal of Materials Chemistry A* **2015**, *3*, 2770−2775.
(1242) Chang, C. M.; Orchard, K. L.; Martindale, B. C. M.; Reisner, E. Ligand removal from CdS quantum dots for enhanced photocatalytic H_2 generation in pH neutral water. *Journal of Materials Chemistry A* **2016**, *4*, 2856−2862.
(1243) Henckel, D. A.; Lenz, O.; Cossairt, B. M. Effect of Ligand Coverage on Hydrogen Evolution Catalyzed by Colloidal WSe_2. *ACS Catal.* **2017**, *7*, 2815−2820.
(1244) Collins, G.; Davitt, F.; O'Dwyer, C.; Holmes, J. D. Comparing Thermal and Chemical Removal of Nanoparticle Stabilizing Ligands: Effect on Catalytic Activity and Stability. *ACS Applied Nano Materials* **2018**, *1*, 7129−7138.
(1245) Ansar, S. M.; Ameer, F. S.; Hu, W.; Zou, S.; Pittman, C. U.; Zhang, D. Removal of Molecular Adsorbates on Gold Nanoparticles Using Sodium Borohydride in Water. *Nano Lett.* **2013**, *13*, 1226−1229.
(1246) Neal, R. D.; Hughes, R. A.; Sapkota, P.; Ptasinska, S.; Neretina, S. Effect of Nanoparticle Ligands on 4-Nitrophenol Reduction: Reaction Rate, Induction Time, and Ligand Desorption. *ACS Catal.* **2020**, *10*, 10040−10050.
(1247) Dasog, M.; Hou, W.; Scott, R. W. J. Controlled growth and catalytic activity of gold monolayer protected clusters in presence of borohydride salts. *Chem. Commun.* **2011**, *47*, 8569−8571.
(1248) Nelson, A.; Zong, Y.; Fritz, K. E.; Suntivich, J.; Robinson, R. D. Assessment of Soft Ligand Removal Strategies: Alkylation as a Promising Alternative to High-Temperature Treatments for Colloidal Nanoparticle Surfaces. *ACS Materials Letters* **2019**, *1*, 177−184.
(1249) Huang, X.; Zhao, Z.; Chen, Y.; Zhu, E.; Li, M.; Duan, X.; Huang, Y. A rational design of carbon-supported dispersive Pt-based octahedra as efficient oxygen reduction reaction catalysts. *Energy Environ. Sci.* **2014**, *7*, 2957−2962.
(1250) Bao, S.; Vara, M.; Yang, X.; Zhou, S.; Figueroa-Cosme, L.; Park, J.; Luo, M.; Xie, Z.; Xia, Y. Facile Synthesis of Pd@Pt3-4L Core-Shell Octahedra with a Clean Surface and Thus Enhanced Activity toward Oxygen Reduction. *ChemCatChem.* **2017**, *9*, 414−419.
(1251) Peng, H.-C.; Xie, S.; Park, J.; Xia, X.; Xia, Y. Quantitative Analysis of the Coverage Density of Br^- Ions on Pd{100} Facets and Its Role in Controlling the Shape of Pd Nanocrystals. *J. Am. Chem. Soc.* **2013**, *135*, 3780−3783.
(1252) Shi, Y.; Lyu, Z.; Cao, Z.; Xie, M.; Xia, Y. How to Remove the Capping Agent from Pd Nanocubes without Destructing Their Surface Structure for the Maximization of Catalytic Activity? *Angew. Chem., Int. Ed.* **2020**, *132*, 19291.
(1253) Pachón, L. D.; Rothenberg, G. Transition-metal nanoparticles: synthesis, stability and the leaching issue. *Appl. Organomet. Chem.* **2008**, *22*, 288−299.
(1254) Köhler, K.; Kleist, W.; Pröckl, S. S. Genesis of Coordinatively Unsaturated Palladium Complexes Dissolved from Solid Precursors during Heck Coupling Reactions and Their Role as Catalytically Active Species. *Inorg. Chem.* **2007**, *46*, 1876−1883.
(1255) Carino, E. V.; Knecht, M. R.; Crooks, R. M. Quantitative Analysis of the Stability of Pd Dendrimer-Encapsulated Nanoparticles. *Langmuir* **2009**, *25*, 10279−10284.
(1256) Gaikwad, A. V.; Holuigue, A.; Thathagar, M. B.; ten Elshof, J. E.; Rothenberg, G. Ion- and Atom-Leaching Mechanisms from Palladium Nanoparticles in Cross-Coupling Reactions. *Chem.-Eur. J.* **2007**, *13*, 6908−6913.
(1257) Niu, Z.; Peng, Q.; Zhuang, Z.; He, W.; Li, Y. Evidence of an Oxidative-Addition-Promoted Pd-Leaching Mechanism in the Suzuki Reaction by Using a Pd-Nanostructure Design. *Chem.-Eur. J.* **2012**, *18*, 9813−9817.
(1258) Briggs, B. D.; Bedford, N. M.; Seifert, S.; Koerner, H.; Ramezani-Dakhel, H.; Heinz, H.; Naik, R. R.; Frenkel, A. I.; Knecht, M. R. Atomic-scale identification of Pd leaching in nanoparticle catalyzed C-C coupling: effects of particle surface disorder. *Chem. Sci.* **2015**, *6*, 6413−6419.
(1259) Kyriakou, G.; Beaumont, S. K.; Humphrey, S. M.; Antonetti, C.; Lambert, R. M. Sonogashira Coupling Catalyzed by Gold Nanoparticles: Does Homogeneous or Heterogeneous Catalysis Dominate? *ChemCatChem.* **2010**, *2*, 1444−1449.
(1260) Trindell, J. A.; Clausmeyer, J.; Crooks, R. M. Size Stability and H_2/CO Selectivity for Au Nanoparticles during Electrocatalytic CO_2 Reduction. *J. Am. Chem. Soc.* **2017**, *139*, 16161−16167.
(1261) Bartholemew, C. H. Model catalyst studies of supported metal sintering and redispersion kinetics. *Catalysis* **1993**, *10*, 41−82.
(1262) Campbell, C. T. The Energetics of Supported Metal Nanoparticles: Relationships to Sintering Rates and Catalytic Activity. *Acc. Chem. Res.* **2013**, *46*, 1712−1719.
(1263) Tao, F.; Crozier, P. A. Atomic-Scale Observations of Catalyst Structures under Reaction Conditions and during Catalysis. *Chem. Rev.* **2016**, *116*, 3487−3539.

https://doi.org/10.1021/acs.chemrev.1c00905
Chem. Rev. XXXX, XXX, XXX−XXX

(1264) Goodman, E. D.; Johnston-Peck, A. C.; Dietze, E. M.; Wrasman, C. J.; Hoffman, A. S.; Abild-Pedersen, F.; Bare, S. R.; Plessow, P. N.; Cargnello, M. Catalyst deactivation via decomposition into single atoms and the role of metal loading. *Nature Catalysis* **2019**, *2*, 748−755.
(1265) Kim, C.; Min, M.; Chang, Y. W.; Yoo, K.-H.; Lee, H. Chemical and Thermal Stability of Pt Nanocubes Synthesized with Various Surface-Capping Agents. *J. Nanosci. Nanotechnol.* **2010**, *10*, 233−239.
(1266) Collins, G.; Schmidt, M.; O'Dwyer, C.; Holmes, J. D.; McGlacken, G. P. The Origin of Shape Sensitivity in Palladium-Catalyzed Suzuki-Miyaura Cross Coupling Reactions. *Angew. Chem., Int. Ed.* **2014**, *53*, 4142−4145.
(1267) Collins, G.; Schmidt, M.; O'Dwyer, C.; McGlacken, G.; Holmes, J. D. Enhanced Catalytic Activity of High-Index Faceted Palladium Nanoparticles in Suzuki-Miyaura Coupling Due to Efficient Leaching Mechanism. *ACS Catal.* **2014**, *4*, 3105−3111.
(1268) Collins, G.; Schmidt, M.; McGlacken, G. P.; O'Dwyer, C.; Holmes, J. D. Stability, Oxidation, and Shape Evolution of PVP-Capped Pd Nanocrystals. *J. Phys. Chem. C* **2014**, *118*, 6522−6530.
(1269) Lee, W. H.; Kim, H. Electrocatalytic activity and durability study of carbon supported Pt nanodendrites in polymer electrolyte membrane fuel cells. *International Journal of Hydrogen Energy* **2013**, *38*, 7126−7132.
(1270) Crespo-Quesada, M.; Yarulin, A.; Jin, M.; Xia, Y.; Kiwi-Minsker, L. Structure Sensitivity of Alkynol Hydrogenation on Shape- and Size-Controlled Palladium Nanocrystals: Which Sites Are Most Active and Selective? *J. Am. Chem. Soc.* **2011**, *133*, 12787−12794.
(1271) Yarulin, A. E.; Crespo-Quesada, R. M.; Egorova, E. V.; Kiwi-Minsker, L. L. Structure sensitivity of selective acetylene hydrogenation over the catalysts with shape-controlled palladium nanoparticles. *Kinetics and Catalysis* **2012**, *53*, 253−261.
(1272) Kim, S. K.; Kim, C.; Lee, J. H.; Kim, J.; Lee, H.; Moon, S. H. Performance of shape-controlled Pd nanoparticles in the selective hydrogenation of acetylene. *J. Catal.* **2013**, *306*, 146−154.
(1273) Renzas, J.; Zhang, Y.; Huang, W.; Somorjai, G. Rhodium Nanoparticle Shape Dependence in the Reduction of NO by CO. *Catal. Lett.* **2009**, *132*, 317−322.
(1274) Antoniassi, R. M.; Silva, J. C. M.; Lopes, T.; Oliveira Neto, A.; Spinacé, E. V. Carbon-supported Pt nanoparticles with (100) preferential orientation with enhanced electrocatalytic properties for carbon monoxide, methanol and ethanol oxidation in acidic medium. *International Journal of Hydrogen Energy* **2017**, *42*, 28786−28796.
(1275) Avanesian, T.; Dai, S.; Kale, M. J.; Graham, G. W.; Pan, X.; Christopher, P. Quantitative and Atomic-Scale View of CO-Induced Pt Nanoparticle Surface Reconstruction at Saturation Coverage via DFT Calculations Coupled with in Situ TEM and IR. *J. Am. Chem. Soc.* **2017**, *139*, 4551−4558.
(1276) Dessal, C.; Sangnier, A.; Chizallet, C.; Dujardin, C.; Morfin, F.; Rousset, J.-L.; Aouine, M.; Bugnet, M.; Afanasiev, P.; Piccolo, L. Atmosphere-dependent stability and mobility of catalytic Pt single atoms and clusters on γ-Al2O3. *Nanoscale* **2019**, *11*, 6897−6904.
(1277) Piccolo, L. Restructuring effects of the chemical environment in metal nanocatalysis and single-atom catalysis. *Catal. Today* **2021**, *373*, 80.
(1278) Kónya, Z.; Puntes, V. F.; Kiricsi, I.; Zhu, J.; Alivisatos, P.; Somorjai, G. A. Novel two-step synthesis of controlled size and shape platinum nanoparticles encapsulated in mesoporous silica. *Catal. Lett.* **2002**, *81*, 137−140.
(1279) Andersson, K. J.; Calle-Vallejo, F.; Rossmeisl, J.; Chorkendorff, I. Adsorption-Driven Surface Segregation of the Less Reactive Alloy Component. *J. Am. Chem. Soc.* **2009**, *131*, 2404−2407.
(1280) Li, L.; Zhou, L.; Ould-Chikh, S.; Anjum, D. H.; Kanoun, M. B.; Scaranto, J.; Hedhili, M. N.; Khalid, S.; Laveille, P. V.; D'Souza, L.; et al. Controlled Surface Segregation Leads to Efficient Coke-Resistant Nickel/Platinum Bimetallic Catalysts for the Dry Reforming of Methane. *ChemCatChem.* **2015**, *7*, 819−829.
(1281) Liu, S.; Zhao, Z.-J.; Yang, C.; Zha, S.; Neyman, K. M.; Studt, F.; Gong, J. Adsorption Preference Determines Segregation Direction: A Shortcut to More Realistic Surface Models of Alloy Catalysts. *ACS Catal.* **2019**, *9*, 5011−5018.
(1282) Bradley, J. S.; Hill, E. W.; Chaudret, B.; Duteil, A. Surface Chemistry on Colloidal Metals. Reversible Adsorbate-Induced Surface Composition Changes in Colloidal Palladium-Copper Alloys. *Langmuir* **1995**, *11*, 693−695.
(1283) Tao, F.; Grass, M. E.; Zhang, Y.; Butcher, D. R.; Aksoy, F.; Aloni, S.; Altoe, V.; Alayoglu, S.; Renzas, J. R.; Tsung, C.-K.; et al. Evolution of Structure and Chemistry of Bimetallic Nanoparticle Catalysts under Reaction Conditions. *J. Am. Chem. Soc.* **2010**, *132*, 8697−8703.
(1284) Liao, H.; Fisher, A.; Xu, Z. J. Surface Segregation in Bimetallic Nanoparticles: A Critical Issue in Electrocatalyst Engineering. *Small* **2015**, *11*, 3221−3246.
(1285) Sneed, B. T.; Young, A. P.; Tsung, C.-K. Building up strain in colloidal metal nanoparticle catalysts. *Nanoscale* **2015**, *7*, 12248−12265.
(1286) Venuto, P. B. Organic catalysis over zeolites: A perspective on reaction paths within micropores. *Microporous Mater.* **1994**, *2*, 297−411.
(1287) Corma, A. Inorganic Solid Acids and Their Use in Acid-Catalyzed Hydrocarbon Reactions. *Chem. Rev.* **1995**, *95*, 559−614.
(1288) Smit, B.; Maesen, T. L. M. Towards a molecular understanding of shape selectivity. *Nature* **2008**, *451*, 671−678.
(1289) Bejblová, M.; Procházková, D.; Cejka, J. Acylation reactions over zeolites and mesoporous catalysts. *ChemSusChem* **2009**, *2*, 486−499.
(1290) Davis, M. E.; Lobo, R. F. Zeolite and molecular sieve synthesis. *Chem. Mater.* **1992**, *4*, 756−768.
(1291) Thomas, J. M. Design, Synthesis, and In Situ Characterization of New Solid Catalysts. *Angew. Chem., Int. Ed.* **1999**, *38*, 3588−3628.
(1292) Ma, Y.; Tong, W.; Zhou, H.; Suib, S. L. A review of zeolite-like porous materials. *Microporous Mesoporous Mater.* **2000**, *37*, 243−252.
(1293) Drews, T. O.; Tsapatsis, M. Progress in manipulating zeolite morphology and related applications. *Curr. Opin. Colloid Interface Sci.* **2005**, *10*, 233−238.
(1294) Martínez, C.; Corma, A. Inorganic molecular sieves: Preparation, modification and industrial application in catalytic processes. *Coord. Chem. Rev.* **2011**, *255*, 1558−1580.
(1295) Corma, A.; Davis, M. E. Issues in the Synthesis of Crystalline Molecular Sieves: Towards the Crystallization of Low Framework-Density Structures. *ChemPhysChem* **2004**, *5*, 304−313.
(1296) Shi, J.; Wang, Y.; Yang, W.; Tang, Y.; Xie, Z. Recent advances of pore system construction in zeolite-catalyzed chemical industry processes. *Chem. Soc. Rev.* **2015**, *44*, 8877−8903.
(1297) Shirazi, L.; Jamshidi, E.; Ghasemi, M. R. The effect of Si/Al ratio of ZSM-5 zeolite on its morphology, acidity and crystal size. *Cryst. Res. Technol.* **2008**, *43*, 1300−1306.
(1298) Dedeček, J.; Sobalík, Z.; Wichterlová, B. Siting and Distribution of Framework Aluminium Atoms in Silicon-Rich Zeolites and Impact on Catalysis. *Catal. Rev.* **2012**, *54*, 135−223.
(1299) Knott, B. C.; Nimlos, C. T.; Robichaud, D. J.; Nimlos, M. R.; Kim, S.; Gounder, R. Consideration of the Aluminum Distribution in Zeolites in Theoretical and Experimental Catalysis Research. *ACS Catal.* **2018**, *8*, 770−784.
(1300) Vogt, E. T. C.; Weckhuysen, B. M. Fluid catalytic cracking: recent developments on the grand old lady of zeolite catalysis. *Chem. Soc. Rev.* **2015**, *44*, 7342−7370.
(1301) *Zeolites and Catalysis: Synthesis, Reactions and Applications*; Cejka, J., Corma, A., Zones, S. I., Eds.; Wiley-VCH Verlag Gmbh & Co.: Weinheim, 2010.
(1302) *Catalysis and Zeolites: Fundamentals and Applications*; Weitkamp, J., Puppe, L., Eds.; Springer-Verlag: Berlin Heidelberg, 2013.
(1303) *Zeolites in Catalysis: Properties and Applications*; Nachtigall, P., Cejka, J., Morris, R. E., Eds.; Royal Society of Chemistry, 2017.

https://doi.org/10.1021/acs.chemrev.1c00905
Chem. Rev. XXXX, XXX, XXX−XXX

(1304) Bhatia, S. *Zeolite Catalysts: Principles and Applications*; CRC Press: Boca Raton, FL, 2020.
(1305) Degnan, T. F. Applications of zeolites in petroleum refining. *Top. Catal.* **2000**, *13*, 349−356.
(1306) Primo, A.; Garcia, H. Zeolites as catalysts in oil refining. *Chem. Soc. Rev.* **2014**, *43*, 7548−7561.
(1307) Biswas, J.; Maxwell, I. E. Recent process- and catalyst-related developments in fluid catalytic cracking. *Appl. Catal.* **1990**, *63*, 197−258.
(1308) *Fluid Catalytic Cracking: Science and Technology*; Magee, J. S., Mitchell, M. M., Jr., Eds.; Elsevier: Amsterdam, 1993; Vol. *76*.
(1309) Rahimi, N.; Karimzadeh, R. Catalytic cracking of hydrocarbons over modified ZSM-5 zeolites to produce light olefins: A review. *Appl. Catal. A* **2011**, *398*, 1−17.
(1310) Graça, I.; Lopes, J. M.; Cerqueira, H. S.; Ribeiro, M. F. Bio-oils Upgrading for Second Generation Biofuels. *Ind. Eng. Chem. Res.* **2013**, *52*, 275−287.
(1311) Jacobs, P. A.; Dusselier, M.; Sels, B. F. Will Zeolite-Based Catalysis be as Relevant in Future Biorefineries as in Crude Oil Refineries? *Angew. Chem., Int. Ed.* **2014**, *53*, 8621−8626.
(1312) Hunger, B.; Heuchel, M.; Clark, L. A.; Snurr, R. Q. Characterization of Acidic OH Groups in Zeolites of Different Types: An Interpretation of NH_3-TPD Results in the Light of Confinement Effects. *J. Phys. Chem. B* **2002**, *106*, 3882−3889.
(1313) Bhan, A.; Iglesia, E. A Link between Reactivity and Local Structure in Acid Catalysis on Zeolites. *Acc. Chem. Res.* **2008**, *41*, 559−567.
(1314) Sklenak, S.; Dedeček, J.; Li, C.; Wichterlová, B.; Gábová, V.; Sierka, M.; Sauer, J. Aluminum Siting in Silicon-Rich Zeolite Frameworks: A Combined High-Resolution 27Al NMR Spectroscopy and Quantum Mechanics / Molecular Mechanics Study of ZSM-5. *Angew. Chem., Int. Ed.* **2007**, *46*, 7286−7289.
(1315) van Bokhoven, J. A.; Lee, T.-L.; Drakopoulos, M.; Lamberti, C.; Thieß, S.; Zegenhagen, J. Determining the aluminium occupancy on the active T-sites in zeolites using X-ray standing waves. *Nat. Mater.* **2008**, *7*, 551−555.
(1316) Xu, B.; Bordiga, S.; Prins, R.; van Bokhoven, J. A. Effect of framework Si/Al ratio and extra-framework aluminum on the catalytic activity of Y zeolite. *Appl. Catal. A* **2007**, *333*, 245−253.
(1317) Simon-Masseron, A.; Marques, J. P.; Lopes, J. M.; Ribeiro, F. R.; Gener, I.; Guisnet, M. Influence of the Si/Al ratio and crystal size on the acidity and activity of HBEA zeolites. *Appl. Catal. A* **2007**, *316*, 75−82.
(1318) Janda, A.; Bell, A. T. Effects of Si/Al Ratio on the Distribution of Framework Al and on the Rates of Alkane Monomolecular Cracking and Dehydrogenation in H-MFI. *J. Am. Chem. Soc.* **2013**, *135*, 19193−19207.
(1319) Pastore, H. O.; Coluccia, S.; Marchese, L. Porous aluminophosphates: From molecular sieves to designed acid catalysts. *Annu. Rev. Mater. Res.* **2005**, *35*, 351−395.
(1320) Chen, J. Q.; Bozzano, A.; Glover, B.; Fuglerud, T.; Kvisle, S. Recent advancements in ethylene and propylene production using the UOP/Hydro MTO process. *Catal. Today* **2005**, *106*, 103−107.
(1321) Hemelsoet, K.; Van der Mynsbrugge, J.; De Wispelaere, K.; Waroquier, M.; Van Speybroeck, V. Unraveling the Reaction Mechanisms Governing Methanol-to-Olefins Catalysis by Theory and Experiment. *ChemPhysChem* **2013**, *14*, 1526−1545.
(1322) Tian, P.; Wei, Y.; Ye, M.; Liu, Z. Methanol to Olefins (MTO): From Fundamentals to Commercialization. *ACS Catal.* **2015**, *5*, 1922−1938.
(1323) Haw, J. F.; Song, W.; Marcus, D. M.; Nicholas, J. B. The Mechanism of Methanol to Hydrocarbon Catalysis. *Acc. Chem. Res.* **2003**, *36*, 317−326.
(1324) Lefevere, J.; Mullens, S.; Meynen, V.; Noyen, J. Structured catalysts for methanol-to-olefins conversion: a review. *Chemical Papers* **2014**, *68*, 1143−1153.
(1325) Zhong, J.; Han, J.; Wei, Y.; Tian, P.; Guo, X.; Song, C.; Liu, Z. Recent advances of the nano-hierarchical SAPO-34 in the methanol-to-olefin (MTO) reaction and other applications. *Catal. Sci. Technol.* **2017**, *7*, 4905−4923.
(1326) Sun, Q.; Xie, Z.; Yu, J. The state-of-the-art synthetic strategies for SAPO-34 zeolite catalysts in methanol-to-olefin conversion. *National Science Review* **2018**, *5*, 542−558.
(1327) Clerici, M. G.; Bellussi, G.; Romano, U. Synthesis of propylene oxide from propylene and hydrogen peroxide catalyzed by titanium silicalite. *J. Catal.* **1991**, *129*, 159−167.
(1328) Clerici, M. G.; Ingallina, P. Epoxidation of Lower Olefins with Hydrogen Peroxide and Titanium Silicalite. *J. Catal.* **1993**, *140*, 71−83.
(1329) Langhendries, G.; De Vos, D. E.; Baron, G. V.; Jacobs, P. A. Quantitative Sorption Experiments on Ti-Zeolites and Relation with α-Olefin Oxidation by H_2O_2. *J. Catal.* **1999**, *187*, 453−463.
(1330) Bordiga, S.; Damin, A.; Bonino, F.; Lamberti, C. *Surface and Interfacial Organometallic Chemistry and Catalysis*; Copéret, C., Chaudret, B., Eds.; Springer Berlin Heidelberg: Berlin, Heidelberg, 2005. DOI: 10.1007/b138073 10.1007/b138073.
(1331) Moliner, M. State of the art of Lewis acid-containing zeolites: lessons from fine chemistry to new biomass transformation processes. *Dalton Trans.* **2014**, *43*, 4197−4208.
(1332) Gordon, C. P.; Engler, H.; Tragl, A. S.; Plodinec, M.; Lunkenbein, T.; Berkessel, A.; Teles, J. H.; Parvulescu, A.-N.; Copéret, C. Efficient epoxidation over dinuclear sites in titanium silicalite-1. *Nature* **2020**, *586*, 708−713.
(1333) Corma, A.; Nemeth, L. T.; Renz, M.; Valencia, S. Sn-zeolite beta as a heterogeneous chemoselective catalyst for Baeyer-Villiger oxidations. *Nature* **2001**, *412*, 423−425.
(1334) Vanelderen, P.; Vancauwenbergh, J.; Sels, B. F.; Schoonheydt, R. A. Coordination chemistry and reactivity of copper in zeolites. *Coord. Chem. Rev.* **2013**, *257*, 483−494.
(1335) Kosinov, N.; Liu, C.; Hensen, E. J. M.; Pidko, E. A. Engineering of Transition Metal Catalysts Confined in Zeolites. *Chem. Mater.* **2018**, *30*, 3177−3198.
(1336) Snyder, B. E. R.; Bols, M. L.; Schoonheydt, R. A.; Sels, B. F.; Solomon, E. I. Iron and Copper Active Sites in Zeolites and Their Correlation to Metalloenzymes. *Chem. Rev.* **2018**, *118*, 2718−2768.
(1337) Woertink, J. S.; Smeets, P. J.; Groothaert, M. H.; Vance, M. A.; Sels, B. F.; Schoonheydt, R. A.; Solomon, E. I. A $[Cu_2O]^{2+}$ core in Cu-ZSM-5, the active site in the oxidation of methane to methanol. *Proc. Natl. Acad. Sci. U. S. A.* **2009**, *106*, 18908.
(1338) Wulfers, M. J.; Teketel, S.; Ipek, B.; Lobo, R. F. Conversion of methane to methanol on copper-containing small-pore zeolites and zeotypes. *Chem. Commun.* **2015**, *51*, 4447−4450.
(1339) Narsimhan, K.; Iyoki, K.; Dinh, K.; Román-Leshkov, Y. Catalytic Oxidation of Methane into Methanol over Copper-Exchanged Zeolites with Oxygen at Low Temperature. *ACS Cent. Sci.* **2016**, *2*, 424−429.
(1340) Sushkevich, V. L.; Palagin, D.; Ranocchiari, M.; van Bokhoven, J. A. Selective anaerobic oxidation of methane enables direct synthesis of methanol. *Science* **2017**, *356*, 523.
(1341) Tomkins, P.; Ranocchiari, M.; van Bokhoven, J. A. Direct Conversion of Methane to Methanol under Mild Conditions over Cu-Zeolites and beyond. *Acc. Chem. Res.* **2017**, *50*, 418−425.
(1342) Pappas, D. K.; Borfecchia, E.; Dyballa, M.; Pankin, I. A.; Lomachenko, K. A.; Martini, A.; Signorile, M.; Teketel, S.; Arstad, B.; Berlier, G.; et al. Methane to Methanol: Structure-Activity Relationships for Cu-CHA. *J. Am. Chem. Soc.* **2017**, *139*, 14961−14975.
(1343) Zhou, C.-H.; Xia, X.; Lin, C.-X.; Tong, D.-S.; Beltramini, J. Catalytic conversion of lignocellulosic biomass to fine chemicals and fuels. *Chem. Soc. Rev.* **2011**, *40*, 5588−5617.
(1344) Farberow, C. A.; Cheah, S.; Kim, S.; Miller, J. T.; Gallagher, J. R.; Hensley, J. E.; Schaidle, J. A.; Ruddy, D. A. Exploring Low-Temperature Dehydrogenation at Ionic Cu Sites in Beta Zeolite To Enable Alkane Recycle in Dimethyl Ether Homologation. *ACS Catal.* **2017**, *7*, 3662−3667.
(1345) Sato, S.; Yu-u, Y.; Yahiro, H.; Mizuno, N.; Iwamoto, M. Cu-ZSM-5 zeolite as highly active catalyst for removal of nitrogen

https://doi.org/10.1021/acs.chemrev.1c00905
Chem. Rev. XXXX, XXX, XXX−XXX

monoxide from emission of diesel engines. *Appl. Catal.* **1991**, *70*, L1−L5.
(1346) Deka, U.; Lezcano-Gonzalez, I.; Weckhuysen, B. M.; Beale, A. M. Local Environment and Nature of Cu Active Sites in Zeolite-Based Catalysts for the Selective Catalytic Reduction of NO_x. *ACS Catal.* **2013**, *3*, 413−427.
(1347) Beale, A. M.; Gao, F.; Lezcano-Gonzalez, I.; Peden, C. H. F.; Szanyi, J. Recent advances in automotive catalysis for NO_x emission control by small-pore microporous materials. *Chem. Soc. Rev.* **2015**, *44*, 7371−7405.
(1348) Paolucci, C.; Di Iorio, J. R.; Ribeiro, F. H.; Gounder, R.; Schneider, W. F. *Adv. Catal.*; Song, C., Ed.; Academic Press, 2016; Vol. *59*.
(1349) Gao, F.; Tang, X.; Yi, H.; Zhao, S.; Li, C.; Li, J.; Shi, Y.; Meng, X. A Review on Selective Catalytic Reduction of NO_x by NH_3 over Mn-Based Catalysts at Low Temperatures: Catalysts, Mechanisms, Kinetics and DFT Calculations. *Catalysts* **2017**, *7*, 199 DOI: 10.3390/catal7070199.
(1350) Wang, J.; Zhao, H.; Haller, G.; Li, Y. Recent advances in the selective catalytic reduction of NOx with NH3 on Cu-Chabazite catalysts. *Appl. Catal. B* **2017**, *202*, 346−354.
(1351) Borfecchia, E.; Beato, P.; Svelle, S.; Olsbye, U.; Lamberti, C.; Bordiga, S. Cu-CHA - a model system for applied selective redox catalysis. *Chem. Soc. Rev.* **2018**, *47*, 8097−8133.
(1352) Han, L.; Cai, S.; Gao, M.; Hasegawa, J.-y.; Wang, P.; Zhang, J.; Shi, L.; Zhang, D. Selective Catalytic Reduction of NO_x with NH_3 by Using Novel Catalysts: State of the Art and Future Prospects. *Chem. Rev.* **2019**, *119*, 10916−10976.
(1353) Groothaert, M. H.; Smeets, P. J.; Sels, B. F.; Jacobs, P. A.; Schoonheydt, R. A. Selective Oxidation of Methane by the Bis(μ-oxo)dicopper Core Stabilized on ZSM-5 and Mordenite Zeolites. *J. Am. Chem. Soc.* **2005**, *127*, 1394−1395.
(1354) Smeets, P. J.; Hadt, R. G.; Woertink, J. S.; Vanelderen, P.; Schoonheydt, R. A.; Sels, B. F.; Solomon, E. I. Oxygen Precursor to the Reactive Intermediate in Methanol Synthesis by Cu-ZSM-5. *J. Am. Chem. Soc.* **2010**, *132*, 14736−14738.
(1355) Grundner, S.; Markovits, M. A. C.; Li, G.; Tromp, M.; Pidko, E. A.; Hensen, E. J. M.; Jentys, A.; Sanchez-Sanchez, M.; Lercher, J. A. Single-site trinuclear copper oxygen clusters in mordenite for selective conversion of methane to methanol. *Nat. Commun.* **2015**, *6*, 7546.
(1356) Li, G.; Vassilev, P.; Sanchez-Sanchez, M.; Lercher, J. A.; Hensen, E. J. M.; Pidko, E. A. Stability and reactivity of copper oxo-clusters in ZSM-5 zeolite for selective methane oxidation to methanol. *J. Catal.* **2016**, *338*, 305−312.
(1357) Palagin, D.; Knorpp, A. J.; Pinar, A. B.; Ranocchiari, M.; van Bokhoven, J. A. Assessing the relative stability of copper oxide clusters as active sites of a CuMOR zeolite for methane to methanol conversion: size matters? *Nanoscale* **2017**, *9*, 1144−1153.
(1358) Hammond, C.; Forde, M. M.; Ab Rahim, M. H.; Thetford, A.; He, Q.; Jenkins, R. L.; Dimitratos, N.; Lopez-Sanchez, J. A.; Dummer, N. F.; Murphy, D. M.; et al. Direct Catalytic Conversion of Methane to Methanol in an Aqueous Medium by using Copper-Promoted Fe-ZSM-5. *Angew. Chem., Int. Ed.* **2012**, *51*, 5129−5133.
(1359) Gao, F.; Washton, N. M.; Wang, Y.; Kollár, M.; Szanyi, J.; Peden, C. H. F. Effects of Si/Al ratio on Cu/SSZ-13 NH_3-SCR catalysts: Implications for the active Cu species and the roles of Brønsted acidity. *J. Catal.* **2015**, *331*, 25−38.
(1360) Gao, F.; Mei, D.; Wang, Y.; Szanyi, J.; Peden, C. H. F. Selective Catalytic Reduction over Cu/SSZ-13: Linking Homo- and Heterogeneous Catalysis. *J. Am. Chem. Soc.* **2017**, *139*, 4935−4942.
(1361) Lei, H.; Rizzotto, V.; Guo, A.; Ye, D.; Simon, U.; Chen, P. Recent Understanding of Low-Temperature Copper Dynamics in Cu-Chabazite NH3-SCR Catalysts. *Catalysts* **2021**, *11*, 52.
(1362) Abate, S.; Barbera, K.; Centi, G.; Lanzafame, P.; Perathoner, S. Disruptive catalysis by zeolites. *Catal. Sci. Technol.* **2016**, *6*, 2485−2501.
(1363) Yashima, T.; Ahmad, H.; Yamazaki, K.; Katsuta, M.; Hara, N. Alkylation on synthetic zeolites: I. Alkylation of toluene with methanol. *J. Catal.* **1970**, *16*, 273−280.
(1364) Chen, N. Y.; Kaeding, W. W.; Dwyer, F. G. Para-directed aromatic reactions over shape-selective molecular sieve zeolite catalysts. *J. Am. Chem. Soc.* **1979**, *101*, 6783−6784.
(1365) Kaeding, W. W.; Chu, C.; Young, L. B.; Weinstein, B.; Butter, S. A. Selective alkylation of toluene with methanol to produce para-Xylene. *J. Catal.* **1981**, *67*, 159−174.
(1366) Cejka, J.; Wichterlová, B. Acid-Catalyzed Synthesis of Mono- and Dialkyl Benzenes over Zeolites: Active Sites, Zeolite Topology, and Reaction Mechanisms. *Catal. Rev.* **2002**, *44*, 375−421.
(1367) Derouane, E. G.; Gabelica, Z. A novel effect of shape selectivity: Molecular traffic control in zeolite ZSM-5. *J. Catal.* **1980**, *65*, 486−489.
(1368) Csicsery, S. M. Shape-selective catalysis in zeolites. *Zeolites* **1984**, *4*, 202−213.
(1369) Degnan, T. F. The implications of the fundamentals of shape selectivity for the development of catalysts for the petroleum and petrochemical industries. *J. Catal.* **2003**, *216*, 32−46.
(1370) Verheyen, E.; Jo, C.; Kurttepeli, M.; Vanbutsele, G.; Gobechiya, E.; Korányi, T. I.; Bals, S.; Van Tendeloo, G.; Ryoo, R.; Kirschhock, C. E. A.; et al. Molecular shape-selectivity of MFI zeolite nanosheets in n-decane isomerization and hydrocracking. *J. Catal.* **2013**, *300*, 70−80.
(1371) Taylor, R. J.; Petty, R. H. Selective hydroisomerization of long chain normal paraffins. *Appl. Catal. A* **1994**, *119*, 121−138.
(1372) Miller, S. J. New molecular sieve process for lube dewaxing by wax isomerization. *Microporous Mater.* **1994**, *2*, 439−449.
(1373) Perego, C.; Angelis, A. d.; Farias, O.; Bosetti, A. *C07C 211/00*; Enitecnologie S.p.A.: Maritano, Italy, 2002; Vol. *6,380,433*.
(1374) Raja, R.; Sankar, G.; Thomas, J. M. Bifunctional Molecular Sieve Catalysts for the Benign Ammoximation of Cyclohexanone: One-Step, Solvent-Free Production of Oxime and ε-Caprolactam with a Mixture of Air and Ammonia. *J. Am. Chem. Soc.* **2001**, *123*, 8153−8154.
(1375) Boronat, M.; Martínez-Sánchez, C.; Law, D.; Corma, A. Enzyme-like Specificity in Zeolites: A Unique Site Position in Mordenite for Selective Carbonylation of Methanol and Dimethyl Ether with CO. *J. Am. Chem. Soc.* **2008**, *130*, 16316−16323.
(1376) Jae, J.; Tompsett, G. A.; Foster, A. J.; Hammond, K. D.; Auerbach, S. M.; Lobo, R. F.; Huber, G. W. Investigation into the shape selectivity of zeolite catalysts for biomass conversion. *J. Catal.* **2011**, *279*, 257−268.
(1377) Moliner, M.; Martínez, C.; Corma, A. Synthesis Strategies for Preparing Useful Small Pore Zeolites and Zeotypes for Gas Separations and Catalysis. *Chem. Mater.* **2014**, *26*, 246−258.
(1378) Dusselier, M.; Davis, M. E. Small-Pore Zeolites: Synthesis and Catalysis. *Chem. Rev.* **2018**, *118*, 5265−5329.
(1379) Sastre, G. Confinement effects in methanol to olefins catalysed by zeolites: A computational review. *Front. Chem. Sci. Eng.* **2016**, *10*, 76−89.
(1380) Zalazar, M. F.; Paredes, E. N.; Romero Ojeda, G. D.; Cabral, N. D.; Peruchena, N. M. Study of Confinement and Catalysis Effects of the Reaction of Methylation of Benzene by Methanol in H-Beta and H-ZSM-5 Zeolites by Topological Analysis of Electron Density. *J. Phys. Chem. C* **2018**, *122*, 3350−3362.
(1381) Snyder, B. E. R.; Bols, M. L.; Rhoda, H. M.; Plessers, D.; Schoonheydt, R. A.; Sels, B. F.; Solomon, E. I. Cage effects control the mechanism of methane hydroxylation in zeolites. *Science* **2021**, *373*, 327.
(1382) Li, C.; Paris, C.; Martínez-Triguero, J.; Boronat, M.; Moliner, M.; Corma, A. Synthesis of reaction-adapted zeolites as methanol-to-olefins catalysts with mimics of reaction intermediates as organic structure-directing agents. *Nat. Catal.* **2018**, *1*, 547−554.
(1383) Rimer, J. D. Rational design of zeolite catalysts. *Nat. Catal.* **2018**, *1*, 488−489.
(1384) Li, C.; Ferri, P.; Paris, C.; Moliner, M.; Boronat, M.; Corma, A. Design and Synthesis of the Active Site Environment in Zeolite Catalysts for Selectively Manipulating Mechanistic Pathways. *J. Am. Chem. Soc.* **2021**, *143*, 10718−10726.

https://doi.org/10.1021/acs.chemrev.1c00905
Chem. Rev. XXXX, XXX, XXX−XXX

(1385) Dryzun, C.; Mastai, Y.; Shvalb, A.; Avnir, D. Chiral silicate zeolites. *J. Mater. Chem.* **2009**, *19*, 2062−2069.
(1386) Kresge, C. T.; Leonowicz, M. E.; Roth, W. J.; Vartuli, J. C.; Beck, J. S. Ordered mesoporous molecular sieves synthesized by a liquid-crystal template mechanism. *Nature* **1992**, *359*, 710−712.
(1387) Yu, J.; Xu, R. Chiral zeolitic materials: structural insights and synthetic challenges. *J. Mater. Chem.* **2008**, *18*, 4021−4030.
(1388) Brand, S. K.; Schmidt, J. E.; Deem, M. W.; Daeyaert, F.; Ma, Y.; Terasaki, O.; Orazov, M.; Davis, M. E. Enantiomerically enriched, polycrystalline molecular sieves. *Proc. Natl. Acad. Sci. U. S. A.* **2017**, *114*, 5101.
(1389) Davis, M. E. A Thirty-Year Journey to the Creation of the First Enantiomerically Enriched Molecular Sieve. *ACS Catal.* **2018**, *8*, 10082−10088.
(1390) Xia, Q. H.; Shen, S. C.; Song, J.; Kawi, S.; Hidajat, K. Structure, morphology, and catalytic activity of β zeolite synthesized in a fluoride medium for asymmetric hydrogenation. *J. Catal.* **2003**, *219*, 74−84.
(1391) Harris, K. D. M.; Thomas, S. J. M. Selected Thoughts on Chiral Crystals, Chiral Surfaces, and Asymmetric Heterogeneous Catalysis. *ChemCatChem.* **2009**, *1*, 223−231.
(1392) Lu, T.; Yan, W.; Xu, R. Chiral zeolite beta: structure, synthesis, and application. *Inorganic Chemistry Frontiers* **2019**, *6*, 1938−1951.
(1393) Chen, T.; Wun, C. K. T.; Day, S. J.; Tang, C. C.; Lo, T. W. B. Enantiospecificity in achiral zeolites for asymmetric catalysis. *Phys. Chem. Chem. Phys.* **2020**, *22*, 18757−18764.
(1394) Tong, M.; Zhang, D.; Fan, W.; Xu, J.; Zhu, L.; Guo, W.; Yan, W.; Yu, J.; Qiu, S.; Wang, J.; et al. Synthesis of chiral polymorph A-enriched zeolite Beta with an extremely concentrated fluoride route. *Sci. Rep.* **2015**, *5*, 11521.
(1395) Hartmann, M. Hierarchical Zeolites: A Proven Strategy to Combine Shape Selectivity with Efficient Mass Transport. *Angew. Chem., Int. Ed.* **2004**, *43*, 5880−5882.
(1396) Pérez-Ramírez, J.; Christensen, C. H.; Egeblad, K.; Christensen, C. H.; Groen, J. C. Hierarchical zeolites: enhanced utilisation of microporous crystals in catalysis by advances in materials design. *Chem. Soc. Rev.* **2008**, *37*, 2530−2542.
(1397) Chen, L.-H.; Li, X.-Y.; Rooke, J. C.; Zhang, Y.-H.; Yang, X.-Y.; Tang, Y.; Xiao, F.-S.; Su, B.-L. Hierarchically structured zeolites: synthesis, mass transport properties and applications. *J. Mater. Chem.* **2012**, *22*, 17381−17403.
(1398) Li, K.; Valla, J.; Garcia-Martinez, J. Realizing the Commercial Potential of Hierarchical Zeolites: New Opportunities in Catalytic Cracking. *ChemCatChem.* **2014**, *6*, 46−66.
(1399) Moliner, M.; Martínez, C.; Corma, A. Multipore Zeolites: Synthesis and Catalytic Applications. *Angew. Chem., Int. Ed.* **2015**, *54*, 3560−3579.
(1400) Yan, Y.; Guo, X.; Zhang, Y.; Tang, Y. Future of nano-/hierarchical zeolites in catalysis: gaseous phase or liquid phase system. *Catal. Sci. Technol.* **2015**, *5*, 772−785.
(1401) Chen, L.-H.; Sun, M.-H.; Wang, Z.; Yang, W.; Xie, Z.; Su, B.-L. Hierarchically Structured Zeolites: From Design to Application. *Chem. Rev.* **2020**, *120*, 11194−11294.
(1402) Roth, W. J.; Nachtigall, P.; Morris, R. E.; Cejka, J. Two-Dimensional Zeolites: Current Status and Perspectives. *Chem. Rev.* **2014**, *114*, 4807−4837.
(1403) Opanasenko, M. V.; Roth, W. J.; Cejka, J. Two-dimensional zeolites in catalysis: current status and perspectives. *Catal. Sci. Technol.* **2016**, *6*, 2467−2484.
(1404) Groen, J. C.; Zhu, W.; Brouwer, S.; Huynink, S. J.; Kapteijn, F.; Moulijn, J. A.; Pérez-Ramírez, J. Direct Demonstration of Enhanced Diffusion in Mesoporous ZSM-5 Zeolite Obtained via Controlled Desilication. *J. Am. Chem. Soc.* **2007**, *129*, 355−360.
(1405) Kortunov, P.; Vasenkov, S.; Kärger, J.; Valiullin, R.; Gottschalk, P.; Fé Elía, M.; Perez, M.; Stöcker, M.; Drescher, B.; McElhiney, G.; et al. The Role of Mesopores in Intracrystalline Transport in USY Zeolite: PFG NMR Diffusion Study on Various Length Scales. *J. Am. Chem. Soc.* **2005**, *127*, 13055−13059.
(1406) Christensen, C. H.; Johannsen, K.; Törnqvist, E.; Schmidt, I.; Topsøe, H.; et al. Mesoporous zeolite single crystal catalysts: Diffusion and catalysis in hierarchical zeolites. *Catal. Today* **2007**, *128*, 117−122.
(1407) Pérez-Ramírez, J.; Verboekend, D.; Bonilla, A.; Abelló, S. Zeolite Catalysts with Tunable Hierarchy Factor by Pore-Growth Moderators. *Adv. Funct. Mater.* **2009**, *19*, 3972−3979.
(1408) Christensen, C. H.; Johannsen, K.; Schmidt, I.; Christensen, C. H. Catalytic Benzene Alkylation over Mesoporous Zeolite Single Crystals: Improving Activity and Selectivity with a New Family of Porous Materials. *J. Am. Chem. Soc.* **2003**, *125*, 13370−13371.
(1409) Shetti, V. N.; Kim, J.; Srivastava, R.; Choi, M.; Ryoo, R. Assessment of the mesopore wall catalytic activities of MFI zeolite with mesoporous/microporous hierarchical structures. *J. Catal.* **2008**, *254*, 296−303.
(1410) Park, D. H.; Kim, S. S.; Wang, H.; Pinnavaia, T. J.; Papapetrou, M. C.; Lappas, A. A.; Triantafyllidis, K. S. Selective Petroleum Refining Over a Zeolite Catalyst with Small Intracrystal Mesopores. *Angew. Chem., Int. Ed.* **2009**, *48*, 7645−7648.
(1411) Na, K.; Jo, C.; Kim, J.; Cho, K.; Jung, J.; Seo, Y.; Messinger, R. J.; Chmelka, B. F.; Ryoo, R. Directing Zeolite Structures into Hierarchically Nanoporous Architectures. *Science* **2011**, *333*, 328.
(1412) García-Martínez, J.; Johnson, M.; Valla, J.; Li, K.; Ying, J. Y. Mesostructured zeolite Y—high hydrothermal stability and superior FCC catalytic performance. *Catal. Sci. Technol.* **2012**, *2*, 987−994.
(1413) Hu, S.; Shan, J.; Zhang, Q.; Wang, Y.; Liu, Y.; Gong, Y.; Wu, Z.; Dou, T. Selective formation of propylene from methanol over high-silica nanosheets of MFI zeolite. *Appl. Catal. A* **2012**, *445-446*, 215−220.
(1414) Hu, Z.; Zhang, H.; Wang, L.; Zhang, H.; Zhang, Y.; Xu, H.; Shen, W.; Tang, Y. Highly stable boron-modified hierarchical nanocrystalline ZSM-5 zeolite for the methanol to propylene reaction. *Catal. Sci. Technol.* **2014**, *4*, 2891−2895.
(1415) Xi, D.; Sun, Q.; Xu, J.; Cho, M.; Cho, H. S.; Asahina, S.; Li, Y.; Deng, F.; Terasaki, O.; Yu, J. In situ growth-etching approach to the preparation of hierarchically macroporous zeolites with high MTO catalytic activity and selectivity. *J. Mater. Chem. A* **2014**, *2*, 17994−18004.
(1416) Hartmann, M.; Machoke, A. G.; Schwieger, W. Catalytic test reactions for the evaluation of hierarchical zeolites. *Chem. Soc. Rev.* **2016**, *45*, 3313−3330.
(1417) Jia, L. Y.; Raad, M.; Hamieh, S.; Toufaily, J.; Hamieh, T.; Bettahar, M. M.; Mauviel, G.; Tarrighi, M.; Pinard, L.; Dufour, A. Catalytic fast pyrolysis of biomass: superior selectivity of hierarchical zeolites to aromatics. *Green Chem.* **2017**, *19*, 5442−5459.
(1418) Yang, X.; Bian, J.; Huang, J.; Xin, W.; Lu, T.; Chen, C.; Su, Y.; Zhou, L.; Wang, F.; Xu, J. Fluoride-free and low concentration template synthesis of hierarchical Sn-Beta zeolites: efficient catalysts for conversion of glucose to alkyl lactate. *Green Chem.* **2017**, *19*, 692−701.
(1419) Serrano, D. P.; Melero, J. A.; Morales, G.; Iglesias, J.; Pizarro, P. Progress in the design of zeolite catalysts for biomass conversion into biofuels and bio-based chemicals. *Catal. Rev.* **2018**, *60*, 1−70.
(1420) Cui, X.; Gao, P.; Li, S.; Yang, C.; Liu, Z.; Wang, H.; Zhong, L.; Sun, Y. Selective Production of Aromatics Directly from Carbon Dioxide Hydrogenation. *ACS Catal.* **2019**, *9*, 3866−3876.
(1421) Khan, W.; Jia, X.; Wu, Z.; Choi, J.; Yip, A. C. K. Incorporating Hierarchy into Conventional Zeolites for Catalytic Biomass Conversions: A Review. *Catalysts* **2019**, *9*, 127.
(1422) Ishihara, A. Preparation and reactivity of hierarchical catalysts in catalytic cracking. *Fuel Processing Technology* **2019**, *194*, 106116.
(1423) Palizdar, A.; Sadrameli, S. M. Catalytic upgrading of biomass pyrolysis oil over tailored hierarchical MFI zeolite: Effect of porosity enhancement and porosity-acidity interaction on deoxygenation reactions. *Renewable Energy* **2020**, *148*, 674−688.
(1424) Zhao, S.; Wang, W. D.; Wang, L.; Schwieger, W.; Wang, W.; Huang, J. Tuning Hierarchical ZSM-5 Zeolite for Both Gas- and Liquid-Phase Biorefining. *ACS Catal.* **2020**, *10*, 1185−1194.

https://doi.org/10.1021/acs.chemrev.1c00905
Chem. Rev. XXXX, XXX, XXX−XXX

(1425) Choi, M.; Na, K.; Kim, J.; Sakamoto, Y.; Terasaki, O.; Ryoo, R. Stable single-unit-cell nanosheets of zeolite MFI as active and long-lived catalysts. *Nature* **2009**, *461*, 246−249.
(1426) Kim, J.; Choi, M.; Ryoo, R. Effect of mesoporosity against the deactivation of MFI zeolite catalyst during the methanol-to-hydrocarbon conversion process. *J. Catal.* **2010**, *269*, 219−228.
(1427) Zhou, J.; Hua, Z.; Liu, Z.; Wu, W.; Zhu, Y.; Shi, J. Direct Synthetic Strategy of Mesoporous ZSM-5 Zeolites by Using Conventional Block Copolymer Templates and the Improved Catalytic Properties. *ACS Catal.* **2011**, *1*, 287−291.
(1428) Mitchell, S.; Michels, N.-L.; Kunze, K.; Pérez-Ramírez, J. Visualization of hierarchically structured zeolite bodies from macro to nano length scales. *Nat. Chem.* **2012**, *4*, 825−831.
(1429) Lakiss, L.; Ngoye, F.; Canaff, C.; Laforge, S.; Pouilloux, Y.; Qin, Z.; Tarighi, M.; Thomas, K.; Valtchev, V.; Vicente, A.; et al. On the remarkable resistance to coke formation of nanometer-sized and hierarchical MFI zeolites during ethanol to hydrocarbons transformation. *J. Catal.* **2015**, *328*, 165−172.
(1430) Weissenberger, T.; Machoke, A. G. F.; Bauer, J.; Dotzel, R.; Casci, J. L.; Hartmann, M.; Schwieger, W. Hierarchical ZSM-5 Catalysts: The Effect of Different Intracrystalline Pore Dimensions on Catalyst Deactivation Behaviour in the MTO Reaction. *ChemCatChem.* **2020**, *12*, 2461−2468.
(1431) Verboekend, D.; Keller, T. C.; Milina, M.; Hauert, R.; Pérez-Ramírez, J. Hierarchy Brings Function: Mesoporous Clinoptilolite and L Zeolite Catalysts Synthesized by Tandem Acid-Base Treatments. *Chem. Mater.* **2013**, *25*, 1947−1959.
(1432) Song, S.; Di, L.; Wu, G.; Dai, W.; Guan, N.; Li, L. Meso-Zr-Al-beta zeolite as a robust catalyst for cascade reactions in biomass valorization. *Appl. Catal. B* **2017**, *205*, 393−403.
(1433) Zhao, B.; Zhai, P.; Wang, P.; Li, J.; Li, T.; Peng, M.; Zhao, M.; Hu, G.; Yang, Y.; Li, Y.-W.; et al. Direct Transformation of Syngas to Aromatics over Na-Zn-Fe5C2 and Hierarchical HZSM-5 Tandem Catalysts. *Chem.* **2017**, *3*, 323−333.
(1434) Bai, Y.; Wei, L.; Yang, M.; Chen, H.; Holdren, S.; Zhu, G.; Tran, D. T.; Yao, C.; Sun, R.; Pan, Y.; et al. Three-step cascade over a single catalyst: synthesis of 5-(ethoxymethyl)furfural from glucose over a hierarchical lamellar multi-functional zeolite catalyst. *J. Mater. Chem. A* **2018**, *6*, 7693−7705.
(1435) Al-Naji, M.; Puértolas, B.; Kumru, B.; Cruz, D.; Bäumel, M.; Schmidt, B. V. K. J.; Tarakina, N. V.; Pérez-Ramírez, J. Sustainable Continuous Flow Valorization of γ-Valerolactone with Trioxane to α-Methylene-γ-Valerolactone over Basic Beta Zeolites. *ChemSusChem* **2019**, *12*, 2628−2636.
(1436) Isaacs, M. A.; Parlett, C. M. A.; Robinson, N.; Durndell, L. J.; Manayil, J. C.; Beaumont, S. K.; Jiang, S.; Hondow, N. S.; Lamb, A. C.; Jampaiah, D.; et al. A spatially orthogonal hierarchically porous acid-base catalyst for cascade and antagonistic reactions. *Nature Catalysis* **2020**, *3*, 921.
(1437) Schüth, F. Non-siliceous Mesostructured and Mesoporous Materials. *Chem. Mater.* **2001**, *13*, 3184−3195.
(1438) Taguchi, A.; Schüth, F. Ordered mesoporous materials in catalysis. *Microporous Mesoporous Mater.* **2005**, *77*, 1−45.
(1439) Liang, C.; Li, Z.; Dai, S. Mesoporous Carbon Materials: Synthesis and Modification. *Angew. Chem., Int. Ed.* **2008**, *47*, 3696−3717.
(1440) Wu, D.; Xu, F.; Sun, B.; Fu, R.; He, H.; Matyjaszewski, K. Design and Preparation of Porous Polymers. *Chem. Rev.* **2012**, *112*, 3959−4015.
(1441) Alothman, Z. A. A Review: Fundamental Aspects of Silicate Mesoporous Materials. *Materials* **2012**, *5*, 2874.
(1442) Gu, D.; Schüth, F. Synthesis of non-siliceous mesoporous oxides. *Chem. Soc. Rev.* **2014**, *43*, 313−344.
(1443) Li, W.; Wu, Z.; Wang, J.; Elzatahry, A. A.; Zhao, D. A Perspective on Mesoporous TiO_2 Materials. *Chem. Mater.* **2014**, *26*, 287−298.
(1444) Ying, J. Y.; Mehnert, C. P.; Wong, M. S. Synthesis and Applications of Supramolecular-Templated Mesoporous Materials. *Angew. Chem., Int. Ed.* **1999**, *38*, 56−77.
(1445) Schüth, F. Endo- and Exotemplating to Create High-Surface-Area Inorganic Materials. *Angew. Chem., Int. Ed.* **2003**, *42*, 3604−3622.
(1446) Wan, Y.; Zhao, D. On the Controllable Soft-Templating Approach to Mesoporous Silicates. *Chem. Rev.* **2007**, *107*, 2821−2860.
(1447) Malgras, V.; Ji, Q.; Kamachi, Y.; Mori, T.; Shieh, F.-K.; Wu, K. C. W.; Ariga, K.; Yamauchi, Y. Templated Synthesis for Nanoarchitectured Porous Materials. *Bull. Chem. Soc. Jpn.* **2015**, *88*, 1171−1200.
(1448) Zhang, L.; Jin, L.; Liu, B.; He, J. Templated Growth of Crystalline Mesoporous Materials: From Soft/Hard Templates to Colloidal Templates. *Front. Chem.* **2019**, *7*. DOI: 10.3389/fchem.2019.00022
(1449) Xu, X.; Megarajan, S. K.; Zhang, Y.; Jiang, H. Ordered Mesoporous Alumina and Their Composites Based on Evaporation Induced Self-Assembly for Adsorption and Catalysis. *Chem. Mater.* **2020**, *32*, 3−26.
(1450) Beck, J. S.; Vartuli, J. C.; Roth, W. J.; Leonowicz, M. E.; Kresge, C. T.; Schmitt, K. D.; Chu, C. T. W.; Olson, D. H.; Sheppard, E. W.; et al. A new family of mesoporous molecular sieves prepared with liquid crystal templates. *J. Am. Chem. Soc.* **1992**, *114*, 10834−10843.
(1451) Zhao, D.; Feng, J.; Huo, Q.; Melosh, N.; Frederickson, G. H.; Chmelka, B. F.; Stucky, G. D. Triblock copolymer syntheses of mesoporous silica with periodic 50 to 300 angstrom pores. *Science* **1998**, *279*, 548−552.
(1452) Yu, T.; Zhang, H.; Yan, X.; Chen, Z.; Zou, X.; Oleynikov, P.; Zhao, D. Pore Structures of Ordered Large Cage-Type Mesoporous Silica FDU-12s. *J. Phys. Chem. B* **2006**, *110*, 21467−21472.
(1453) Jelassi, J.; Grosz, T.; Bako, I.; Bellissent-Funel, M. C.; Dore, J. C.; Castricum, H. L.; Sridi-Dorbez, R. Structural studies of water in hydrophilic and hydrophobic mesoporous silicas: An x-ray and neutron diffraction study at 297 K. *J. Chem. Phys.* **2011**, *134*, 064509−064509.
(1454) El Mourabit, S.; Guillot, M.; Toquer, G.; Cambedouzou, J.; Goettmann, F.; Grandjean, A. Stability of mesoporous silica under acidic conditions. *RSC Adv.* **2012**, *2*, 10916−10924.
(1455) Lin, H.-P.; Mou, C.-Y. Structural and Morphological Control of Cationic Surfactant-Templated Mesoporous Silica. *Acc. Chem. Res.* **2002**, *35*, 927−935.
(1456) Dong, W.; Sun, Y.; Lee, C. W.; Hua, W.; Lu, X.; Shi, Y.; Zhang, S.; Chen, J.; Zhao, D. Controllable and Repeatable Synthesis of Thermally Stable Anatase Nanocrystal-Silica Composites with Highly Ordered Hexagonal Mesostructures. *J. Am. Chem. Soc.* **2007**, *129*, 13894−13904.
(1457) Chen, X.-R.; Ju, Y.-H.; Mou, C.-Y. Direct Synthesis of Mesoporous Sulfated Silica-Zirconia Catalysts with High Catalytic Activity for Biodiesel via Esterification. *J. Phys. Chem. C* **2007**, *111*, 18731−18737.
(1458) Martín-Aranda, R. M.; Cejka, J. Recent Advances in Catalysis Over Mesoporous Molecular Sieves. *Top. Catal.* **2010**, *53*, 141−153.
(1459) Li, L.; Stroobants, C.; Lin, K.; Jacobs, P. A.; Sels, B. F.; Pescarmona, P. P. Selective conversion of trioses to lactates over Lewis acid heterogeneous catalysts. *Green Chem.* **2011**, *13*, 1175−1181.
(1460) González, M. D.; Salagre, P.; Mokaya, R.; Cesteros, Y. Tuning the acidic and textural properties of ordered mesoporous silicas for their application as catalysts in the etherification of glycerol with isobutene. *Catal. Today* **2014**, *227*, 171−178.
(1461) Corma, A.; Martinez, A.; Martinezsoria, V.; Monton, J. B. Hydrocracking of Vacuum Gasoil on the Novel Mesoporous MCM-41 Aluminosilicate Catalyst. *J. Catal.* **1995**, *153*, 25−31.
(1462) Trong On, D.; Desplantier-Giscard, D.; Danumah, C.; Kaliaguine, S. Perspectives in catalytic applications of mesostructured materials. *Appl. Catal. A* **2001**, *222*, 299−357.
(1463) Norhasyimi, R.; Ahmad Zuhairi, A.; Abdullah Rahman, M. A Review: Mesoporous Santa Barbara Amorphous-15, Types, Synthesis

https://doi.org/10.1021/acs.chemrev.1c00905
Chem. Rev. XXXX, XXX, XXX−XXX

and Its Applications towards Biorefinery Production. *American Journal of Applied Sciences* **2010**, *7*, 1579.
(1464) Lanzafame, P.; Temi, D. M.; Perathoner, S.; Centi, G.; Macario, A.; Aloise, A.; Giordano, G. Etherification of 5-hydroxymethyl-2-furfural (HMF) with ethanol to biodiesel components using mesoporous solid acidic catalysts. *Catal. Today* **2011**, *175*, 435−441.
(1465) Li, L.; Korányi, T. I.; Sels, B. F.; Pescarmona, P. P. Highly-efficient conversion of glycerol to solketal over heterogeneous Lewis acid catalysts. *Green Chem.* **2012**, *14*, 1611−1619.
(1466) Serrano, D. P.; Aguado, J.; Escola, J. M. Developing Advanced Catalysts for the Conversion of Polyolefinic Waste Plastics into Fuels and Chemicals. *ACS Catal.* **2012**, *2*, 1924−1941.
(1467) Jun, S.; Ryoo, R. Aluminum Impregnation into Mesoporous Silica Molecular Sieves for Catalytic Application to Friedel-Crafts Alkylation. *J. Catal.* **2000**, *195*, 237−243.
(1468) Clark, J. H.; Monks, G. L.; Nightingale, D. J.; Price, P. M.; White, J. F. A New Solid Acid-Based Route to Linear Alkylbenzenes. *J. Catal.* **2000**, *193*, 348−350.
(1469) Cejka, J.; Mintova, S. Perspectives of Micro/Mesoporous Composites in Catalysis. *Catal. Rev.* **2007**, *49*, 457−509.
(1470) Mbaraka, I.; Shanks, B. Conversion of oils and fats using advanced mesoporous heterogeneous catalysts. *J. Am. Oil Chem. Soc.* **2006**, *83*, 79−91.
(1471) Van Looveren, L. K.; Geysen, D. F.; Vercruysse, K. A.; Wouters, B. H.; Grobet, P. J.; Jacobs, P. A. Methylalumoxane MCM-41 as Support in the Co-Oligomerization of Ethene and Propene with [{C2H4(1-indenyl)2}Zr(CH3)2]. *Angew. Chem., Int. Ed.* **1998**, *37*, 517−520.
(1472) Severn, J. R.; Chadwick, J. C.; Duchateau, R.; Friederichs, N. Bound but Not Gagged"Immobilizing Single-Site α-Olefin Polymerization Catalysts. *Chem. Rev.* **2005**, *105*, 4073−4147.
(1473) Saib, A. M.; Claeys, M.; van Steen, E. Silica supported cobalt Fischer-Tropsch catalysts: effect of pore diameter of support. *Catal. Today* **2002**, *71*, 395−402.
(1474) Xiong, H.; Zhang, Y.; Liew, K.; Li, J. Fischer-Tropsch synthesis: The role of pore size for Co/SBA-15 catalysts. *J. Mol. Catal. A* **2008**, *295*, 68−76.
(1475) Ghampson, I. T.; Newman, C.; Kong, L.; Pier, E.; Hurley, K. D.; Pollock, R. A.; Walsh, B. R.; Goundie, B.; Wright, J.; Wheeler, M. C.; et al. Effects of pore diameter on particle size, phase, and turnover frequency in mesoporous silica supported cobalt Fischer-Tropsch catalysts. *Appl. Catal. A* **2010**, *388*, 57−67.
(1476) Wei, L.; Zhao, Y.; Zhang, Y.; Liu, C.; Hong, J.; Xiong, H.; Li, J. Fischer-Tropsch synthesis over a 3D foamed MCF silica support: Toward a more open porous network of cobalt catalysts. *J. Catal.* **2016**, *340*, 205−218.
(1477) Moller, K.; Bein, T. Inclusion Chemistry in Periodic Mesoporous Hosts. *Chem. Mater.* **1998**, *10*, 2950−2963.
(1478) Zhang, Q.; Wang, Y.; Itsuki, S.; Shishido, T.; Takehira, K. Manganese-containing MCM-41 for epoxidation of styrene and stilbene. *J. Mol. Catal. A: Chem.* **2002**, *188*, 189−200.
(1479) Laha, S. C.; Mukherjee, P.; Sainkar, S. R.; Kumar, R. Cerium Containing MCM-41-Type Mesoporous Materials and their Acidic and Redox Catalytic Properties. *J. Catal.* **2002**, *207*, 213−223.
(1480) Wojcieszak, R.; Monteverdi, S.; Mercy, M.; Nowak, I.; Ziolek, M.; Bettahar, M. M. Nickel containing MCM-41 and AlMCM-41 mesoporous molecular sieves: Characteristics and activity in the hydrogenation of benzene. *Appl. Catal. A* **2004**, *268*, 241−253.
(1481) Samanta, S.; Mal, N. K.; Bhaumik, A. Mesoporous Cr-MCM-41: An efficient catalyst for selective oxidation of cycloalkanes. *J. Mol. Catal. A: Chem.* **2005**, *236*, 7−11.
(1482) Pacheco, J. J.; Davis, M. E. Synthesis of terephthalic acid via Diels-Alder reactions with ethylene and oxidized variants of 5-hydroxymethylfurfural. *Proc. Natl. Acad. Sci. U. S. A.* **2014**, *111*, 8363.
(1483) Yang, M.; Li, S.; Wang, Y.; Herron, J. A.; Xu, Y.; Allard, L. F.; Lee, S.; Huang, J.; Mavrikakis, M.; Flytzani-Stephanopoulos, M. Catalytically active Au-O$(OH)_x$- species stabilized by alkali ions on zeolites and mesoporous oxides. *Science* **2014**, *346*, 1498.
(1484) Das, P.; Ray, S.; Bhanja, P.; Bhaumik, A.; Mukhopadhyay, C. Serendipitous Observation of Liquid-Phase Size Selectivity inside a Mesoporous Silica Nanoreactor in the Reaction of Chromene with Formic Acid. *ChemCatChem.* **2018**, *10*, 2260−2270.
(1485) Che, S.; Liu, Z.; Ohsuna, T.; Sakamoto, K.; Terasaki, O.; Tatsumi, T. Synthesis and characterization of chiral mesoporous silica. *Nature* **2004**, *429*, 281−284.
(1486) Qiu, H.; Che, S. Chiral mesoporous silica: Chiral construction and imprinting via cooperative self-assembly of amphiphiles and silica precursors. *Chem. Soc. Rev.* **2011**, *40*, 1259−1268.
(1487) Gao, Y.; Hao, J.; Liu, J.; Liang, Y.; Du, F.; Hu, J.; Ju, Y. Imprinting supramolecular chirality on silica from natural triterpenoid-regulated helical ribbons. *Materials Chemistry Frontiers* **2019**, *3*, 308−313.
(1488) Zhang, F.; Ai, J.; Ding, K.; Duan, Y.; Han, L.; Che, S. Synthesis of chiral mesostructured titanium dioxide films. *Chem. Commun.* **2020**, *56*, 4848−4851.
(1489) Cui, M.; Zhang, W.; Xie, L.; Chen, L.; Xu, L. Chiral Mesoporous Silica Materials: A Review on Synthetic Strategies and Applications. *Molecules* **2020**, *25*, 3899.
(1490) Kawasaki, T.; Araki, Y.; Hatase, K.; Suzuki, K.; Matsumoto, A.; Yokoi, T.; Kubota, Y.; Tatsumi, T.; Soai, K. Helical mesoporous silica as an inorganic heterogeneous chiral trigger for asymmetric autocatalysis with amplification of enantiomeric excess. *Chem. Commun.* **2015**, *51*, 8742−8744.
(1491) García-Muñoz, R. A.; Morales, V.; Linares, M.; Rico-Oller, B. Synthesis of Helical and Supplementary Chirally Doped PMO Materials. Suitable Catalysts for Asymmetric Synthesis. *Langmuir* **2014**, *30*, 881−890.
(1492) Sokolov, S.; Kondratenko, E. V.; Pohl, M.-M.; Barkschat, A.; Rodemerck, U. Stable low-temperature dry reforming of methane over mesoporous La_2O_3-ZrO_2 supported Ni catalyst. *Appl. Catal. B* **2012**, *113-114*, 19−30.
(1493) El Hassan, N.; Kaydouh, M. N.; Geagea, H.; El Zein, H.; Jabbour, K.; Casale, S.; El Zakhem, H.; Massiani, P. Low temperature dry reforming of methane on rhodium and cobalt based catalysts: Active phase stabilization by confinement in mesoporous SBA-15. *Appl. Catal. A* **2016**, *520*, 114−121.
(1494) Li, Z.; Das, S.; Hongmanorom, P.; Dewangan, N.; Wai, M. H.; Kawi, S. Silica-based micro- and mesoporous catalysts for dry reforming of methane. *Catal. Sci. Technol.* **2018**, *8*, 2763−2778.
(1495) Erdogan, B.; Arbag, H.; Yasyerli, N. SBA-15 supported mesoporous Ni and Co catalysts with high coke resistance for dry reforming of methane. *Int. J. Hydrogen Energy* **2018**, *43*, 1396−1405.
(1496) Raja, R.; Thomas, J. M.; Jones, M. D.; Johnson, B. F. G.; Vaughan, D. E. W. Constraining Asymmetric Organometallic Catalysts within Mesoporous Supports Boosts Their Enantioselectivity. *J. Am. Chem. Soc.* **2003**, *125*, 14982−14983.
(1497) Li, C. Chiral Synthesis on Catalysts Immobilized in Microporous and Mesoporous Materials. *Catal. Rev.* **2004**, *46*, 419−492.
(1498) Song, C. E.; Kim, D. H.; Choi, D. S. Chiral Organometallic Catalysts in Confined Nanospaces: Significantly Enhanced Enantioselectivity and Stability. *Eur. J. Inorg. Chem.* **2006**, *2006*, 2927−2935.
(1499) Li, C.; Zhang, H.; Jiang, D.; Yang, Q. Chiral catalysis in nanopores of mesoporous materials. *Chem. Commun.* **2007**, 547−558.
(1500) Mihalcik, D. J.; Lin, W. Mesoporous Silica Nanosphere-Supported Chiral Ruthenium Catalysts: Synthesis, Characterization, and Asymmetric Hydrogenation Studies. *ChemCatChem.* **2009**, *1*, 406−413.
(1501) Zhao, L.; Li, Y.; Yu, P.; Han, X.; He, J. Exploration of Dependence of Organo-Catalyzed Enantioselective Michael Addition on the Pore Size of Mesoporous Host. *ACS Catal.* **2012**, *2*, 1118−1126.
(1502) Liu, K.; Jin, R.; Cheng, T.; Xu, X.; Gao, F.; Liu, G.; Li, H. Functionalized Periodic Mesoporous Organosilica: A Highly Enantioselective Catalyst for the Michael Addition of 1,3-Dicarbonyl Compounds to Nitroalkenes. *Chem.-Eur. J.* **2012**, *18*, 15546−15553.

https://doi.org/10.1021/acs.chemrev.1c00905
Chem. Rev. XXXX, XXX, XXX−XXX

(1503) Cao, H.; Zhu, X.-H.; Wang, D.; Sun, Z.; Deng, Y.; Hou, X.-F.; Zhao, D. Selectivity Enhancement in Dynamic Kinetic Resolution of Secondary Alcohols through Adjusting the Micro-Environment of Metal Complex Confined in Nanochannels: A Promising Strategy for Tandem Reactions. *ACS Catal.* **2015**, *5*, 27−33.
(1504) Xia, X.; Meng, J.; Wu, H.; Cheng, T.; Liu, G. Integration of multiple active sites on large-pore mesoporous silica for enantioselective tandem reactions. *Chem. Commun.* **2017**, *53*, 1638−1641.
(1505) Xiang, S.; Zhang, Y.; Xin, Q.; Li, C. Enantioselective epoxidation of olefins catalyzed by Mn (salen)/MCM-41 synthesized with a new anchoring method. *Chem. Commun.* **2002**, 2696−2697.
(1506) Yang, H.; Li, J.; Yang, J.; Liu, Z.; Yang, Q.; Li, C. Asymmetric reactions on chiral catalysts entrapped within a mesoporous cage. *Chem. Commun.* **2007**, 1086−1088.
(1507) Raynor, S. A.; Thomas, J. M.; Raja, R.; Johnson, B. F. G.; Bell, R. G.; Mantle, M. D. A one-step, enantioselective reduction of ethyl nicotinate to ethyl nipecotinate using a constrained, chiral, heterogeneous catalyst. *Chem. Commun.* **2000**, 1925−1926.
(1508) Jones, M. D.; Raja, R.; Thomas, J. M.; Johnson, B. F. G.; Lewis, D. W.; Rouzaud, J.; Harris, K. D. M. Enhancing the Enantioselectivity of Novel Homogeneous Organometallic Hydrogenation Catalysts. *Angew. Chem., Int. Ed.* **2003**, *42*, 4326−4331.
(1509) Hu, A.; Ngo, H. L.; Lin, W. Chiral Porous Hybrid Solids for Practical Heterogeneous Asymmetric Hydrogenation of Aromatic Ketones. *J. Am. Chem. Soc.* **2003**, *125*, 11490−11491.
(1510) Li, X.; Wu, P. Enantioselective hydrogenation catalyzed by chiral nanoporous materials. *Curr. Org. Chem.* **2014**, *18*, 1242−1261.
(1511) Jin Bae, S.; Kim, S.-W.; Hyeon, T.; Moon Kim, B. New chiral heterogeneous catalysts based on mesoporous silica: asymmetric diethylzinc addition to benzaldehyde. *Chem. Commun.* **2000**, 31−32.
(1512) Corma, A.; García, H.; Moussaif, A.; Sabater, M. J.; Zniber, R.; Redouane, A. Chiral copper(ii) bisoxazoline covalently anchored to silica and mesoporous MCM-41 as a heterogeneous catalyst for the enantioselective Friedel-Crafts hydroxyalkylation. *Chem. Commun.* **2002**, 1058−1059.
(1513) Wan, Y.; McMorn, P.; Hancock, F. E.; Hutchings, G. J. Heterogeneous Enantioselective Synthesis of a Dihydropyran Using Cu-Exchanged Microporous and Mesoporous Materials Modified by Bis(oxazoline). *Catal. Lett.* **2003**, *91*, 145−148.
(1514) Jeong, E.-Y.; Lim, C.-R.; Jin, H.; Park, S.-E. trans-1,2-Diaminocyclohexane mesoporous silica for asymmetric catalysis: enhancement of chirality through confinement space by the plug effect. *Chem. Commun.* **2012**, *48*, 3079−3081.
(1515) Furukawa, Y.; Ogura, M. A Unique Heterogeneous Nucleophilic Catalyst Comprising Methylated Nitrogen-Substituted Porous Silica Provides High Product Selectivity for the Morita-Baylis-Hillman Reaction. *J. Am. Chem. Soc.* **2014**, *136*, 119−121.
(1516) Shu, X.-Z.; Nguyen, S. C.; He, Y.; Oba, F.; Zhang, Q.; Canlas, C.; Somorjai, G. A.; Alivisatos, A. P.; Toste, F. D. Silica-Supported Cationic Gold(I) Complexes as Heterogeneous Catalysts for Regio- and Enantioselective Lactonization Reactions. *J. Am. Chem. Soc.* **2015**, *137*, 7083−7086.
(1517) Pump, E.; Cao, Z.; Samantaray, M. K.; Bendjeriou-Sedjerari, A.; Cavallo, L.; Basset, J.-M. Exploiting Confinement Effects to Tune Selectivity in Cyclooctane Metathesis. *ACS Catal.* **2017**, *7*, 6581−6586.
(1518) Ishito, N.; Kobayashi, H.; Nakajima, K.; Maegawa, Y.; Inagaki, S.; Hara, K.; Fukuoka, A. Ruthenium-Immobilized Periodic Mesoporous Organosilica: Synthesis, Characterization, and Catalytic Application for Selective Oxidation of Alkanes. *Chem.-Eur. J.* **2015**, *21*, 15564−15569.
(1519) Li, B.; Bai, S.; Wang, P.; Yang, H.; Yang, Q.; Li, C. Encapsulation of chiral Fe(salan) in nanocages with different microenvironments for asymmetric sulfide oxidation. *Phys. Chem. Chem. Phys.* **2011**, *13*, 2504−2511.
(1520) Bai, S.; Li, B.; Peng, J.; Zhang, X.; Yang, Q.; Li, C. Promoted activity of Cr(Salen) in a nanoreactor for kinetic resolution of terminal epoxides. *Chem. Sci.* **2012**, *3*, 2864−2867.
(1521) Takahashi, H.; Li, B.; Sasaki, T.; Miyazaki, C.; Kajino, T.; Inagaki, S. Catalytic Activity in Organic Solvents and Stability of Immobilized Enzymes Depend on the Pore Size and Surface Characteristics of Mesoporous Silica. *Chem. Mater.* **2000**, *12*, 3301−3305.
(1522) Hartmann, M. Ordered Mesoporous Materials for Bioadsorption and Biocatalysis. *Chem. Mater.* **2005**, *17*, 4577−4593.
(1523) Hudson, S.; Cooney, J.; Magner, E. Proteins in Mesoporous Silicates. *Angew. Chem., Int. Ed.* **2008**, *47*, 8582−8594.
(1524) Popat, A.; Hartono, S. B.; Stahr, F.; Liu, J.; Qiao, S. Z.; Qing Lu, G. Mesoporous silica nanoparticles for bioadsorption, enzyme immobilisation, and delivery carriers. *Nanoscale* **2011**, *3*, 2801−2818.
(1525) Gupta, M. N.; Kaloti, M.; Kapoor, M.; Solanki, K. Nanomaterials as Matrices for Enzyme Immobilization. *Artificial Cells, Blood Substitutes, and Biotechnology* **2011**, *39*, 98−109.
(1526) Engström, K.; Johnston, E. V.; Verho, O.; Gustafson, K. P. J.; Shakeri, M.; Tai, C.-W.; Bäckvall, J.-E. Co-immobilization of an Enzyme and a Metal into the Compartments of Mesoporous Silica for Cooperative Tandem Catalysis: An Artificial Metalloenzyme. *Angew. Chem., Int. Ed.* **2013**, *52*, 14006−14010.
(1527) Sharma, K. K.; Asefa, T. Efficient Bifunctional Nanocatalysts by Simple Postgrafting of Spatially Isolated Catalytic Groups on Mesoporous Materials. *Angew. Chem., Int. Ed.* **2007**, *46*, 2879−2882.
(1528) Yu, C.; He, J. Synergic catalytic effects in confined spaces. *Chem. Commun.* **2012**, *48*, 4933−4940.
(1529) Shi, J. On the Synergetic Catalytic Effect in Heterogeneous Nanocomposite Catalysts. *Chem. Rev.* **2013**, *113*, 2139−2181.
(1530) Guan, J.; Liu, B.; Yang, X.; Hu, J.; Wang, C.; Kan, Q. Immobilization of Proline onto Al-SBA-15 for C-C Bond-Forming Reactions. *ACS Sustainable Chem. Eng.* **2014**, *2*, 925−933.
(1531) Kuschel, A.; Drescher, M.; Kuschel, T.; Polarz, S. Bifunctional Mesoporous Organosilica Materials and Their Application in Catalysis: Cooperative Effects or Not? *Chem. Mater.* **2010**, *22*, 1472−1482.
(1532) Gross, E.; Liu, J. H.; Alayoglu, S.; Marcus, M. A.; Fakra, S. C.; Toste, F. D.; Somorjai, G. A. Asymmetric Catalysis at the Mesoscale: Gold Nanoclusters Embedded in Chiral Self-Assembled Monolayer as Heterogeneous Catalyst for Asymmetric Reactions. *J. Am. Chem. Soc.* **2013**, *135*, 3881−3886.
(1533) Lee, J.; Farha, O. K.; Roberts, J.; Scheidt, K. A.; Nguyen, S. T.; Hupp, J. T. Metal-organic framework materials as catalysts. *Chem. Soc. Rev.* **2009**, *38*, 1450−1459.
(1534) Corma, A.; García, H.; Llabrés i Xamena, F. X. Engineering Metal Organic Frameworks for Heterogeneous Catalysis. *Chem. Rev.* **2010**, *110*, 4606−4655.
(1535) Ma, L.; Lin, W. *Functional Metal-Organic Frameworks: Gas Storage, Separation and Catalysis*; Schröder, M., Ed.; Springer Berlin Heidelberg, 2010; Vol. *293*.
(1536) Isaeva, V. I.; Kustov, L. M. The application of metal-organic frameworks in catalysis (Review). *Pet. Chem.* **2010**, *50*, 167−180.
(1537) Ma, L.; Lin, W. *Functional Metal-Organic Frameworks: Gas Storage, Separation and Catalysis*; Schröder, M., Ed.; Springer Berlin Heidelberg: Berlin, Heidelberg, 2010. DOI: 10.1007/128_2009_20 10.1007/128_2009_20.
(1538) Liu, J.; Chen, L.; Cui, H.; Zhang, J.; Zhang, L.; Su, C.-Y. Applications of metal-organic frameworks in heterogeneous supramolecular catalysis. *Chem. Soc. Rev.* **2014**, *43*, 6011−6061.
(1539) Gu, Z.-Y.; Park, J.; Raiff, A.; Wei, Z.; Zhou, H.-C. Metal-Organic Frameworks as Biomimetic Catalysts. *ChemCatChem.* **2014**, *6*, 67−75.
(1540) Zhu, L.; Liu, X.-Q.; Jiang, H.-L.; Sun, L.-B. Metal-Organic Frameworks for Heterogeneous Basic Catalysis. *Chem. Rev.* **2017**, *117*, 8129−8176.
(1541) Rogge, S. M. J.; Bavykina, A.; Hajek, J.; Garcia, H.; Olivos-Suarez, A. I.; Sepúlveda-Escribano, A.; Vimont, A.; Clet, G.; Bazin, P.; Kapteijn, F.; et al. Metal-organic and covalent organic frameworks as single-site catalysts. *Chem. Soc. Rev.* **2017**, *46*, 3134−3184.

https://doi.org/10.1021/acs.chemrev.1c00905
Chem. Rev. XXXX, XXX, XXX−XXX

(1542) Xu, W.; Thapa, K. B.; Ju, Q.; Fang, Z.; Huang, W. Heterogeneous catalysts based on mesoporous metal-organic frameworks. *Coord. Chem. Rev.* **2018**, *373*, 199−232.
(1543) Dhakshinamoorthy, A.; Li, Z.; Garcia, H. Catalysis and photocatalysis by metal organic frameworks. *Chem. Soc. Rev.* **2018**, *47*, 8134−8172.
(1544) Yuan, S.; Feng, L.; Wang, K.; Pang, J.; Bosch, M.; Lollar, C.; Sun, Y.; Qin, J.; Yang, X.; Zhang, P.; et al. Stable Metal-Organic Frameworks: Design, Synthesis, and Applications. *Adv. Mater.* **2018**, *30*, 1704303.
(1545) Chen, Y.-Z.; Zhang, R.; Jiao, L.; Jiang, H.-L. Metal-organic framework-derived porous materials for catalysis. *Coord. Chem. Rev.* **2018**, *362*, 1−23.
(1546) Yang, D.; Gates, B. C. Catalysis by Metal Organic Frameworks: Perspective and Suggestions for Future Research. *ACS Catal.* **2019**, *9*, 1779−1798.
(1547) Stock, N.; Biswas, S. Synthesis of Metal-Organic Frameworks (MOFs): Routes to Various MOF Topologies, Morphologies, and Composites. *Chem. Rev.* **2012**, *112*, 933−969.
(1548) Cook, T. R.; Zheng, Y.-R.; Stang, P. J. Metal-Organic Frameworks and Self-Assembled Supramolecular Coordination Complexes: Comparing and Contrasting the Design, Synthesis, and Functionality of Metal-Organic Materials. *Chem. Rev.* **2013**, *113*, 734−777.
(1549) Furukawa, H.; Cordova, K. E.; O'Keeffe, M.; Yaghi, O. M. The Chemistry and Applications of Metal-Organic Frameworks. *Science* **2013**, *341*. DOI: 10.1126/science.1230444
(1550) Lu, W.; Wei, Z.; Gu, Z.-Y.; Liu, T.-F.; Park, J.; Park, J.; Tian, J.; Zhang, M.; Zhang, Q.; Gentle Iii, T.; et al. Tuning the structure and function of metal-organic frameworks via linker design. *Chem. Soc. Rev.* **2014**, *43*, 5561−5593.
(1551) Kirchon, A.; Feng, L.; Drake, H. F.; Joseph, E. A.; Zhou, H.-C. From fundamentals to applications: a toolbox for robust and multifunctional MOF materials. *Chem. Soc. Rev.* **2018**, *47*, 8611−8638.
(1552) Howarth, A. J.; Liu, Y.; Li, P.; Li, Z.; Wang, T. C.; Hupp, J. T.; Farha, O. K. Chemical, thermal and mechanical stabilities of metal-organic frameworks. *Nature Reviews Materials* **2016**, *1*, 15018.
(1553) Rimer, J. D.; Chawla, A.; Le, T. T. Crystal Engineering for Catalysis. *Annu. Rev. Chem. Biomol. Eng.* **2018**, *9*, 283−309.
(1554) Ding, M.; Cai, X.; Jiang, H.-L. Improving MOF stability: approaches and applications. *Chem. Sci.* **2019**, *10*, 10209−10230.
(1555) Burtch, N. C.; Jasuja, H.; Walton, K. S. Water Stability and Adsorption in Metal-Organic Frameworks. *Chem. Rev.* **2014**, *114*, 10575−10612.
(1556) Zuluaga, S.; Fuentes-Fernandez, E. M. A.; Tan, K.; Xu, F.; Li, J.; Chabal, Y. J.; Thonhauser, T. Understanding and controlling water stability of MOF-74. *Journal of Materials Chemistry A* **2016**, *4*, 5176−5183.
(1557) Fujita, M.; Kwon, Y. J.; Washizu, S.; Ogura, K. Preparation, Clathration Ability, and Catalysis of a Two-Dimensional Square Network Material Composed of Cadmium(II) and 4,4'-Bipyridine. *J. Am. Chem. Soc.* **1994**, *116*, 1151−1152.
(1558) Ohmori, O.; Fujita, M. Heterogeneous catalysis of a coordination network: cyanosilylation of imines catalyzed by a Cd(ii)-(4,4′-bipyridine) square grid complex. *Chem. Commun.* **2004**, 1586−1587.
(1559) Chui, S. S. Y.; Lo, S. M. F.; Charmant, J. P. H.; Orpen, A. G.; Williams, I. D. A Chemically Functionalizable Nanoporous Material $[Cu_3(TMA)_2(H2O)_3]_n$. *Science* **1999**, *283*, 1148.
(1560) Henschel, A.; Gedrich, K.; Kraehnert, R.; Kaskel, S. Catalytic properties of MIL-101. *Chem. Commun.* **2008**, 4192−4194.
(1561) Horike, S.; Dinca, M.; Tamaki, K.; Long, J. R. Size-Selective Lewis Acid Catalysis in a Microporous Metal-Organic Framework with Exposed Mn^{2+} Coordination Sites. *J. Am. Chem. Soc.* **2008**, *130*, 5854−5855.
(1562) Alaerts, L.; Séguin, E.; Poelman, H.; Thibault-Starzyk, F.; Jacobs, P. A.; De Vos, D. E. Probing the Lewis Acidity and Catalytic Activity of the Metal-Organic Framework $[Cu_3(btc)_2]$ (BTC=Benzene-1,3,5-tricarboxylate). *Chem.-Eur. J.* **2006**, *12*, 7353−7363.
(1563) Hu, Z.; Peng, Y.; Tan, K. M.; Zhao, D. Enhanced catalytic activity of a hierarchical porous metal-organic framework CuBTC. *CrystEngComm* **2015**, *17*, 7124−7129.
(1564) Mo, K.; Yang, Y.; Cui, Y. A Homochiral Metal-Organic Framework as an Effective Asymmetric Catalyst for Cyanohydrin Synthesis. *J. Am. Chem. Soc.* **2014**, *136*, 1746−1749.
(1565) Hu, Z.; Zhao, D. Metal-organic frameworks with Lewis acidity: synthesis, characterization, and catalytic applications. *CrystEngComm* **2017**, *19*, 4066−4081.
(1566) Opanasenko, M.; Dhakshinamoorthy, A.; Hwang, Y. K.; Chang, J.-S.; Garcia, H.; Cejka, J. Superior Performance of Metal-Organic Frameworks over Zeolites as Solid Acid Catalysts in the Prins Reaction: Green Synthesis of Nopol. *ChemSusChem* **2013**, *6*, 865−871.
(1567) Reinares-Fisac, D.; Aguirre-Díaz, L. M.; Iglesias, M.; Snejko, N.; Gutiérrez-Puebla, E.; Monge, M. Á.; Gándara, F. A Mesoporous Indium Metal-Organic Framework: Remarkable Advances in Catalytic Activity for Strecker Reaction of Ketones. *J. Am. Chem. Soc.* **2016**, *138*, 9089−9092.
(1568) Ravon, U.; Domine, M. E.; Gaudillère, C.; Desmartin-Chomel, A.; Farrusseng, D. MOFs as acid catalysts with shape selectivity properties. *New J. Chem.* **2008**, *32*, 937−940.
(1569) Phan, N. T. S.; Le, K. K. A.; Phan, T. D. MOF-5 as an efficient heterogeneous catalyst for Friedel-Crafts alkylation reactions. *Appl. Catal. A* **2010**, *382*, 246−253.
(1570) Thallapally, P. K.; Fernandez, C. A.; Motkuri, R. K.; Nune, S. K.; Liu, J.; Peden, C. H. F. Micro and mesoporous metal-organic frameworks for catalysis applications. *Dalton Trans.* **2010**, *39*, 1692−1694.
(1571) Liao, T.-B.; Ling, Y.; Chen, Z.-X.; Zhou, Y.-M.; Weng, L.-H. A rutile-type porous zinc(ii)-phosphonocarboxylate framework: local proton transfer and size-selected catalysis. *Chem. Commun.* **2010**, *46*, 1100−1102.
(1572) Roberts, J. M.; Fini, B. M.; Sarjeant, A. A.; Farha, O. K.; Hupp, J. T.; Scheidt, K. A. Urea Metal-Organic Frameworks as Effective and Size-Selective Hydrogen-Bond Catalysts. *J. Am. Chem. Soc.* **2012**, *134*, 3334−3337.
(1573) Calleja, G.; Sanz, R.; Orcajo, G.; Briones, D.; Leo, P.; Martínez, F. Copper-based MOF-74 material as effective acid catalyst in Friedel-Crafts acylation of anisole. *Catal. Today* **2014**, *227*, 130−137.
(1574) Doan, T. L. H.; Dao, T. Q.; Tran, H. N.; Tran, P. H.; Le, T. N. An efficient combination of Zr-MOF and microwave irradiation in catalytic Lewis acid Friedel-Crafts benzoylation. *Dalton Trans.* **2016**, *45*, 7875−7880.
(1575) Shamzhy, M. V.; Opanasenko, M. V.; Garcia, H.; Cejka, J. Annulation of phenols with methylbutenol over MOFs: The role of catalyst structure and acid strength in producing 2,2-dimethylbenzopyran derivatives. *Microporous Mesoporous Mater.* **2015**, *202*, 297−302.
(1576) Dhakshinamoorthy, A.; Alvaro, M.; Chevreau, H.; Horcajada, P.; Devic, T.; Serre, C.; Garcia, H. Iron(iii) metal-organic frameworks as solid Lewis acids for the isomerization of α-pinene oxide. *Catal. Sci. Technol.* **2012**, *2*, 324−330.
(1577) Steenhaut, T.; Grégoire, N.; Barozzino-Consiglio, G.; Filinchuk, Y.; Hermans, S. Mechanochemical defect engineering of HKUST-1 and impact of the resulting defects on carbon dioxide sorption and catalytic cyclopropanation. *RSC Adv.* **2020**, *10*, 19822−19831.
(1578) Brozek, C. K.; Dinca, M. Ti^{3+}-, $V^{2+/3+}$-, $Cr^{2+/3+}$-, Mn^{2+}-, and Fe^{2+}-Substituted MOF-5 and Redox Reactivity in Cr- and Fe-MOF-5. *J. Am. Chem. Soc.* **2013**, *135*, 12886−12891.
(1579) Nakagaki, S.; Ferreira, G. K.; Ucoski, G. M.; Dias de Freitas Castro, K. A. Chemical Reactions Catalyzed by Metalloporphyrin-Based Metal-Organic Frameworks. *Molecules* **2013**, *18*, 7279.
(1580) Liu, Y.; Howarth, A. J.; Vermeulen, N. A.; Moon, S.-Y.; Hupp, J. T.; Farha, O. K. Catalytic degradation of chemical warfare

https://doi.org/10.1021/acs.chemrev.1c00905
Chem. Rev. XXXX, XXX, XXX−XXX

agents and their simulants by metal-organic frameworks. *Coord. Chem. Rev.* **2017**, *346*, 101−111.
(1581) Cheng, M.; Lai, C.; Liu, Y.; Zeng, G.; Huang, D.; Zhang, C.; Qin, L.; Hu, L.; Zhou, C.; Xiong, W. Metal-organic frameworks for highly efficient heterogeneous Fenton-like catalysis. *Coord. Chem. Rev.* **2018**, *368*, 80−92.
(1582) Konnerth, H.; Matsagar, B. M.; Chen, S. S.; Prechtl, M. H. G.; Shieh, F.-K.; Wu, K. C. W. Metal-organic framework (MOF)-derived catalysts for fine chemical production. *Coord. Chem. Rev.* **2020**, *416*, 213319.
(1583) Dhakshinamoorthy, A.; Alvaro, M.; Garcia, H. Metal-organic frameworks as heterogeneous catalysts for oxidation reactions. *Catal. Sci. Technol.* **2011**, *1*, 856−867.
(1584) Llabrés i Xamena, F. X.; Abad, A.; Corma, A.; Garcia, H. MOFs as catalysts: Activity, reusability and shape-selectivity of a Pd-containing MOF. *J. Catal.* **2007**, *250*, 294−298.
(1585) Kato, C. N.; Hasegawa, M.; Sato, T.; Yoshizawa, A.; Inoue, T.; Mori, W. Microporous dinuclear copper(II) trans-1,4-cyclohexanedicarboxylate: heterogeneous oxidation catalysis with hydrogen peroxide and X-ray powder structure of peroxo copper(II) intermediate. *J. Catal.* **2005**, *230*, 226−236.
(1586) Dhakshinamoorthy, A.; Alvaro, M.; Horcajada, P.; Gibson, E.; Vishnuvarthan, M.; Vimont, A.; Grenèche, J.-M.; Serre, C.; Daturi, M.; Garcia, H. Comparison of Porous Iron Trimesates Basolite F300 and MIL-100(Fe) As Heterogeneous Catalysts for Lewis Acid and Oxidation Reactions: Roles of Structural Defects and Stability. *ACS Catal.* **2012**, *2*, 2060−2065.
(1587) Guo, P.; Froese, C.; Fu, Q.; Chen, Y.-T.; Peng, B.; Kleist, W.; Fischer, R. A.; Muhler, M.; Wang, Y. CuPd Mixed-Metal HKUST-1 as a Catalyst for Aerobic Alcohol Oxidation. *J. Phys. Chem. C* **2018**, *122*, 21433−21440.
(1588) Xiao, D. J.; Oktawiec, J.; Milner, P. J.; Long, J. R. Pore Environment Effects on Catalytic Cyclohexane Oxidation in Expanded Fe_2(dobdc) Analogues. *J. Am. Chem. Soc.* **2016**, *138*, 14371−14379.
(1589) Xiao, D. J.; Bloch, E. D.; Mason, J. A.; Queen, W. L.; Hudson, M. R.; Planas, N.; Borycz, J.; Dzubak, A. L.; Verma, P.; Lee, K.; et al. Oxidation of ethane to ethanol by N_2O in a metal-organic framework with coordinatively unsaturated iron(II) sites. *Nat. Chem.* **2014**, *6*, 590−595.
(1590) Han, J. W.; Hill, C. L. A Coordination Network That Catalyzes O_2-Based Oxidations. *J. Am. Chem. Soc.* **2007**, *129*, 15094−15095.
(1591) Wang, S.; Wang, X. Multifunctional Metal-Organic Frameworks for Photocatalysis. *Small* **2015**, *11*, 3097−3112.
(1592) Mazari, S. A.; Hossain, N.; Basirun, W. J.; Mubarak, N. M.; Abro, R.; Sabzoi, N.; Shah, A. An overview of catalytic conversion of CO_2 into fuels and chemicals using metal organic frameworks. *Process Safety and Environmental Protection* **2021**, *149*, 67−92.
(1593) Wen, M.; Li, G.; Liu, H.; Chen, J.; An, T.; Yamashita, H. Metal-organic framework-based nanomaterials for adsorption and photocatalytic degradation of gaseous pollutants: recent progress and challenges. *Environmental Science: Nano* **2019**, *6*, 1006−1025.
(1594) He, H.; Perman, J. A.; Zhu, G.; Ma, S. Metal-Organic Frameworks for CO_2 Chemical Transformations. *Small* **2016**, *12*, 6309−6324.
(1595) Morimoto, T.; Nakajima, T.; Sawa, S.; Nakanishi, R.; Imori, D.; Ishitani, O. CO_2 Capture by a Rhenium(I) Complex with the Aid of Triethanolamine. *J. Am. Chem. Soc.* **2013**, *135*, 16825−16828.
(1596) Wang, Y.; Huang, N.-Y.; Shen, J.-Q.; Liao, P.-Q.; Chen, X.-M.; Zhang, J.-P. Hydroxide Ligands Cooperate with Catalytic Centers in Metal-Organic Frameworks for Efficient Photocatalytic CO_2 Reduction. *J. Am. Chem. Soc.* **2018**, *140*, 38−41.
(1597) Gao, W.-Y.; Ngo, H. T.; Niu, Z.; Zhang, W.; Pan, Y.; Yang, Z.; Bhethanabotla, V. R.; Joseph, B.; Aguila, B.; Ma, S. A Mixed-Metal Porphyrinic Framework Promoting Gas-Phase CO_2 Photoreduction without Organic Sacrificial Agents. *ChemSusChem* **2020**, *13*, 6273−6277.
(1598) Fateeva, A.; Chater, P. A.; Ireland, C. P.; Tahir, A. A.; Khimyak, Y. Z.; Wiper, P. V.; Darwent, J. R.; Rosseinsky, M. J. A Water-Stable Porphyrin-Based Metal-Organic Framework Active for Visible-Light Photocatalysis. *Angew. Chem., Int. Ed.* **2012**, *51*, 7440−7444.
(1599) Wang, C.; Xie, Z.; deKrafft, K. E.; Lin, W. Doping Metal-Organic Frameworks for Water Oxidation, Carbon Dioxide Reduction, and Organic Photocatalysis. *J. Am. Chem. Soc.* **2011**, *133*, 13445−13454.
(1600) Fu, Y.; Sun, D.; Chen, Y.; Huang, R.; Ding, Z.; Fu, X.; Li, Z. An Amine-Functionalized Titanium Metal-Organic Framework Photocatalyst with Visible-Light-Induced Activity for CO_2 Reduction. *Angew. Chem., Int. Ed.* **2012**, *51*, 3364−3367.
(1601) Wang, M.; Wang, D.; Li, Z. Self-assembly of CPO-27-Mg/TiO_2 nanocomposite with enhanced performance for photocatalytic CO_2 reduction. *Appl. Catal. B* **2016**, *183*, 47−52.
(1602) Qin, J.-S.; Du, D.-Y.; Guan, W.; Bo, X.-J.; Li, Y.-F.; Guo, L.-P.; Su, Z.-M.; Wang, Y.-Y.; Lan, Y.-Q.; Zhou, H.-C. Ultrastable Polymolybdate-Based Metal-Organic Frameworks as Highly Active Electrocatalysts for Hydrogen Generation from Water. *J. Am. Chem. Soc.* **2015**, *137*, 7169−7177.
(1603) Kornienko, N.; Zhao, Y.; Kley, C. S.; Zhu, C.; Kim, D.; Lin, S.; Chang, C. J.; Yaghi, O. M.; Yang, P. Metal-Organic Frameworks for Electrocatalytic Reduction of Carbon Dioxide. *J. Am. Chem. Soc.* **2015**, *137*, 14129−14135.
(1604) Hod, I.; Sampson, M. D.; Deria, P.; Kubiak, C. P.; Farha, O. K.; Hupp, J. T. Fe-Porphyrin-Based Metal-Organic Framework Films as High-Surface Concentration, Heterogeneous Catalysts for Electrochemical Reduction of CO_2. *ACS Catal.* **2015**, *5*, 6302−6309.
(1605) Lin, S.; Diercks, C. S.; Zhang, Y.-B.; Kornienko, N.; Nichols, E. M.; Zhao, Y.; Paris, A. R.; Kim, D.; Yang, P.; Yaghi, O. M.; et al. Covalent organic frameworks comprising cobalt porphyrins for catalytic CO_2 reduction in water. *Science* **2015**, *349*, 1208.
(1606) Senthil Kumar, R.; Senthil Kumar, S.; Anbu Kulandainathan, M. Highly selective electrochemical reduction of carbon dioxide using Cu based metal organic framework as an electrocatalyst. *Electrochem. Commun.* **2012**, *25*, 70−73.
(1607) Albo, J.; Vallejo, D.; Beobide, G.; Castillo, O.; Castaño, P.; Irabien, A. Copper-Based Metal-Organic Porous Materials for CO_2 Electrocatalytic Reduction to Alcohols. *ChemSusChem* **2017**, *10*, 1100−1109.
(1608) Manna, K.; Zhang, T.; Carboni, M.; Abney, C. W.; Lin, W. Salicylaldimine-Based Metal-Organic Framework Enabling Highly Active Olefin Hydrogenation with Iron and Cobalt Catalysts. *J. Am. Chem. Soc.* **2014**, *136*, 13182−13185.
(1609) Ren, Y.; Cheng, X.; Yang, S.; Qi, C.; Jiang, H.; Mao, Q. A chiral mixed metal-organic framework based on a Ni(saldpen) metalloligand: synthesis, characterization and catalytic performances. *Dalton Trans.* **2013**, *42*, 9930−9937.
(1610) Jiang, W.; Yang, J.; Liu, Y.-Y.; Song, S.-Y.; Ma, J.-F. A Porphyrin-Based Porous *rtl* Metal-Organic Framework as an Efficient Catalyst for the Cycloaddition of CO_2 to Epoxides. *Chem.-Eur. J.* **2016**, *22*, 16991−16997.
(1611) Gao, W.-Y.; Chen, Y.; Niu, Y.; Williams, K.; Cash, L.; Perez, P. J.; Wojtas, L.; Cai, J.; Chen, Y.-S.; Ma, S. Crystal Engineering of an nbo Topology Metal-Organic Framework for Chemical Fixation of CO2 under Ambient Conditions. *Angew. Chem., Int. Ed.* **2014**, *53*, 2615−2619.
(1612) Zou, R.; Li, P.-Z.; Zeng, Y.-F.; Liu, J.; Zhao, R.; Duan, H.; Luo, Z.; Wang, J.-G.; Zou, R.; Zhao, Y. Bimetallic Metal-Organic Frameworks: Probing the Lewis Acid Site for CO_2 Conversion. *Small* **2016**, *12*, 2334−2343.
(1613) Zhang, G.; Wei, G.; Liu, Z.; Oliver, S. R. J.; Fei, H. A Robust Sulfonate-Based Metal-Organic Framework with Permanent Porosity for Efficient CO_2 Capture and Conversion. *Chem. Mater.* **2016**, *28*, 6276−6281.
(1614) Gascon, J.; Aktay, U.; Hernandez-Alonso, M. D.; van Klink, G. P. M.; Kapteijn, F. Amino-based metal-organic frameworks as stable, highly active basic catalysts. *J. Catal.* **2009**, *261*, 75−87.

https://doi.org/10.1021/acs.chemrev.1c00905
Chem. Rev. XXXX, XXX, XXX−XXX

(1615) Hasegawa, S.; Horike, S.; Matsuda, R.; Furukawa, S.; Mochizuki, K.; Kinoshita, Y.; Kitagawa, S. Three-Dimensional Porous Coordination Polymer Functionalized with Amide Groups Based on Tridentate Ligand: Selective Sorption and Catalysis. *J. Am. Chem. Soc.* **2007**, *129*, 2607−2614.
(1616) Park, H. D.; Dinca, M.; Román-Leshkov, Y. Heterogeneous Epoxide Carbonylation by Cooperative Ion-Pair Catalysis in Co-$(CO)_4$—Incorporated Cr-MIL-101. *ACS Cent. Sci.* **2017**, *3*, 444−448.
(1617) Tahmouresilerd, B.; Larson, P. J.; Unruh, D. K.; Cozzolino, A. F. Make room for iodine: systematic pore tuning of multivariate metal-organic frameworks for the catalytic oxidation of hydroquinones using hypervalent iodine. *Catal. Sci. Technol.* **2018**, *8*, 4349−4357.
(1618) Tahmouresilerd, B.; Moody, M.; Agogo, L.; Cozzolino, A. F. The impact of an isoreticular expansion strategy on the performance of iodine catalysts supported in multivariate zirconium and aluminum metal-organic frameworks. *Dalton Trans.* **2019**, *48*, 6445−6454.
(1619) Jiang, J.; Yaghi, O. M. Brønsted Acidity in Metal-Organic Frameworks. *Chem. Rev.* **2015**, *115*, 6966−6997.
(1620) Férey, G.; Mellot-Draznieks, C.; Serre, C.; Millange, F.; Dutour, J.; Surblé, S.; Margiolaki, I. A Chromium Terephthalate-Based Solid with Unusually Large Pore Volumes and Surface Area. *Science* **2005**, *309*, 2040.
(1621) Hwang, Y. K.; Hong, D.-Y.; Chang, J.-S.; Jhung, S. H.; Seo, Y.-K.; Kim, J.; Vimont, A.; Daturi, M.; Serre, C.; Férey, G. Amine Grafting on Coordinatively Unsaturated Metal Centers of MOFs: Consequences for Catalysis and Metal Encapsulation. *Angew. Chem., Int. Ed.* **2008**, *47*, 4144−4148.
(1622) Ingleson, M. J.; Barrio, J. P.; Bacsa, J.; Dickinson, C.; Park, H.; Rosseinsky, M. J. Generation of a solid Brønsted acid site in a chiral framework. *Chem. Commun.* **2008**, 1287−1289.
(1623) Su, Y.; Chang, G.; Zhang, Z.; Xing, H.; Su, B.; Yang, Q.; Ren, Q.; Yang, Y.; Bao, Z. Catalytic dehydration of glucose to 5-hydroxymethylfurfural with a bifunctional metal-organic framework. *AIChE Journal* **2016**, *62*, 4403−4417.
(1624) Lu, G.; Li, S.; Guo, Z.; Farha, O. K.; Hauser, B. G.; Qi, X.; Wang, Y.; Wang, X.; Han, S.; Liu, X.; et al. Imparting functionality to a metal-organic framework material by controlled nanoparticle encapsulation. *Nat. Chem.* **2012**, *4*, 310−316.
(1625) Wang, Q.; Astruc, D. State of the Art and Prospects in Metal-Organic Framework (MOF)-Based and MOF-Derived Nanocatalysis. *Chem. Rev.* **2020**, *120*, 1438−1511.
(1626) Zahid, M.; Li, J.; Ismail, A.; Zaera, F.; Zhu, Y. Platinum and cobalt intermetallic nanoparticles confined within MIL-101(Cr) for enhanced selective hydrogenation of the carbonyl bond in α,β-unsaturated aldehydes: synergistic effects of electronically modified Pt sites and Lewis acid sites. *Catal. Sci. Technol.* **2021**, *11*, 2433−2445.
(1627) Na, K.; Choi, K. M.; Yaghi, O. M.; Somorjai, G. A. Metal Nanocrystals Embedded in Single Nanocrystals of MOFs Give Unusual Selectivity as Heterogeneous Catalysts. *Nano Lett.* **2014**, *14*, 5979−5983.
(1628) Choi, K. M.; Na, K.; Somorjai, G. A.; Yaghi, O. M. Chemical Environment Control and Enhanced Catalytic Performance of Platinum Nanoparticles Embedded in Nanocrystalline Metal-Organic Frameworks. *J. Am. Chem. Soc.* **2015**, *137*, 7810−7816.
(1629) Huang, G.; Yang, Q.; Xu, Q.; Yu, S.-H.; Jiang, H.-L. Polydimethylsiloxane Coating for a Palladium/MOF Composite: Highly Improved Catalytic Performance by Surface Hydrophobization. *Angew. Chem., Int. Ed.* **2016**, *55*, 7379−7383.
(1630) Rungtaweevoranit, B.; Baek, J.; Araujo, J. R.; Archanjo, B. S.; Choi, K. M.; Yaghi, O. M.; Somorjai, G. A. Copper Nanocrystals Encapsulated in Zr-based Metal-Organic Frameworks for Highly Selective CO_2 Hydrogenation to Methanol. *Nano Lett.* **2016**, *16*, 7645−7649.
(1631) Zhang, W.; Lu, G.; Cui, C.; Liu, Y.; Li, S.; Yan, W.; Xing, C.; Chi, Y. R.; Yang, Y.; Huo, F. A Family of Metal-Organic Frameworks Exhibiting Size-Selective Catalysis with Encapsulated Noble-Metal Nanoparticles. *Adv. Mater.* **2014**, *26*, 4056−4060.
(1632) Schröder, F.; Esken, D.; Cokoja, M.; van den Berg, M. W. E.; Lebedev, O. I.; Van Tendeloo, G.; Walaszek, B.; Buntkowsky, G.; Limbach, H.-H.; Chaudret, B.; et al. Ruthenium Nanoparticles inside Porous $[Zn_4O(bdc)_3]$ by Hydrogenolysis of Adsorbed [Ru(cod)-(cot)]: A Solid-State Reference System for Surfactant-Stabilized Ruthenium Colloids. *J. Am. Chem. Soc.* **2008**, *130*, 6119−6130.
(1633) Tan, Y. C.; Zeng, H. C. Lewis basicity generated by localised charge imbalance in noble metal nanoparticle-embedded defective metal-organic frameworks. *Nat. Commun.* **2018**, *9*, 4326.
(1634) Dhakshinamoorthy, A.; Garcia, H. Catalysis by metal nanoparticles embedded on metal-organic frameworks. *Chem. Soc. Rev.* **2012**, *41*, 5262−5284.
(1635) Zhu, Y.; Zhu, M.; Xia, L.; Wu, Y.; Hua, H.; Xie, J. Lanthanide Metal-Organic Frameworks with Six-Coordinated Ln(III) Ions and Free Functional Organic Sites for Adsorptions and Extensive Catalytic Activities. *Sci. Rep.* **2016**, *6*, 29728.
(1636) Song, J.; Luo, Z.; Britt, D. K.; Furukawa, H.; Yaghi, O. M.; Hardcastle, K. I.; Hill, C. L. A Multiunit Catalyst with Synergistic Stability and Reactivity: A Polyoxometalate-Metal Organic Framework for Aerobic Decontamination. *J. Am. Chem. Soc.* **2011**, *133*, 16839−16846.
(1637) Hossain, S.; Jin, M.-J.; Park, J.-h.; Yingjie, Q.; Yang, D.-A. Oxidation and Reduction of Various Substrates Over a Pd(II) Containing Post-Synthesis Metal Organic Framework. *Catal. Lett.* **2013**, *143*, 122−125.
(1638) Pan, L.; Liu, H.; Lei, X.; Huang, X.; Olson, D. H.; Turro, N. J.; Li, J. RPM-1: A Recyclable Nanoporous Material Suitable for Ship-In-Bottle Synthesis and Large Hydrocarbon Sorption. *Angew. Chem., Int. Ed.* **2003**, *42*, 542−546.
(1639) Uemura, T.; Kitaura, R.; Ohta, Y.; Nagaoka, M.; Kitagawa, S. Nanochannel-Promoted Polymerization of Substituted Acetylenes in Porous Coordination Polymers. *Angew. Chem., Int. Ed.* **2006**, *45*, 4112−4116.
(1640) Uemura, T.; Hiramatsu, D.; Kubota, Y.; Takata, M.; Kitagawa, S. Topotactic Linear Radical Polymerization of Divinylbenzenes in Porous Coordination Polymers. *Angew. Chem., Int. Ed.* **2007**, *46*, 4987−4990.
(1641) Wu, C.-D.; Hu, A.; Zhang, L.; Lin, W. A Homochiral Porous Metal-Organic Framework for Highly Enantioselective Heterogeneous Asymmetric Catalysis. *J. Am. Chem. Soc.* **2005**, *127*, 8940−8941.
(1642) Lin, W. Homochiral porous metal-organic frameworks: Why and how? *J. Solid State Chem.* **2005**, *178*, 2486−2490.
(1643) Ma, L.; Abney, C.; Lin, W. Enantioselective catalysis with homochiral metal-organic frameworks. *Chem. Soc. Rev.* **2009**, *38*, 1248−1256.
(1644) Kim, K.; Banerjee, M.; Yoon, M.; Das, S. *Functional Metal-Organic Frameworks: Gas Storage, Separation and Catalysis*; Schröder, M., Ed.; Springer Berlin Heidelberg: Berlin, Heidelberg, 2010. DOI: 10.1007/128_2009_7 10.1007/128_2009_7.
(1645) Nickerl, G.; Henschel, A.; Grünker, R.; Gedrich, K.; Kaskel, S. Chiral Metal-Organic Frameworks and Their Application in Asymmetric Catalysis and Stereoselective Separation. *Chemie Ingenieur Technik* **2011**, *83*, 90−103.
(1646) Leus, K.; Liu, Y.-Y.; Van Der Voort, P. Metal-Organic Frameworks as Selective or Chiral Oxidation Catalysts. *Catalysis Reviews* **2014**, *56*, 1−56.
(1647) Seo, J. S.; Whang, D.; Lee, H.; Jun, S. I.; Oh, J.; Jeon, Y. J.; Kim, K. A homochiral metal-organic porous material for enantioselective separation and catalysis. *Nature* **2000**, *404*, 982−986.
(1648) Cho, S.-H.; Ma, B.; Nguyen, S. T.; Hupp, J. T.; Albrecht-Schmitt, T. E. A metal-organic framework material that functions as an enantioselective catalyst for olefin epoxidation. *Chem. Commun.* **2006**, 2563−2565.
(1649) Song, F.; Zhang, T.; Wang, C.; Lin, W. Chiral porous metal-organic frameworks with dual active sites for sequential asymmetric catalysis. *Proc. R. Soc. A* **2012**, *468*, 2035−2052.
(1650) Kepert, C. J.; Prior, T. J.; Rosseinsky, M. J. A Versatile Family of Interconvertible Microporous Chiral Molecular Frameworks: The First Example of Ligand Control of Network Chirality. *J. Am. Chem. Soc.* **2000**, *122*, 5158−5168.

https://doi.org/10.1021/acs.chemrev.1c00905
Chem. Rev. XXXX, XXX, XXX−XXX

(1651) Lin, Z.; Slawin, A. M. Z.; Morris, R. E. Chiral Induction in the Ionothermal Synthesis of a 3-D Coordination Polymer. *J. Am. Chem. Soc.* **2007**, *129*, 4880−4881.
(1652) Ezuhara, T.; Endo, K.; Aoyama, Y. Helical Coordination Polymers from Achiral Components in Crystals. Homochiral Crystallization, Homochiral Helix Winding in the Solid State, and Chirality Control by Seeding. *J. Am. Chem. Soc.* **1999**, *121*, 3279−3283.
(1653) Wu, S.-T.; Wu, Y.-R.; Kang, Q.-Q.; Zhang, H.; Long, L.-S.; Zheng, Z.; Huang, R.-B.; Zheng, L.-S. Chiral Symmetry Breaking by Chemically Manipulating Statistical Fluctuation in Crystallization. *Angew. Chem., Int. Ed.* **2007**, *46*, 8475−8479.
(1654) Banerjee, M.; Das, S.; Yoon, M.; Choi, H. J.; Hyun, M. H.; Park, S. M.; Seo, G.; Kim, K. Postsynthetic Modification Switches an Achiral Framework to Catalytically Active Homochiral Metal-Organic Porous Materials. *J. Am. Chem. Soc.* **2009**, *131*, 7524−7525.
(1655) Cohen, S. M. Postsynthetic Methods for the Functionalization of Metal-Organic Frameworks. *Chem. Rev.* **2012**, *112*, 970−1000.
(1656) Xi, W.; Liu, Y.; Xia, Q.; Li, Z.; Cui, Y. Direct and Post-Synthesis Incorporation of Chiral Metallosalen Catalysts into Metal-Organic Frameworks for Asymmetric Organic Transformations. *Chem.-Eur. J.* **2015**, *21*, 12581−12585.
(1657) Tan, C.; Han, X.; Li, Z.; Liu, Y.; Cui, Y. Controlled Exchange of Achiral Linkers with Chiral Linkers in Zr-Based UiO-68 Metal-Organic Framework. *J. Am. Chem. Soc.* **2018**, *140*, 16229−16236.
(1658) Song, F.; Wang, C.; Falkowski, J. M.; Ma, L.; Lin, W. Isoreticular Chiral Metal-Organic Frameworks for Asymmetric Alkene Epoxidation: Tuning Catalytic Activity by Controlling Framework Catenation and Varying Open Channel Sizes. *J. Am. Chem. Soc.* **2010**, *132*, 15390−15398.
(1659) Dang, D.; Wu, P.; He, C.; Xie, Z.; Duan, C. Homochiral Metal-Organic Frameworks for Heterogeneous Asymmetric Catalysis. *J. Am. Chem. Soc.* **2010**, *132*, 14321−14323.
(1660) Jeong, K. S.; Go, Y. B.; Shin, S. M.; Lee, S. J.; Kim, J.; Yaghi, O. M.; Jeong, N. Asymmetric catalytic reactions by NbO-type chiral metal-organic frameworks. *Chem. Sci.* **2011**, *2*, 877−882.
(1661) Gedrich, K.; Heitbaum, M.; Notzon, A.; Senkovska, I.; Fröhlich, R.; Getzschmann, J.; Mueller, U.; Glorius, F.; Kaskel, S. A Family of Chiral Metal-Organic Frameworks. *Chem.-Eur. J.* **2011**, *17*, 2099−2106.
(1662) Wu, P.; He, C.; Wang, J.; Peng, X.; Li, X.; An, Y.; Duan, C. Photoactive Chiral Metal-Organic Frameworks for Light-Driven Asymmetric α-Alkylation of Aldehydes. *J. Am. Chem. Soc.* **2012**, *134*, 14991−14999.
(1663) Zhu, C.; Xia, Q.; Chen, X.; Liu, Y.; Du, X.; Cui, Y. Chiral Metal-Organic Framework as a Platform for Cooperative Catalysis in Asymmetric Cyanosilylation of Aldehydes. *ACS Catal.* **2016**, *6*, 7590−7596.
(1664) Zhang, Y.; Guo, J.; Shi, L.; Zhu, Y.; Hou, K.; Zheng, Y.; Tang, Z. Tunable chiral metal organic frameworks toward visible light-driven asymmetric catalysis. *Science Advances* **2017**, *3*, No. e1701162.
(1665) Xia, Q.; Li, Z.; Tan, C.; Liu, Y.; Gong, W.; Cui, Y. Multivariate Metal-Organic Frameworks as Multifunctional Heterogeneous Asymmetric Catalysts for Sequential Reactions. *J. Am. Chem. Soc.* **2017**, *139*, 8259−8266.
(1666) Nguyen, K. D.; Kutzscher, C.; Drache, F.; Senkovska, I.; Kaskel, S. Chiral Functionalization of a Zirconium Metal-Organic Framework (DUT-67) as a Heterogeneous Catalyst in Asymmetric Michael Addition Reaction. *Inorg. Chem.* **2018**, *57*, 1483−1489.
(1667) Gong, W.; Chen, X.; Jiang, H.; Chu, D.; Cui, Y.; Liu, Y. Highly Stable Zr(IV)-Based Metal-Organic Frameworks with Chiral Phosphoric Acids for Catalytic Asymmetric Tandem Reactions. *J. Am. Chem. Soc.* **2019**, *141*, 7498−7508.
(1668) Jiang, H.; Zhang, W.; Kang, X.; Cao, Z.; Chen, X.; Liu, Y.; Cui, Y. Topology-Based Functionalization of Robust Chiral Zr-Based Metal-Organic Frameworks for Catalytic Enantioselective Hydrogenation. *J. Am. Chem. Soc.* **2020**, *142*, 9642−9652.
(1669) Jeong, K. S.; Go, Y. B.; Shin, S. M.; Lee, S. J.; Kim, J.; Yaghi, O. M.; Jeong, N. Asymmetric catalytic reactions by NbO-type chiral metal-organic frameworks. *Chem. Sci.* **2011**, *2*, 877−882.
(1670) Côté Adrien, P.; Benin Annabelle, I.; Ockwig Nathan, W.; O'Keeffe, M.; Matzger Adam, J.; Yaghi Omar, M. Porous, Crystalline, Covalent Organic Frameworks. *Science* **2005**, *310*, 1166−1170.
(1671) Bleschke, C.; Schmidt, J.; Kundu, D. S.; Blechert, S.; Thomas, A. A Chiral Microporous Polymer Network as Asymmetric Heterogeneous Organocatalyst. *Adv. Synth. Catal.* **2011**, *353*, 3101−3106.
(1672) Kraft, S. J.; Zhang, G.; Childers, D.; Dogan, F.; Miller, J. T.; Nguyen, S. T.; Hock, A. S. Rhodium Catechol Containing Porous Organic Polymers: Defined Catalysis for Single-Site and Supported Nanoparticulate Materials. *Organometallics* **2014**, *33*, 2517−2522.
(1673) Bavykina, A. V.; Goesten, M. G.; Kapteijn, F.; Makkee, M.; Gascon, J. Efficient production of hydrogen from formic acid using a Covalent Triazine Framework supported molecular catalyst. *ChemSusChem* **2015**, *8*, 809−812.
(1674) Hu, H.; Yan, Q.; Ge, R.; Gao, Y. Covalent organic frameworks as heterogeneous catalysts. *Chin. J. Catal.* **2018**, *39*, 1167−1179.
(1675) Han, Y.; Zhang, M.; Zhang, Y.-Q.; Zhang, Z.-H. Copper immobilized at a covalent organic framework: an efficient and recyclable heterogeneous catalyst for the Chan-Lam coupling reaction of aryl boronic acids and amines. *Green Chem.* **2018**, *20*, 4891−4900.
(1676) Zhi, Y.; Wang, Z.; Zhang, H.-L.; Zhang, Q. Recent Progress in Metal-Free Covalent Organic Frameworks as Heterogeneous Catalysts. *Small* **2020**, *16*, 2001070.
(1677) Chen, M.; Zhang, J.; Liu, C.; Li, H.; Yang, H.; Feng, Y.; Zhang, B. Construction of Pyridine-Based Chiral Ionic Covalent Organic Frameworks as a Heterogeneous Catalyst for Promoting Asymmetric Henry Reactions. *Organic Letters* **2021**, *23*, 1748−1752.
(1678) Khaing, K. K.; Yin, D.; Ouyang, Y.; Xiao, S.; Liu, B.; Deng, L.; Li, L.; Guo, X.; Wang, J.; Liu, J.; et al. Fabrication of 2D-2D Heterojunction Catalyst with Covalent Organic Framework (COF) and MoS_2 for Highly Efficient Photocatalytic Degradation of Organic Pollutants. *Inorg. Chem.* **2020**, *59*, 6942−6952.
(1679) Sarkar, P.; Riyajuddin, S.; Das, A.; Hazra Chowdhury, A.; Ghosh, K.; Islam, S. M. Mesoporous covalent organic framework: An active photo-catalyst for formic acid synthesis through carbon dioxide reduction under visible light. *Molecular Catalysis* **2020**, *484*, 110730.
(1680) Banerjee, T.; Haase, F.; Savasci, G.; Gottschling, K.; Ochsenfeld, C.; Lotsch, B. V. Single-Site Photocatalytic H_2 Evolution from Covalent Organic Frameworks with Molecular Cobaloxime Co-Catalysts. *J. Am. Chem. Soc.* **2017**, *139*, 16228−16234.
(1681) Peng, Y.; Hu, Z.; Gao, Y.; Yuan, D.; Kang, Z.; Qian, Y.; Yan, N.; Zhao, D. Synthesis of a Sulfonated Two-Dimensional Covalent Organic Framework as an Efficient Solid Acid Catalyst for Biobased Chemical Conversion. *ChemSusChem* **2015**, *8*, 3208−3212.
(1682) Mu, Z.-J.; Ding, X.; Chen, Z.-Y.; Han, B.-H. Zwitterionic Covalent Organic Frameworks as Catalysts for Hierarchical Reduction of CO_2 with Amine and Hydrosilane. *ACS Appl. Mater. Interfaces* **2018**, *10*, 41350−41358.
(1683) Wu, Y.; Xu, H.; Chen, X.; Gao, J.; Jiang, D. A π-electronic covalent organic framework catalyst: π-walls as catalytic beds for Diels-Alder reactions under ambient conditions. *Chem. Commun.* **2015**, *51*, 10096−10098.
(1684) Voiry, D.; Mohite, A.; Chhowalla, M. Phase engineering of transition metal dichalcogenides. *Chem. Soc. Rev.* **2015**, *44*, 2702−2712.
(1685) Rao, C. N. R.; Gopalakrishnan, K.; Maitra, U. Comparative Study of Potential Applications of Graphene, MoS_2, and Other Two-Dimensional Materials in Energy Devices, Sensors, and Related Areas. *ACS Appl. Mater. Interfaces* **2015**, *7*, 7809−7832.
(1686) Breysse, M.; Djega-Mariadassou, G.; Pessayre, S.; Geantet, C.; Vrinat, M.; Pérot, G.; Lemaire, M. Deep desulfurization: reactions, catalysts and technological challenges. *Catal. Today* **2003**, *84*, 129−138.

https://doi.org/10.1021/acs.chemrev.1c00905
Chem. Rev. XXXX, XXX, XXX−XXX

(1687) Topsøe, H. The role of Co-Mo-S type structures in hydrotreating catalysts. *Appl. Catal. A* **2007**, *322*, 3−8.
(1688) Stanislaus, A.; Marafi, A.; Rana, M. S. Recent advances in the science and technology of ultra low sulfur diesel (ULSD) production. *Catal. Today* **2010**, *153*, 1−68.
(1689) Javadli, R.; de Klerk, A. Desulfurization of heavy oil. *Applied Petrochemical Research* **2012**, *1*, 3−19.
(1690) de León, J. N. D.; Kumar, C. R.; Antúnez-García, J.; Fuentes-Moyado, S. Recent insights in transition metal sulfide hydrodesulfurization catalysts for the production of ultra low sulfur diesel: A short review. *Catalysts* **2019**, *9*, 87.
(1691) Speight, J. G. *Heavy Oil Recovery and Upgrading*; Speight, J. G., Ed.; Gulf Professional Publishing, 2019.
(1692) Mortensen, P. M.; Grunwaldt, J. D.; Jensen, P. A.; Knudsen, K. G.; Jensen, A. D. A review of catalytic upgrading of bio-oil to engine fuels. *Appl. Catal. A* **2011**, *407*, 1−19.
(1693) Saidi, M.; Samimi, F.; Karimipourfard, D.; Nimmanwudipong, T.; Gates, B. C.; Rahimpour, M. R. Upgrading of lignin-derived bio-oils by catalytic hydrodeoxygenation. *Energy Environm. Sci.* **2014**, *7*, 103−129.
(1694) Besenbacher, F.; Brorson, M.; Clausen, B. S.; Helveg, S.; Hinnemann, B.; Kibsgaard, J.; Lauritsen, J. V.; Moses, P. G.; Nørskov, J. K.; Topsøe, H. Recent STM, DFT and HAADF-STEM studies of sulfide-based hydrotreating catalysts: Insight into mechanistic, structural and particle size effects. *Catal. Today* **2008**, *130*, 86−96.
(1695) Hansen, L. P.; Ramasse, Q. M.; Kisielowski, C.; Brorson, M.; Johnson, E.; Topsøe, H.; Helveg, S. Atomic-Scale Edge Structures on Industrial-Style MoS_2 Nanocatalysts. *Angew. Chem., Int. Ed.* **2011**, *50*, 10153−10156.
(1696) Zhu, Y.; Ramasse, Q. M.; Brorson, M.; Moses, P. G.; Hansen, L. P.; Kisielowski, C. F.; Helveg, S. Visualizing the Stoichiometry of Industrial-Style Co-Mo-S Catalysts with Single-Atom Sensitivity. *Angew. Chem., Int. Ed.* **2014**, *53*, 10723−10727.
(1697) Bruix, A.; Füchtbauer, H. G.; Tuxen, A. K.; Walton, A. S.; Andersen, M.; Porsgaard, S.; Besenbacher, F.; Hammer, B.; Lauritsen, J. V. In Situ Detection of Active Edge Sites in Single-Layer MoS_2 Catalysts. *ACS Nano* **2015**, *9*, 9322−9330.
(1698) Lauritsen, J. V.; Nyberg, M.; Nørskov, J. K.; Clausen, B. S.; Topsøe, H.; Lægsgaard, E.; Besenbacher, F. Hydrodesulfurization reaction pathways on MoS_2 nanoclusters revealed by scanning tunneling microscopy. *J. Catal.* **2004**, *224*, 94−106.
(1699) Grønborg, S. S.; Salazar, N.; Bruix, A.; Rodríguez-Fernández, J.; Thomsen, S. D.; Hammer, B.; Lauritsen, J. V. Visualizing hydrogen-induced reshaping and edge activation in MoS_2 and Co-promoted MoS_2 catalyst clusters. *Nat. Commun.* **2018**, *9*, 2211.
(1700) Hansen, L. P.; Ramasse, Q. M.; Kisielowski, C.; Brorson, M.; Johnson, E.; Topsøe, H.; Helveg, S. Atomic-Scale Edge Structures on Industrial-Style MoS_2 Nanocatalysts. *Angew. Chem., Int. Ed.* **2011**, *50*, 10153−10156.
(1701) Albiter, M. A.; Huirache-Acuña, R.; Paraguay-Delgado, F.; Zaera, F.; Alonso-Nuñez, G. Co(Ni)/MoS_2 nanostructured catalysts for the hydrodesulphurization of dibenzothiophene. *J. Nanosci. Nanotechnol.* **2008**, *8*, 6437−6444.
(1702) Lauritsen, J. V.; Kibsgaard, J.; Olesen, G. H.; Moses, P. G.; Hinnemann, B.; Helveg, S.; Nørskov, J. K.; Clausen, B. S.; Topsøe, H.; Lægsgaard, E.; et al. Location and coordination of promoter atoms in Co- and Ni-promoted MoS_2-based hydrotreating catalysts. *J. Catal.* **2007**, *249*, 220−233.
(1703) Wu, Z.; Fang, B.; Wang, Z.; Wang, C.; Liu, Z.; Liu, F.; Wang, W.; Alfantazi, A.; Wang, D.; Wilkinson, D. P. MoS_2 Nanosheets: A Designed Structure with High Active Site Density for the Hydrogen Evolution Reaction. *ACS Catal.* **2013**, *3*, 2101−2107.
(1704) Maitra, U.; Gupta, U.; De, M.; Datta, R.; Govindaraj, A.; Rao, C. N. R. Highly Effective Visible-Light-Induced H_2 Generation by Single-Layer 1T-MoS_2 and a Nanocomposite of Few-Layer 2H-MoS_2 with Heavily Nitrogenated Graphene. *Angew. Chem., Int. Ed.* **2013**, *52*, 13057−13061.
(1705) Voiry, D.; Yang, J.; Chhowalla, M. Recent Strategies for Improving the Catalytic Activity of 2D TMD Nanosheets Toward the Hydrogen Evolution Reaction. *Adv. Mater.* **2016**, *28*, 6197−6206.
(1706) Hu, J.; Huang, B.; Zhang, C.; Wang, Z.; An, Y.; Zhou, D.; Lin, H.; Leung, M. K. H.; Yang, S. Engineering stepped edge surface structures of MoS_2 sheet stacks to accelerate the hydrogen evolution reaction. *Energy Environm. Sci.* **2017**, *10*, 593−603.
(1707) Gupta, U.; Rao, C. N. R. Hydrogen generation by water splitting using MoS_2 and other transition metal dichalcogenides. *Nano Energy* **2017**, *41*, 49−65.
(1708) Ganguly, P.; Harb, M.; Cao, Z.; Cavallo, L.; Breen, A.; Dervin, S.; Dionysiou, D. D.; Pillai, S. C. 2D Nanomaterials for Photocatalytic Hydrogen Production. *ACS Energy Letters* **2019**, *4*, 1687−1709.
(1709) Xie, J.; Zhang, H.; Li, S.; Wang, R.; Sun, X.; Zhou, M.; Zhou, J.; Lou, X. W.; Xie, Y. Defect-Rich MoS_2 Ultrathin Nanosheets with Additional Active Edge Sites for Enhanced Electrocatalytic Hydrogen Evolution. *Adv. Mater.* **2013**, *25*, 5807−5813.
(1710) Wang, T.; Gao, D.; Zhuo, J.; Zhu, Z.; Papakonstantinou, P.; Li, Y.; Li, M. Size-Dependent Enhancement of Electrocatalytic Oxygen-Reduction and Hydrogen-Evolution Performance of MoS_2 Particles. *Chem.-Eur. J.* **2013**, *19*, 11939−11948.
(1711) Eng, A. Y. S.; Ambrosi, A.; Sofer, Z.; Šimek, P.; Pumera, M. Electrochemistry of Transition Metal Dichalcogenides: Strong Dependence on the Metal-to-Chalcogen Composition and Exfoliation Method. *ACS Nano* **2014**, *8*, 12185−12198.
(1712) Li, G.; Fu, C.; Wu, J.; Rao, J.; Liou, S.-C.; Xu, X.; Shao, B.; Liu, K.; Liu, E.; Kumar, N.; et al. Synergistically creating sulfur vacancies in semimetal-supported amorphous MoS_2 for efficient hydrogen evolution. *Appl. Catal. B* **2019**, *254*, 1−6.
(1713) Huang, J.; Jiang, Y.; An, T.; Cao, M. Increasing the active sites and intrinsic activity of transition metal chalcogenide electrocatalysts for enhanced water splitting. *J. Mater. Chem. A* **2020**, *8*, 25465−25498.
(1714) Yan, Y.; Wang, P.; Lin, J.; Cao, J.; Qi, J. Modification strategies on transition metal-based electrocatalysts for efficient water splitting. *Journal of Energy Chemistry* **2021**, *58*, 446−462.
(1715) Liang, Z.; Shen, R.; Ng, Y. H.; Zhang, P.; Xiang, Q.; Li, X. A review on 2D MoS_2 cocatalysts in photocatalytic H_2 production. *Journal of Materials Science & Technology* **2020**, *56*, 89−121.
(1716) Seo, B.; Jung, G. Y.; Sa, Y. J.; Jeong, H. Y.; Cheon, J. Y.; Lee, J. H.; Kim, H. Y.; Kim, J. C.; Shin, H. S.; Kwak, S. K.; et al. Monolayer-Precision Synthesis of Molybdenum Sulfide Nanoparticles and Their Nanoscale Size Effects in the Hydrogen Evolution Reaction. *ACS Nano* **2015**, *9*, 3728−3739.
(1717) Liu, Y.; Cheng, H.; Lyu, M.; Fan, S.; Liu, Q.; Zhang, W.; Zhi, Y.; Wang, C.; Xiao, C.; Wei, S.; et al. Low Overpotential in Vacancy-Rich Ultrathin $CoSe_2$ Nanosheets for Water Oxidation. *J. Am. Chem. Soc.* **2014**, *136*, 15670−15675.
(1718) Merki, D.; Fierro, S.; Vrubel, H.; Hu, X. Amorphous molybdenum sulfide films as catalysts for electrochemical hydrogen production in water. *Chem. Sci.* **2011**, *2*, 1262−1267.
(1719) Machado, B. F.; Serp, P. Graphene-based materials for catalysis. *Catal. Sci. Technol.* **2012**, *2*, 54−75.
(1720) Huang, C.; Li, C.; Shi, G. Graphene based catalysts. *Energy Environm. Sci.* **2012**, *5*, 8848−8868.
(1721) Navalon, S.; Dhakshinamoorthy, A.; Alvaro, M.; Garcia, H. Carbocatalysis by Graphene-Based Materials. *Chem. Rev.* **2014**, *114*, 6179−6212.
(1722) Kong, X.-K.; Chen, C.-L.; Chen, Q.-W. Doped graphene for metal-free catalysis. *Chem. Soc. Rev.* **2014**, *43*, 2841−2857.
(1723) Deng, D.; Novoselov, K. S.; Fu, Q.; Zheng, N.; Tian, Z.; Bao, X. Catalysis with two-dimensional materials and their heterostructures. *Nat. Nanotechnol.* **2016**, *11*, 218−230.
(1724) Sereda, G. A.; Rajpara, V. B.; Slaba, R. L. The synthetic potential of graphite-catalyzed alkylation. *Tetrahedron* **2007**, *63*, 8351−8357.
(1725) *Carbon Materials for Catalysis Ed.(s): First published: Print*; Serp, P., Figueiredo, J. L., Eds.; John Wiley & Sons, Inc.: Hoboken,

https://doi.org/10.1021/acs.chemrev.1c00905
Chem. Rev. XXXX, XXX, XXX−XXX

New Jersey, 2009. DOI: 10.1002/9780470403709 10.1002/9780470403709.
(1726) Zheng, Y.; Jiao, Y.; Jaroniec, M.; Jin, Y.; Qiao, S. Z. Nanostructured Metal-Free Electrochemical Catalysts for Highly Efficient Oxygen Reduction. *Small* **2012**, *8*, 3550−3566.
(1727) Zhai, Y.; Zhu, Z.; Dong, S. Carbon-Based Nanostructures for Advanced Catalysis. *ChemCatChem.* **2015**, *7*, 2806−2815.
(1728) Chandrasekaran, S.; Campbell, P. G.; Baumann, T. F.; Worsley, M. A. Carbon aerogel evolution: Allotrope, graphene-inspired, and 3D-printed aerogels. *J. Mater. Res.* **2017**, *32*, 4166−4185.
(1729) Zhao, Q.; Mao, Q.; Zhou, Y.; Wei, J.; Liu, X.; Yang, J.; Luo, L.; Zhang, J.; Chen, H.; Chen, H.; et al. Metal-free carbon materials-catalyzed sulfate radical-based advanced oxidation processes: A review on heterogeneous catalysts and applications. *Chemosphere* **2017**, *189*, 224−238.
(1730) Chen, L.; Hernandez, Y.; Feng, X.; Müllen, K. From Nanographene and Graphene Nanoribbons to Graphene Sheets: Chemical Synthesis. *Angew. Chem., Int. Ed.* **2012**, *51*, 7640−7654.
(1731) Luo, B.; Liu, S.; Zhi, L. Chemical Approaches toward Graphene-Based Nanomaterials and their Applications in Energy-Related Areas. *Small* **2012**, *8*, 630−646.
(1732) Novoselov, K. S.; Fal'ko, V. I.; Colombo, L.; Gellert, P. R.; Schwab, M. G.; Kim, K. A roadmap for graphene. *Nature* **2012**, *490*, 192−200.
(1733) Wang, Q.; Wang, X.; Chai, Z.; Hu, W. Low-temperature plasma synthesis of carbon nanotubes and graphene based materials and their fuel cell applications. *Chem. Soc. Rev.* **2013**, *42*, 8821−8834.
(1734) Sarkar, S.; Niyogi, S.; Bekyarova, E.; Haddon, R. C. Organometallic chemistry of extended periodic π-electron systems: hexahapto-chromium complexes of graphene and single-walled carbon nanotubes. *Chem. Sci.* **2011**, *2*, 1326−1333.
(1735) Navalon, S.; Dhakshinamoorthy, A.; Alvaro, M.; Garcia, H. Metal nanoparticles supported on two-dimensional graphenes as heterogeneous catalysts. *Coord. Chem. Rev.* **2016**, *312*, 99−148.
(1736) Paraknowitsch, J. P.; Thomas, A. Doping carbons beyond nitrogen: an overview of advanced heteroatom doped carbons with boron, sulphur and phosphorus for energy applications. *Energy Environm. Sci.* **2013**, *6*, 2839−2855.
(1737) Antolini, E. Graphene as a new carbon support for low-temperature fuel cell catalysts. *Appl. Catal. B* **2012**, *123-124*, 52−68.
(1738) Zhu, J.; Holmen, A.; Chen, D. Carbon Nanomaterials in Catalysis: Proton Affinity, Chemical and Electronic Properties, and their Catalytic Consequences. *ChemCatChem.* **2013**, *5*, 378−401.
(1739) Zhao, S.; Wang, D.-W.; Amal, R.; Dai, L. Carbon-Based Metal-Free Catalysts for Key Reactions Involved in Energy Conversion and Storage. *Adv. Mater.* **2019**, *31*, 1801526.
(1740) An, X.; Yu, J. C. Graphene-based photocatalytic composites. *RSC Adv.* **2011**, *1*, 1426−1434.
(1741) Latorre-Sánchez, M.; Primo, A.; García, H. P-Doped Graphene Obtained by Pyrolysis of Modified Alginate as a Photocatalyst for Hydrogen Generation from Water-Methanol Mixtures. *Angew. Chem., Int. Ed.* **2013**, *52*, 11813−11816.
(1742) Guo, D.; Shibuya, R.; Akiba, C.; Saji, S.; Kondo, T.; Nakamura, J. Active sites of nitrogen-doped carbon materials for oxygen reduction reaction clarified using model catalysts. *Science* **2016**, *351*, 361.
(1743) Dreyer, D. R.; Park, S.; Bielawski, C. W.; Ruoff, R. S. The chemistry of graphene oxide. *Chem. Soc. Rev.* **2010**, *39*, 228−240.
(1744) Su, C.; Loh, K. P. Carbocatalysts: Graphene Oxide and Its Derivatives. *Acc. Chem. Res.* **2013**, *46*, 2275−2285.
(1745) Loh, K. P.; Bao, Q.; Ang, P. K.; Yang, J. The chemistry of graphene. *J. Mater. Chem.* **2010**, *20*, 2277−2289.
(1746) Banhart, F.; Kotakoski, J.; Krasheninnikov, A. V. Structural Defects in Graphene. *ACS Nano* **2011**, *5*, 26−41.
(1747) Navalon, S.; Dhakshinamoorthy, A.; Alvaro, M.; Antonietti, M.; García, H. Active sites on graphene-based materials as metal-free catalysts. *Chem. Soc. Rev.* **2017**, *46*, 4501−4529.
(1748) Deng, D.; Chen, X.; Yu, L.; Wu, X.; Liu, Q.; Liu, Y.; Yang, H.; Tian, H.; Hu, Y.; Du, P.; et al. A single iron site confined in a graphene matrix for the catalytic oxidation of benzene at room temperature. *Science Advances* **2015**, *1*, No. e1500462.
(1749) Cheng, N.; Stambula, S.; Wang, D.; Banis, M. N.; Liu, J.; Riese, A.; Xiao, B.; Li, R.; Sham, T.-K.; Liu, L.-M.; et al. Platinum single-atom and cluster catalysis of the hydrogen evolution reaction. *Nat. Commun.* **2016**, *7*, 13638.
(1750) Li, X.; Huang, X.; Xi, S.; Miao, S.; Ding, J.; Cai, W.; Liu, S.; Yang, X.; Yang, H.; Gao, J.; et al. Single Cobalt Atoms Anchored on Porous N-Doped Graphene with Dual Reaction Sites for Efficient Fenton-like Catalysis. *J. Am. Chem. Soc.* **2018**, *140*, 12469−12475.
(1751) Qu, L.; Liu, Y.; Baek, J.-B.; Dai, L. Nitrogen-Doped Graphene as Efficient Metal-Free Electrocatalyst for Oxygen Reduction in Fuel Cells. *ACS Nano* **2010**, *4*, 1321−1326.
(1752) Wang, H.; Wang, Q.; Cheng, Y.; Li, K.; Yao, Y.; Zhang, Q.; Dong, C.; Wang, P.; Schwingenschlögl, U.; Yang, W.; et al. Doping Monolayer Graphene with Single Atom Substitutions. *Nano Lett.* **2012**, *12*, 141−144.
(1753) Zheng, Y.; Jiao, Y.; Ge, L.; Jaroniec, M.; Qiao, S. Z. Two-Step Boron and Nitrogen Doping in Graphene for Enhanced Synergistic Catalysis. *Angew. Chem., Int. Ed.* **2013**, *52*, 3110−3116.
(1754) Tang, Q.; Zhou, Z.; Chen, Z. Graphene-related nanomaterials: tuning properties by functionalization. *Nanoscale* **2013**, *5*, 4541−4583.
(1755) Hu, C.; Dai, L. Doping of Carbon Materials for Metal-Free Electrocatalysis. *Adv. Mater.* **2019**, *31*, 1804672.
(1756) Sheng, Z.-H.; Gao, H.-L.; Bao, W.-J.; Wang, F.-B.; Xia, X.-H. Synthesis of boron doped graphene for oxygen reduction reaction in fuel cells. *J. Mater. Chem.* **2012**, *22*, 390−395.
(1757) Sreekanth, N.; Nazrulla, M. A.; Vineesh, T. V.; Sailaja, K.; Phani, K. L. Metal-free boron-doped graphene for selective electroreduction of carbon dioxide to formic acid/formate. *Chem. Commun.* **2015**, *51*, 16061−16064.
(1758) Kong, X.; Huang, Y.; Liu, Q. Two-dimensional boron-doped graphyne nanosheet: A new metal-free catalyst for oxygen evolution reaction. *Carbon* **2017**, *123*, 558−564.
(1759) Mao, X.; Kour, G.; Zhang, L.; He, T.; Wang, S.; Yan, C.; Zhu, Z.; Du, A. Silicon-doped graphene edges: an efficient metal-free catalyst for the reduction of CO_2 into methanol and ethanol. *Catal. Sci. Technol.* **2019**, *9*, 6800−6807.
(1760) Zhang, C.; Mahmood, N.; Yin, H.; Liu, F.; Hou, Y. Synthesis of Phosphorus-Doped Graphene and its Multifunctional Applications for Oxygen Reduction Reaction and Lithium Ion Batteries. *Adv. Mater.* **2013**, *25*, 4932−4937.
(1761) Yang, Z.; Yao, Z.; Li, G.; Fang, G.; Nie, H.; Liu, Z.; Zhou, X.; Chen, X. a.; Huang, S. Sulfur-Doped Graphene as an Efficient Metal-free Cathode Catalyst for Oxygen Reduction. *ACS Nano* **2012**, *6*, 205−211.
(1762) Jeon, I.-Y.; Zhang, S.; Zhang, L.; Choi, H.-J.; Seo, J.-M.; Xia, Z.; Dai, L.; Baek, J.-B. Edge-Selectively Sulfurized Graphene Nanoplatelets as Efficient Metal-Free Electrocatalysts for Oxygen Reduction Reaction: The Electron Spin Effect. *Adv. Mater.* **2013**, *25*, 6138−6145.
(1763) Jin, Z.; Nie, H.; Yang, Z.; Zhang, J.; Liu, Z.; Xu, X.; Huang, S. Metal-free selenium doped carbon nanotube/graphene networks as a synergistically improved cathode catalyst for oxygen reduction reaction. *Nanoscale* **2012**, *4*, 6455−6460.
(1764) Yao, Z.; Nie, H.; Yang, Z.; Zhou, X.; Liu, Z.; Huang, S. Catalyst-free synthesis of iodine-doped graphenevia a facile thermal annealing process and its use for electrocatalytic oxygen reduction in an alkaline medium. *Chem. Commun.* **2012**, *48*, 1027−1029.
(1765) Liang, J.; Jiao, Y.; Jaroniec, M.; Qiao, S. Z. Sulfur and Nitrogen Dual-Doped Mesoporous Graphene Electrocatalyst for Oxygen Reduction with Synergistically Enhanced Performance. *Angew. Chem., Int. Ed.* **2012**, *51*, 11496−11500.
(1766) Zhang, J.; Zhao, Z.; Xia, Z.; Dai, L. A metal-free bifunctional electrocatalyst for oxygen reduction and oxygen evolution reactions. *Nat. Nanotechnol.* **2015**, *10*, 444−452.

https://doi.org/10.1021/acs.chemrev.1c00905
Chem. Rev. XXXX, XXX, XXX−XXX

(1767) Tang, L.; Meng, X.; Deng, D.; Bao, X. Confinement Catalysis with 2D Materials for Energy Conversion. *Adv. Mater.* **2019**, *31*, 1901996.
(1768) Dreyer, D. R.; Bielawski, C. W. Carbocatalysis: Heterogeneous carbons finding utility in synthetic chemistry. *Chem. Sci.* **2011**, *2*, 1233−1240.
(1769) Jia, H.-P.; Dreyer, D. R.; Bielawski, C. W. C-H oxidation using graphite oxide. *Tetrahedron* **2011**, *67*, 4431−4434.
(1770) Dreyer, D. R.; Jia, H.-P.; Bielawski, C. W. Graphene Oxide: A Convenient Carbocatalyst for Facilitating Oxidation and Hydration Reactions. *Angew. Chem., Int. Ed.* **2010**, *49*, 6813−6816.
(1771) Boukhvalov, D. W.; Dreyer, D. R.; Bielawski, C. W.; Son, Y.-W. A Computational Investigation of the Catalytic Properties of Graphene Oxide: Exploring Mechanisms by using DFT Methods. *ChemCatChem.* **2012**, *4*, 1844−1849.
(1772) Vijay Kumar, A.; Rama Rao, K. Recyclable graphite oxide catalyzed Friedel-Crafts addition of indoles to α,β-unsaturated ketones. *Tetrahedron Lett.* **2011**, *52*, 5188−5191.
(1773) Verma, S.; Mungse, H. P.; Kumar, N.; Choudhary, S.; Jain, S. L.; Sain, B.; Khatri, O. P. Graphene oxide: an efficient and reusable carbocatalyst for aza-Michael addition of amines to activated alkenes. *Chem. Commun.* **2011**, *47*, 12673−12675.
(1774) Dreyer, D. R.; Jarvis, K. A.; Ferreira, P. J.; Bielawski, C. W. Graphite oxide as a carbocatalyst for the preparation of fullerene-reinforced polyester and polyamide nanocomposites. *Polym. Chem.* **2012**, *3*, 757−766.
(1775) Hu, F.; Patel, M.; Luo, F.; Flach, C.; Mendelsohn, R.; Garfunkel, E.; He, H.; Szostak, M. Graphene-Catalyzed Direct Friedel-Crafts Alkylation Reactions: Mechanism, Selectivity, and Synthetic Utility. *J. Am. Chem. Soc.* **2015**, *137*, 14473−14480.
(1776) Su, D. S.; Zhang, J.; Frank, B.; Thomas, A.; Wang, X.; Paraknowitsch, J.; Schlögl, R. Metal-Free Heterogeneous Catalysis for Sustainable Chemistry. *ChemSusChem* **2010**, *3*, 169−180.
(1777) Kim, J.; Cote, L. J.; Kim, F.; Yuan, W.; Shull, K. R.; Huang, J. Graphene Oxide Sheets at Interfaces. *J. Am. Chem. Soc.* **2010**, *132*, 8180−8186.
(1778) Zheng, Y.; Liu, J.; Liang, J.; Jaroniec, M.; Qiao, S. Z. Graphitic carbon nitride materials: controllable synthesis and applications in fuel cells and photocatalysis. *Energy Environm. Sci.* **2012**, *5*, 6717−6731.
(1779) Zhu, C.; Dong, S. Recent progress in graphene-based nanomaterials as advanced electrocatalysts towards oxygen reduction reaction. *Nanoscale* **2013**, *5*, 1753−1767.
(1780) Zhao, Z.; Sun, Y.; Dong, F. Graphitic carbon nitride based nanocomposites: a review. *Nanoscale* **2015**, *7*, 15−37.
(1781) Reddy, K. R.; Reddy, C. H. V.; Nadagouda, M. N.; Shetti, N. P.; Jaesool, S.; Aminabhavi, T. M. Polymeric graphitic carbon nitride ($g\text{-}C_3N_4$)-based semiconducting nanostructured materials: Synthesis methods, properties and photocatalytic applications. *Journal of Environmental Management* **2019**, *238*, 25−40.
(1782) Zhang, C.; Li, Y.; Shuai, D.; Shen, Y.; Xiong, W.; Wang, L. Graphitic carbon nitride ($g\text{-}C_3N_4$)-based photocatalysts for water disinfection and microbial control: A review. *Chemosphere* **2019**, *214*, 462−479.
(1783) Serp, P.; Corrias, M.; Kalck, P. Carbon nanotubes and nanofibers in catalysis. *Appl. Catal. A* **2003**, *253*, 337−358.
(1784) Sherigara, B. S.; Kutner, W.; D'Souza, F. Electrocatalytic Properties and Sensor Applications of Fullerenes and Carbon Nanotubes. *Electroanalysis* **2003**, *15*, 753−772.
(1785) Schaetz, A.; Zeltner, M.; Stark, W. J. Carbon Modifications and Surfaces for Catalytic Organic Transformations. *ACS Catal.* **2012**, *2*, 1267−1284.
(1786) Sharma, S.; Pollet, B. G. Support materials for PEMFC and DMFC electrocatalysts—A review. *J. Power Sources* **2012**, *208*, 96−119.
(1787) Gao, F.; Zhao, G.-L.; Yang, S.; Spivey, J. J. Nitrogen-Doped Fullerene as a Potential Catalyst for Hydrogen Fuel Cells. *J. Am. Chem. Soc.* **2013**, *135*, 3315−3318.
(1788) Maroto, E. E.; Izquierdo, M.; Reboredo, S.; Marco-Martínez, J.; Filippone, S.; Martín, N. Chiral Fullerenes from Asymmetric Catalysis. *Acc. Chem. Res.* **2014**, *47*, 2660−2670.
(1789) Dai, L.; Xue, Y.; Qu, L.; Choi, H.-J.; Baek, J.-B. Metal-Free Catalysts for Oxygen Reduction Reaction. *Chem. Rev.* **2015**, *115*, 4823−4892.
(1790) Zhang, J.; Xia, Z.; Dai, L. Carbon-based electrocatalysts for advanced energy conversion and storage. *Science Advances* **2015**, *1*, No. e1500564.
(1791) Xu, Z. P.; Zhang, J.; Adebajo, M. O.; Zhang, H.; Zhou, C. Catalytic applications of layered double hydroxides and derivatives. *Appl. Clay Sci.* **2011**, *53*, 139−150.
(1792) Li, C.; Wei, M.; Evans, D. G.; Duan, X. Layered Double Hydroxide-based Nanomaterials as Highly Efficient Catalysts and Adsorbents. *Small* **2014**, *10*, 4469−4486.
(1793) Xu, M.; Wei, M. Layered Double Hydroxide-Based Catalysts: Recent Advances in Preparation, Structure, and Applications. *Adv. Funct. Mater.* **2018**, *28*, 1802943.
(1794) Heard, C. J.; Cejka, J.; Opanasenko, M.; Nachtigall, P.; Centi, G.; Perathoner, S. 2D Oxide Nanomaterials to Address the Energy Transition and Catalysis. *Adv. Mater.* **2019**, *31*, 1801712.
(1795) Kuang, Y.; Zhao, L.; Zhang, S.; Zhang, F.; Dong, M.; Xu, S. Morphologies, Preparations and Applications of Layered Double Hydroxide Micro-/Nanostructures. *Materials* **2010**, *3*, 5220.
(1796) Theiss, F. L.; Ayoko, G. A.; Frost, R. L. Synthesis of layered double hydroxides containing Mg^{2+}, Zn^{2+}, Ca^{2+} and Al^{3+} layer cations by co-precipitation methods—A review. *Appl. Surf. Sci.* **2016**, *383*, 200−213.
(1797) Yu, J.; Wang, Q.; O'Hare, D.; Sun, L. Preparation of two dimensional layered double hydroxide nanosheets and their applications. *Chem. Soc. Rev.* **2017**, *46*, 5950−5974.
(1798) Sels, B. F.; De Vos, D. E.; Jacobs, P. A. Hydrotalcite-like anionic clays in catalytic organic reactions. *Catal. Rev.* **2001**, *43*, 443−488.
(1799) Debecker, D. P.; Gaigneaux, E. M.; Busca, G. Exploring, Tuning, and Exploiting the Basicity of Hydrotalcites for Applications in Heterogeneous Catalysis. *Chem.-Eur. J.* **2009**, *15*, 3920−3935.
(1800) Yan, K.; Liu, Y.; Lu, Y.; Chai, J.; Sun, L. Catalytic application of layered double hydroxide-derived catalysts for the conversion of biomass-derived molecules. *Catal. Sci. Technol.* **2017**, *7*, 1622−1645.
(1801) Feng, J.; He, Y.; Liu, Y.; Du, Y.; Li, D. Supported catalysts based on layered double hydroxides for catalytic oxidation and hydrogenation: general functionality and promising application prospects. *Chem. Soc. Rev.* **2015**, *44*, 5291−5319.
(1802) Li, P.; Yu, F.; Altaf, N.; Zhu, M.; Li, J.; Dai, B.; Wang, Q. Two-Dimensional Layered Double Hydroxides for Reactions of Methanation and Methane Reforming in C1 Chemistry. *Materials* **2018**, *11*, 221.
(1803) Christensen, K. O.; Chen, D.; Lødeng, R.; Holmen, A. Effect of supports and Ni crystal size on carbon formation and sintering during steam methane reforming. *Appl. Catal. A* **2006**, *314*, 9−22.
(1804) Sikander, U.; Sufian, S.; Salam, M. A. A review of hydrotalcite based catalysts for hydrogen production systems. *Int. J. Hydrogen Energy* **2017**, *42*, 19851−19868.
(1805) Debek, R.; Motak, M.; Grzybek, T.; Galvez, M. E.; Da Costa, P. A Short Review on the Catalytic Activity of Hydrotalcite-Derived Materials for Dry Reforming of Methane. *Catalysts* **2017**, *7*, 32.
(1806) Huynh, H. L.; Yu, Z. CO_2 Methanation on Hydrotalcite-Derived Catalysts and Structured Reactors: A Review. *Energy Technology* **2020**, *8*, 1901475.
(1807) Baskaran, T.; Christopher, J.; Sakthivel, A. Progress on layered hydrotalcite (HT) materials as potential support and catalytic materials. *RSC Adv.* **2015**, *5*, 98853−98875.
(1808) Hernández, W. Y.; Lauwaert, J.; Van Der Voort, P.; Verberckmoes, A. Recent advances on the utilization of layered double hydroxides (LDHs) and related heterogeneous catalysts in a lignocellulosic-feedstock biorefinery scheme. *Green Chem.* **2017**, *19*, 5269−5302.

https://doi.org/10.1021/acs.chemrev.1c00905
Chem. Rev. XXXX, XXX, XXX−XXX

(1809) Takagaki, A.; Takahashi, M.; Nishimura, S.; Ebitani, K. One-Pot Synthesis of 2,5-Diformylfuran from Carbohydrate Derivatives by Sulfonated Resin and Hydrotalcite-Supported Ruthenium Catalysts. *ACS Catal.* **2011**, *1*, 1562−1565.
(1810) Mobley, J. K.; Crocker, M. Catalytic oxidation of alcohols to carbonyl compounds over hydrotalcite and hydrotalcite-supported catalysts. *RSC Adv.* **2015**, *5*, 65780−65797.
(1811) Navalon, S.; Alvaro, M.; Garcia, H. Heterogeneous Fenton catalysts based on clays, silicas and zeolites. *Appl. Catal. B* **2010**, *99*, 1−26.
(1812) Yang, Z.; Wang, F.; Zhang, C.; Zeng, G.; Tan, X.; Yu, Z.; Zhong, Y.; Wang, H.; Cui, F. Utilization of LDH-based materials as potential adsorbents and photocatalysts for the decontamination of dyes wastewater: a review. *RSC Adv.* **2016**, *6*, 79415−79436.
(1813) Zhang, G.; Zhang, X.; Meng, Y.; Pan, G.; Ni, Z.; Xia, S. Layered double hydroxides-based photocatalysts and visible-light driven photodegradation of organic pollutants: A review. *Chem. Eng. J.* **2020**, *392*, 123684.
(1814) Yang, Z.-z.; Zhang, C.; Zeng, G.-m.; Tan, X.-f.; Wang, H.; Huang, D.-l.; Yang, K.-h.; Wei, J.-j.; Ma, C.; Nie, K. Design and engineering of layered double hydroxide based catalysts for water depollution by advanced oxidation processes: a review. *J. Mater. Chem. A* **2020**, *8*, 4141−4173.
(1815) Yan, Q.; Hou, X.; Liu, G.; Li, Y.; Zhu, T.; Xin, Y.; Wang, Q. Recent advances in layered double hydroxides (LDHs) derived catalysts for selective catalytic reduction of NO_x with NH_3. *J. Hazard. Mater.* **2020**, *400*, 123260.
(1816) Fan, G.; Li, F.; Evans, D. G.; Duan, X. Catalytic applications of layered double hydroxides: recent advances and perspectives. *Chem. Soc. Rev.* **2014**, *43*, 7040−7066.
(1817) Zhao, Y.; Jia, X.; Waterhouse, G. I. N.; Wu, L.-Z.; Tung, C.-H.; O'Hare, D.; Zhang, T. Layered Double Hydroxide Nanostructured Photocatalysts for Renewable Energy Production. *Adv. Energy Mater.* **2016**, *6*, 1501974.
(1818) Zhao, Y.; Chen, G.; Bian, T.; Zhou, C.; Waterhouse, G. I. N.; Wu, L.-Z.; Tung, C.-H.; Smith, L. J.; O'Hare, D.; Zhang, T. Defect-Rich Ultrathin ZnAl-Layered Double Hydroxide Nanosheets for Efficient Photoreduction of CO_2 to CO with Water. *Adv. Mater.* **2015**, *27*, 7824−7831.
(1819) Li, X.; Hao, X.; Abudula, A.; Guan, G. Nanostructured catalysts for electrochemical water splitting: current state and prospects. *J. Mater. Chem. A* **2016**, *4*, 11973−12000.
(1820) Anantharaj, S.; Karthick, K.; Kundu, S. Evolution of layered double hydroxides (LDH) as high performance water oxidation electrocatalysts: A review with insights on structure, activity and mechanism. *Materials Today Energy* **2017**, *6*, 1−26.
(1821) Zhou, L.; Shao, M.; Wei, M.; Duan, X. Advances in efficient electrocatalysts based on layered double hydroxides and their derivatives. *Journal of Energy Chemistry* **2017**, *26*, 1094−1106.
(1822) Cai, Z.; Bu, X.; Wang, P.; Ho, J. C.; Yang, J.; Wang, X. Recent advances in layered double hydroxide electrocatalysts for the oxygen evolution reaction. *J. Mater. Chem. A* **2019**, *7*, 5069−5089.
(1823) Wu, L.; Yu, L.; Xiao, X.; Zhang, F.; Song, S.; Chen, S.; Ren, Z. Recent Advances in Self-Supported Layered Double Hydroxides for Oxygen Evolution Reaction. *Research* **2020**, *2020*, 3976278.
(1824) Li, Y.; Shen, W. Morphology-dependent nanocatalysis on metal oxides. *Science China Chemistry* **2012**, *55*, 2485−2496.
(1825) Pan, C.; Zhang, D.; Shi, L. CTAB assisted hydrothermal synthesis, controlled conversion and CO oxidation properties of CeO_2 nanoplates, nanotubes, and nanorods. *J. Solid State Chem.* **2008**, *181*, 1298−1306.
(1826) Lv, J.; Shen, Y.; Peng, L.; Guo, X.; Ding, W. Exclusively selective oxidation of toluene to benzaldehyde on ceria nanocubes by molecular oxygen. *Chem. Commun.* **2010**, *46*, 5909−5911.
(1827) Wu, Z.; Li, M.; Overbury, S. H. On the structure dependence of CO oxidation over CeO_2 nanocrystals with well-defined surface planes. *J. Catal.* **2012**, *285*, 61−73.
(1828) Qiao, Z.-A.; Wu, Z.; Dai, S. Shape-Controlled Ceria-based Nanostructures for Catalysis Applications. *ChemSusChem* **2013**, *6*, 1821−1833.
(1829) Trovarelli, A.; Llorca, J. Ceria Catalysts at Nanoscale: How Do Crystal Shapes Shape Catalysis? *ACS Catal.* **2017**, *7*, 4716−4735.
(1830) Wu, N.; Wang, J.; Tafen, D. N.; Wang, H.; Zheng, J.-G.; Lewis, J. P.; Liu, X.; Leonard, S. S.; Manivannan, A. Shape-Enhanced Photocatalytic Activity of Single-Crystalline Anatase TiO_2 (101) Nanobelts. *J. Am. Chem. Soc.* **2010**, *132*, 6679−6685.
(1831) Li, X.; Zheng, W.; He, G.; Zhao, R.; Liu, D. Morphology Control of TiO_2 Nanoparticle in Microemulsion and Its Photocatalytic Property. *ACS Sustainable Chem. Eng.* **2014**, *2*, 288−295.
(1832) Hu, L.; Peng, Q.; Li, Y. Selective Synthesis of Co_3O_4 Nanocrystal with Different Shape and Crystal Plane Effect on Catalytic Property for Methane Combustion. *J. Am. Chem. Soc.* **2008**, *130*, 16136−16137.
(1833) Xie, X.; Li, Y.; Liu, Z.-Q.; Haruta, M.; Shen, W. Low-temperature oxidation of CO catalysed by Co_3O_4 nanorods. *Nature* **2009**, *458*, 746−749.
(1834) Hu, L.; Sun, K.; Peng, Q.; Xu, B.; Li, Y. Surface active sites on Co_3O_4 nanobelt and nanocube model catalysts for CO oxidation. *Nano Res.* **2010**, *3*, 363−368.
(1835) Meng, B.; Zhao, Z.; Wang, X.; Liang, J.; Qiu, J. Selective catalytic reduction of nitrogen oxides by ammonia over Co3O4 nanocrystals with different shapes. *Appl. Catal. B* **2013**, *129*, 491−500.
(1836) Bai, G.; Dai, H.; Deng, J.; Liu, Y.; Wang, F.; Zhao, Z.; Qiu, W.; Au, C. T. Porous Co_3O_4 nanowires and nanorods: Highly active catalysts for the combustion of toluene. *Appl. Catal. A* **2013**, *450*, 42−49.
(1837) González-Prior, J.; López-Fonseca, R.; Gutiérrez-Ortiz, J. I.; de Rivas, B. Oxidation of 1,2-dichloroethane over nanocube-shaped Co_3O_4 catalysts. *Appl. Catal. B* **2016**, *199*, 384−393.
(1838) Ren, Q.; Mo, S.; Peng, R.; Feng, Z.; Zhang, M.; Chen, L.; Fu, M.; Wu, J.; Ye, D. Controllable synthesis of 3D hierarchical Co_3O_4 nanocatalysts with various morphologies for the catalytic oxidation of toluene. *Journal of Materials Chemistry A* **2018**, *6*, 498−509.
(1839) Leng, M.; Liu, M.; Zhang, Y.; Wang, Z.; Yu, C.; Yang, X.; Zhang, H.; Wang, C. Polyhedral 50-Facet Cu_2O Microcrystals Partially Enclosed by {311} High-Index Planes: Synthesis and Enhanced Catalytic CO Oxidation Activity. *J. Am. Chem. Soc.* **2010**, *132*, 17084−17087.
(1840) Xu, Y.; Wang, H.; Yu, Y.; Tian, L.; Zhao, W.; Zhang, B. Cu_2O Nanocrystals: Surfactant-Free Room-Temperature Morphology-Modulated Synthesis and Shape-Dependent Heterogeneous Organic Catalytic Activities. *J. Phys. Chem. C* **2011**, *115*, 15288−15296.
(1841) Li, L.; Nan, C.; Peng, Q.; Li, Y. Selective Synthesis of Cu2O Nanocrystals as Shape-Dependent Catalysts for Oxidative Arylation of Phenylacetylene. *Chem.-Eur. J.* **2012**, *18*, 10491−10496.
(1842) Zhang, Z.; Che, H.; Gao, J.; Wang, Y.; She, X.; Sun, J.; Gunawan, P.; Zhong, Z.; Su, F. Shape-controlled synthesis of Cu2O microparticles and their catalytic performances in the Rochow reaction. *Catal. Sci. Technol.* **2012**, *2*, 1207−1212.
(1843) Yang, P. Crystal cuts on the nanoscale. *Nature* **2012**, *482*, 41−42.
(1844) Konar, S.; Kalita, H.; Puvvada, N.; Tantubay, S.; Mahto, M. K.; Biswas, S.; Pathak, A. Shape-dependent catalytic activity of CuO nanostructures. *J. Catal.* **2016**, *336*, 11−22.
(1845) Choudary, B. M.; Mulukutla, R. S.; Klabunde, K. J. Benzylation of Aromatic Compounds with Different Crystallites of MgO. *J. Am. Chem. Soc.* **2003**, *125*, 2020−2021.
(1846) Sutradhar, N.; Sinhamahapatra, A.; Pahari, S. K.; Pal, P.; Bajaj, H. C.; Mukhopadhyay, I.; Panda, A. B. Controlled Synthesis of Different Morphologies of MgO and Their Use as Solid Base Catalysts. *J. Phys. Chem. C* **2011**, *115*, 12308−12316.
(1847) Selvamani, T.; Sinhamahapatra, A.; Bhattacharjya, D.; Mukhopadhyay, I. Rectangular MgO microsheets with strong catalytic activity. *Materials Chemistry and Physics* **2011**, *129*, 853−861.
(1848) Mutch, G. A.; Shulda, S.; McCue, A. J.; Menart, M. J.; Ciobanu, C. V.; Ngo, C.; Anderson, J. A.; Richards, R. M.; Vega-Maza,

https://doi.org/10.1021/acs.chemrev.1c00905
Chem. Rev. XXXX, XXX, XXX−XXX

D. Carbon Capture by Metal Oxides: Unleashing the Potential of the (111) Facet. *J. Am. Chem. Soc.* **2018**, *140*, 4736−4742.
(1849) Jana, S.; Basu, S.; Pande, S.; Ghosh, S. K.; Pal, T. Shape-Selective Synthesis, Magnetic Properties, and Catalytic Activity of Single Crystalline β-MnO_2 Nanoparticles. *J. Phys. Chem. C* **2007**, *111*, 16272−16277.
(1850) Qiu, G.; Huang, H.; Dharmarathna, S.; Benbow, E.; Stafford, L.; Suib, S. L. Hydrothermal Synthesis of Manganese Oxide Nanomaterials and Their Catalytic and Electrochemical Properties. *Chem. Mater.* **2011**, *23*, 3892−3901.
(1851) Sun, M.; Lan, B.; Lin, T.; Cheng, G.; Ye, F.; Yu, L.; Cheng, X.; Zheng, X. Controlled synthesis of nanostructured manganese oxide: crystalline evolution and catalytic activities. *CrystEngComm* **2013**, *15*, 7010−7018.
(1852) Selvakumar, K.; Senthil Kumar, S. M.; Thangamuthu, R.; Kruthika, G.; Murugan, P. Development of shape-engineered α-MnO_2 materials as bi-functional catalysts for oxygen evolution reaction and oxygen reduction reaction in alkaline medium. *International Journal of Hydrogen Energy* **2014**, *39*, 21024−21036.
(1853) Selvakumar, K.; Senthil Kumar, S. M.; Thangamuthu, R.; Ganesan, K.; Murugan, P.; Rajput, P.; Jha, S. N.; Bhattacharyya, D. Physiochemical Investigation of Shape-Designed MnO_2 Nanostructures and Their Influence on Oxygen Reduction Reaction Activity in Alkaline Solution. *J. Phys. Chem. C* **2015**, *119*, 6604−6618.
(1854) Zheng, Y.; Cheng, Y.; Wang, Y.; Bao, F.; Zhou, L.; Wei, X.; Zhang, Y.; Zheng, Q. Quasicubic α-Fe_2O_3 Nanoparticles with Excellent Catalytic Performance. *J. Phys. Chem. B* **2006**, *110*, 3093−3097.
(1855) Mou, X.; Zhang, B.; Li, Y.; Yao, L.; Wei, X.; Su, D. S.; Shen, W. Rod-Shaped Fe_2O_3 as an Efficient Catalyst for the Selective Reduction of Nitrogen Oxide by Ammonia. *Angew. Chem., Int. Ed.* **2012**, *51*, 2989−2993.
(1856) Mishra, M.; Chun, D.-M. α-Fe_2O_3 as a photocatalytic material: A review. *Appl. Catal. A* **2015**, *498*, 126−141.
(1857) Ma, L.; Ma, H.; Gao, N.; Wang, J.; Zhang, X. Controllable synthesis of α-Fe_2O_3 nanotubes with high surface area: preparation, growth mechanism, and its catalytic performance for the selective catalytic reduction of NO with NH_3. *J. Mater. Sci.* **2016**, *51*, 1959−1965.
(1858) Patra, A. K.; Kundu, S. K.; Kim, D.; Bhaumik, A. Controlled Synthesis of a Hexagonal-Shaped NiO Nanocatalyst with Highly Reactive Facets {110} and Its Catalytic Activity. *ChemCatChem.* **2015**, *7*, 791−798.
(1859) Pal, J.; Pal, T. Faceted metal and metal oxide nanoparticles: design, fabrication and catalysis. *Nanoscale* **2015**, *7*, 14159−14190.
(1860) Li, Y.; Shen, W. Morphology-dependent nanocatalysts: Rod-shaped oxides. *Chem. Soc. Rev.* **2014**, *43*, 1543−1574.
(1861) Jain, P.; Gupta, S.; Vinod, C. P. Role of exposed crystal facets in the atmospheric pressure CO hydrogenation on Co_3O_4 nanostructures. *Nano-Structures & Nano-Objects* **2020**, *23*, 100504.
(1862) Vilé, G.; Bridier, B.; Wichert, J.; Pérez-Ramírez, J. Ceria in Hydrogenation Catalysis: High Selectivity in the Conversion of Alkynes to Olefins. *Angew. Chem., Int. Ed.* **2012**, *51*, 8620−8623.
(1863) Zhao, E. W.; Zheng, H.; Zhou, R.; Hagelin-Weaver, H. E.; Bowers, C. R. Shaped Ceria Nanocrystals Catalyze Efficient and Selective Para-Hydrogen-Enhanced Polarization. *Angew. Chem., Int. Ed.* **2015**, *54*, 14270−14275.
(1864) Zhao, E. W.; Xin, Y.; Hagelin-Weaver, H. E.; Bowers, C. R. Semihydrogenation of Propyne over Cerium Oxide Nanorods, Nanocubes, and Nano-Octahedra: Facet-Dependent Parahydrogen-Induced Polarization. *ChemCatChem.* **2016**, *8*, 2197−2201.
(1865) Zhou, K.; Wang, X.; Sun, X.; Peng, Q.; Li, Y. Enhanced catalytic activity of ceria nanorods from well-defined reactive crystal planes. *J. Catal.* **2005**, *229*, 206−212.
(1866) Agarwal, S.; Lefferts, L.; Mojet, B. L.; Ligthart, D. A. J. M.; Hensen, E. J. M.; Mitchell, D. R. G.; Erasmus, W. J.; Anderson, B. G.; Olivier, E. J.; Neethling, J. H.; et al. Exposed Surfaces on Shape-Controlled Ceria Nanoparticles Revealed through AC-TEM and Water-Gas Shift Reactivity. *ChemSusChem* **2013**, *6*, 1898−1906.
(1867) Vilé, G.; Colussi, S.; Krumeich, F.; Trovarelli, A.; Pérez-Ramírez, J. Opposite Face Sensitivity of CeO_2 in Hydrogenation and Oxidation Catalysis. *Angew. Chem., Int. Ed.* **2014**, *53*, 12069−12072.
(1868) Zhang, S.; Huang, Z. Q.; Ma, Y.; Gao, W.; Li, J.; Cao, F.; Li, L.; Chang, C. R.; Qu, Y. Solid frustrated-Lewis-pair catalysts constructed by regulations on surface defects of porous nanorods of CeO_2. *Nat. Commun.* **2017**, *8*. DOI: 10.1038/ncomms15266
(1869) Murakami, N.; Katayama, S.; Nakamura, M.; Tsubota, T.; Ohno, T. Dependence of Photocatalytic Activity on Aspect Ratio of Shape-Controlled Rutile Titanium(IV) Oxide Nanorods. *J. Phys. Chem. C* **2011**, *115*, 419−424.
(1870) Pham, H. H.; Wang, L.-W. Oxygen vacancy and hole conduction in amorphous TiO_2. *Phys. Chem. Chem. Phys.* **2015**, *17*, 541−550.
(1871) Sreeremya, T. S.; Krishnan, A.; Remani, K. C.; Patil, K. R.; Brougham, D. F.; Ghosh, S. Shape-Selective Oriented Cerium Oxide Nanocrystals Permit Assessment of the Effect of the Exposed Facets on Catalytic Activity and Oxygen Storage Capacity. *ACS Appl. Mater. Interfaces* **2015**, *7*, 8545−8555.
(1872) Inomata, Y.; Albrecht, K.; Yamamoto, K. Size-Dependent Oxidation State and CO Oxidation Activity of Tin Oxide Clusters. *ACS Catal.* **2018**, *8*, 451−456.
(1873) Bao, H.; Zhang, W.; Hua, Q.; Jiang, Z.; Yang, J.; Huang, W. Crystal-Plane-Controlled Surface Restructuring and Catalytic Performance of Oxide Nanocrystals. *Angew. Chem., Int. Ed.* **2011**, *50*, 12294−12298.
(1874) Wang, X.; Liu, C.; Zheng, B.; Jiang, Y.; Zhang, L.; Xie, Z.; Zheng, L. Controlled synthesis of concave Cu_2O microcrystals enclosed by {hhl} high-index facets and enhanced catalytic activity. *J. Mater. Chem. A* **2013**, *1*, 282−287.
(1875) Hua, Q.; Cao, T.; Bao, H.; Jiang, Z.; Huang, W. Crystal-Plane-Controlled Surface Chemistry and Catalytic Performance of Surfactant-Free Cu_2O Nanocrystals. *ChemSusChem* **2013**, *6*, 1966−1972.
(1876) Hua, Q.; Cao, T.; Gu, X.-K.; Lu, J.; Jiang, Z.; Pan, X.; Luo, L.; Li, W.-X.; Huang, W. Crystal-Plane-Controlled Selectivity of Cu_2O Catalysts in Propylene Oxidation with Molecular Oxygen. *Angew. Chem., Int. Ed.* **2014**, *53*, 4856−4861.
(1877) Chanda, K.; Rej, S.; Huang, M. H. Facet-Dependent Catalytic Activity of Cu_2O Nanocrystals in the One-Pot Synthesis of 1,2,3-Triazoles by Multicomponent Click Reactions. *Chem.-Eur. J.* **2013**, *19*, 16036−16043.
(1878) Chanda, K.; Rej, S.; Huang, M. H. Investigation of facet effects on the catalytic activity of Cu_2O nanocrystals for efficient regioselective synthesis of 3,5-disubstituted isoxazoles. *Nanoscale* **2013**, *5*, 12494−12501.
(1879) Fujishima, A.; Zhang, X.; Tryk, D. A. TiO_2 photocatalysis and related surface phenomena. *Surf. Sci. Rep.* **2008**, *63*, 515−582.
(1880) Leung, D. Y. C.; Fu, X.; Wang, C.; Ni, M.; Leung, M. K. H.; Wang, X.; Fu, X. Hydrogen Production over Titania-Based Photocatalysts. *ChemSusChem* **2010**, *3*, 681−694.
(1881) Serpone, N.; Emeline, A. V.; Horikoshi, S.; Kuznetsov, V. N.; Ryabchuk, V. K. On the genesis of heterogeneous photocatalysis: a brief historical perspective in the period 1910 to the mid-1980s. *Photochem. Photobiol. Sci.* **2012**, *11*, 1121−1150.
(1882) Guo, Q.; Zhou, C.; Ma, Z.; Ren, Z.; Fan, H.; Yang, X. Elementary photocatalytic chemistry on TiO_2 surfaces. *Chem. Soc. Rev.* **2016**, *45*, 3701−3730.
(1883) Vittadini, A.; Selloni, A.; Rotzinger, F. P.; Grätzel, M. Structure and Energetics of Water Adsorbed at TiO_2 Anatase (101) and (001) Surfaces. *Phys. Rev. Lett.* **1998**, *81*, 2954−2957.
(1884) Yang, X. H.; Li, Z.; Liu, G.; Xing, J.; Sun, C.; Yang, H. G.; Li, C. Ultra-thin anatase TiO_2 nanosheets dominated with {001} facets: thickness-controlled synthesis, growth mechanism and water-splitting properties. *CrystEngComm* **2011**, *13*, 1378−1383.
(1885) Xie, S.; Han, X.; Kuang, Q.; Fu, J.; Zhang, L.; Xie, Z.; Zheng, L. Solid state precursor strategy for synthesizing hollow TiO_2 boxes with a high percentage of reactive {001} facets exposed. *Chem. Commun.* **2011**, *47*, 6722−6724.

https://doi.org/10.1021/acs.chemrev.1c00905
Chem. Rev. XXXX, XXX, XXX−XXX

(1886) Ong, W.-J.; Tan, L.-L.; Chai, S.-P.; Yong, S.-T.; Mohamed, A. R. Facet-Dependent Photocatalytic Properties of TiO_2-Based Composites for Energy Conversion and Environmental Remediation. *ChemSusChem* **2014**, *7*, 690−719.
(1887) Sajan, C. P.; Wageh, S.; Al-Ghamdi, A. A.; Yu, J.; Cao, S. TiO_2 nanosheets with exposed {001} facets for photocatalytic applications. *Nano Res.* **2016**, *9*, 3−27.
(1888) Kumar, S. G.; Devi, L. G. Review on Modified TiO_2 Photocatalysis under UV/Visible Light: Selected Results and Related Mechanisms on Interfacial Charge Carrier Transfer Dynamics. *J. Phys. Chem. A* **2011**, *115*, 13211−13241.
(1889) Pan, J.; Liu, G.; Lu, G. Q.; Cheng, H.-M. On the True Photoreactivity Order of {001}, {010}, and {101} Facets of Anatase TiO_2 Crystals. *Angew. Chem., Int. Ed.* **2011**, *50*, 2133−2137.
(1890) Gordon, T. R.; Cargnello, M.; Paik, T.; Mangolini, F.; Weber, R. T.; Fornasiero, P.; Murray, C. B. Nonaqueous Synthesis of TiO_2 Nanocrystals Using TiF_4 to Engineer Morphology, Oxygen Vacancy Concentration, and Photocatalytic Activity. *J. Am. Chem. Soc.* **2012**, *134*, 6751−6761.
(1891) Roy, N.; Sohn, Y.; Pradhan, D. Synergy of Low-Energy {101} and High-Energy {001} TiO_2 Crystal Facets for Enhanced Photocatalysis. *ACS Nano* **2013**, *7*, 2532−2540.
(1892) Yu, J.; Low, J.; Xiao, W.; Zhou, P.; Jaroniec, M. Enhanced Photocatalytic CO_2-Reduction Activity of Anatase TiO_2 by Coexposed {001} and {101} Facets. *J. Am. Chem. Soc.* **2014**, *136*, 8839−8842.
(1893) Gnanasekaran, L.; Hemamalini, R.; Saravanan, R.; Ravichandran, K.; Gracia, F.; Agarwal, S.; Gupta, V. K. Synthesis and characterization of metal oxides (CeO_2, CuO, NiO, Mn_3O_4, SnO_2 and ZnO) nanoparticles as photo catalysts for degradation of textile dyes. *Journal of Photochemistry and Photobiology B: Biology* **2017**, *173*, 43−49.
(1894) Liu, M.; Piao, L.; Lu, W.; Ju, S.; Zhao, L.; Zhou, C.; Li, H.; Wang, W. Flower-like TiO_2 nanostructures with exposed {001} facets: Facile synthesis and enhanced photocatalysis. *Nanoscale* **2010**, *2*, 1115−1117.
(1895) Wei, W.; Yaru, N.; Chunhua, L.; Zhongzi, X. Hydrogenation of TiO_2 nanosheets with exposed {001} facets for enhanced photocatalytc activity. *RSC Adv.* **2012**, *2*, 8286−8288.
(1896) Wu, B.; Guo, C.; Zheng, N.; Xie, Z.; Stucky, G. D. Nonaqueous Production of Nanostructured Anatase with High-Energy Facets. *J. Am. Chem. Soc.* **2008**, *130*, 17563−17567.
(1897) Liu, L.; Gu, X.; Ji, Z.; Zou, W.; Tang, C.; Gao, F.; Dong, L. Anion-Assisted Synthesis of TiO_2 Nanocrystals with Tunable Crystal Forms and Crystal Facets and Their Photocatalytic Redox Activities in Organic Reactions. *J. Phys. Chem. C* **2013**, *117*, 18578−18587.
(1898) Xu, H.; Wang, W.; Zhu, W. Shape Evolution and Size-Controllable Synthesis of Cu_2O Octahedra and Their Morphology-Dependent Photocatalytic Properties. *J. Phys. Chem. B* **2006**, *110*, 13829−13834.
(1899) Zheng, Z.; Huang, B.; Wang, Z.; Guo, M.; Qin, X.; Zhang, X.; Wang, P.; Dai, Y. Crystal Faces of Cu_2O and Their Stabilities in Photocatalytic Reactions. *J. Phys. Chem. C* **2009**, *113*, 14448−14453.
(1900) Zhang, Y.; Deng, B.; Zhang, T.; Gao, D.; Xu, A.-W. Shape Effects of Cu_2O Polyhedral Microcrystals on Photocatalytic Activity. *J. Phys. Chem. C* **2010**, *114*, 5073−5079.
(1901) Cao, Y.; Fan, J.; Bai, L.; Yuan, F.; Chen, Y. Morphology Evolution of Cu_2O from Octahedra to Hollow Structures. *Cryst. Growth Des.* **2010**, *10*, 232−236.
(1902) Huang, W.-C.; Lyu, L.-M.; Yang, Y.-C.; Huang, M. H. Synthesis of Cu_2O Nanocrystals from Cubic to Rhombic Dodecahedral Structures and Their Comparative Photocatalytic Activity. *J. Am. Chem. Soc.* **2012**, *134*, 1261−1267.
(1903) Yu, X.; Kou, S.; Zhang, J.; Tang, X.; Yang, Q.; Yao, B. Preparation and characterization of Cu2O nano-particles and their photocatalytic degradation of fluroxypyr. *Environmental Technology* **2018**, *39*, 2967−2976.
(1904) Prado-Chay, D. A.; Cortés-Jácome, M. A.; Angeles-Chávez, C.; Oviedo-Roa, R.; Martínez-Magadán, J. M.; Zuriaga-Monroy, C.; Hernández-Hernández, I. J.; Mayoral, P. R.; Gómora-Herrera, D. R.; Toledo-Antonio, J. A. Synthesis and Photocatalytic Activity of Cu_2O Microspheres upon Methyl Orange Degradation. *Top. Catal.* **2020**, *63*, 586−600.
(1905) Wu, Z.; Mann, A. K. P.; Li, M.; Overbury, S. H. Spectroscopic Investigation of Surface-Dependent Acid-Base Property of Ceria Nanoshapes. *J. Phys. Chem. C* **2015**, *119*, 7340−7350.
(1906) Mann, A. K. P.; Wu, Z.; Calaza, F. C.; Overbury, S. H. Adsorption and Reaction of Acetaldehyde on Shape-Controlled CeO_2 Nanocrystals: Elucidation of Structure-Function Relationships. *ACS Catal.* **2014**, *4*, 2437−2448.
(1907) Wang, S.; Zhao, L.; Wang, W.; Zhao, Y.; Zhang, G.; Ma, X.; Gong, J. Morphology control of ceria nanocrystals for catalytic conversion of CO_2 with methanol. *Nanoscale* **2013**, *5*, 5582−5588.
(1908) Geng, L.; Song, J.; Zhou, Y.; Xie, Y.; Huang, J.; Zhang, W.; Peng, L.; Liu, G. CeO_2 nanorods anchored on mesoporous carbon as an efficient catalyst for imine synthesis. *Chem. Commun.* **2016**, *52*, 13495−13498.
(1909) Fernández-Arroyo, A.; Lara, M. A.; Domine, M. E.; Sayagués, M. J.; Navío, J. A.; Hidalgo, M. C. High {0 0 1} faceted TiO_2 nanoparticles for the valorization of oxygenated compounds present in aqueous biomass-derived feedstocks. *J. Catal.* **2018**, *358*, 266−276.
(1910) Han, W.; Li, X.; Tang, H.; Wang, Z.; Xi, M.; Li, Y.; Liu, H. Preparation of fluorinated Cr_2O_3 hexagonal prism and catalytic performance for the dehydrofluorination of 1,1-difluoroethane to vinyl fluoride. *J. Nanopart. Res.* **2015**, *17*, 365.
(1911) Fuchigami, T.; Kuroda, M.; Nakamura, S.; Haneda, M.; Kakimoto, K.-i. Spiky-shaped niobium pentoxide nano-architecture: highly stable and recoverable Lewis acid catalyst. *Nanotechnol.* **2020**, *31*, 325705.
(1912) Wang, F.; Ta, N.; Shen, W. MgO nanosheets, nanodisks, and nanofibers for the Meerwein-Ponndorf-Verley reaction. *Appl. Catal. A* **2014**, *475*, 76−81.
(1913) Ahmad, T.; Phul, R.; Khan, H. Iron Oxide Nanoparticles: An Efficient Nano-catalyst. *Curr. Org. Chem.* **2019**, *23*, 994−1004.
(1914) Laursen, S.; Combita, D.; Hungría, A. B.; Boronat, M.; Corma, A. First-Principles Design of Highly Active and Selective Catalysts for Phosgene-Free Synthesis of Aromatic Polyurethanes. *Angew. Chem., Int. Ed.* **2012**, *51*, 4190−4193.
(1915) Aditya, T.; Jana, J.; Singh, N. K.; Pal, A.; Pal, T. Remarkable Facet Selective Reduction of 4-Nitrophenol by Morphologically Tailored (111) Faceted Cu_2O Nanocatalyst. *ACS Omega* **2017**, *2*, 1968−1984.
(1916) Huang, W.; Gao, Y. Morphology-dependent surface chemistry and catalysis of CeO_2 nanocrystals. *Catal. Sci. Technol.* **2014**, *4*, 3772−3784.
(1917) Mullins, D. R. The surface chemistry of cerium oxide. *Surf. Sci. Rep.* **2015**, *70*, 42−85.
(1918) Huang, H.; Dai, Q.; Wang, X. Morphology effect of Ru/CeO_2 catalysts for the catalytic combustion of chlorobenzene. *Appl. Catal. B* **2014**, *158-159*, 96−105.
(1919) Si, R.; Flytzani-Stephanopoulos, M. Shape and Crystal-Plane Effects of Nanoscale Ceria on the Activity of Au-CeO_2 Catalysts for the Water-Gas Shift Reaction. *Angew. Chem., Int. Ed.* **2008**, *47*, 2884−2887.
(1920) Ciftci, A.; Ligthart, D. A. J. M.; Pastorino, P.; Hensen, E. J. M. Nanostructured ceria supported Pt and Au catalysts for the reactions of ethanol and formic acid. *Appl. Catal. B* **2013**, *130-131*, 325−335.
(1921) Xu, Q.; Lei, W.; Li, X.; Qi, X.; Yu, J.; Liu, G.; Wang, J.; Zhang, P. Efficient Removal of Formaldehyde by Nanosized Gold on Well-Defined CeO_2 Nanorods at Room Temperature. *Environ. Sci. Technol.* **2014**, *48*, 9702−9708.
(1922) Yi, G.; Yang, H.; Li, B.; Lin, H.; Tanaka, K.-i.; Yuan, Y. Preferential CO oxidation in a H_2-rich gas by Au/CeO_2 catalysts: Nanoscale CeO_2 shape effect and mechanism aspect. *Catal. Today* **2010**, *157*, 83−88.

https://doi.org/10.1021/acs.chemrev.1c00905
Chem. Rev. XXXX, XXX, XXX−XXX

(1923) Tan, H.; Wang, J.; Yu, S.; Zhou, K. Support Morphology-Dependent Catalytic Activity of Pd/CeO_2 for Formaldehyde Oxidation. *Environ. Sci. Technol.* **2015**, *49*, 8675−8682.
(1924) Hu, Z.; Liu, X.; Meng, D.; Guo, Y.; Guo, Y.; Lu, G. Effect of Ceria Crystal Plane on the Physicochemical and Catalytic Properties of Pd/Ceria for CO and Propane Oxidation. *ACS Catal.* **2016**, *6*, 2265−2279.
(1925) Yao, S. Y.; Xu, W. Q.; Johnston-Peck, A. C.; Zhao, F. Z.; Liu, Z. Y.; Luo, S.; Senanayake, S. D.; Martínez-Arias, A.; Liu, W. J.; Rodriguez, J. A. Morphological effects of the nanostructured ceria support on the activity and stability of CuO/CeO_2 catalysts for the water-gas shift reaction. *Phys. Chem. Chem. Phys.* **2014**, *16*, 17183−17195.
(1926) Konsolakis, M. The role of Copper-Ceria interactions in catalysis science: Recent theoretical and experimental advances. *Appl. Catal. B* **2016**, *198*, 49−66.
(1927) Wang, W.-W.; Yu, W.-Z.; Du, P.-P.; Xu, H.; Jin, Z.; Si, R.; Ma, C.; Shi, S.; Jia, C.-J.; Yan, C.-H. Crystal Plane Effect of Ceria on Supported Copper Oxide Cluster Catalyst for CO Oxidation: Importance of Metal-Support Interaction. *ACS Catal.* **2017**, *7*, 1313−1329.
(1928) Du, X.; Zhang, D.; Shi, L.; Gao, R.; Zhang, J. Morphology Dependence of Catalytic Properties of Ni/CeO_2 Nanostructures for Carbon Dioxide Reforming of Methane. *J. Phys. Chem. C* **2012**, *116*, 10009−10016.
(1929) Wang, F.; Li, C.; Zhang, X.; Wei, M.; Evans, D. G.; Duan, X. Catalytic behavior of supported Ru nanoparticles on the {100}, {110}, and {111} facet of CeO_2. *J. Catal.* **2015**, *329*, 177−186.
(1930) Peng, R.; Sun, X.; Li, S.; Chen, L.; Fu, M.; Wu, J.; Ye, D. Shape effect of Pt/CeO_2 catalysts on the catalytic oxidation of toluene. *Chem. Eng. J.* **2016**, *306*, 1234−1246.
(1931) Guo, T.; Du, J.; Li, J. The effects of ceria morphology on the properties of Pd/ceria catalyst for catalytic oxidation of low-concentration methane. *J. Mater. Sci.* **2016**, *51*, 10917−10925.
(1932) Vayssilov, G. N.; Lykhach, Y.; Migani, A.; Staudt, T.; Petrova, G. P.; Tsud, N.; Skála, T.; Bruix, A.; Illas, F.; Prince, K. C.; et al. Support nanostructure boosts oxygen transfer to catalytically active platinum nanoparticles. *Nat. Mater.* **2011**, *10*, 310−315.
(1933) Green, I. X.; Tang, W.; Neurock, M.; Yates, J. T. Insights into Catalytic Oxidation at the Au/TiO_2 Dual Perimeter Sites. *Acc. Chem. Res.* **2014**, *47*, 805−815.
(1934) Plata, J. J.; Graciani, J.; Evans, J.; Rodriguez, J. A.; Sanz, J. F. Cu Deposited on CeO_x-Modified TiO_2(110): Synergistic Effects at the Metal-Oxide Interface and the Mechanism of the WGS Reaction. *ACS Catal.* **2016**, *6*, 4608−4615.
(1935) Rodriguez, J. A.; Grinter, D. C.; Liu, Z.; Palomino, R. M.; Senanayake, S. D. Ceria-based model catalysts: fundamental studies on the importance of the metal-ceria interface in CO oxidation, the water-gas shift, CO_2 hydrogenation, and methane and alcohol reforming. *Chem. Soc. Rev.* **2017**, *46*, 1824−1841.
(1936) Chen, A.; Yu, X.; Zhou, Y.; Miao, S.; Li, Y.; Kuld, S.; Sehested, J.; Liu, J.; Aoki, T.; Hong, S.; et al. Structure of the catalytically active copper-ceria interfacial perimeter. *Nature Catalysis* **2019**, *2*, 334−341.
(1937) Yuan, W.; Zhu, B.; Fang, K.; Li, X.-Y.; Hansen, T. W.; Ou, Y.; Yang, H.; Wagner, J. B.; Gao, Y.; Wang, Y.; et al. In situ manipulation of the active Au-TiO_2 interface with atomic precision during CO oxidation. *Science* **2021**, *371*, 517.
(1938) Zhou, Y.; Doronkin, D. E.; Chen, M.; Wei, S.; Grunwaldt, J.-D. Interplay of Pt and Crystal Facets of TiO_2: CO Oxidation Activity and Operando XAS/DRIFTS Studies. *ACS Catal.* **2016**, *6*, 7799−7809.
(1939) Wang, W.-K.; Chen, J.-J.; Li, W.-W.; Pei, D.-N.; Zhang, X.; Yu, H.-Q. Synthesis of Pt-Loaded Self-Interspersed Anatase TiO_2 with a Large Fraction of (001) Facets for Efficient Photocatalytic Nitrobenzene Degradation. *ACS Appl. Mater. Interfaces* **2015**, *7*, 20349−20359.
(1940) Liu, L.; Gu, X.; Cao, Y.; Yao, X.; Zhang, L.; Tang, C.; Gao, F.; Dong, L. Crystal-Plane Effects on the Catalytic Properties of Au/TiO_2. *ACS Catal.* **2013**, *3*, 2768−2775.
(1941) Chen, S.; Zhang, B.; Su, D.; Huang, W. Titania Morphology-Dependent Gold-Titania Interaction, Structure, and Catalytic Performance of Gold/Titania Catalysts. *ChemCatChem.* **2015**, *7*, 3290−3298.
(1942) Zhang, Q.; Lee, I.; Ge, J.; Zaera, F.; Yin, Y. Surface-Protected Etching of Mesoporous Oxide Shells for Stabilization of Metal Nanocatalysts. *Adv. Funct. Mater.* **2010**, *20*, 2201−2214.
(1943) Liu, J.; Qiao, S. Z.; Chen, J. S.; Lou, X. W.; Xing, X.; Lu, G. Q. Yolk/shell nanoparticles: new platforms for nanoreactors, drug delivery and lithium-ion batteries. *Chem. Commun.* **2011**, *47*, 12578−12591.
(1944) Pérez-Lorenzo, M.; Vaz, B.; Salgueiriño, V.; Correa-Duarte, M. A. Hollow-Shelled Nanoreactors Endowed with High Catalytic Activity. *Chem.-Eur. J.* **2013**, *19*, 12196−12211.
(1945) Ye, R.-P.; Wang, X.; Price, C.-A. H.; Liu, X.; Yang, Q.; Jaroniec, M.; Liu, J. Engineering of Yolk/Core-Shell Structured Nanoreactors for Thermal Hydrogenations. *Small* **2021**, *17*, 1906250.
(1946) Luo, J.; Wang, L.; Mott, D.; Njoki, P. N.; Lin, Y.; He, T.; Xu, Z.; Wanjana, B. N.; Lim, I. I. S.; Zhong, C.-J. Core/Shell Nanoparticles as Electrocatalysts for Fuel Cell Reactions. *Adv. Mater.* **2008**, *20*, 4342−4347.
(1947) Zhang, Q.; Lee, I.; Joo, J. B.; Zaera, F.; Yin, Y. Core-Shell Nanostructured Catalysts. *Acc. Chem. Res.* **2013**, *46*, 1816−1824.
(1948) Li, G.; Tang, Z. Noble metal nanoparticle@metal oxide core/yolk-shell nanostructures as catalysts: recent progress and perspective. *Nanoscale* **2014**, *6*, 3995−4011.
(1949) Prieto, G.; Tüysüz, H.; Duyckaerts, N.; Knossalla, J.; Wang, G.-H.; Schüth, F. Hollow Nano- and Microstructures as Catalysts. *Chem. Rev.* **2016**, *116*, 14056−14119.
(1950) Li, Z.; Li, M.; Bian, Z.; Kathiraser, Y.; Kawi, S. Design of highly stable and selective core/yolk-shell nanocatalysts—A review. *Appl. Catal. B* **2016**, *188*, 324−341.
(1951) Li, W.; Elzatahry, A.; Aldhayan, D.; Zhao, D. Core-shell structured titanium dioxide nanomaterials for solar energy utilization. *Chem. Soc. Rev.* **2018**, *47*, 8203−8237.
(1952) Gao, C.; Lyu, F.; Yin, Y. Encapsulated Metal Nanoparticles for Catalysis. *Chem. Rev.* **2021**, *121*, 834.
(1953) Das, S.; Pérez-Ramírez, J.; Gong, J.; Dewangan, N.; Hidajat, K.; Gates, B. C.; Kawi, S. Core-shell structured catalysts for thermocatalytic, photocatalytic, and electrocatalytic conversion of CO_2. *Chem. Soc. Rev.* **2020**, *49*, 2937−3004.
(1954) Zhang, Q.; Lee, I.; Joo, J. B.; Zaera, F.; Yin, Y. Core-Shell Nanostructured Catalysts. *Acc. Chem. Res.* **2013**, *46*, 1816−1824.
(1955) Priebe, M.; Fromm, K. M. Nanorattles or Yolk-Shell Nanoparticles—What Are They, How Are They Made, and What Are They Good For? *Chem.-Eur. J.* **2015**, *21*, 3854−3874.
(1956) Wang, M.; Boyjoo, Y.; Pan, J.; Wang, S.; Liu, J. Advanced yolk-shell nanoparticles as nanoreactors for energy conversion. *Chinese Journal of Catalysis* **2017**, *38*, 970−990.
(1957) Liu, L.; Gao, F.; Concepción, P.; Corma, A. A new strategy to transform mono and bimetallic non-noble metal nanoparticles into highly active and chemoselective hydrogenation catalysts. *J. Catal.* **2017**, *350*, 218−225.
(1958) Otor, H. O.; Steiner, J. B.; García-Sancho, C.; Alba-Rubio, A. C. Encapsulation Methods for Control of Catalyst Deactivation: A Review. *ACS Catal.* **2020**, *10*, 7630−7656.
(1959) Yin, H.; Ma, Z.; Zhu, H.; Chi, M.; Dai, S. Evidence for and mitigation of the encapsulation of gold nanoparticles within silica supports upon high-temperature treatment of Au/SiO_2 catalysts: Implication to catalyst deactivation. *Appl. Catal. A* **2010**, *386*, 147−156.
(1960) Qiao, Z.-A.; Zhang, P.; Chai, S.-H.; Chi, M.; Veith, G. M.; Gallego, N. C.; Kidder, M.; Dai, S. Lab-in-a-Shell: Encapsulating Metal Clusters for Size Sieving Catalysis. *J. Am. Chem. Soc.* **2014**, *136*, 11260−11263.

https://doi.org/10.1021/acs.chemrev.1c00905
Chem. Rev. XXXX, XXX, XXX−XXX

(1961) Zhu, Y.; Zaera, F. Selectivity in the catalytic hydrogenation of cinnamaldehyde promoted by Pt/SiO_2 as a function of metal nanoparticle size. *Catal. Sci. Technol.* **2014**, *4*, 955−962.
(1962) Gao, D.; Zhou, H.; Wang, J.; Miao, S.; Yang, F.; Wang, G.; Wang, J.; Bao, X. Size-Dependent Electrocatalytic Reduction of CO_2 over Pd Nanoparticles. *J. Am. Chem. Soc.* **2015**, *137*, 4288−4291.
(1963) Li, Y.; Zaera, F. Sensitivity of the glycerol oxidation reaction to the size and shape of the platinum nanoparticles in Pt/SiO_2 catalysts. *J. Catal.* **2015**, *326*, 116−126.
(1964) Crampton, A. S.; Rotzer, M. D.; Ridge, C. J.; Schweinberger, F. F.; Heiz, U.; Yoon, B.; Landman, U. Structure sensitivity in the nonscalable regime explored via catalysed ethylene hydrogenation on supported platinum nanoclusters. *Nat. Commun.* **2016**, *7*. DOI: 10.1038/ncomms10389
(1965) Bai, L.; Zhang, S.; Chen, Q.; Gao, C. Synthesis of Ultrasmall Platinum Nanoparticles on Polymer Nanoshells for Size-Dependent Catalytic Oxidation Reactions. *ACS Appl. Mater. Interfaces* **2017**, *9*, 9710−9717.
(1966) Cheng, Q.; Tian, Y.; Lyu, S.; Zhao, N.; Ma, K.; Ding, T.; Jiang, Z.; Wang, L.; Zhang, J.; Zheng, L.; et al. Confined small-sized cobalt catalysts stimulate carbon-chain growth reversely by modifying ASF law of Fischer-Tropsch synthesis. *Nat. Commun.* **2018**, *9*, 3250.
(1967) Ishida, T.; Koga, H.; Okumura, M.; Haruta, M. Advances in Gold Catalysis and Understanding the Catalytic Mechanism. *Chem. Rec.* **2016**, *16*, 2278−2293.
(1968) Ishida, T.; Murayama, T.; Taketoshi, A.; Haruta, M. Importance of Size and Contact Structure of Gold Nanoparticles for the Genesis of Unique Catalytic Processes. *Chem. Rev.* **2020**, *120*, 464−525.
(1969) Laoufi, I.; Saint-Lager, M. C.; Lazzari, R.; Jupille, J.; Robach, O.; Garaudée, S.; Cabailh, G.; Dolle, P.; Cruguel, H.; Bailly, A. Size and Catalytic Activity of Supported Gold Nanoparticles: An in Operando Study during CO Oxidation. *J. Phys. Chem. C* **2011**, *115*, 4673−4679.
(1970) Masoud, N.; Partsch, T.; de Jong, K. P.; de Jongh, P. E. Thermal stability of oxide-supported gold nanoparticles. *Gold Bulletin* **2019**, *52*, 105−114.
(1971) Zhang, T.; Zhao, H.; He, S.; Liu, K.; Liu, H.; Yin, Y.; Gao, C. Unconventional Route to Encapsulated Ultrasmall Gold Nanoparticles for High-Temperature Catalysis. *ACS Nano* **2014**, *8*, 7297−7304.
(1972) Qi, J.; Chen, J.; Li, G.; Li, S.; Gao, Y.; Tang, Z. Facile synthesis of core-shell $Au@CeO_2$ nanocomposites with remarkably enhanced catalytic activity for CO oxidation. *Energy Environ. Sci.* **2012**, *5*, 8937−8941.
(1973) Wang, X.; Liu, D.; Li, J.; Zhen, J.; Wang, F.; Zhang, H. γ-Al_2O_3 supported $Pd@CeO_2$ core@shell nanospheres: salting-out assisted growth and self-assembly, and their catalytic performance in CO oxidation. *Chem. Sci.* **2015**, *6*, 2877−2884.
(1974) Chen, C.; Fang, X.; Wu, B.; Huang, L.; Zheng, N. A Multi-Yolk-Shell Structured Nanocatalyst Containing Sub-10 nm Pd Nanoparticles in Porous CeO_2. *ChemCatChem.* **2012**, *4*, 1578−1586.
(1975) Zhang, Y.; Zhang, J.; Zhang, B.; Si, R.; Han, B.; Hong, F.; Niu, Y.; Sun, L.; Li, L.; Qiao, B.; et al. Boosting the catalysis of gold by O_2 activation at Au-SiO_2 interface. *Nat. Commun.* **2020**, *11*, 558.
(1976) Lee, I.; Joo, J. B.; Yin, Y.; Zaera, F. A Yolk@Shell Nanoarchitecture for Au/TiO_2 Catalysts. *Angew. Chem., Int. Ed.* **2011**, *50*, 10208−10211.
(1977) Cargnello, M.; Jaén, J. J. D.; Garrido, J. C. H.; Bakhmutsky, K.; Montini, T.; Gámez, J. J. C.; Gorte, R. J.; Fornasiero, P. Exceptional Activity for Methane Combustion over Modular $Pd@CeO_2$ Subunits on Functionalized Al_2O_3. *Science* **2012**, *337*, 713.
(1978) Adijanto, L.; Bennett, D. A.; Chen, C.; Yu, A. S.; Cargnello, M.; Fornasiero, P.; Gorte, R. J.; Vohs, J. M. Exceptional Thermal Stability of $Pd@CeO_2$ Core-Shell Catalyst Nanostructures Grafted onto an Oxide Surface. *Nano Lett.* **2013**, *13*, 2252−2257.
(1979) Zhang, S.; Chen, C.; Cargnello, M.; Fornasiero, P.; Gorte, R. J.; Graham, G. W.; Pan, X. Dynamic structural evolution of supported palladium-ceria core-shell catalysts revealed by in situ electron microscopy. *Nat. Commun.* **2015**, *6*, 7778.
(1980) Lee, S.; Seo, J.; Jung, W. Sintering-resistant $Pt@CeO_2$ nanoparticles for high-temperature oxidation catalysis. *Nanoscale* **2016**, *8*, 10219−10228.
(1981) Feng, X.; Li, W.; Liu, D.; Zhang, Z.; Duan, Y.; Zhang, Y. Self-Assembled $Pd@CeO_2/\gamma$-Al_2O_3 Catalysts with Enhanced Activity for Catalytic Methane Combustion. *Small* **2017**, *13*, 1700941.
(1982) Cai, G.; Luo, W.; Xiao, Y.; Zheng, Y.; Zhong, F.; Zhan, Y.; Jiang, L. Synthesis of a Highly Stable $Pd@CeO_2$ Catalyst for Methane Combustion with the Synergistic Effect of Urea and Citric Acid. *ACS Omega* **2018**, *3*, 16769−16776.
(1983) Li, L.; Zhang, N.; Huang, X.; Liu, Y.; Li, Y.; Zhang, G.; Song, L.; He, H. Hydrothermal Stability of Core-Shell $Pd@Ce_{0.5}Zr_{0.5}O_2/Al_2O_3$ Catalyst for Automobile Three-Way Reaction. *ACS Catal.* **2018**, *8*, 3222−3231.
(1984) Zhao, H.; Yao, S.; Zhang, M.; Huang, F.; Fan, Q.; Zhang, S.; Liu, H.; Ma, D.; Gao, C. Ultra-Small Platinum Nanoparticles Encapsulated in Sub-50 nm Hollow Titania Nanospheres for Low-Temperature Water-Gas Shift Reaction. *ACS Appl. Mater. Interfaces* **2018**, *10*, 36954−36960.
(1985) Wieder, N. L.; Cargnello, M.; Bakhmutsky, K.; Montini, T.; Fornasiero, P.; Gorte, R. J. Study of the Water-Gas-Shift Reaction on $Pd@CeO_2/Al_2O_3$ Core-Shell Catalysts. *J. Phys. Chem. C* **2011**, *115*, 915−919.
(1986) Shim, J.-O.; Hong, Y. J.; Na, H.-S.; Jang, W.-J.; Kang, Y. C.; Roh, H.-S. Highly Active and Stable Pt-Loaded $Ce_{0.75}Zr_{0.25}O_2$ Yolk-Shell Catalyst for Water-Gas Shift Reaction. *ACS Appl. Mater. Interfaces* **2016**, *8*, 17239−17244.
(1987) Forman, A. J.; Park, J.-N.; Tang, W.; Hu, Y.-S.; Stucky, G. D.; McFarland, E. W. Silica-Encapsulated Pd Nanoparticles as a Regenerable and Sintering-Resistant Catalyst. *ChemCatChem.* **2010**, *2*, 1318−1324.
(1988) Li, Z.; Mo, L.; Kathiraser, Y.; Kawi, S. Yolk-Satellite-Shell Structured Ni-Yolk@Ni@SiO_2 Nanocomposite: Superb Catalyst toward Methane CO_2 Reforming Reaction. *ACS Catal.* **2014**, *4*, 1526−1536.
(1989) Lim, Z.-Y.; Wu, C.; Wang, W. G.; Choy, K.-L.; Yin, H. A novel and anti-agglomerating Ni@yolk-ZrO_2 structure with sub-10 nm Ni core for high performance steam reforming of methane. *RSC Adv.* **2015**, *5*, 61925−61932.
(1990) Price, C. A. H.; Reina, T. R.; Liu, J. Engineering heterogenous catalysts for chemical CO_2 utilization: Lessons from thermal catalysis and advantages of yolk@shell structured nanoreactors. *Journal of Energy Chemistry* **2021**, *57*, 304−324.
(1991) Park, J. C.; Bang, J. U.; Lee, J.; Ko, C. H.; Song, H. Ni@SiO_2 yolk-shell nanoreactor catalysts: High temperature stability and recyclability. *J. Mater. Chem.* **2010**, *20*, 1239−1246.
(1992) Wang, F.; Xu, L.; Shi, W. Syngas production from CO_2 reforming with methane over core-shell Ni@SiO_2 catalysts. *Journal of CO2 Utilization* **2016**, *16*, 318−327.
(1993) Lucchini, M. A.; Testino, A.; Kambolis, A.; Proff, C.; Ludwig, C. Sintering and coking resistant core-shell microporous silica-nickel nanoparticles for CO methanation: Towards advanced catalysts production. *Appl. Catal. B* **2016**, *182*, 94−101.
(1994) Zhao, X.; Li, H.; Zhang, J.; Shi, L.; Zhang, D. Design and synthesis of NiCe@m-SiO_2 yolk-shell framework catalysts with improved coke- and sintering-resistance in dry reforming of methane. *International Journal of Hydrogen Energy* **2016**, *41*, 2447−2456.
(1995) Liu, W.; Li, L.; Zhang, X.; Wang, Z.; Wang, X.; Peng, H. Design of Ni-ZrO_2@SiO_2 catalyst with ultra-high sintering and coking resistance for dry reforming of methane to prepare syngas. *Journal of CO2 Utilization* **2018**, *27*, 297−307.
(1996) Li, P.; Yu, Y.; Liu, H.; Cao, C.-Y.; Song, W.-G. A core-shell-satellite structured Fe_3O_4@MS-NH_2@Pd nanocomposite: a magnetically recyclable multifunctional catalyst for one-pot multistep cascade reaction sequences. *Nanoscale* **2014**, *6*, 442−448.
(1997) Li, J.; Zhao, H.; Hou, X.; Fa, W.; Cai, J. Fe_3O_4@SiO_2-SO_3H nanocomposites: an efficient magnetically separable solid acid

https://doi.org/10.1021/acs.chemrev.1c00905
Chem. Rev. XXXX, XXX, XXX−XXX

catalysts for esterification reaction. *Micro & Nano Letters* **2017**, *12*, 53−57.
(1998) Kothandapani, J.; Ganesan, S. S. Concise Review on the Applications of Magnetically Separable Brønsted Acidic Catalysts. *Curr. Org. Chem.* **2019**, *23*, 313−334.
(1999) Galeano, C.; Baldizzone, C.; Bongard, H.; Spliethoff, B.; Weidenthaler, C.; Meier, J. C.; Mayrhofer, K. J. J.; Schüth, F. Carbon-Based Yolk-Shell Materials for Fuel Cell Applications. *Adv. Funct. Mater.* **2014**, *24*, 220−232.
(2000) Gao, L.; Fu, Q.; Wei, M.; Zhu, Y.; Liu, Q.; Crumlin, E.; Liu, Z.; Bao, X. Enhanced Nickel-Catalyzed Methanation Confined under Hexagonal Boron Nitride Shells. *ACS Catal.* **2016**, *6*, 6814−6822.
(2001) Tian, H.; Liu, X.; Dong, L.; Ren, X.; Liu, H.; Price, C. A. H.; Li, Y.; Wang, G.; Yang, Q.; Liu, J. Enhanced Hydrogenation Performance over Hollow Structured Co-CoO_x@N-C Capsules. *Advanced Science* **2019**, *6*, 1900807.
(2002) Wang, J. X.; Ma, C.; Choi, Y.; Su, D.; Zhu, Y.; Liu, P.; Si, R.; Vukmirovic, M. B.; Zhang, Y.; Adzic, R. R. Kirkendall Effect and Lattice Contraction in Nanocatalysts: A New Strategy to Enhance Sustainable Activity. *J. Am. Chem. Soc.* **2011**, *133*, 13551−13557.
(2003) Cargnello, M.; Montini, T.; Polizzi, S.; Wieder, N. L.; Gorte, R. J.; Graziani, M.; Fornasiero, P. Novel embedded Pd@CeO_2 catalysts: a way to active and stable catalysts. *Dalton Trans.* **2010**, *39*, 2122−2127.
(2004) Kamata, K.; Lu, Y.; Xia, Y. Synthesis and Characterization of Monodispersed Core-Shell Spherical Colloids with Movable Cores. *J. Am. Chem. Soc.* **2003**, *125*, 2384−2385.
(2005) Lee, J.; Park, J. C.; Bang, J. U.; Song, H. Precise Tuning of Porosity and Surface Functionality in Au@SiO_2 Nanoreactors for High Catalytic Efficiency. *Chem. Mater.* **2008**, *20*, 5839−5844.
(2006) Fang, X.; Liu, S.; Zang, J.; Xu, C.; Zheng, M.-S.; Dong, Q.-F.; Sun, D.; Zheng, N. Precisely controlled resorcinol-formaldehyde resin coating for fabricating core-shell, hollow, and yolk-shell carbon nanostructures. *Nanoscale* **2013**, *5*, 6908−6916.
(2007) Liu, X.; Cui, X.; Liu, Y.; Yin, Y. Stabilization of ultrafine metal nanocatalysts on thin carbon sheets. *Nanoscale* **2015**, *7*, 18320−18326.
(2008) Harada, T.; Ikeda, S.; Hashimoto, F.; Sakata, T.; Ikeue, K.; Torimoto, T.; Matsumura, M. Catalytic Activity and Regeneration Property of a Pd Nanoparticle Encapsulated in a Hollow Porous Carbon Sphere for Aerobic Alcohol Oxidation. *Langmuir* **2010**, *26*, 17720−17725.
(2009) Wang, G.-H.; Hilgert, J.; Richter, F. H.; Wang, F.; Bongard, H.-J.; Spliethoff, B.; Weidenthaler, C.; Schüth, F. Platinum-cobalt bimetallic nanoparticles in hollow carbon nanospheres for hydrogenolysis of 5-hydroxymethylfurfural. *Nat. Mater.* **2014**, *13*, 293−300.
(2010) Pochert, A.; Schneider, D.; Haase, J.; Linden, M.; Valiullin, R. Diffusion and Molecular Exchange in Hollow Core-Shell Silica Nanoparticles. *Langmuir* **2015**, *31*, 10285−10295.
(2011) Liang, X.; Li, J.; Joo, J. B.; Gutiérrez, A.; Tillekaratne, A.; Lee, I.; Yin, Y.; Zaera, F. Diffusion through the Shells of Yolk-Shell and Core-Shell Nanostructures in the Liquid Phase. *Angew. Chem., Int. Ed.* **2012**, *51*, 8034−8036.
(2012) Li, J.; Liang, X.; Joo, J. B.; Lee, I.; Yin, Y.; Zaera, F. Mass Transport Across the Porous Oxide Shells of Core-Shell and Yolk-Shell Nanostructures in Liquid Phase. *J. Phys. Chem. C* **2013**, *117*, 20043−20053.
(2013) Kim, S.; Yin, Y.; Alivisatos, A. P.; Somorjai, G. A.; Yates, J. T. IR Spectroscopic Observation of Molecular Transport through Pt@CoO Yolk-Shell Nanostructures. *J. Am. Chem. Soc.* **2007**, *129*, 9510−9513.
(2014) Gautam, J.; Thanh, T. D.; Maiti, K.; Kim, N. H.; Lee, J. H. Highly efficient electrocatalyst of N-doped graphene-encapsulated cobalt-iron carbides towards oxygen reduction reaction. *Carbon* **2018**, *137*, 358−367.
(2015) Liu, J.; Yang, H. Q.; Kleitz, F.; Chen, Z. G.; Yang, T.; Strounina, E.; Lu, G. Q.; Qiao, S. Z. Yolk-Shell Hybrid Materials with a Periodic Mesoporous Organosilica Shell: Ideal Nanoreactors for Selective Alcohol Oxidation. *Adv. Funct. Mater.* **2012**, *22*, 591−599.
(2016) Lin, C.-H.; Liu, X.; Wu, S.-H.; Liu, K.-H.; Mou, C.-Y. Corking and Uncorking a Catalytic Yolk-Shell Nanoreactor: Stable Gold Catalyst in Hollow Silica Nanosphere. *J. Phys. Chem. Lett.* **2011**, *2*, 2984−2988.
(2017) Long, Y.; Song, S.; Li, J.; Wu, L.; Wang, Q.; Liu, Y.; Jin, R.; Zhang, H. Pt/CeO_2@MOF Core@Shell Nanoreactor for Selective Hydrogenation of Furfural via the Channel Screening Effect. *ACS Catal.* **2018**, *8*, 8506−8512.
(2018) Chen, Z.; Cui, Z.-M.; Li, P.; Cao, C.-Y.; Hong, Y.-L.; Wu, Z.-y.; Song, W.-G. Diffusion Induced Reactant Shape Selectivity Inside Mesoporous Pores of Pd@meso-SiO_2 Nanoreactor in Suzuki Coupling Reactions. *J. Phys. Chem. C* **2012**, *116*, 14986−14991.
(2019) Cheng, H.; Huang, B.; Liu, Y.; Wang, Z.; Qin, X.; Zhang, X.; Dai, Y. An anion exchange approach to Bi_2WO_6 hollow microspheres with efficient visible light photocatalytic reduction of CO_2 to methanol. *Chem. Commun.* **2012**, *48*, 9729−9731.
(2020) Li, B.; Zeng, H. C. Synthetic Chemistry and Multifunctionality of an Amorphous Ni-MOF-74 Shell on a Ni/SiO_2 Hollow Catalyst for Efficient Tandem Reactions. *Chem. Mater.* **2019**, *31*, 5320−5330.
(2021) Yang, Y.; Liu, X.; Li, X.; Zhao, J.; Bai, S.; Liu, J.; Yang, Q. A Yolk-Shell Nanoreactor with a Basic Core and an Acidic Shell for Cascade Reactions. *Angew. Chem., Int. Ed.* **2012**, *51*, 9164−9168.
(2022) Li, P.; Cao, C.-Y.; Liu, H.; Yu, Y.; Song, W.-G. Synthesis of a core-shell-shell structured acid-base bifunctional mesoporous silica nanoreactor (MS-SO_3H@MS@MS-NH_2) and its application in tandem catalysis. *Journal of Materials Chemistry A* **2013**, *1*, 12804−12810.
(2023) Su, J.; Xie, C.; Chen, C.; Yu, Y.; Kennedy, G.; Somorjai, G. A.; Yang, P. Insights into the Mechanism of Tandem Alkene Hydroformylation over a Nanostructured Catalyst with Multiple Interfaces. *J. Am. Chem. Soc.* **2016**, *138*, 11568−11574.
(2024) Xie, C.; Chen, C.; Yu, Y.; Su, J.; Li, Y.; Somorjai, G. A.; Yang, P. Tandem Catalysis for CO_2 Hydrogenation to C_2-C_4 Hydrocarbons. *Nano Lett.* **2017**, *17*, 3798−3802.
(2025) Hill, A. J.; Seo, C. Y.; Chen, X.; Bhat, A.; Fisher, G. B.; Lenert, A.; Schwank, J. W. Thermally Induced Restructuring of Pd@CeO_2 and Pd@SiO_2 Nanoparticles as a Strategy for Enhancing Low-Temperature Catalytic Activity. *ACS Catal.* **2020**, *10*, 1731−1741.
(2026) Cui, X.; Ren, P.; Deng, D.; Deng, J.; Bao, X. Single layer graphene encapsulating non-precious metals as high-performance electrocatalysts for water oxidation. *Energy Environ. Sci.* **2016**, *9*, 123−129.
(2027) Sharma, M.; Jang, J.-H.; Shin, D. Y.; Kwon, J. A.; Lim, D.-H.; Choi, D.; Sung, H.; Jang, J.; Lee, S.-Y.; Lee, K. Y.; et al. Work function-tailored graphene via transition metal encapsulation as a highly active and durable catalyst for the oxygen reduction reaction. *Energy Environ. Sci.* **2019**, *12*, 2200−2211.
(2028) Lee, I.; Joo, J. B.; Yin, Y.; Zaera, F. Au@Void@TiO_2 yolk-shell nanostructures as catalysts for the promotion of oxidation reactions at cryogenic temperatures. *Surf. Sci.* **2016**, *648*, 150−155.
(2029) Zaera, F. Gold-Titania Catalysts for Low-Temperature Oxidation and Water Splitting. *Top. Catal.* **2018**, *61*, 336−347.
(2030) Lee, I.; Zaera, F. Use of Au@Void@TiO_2 yolk-shell nanostructures to probe the influence of oxide crystallinity on catalytic activity for low-temperature oxidations. *J. Chem. Phys.* **2019**, *151*, 234706.
(2031) Lee, I.; Zaera, F. Catalytic oxidation of carbon monoxide at cryogenic temperatures. *J. Catal.* **2014**, *319*, 155−162.
(2032) Dillon, R. J.; Joo, J.-B.; Zaera, F.; Yin, Y.; Bardeen, C. J. Correlating the excited state relaxation dynamics as measured by photoluminescence and transient absorption with the photocatalytic activity of Au@TiO_2 core-shell nanostructures. *Phys. Chem. Chem. Phys.* **2013**, *15*, 1488−1496.
(2033) Joo, J. B.; Dillon, R.; Lee, I.; Yin, Y.; Bardeen, C. J.; Zaera, F. Promotion of Atomic Hydrogen Recombination as an Alternative to Electron Trapping for the Role of Metals in the Photocatalytic Production of H_2. *Proc. Natl. Acad. Sci. U. S. A.* **2014**, *111*, 7942−7947.

https://doi.org/10.1021/acs.chemrev.1c00905
Chem. Rev. XXXX, XXX, XXX−XXX

(2034) Lee, Y. J.; Joo, J. B.; Yin, Y.; Zaera, F. Evaluation of the Effective Photoexcitation Distances in the Photocatalytic Production of H_2 from Water using Au@Void@TiO_2 Yolk-Shell Nanostructures. *ACS Energy Letters* **2016**, *1*, 52−56.
(2035) van der Hoeven, J. E. S.; Jelic, J.; Olthof, L. A.; Totarella, G.; van Dijk-Moes, R. J. A.; Krafft, J.-M.; Louis, C.; Studt, F.; van Blaaderen, A.; de Jongh, P. E. Unlocking synergy in bimetallic catalysts by core-shell design. *Nat. Mater.* **2021**, *20*, 1216.
(2036) Wang, D.; Wang, Z.; Li, G.; Li, X.; Hou, B. SiO_2-Modified Al_2O_3@Al-Supported Cobalt for Fischer-Tropsch Synthesis: Improved Catalytic Performance and Intensified Heat Transfer. *Industrial & Engineering Chemistry Research* **2018**, *57*, 12756−12765.
(2037) Wang, Y.; Zhao, Y.; Lv, J.; Ma, X. Facile Synthesis of Cu@CeO_2 and Its Catalytic Behavior for the Hydrogenation of Methyl Acetate to Ethanol. *ChemCatChem.* **2017**, *9*, 2085−2090.
(2038) Huang, X.; Ma, M.; Miao, S.; Zheng, Y.; Chen, M.; Shen, W. Hydrogenation of methyl acetate to ethanol over a highly stable Cu/SiO_2 catalyst: Reaction mechanism and structural evolution. *Appl. Catal. A* **2017**, *531*, 79−88.
(2039) Bustamante, T. M.; Fraga, M. A.; Fierro, J. L. G.; Campos, C. H.; Pecchi, G. Cobalt SiO_2 core-shell catalysts for chemoselective hydrogenation of cinnamaldehyde. *Catal. Today* **2020**, *356*, 330−338.
(2040) Poggi, E.; Gohy, J.-F. Janus particles: from synthesis to application. *Colloid and Polymer Science* **2017**, *295*, 2083−2108.
(2041) Qiu, J.; Camargo, P. H. C.; Jeong, U.; Xia, Y. Synthesis, Transformation, and Utilization of Monodispersed Colloidal Spheres. *Acc. Chem. Res.* **2019**, *52*, 3475−3487.
(2042) Lee, K. J.; Yoon, J.; Lahann, J. Recent advances with anisotropic particles. *Current Opinion in Colloid & Interface Science* **2011**, *16*, 195−202.
(2043) Ismail, A. S. M.; Casavola, M.; Liu, B.; Gloter, A.; van Deelen, T. W.; Versluijs, M.; Meeldijk, J. D.; Stéphan, O.; de Jong, K. P.; de Groot, F. M. F. Atomic-Scale Investigation of the Structural and Electronic Properties of Cobalt-Iron Bimetallic Fischer-Tropsch Catalysts. *ACS Catal.* **2019**, *9*, 7998−8011.
(2044) Zhang, J.; Shao, Q.; Wang, P.; Guo, J.; Huang, X. Catalytic Hydrogen Production by Janus CuAg Nanostructures. *ChemNanoMat* **2018**, *4*, 477−481.
(2045) Wang, C.; Yin, H.; Dai, S.; Sun, S. A General Approach to Noble Metal-Metal Oxide Dumbbell Nanoparticles and Their Catalytic Application for CO Oxidation. *Chem. Mater.* **2010**, *22*, 3277−3282.
(2046) Han, C. W.; Choksi, T.; Milligan, C.; Majumdar, P.; Manto, M.; Cui, Y.; Sang, X.; Unocic, R. R.; Zemlyanov, D.; Wang, C.; et al. A Discovery of Strong Metal-Support Bonding in Nanoengineered Au-Fe_3O_4 Dumbbell-like Nanoparticles by in Situ Transmission Electron Microscopy. *Nano Lett.* **2017**, *17*, 4576−4582.
(2047) Wang, C.; Daimon, H.; Sun, S. Dumbbell-like Pt-Fe_3O_4 Nanoparticles and Their Enhanced Catalysis for Oxygen Reduction Reaction. *Nano Lett.* **2009**, *9*, 1493−1496.
(2048) Li, Q.; Wu, L.; Wu, G.; Su, D.; Lv, H.; Zhang, S.; Zhu, W.; Casimir, A.; Zhu, H.; Mendoza-Garcia, A.; et al. New Approach to Fully Ordered fct-FePt Nanoparticles for Much Enhanced Electrocatalysis in Acid. *Nano Lett.* **2015**, *15*, 2468−2473.
(2049) Lee, Y.; Garcia, M. A.; Frey Huls, N. A.; Sun, S. Synthetic Tuning of the Catalytic Properties of Au-Fe_3O_4 Nanoparticles. *Angew. Chem., Int. Ed.* **2010**, *49*, 1271−1274.
(2050) Sun, X.; Guo, S.; Chung, C.-S.; Zhu, W.; Sun, S. A Sensitive H_2O_2 Assay Based on Dumbbell-like PtPd-Fe_3O_4 Nanoparticles. *Adv. Mater.* **2013**, *25*, 132−136.
(2051) Wu, B.; Zhang, H.; Chen, C.; Lin, S.; Zheng, N. Interfacial activation of catalytically inert Au (6.7 nm)-Fe_3O_4 dumbbell nanoparticles for CO oxidation. *Nano Res.* **2009**, *2*, 975−983.
(2052) Lee, K. S.; Anisur, R. M.; Kim, K. W.; Kim, W. S.; Park, T.-J.; Kang, E. J.; Lee, I. S. Seed Size-Dependent Formation of Fe_3O_4/MnO Hybrid Nanocrystals: Selective, Magnetically Recyclable Catalyst Systems. *Chem. Mater.* **2012**, *24*, 682−687.
(2053) Lu, C.; Liu, X.; Li, Y.; Yu, F.; Tang, L.; Hu, Y.; Ying, Y. Multifunctional Janus Hematite-Silica Nanoparticles: Mimicking Peroxidase-Like Activity and Sensitive Colorimetric Detection of Glucose. *ACS Appl. Mater. Interfaces* **2015**, *7*, 15395−15402.
(2054) Kuttiyiel, K. A.; Sasaki, K.; Park, G.-G.; Vukmirovic, M. B.; Wu, L.; Zhu, Y.; Chen, J. G.; Adzic, R. R. Janus structured Pt-FeNC nanoparticles as a catalyst for the oxygen reduction reaction. *Chem. Commun.* **2017**, *53*, 1660−1663.
(2055) Suryanto, B. H. R.; Wang, Y.; Hocking, R. K.; Adamson, W.; Zhao, C. Overall electrochemical splitting of water at the heterogeneous interface of nickel and iron oxide. *Nat. Commun.* **2019**, *10*, 5599.
(2056) Xue, Z.-H.; Su, H.; Yu, Q.-Y.; Zhang, B.; Wang, H.-H.; Li, X.-H.; Chen, J.-S. Janus Co/CoP Nanoparticles as Efficient Mott-Schottky Electrocatalysts for Overall Water Splitting in Wide pH Range. *Adv. Energy Mater.* **2017**, *7*, 1602355.
(2057) Lai, J.; Huang, B.; Tang, Y.; Lin, F.; Zhou, P.; Chen, X.; Sun, Y.; Lv, F.; Guo, S. Barrier-free Interface Electron Transfer on PtFe-Fe_2C Janus-like Nanoparticles Boosts Oxygen Catalysis. *Chem.* **2018**, *4*, 1153−1166.
(2058) Tang, R.; Zhou, S.; Li, C.; Chen, R.; Zhang, L.; Zhang, Z.; Yin, L. Janus-Structured Co-Ti_3C_2 MXene Quantum Dots as a Schottky Catalyst for High-Performance Photoelectrochemical Water Oxidation. *Adv. Funct. Mater.* **2020**, *30*, 2000637.
(2059) Si, Y.; Cao, S.; Wu, Z.; Ji, Y.; Mi, Y.; Wu, X.; Liu, X.; Piao, L. What is the predominant electron transfer process for Au NRs/TiO_2 nanodumbbell heterostructure under sunlight irradiation? *Appl. Catal. B* **2018**, *220*, 471−476.
(2060) Greydanus, B.; Schwartz, D. K.; Medlin, J. W. Controlling Catalyst-Phase Selectivity in Complex Mixtures with Amphiphilic Janus Particles. *ACS Appl. Mater. Interfaces* **2020**, *12*, 2338−2345.
(2061) Faria, J.; Ruiz, M. P.; Resasco, D. E. Phase-Selective Catalysis in Emulsions Stabilized by Janus Silica-Nanoparticles. *Adv. Synth. Catal.* **2010**, *352*, 2359−2364.
(2062) Yang, T.; Wei, L.; Jing, L.; Liang, J.; Zhang, X.; Tang, M.; Monteiro, M. J.; Chen, Y.; Wang, Y.; Gu, S.; et al. Dumbbell-Shaped Bi-component Mesoporous Janus Solid Nanoparticles for Biphasic Interface Catalysis. *Angew. Chem., Int. Ed.* **2017**, *56*, 8459−8463.
(2063) Liu, Y.; Hu, J.; Yu, X.; Xu, X.; Gao, Y.; Li, H.; Liang, F. Preparation of Janus-type catalysts and their catalytic performance at emulsion interface. *J. Coll. Interface Sci.* **2017**, *490*, 357−364.
(2064) Cho, J.; Cho, J.; Kim, H.; Lim, M.; Jo, H.; Kim, H.; Min, S.-J.; Rhee, H.; Kim, J. W. Janus colloid surfactant catalysts for in situ organic reactions in Pickering emulsion microreactors. *Green Chem.* **2018**, *20*, 2840−2844.
(2065) Kirillova, A.; Schliebe, C.; Stoychev, G.; Jakob, A.; Lang, H.; Synytska, A. Hybrid Hairy Janus Particles Decorated with Metallic Nanoparticles for Catalytic Applications. *ACS Appl. Mater. Interfaces* **2015**, *7*, 21218−21225.
(2066) Wang, J.; Manesh, K. M. Motion Control at the Nanoscale. *Small* **2010**, *6*, 338−345.
(2067) Sánchez, S.; Soler, L.; Katuri, J. Chemically Powered Micro- and Nanomotors. *Angew. Chem., Int. Ed.* **2015**, *54*, 1414−1444.
(2068) Dey, K. K.; Wong, F.; Altemose, A.; Sen, A. Catalytic Motors—Quo Vadimus? *Current Opinion in Colloid & Interface Science* **2016**, *21*, 4−13.
(2069) Paxton, W. F.; Kistler, K. C.; Olmeda, C. C.; Sen, A.; St. Angelo, S. K.; Cao, Y.; Mallouk, T. E.; Lammert, P. E.; Crespi, V. H. Catalytic Nanomotors: Autonomous Movement of Striped Nanorods. *J. Am. Chem. Soc.* **2004**, *126*, 13424−13431.
(2070) Lee, C.-S.; Gong, J.; Oh, D.-S.; Jeon, J.-R.; Chang, Y.-S. Zerovalent-Iron/Platinum Janus Micromotors with Spatially Separated Functionalities for Efficient Water Decontamination. *ACS Applied Nano Materials* **2018**, *1*, 768−776.
(2071) Mirkovic, T.; Zacharia, N. S.; Scholes, G. D.; Ozin, G. A. Fuel for Thought: Chemically Powered Nanomotors Out-Swim Nature's Flagellated Bacteria. *ACS Nano* **2010**, *4*, 1782−1789.
(2072) Pumera, M. Electrochemically powered self-propelled electrophoretic nanosubmarines. *Nanoscale* **2010**, *2*, 1643−1649.

https://doi.org/10.1021/acs.chemrev.1c00905
Chem. Rev. XXXX, XXX, XXX−XXX

(2073) Mozaffari, A.; Sharifi-Mood, N.; Koplik, J.; Maldarelli, C. Self-diffusiophoretic colloidal propulsion near a solid boundary. *Phys. Fluids* **2016**, *28*, 053107.
(2074) Fournier-Bidoz, S.; Arsenault, A. C.; Manners, I.; Ozin, G. A. Synthetic self-propelled nanorotors. *Chem. Commun.* **2005**, 441−443.
(2075) Wang, W.; Duan, W.; Ahmed, S.; Sen, A.; Mallouk, T. E. From One to Many: Dynamic Assembly and Collective Behavior of Self-Propelled Colloidal Motors. *Acc. Chem. Res.* **2015**, *48*, 1938−1946.
(2076) Ebbens, S. J. Active colloids: Progress and challenges towards realising autonomous applications. *Current Opinion in Colloid & Interface Science* **2016**, *21*, 14−23.
(2077) Ebbens, S. J.; Gregory, D. A. Catalytic Janus Colloids: Controlling Trajectories of Chemical Microswimmers. *Acc. Chem. Res.* **2018**, *51*, 1931−1939.
(2078) Lin, X.; Zhu, H.; Zhao, Z.; You, C.; Kong, Y.; Zhao, Y.; Liu, J.; Chen, H.; Shi, X.; Makarov, D.; et al. Hydrogel-Based Janus Micromotors Capped with Functional Nanoparticles for Environmental Applications. *Advanced Materials Technologies* **2020**, *5*, 2000279.
(2079) Ma, X.; Hahn, K.; Sanchez, S. Catalytic Mesoporous Janus Nanomotors for Active Cargo Delivery. *J. Am. Chem. Soc.* **2015**, *137*, 4976−4979.
(2080) Guix, M.; Mayorga-Martinez, C. C.; Merkoçi, A. Nano/Micromotors in (Bio)chemical Science Applications. *Chem. Rev.* **2014**, *114*, 6285−6322.
(2081) Guix, M.; Weiz, S. M.; Schmidt, O. G.; Medina-Sánchez, M. Self-Propelled Micro/Nanoparticle Motors. *Particle & Particle Systems Characterization* **2018**, *35*, 1700382.
(2082) Pavlick, R. A.; Sengupta, S.; McFadden, T.; Zhang, H.; Sen, A. A Polymerization-Powered Motor. *Angew. Chem., Int. Ed.* **2011**, *50*, 9374−9377.
(2083) Lee, T.-C.; Alarcón-Correa, M.; Miksch, C.; Hahn, K.; Gibbs, J. G.; Fischer, P. Self-Propelling Nanomotors in the Presence of Strong Brownian Forces. *Nano Lett.* **2014**, *14*, 2407−2412.
(2084) Gao, W.; D'Agostino, M.; Garcia-Gradilla, V.; Orozco, J.; Wang, J. Multi-Fuel Driven Janus Micromotors. *Small* **2013**, *9*, 467−471.
(2085) Gao, W.; Pei, A.; Dong, R.; Wang, J. Catalytic Iridium-Based Janus Micromotors Powered by Ultralow Levels of Chemical Fuels. *J. Am. Chem. Soc.* **2014**, *136*, 2276−2279.
(2086) Maeda, K.; Domen, K. Photocatalytic Water Splitting: Recent Progress and Future Challenges. *J. Phys. Chem. Lett.* **2010**, *1*, 2655−2661.
(2087) Hisatomi, T.; Kubota, J.; Domen, K. Recent advances in semiconductors for photocatalytic and photoelectrochemical water splitting. *Chem. Soc. Rev.* **2014**, *43*, 7520.
(2088) Wang, Q.; Domen, K. Particulate Photocatalysts for Light-Driven Water Splitting: Mechanisms, Challenges, and Design Strategies. *Chem. Rev.* **2020**, *120*, 919−985.
(2089) Takata, T.; Jiang, J.; Sakata, Y.; Nakabayashi, M.; Shibata, N.; Nandal, V.; Seki, K.; Hisatomi, T.; Domen, K. Photocatalytic water splitting with a quantum efficiency of almost unity. *Nature* **2020**, *581*, 411−414.
(2090) Chu, C.; Zhu, Q.; Pan, Z.; Gupta, S.; Huang, D.; Du, Y.; Weon, S.; Wu, Y.; Muhich, C.; Stavitski, E.; et al. Spatially separating redox centers on 2D carbon nitride with cobalt single atom for photocatalytic H_2O_2 production. *Proc. Natl. Acad. Sci. U. S. A.* **2020**, *117*, 6376.
(2091) Zheng, D.; Cao, X.-N.; Wang, X. Precise Formation of a Hollow Carbon Nitride Structure with a Janus Surface To Promote Water Splitting by Photoredox Catalysis. *Angew. Chem., Int. Ed.* **2016**, *55*, 11512−11516.
(2092) Chen, J.; Li, H.; Fan, C.; Meng, Q.; Tang, Y.; Qiu, X.; Fu, G.; Ma, T. Dual Single-Atomic Ni-N_4 and Fe-N_4 Sites Constructing Janus Hollow Graphene for Selective Oxygen Electrocatalysis. *Adv. Mater.* **2020**, *32*, 2003134.
(2093) Li, Z.; Wang, H.; Wu, X.; Ye, Q.; Xu, X.; Li, B.; Wang, F. Novel synthesis and shape-dependent catalytic performance of Cu-Mn oxides for CO oxidation. *Applied Surface Science* **2017**, *403*, 335−341.
(2094) Gong, W.; Jiang, Z.; Wu, R.; Liu, Y.; Huang, L.; Hu, N.; Tsiakaras, P.; Shen, P. K. Cross-double dumbbell-like Pt-Ni nanostructures with enhanced catalytic performance toward the reactions of oxygen reduction and methanol oxidation. *Appl. Catal. B* **2019**, *246*, 277−283.
(2095) Sun, J.; Hu, J.; Han, J.; Yuan, G.; Guo, R. Dumbbell-like Pt-Fe_3O_4 Nanoparticles Encapsulated in N-Doped Carbon Hollow Nanospheres as a Novel Yolk@Shell Nanostructure toward High-Performance Nanocatalysis. *Langmuir* **2019**, *35*, 12704−12710.
(2096) Wang, X.; Guan, B.; He, Y.; Zhang, Y.; Cao, Y.; Liu, Y.; Qiao, Z.-A.; Huo, Q. Synthesis of Janus Mesoporous Silica Nanostructures with Organic-Inorganic Hybrid Components through a Sprout-Like Growth Method. *ChemNanoMat* **2015**, *1*, 562−566.
(2097) He, H.; Tao, Q.; Zhu, J.; Yuan, P.; Shen, W.; Yang, S. Silylation of clay mineral surfaces. *Appl. Clay Sci.* **2013**, *71*, 15−20.
(2098) Mahadik, S. A.; Pedraza, F.; Parale, V. G.; Park, H.-H. Organically modified silica aerogel with different functional silylating agents and effect on their physico-chemical properties. *J. Non-Cryst. Solids* **2016**, *453*, 164−171.
(2099) Halket, J. M.; Zaikin, V. G. Derivatization in mass spectrometry - 1. Silylation. *European Journal of Mass Spectrometry* **2003**, *9*, 1−21.
(2100) Schlosser, M. The 2×3 Toolbox of Organometallic Methods for Regiochemically Exhaustive Functionalization. *Angew. Chem., Int. Ed.* **2005**, *44*, 376−393.
(2101) Seliger, J.; Oestreich, M. Making the Silylation of Alcohols Chiral: Asymmetric Protection of Hydroxy Groups. *Chem.-Eur. J.* **2019**, *25*, 9358−9365.
(2102) Xie, R.; Li, D.; Hou, B.; Wang, J.; Jia, L.; Sun, Y. Silylated Co_3O_4-m-SiO_2 catalysts for Fischer-Tropsch synthesis. *Catal. Commun.* **2011**, *12*, 589−592.
(2103) Jia, L.; Jia, L.; Li, D.; Hou, B.; Wang, J.; Sun, Y. Silylated Co/SBA-15 catalysts for Fischer-Tropsch synthesis. *J. Solid State Chem.* **2011**, *184*, 488−493.
(2104) Nakatsuka, K.; Mori, K.; Okada, S.; Ikurumi, S.; Kamegawa, T.; Yamashita, H. Hydrophobic Modification of Pd/SiO_2@Single-Site Mesoporous Silicas by Triethoxyfluorosilane: Enhanced Catalytic Activity and Selectivity for One-Pot Oxidation. *Chem.-Eur. J.* **2014**, *20*, 8348−8354.
(2105) Hu, L.; Yue, B.; Wang, C.; Chen, X.; He, H. Enhanced catalytic activity over vanadium-containing silylated SBA-15 catalysts for styrene epoxidation and benzene hydroxylation. *Appl. Catal. A* **2014**, *477*, 141−146.
(2106) Silvestre-Alberó, J.; Domine, M. E.; Jordá, J. L.; Navarro, M. T.; Rey, F.; Rodríguez-Reinoso, F.; Corma, A. Spectroscopic, calorimetric, and catalytic evidences of hydrophobicity on Ti-MCM-41 silylated materials for olefin epoxidations. *Appl. Catal. A* **2015**, *507*, 14−25.
(2107) Yuan, L. S.; Chandren, S.; Efendi, J. O. N.; Ho, C. S.; Nur, H. Hydrophobic effect of silica functionalized with silylated Ti-salicylaldimine complex on limonene oxidation by aqueous hydrogen peroxide. *Journal of Chemical Sciences* **2015**, *127*, 1905−1917.
(2108) Pan, F.; Zhang, B.; Cai, W. The effect of hydrophilicity/hydrophobicity of TiO_2-SiO_2 composite aerogels in the epoxidation reaction. *Catal. Commun.* **2017**, *98*, 121−125.
(2109) Liu, J.; Fang, S.; Jian, R.; Wu, F.; Jian, P. Silylated Pd/Ti-MCM-41 catalyst for the selective production of propylene oxide from the oxidation of propylene with cumene hydroperoxide. *Powder Technol.* **2018**, *329*, 19−24.
(2110) Rytter, E.; Salman, A. u. R.; Tsakoumis, N. E.; Myrstad, R.; Yang, J.; Lögdberg, S.; Holmen, A.; Rønning, M. Hydrophobic catalyst support surfaces by silylation of γ-alumina for Co/Re Fischer-Tropsch synthesis. *Catal. Today* **2018**, *299*, 20−27.
(2111) Kanungo, S.; Keshri, K. S.; Hensen, E. J. M.; Chowdhury, B.; Schouten, J. C.; Neira d'Angelo, M. F. Direct epoxidation of propene on silylated Au-Ti catalysts: a study on silylation procedures and the effect on propane formation. *Catal. Sci. Technol.* **2018**, *8*, 3052−3059.

https://doi.org/10.1021/acs.chemrev.1c00905
Chem. Rev. XXXX, XXX, XXX−XXX

(2112) Soomro, S. S.; Röhlich, C.; Köhler, K. Suzuki Coupling Reactions in Pure Water Catalyzed by Supported Palladium - Relevance of the Surface Polarity of the Support. *Adv. Synth. Catal.* **2011**, *353*, 767−775.
(2113) Shen, W.; Gu, Y.; Xu, H.; Dubé, D.; Kaliaguine, S. Alkylation of isobutane/1-butene on methyl-modified Nafion/SBA-15 materials. *Appl. Catal. A* **2010**, *377*, 1−8.
(2114) Yang, Y.; Guan, J.; Qiu, P.; Kan, Q. Enhanced catalytic performances by surface silylation of Cu(II) Schiff base-containing SBA-15 in epoxidation of styrene with H_2O_2. *Appl. Surf. Sci.* **2010**, *256*, 3346−3351.
(2115) Yu, X.; Zhang, J.; Wang, X.; Ma, Q.; Gao, X.; Xia, H.; Lai, X.; Fan, S.; Zhao, T.-S. Fischer-Tropsch synthesis over methyl modified Fe_2O_3@SiO_2 catalysts with low CO_2 selectivity. *Appl. Catal. B* **2018**, *232*, 420−428.
(2116) Zola, A. S.; da Silva, L. S.; Moretti, A. L.; do Couto Fraga, A.; Sousa-Aguiar, E. F.; Arroyo, P. A. Effect of Silylation and Support Porosity of Co/MCM-41 and Co/SiO_2 Catalysts in Fischer-Tropsch Synthesis. *Top. Catal.* **2016**, *59*, 219−229.
(2117) Gao, N.; Xie, S.; Liu, S.; Li, X.; Xu, L. Improvement of vapor-phase silylation and thermal stability of silylated MCM-22 zeolite. *Journal of Porous Materials* **2013**, *20*, 1217−1224.
(2118) Zheng, S.; Heydenrych, H. R.; Jentys, A.; Lercher, J. A. Influence of Surface Modification on the Acid Site Distribution of HZSM-5. *J. Phys. Chem. B* **2002**, *106*, 9552−9558.
(2119) Xu, B.; Tan, M.; Wu, X.; Geng, H.; Song, F.; Ma, Q.; Luan, C.; Yang, G.; Tan, Y. Effects of silylation on Ga/HZSM-5 for improved propane dehydroaromatization. *Fuel* **2021**, *283*, 118889.
(2120) Tempelman, C. H. L.; Hensen, E. J. M. On the deactivation of Mo/HZSM-5 in the methane dehydroaromatization reaction. *Appl. Catal. B* **2015**, *176-177*, 731−739.
(2121) Tempelman, C. H. L.; de Rodrigues, V. O.; van Eck, E. R. H.; Magusin, P. C. M. M.; Hensen, E. J. M. Desilication and silylation of Mo/HZSM-5 for methane dehydroaromatization. *Microporous Mesoporous Mater.* **2015**, *203*, 259−273.
(2122) Losch, P.; Boltz, M.; Bernardon, C.; Louis, B.; Palčić, A.; Valtchev, V. Impact of external surface passivation of nano-ZSM-5 zeolites in the methanol-to-olefins reaction. *Appl. Catal. A* **2016**, *509*, 30−37.
(2123) Lanzafame, P.; Barbera, K.; Perathoner, S.; Centi, G.; Aloise, A.; Migliori, M.; Macario, A.; Nagy, J. B.; Giordano, G. The role of acid sites induced by defects in the etherification of HMF on Silicalite-1 catalysts. *J. Catal.* **2015**, *330*, 558−568.
(2124) Lanzafame, P.; Papanikolaou, G.; Perathoner, S.; Centi, G.; Giordano, G.; Migliori, M. Weakly acidic zeolites: A review on uses and relationship between nature of the active sites and catalytic behaviour. *Microporous Mesoporous Mater.* **2020**, *300*, 110157.
(2125) Ordomsky, V. V.; Cai, M.; Sushkevich, V.; Moldovan, S.; Ersen, O.; Lancelot, C.; Valtchev, V.; Khodakov, A. Y. The role of external acid sites of ZSM-5 in deactivation of hybrid CuZnAl/ZSM-5 catalyst for direct dimethyl ether synthesis from syngas. *Appl. Catal. A* **2014**, *486*, 266−275.
(2126) Rostamnia, S.; Doustkhah, E. Increased SBA-15-SO_3H Catalytic Activity through Hydrophilic/Hydrophobic Fluoroalkyl-Chained Alcohols (RFOH/SBA-15-Pr-SO_3H). *Synlett* **2015**, *26*, 1345−1347.
(2127) Shi, J.; Zhang, L.; Cheng, Z. Design of Water-Tolerant Solid Acids: A Trade-Off Between Hydrophobicity and Acid Strength and their Catalytic Performance in Esterification. *Catal. Surv. Asia* **2021**, *25*, 279−300.
(2128) Dacquin, J.-P.; Cross, H. E.; Brown, D. R.; Düren, T.; Williams, J. J.; Lee, A. F.; Wilson, K. Interdependent lateral interactions, hydrophobicity and acid strength and their influence on the catalytic activity of nanoporous sulfonic acid silicas. *Green Chem.* **2010**, *12*, 1383−1391.
(2129) Kasinathan, P.; Lang, C.; Gaigneaux, E. M.; Jonas, A. M.; Fernandes, A. E. Influence of Site Pairing in Hydrophobic Silica-Supported Sulfonic Acid Bifunctional Catalysts. *Langmuir* **2020**, *36*, 13743−13751.
(2130) Plata, J. J.; Pacheco, L. C.; Remesal, E. R.; Masa, M. O.; Vega, L.; Márquez, A. M.; Odriozola, J. A.; Sanz, J. F. Analysis of the variables that modify the robustness of Ti-SiO_2 catalysts for alkene epoxidation: Role of silylation, deactivation and potential solutions. *Molecular Catalysis* **2018**, *459*, 55−60.
(2131) Almeida, A. R.; Carneiro, J. T.; Moulijn, J. A.; Mul, G. Improved performance of TiO_2 in the selective photo-catalytic oxidation of cyclohexane by increasing the rate of desorption through surface silylation. *J. Catal.* **2010**, *273*, 116−124.
(2132) Ngo, D. T.; Tan, Q.; Wang, B.; Resasco, D. E. Aldol Condensation of Cyclopentanone on Hydrophobized MgO. Promotional Role of Water and Changes in the Rate-Limiting Step upon Organosilane Functionalization. *ACS Catal.* **2019**, *9*, 2831−2841.
(2133) Zhang, F.; Jiang, H.; Li, X.; Wu, X.; Li, H. Amine-Functionalized GO as an Active and Reusable Acid-Base Bifunctional Catalyst for One-Pot Cascade Reactions. *ACS Catal.* **2014**, *4*, 394−401.
(2134) Takenaka, S.; Hirata, A.; Tanabe, E.; Matsune, H.; Kishida, M. Preparation of supported Pt-Co alloy nanoparticle catalysts for the oxygen reduction reaction by coverage with silica. *J. Catal.* **2010**, *274*, 228−238.
(2135) Sun, Z.; Zhang, H.; Zhao, Y.; Huang, C.; Tao, R.; Liu, Z.; Wu, Z. Thermal-Stable Carbon Nanotube-Supported Metal Nanocatalysts by Mesoporous Silica Coating. *Langmuir* **2011**, *27*, 6244−6251.
(2136) Takenaka, S.; Miyamoto, H.; Utsunomiya, Y.; Matsune, H.; Kishida, M. Catalytic Activity of Highly Durable Pt/CNT Catalysts Covered with Hydrophobic Silica Layers for the Oxygen Reduction Reaction in PEFCs. *J. Phys. Chem. C* **2014**, *118*, 774−783.
(2137) Islam, J.; Kim, S.-K.; Lee, E.; Park, G.-G. Durability enhancement of a Pt/C electrocatalyst using silica-coated carbon nanofiber as a corrosion-resistant support. *International Journal of Hydrogen Energy* **2019**, *44*, 4177−4187.
(2138) Hench, L. L.; West, J. K. The sol-gel process. *Chem. Rev.* **1990**, *90*, 33−72.
(2139) Brinker, C. J.; Scherer, G. W. *Sol-Gel Science: The Physics and Chemistry of Sol-Gel Processing*; Academic Press: San Diego, California, USA, 1990.
(2140) Monaco, S. J.; Ko, E. I. The puzzle of sol-gel catalysts. *Chemtech* **1998**, *28*, 23−30.
(2141) Akpan, U. G.; Hameed, B. H. The advancements in sol-gel method of doped-TiO_2 photocatalysts. *Appl. Catal. A* **2010**, *375*, 1−11.
(2142) Gonzalez, R. D.; Lopez, T.; Gomez, R. Sol-gel preparation of supported metal catalysts. *Catal. Today* **1997**, *35*, 293−317.
(2143) He, Y.; Sutton, N. B.; Rijnaarts, H. H. H.; Langenhoff, A. A. M. Degradation of pharmaceuticals in wastewater using immobilized TiO_2 photocatalysis under simulated solar irradiation. *Appl. Catal. B* **2016**, *182*, 132−141.
(2144) Srikanth, B.; Goutham, R.; Badri Narayan, R.; Ramprasath, A.; Gopinath, K. P.; Sankaranarayanan, A. R. Recent advancements in supporting materials for immobilised photocatalytic applications in waste water treatment. *Journal of Environmental Management* **2017**, *200*, 60−78.
(2145) Li, W.; Wang, F.; Feng, S.; Wang, J.; Sun, Z.; Li, B.; Li, Y.; Yang, J.; Elzatahry, A. A.; Xia, Y.; et al. Sol-Gel Design Strategy for Ultradispersed TiO_2 Nanoparticles on Graphene for High-Performance Lithium Ion Batteries. *J. Am. Chem. Soc.* **2013**, *135*, 18300−18303.
(2146) Kanazawa, T. Suppression of Pt Sintering on MFI Zeolite by Modification with Tetramethoxysilane. *Catal. Lett.* **2006**, *108*, 45−47.
(2147) Takenaka, S.; Arike, T.; Matsune, H.; Tanabe, E.; Kishida, M. Preparation of carbon nanotube-supported metal nanoparticles coated with silica layers. *J. Catal.* **2008**, *257*, 345−355.
(2148) Nakagawa, K.; Tanimoto, Y.; Okayama, T.; Sotowa, K.-I.; Sugiyama, S.; Takenaka, S.; Kishida, M. Sintering Resistance and Catalytic Activity of Platinum Nanoparticles Covered with a Microporous Silica Layer Using Methyltriethoxysilane. *Catal. Lett.* **2010**, *136*, 71−76.

https://doi.org/10.1021/acs.chemrev.1c00905
Chem. Rev. XXXX, XXX, XXX−XXX

(2149) Zhang, P.; Chi, M.; Sharma, S.; McFarland, E. Silica encapsulated heterostructure catalyst of Pt nanoclusters on hematite nanocubes: synthesis and reactivity. *J. Mater. Chem.* **2010**, *20*, 2013−2017.
(2150) Calderone, V.; Schütz-Widoniak, J.; Bezemer, G.; Bakker, G.; Steurs, C.; Philipse, A. Design of Colloidal Pt Catalysts Encapsulated by Silica Nano Membranes for Enhanced Stability in H_2S Streams. *Catal. Lett.* **2010**, *137*, 132−140.
(2151) Zhu, H.; Ma, Z.; Overbury, S.; Dai, S. Rational design of gold catalysts with enhanced thermal stability: post modification of Au/TiO_2 by amorphous SiO_2 decoration. *Catal. Lett.* **2007**, *116*, 128−135.
(2152) Ma, Z.; Dai, S. Design of Novel Structured Gold Nanocatalysts. *ACS Catal.* **2011**, *1*, 805−818.
(2153) Yan, W.; Mahurin, S. M.; Pan, Z.; Overbury, S. H.; Dai, S. Ultrastable Au Nanocatalyst Supported on Surface-Modified TiO_2 Nanocrystals. *J. Am. Chem. Soc.* **2005**, *127*, 10480−10481.
(2154) Horváth, A.; Beck, A.; Sárkány, A.; Stefler, G.; Varga, Z.; Geszti, O.; Tóth, L.; Guczi, L. Silica-Supported Au Nanoparticles Decorated by TiO_2: Formation, Morphology, and CO Oxidation Activity. *J. Phys. Chem. B* **2006**, *110*, 15417−15425.
(2155) Lee, I.; Zhang, Q.; Ge, J.; Yin, Y.; Zaera, F. Encapsulation of Supported Pt Nanoparticles for Increased Catalyst Stability. *Nano Res.* **2011**, *4*, 115−123.
(2156) Blas, H.; Save, M.; Pasetto, P.; Boissière, C.; Sanchez, C.; Charleux, B. Elaboration of Monodisperse Spherical Hollow Particles with Ordered Mesoporous Silica Shells via Dual Latex/Surfactant Templating: Radial Orientation of Mesopore Channels. *Langmuir* **2008**, *24*, 13132−13137.
(2157) Li, J.; Liu, J.; Wang, D.; Guo, R.; Li, X.; Qi, W. Interfacially Controlled Synthesis of Hollow Mesoporous Silica Spheres with Radially Oriented Pore Structures. *Langmuir* **2010**, *26*, 12267−12272.
(2158) Fang, X.; Chen, C.; Liu, Z.; Liu, P.; Zheng, N. A cationic surfactant assisted selective etching strategy to hollow mesoporous silica spheres. *Nanoscale* **2011**, *3*, 1632−1639.
(2159) Teng, Z.; Su, X.; Zheng, Y.; Sun, J.; Chen, G.; Tian, C.; Wang, J.; Li, H.; Zhao, Y.; Lu, G. Mesoporous Silica Hollow Spheres with Ordered Radial Mesochannels by a Spontaneous Self-Transformation Approach. *Chem. Mater.* **2013**, *25*, 98−105.
(2160) Mirata, F.; Resmini, M. In *Molecularly Imprinted Polymers in Biotechnology*; Mattiasson, B., Ye, L., Eds.; Springer International Publishing: Cham, 2015.
(2161) *Molecularly Imprinted Catalysts: Principles, Syntheses, and Applications*; Li, S., Cao, S., Piletsky, S. A., Turner, A. P. F., Eds.; Elsevier: Amsterdam, 2016.
(2162) Nakai, S.; Sunayama, H.; Kitayama, Y.; Nishijima, M.; Wada, T.; Inoue, Y.; Takeuchi, T. Regioselective Molecularly Imprinted Reaction Field for [4 + 4] Photocyclodimerization of 2-Anthracenecarboxylic Acid. *Langmuir* **2017**, *33*, 2103−2108.
(2163) Zeng, H.; Stewart-Yates, L.; Casey, L. M.; Bampos, N.; Roberts, D. A. Covalent Post-Assembly Modification: A Synthetic Multipurpose Tool in Supramolecular Chemistry. *ChemPlusChem.* **2020**, *85*, 1249−1269.
(2164) Muratsugu, S.; Shirai, S.; Tada, M. Recent progress in molecularly imprinted approach for catalysis. *Tetrahedron Lett.* **2020**, *61*, 151603.
(2165) Alexander, C.; Davidson, L.; Hayes, W. Imprinted polymers: artificial molecular recognition materials with applications in synthesis and catalysis. *Tetrahedron* **2003**, *59*, 2025−2057.
(2166) Becker, J. J.; Gagné, M. R. Exploiting the Synergy between Coordination Chemistry and Molecular Imprinting in the Quest for New Catalysts. *Acc. Chem. Res.* **2004**, *37*, 798−804.
(2167) Wulff, G.; Liu, J. Design of Biomimetic Catalysts by Molecular Imprinting in Synthetic Polymers: The Role of Transition State Stabilization. *Acc. Chem. Res.* **2012**, *45*, 239−247.
(2168) Sharma, P. S.; Wojnarowicz, A.; Kutner, W.; D'Souza, F. *Molecularly Imprinted Catalysts*; Li, S., Cao, S., Piletsky, S. A., Turner, A. P. F., Eds.; Elsevier: Amsterdam, 2016.
(2169) Qin, Y.-P.; Li, D.-Y.; He, X.-W.; Li, W.-Y.; Zhang, Y.-K. Preparation of High-Efficiency Cytochrome c-Imprinted Polymer on the Surface of Magnetic Carbon Nanotubes by Epitope Approach via Metal Chelation and Six-Membered Ring. *ACS Appl. Mater. Interfaces* **2016**, *8*, 10155−10163.
(2170) Zheng, A.-x.; Gong, C.-b.; Zhang, W.-j.; Tang, Q.; Huang, H.-r.; Chow, C.-f.; Tang, Q. An amphiphilic and photoswitchable organocatalyst for the aldol reaction based on a product-imprinted polymer. *Molecular Catalysis* **2017**, *442*, 115−125.
(2171) Hu, L.; Zhao, Y. Molecularly imprinted artificial esterases with highly specific active sites and precisely installed catalytic groups. *Organic & Biomolecular Chemistry* **2018**, *16*, 5580−5584.
(2172) Dong, Z. Y.; Liu, J. Q. *Molecularly Imprinted Polymers for Analytical Chemistry Applications*; The Royal Society of Chemistry, 2018.
(2173) Hu, L.; Zhao, Y. A Bait-and-Switch Method for the Construction of Artificial Esterases for Substrate-Selective Hydrolysis. *Chem.-Eur. J.* **2019**, *25*, 7702−7710.
(2174) Hu, L.; Arifuzzaman, M. D.; Zhao, Y. Controlling Product Inhibition through Substrate-Specific Active Sites in Nanoparticle-Based Phosphodiesterase and Esterase. *ACS Catal.* **2019**, *9*, 5019−5024.
(2175) Li, X.; Zhao, Y. Chiral Gating for Size- and Shape-Selective Asymmetric Catalysis. *J. Am. Chem. Soc.* **2019**, *141*, 13749−13752.
(2176) Carboni, D.; Malfatti, L.; Pinna, A.; Lasio, B.; Tokudome, Y.; Takahashi, M.; Innocenzi, P. Molecularly imprinted La-doped mesoporous titania films with hydrolytic properties toward organophosphate pesticides. *New J. Chem.* **2013**, *37*, 2995−3002.
(2177) Zhang, Z.; Li, Y.; Zhang, X.; Liu, J. Molecularly imprinted nanozymes with faster catalytic activity and better specificity. *Nanoscale* **2019**, *11*, 4854−4863.
(2178) Lin, F.; Yushen, T.; Doudou, L.; Haoan, W.; Yan, C.; Ning, G.; Yu, Z. Catalytic gold-platinum alloy nanoparticles and a novel glucose oxidase mimic with enhanced activity and selectivity constructed by molecular imprinting. *Analytical Methods* **2019**, *11*, 4586−4592.
(2179) Tada, M.; Iwasawa, Y. Advanced design of catalytically active reaction space at surfaces for selective catalysis. *Coord. Chem. Rev.* **2007**, *251*, 2702−2716.
(2180) Muratsugu, S.; Tada, M. Molecularly Imprinted Ru Complex Catalysts Integrated on Oxide Surfaces. *Acc. Chem. Res.* **2013**, *46*, 300−311.
(2181) Tada, M.; Sasaki, T.; Iwasawa, Y. Design of a Novel Molecular-Imprinted Rh-Amine Complex on SiO_2 and Its Shape-Selective Catalysis for α-Methylstyrene Hydrogenation. *J. Phys. Chem. B* **2004**, *108*, 2918−2930.
(2182) Weng, Z.; Muratsugu, S.; Ishiguro, N.; Ohkoshi, S.-i.; Tada, M. Preparation of surface molecularly imprinted Ru-complex catalysts for asymmetric transfer hydrogenation in water media. *Dalton Trans.* **2011**, *40*, 2338−2347.
(2183) Yang, Y.; Weng, Z.; Muratsugu, S.; Ishiguro, N.; Ohkoshi, S.-i.; Tada, M. Preparation and Catalytic Performances of a Molecularly Imprinted Ru-Complex Catalyst with an NH_2 Binding Site on a SiO_2 Surface. *Chem.-Eur. J.* **2012**, *18*, 1142−1153.
(2184) Muratsugu, S.; Maity, N.; Baba, H.; Tasaki, M.; Tada, M. Preparation and catalytic performance of a molecularly imprinted Pd complex catalyst for Suzuki cross-coupling reactions. *Dalton Trans.* **2017**, *46*, 3125−3134.
(2185) Guo, Y.; Guo, T. A dual-template imprinted capsule with remarkably enhanced catalytic activity for pesticide degradation and elimination simultaneously. *Chem. Commun.* **2013**, *49*, 1073−1075.
(2186) Elam, J. W.; Dasgupta, N. P.; Prinz, F. B. ALD for clean energy conversion, utilization, and storage. *MRS Bull.* **2011**, *36*, 899−906.
(2187) Detavernier, C.; Dendooven, J.; Pulinthanathu Sree, S.; Ludwig, K. F.; Martens, J. A. Tailoring nanoporous materials by atomic layer deposition. *Chem. Soc. Rev.* **2011**, *40*, 5242−5253.

https://doi.org/10.1021/acs.chemrev.1c00905
Chem. Rev. XXXX, XXX, XXX−XXX

(2188) Lu, J.; Elam, J. W.; Stair, P. C. Synthesis and Stabilization of Supported Metal Catalysts by Atomic Layer Deposition. *Acc. Chem. Res.* **2013**, *46*, 1806−1815.
(2189) O'Neill, B. J.; Jackson, D. H. K.; Lee, J.; Canlas, C.; Stair, P. C.; Marshall, C. L.; Elam, J. W.; Kuech, T. F.; Dumesic, J. A.; Huber, G. W. Catalyst Design with Atomic Layer Deposition. *ACS Catal.* **2015**, *5*, 1804−1825.
(2190) Cao, K.; Cai, J.; Liu, X.; Chen, R. Review Article: Catalysts design and synthesis via selective atomic layer deposition. *J. Vac. Sci. Technol., A* **2018**, *36*, 010801.
(2191) Wang, H.; Lu, J. Atomic Layer Deposition: A Gas Phase Route to Bottom-up Precise Synthesis of Heterogeneous Catalyst. *Acta Physico-Chimica Sinica* **2018**, *34*, 1334−1357.
(2192) Zhang, B.; Qin, Y. Interface Tailoring of Heterogeneous Catalysts by Atomic Layer Deposition. *ACS Catal.* **2018**, *8*, 10064−10081.
(2193) Cao, K.; Cai, J.; Liu, X.; Chen, R. Review Article: Catalysts design and synthesis via selective atomic layer deposition. *J. Vac. Sci. Technol., A* **2018**, *36*, 010801.
(2194) Mallick, B. C.; Hsieh, C.-T.; Yin, K.-M.; Gandomi, Y. A.; Huang, K.-T. Review—On Atomic Layer Deposition: Current Progress and Future Challenges. *ECS J. Solid State Sci. Technol.* **2019**, *8*, N55−N78.
(2195) Zaera, F. The surface chemistry of thin film atomic layer deposition (ALD) processes for electronic device manufacturing. *J. Mater. Chem.* **2008**, *18*, 3521−3526.
(2196) Ritala, M.; Niinistö, J. Industrial Applications of Atomic Layer Deposition. *ECS Trans.* **2009**, *25*, 641−652.
(2197) George, S. M. Atomic layer deposition: An overview. *Chem. Rev.* **2010**, *110*, 111−131.
(2198) Parsons, G. N.; Elam, J. W.; George, S. M.; Haukka, S.; Jeon, H.; Kessels, W. M. M.; Leskelä, M.; Poodt, P.; Ritala, M.; Rossnagel, S. M. History of atomic layer deposition and its relationship with the American Vacuum Society. *J. Vac. Sci. Technol., A* **2013**, *31*, 050818.
(2199) Biyikli, N.; Haider, A. Atomic layer deposition: an enabling technology for the growth of functional nanoscale semiconductors. *Semicond. Sci. Technol.* **2017**, *32*, 093002.
(2200) Leskelä, M.; Niinistö, J.; Ritala, M. *Comprehensive Materials Processing*; Hashmi, S., Batalha, G. F., Van Tyne, C. J., Yilbas, B., Eds.; Elsevier: Oxford, 2014; Vol. *4*.
(2201) Meng, X.; Wang, X.; Geng, D.; Ozgit-Akgun, C.; Schneider, N.; Elam, J. W. Atomic layer deposition for nanomaterial synthesis and functionalization in energy technology. *Mater. Horiz.* **2017**, *4*, 133−154.
(2202) Zardetto, V.; Williams, B. L.; Perrotta, A.; Di Giacomo, F.; Verheijen, M. A.; Andriessen, R.; Kessels, W. M. M.; Creatore, M. Atomic layer deposition for perovskite solar cells: research status, opportunities and challenges. *Sustainable Energy & Fuels* **2017**, *1*, 30−55.
(2203) Van Bui, H.; Grillo, F.; van Ommen, J. R. Atomic and molecular layer deposition: off the beaten track. *Chem. Commun.* **2017**, *53*, 45−71.
(2204) Weber, M.; Julbe, A.; Ayral, A.; Miele, P.; Bechelany, M. Atomic Layer Deposition for Membranes: Basics, Challenges, and Opportunities. *Chem. Mater.* **2018**, *30*, 7368−7390.
(2205) Zaera, F. The Surface Chemistry of Atomic Layer Depositions of Solid Thin Films. *J. Phys. Chem. Lett.* **2012**, *3*, 1301−1309.
(2206) Zaera, F. Mechanisms of surface reactions in thin solid film chemical deposition processes. *Coord. Chem. Rev.* **2013**, *257*, 3177−3191.
(2207) Richey, N. E.; de Paula, C.; Bent, S. F. Understanding chemical and physical mechanisms in atomic layer deposition. *J. Chem. Phys.* **2020**, *152*, 040902.
(2208) Onn, T. M.; Küngas, R.; Fornasiero, P.; Huang, K.; Gorte, R. J. Atomic Layer Deposition on Porous Materials: Problems with Conventional Approaches to Catalyst and Fuel Cell Electrode Preparation. *Inorganics* **2018**, *6*, 34.
(2209) Adhikari, S.; Selvaraj, S.; Kim, D.-H. Progress in Powder Coating Technology Using Atomic Layer Deposition. *Advanced Materials Interfaces* **2018**, *5*, 1800581.
(2210) Weng, Z.; Chen, Z.-h.; Qin, X.; Zaera, F. Sub-monolayer control of the growth of oxide films on mesoporous materials. *J. Mater. Chem. A* **2018**, *6*, 17548−17558.
(2211) Pore, V.; Rahtu, A.; Leskelä, M.; Ritala, M.; Sajavaara, T.; Keinonen, J. Atomic Layer Deposition of Photocatalytic TiO_2 Thin Films from Titanium Tetramethoxide and Water. *Chem. Vap. Deposition* **2004**, *10*, 143−148.
(2212) Lim, G. T.; Kim, D. H. Characteristics of TiO_x films prepared by chemical vapor deposition using tetrakis-dimethyl-amido-titanium and water. *Thin Solid Films* **2006**, *498*, 254−258.
(2213) Vilhunen, S.; Bosund, M.; Kääriäinen, M.-L.; Cameron, D.; Sillanpää, M. Atomic layer deposited TiO_2 films in photodegradation of aqueous salicylic acid. *Sep. Purif. Technol.* **2009**, *66*, 130−134.
(2214) Paracchino, A.; Mathews, N.; Hisatomi, T.; Stefik, M.; Tilley, S. D.; Grätzel, M. Ultrathin films on copper(i) oxide water splitting photocathodes: a study on performance and stability. *Energy Environ. Sci.* **2012**, *5*, 8673−8681.
(2215) Ivanova, T. V.; Toivonen, J.; Maydannik, P. S.; Kääriäinen, T.; Sillanpää, M.; Homola, T.; Cameron, D. C. Atomic layer deposition of cerium oxide for potential use in diesel soot combustion. *J. Vac. Sci. Technol., A* **2016**, *34*, 031506.
(2216) Pagán-Torres, Y. J.; Gallo, J. M. R.; Wang, D.; Pham, H. N.; Libera, J. A.; Marshall, C. L.; Elam, J. W.; Datye, A. K.; Dumesic, J. A. Synthesis of Highly Ordered Hydrothermally Stable Mesoporous Niobia Catalysts by Atomic Layer Deposition. *ACS Catal.* **2011**, *1*, 1234−1245.
(2217) Weng, Z.; Zaera, F. Atomic Layer Deposition (ALD) as a Way to Prepare New Mixed-Oxide Catalyst Supports: The Case of Alumina Addition to Silica-Supported Platinum for the Selective Hydrogenation of Cinnamaldehyde. *Top. Catal.* **2019**, *62*, 838−848.
(2218) Lu, J.; Kosuda, K. M.; Van Duyne, R. P.; Stair, P. C. Surface Acidity and Properties of TiO_2/SiO_2 Catalysts Prepared by Atomic Layer Deposition: UV-visible Diffuse Reflectance, DRIFTS, and Visible Raman Spectroscopy Studies. *J. Phys. Chem. C* **2009**, *113*, 12412−12418.
(2219) Jeong, M.-G.; Kim, I. H.; Han, S. W.; Kim, D. H.; Kim, Y. D. Room temperature CO oxidation catalyzed by NiO particles on mesoporous SiO_2 prepared via atomic layer deposition: Influence of pre-annealing temperature on catalytic activity. *J. Mol. Catal. A* **2016**, *414*, 87−93.
(2220) Kim, J.; Iivonen, T.; Hämäläinen, J.; Kemell, M.; Meinander, K.; Mizohata, K.; Wang, L.; Räisänen, J.; Beranek, R.; Leskelä, M.; et al. Low-Temperature Atomic Layer Deposition of Cobalt Oxide as an Effective Catalyst for Photoelectrochemical Water-Splitting Devices. *Chem. Mater.* **2017**, *29*, 5796−5805.
(2221) Amama, P. B.; Pint, C. L.; Kim, S. M.; McJilton, L.; Eyink, K. G.; Stach, E. A.; Hauge, R. H.; Maruyama, B. Influence of Alumina Type on the Evolution and Activity of Alumina-Supported Fe Catalysts in Single-Walled Carbon Nanotube Carpet Growth. *ACS Nano* **2010**, *4*, 895−904.
(2222) Feng, H.; Lu, J.; Stair, P.; Elam, J. Alumina Over-coating on Pd Nanoparticle Catalysts by Atomic Layer Deposition: Enhanced Stability and Reactivity. *Catal. Lett.* **2011**, *141*, 512−517.
(2223) Lobo, R.; Marshall, C. L.; Dietrich, P. J.; Ribeiro, F. H.; Akatay, C.; Stach, E. A.; Mane, A.; Lei, Y.; Elam, J.; Miller, J. T. Understanding the Chemistry of H_2 Production for 1-Propanol Reforming: Pathway and Support Modification Effects. *ACS Catal.* **2012**, *2*, 2316−2326.
(2224) O'Neill, B. J.; Jackson, D. H. K.; Crisci, A. J.; Farberow, C. A.; Shi, F.; Alba-Rubio, A. C.; Lu, J.; Dietrich, P. J.; Gu, X.; Marshall, C. L.; et al. Stabilization of Copper Catalysts for Liquid-Phase Reactions by Atomic Layer Deposition. *Angew. Chem., Int. Ed.* **2013**, *52*, 13808−13812.
(2225) Caner, N.; Bulut, A.; Yurderi, M.; Ertas, I. E.; Kivrak, H.; Kaya, M.; Zahmakiran, M. Atomic layer deposition-SiO_2 layers protected PdCoNi nanoparticles supported on TiO_2 nanopowders:

https://doi.org/10.1021/acs.chemrev.1c00905
Chem. Rev. XXXX, XXX, XXX−XXX

Exceptionally stable nanocatalyst for the dehydrogenation of formic acid. *Appl. Catal. B* **2017**, *210*, 470−483.
(2226) Onn, T. M.; Monai, M.; Dai, S.; Fonda, E.; Montini, T.; Pan, X.; Graham, G. W.; Fornasiero, P.; Gorte, R. J. Smart Pd Catalyst with Improved Thermal Stability Supported on High-Surface-Area $LaFeO_3$ Prepared by Atomic Layer Deposition. *J. Am. Chem. Soc.* **2018**, *140*, 4841−4848.
(2227) Lin, W.; Chen, H.; Li, J.; Chen, K.; Lu, X.; Ouyang, P.; Fu, J. Enhanced stability of Pt/C by the atomic layer deposition of porous MO_x for the decarboxylation of oleic acid. *Catal. Commun.* **2019**, *123*, 59−63.
(2228) Ma, Z.; Brown, S.; Howe, J. Y.; Overbury, S. H.; Dai, S. Surface Modification of Au/TiO_2 Catalysts by SiO_2 via Atomic Layer Deposition. *J. Phys. Chem. C* **2008**, *112*, 9448−9457.
(2229) Onn, T. M.; Zhang, S.; Arroyo-Ramirez, L.; Chung, Y.-C.; Graham, G. W.; Pan, X.; Gorte, R. J. Improved Thermal Stability and Methane-Oxidation Activity of Pd/Al2O3 Catalysts by Atomic Layer Deposition of ZrO_2. *ACS Catal.* **2015**, *5*, 5696−5701.
(2230) Lin, C.; Mao, X.; Onn, M. T.; Jang, J.; Gorte, J. R. Stabilization of ZrO_2 Powders via ALD of CeO_2 and ZrO_2. *Inorganics* **2017**, *5*, 65.
(2231) Lee, J.; Jackson, D. H. K.; Li, T.; Winans, R. E.; Dumesic, J. A.; Kuech, T. F.; Huber, G. W. Enhanced stability of cobalt catalysts by atomic layer deposition for aqueous-phase reactions. *Energy Environ. Sci.* **2014**, *7*, 1657−1660.
(2232) Lu, J.; Fu, B.; Kung, M. C.; Xiao, G.; Elam, J. W.; Kung, H. H.; Stair, P. C. Coking- and Sintering-Resistant Palladium Catalysts Achieved Through Atomic Layer Deposition. *Science* **2012**, *335*, 1205−1208.
(2233) Fu, B.; Lu, J.; Stair, P. C.; Xiao, G.; Kung, M. C.; Kung, H. H. Oxidative dehydrogenation of ethane over alumina-supported Pd catalysts. Effect of alumina overlayer. *J. Catal.* **2013**, *297*, 289−295.
(2234) Chen, Y. W.; Prange, J. D.; Dühnen, S.; Park, Y.; Gunji, M.; Chidsey, C. E. D.; McIntyre, P. C. Atomic layer-deposited tunnel oxide stabilizes silicon photoanodes for water oxidation. *Nat. Mater.* **2011**, *10*, 539−544.
(2235) Riha, S. C.; Klahr, B. M.; Tyo, E. C.; Seifert, S.; Vajda, S.; Pellin, M. J.; Hamann, T. W.; Martinson, A. B. F. Atomic Layer Deposition of a Submonolayer Catalyst for the Enhanced Photoelectrochemical Performance of Water Oxidation with Hematite. *ACS Nano* **2013**, *7*, 2396−2405.
(2236) Hu, S.; Shaner, M. R.; Beardslee, J. A.; Lichterman, M.; Brunschwig, B. S.; Lewis, N. S. Amorphous TiO_2 coatings stabilize Si, GaAs, and GaP photoanodes for efficient water oxidation. *Science* **2014**, *344*, 1005.
(2237) Le Formal, F.; Tétreault, N.; Cornuz, M.; Moehl, T.; Grätzel, M.; Sivula, K. Passivating surface states on water splitting hematite photoanodes with alumina overlayers. *Chem. Sci.* **2011**, *2*, 737−743.
(2238) Pan, L.; Kim, J. H.; Mayer, M. T.; Son, M.-K.; Ummadisingu, A.; Lee, J. S.; Hagfeldt, A.; Luo, J.; Grätzel, M. Boosting the performance of Cu_2O photocathodes for unassisted solar water splitting devices. *Nature Catalysis* **2018**, *1*, 412−420.
(2239) Pickrahn, K. L.; Park, S. W.; Gorlin, Y.; Lee, H.-B.-R.; Jaramillo, T. F.; Bent, S. F. Active MnO_x Electrocatalysts Prepared by Atomic Layer Deposition for Oxygen Evolution and Oxygen Reduction Reactions. *Adv. Energy Mater.* **2012**, *2*, 1269−1277.
(2240) Singh, A. K.; Kumar, P.; Late, D. J.; Kumar, A.; Patel, S.; Singh, J. 2D layered transition metal dichalcogenides (MoS_2): Synthesis, applications and theoretical aspects. *Applied Materials Today* **2018**, *13*, 242−270.
(2241) Cheng, N.; Norouzi Banis, M.; Liu, J.; Riese, A.; Mu, S.; Li, R.; Sham, T.-K.; Sun, X. Atomic scale enhancement of metal-support interactions between Pt and ZrC for highly stable electrocatalysts. *Energy Environ. Sci.* **2015**, *8*, 1450−1455.
(2242) Mao, X.; Foucher, A.; Stach, E. A.; Gorte, R. J. A Study of Support Effects for CH_4 and CO Oxidation over Pd Catalysts on ALD-Modified Al_2O_3. *Catal. Lett.* **2019**, *149*, 905−915.
(2243) Keränen, J.; Guimon, C.; Iiskola, E.; Auroux, A.; Niinistö, L. Atomic layer deposition and surface characterization of highly dispersed titania/silica-supported vanadia catalysts. *Catal. Today* **2003**, *78*, 149−157.
(2244) Herrera, J. E.; Kwak, J. H.; Hu, J. Z.; Wang, Y.; Peden, C. H. F.; Macht, J.; Iglesia, E. Synthesis, characterization, and catalytic function of novel highly dispersed tungsten oxide catalysts on mesoporous silica. *J. Catal.* **2006**, *239*, 200−211.
(2245) Gervasini, A.; Carniti, P.; Keränen, J.; Niinistö, L.; Auroux, A. Surface characteristics and activity in selective oxidation of o-xylene of supported V_2O_5 catalysts prepared by standard impregnation and atomic layer deposition. *Catal. Today* **2004**, *96*, 187−194.
(2246) Shiju, N. R.; Liang, X.; Weimer, A. W.; Liang, C.; Dai, S.; Guliants, V. V. The Role of Surface Basal Planes of Layered Mixed Metal Oxides in Selective Transformation of Lower Alkanes: Propane Ammoxidation over Surface ab Planes of Mo-V-Te-Nb-O M1 Phase. *J. Am. Chem. Soc.* **2008**, *130*, 5850−5851.
(2247) Keränen, J.; Auroux, A.; Ek, S.; Niinistö, L. Preparation, characterization and activity testing of vanadia catalysts deposited onto silica and alumina supports by atomic layer deposition. *Appl. Catal. A* **2002**, *228*, 213−225.
(2248) Goldstein, D. N.; McCormick, J. A.; George, S. M. Al_2O_3 atomic layer deposition with trimethylaluminum and ozone studied by in situ transmission FTIR spectroscopy and quadrupole mass spectrometry. *J. Phys. Chem. C* **2008**, *112*, 19530−19539.
(2249) Ospina-Acevedo, F. A.; Perez Beltran, S.; Balbuena, P. B. Mechanisms of alumina growth via atomic layer deposition on nickel oxide and metallic nickel surfaces. *Phys. Chem. Chem. Phys.* **2019**, *21*, 24543−24553.
(2250) Gallas, J.-P.; Goupil, J.-M.; Vimont, A.; Lavalley, J.-C.; Gil, B.; Gilson, J.-P.; Miserque, O. Quantification of Water and Silanol Species on Various Silicas by Coupling IR Spectroscopy and in-Situ Thermogravimetry. *Langmuir* **2009**, *25*, 5825−5834.
(2251) Ide, M.; El-Roz, M.; De Canck, E.; Vicente, A.; Planckaert, T.; Bogaerts, T.; Van Driessche, I.; Lynen, F.; Van Speybroeck, V.; Thybault-Starzyk, F.; et al. Quantification of silanol sites for the most common mesoporous ordered silicas and organosilicas: total versus accessible silanols. *Phys. Chem. Chem. Phys.* **2013**, *15*, 642−650.
(2252) Onn, T. M.; Dai, S.; Chen, J.; Pan, X.; Graham, G. W.; Gorte, R. J. High-Surface Area Ceria-Zirconia Films Prepared by Atomic Layer Deposition. *Catal. Lett.* **2017**, *147*, 1464−1470.
(2253) Adebayo, B. O.; Newport, K.; Yu, H.; Rownaghi, A. A.; Liang, X.; Rezaei, F. Atomic Layer Deposited Ni/ZrO_2-SiO_2 for Combined Capture and Oxidation of VOCs. *ACS Appl. Mater. Interfaces* **2020**, *12*, 39318−39334.
(2254) Samek, I. A.; Bobbitt, N. S.; Snurr, R. Q.; Stair, P. C. Structure and activity of mixed VO_x-CeO_2 domains supported on alumina in cyclohexane oxidative dehydrogenation. *J. Catal.* **2020**, *384*, 147−158.
(2255) Ke, W.; Liu, Y.; Wang, X.; Qin, X.; Chen, L.; Palomino, R. M.; Simonovis, J. P.; Lee, I.; Waluyo, I.; Rodriguez, J. A.; et al. Nucleation and Initial Stages of Growth during the Atomic Layer Deposition of Titanium Oxide on Mesoporous Silica. *Nano Lett.* **2020**, *20*, 6884−6890.
(2256) Muylaert, I.; Musschoot, J.; Leus, K.; Dendooven, J.; Detavernier, C.; Van Der Voort, P. Atomic Layer Deposition of Titanium and Vanadium Oxide on Mesoporous Silica and Phenol/Formaldehyde Resins - the Effect of the Support on the Liquid Phase Epoxidation of Cyclohexene. *Eur. J. Inorg. Chem.* **2012**, *2012*, 251−260.
(2257) Weng, Z.; Zaera, F. Sub-Monolayer Control of Mixed-Oxide Support Composition in Catalysts via Atomic Layer Deposition: Selective Hydrogenation of Cinnamaldehyde Promoted by (SiO_2-ALD)-Pt/Al_2O_3. *ACS Catal.* **2018**, *8*, 8513−8524.
(2258) Hsu, I. J.; Kimmel, Y. C.; Jiang, X.; Willis, B. G.; Chen, J. G. Atomic layer deposition synthesis of platinum-tungsten carbide core-shell catalysts for the hydrogen evolution reaction. *Chem. Commun.* **2012**, *48*, 1063−1065.
(2259) King, J. S.; Wittstock, A.; Biener, J.; Kucheyev, S. O.; Wang, Y. M.; Baumann, T. F.; Giri, S. K.; Hamza, A. V.; Baeumer, M.; Bent,

https://doi.org/10.1021/acs.chemrev.1c00905
Chem. Rev. XXXX, XXX, XXX−XXX

S. F. Ultralow Loading Pt Nanocatalysts Prepared by Atomic Layer Deposition on Carbon Aerogels. *Nano Lett.* **2008**, *8*, 2405−2409.
(2260) Li, J.; Liang, X.; King, D. M.; Jiang, Y.-B.; Weimer, A. W. Highly dispersed Pt nanoparticle catalyst prepared by atomic layer deposition. *Appl. Catal. B* **2010**, *97*, 220−226.
(2261) Weber, M. J.; Mackus, A. J. M.; Verheijen, M. A.; van der Marel, C.; Kessels, W. M. M. Supported Core/Shell Bimetallic Nanoparticles Synthesis by Atomic Layer Deposition. *Chem. Mater.* **2012**, *24*, 2973−2977.
(2262) Lei, Y.; Liu, B.; Lu, J.; Lobo-Lapidus, R. J.; Wu, T.; Feng, H.; Xia, X.; Mane, A. U.; Libera, J. A.; Greeley, J. P.; et al. Synthesis of Pt-Pd Core-Shell Nanostructures by Atomic Layer Deposition: Application in Propane Oxidative Dehydrogenation to Propylene. *Chem. Mater.* **2012**, *24*, 3525−3533.
(2263) Gould, T. D.; Montemore, M. M.; Lubers, A. M.; Ellis, L. D.; Weimer, A. W.; Falconer, J. L.; Medlin, J. W. Enhanced dry reforming of methane on Ni and Ni-Pt catalysts synthesized by atomic layer deposition. *Appl. Catal. A* **2015**, *492*, 107−116.
(2264) Feng, H.; Elam, J. W.; Libera, J. A.; Setthapun, W.; Stair, P. C. Palladium Catalysts Synthesized by Atomic Layer Deposition for Methanol Decomposition. *Chem. Mater.* **2010**, *22*, 3133−3142.
(2265) Setthapun, W.; Williams, W. D.; Kim, S. M.; Feng, H.; Elam, J. W.; Rabuffetti, F. A.; Poeppelmeier, K. R.; Stair, P. C.; Stach, E. A.; Ribeiro, F. H.; et al. Genesis and Evolution of Surface Species during Pt Atomic Layer Deposition on Oxide Supports Characterized by in Situ XAFS Analysis and Water, a Gas Shift Reaction. *J. Phys. Chem. C* **2010**, *114*, 9758−9771.
(2266) Feng, H.; Libera, J. A.; Stair, P. C.; Miller, J. T.; Elam, J. W. Subnanometer Palladium Particles Synthesized by Atomic Layer Deposition. *ACS Catal.* **2011**, *1*, 665−673.
(2267) Gong, T.; Qin, L.; Zhang, W.; Wan, H.; Lu, J.; Feng, H. Activated Carbon Supported Palladium Nanoparticle Catalysts Synthesized by Atomic Layer Deposition: Genesis and Evolution of Nanoparticles and Tuning the Particle Size. *J. Phys. Chem. C* **2015**, *119*, 11544−11556.
(2268) Chen, H.; Shen, J.; Chen, K.; Qin, Y.; Lu, X.; Ouyang, P.; Fu, J. Atomic layer deposition of Pt nanoparticles on low surface area zirconium oxide for the efficient base-free oxidation of 5-hydroxymethylfurfural to 2,5-furandicarboxylic acid. *Appl. Catal. A* **2018**, *555*, 98−107.
(2269) Zhang, X.; Shao, B.; Sun, Z.; Gao, Z.; Qin, Y.; Zhang, C.; Cui, F.; Yang, X. Platinum Nanoparticle-Deposited $Ti_3C_2T_x$ MXene for Hydrogen Evolution Reaction. *Ind. Eng. Chem. Res.* **2020**, *59*, 1822−1828.
(2270) Dasgupta, N. P.; Liu, C.; Andrews, S.; Prinz, F. B.; Yang, P. Atomic Layer Deposition of Platinum Catalysts on Nanowire Surfaces for Photoelectrochemical Water Reduction. *J. Am. Chem. Soc.* **2013**, *135*, 12932−12935.
(2271) Huang, R.; Cheng, Y.; Ji, Y.; Gorte, R. J. Atomic Layer Deposition for Preparing Isolated Co Sites on SiO_2 for Ethane Dehydrogenation Catalysis. *Nanomaterials* **2020**, *10*, 244.
(2272) Yan, H.; Lin, Y.; Wu, H.; Zhang, W.; Sun, Z.; Cheng, H.; Liu, W.; Wang, C.; Li, J.; Huang, X.; et al. Bottom-up precise synthesis of stable platinum dimers on graphene. *Nat. Commun.* **2017**, *8*, 1070.
(2273) Gould, T. D.; Lubers, A. M.; Corpuz, A. R.; Weimer, A. W.; Falconer, J. L.; Medlin, J. W. Controlling Nanoscale Properties of Supported Platinum Catalysts through Atomic Layer Deposition. *ACS Catal.* **2015**, *5*, 1344−1352.
(2274) Li, Z.; Schweitzer, N. M.; League, A. B.; Bernales, V.; Peters, A. W.; Getsoian, A. B.; Wang, T. C.; Miller, J. T.; Vjunov, A.; Fulton, J. L.; et al. Sintering-Resistant Single-Site Nickel Catalyst Supported by Metal-Organic Framework. *J. Am. Chem. Soc.* **2016**, *138*, 1977−1982.
(2275) Christensen, S. T.; Feng, H.; Libera, J. L.; Guo, N.; Miller, J. T.; Stair, P. C.; Elam, J. W. Supported Ru-Pt Bimetallic Nanoparticle Catalysts Prepared by Atomic Layer Deposition. *Nano Lett.* **2010**, *10*, 3047−3051.
(2276) Wang, H.; Wang, C.; Yan, H.; Yi, H.; Lu, J. Precisely-controlled synthesis of Au@Pd core-shell bimetallic catalyst via atomic layer deposition for selective oxidation of benzyl alcohol. *J. Catal.* **2015**, *324*, 59−68.
(2277) Jiang, X.; Gür, T. M.; Prinz, F. B.; Bent, S. F. Atomic Layer Deposition (ALD) Co-Deposited Pt-Ru Binary and Pt Skin Catalysts for Concentrated Methanol Oxidation. *Chem. Mater.* **2010**, *22*, 3024−3032.
(2278) Gao, Z.; Qin, Y. Design and Properties of Confined Nanocatalysts by Atomic Layer Deposition. *Acc. Chem. Res.* **2017**, *50*, 2309−2316.
(2279) Zhang, J.; Yu, Z.; Gao, Z.; Ge, H.; Zhao, S.; Chen, C.; Chen, S.; Tong, X.; Wang, M.; Zheng, Z.; et al. Porous TiO_2 Nanotubes with Spatially Separated Platinum and CoO_x Cocatalysts Produced by Atomic Layer Deposition for Photocatalytic Hydrogen Production. *Angew. Chem., Int. Ed.* **2017**, *56*, 816−820.
(2280) Ge, H.; Zhang, B.; Gu, X.; Liang, H.; Yang, H.; Gao, Z.; Wang, J.; Qin, Y. A Tandem Catalyst with Multiple Metal Oxide Interfaces Produced by Atomic Layer Deposition. *Angew. Chem., Int. Ed.* **2016**, *55*, 7081−7085.

https://doi.org/10.1021/acs.chemrev.1c00905
Chem. Rev. XXXX, XXX, XXX−XXX